Advances in Electromagnetics of Complex Media and Metamaterials

NATO Science Series

A Series presenting the results of scientific meetings supported under the NATO Science Programme.

The Series is published by IOS Press, Amsterdam, and Kluwer Academic Publishers in conjunction with the NATO Scientific Affairs Division

Sub-Series

I. Life and Behavioural Sciences	IOS Press
II. Mathematics, Physics and Chemistry	Kluwer Academic Publishers
III. Computer and Systems Science	IOS Press
IV. Earth and Environmental Sciences	Kluwer Academic Publishers
V. Science and Technology Policy	IOS Press

The NATO Science Series continues the series of books published formerly as the NATO ASI Series.

The NATO Science Programme offers support for collaboration in civil science between scientists of countries of the Euro-Atlantic Partnership Council. The types of scientific meeting generally supported are "Advanced Study Institutes" and "Advanced Research Workshops", although other types of meeting are supported from time to time. The NATO Science Series collects together the results of these meetings. The meetings are co-organized bij scientists from NATO countries and scientists from NATO's Partner countries – countries of the CIS and Central and Eastern Europe.

Advanced Study Institutes are high-level tutorial courses offering in-depth study of latest advances in a field.
Advanced Research Workshops are expert meetings aimed at critical assessment of a field, and identification of directions for future action.

As a consequence of the restructuring of the NATO Science Programme in 1999, the NATO Science Series has been re-organised and there are currently Five Sub-series as noted above. Please consult the following web sites for information on previous volumes published in the Series, as well as details of earlier Sub-series.

http://www.nato.int/science
http://www.wkap.nl
http://www.iospress.nl
http://www.wtv-books.de/nato-pco.htm

Series II: Mathematics, Physics and Chemistry – Vol. 89

Advances in Electromagnetics of Complex Media and Metamaterials

edited by

Saïd Zouhdi
Pierre et Marie Curie University,
Paris, France

Ari Sihvola
Helsinki University of Technology,
Espoo, Finland

and

Mohamed Arsalane
Cadi Ayyad University,
Marrakesh, Morocco

SPRINGER-SCIENCE+BUSINESS MEDIA, B.V.

Proceedings of the NATO Advanced Workshop on
Bianisotropics 2002 – 9th International Conference on Electromagnetics of Complex Media
Marrakesh, Morocco
8–11 May 2002

A C.I.P. Catalogue record for this book is available from the Library of Congress.

ISBN 978-1-4020-1102-3 ISBN 978-94-007-1067-2 (eBook)
DOI 10.1007/978-94-007-1067-2

Printed on acid-free paper

TABLE OF CONTENTS

PREFACE

The NATO Advanced Research Workshop *Bianisotropics 2002* was held in Marrakesh, Morocco, during 8–11 May 2002. This was the 9th International Conference on Electromagnetics of Complex Media, belonging to a series of meetings where the focus is on electromagnetics of chiral, bianisotropic, and other materials that may respond to electric and magnetic field excitations in special manner.

The first of these meetings was held in Espoo, Finland (1993), and the following venues were Gomel, Belarus (1993), Périgueux, France (1994), State College, Pennsylvania, USA (1995), the rivers and channels between St. Petersburg and Moscow in Russia (1996), Glasgow, Scotland (1997), Brunswick, Germany (1998), and Lisbon, Portugal (2000).

The present book contains full articles of several of the presentations that were given in the Marrakesh conference. In *Bianisotropics 2002*, 8 review lectures, 14 invited lectures and 68 contributed talks and posters were presented. Of these presentations, after a double review process, 28 contributions have achieved their final form on the pages to follow. From the contributions of the meeting, also another publication is being planned: a Special Issue of the journal *Electromagnetics* will be devoted to complex materials. Guest editors for this issue are Keith W. Whites and Saïd Zouhdi.

The chairmen of *Bianisotropics 2002* conference were Saïd Zouhdi (Pierre et Marie Curie University – Paris) and Mohamed Arsalane (Cadi Ayyad University – Marrakesh), who were assisted by Scientists from Moroccan Universities and the International Bianisotropics Conference Committee. The organisation and arrangement of the meeting required financial assistance and other support from several sources. Especially helpful in this respect was that *Bianisotropics 2002* meeting was a NATO Advanced Research Workshop. This gave the organisers a possibility to enrich the scientific programme of the meeting. Furthermore, the opening session of the workshop had a special flavour by the presentation of Dr. Fausto Pedrazzini, the Programme Director in the Scientific and Environmental Affairs Division of the NATO Science Programme. He spoke about the scientific dimension in the mission of the North Atlantic Treaty Organisation. This

is the third level on which NATO works, complementing the political and military aspects of the organisation.

This volume is structured in seven sections, each containing from three to six articles. Beginning from general aspects of complex materials, the focus changes to the characteristics of modern metamaterials and photonic band gap media. Then follows analysis and modelling of bianisotropic structures, along with computational studies of wave-interaction in complex media. After contributions on how material heterogeneities are connected to wave localisation, the final section discusses engineering and other applications of complex media and metamaterials.

Acknowledgements

We would like to take this opportunity to thank all who worked efficiently and very hard for *Bianisotropics 2002* to build a successful and productive event: the group of organisers, support staff, and all participants. We also wish to express our appreciation to the local committee and staff members of the conference for their efforts in organising and running the meeting; especially, thanks are directed to Abdelilah Ghammaz, Abdelaziz El Idrissi, and Abdessamad Zouhdi. The help from Sergei Tretyakov and Alexei Vinogradov was essential with the travel arrangements for our colleagues from the Former Soviet Union countries. The authors and reviewers of all the articles deserve a special acknowledgement. Their commitment has contributed to the successful completion of this volume.

We are grateful to the NATO Science Programme for the generous financial assistance which helped us to invite several scientists who would otherwise have had little chances to attend the meeting. Thanks also stand for the possibility to have the present collection of articles published in the NATO ASI series. We also gratefully acknowledge substantial financial contributions from the IST programme of the European Commission (Brussels), the Office of Naval Research International Field Office (London), and the DGA (Paris).

Paris - Espoo - Marrakesh
September 2002 *Editors*

Following page: Closing session of Bianisotropics 2002 *in Sahara. The famous kasbah, named* Ait Ben Haddou *guarded in medieval times the lucrative trading route through the desert to Timbuktu. Lawrence of Arabia, among other famous movie classics, has been filmed here. On the far background the Atlas mountains.*

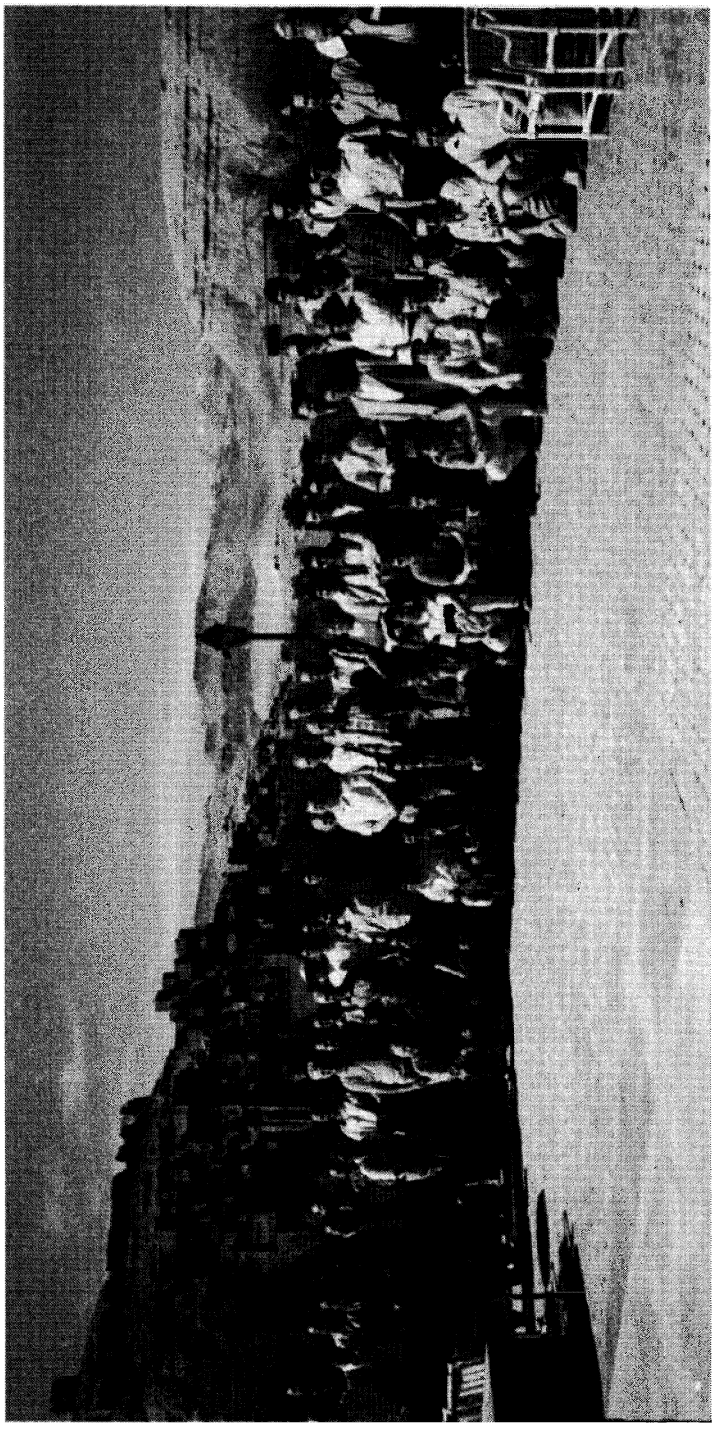

I.

GENERAL ASPECTS OF COMPLEX MEDIA AND META-MATERIALS

ELECTROMAGNETIC EMERGENCE IN METAMATERIALS

Deconstruction of terminology of complex media

A. SIHVOLA
Helsinki University of Technology, Electromagnetics Laboratory
P.O. Box 3000, FIN-02015 HUT, Finland

Abstract. This chapter focuses on the emergent electromagnetic properties in such heterogeneous materials that are, in today's discussion, being more and more often called "metamaterials." More precisely, the very concept of metamaterial is under study as also are the preconditions under which such a term is appropriate.

1. Introduction. The power of naming things.

"Metamaterials." This word has become very common in the recent discussion of materials research in electromagnetics, and perhaps also in some other fields of applied and theoretical physics. At least such an impression is by no means excluded. If this is true, what is the reason for such a state of affairs? Why is "metamaterial" used increasingly in electromagnetics parlance, if not yet so much in literature? Indeed, what is the exact meaning of the term?

In this presentation, I would like to problematise the use of the term "metamaterial," at least in the extent to which it is used exclusively to new, especially nanoengineered, materials. The history of electromagnetics research contains a very rich collection of results for random, inhomogeneous, and composite materials. A closer look at the properties of these old-fashioned materials reveals that they could be certainly classified into the group of the modern metamaterials, even though they may be well known and familiar to many of us as "ordinary" materials.

That scientists name things such that they attract attention is understandable. One can think of the recent surge of interest in PBG (photonic band gap) materials, or photonic crystals, where artificially manufactured geometries create pass band and stop bands for electromagnetic waves in microwave, millimetre wave, and optical regions. Physicist-driven research on PBG's has caused irritation within the microwave engineering community, and engineers point out (partially correctly) that periodical dielectric materials are nothing new. But who would not feel the desire of finding exciting and potentially money-attracting names for materials that are the subject of one's present studies? Certainly we also in the bi-anisotropics

S. Zouhdi et al. (eds.), Advances in Electromagnetics of Complex Media and Metamaterials, 3–17.

field have to admit this as we are talking about exotic, novel, or complex materials. But we have to remember that in some cases language can become a barrier for communication.

In the present article the use of the new term, metamaterials, is discussed. I try to find a meaning for it. The term is increasingly being used in literature, and I'll analyse some of the presented definitions. It seems that with the use of the term, there is a strong emphasis on the requirement that a metamaterial should display properties that are qualitatively different from its components. My aim is to problematise this requirement, at least in its strong form. I'll focus on the question what is the difference between "ordinary" composite materials and new metamaterials, if any. Towards the end of the article, I shall discuss some examples of complex materials, especially from the point of view of our bianisotropics community, and raise the question to what extent these media deserve to be called metamaterials.

But let us start from definitions.

2. Metamaterials? What do you mean?

It is difficult to find an acceptable definition for the term "metamaterial." This statement may sound very normative; after all, can one argue names? Of course, in a free world everyone is allowed to use words in ways that have not necessarily been formally approved into use by international committees, or even to use them in a totally idiosyncratic manner. But to be able to conduct constructive discussion where a given word has an important role, however, it is helpful if at least a group of people agree on the meaning of this word. Sure, the question remains open how large and representative this group must be. Furthermore, with a definition and use of terms in new environments one should pay respect to the historical use of the word, even if its background is on another, perhaps very different, field. This question is not unimportant in the case where we name scientific or engineering things and properties. One example of such a situation is the use of term "metamaterial."

By the writing of the present text (May 2002), the term "metamaterial" has been appearing in print for only a very short period. But some definitions exist. In first-order literature, materials conferences and research web pages the following definitions can be already found:

- Electromagnetic metamaterials are artificially structured composite materials that can be engineered to have desired electromagnetic properties, while having other advantageous material properties. [1]
- Structures composed of macroscopically scattering elements. [2]
- "Meta-materials", materials whose permeability and permittivity derive from their structure. [3]

- MetaMaterials are a new class of ordered nanocomposites that exhibit exceptional properties not readily observed in nature. These properties arise from qualitatively new response functions that are not observed in the constituent materials and result from the inclusion of artificially fabricated, extrinsic, low dimensional inhomogeneities. [4]
- Metamaterials are defined as macroscopic composites having a man-made, three dimensional, periodic cellular architecture designed to produce an optimized combination, not available in nature, of two or more responses to a specific excitation. Each cell contains *metaparticles*, macroscopic constituents designed with low dimensionality that allow each component of the excitation to be isolated and separately maximized. The metamaterial architecture is selected to strategically recombine local quasi-static responses, or to combine or isolate specific non-local responses. [5]

These four attempts to catch the meaning of metamaterials occur with only little variation in the electromagnetics literature. Regarding such definitions, one observation that can be made is that two essential properties are mentioned. The materials should exhibit (electromagnetic) properties

◊ not observed in the constituent materials, and/or
◊ not observed in nature.

These are quite remarkable and very restrictive features for materials if they are really applied to define a metamaterial. But indeed, the fact that such properties make a compulsory requirement is in the following sense in consonance with the authentic meaning of the compound word, meta-material.

The prefix *meta* comes from Greek (it is also used in Latin), and it means "after." Often the prefix is used also for "along with," "beyond," "among," "in the midst of," "according to," and "behind." There are numerous words in English and other languages starting with "meta," like, for example, metabolism, metalinguistics, metamerism, metaphysics,[1] metamorphosis, metastasis, etc. However, the common word in materials engineering, "metal," is of different origin.

With this background in mind, it seems that in the choice and use of "metamaterial," this meta-prefix emphasises the transcendental aspect of the

[1] The use of "meta" in the term "metaphysics" does not come from a very sublime sense of "above." Rather, it originally applied to those writings of Aristotle which in the accepted order came after (=*meta*) those dealing with natural science (*ta physika*--physics, nature) [6]. It is helpful to remember this in today's world where the word metaphysics brings to mind quite obscure, unclear, and transcendental overtones. Even the dictionaric definitions for metaphysics reflect this, being like "the branch of philosophy that treats of first principles, includes ontology and cosmology, and is always intimately connected with an epistemology;" or more generally, "philosophy, esp. in its more abstruse branches" [7].

meaning. A metamaterial needs to be qualitatively different from its components. New phenomena and novel properties should emerge when "ordinary" pieces are brought together. The whole should be more than the sum of its parts. Quantitative differences become qualitative ones.

There is a word for such a behaviour of systems. It is "emergence."

3. Emergence. More is different.

Emergence is the process of emerging. Something arises, comes up into existence. It comes forth from concealment or obscurity. The etymology for this word leads to the combination *e* (out of) + *mergere* (to plunge, dip, or immerse). A more common word with the same root is "emergency" which is a sudden, urgent, usually unexpected occurrence or occasion requiring immediate action. But about emergence, it is important to note that it has also a more technical meaning in science and philosophy. In evolutionary theory, it stands for the rise of a system that cannot be predicted or explained from antecedent conditions. George Henry Lewes, the 19th-century English philosopher of science, distinguished between resultants and emergents—phenomena that are predictable from their constituent parts and those that are not [Encyclopaedia Britannica]. Later, emergence theories have been espoused by Henri Bergson, Pierre Teilhard de Chardin, Alfred North Whitehead, and Michael Polanyi. The doctrine of emergence is sometimes stated as part of an "evolutionary cosmogony, according to which the simpler properties and forms of organisation already in existence make contributions to the 'creative advance' of nature by giving birth to to more complex and 'irreducibly novel' traits and structures" [8].

Clearly the present-day electromagnetics use of "metamaterials" is defining the word through the concept of emergence.

The philosophical meaning of "emergence" is connected to another essential term, reductionism. Emergence is very often associated with antireductionistic goals. According to a (strict) reductionist view, "higher-level" scientific theories can be completely and exhaustively reduced to more basic fields of science, for example chemistry into physics, biology in biochemistry, psychology in neurophysiology, and so forth. Everything (it can be objects (ontological reduction), theories, or whole scientific fields) in the higher level of description is contained (even if in a non-obvious way to an amateur) in the "harder" sciences, finally in elementary particle physics.[2] Clearly the concept of emergence is a problematic phenomenon to a reductionist, or may be difficult to accept within (philosophical) materialism. A person with inclination to a very mechanistically

---

[2] It may be visible from the present text that I am not fully subscribing to the strict reductionist programme. Can the great book *The Brothers Karamazov* by Fyodor M. Dostoyevsky be reduced to (=be equivalent to certain ordered combinations of) the 26 letters of the English alphabet (or, more precisely, to the 33 letters of the Russian one) ?
---I doubt it. (...but feel a little uncomfortable with the doubt...)

reductionist view may feel the temptation to call an "upper-level" field of science just "applied" more fundamental science: chemistry as applied physics, for example.

In dialectic materialism and Marxism–Leninism, emergence is nevertheless something that can be accepted. According to those lines of thought, matter (in movement) has various levels of existence and movement, physico–chemical, biological, and social, which all have their own laws. And these laws are independent of the other levels. However, this does not mean that living creatures would possess properties that are not connected to physical laws. It is that they "emerge" in systems that are sufficiently complex but it may be difficult to predict, or even to explain how or when such qualitative changes happen.[3] A simple extrapolation upwards fails.

Indeed, an important distinction regarding reductionism comes from Philip Anderson [9]. He criticises its strong form which claims that in materials science, there are only "extensive" problems left, equal to device engineering.[4] Anderson identifies the fallacy in this reasoning in that the reductionist hypothesis does not imply a constructionist one. In other words, even if one could reduce a phenomenon into the fundamental elements, one cannot start with basic laws and reconstruct the universe. "[T]he more the elementary particle physicists tell us about the nature of the fundamental laws, the less relevance they seem to have to the very real problems of the rest of science, much less to those of society."

Emergence can also be appreciated in the mechanism according to which many cellular automata operate. There, simple and local rules can create behaviour in which new patterns may appear and objects are created. Or at least one would think of them as reals "objects" even if they may be just little squares on the computer screen which are turning on and off. For example, in the emergence applets of the Media Laboratory of the Massachusetts Institute of Technology (available from el.www.media.mit.edu/groups/el/projects/emergence) the emergence of "life" can be seen on the computer screen.

4. Against emergence. More is less.

But somehow the slogan "the whole is more than the sum of its parts" is counterintuitive. When we look at an ensemble, very much of the detailed structure

---

[3] Something essential about emergence, and about quantity transforming to quality is contained in the following anecdote (taken from the article [9]) where the two famous American literary figures meet in Paris in the 1920's:

FITZGERALD: The rich are different from us.

HEMINGWAY: Yes, they have more money.

[4] V. Weisskopf [10] distinguishes between intensive and extensive research: "[I]ntensive research goes for the fundamental laws, extensive research goes for the explanation of phenomena in terms of known fundamental laws.... Solid state physics, plasma physics, and perhaps also biology are extensive. High energy physics and a good part of nuclear physics are intensive."

is left out in the grand picture. If we have a mixture of a great number of elementary objects, in the "real life" they are interacting in many ways. But in the large-scale picture, all these interactions only have an effective influence. The macroscopic picture is a certain "average" of the individual contributions, although this averaging does not need to be a simple operation. And hence extremely many degrees of freedom are lost when the ensemble is sensed with a coarser resolution. Then, sure, the whole is *less* than the sum of its parts.

Indeed, an effective picture means a *reduced* dimensionality compared to the corresponding macroscopic properties of the constituents. One is unable to catch the details because there is simply too much information.

What, then, about the intuitively emergent meaning of a piece of art? Wouldn't everyone take an antireductionist stance when it comes to literature? Why do we feel that a poem is "more" than the information content (expressable as a relatively short sequence of 0's and 1's) of its letters, exclamation marks and spaces between characters? The answer to this dilemma may be in the following. Is it that when asking such questions we are mixing up the real physical object and the measuring instrument?[5] What is a poem, after all? And where does its meaning exist?

5. Physics and metaphysics of electromagnetic materials

Can the philosophically flavoured discussion in the previous sections be made relevant to electromagnetic properties of materials? Is it too far into the field of metaphysics? Why, the effective modelling of heterogeneous materials is fundamentally analysis and prediction of emergence. When higher-level description of matter is sought using various mixing rules–even the simplest ones, like Maxwell Garnett [12]–it quite often happens that the homogenised medium displays properties that are astonishingly different from not only those of the components but also from those that one would expect from the mixing process [13]. But does the fact that the result for macroscopic material character is unforeseen and unexpected automatically mean that the higher-level property is emergent, especially in the evolutional and vitalist tone and meaning of the word? It seems that this is a crucial distinction to be made in the metamaterials discussion.

5.1. IS A COMPOSITE MATERIAL METAMATERIAL?

The electromagnetics community has been working for a long time with modelling of properties of heterogeneous materials, both in the field of natural, geophysical materials that are random in structure in the first place, and also in the design of artificial and composite materials where the goal is to manufacture materials with desired properties. In the analysis of the effective properties of such materials,

[5] As Kari Enqvist [11] has noted, we may be especially susceptible to this fallacious reasoning when the observing system is the human brain.

emergence-type behaviour often takes place when we move upwards from the microscale to meso- and macroscales and assign the medium effective properties on the larger scale. But can we call any kind of higher-level material by the name metamaterial?

Why not? At least all materials are composites because if we go to smaller and smaller scales, finally we encounter atomic constituents, electrons, protons, neutrons. On macroscale, the medium appears always as an effective average of the lower-level constituents. These effective properties are always "emergent" properties, and are in principle "other than" the properties of the components. They are not plain volume averages of the corresponding inclusion properties, and therefore all matter, even simple mixtures, deserve to be called "metamaterials." And very often do these materials have superior properties over their components. Take for example cellulose or cement, where the superiority is evident even from an everyday-life point of view.

The question is therefore on scale. When we look with myopic eyes at a medium, there is a limit below which we cannot resolve finer details. Can we find or determine an absolute scale? One can always go to higher levels on the scale of various materials. Then we face the problem of the measure and length of homogenisation and the question what can be called a material. Even the mobile radio channel has been called as a complex medium.[6] What a composite!

5.2. LINEARITY AND SUPERPOSITION

Scale and geometry are essential in the character of mixed matter but so is also the constitutive response of the component materials themselves. Nonlinear media are more complex than media with purely linear response. It would be tempting to associate the emergent properties in material description to nonlinearity in the constitutive relations. If the electric polarisation is not linearly dependent on the excitation field, it is certainly difficult to foresee what kind of macroscopic responses can a heterogeneous aggregate of such materials possess. But this kind of a straightforward correspondence between emergence and nonlinearity is not satisfactory, for at least two reasons.

Firstly, the principle of superposition, which according to normal textbook logic follows from linear input--output relation, is still fully compatible with the reductionist view where the properties of the whole can be derived and constructed from the properties of its components. Nonlinearity may lead into difficulties in the analysis of the problem but does not give to it any mystical and unexplainable character. It is only that we can no longer exploit superposition and splitting of the problem into easily solvable subproblems.

---

[6] See the title of the presentation by R. Prasad and D.K. Kalluri in the Conference *Complex Mediums II: Beyond Linear Dielectrics*, in SPIE's 46th Annual Meeting and International Symposium on Optical Sciences and Technology, **4467**, San Diego, California, 2001.

For the second, even simple, linear mixing problems may bring forth macroscopic phenomena that quite often look emergent in the unexpected sense of the word. Such phenomena, like for example, percolation, enhanced electric or magnetic polarisation, and chirality, will be discussed later in this section.

Our eyes as receiving antennas and the image processing equipment connected to those make their own interpretations of the random microstructure of materials. Take, for example, the two-dimensional "material" depicted in Figure 1. There, depending on scale, structures may be seen as emergent patterns, although the dew formation on a day with freezing environment follows blind rules of condensation.

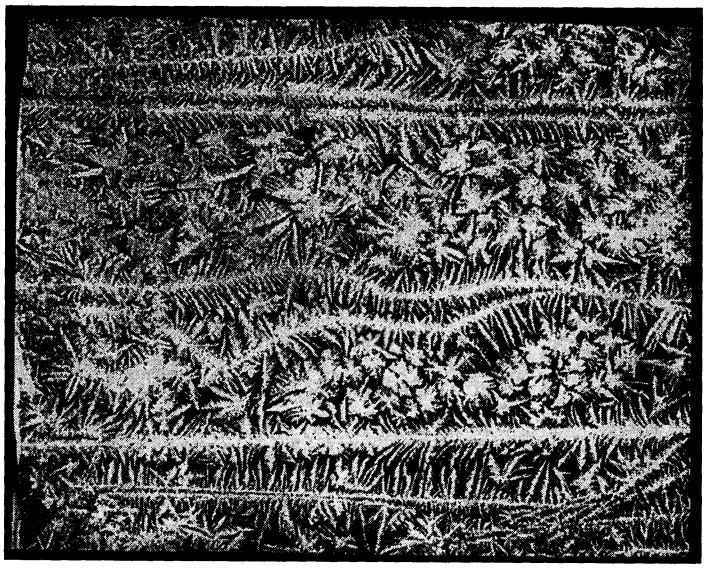

Figure 1. Frost and dew form patterns in which structure on a higher level clearly emerges. (Perhaps emerges ...) This picture is from W.A. Bentley's snow archives [14].

And how blind is the process? The rules and laws governing the evolution and rest states of the physical system may be written as partial differential equations as has been the habit throughout the three centuries old history of mathematical physics. No emergence is explicit in these equations. They only connect the amplitudes at a certain spatial point at a certain time instant to the neighbouring ones. Perhaps the alternative description in which the observed phenomena of the material world are seen as products of rules, simple lines of code which Stephen Wolfram [15] has advocated may catch more of the essence of these emergent phenomena.

5.3. ARTIFICIAL DIELECTRICS

An earlier version of the metamaterial-term is the term "artificial dielectric" which has a history of over a half century. In 1948 Winston E. Kock suggested to make a dielectric lens lighter in weight by replacing the refractive material by a mixture of metal spheres in a matrix. Kock built lenses by spraying conducting paint on polystyrene foam and cellophane sheets. He was probably the one to coin the term *artificial dielectric*, the physics of which is well documented in Collin's text on guided waves [16] and which term is very well established in the microwave literature (see also, [17]). Let us remind ourselves of Kock's own words [18]:

> *The artificial dielectric material which constitutes the delay lens was arrived at by reproducing, on a much larger scale, those processes occurring in the molecules of a true dielectric which produce the observed delay of electromagnetic waves in such dielectrics. This involved arranging metallic elements in a three-dimensional array or lattice structure to simulate the crystalline lattices of the dielectric material. Such an array responds to radio waves just as a molecular lattice responds to light waves; the free electrons in the metal elements flow back and forth under the action of the alternating electric field, causing the elements to become oscillating dipoles similar to the oscillating molecular dipoles of the dielectric.*

Compare this with the introductions of reports from the present third millennium that deal with photonic band gap structures and metamaterials! Although in the above citation the emphasis of low frequencies is conspicious and therefore does not directly relate to more complicated resonance phenomena, this excerpt is a good reminder for us about the fact that many ideas in materials design have been around for a long time.

Admittedly today's treatments of the metamaterial design are more detailed. Take, for example, the classification into *mesomaterials* and *metamaterials* by Walser [5]. With mesomaterial design he means that ordered macroscopic materials are synthesised from the bottom up by assembling macromolecules, like fullerenes or carbon nanotubes (these are so-called mesoscale supramolecules). In the more advanced and mature metamaterials design the order is the opposite: macroscopic composites are synthesised top down by "first disassembling, then recombining macroscopic constituents." Probably the strategy in this second approach by Walser is more target-oriented: the desired properties of the metamaterial to be fabricated are predetermined with stricter tolerances as in the first, mesomaterial approach.

5.4. EMERGENCE AND REDUCTION IN ELECTROMAGNETICS: ARE THEY COMPATIBLE?

The crucial question remains: does there exist really emergent behaviour when electromagnetic materials are treated as mixtures and when they are synthesised

from lower-level components? An emphatic yes is clearly the opinion of many metamaterials investigators. Or, looking from another direction, is everything in the behaviour of the composite on a higher level just a straightforward average of the properties of its components and the microgeometry of its structure, which would be a more reductionistic view? To make it easier to look for answers for these questions, Table 1 attempts to achieve structure to the dichotomy between emergence and reduction in the degrees of freedom in the description of electromagnetic materials.

TABLE 1. Some differences follow regarding the status of "ordinary" composites, when the point of view of emphasising emergence is changed to a reductionistic one. The left column (the whole is MORE than the sum of its parts) stresses the view of qualitatively different character of engineered metamaterials with emergent properties, while the right-hand side (the whole is LESS than the sum of its parts) takes the more mechanistic bottom-up view of material description where the averaging process reduces the dimensionality of the microlevel of the matter.

The whole vs. the sum of its parts	MORE	LESS
Philosophical background	Idealistic, immaterialistic, holistic	Reductionist, physicalist
Effect on the higher level of description	Emergence	Reduced dimensionality
Materials	Metamaterials	Classical composites
Effective medium description	Non-local effects and connections	Linear mixing rules
Effects and phenomena	Spontaneous symmetry breaking	Continuous extrapolation
Examples	Percolation, chiral materials, artificial (and natural) magnetism, PBG's, Veselago media	Simple aggregates, laminates, weakly interacting inclusions

In the table the contrast between the two views appears perhaps a little exaggerated but it is intentional: to make the translation of the philosophical thinking to the electromagnetics level. Emergence is identified with new macroscopic phenomena that are brought forth by the process of mixing. But it is at the same time contrasted with the recipes of classical mixing formulas which may look quite simple algebraic relations between the properties of the composite on one hand, and those of the constituent materials on the other. But such a picture may need more

elaboration. Let us take a closer look at various materials in electromagnetics and see how they relate to the dichotomy of Table 1.

5.5. EXAMPLES OF ELECTROMAGNETIC MATERIALS WITH EMERGENT PROPERTIES

5.5.1. Chiral materials

From the point of view of complex materials and bianisotropic description of electromagnetic materials, the obvious example of media with intuitively emergent properties is the class of chiral materials. In chiral media, the geometrical character of the internal structure (the handedness) cause macroscopic effects that are observed as the rotation of the polarisation of the propagating field plane [19]. A man-made chiral sample could be a collection of metal helices, randomly oriented and distributed in a neutral polymer matrix. Were one to call chiral media metamaterials with emergent properties, the emergent character could be interpreted in the manner that nothing in the component materials (metal and polymer) hints to the ability of causing rotatory power but still this is the effect of the chiral composite. The effect comes through mixing and geometry.

5.5.2. Percolation effects

Percolation effects display themselves as large changes in macroscopic properties of random materials when the fractional volumes of the components are varied [20]. Percolation is an important phenomenon and it has been studied in connection with several fields and applications: study of ferromagnetism, soil moisture, oil penetration in rocks, the spread of epidemics, forest fires, and even in wafer-scale integration in the manufacture of microchips. Also the macroscopic electromagnetic properties of random materials can achieve percolatory character, being very sensitive to the microstructure of the mixture, even if the components have no special character in their properties.

5.5.3. Artificial magnetics

One further example of the metamaterial-type phenomenon is the creation of magnetism without magnetic constituents. This may happen in ordinary random materials, like wet snow where loop-forming parts of the liquid water cause diamagnetic behaviour in the macroscopic response of the medium. The magnetic permeability, μ is not equal to that of the free space. But this effect can also be enhanced and "artificially" produced by embedding various metallic loop-type elements in a matrix. Swiss roll -type of scatterers are especially effective in this respect [21]. Also in modern metamaterial design the use of split-ring resonators (which often are adjacent, nonconnected open metallic loops) is quite common. Because of its planar structure it is perhaps a more practical way of creating artificial magnetism [22].

5.5.4. Enhanced polarisation

The next example of "emergent behaviour" due to simple mixing is so-called enhanced polarisation. This phenomenon is even theoretically visible with the use of the most simple mixing rule, the Maxwell Garnett formula for mixtures where spherical scatterers, small compared to the wavelength, are immersed in homogeneous background. Figure 2 displays the results of such mixing in two cases.

The two figures illustrate clearly the two classes of mixtures in Table 1. On the left, the macroscopic permittivity of dry snow is a quite dull and uninteresting average of the permittivities of its two constituents, air and ice. Nothing emergent---qualitatively new---can be observed. But on the right-hand figure, the real part of the effective permittivity of the mixture where lossy spheres are embedded in air displays much stronger polarisation (the real part of the effective permittivity is close to 5 even if the real part of the inclusions is 2) than either of the constituents. This happens, of course, only at a range of the volume fraction of the inclusions (here the maximum enhancement requires around 80% fraction). And this enhancement can be made much stronger by increasing losses in the inclusion phase. This effect of high permittivity values is known with living matter, where interfacial polarisation mechanisms may be drastically enhanced and observed with biological membranes and tissues.

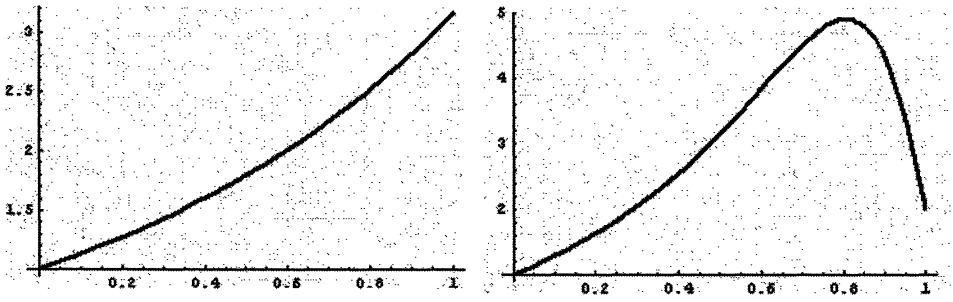

Figure 2. The (real part of the) effective permittivity of a mixture with spherical dielectric inclusions immersed in free space, as a function of the volume fraction of the inclusions. Left-hand side: dry snow (the inclusions are ice (permittivity ε=3.17) and background is air (permittivity ε=1)). Right-hand side: a high-loss mixture with inclusions having permittivity ε=2 - j10 in air. (Note that depicted is the real part of the permittivity.)

5.5.5. Veselago medium

The so-called Veselago medium can be deservedly called a metamaterial *par excellence*. This medium has, as very often new effects and inventions do, several different names:

◊ Left-handed medium

- ◊ Medium with simultaneously negative permittivity and negative permeability
- ◊ Negative index of refraction (NIR) medium
- ◊ Double negative metamaterial
- ◊ Backward-wave material

Suggested in 1967 [23], this medium has been studied theoretically and experimentally very much during the two last years or so. As can be inferred from the various labels on Veselago medium, its nonconventional property is that both its permittivity and permeability are negative, for a certain range of frequencies. Practical realisations have been indeed achieved for such Veselago-medium samples with observed properties that confirm the predictions (see, for example, [24]). The strange effects of Veselago media include anomalous refraction, inverted Cherenkov radiation and Doppler shift, and it is being studied for applications involving waveguiding, radiation, and diffraction phenomena.

In many of these emergent phenomena that are created in mixtures, the effect is a cause of a break in the symmetry that is preserved on the lower level. No wonder that broken symmetry is an important concept in the description of magnetism. But even in more general terms, many material effects can be said to testify to Johannes Kepler's famous slogan (see, for example, [25]): *Ubi materia, ibi geometria.*

6. Conclusion: the three critiques

To conclude this treatment of emergence in electromagnetic materials, let us summarise the critique towards the definition of metamaterial when it is understood in the above sense that has been deconstructed from the explicit definitions and practical use of the term.

Firstly, the requirement that a metamaterial needs to be "superior" to previously existing materials is inherently subjective. There are figures of merit with which people measure superiority of the materials. For example, in ferrites this measure could be the product of low-frequency permeability and resonant frequency. But because of this arbitrariness, a definition based on superiority is too loose to be acceptable to classify metamaterial. Any kind of new mixture is always different from previously existing ones and therefore possesses a unique combination of properties. If such a set is what is wanted, we have everywhere examples of metamaterials.

The second piece of critique is connected to the distinction between local and non-local effects in the material response, also mentioned in Table 1. Very often the emergent and novel property of metamaterials is assigned to the fact that the scattering elements in the composite interact in a non-local manner, like for example in frequency-selective surfaces or photonic crystals. Spatial dispersion is often required for the higher-order effects. But this is not necessary, as has been pointed out in the previous examples in this article. Even simple mixing rules are

able to explain very non-intuitive and emergent properties for ordinary-looking mixtures, like, for example, enhanced polarisation and percolation behaviour.

And finally, if a metamaterial should possess properties that (in addition of being superior to those observed before) are not found in nature, the definition might sound a little contradictory. We are, in our design and synthesis of composite materials, working according to the rules and laws of nature.[7] Therefore the results–our metamaterials–also are "natural." And if we did not find materials with properties corresponding to these new designs yet in nature, is it only that we did not search hard enough? Nature is extremely prodigious. All possibilities come true. All properties, all media that are not forbidden, are there, somewhere. They are compulsory.

7. References

1. The www page of David Smith, University of California, San Diego. http://physics.ucsd.edu/~drs/
2. Weiland, T., Schuhmann, R., Greegor, R.P., Parazzoli, C.G., Vetter, A.M., Smith, D.R., Vier, D.C., and Schultz, S. (2001) *Ab initio* numerical simulation of left-handed metamaterials: Comparison of calculations and experiments, *J. of Applied Physics,* **90**(10), 5419-5424.
3. Pendry, J.B. (2001), Negative μ, negative ε, negative refractive index, and how to exploit them. Electromagnetic Crystal Structures, Euroconference on Electromagnetic Confinement, from Basic Research to the Marketplace, St. Andrews, Scotland, 9-14 June 2001. (no page number)
4. Metamaterials home page of the future projects of the Defense Advanced Research Projects Agency's (DARPA) Defense Sciences Office (DSO). http://www.darpa.mil/DSO/future/metamaterials/metamaterials.html
5. Walser, R.M. (2001) Electromagnetic metamaterials, Inaugural Lecture, Proc. of SPIE (Complex Mediums II: Beyond Linear Isotropic Dielectrics; Lakhtakia, A, Weiglhofer, W.S., and Hodgkinson, I.J.editors), **4467**, 1-15.
6. Chambers Twentieth Century Dictionary, 1977, (edited by A M Macdonald)
7. The Random House Dictionary of the English Language, Second Edition, unabridged, New York, 1987, (Stuart Berg Flexner, editor-in-chief).
   [The "abstruseness" of the Random House definition for metaphysics is evident in the following citation from "Subjects among other things" by E. Sosa (1987) in *Philosophical Perspectives,* Vol. 1, where also "metamaterial" is used in a different meaning (adjective) as in the present article: "If we allow real status to the materially derivative, it seems arbitrary to rule out objects that though immaterial are no more derivative; all the more so if in each case the mode of derivation is equally well understood. So it seems ill-advised and unnecessary to strain against

[7] The question of what kind of materials can occur in nature and which are forbidden may bring reminiscences into mind of the controversy concerning the possible existence of non-reciprocal bi-isotropic media, also called as NRBI media or Tellegen media [26], [27]. However, there the discussion focused on the question whether the laws of physics forbid the possibility to manufacture these materials (in which case it would be understandable that one cannot find those in nature). Here, with metamaterials discussion, no one is claiming that metamaterials as such break the rules acconrding to which materials have to exist; it is only that some metamaterials definitions exclude the natural existence of such media, even if engineers can (and want to) manufacture those.

the immaterial, or at least against that which is sufficiently *meta-material* (metaphysical?) to be distinct from the chunk of material that constitutes it at that time." (italics not in the original)]

8. Nagel, E. (1979) *The structure of science*, Problems in the logic of scientific explanation.Routledge and Kegan Paul, New York.
9. Anderson, P.W. (1972) More is different. Broken symmetry and the nature of the hierarchical structure of science. *Science*, **177**(4047), 393-396.
10. Weisskopf, V.F., in *Brookhaven Nat. Lab. Publ. 888T360.* Cited in [9].
11. Enqvist, K. (2000) *Valo ja varjo* (Light and shadow, in Finnish). WSOY.
12. Maxwell Garnett, J.C. (1904) Colours in metal glasses and metal films, *Transactions of the Royal Society (London)*, **CCIII**, 385-420.
13. Sihvola, A. (1999) *Electromagnetic mixing formulas and applications,* IEE Publishing, Electromagnetic Waves Series, London.
14. Wilson "Snowflake" Bentley Digital Archives. The man & his images, CD-rom, **1**, PhotoGraphics Multimedia production, Jericho, Vermont, USA, 1999. See also, Bentley, W.A. and Humpreys, W.J. (1962) *Snow Crystals.* New York: Dover.
15. Wolfram, S. (2002) *A new kind of science,* Wolfram Media, Inc.
16. Collin, R.E. (1991) *Field theory of guided waves*, Second Edition, IEEE Press, New York.
17. Brown, J. (1960) Artificial dielectrics, in *Progress in Dielectrics,* (Birks, J.B., editor) **2**, 193-225.
18. Kock, W.E. (1948) Metallic delay lenses, *Bell System Technical J.*, **27**, 58-82.
19. Lindell, I.V., Sihvola, A.H., Tretyakov, S.A., and Viitanen, A.J. (1994) *Electromagnetic waves in chiral and bi-isotropic media*, Artech House, Boston and London.
20. Grimmett, G. (1989) *Percolation*, Springer, New York.
21. Pendry, J.B., Holden, A.J., Robbins, D.J., and Stewart, W.J. (1999) Magnetism from conductors and enhanced nonlinear phenomena, *IEEE Transactions on Microwave Theory and Techniques,* **47**(11), 2075-2084.
22. Shelby, R.A., Smith, D.R., and Schultz, S. (2001) Experimental verification of a negative index of refraction, *Science*, **292**, 77-79.
23. Veselago, V.G. (1968) The electrodynamics of substances with simultaneously negative values of ε and μ, *Soviet Physics Uspekhi,* **10**(4), 509-514. (Translation from the original Russian version, *Uspekhi Fizicheskii Nauk*, **92**, 517-526, July 1967.)
24. Shelby, R.A., Smith, D.R., Nemat-Nasser, S.C., and Schultz S. (2001), Microwave transmission through a two-dimensional, isotropic, left-handed metamaterial, *Applied Physics Letters*, **78**(4), 489-491.
25. Sihvola, A. (2000) Ubi materia, ibi geometria. *Helsinki University of Technology, Electromagnetics Laboratory Rep. Series*, **339**, September 2000. See also http://www.hut.fi/~asihvola/memos.html
26. Lakhtakia, A. and Weiglhofer, W.S. (1994) Are linear, nonreciprocal, bi-isotropic media forbidden? *IEEE Trans. Microwave Theory and Techniques,* **42**(9), 1715-1716. (See also, *ibid.*, September 1995, December 1995)
27. Sihvola, A.H. (1995) Are nonreciprocal, bi-isotropic media forbidden indeed? *IEEE Trans. Microwave Theory and Techniques,* **43**(9), 2160-2162. (See also, *ibid.*, September 1994, December 1995)

IDEAS FOR POTENTIAL APPLICATIONS OF METAMATERIALS WITH NEGATIVE PERMITTIVITY AND PERMEABILITY

Nader Engheta
University of Pennsylvania
Department of Electrical and Systems Engineering
Philadelphia, Pennsylvania 19104, U.S.A.

Abstract. Metamaterials with negative real permittivity and permeability possess interesting electromagnetic properties. Owing to the presence of anomalous refraction at the boundary between such a medium and a conventional medium, and the fact that in these media the Poynting vector and the wave vector of a uniform plane wave are antiparallel, one can conceptually suggest a variety of interesting potential applications for these media. In this chapter, we briefly describe some of our ideas and speculations on potential applications involving these metamaterials. These ideas include suggestions for phase compensators/phase conjugators, the idea of "complex medium of media" with compensated phase, the idea for thin, compact, subwavelength cavities and waveguides, suggestions for anomalous mode couplers, radomes and antenna covers, to name a few. We provide physical remarks and intuitive comments on these ideas.

1. Introduction

The concept of composite materials in which both permittivity *and* permeability possess simultaneously negative real values at some frequencies has recently gained considerable attention (see e.g., [1]-[15]). This idea was originally initiated by Veselago in 1967, who theoretically studied monochromatic uniform plane wave propagation in a material whose permittivity and permeability were assumed to be simultaneously negative [6]. Recently Shelby, Smith, and Schultz in their group at the University of California, San Diego constructed a composite medium in the microwave regime, and experimentally showed the presence of anomalous refraction in this medium [1], [2], [3], [5]. It is also worth mentioning that previous theoretical study of electromagnetic wave interaction with omega media using the circuit-model approach had also revealed the possibility of having negative permittivity and permeability in omega media for certain range of frequencies [16].

Various names and terminologies have been suggested for metamaterials with negative permittivity and permeability. Among these one can mention "left-handed" media (see e.g., [1], [2], [3]), media with negative refractive index [1]-[6], [11], [12], "backward-wave" media (BW media) [7], "double negative" (DNG)

S. Zouhdi et al. (eds.), Advances in Electromagnetics of Complex Media and Metamaterials, 19–37.

metamaterials [8], and negative-index media (NIM) [13], to name a few. The fact that for a time-harmonic monochromatic uniform plane wave in such a medium the direction of the Poynting vector is antiparallel with the direction of phase flow as theoretically pointed out by Veselago [6], leads to the anomalous refraction at the boundary of such a medium with a conventional medium. This is an exciting feature that may become advantageous in design of some novel devices and components, if/when such media can be easily constructed. It is important to point out that the study of the "backward" wave propagation in certain structures was a subject of research study several decades ago, when periodic structures supporting "backward" waves were analyzed for some applications in microwave oscillators and amplifiers (see e.g., [17], [18], and [19]). Furthermore, some recent studies of photonic bandgap (PBG) structures have shown the presence of anomalous refractive properties in photonic crystals under certain conditions [20], [21], [22], [23].

In this chapter, we present some of our conceptual, speculative ideas for potential applications of metamaterials possessing simultaneously negative real permittivity and permeability. In all these cases, we conceptually assume these metamaterials to be essentially lossless and, therefore, the material parameters are taken to be real-valued quantities. It is known that strictly speaking, no material (except the vacuum in the classical sense) is dispersionless, and therefore the Kramers-Kronig relations require the inclusion of dissipation. However, in our speculative ideas presented here, we assume that the dissipation is negligible at the frequency of monochromatic radiation of interest.

Theoretical analyses of some of these ideas have been performed, while some of the analyses of other speculative ideas suggested here are under way.

2. Phase Compensation/Phase Conjugation Using Metamaterials with Negative Permittivity and Permeability

It is known that in a homogeneous, isotropic, lossless medium, the wave number k of a monochromatic uniform plane wave can be expressed as $k = \omega\sqrt{\mu\varepsilon}$, where ω is the radian frequency, and μ and ε are the permeability and permittivity of the medium, respectively. For a lossless metamaterial with negative real permittivity and permeability at certain frequencies, i.e., when $\mu < 0$ and $\varepsilon < 0$ at given frequencies, this wave number attains real values, and as a result, the electromagnetic plane wave can propagate in such a medium at these frequencies [6]. However, for such a plane wave in this medium the phase velocity is in the opposite direction of the Poynting vector, as pointed out by Veselago in 1967 [6]. Due to this antiparallel nature of Poynting vector and the phase velocity in such a medium, one can consider the possibility of phase compensation/phase conjugation using these materials. In [10], we introduced theoretically the concept of phase

compensation by these materials. Below we give a brief overview of this idea.

We first take a slab of conventional lossless material with positive real permittivity $\varepsilon_1 > 0$ and positive real permeability $\mu_1 > 0$. In analogy with the terminology of "double-negative" (DNG) medium suggested in [8] for metamaterials with negative permittivity and permeability, here for conventional materials with positive permittivity and permeability we use the term "double-positive" (DPS) media. The index of refraction of this slab of DPS medium is shown as $n_1 \equiv \sqrt{(\varepsilon_1 \mu_1)/(\varepsilon_o \mu_o)}$, where ε_o and μ_o are the permittivity and permeability of the free space. Here we take n_1 to be a positive real quantity. The slab is infinitely extent in the *x-y* plane and has the thickness d_1 along the *z* axis. For the sake of simplicity in the argument, we assume that the intrinsic impedance of the DPS material of this slab $\eta_1 = \sqrt{\mu_1 / \varepsilon_1}$ is the same as that of the outside region $\eta_o = \sqrt{\mu_o / \varepsilon_o}$, i.e., $\eta_1 = \eta_o$, although this assumption is not necessary. The refractive index of the slab is, however, different from that of outside, i.e., $n_1 \neq n_o$. We now consider a monochromatic uniform plane wave normally incident on this slab. This monochromatic wave enters the slab without any reflection, traverses the width d_1, and exits from the other face of the slab. The phase of this wave at the end of the slab is obviously different from the phase at the beginning of it by the amount $n_1 k_o d_1$, where $k_o \equiv \omega \sqrt{\varepsilon_o \mu_o}$. Now let us put another layer of width d_2 made of a lossless DNG metamaterial, in which $\varepsilon_2 < 0$ and $\mu_2 < 0$ at certain frequencies, next to this DPS slab. (See Fig. 1.) The index of refraction for this DNG layer is a real quantity denoted by $n_2 \equiv \sqrt{(\varepsilon_2 \mu_2)/(\varepsilon_o \mu_o)}$. We emphasize here that we do not need to specify any sign for the operation of the square root appearing in the expression of n_2. We merely state that n_2 is a real quantity for the lossless DNG metamaterial here. For example, n_2 can be taken to be a positive real quantity. As in the case of the DPS slab, we again assume that the intrinsic impedance of this DNG metamaterial $\eta_2 = \sqrt{\frac{\mu_2}{\varepsilon_2}}$ is the same as that of outside region, i.e., $\eta_2 = \eta_o$, but its index of refraction is different from that of outside, i.e., $n_2 \neq n_o$. As the monochromatic plane wave exits the DPS slab, it enters the DNG layer, traverses this slab, and leaves this DNG layer. The direction of power flow (i.e., the Poynting vector) in the DPS slab should be the same as that in the DNG one, because the power of the incident wave enters the first slab (without any reflection at the first interface), traverses the first slab, exits the second interface, enters the DNG layer and traverses it, and finally leaves the second slab. In the DPS layer, the direction of the Poynting vector is parallel with the direction of phase velocity; however, in the DNG slab these two vectors are antiparallel, as depicted in Fig. 1.

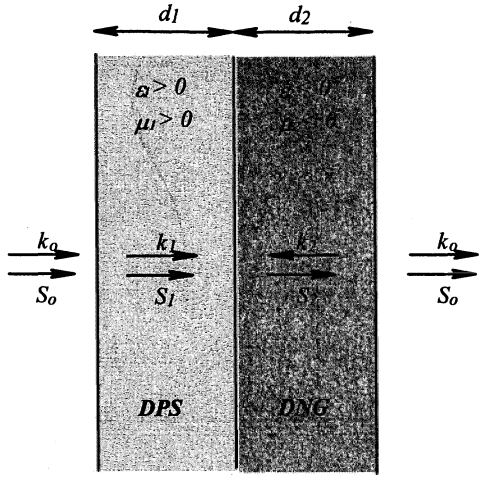

Figure 1. A paired two-layer structure formed by a lossless metamaterial with negative permittivity and permeability (a "double-negative (DNG) medium) and a conventional lossless dielectric material with positive permittivity and permeability (which can be termed as a "double-positive (DPS)" medium). In the DPS layer, the direction of Poynting vector (S_1) is parallel with the direction of phase velocity or wave vector (k_1), whereas in the DNG layer these two directions are antiparallel. The DNG layer can play the role of a phase compensator. With proper choice of the *ratio* of d_1 and d_2, not the *sum* of d_1 and d_2, one can have the phase of the wave at the left (entrance) interface to be the same as the phase at the right (exit) interface, essentially with no constraint on the total thickness of the structure.

Therefore, the wave vector $k_2(\equiv n_2 k_o)$ is in the opposite direction of the wave vector $k_1(\equiv n_1 k_o)$. So, the phase at the end of the DNG slab is different from the phase at the beginning of it by the amount $-n_2 k_o d_2$. (As was mentioned above, n_2 here is taken to be positive.) So if we consider these two layers as a single paired DPS-DNG structure, the total phase difference between the front and back faces of this DPS-DNG structure is $n_1 k_o d_1 - n_2 k_o d_2$ for normally incident monochromatic plane waves. This implies that the phase difference achieved by traversing the first (DPS) slab can be decreased and even *compensated* by traversing the second (DNG) slab. If the ratio of d_1 and d_2 is chosen to be $d_1 / d_2 = n_2 / n_1$, then the total phase difference between the front and back faces of this two-layer structure becomes zero. (The total phase difference is not 2π, 4π, or 6π. But instead it can be zero!) So indeed for normally incident monochromatic plane wave the

DNG slab at given frequencies can act as the phase compensator/phase conjugator in this paired DPS-DNG structure. We emphasize that such phase compensation in this paired structure does not depend on the *sum* of thicknesses, $d_1 + d_2$, instead it depends on the *ratio* of d_1 and d_2. So conceptually, $d_1 + d_2$ can be any value as long as d_1 / d_2 satisfies the above condition.[1] Therefore, even though this two-layer paired structure is present, the normally incident wave traversing these paired layers would not experience the phase difference. This feature can lead to several interesting ideas in design of some devices and components. For instance, one can speculate that if we put several of these paired structures next to each other, we will have a multilayered slab with an arbitrary thickness, as sketched in Fig. 2, through which a normally incident monochromatic plane wave can propagate while there will be essentially no phase difference for this plane wave between the entrance and exit faces of this multilayered stack with arbitrary width. Such multilayered structures can also be arranged in cylindrical or spherical forms. Figure 3 shows a cylindrical multilayered stack of DPS-DNG coaxial shells.

Another interesting speculation for such a paired DPS-DNG slab is its possibility as antenna radomes/covers. If we consider two concentric spherical or two coaxial cylindrical shells, one shell formed by a DPS material and the other shell by a DNG medium in each case, as shown in Fig. 4, what would be the effects of such paired structures if one put them over an antenna (a dipole antenna or a wire antenna) as radomes? One can predict that by properly selecting the *ratio* of radii of these shells (but perhaps essentially with no restriction on the *sum* of the radii), one can achieve certain phase compensation for the spherical wave (if we have spherical shells) or for the cylindrical waves (if we have cylindrical shells) emitted from the antenna. If this is the case, the phase of the radiated wave at the outer surface of the radome will be similar to the phase at the inner surface of such a multilayered radome. Some of the aspects of this idea are currently under analytical study.

---

[1] It must be noted that since composite materials are in general formed by embedding many small inclusions in host media, if the thickness of a layer is "too thin" such that it does not contain many small inclusions, the layer can no longer be regarded as a "medium". So d_1 and d_2 can be made small, but not *too* small, so that each layer can still be considered as a composite medium.

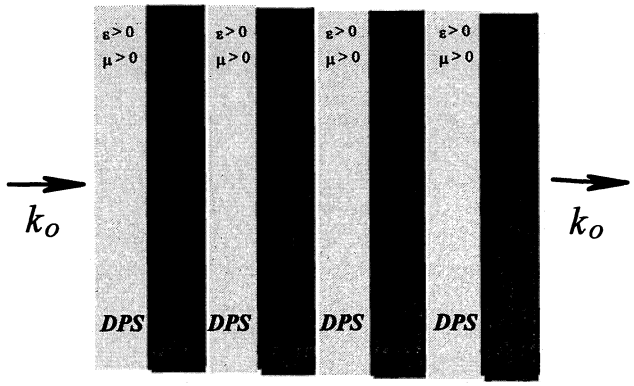

Figure 2. A multilayered stack of paired DPS-DNG slabs, one of which was shown in Fig. 1. As in Fig.1, if the *ratio* of thicknesses of DPS and DNG slabs in each paired structure is chosen properly, the phase difference for a normally incident monochromatic plane wave between the entrance and exit faces of each paired structure would be zero. By stacking these paired structures to form a multilayered structure with an arbitrary thickness, as sketched above, one can conceptually have a structure in which a normally incident plane wave can propagate through while the wave experiences no phase difference between the front and back faces of this structure with arbitrary thickness.

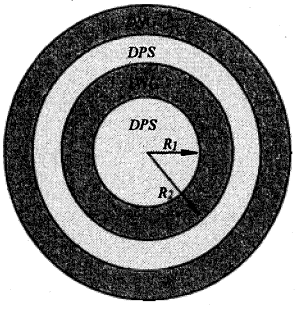

Figure 3. A multilayered structure formed by coaxial cylindrical DPS-DNG layers. See the description in Fig. 2.

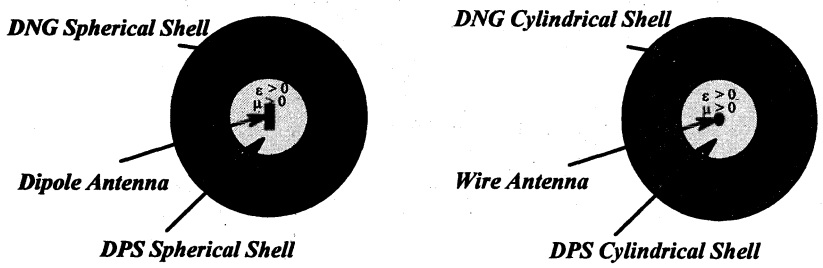

Figure 4. A suggestion for spherical (left) and cylindrical (right) radomes formed by two shells; one made of a conventional medium with positive permittivity and permeability (a DPS layer), and the other made of a metamaterial with negative permittivity and permeability (a DNG layer). One can speculate that by properly choosing the ratio of radii of these shells, the phase of the wave originating from the antenna can be compensated, resulting in a phase at the outer surface of the radomes similar to the phase at its inner surface.

One can also imagine forming small "objects" by having multilayered concentric spherical shells of DPS-DNG layers. If these objects are to be used as inclusions embedded in a host medium in order to make a more complex composite medium, as imagined in Fig. 5, one will obtain a complex medium formed by such complex inclusions. For each of these inclusions, proper choice of *ratio* of radii of concentric DPS-DNG shells may lead to phase compensation for wave interaction with such a complex "object", and may lead to exciting properties for polarizability tensors of such objects. As a result, the wave propagation through such a complex medium formed by embedding these inclusions in host media can be quite interesting. For instance, for such a complex medium, would it be possible to have a monochromatic plane wave propagation while the phase difference of this wave between any two "macroscopic" points in this "medium" is effectively compensated and zero? Some of these conceptual ideas are currently being studied.

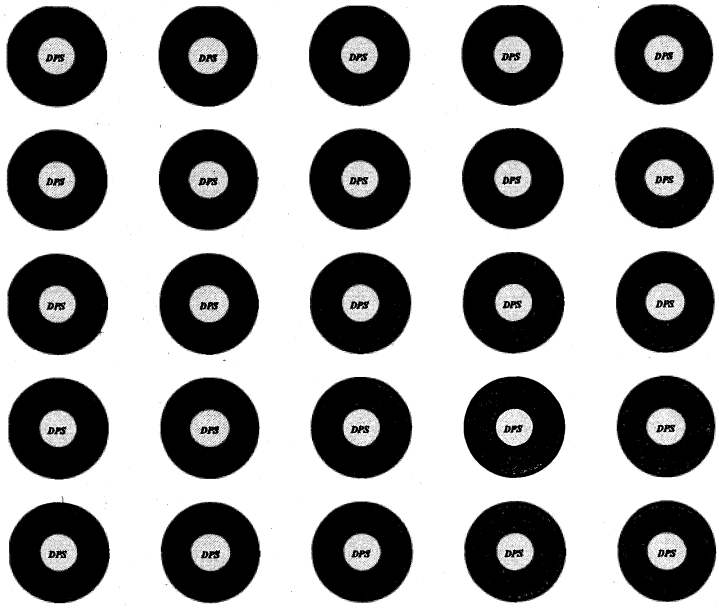

Figure 5. An idea for forming a complex medium by embedding many small inclusions, each of which contains layers of DPS-DNG concentric spherical shells, in a host medium. If the ratio of radii of DPS-DNG shells are chosen properly, one may speculate having interesting polarizability tensors for this object. This in turn may provide interesting plane wave propagation in such a complex "medium of media".

The concept of phase compensation in the paired DPS-DNG layers can also lead to the following idea for compact, subwavelength, thin cavity resonators, which we proposed recently [10]. This idea will be briefly reviewed below. More details can be found in [10].

3. Compact, Subwavelength, Thin Cavity Resonators

If we take the paired DPS-DNG layers, shown in Fig. 1, and place two perfect reflectors (e.g., two perfectly conducting plates) at the two open surfaces of this paired structure, as shown in Fig. 6, we will have an interesting one-dimensional (1-D) cavity resonator. In searching for the resonant modes in this cavity, we now remove the restriction of $\eta_1 = \eta_2 = \eta_3$, which we assumed earlier. So in general the intrinsic impedances of the DPS and the DNG layers are not taken to be the same as η_o. So we now have $\eta_1 \neq \eta_2 \neq \eta_o$ and $n_1 \neq n_2 \neq n_o$. We are now interested to solve for solutions of the Maxwell equations in this 1-D cavity resonator.

The Cartesian coordinate system (x, y, z) is used here, where the plane $z = 0$ is

chosen to be at the perfectly conducting plate located at the left face of the DPS material slab shown in Fig. 6, and the plane $z = d_1 + d_2$ is taken to be at the other perfectly conducting plate at the right face of the DNG metamaterial slab. The time dependence for the monochromatic solutions is taken to be $\exp(-i\omega t)$. For this 1-D cavity resonator, all quantities are assumed to be independent of the x and y coordinates. The electric and magnetic field vectors are then assumed to be oriented along the x and y directions, respectively. Following the source-free Maxwell equations and satisfying the boundary conditions at the interface between the DPS and DNG layers, i.e., at $z = d_1$, and at the perfectly conducting plates at $z = 0$ and $z = d_1 + d_2$, we obtain the following dispersion relation in order to have the non-trivial solutions for the fields inside this 1-D cavity resonator.

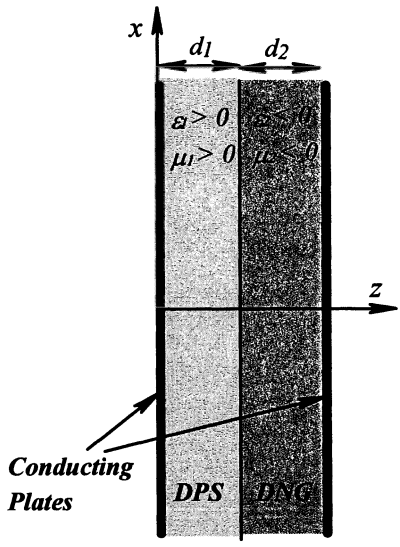

Figure 6. An idea for a compact, thin, sub-wavelength cavity resonator. The paired DPS-DNG structure discussed in Fig. 1 is sandwiched between the two perfectly conducting plates. With the proper choice of ratio of d_1 over d_2, one can have a resonant cavity in which the ratio of d_1 and d_2 is the main constraint, *not the sum of thicknesses*, d_1+d_2.

$$\frac{n_2}{\mu_2}\tan(n_1 k_o d_1) + \frac{n_1}{\mu_1}\tan(n_2 k_o d_2) = 0 \qquad (1)$$

In this dispersion relation, the quantities n_1, μ_1, n_2, μ_2, and k_o are generally all frequency dependent. It is important to note that the choice of sign for n_1 and n_2 does not affect this dispersion relation. Either choice of sign (positive or negative sign) for n_1 and n_2 will leave this dispersion relation unchanged. When this

dispersion relation is satisfied, the non-trivial electric and magnetic fields in this cavity can be expressed as

$$E_{x1} = E_o \sin(n_2 k_o d_2)\sin(n_1 k_o z) \tag{2}$$

$$H_{y1} = \frac{n_1 k_o}{i\omega\mu_1} E_o \sin(n_2 k_o d_2)\cos(n_1 k_o z) \tag{3}$$

for $0 \le z \le d_1$, and

$$E_{x2} = E_o \sin(n_1 k_o d_1)\sin\left[n_2 k_o (d_1 + d_2 - z)\right] \tag{4}$$

$$H_{y2} = -\frac{n_2 k_o}{i\omega\mu_2} E_o \sin(n_1 k_o d_1)\cos\left[n_2 k_o (d_1 + d_2 - z)\right] \tag{5}$$

for $d_1 \le z \le d_1 + d_2$. The subscripts '1' and '2' denote the quantities in the regions '1' and '2', which are the DPS slab and the DNG metamaterial slab, respectively. The expressions given in Eqs. (1)-(5) are derived for the general case of two slabs within a 1-D cavity resonator, regardless of the sign of permittivity and permeability in any one of these slabs. However, since the first layer is assumed to be made of a lossless DPS material, and the second layer is taken to be a lossless DNG metamaterial, we can write $\mu_1 = |\mu_1|$ and $\mu_2 = -|\mu_2|$. Substituting these expressions in Eq. (1), we get

$$-\frac{n_2}{|\mu_2|}\tan(n_1 k_o d_1) + \frac{n_1}{|\mu_1|}\tan(n_2 k_o d_2) = 0 \tag{6}$$

So for a given frequency ω, if $\varepsilon_1 > 0$, $\mu_1 > 0$, $\varepsilon_2 < 0$ and $\mu_2 < 0$, a non-trivial one-dimensional solution for this cavity is obtained when the thicknesses d_1 and d_2 satisfy the relation

$$\frac{\tan(n_1 k_o d_1)}{\tan(n_2 k_o d_2)} = \frac{n_1 |\mu_2|}{n_2 |\mu_1|} \tag{7}$$

It is important to note that this relation does not show any constraint on the *sum* of thicknesses of d_1 and d_2. Instead, it deals with the *ratio* of tangent of these thicknesses (with multiplicative constants). So, in principle, d_1 and d_2 can conceptually be as thin[1] or as thick as otherwise needed as long as the above ratio is satisfied. If we assume that ω, d_1 and d_2 are chosen such that the small-argument approximation can be used for the tangent function, the above relation can be simplified as

$$\frac{d_1}{d_2} \cong \frac{|\mu_2|}{|\mu_1|} \tag{8}$$

From the above equation, we can see even more clearly how d_1 and d_2 must be related in order to have a resonant mode with frequency ω in this cavity. So this means that the constraint is not on the sum of d_1 and d_2, but rather on the ratio of d_1 and d_2. Therefore, in principle, we can have a thin, sub-wavelength cavity

resonator for a given frequency, if at this frequency the second layer acts as a DNG metamaterial, and the ratio, d_1/d_2, satisfies the above condition or in general Eq. (7).

Taking into account that $\mu_1 = |\mu_1|$ and $\mu_2 = -|\mu_2|$, the electric and magnetic field expressions for the non-trivial solutions in this 1-D cavity can be rewritten as

$$E_{x1} = E_o \sin(n_2 k_o d_2)\sin(n_1 k_o z) \tag{9}$$

$$H_{y1} = \frac{n_1 k_o}{i\omega|\mu_1|} E_o \sin(n_2 k_o d_2)\cos(n_1 k_o z) \tag{10}$$

for $0 \le z \le d_1$, and

$$E_{x2} = E_o \sin(n_1 k_o d_1)\sin[n_2 k_o (d_1 + d_2 - z)] \tag{11}$$

$$H_{y2} = \frac{n_2 k_o}{i\omega|\mu_2|} E_o \sin(n_1 k_o d_1)\cos[n_2 k_o (d_1 + d_2 - z)] \tag{12}$$

for $d_1 \le z \le d_1 + d_2$. Figure 7 presents the sketch of normalized magnitude of the electric and magnetic field distributions given in the above equations for two different sets of parameters.

It is interesting to point out that if both slabs had been made of DPS layers, the quantities μ_1 and μ_2 would have been both positive real, and as mentioned before the form of the dispersion relation in Eq. (1) would have remained unchanged. However, if $\tan(n_1 k_o d_1)$ had been positive, the other term, $\tan(n_2 k_o d_2)$, must have been negative in order to fulfill the dispersion relation in Eq. (1). As a result, for such a case if $d_1 < \frac{\pi}{2n_1 k_o}$ for $\tan(n_1 k_o d_1)$ to be positive, then d_2 must have been greater than $\frac{\pi}{2n_2 k_o}$ in order to have $\tan(n_2 k_o d_2)$ negative. This implies that there will be some limits on the sum of thicknesses d_1 and d_2. In the case here, however, where we have a paired DPS-DNG structure, since $\mu_1 > 0$ and $\mu_2 < 0$, the two functions $\tan(n_1 k_o d_1)$ and $\tan(n_2 k_o d_2)$ can be both positive (or both negative), and thus, there is no constraint on the sum of d_1 and d_2.

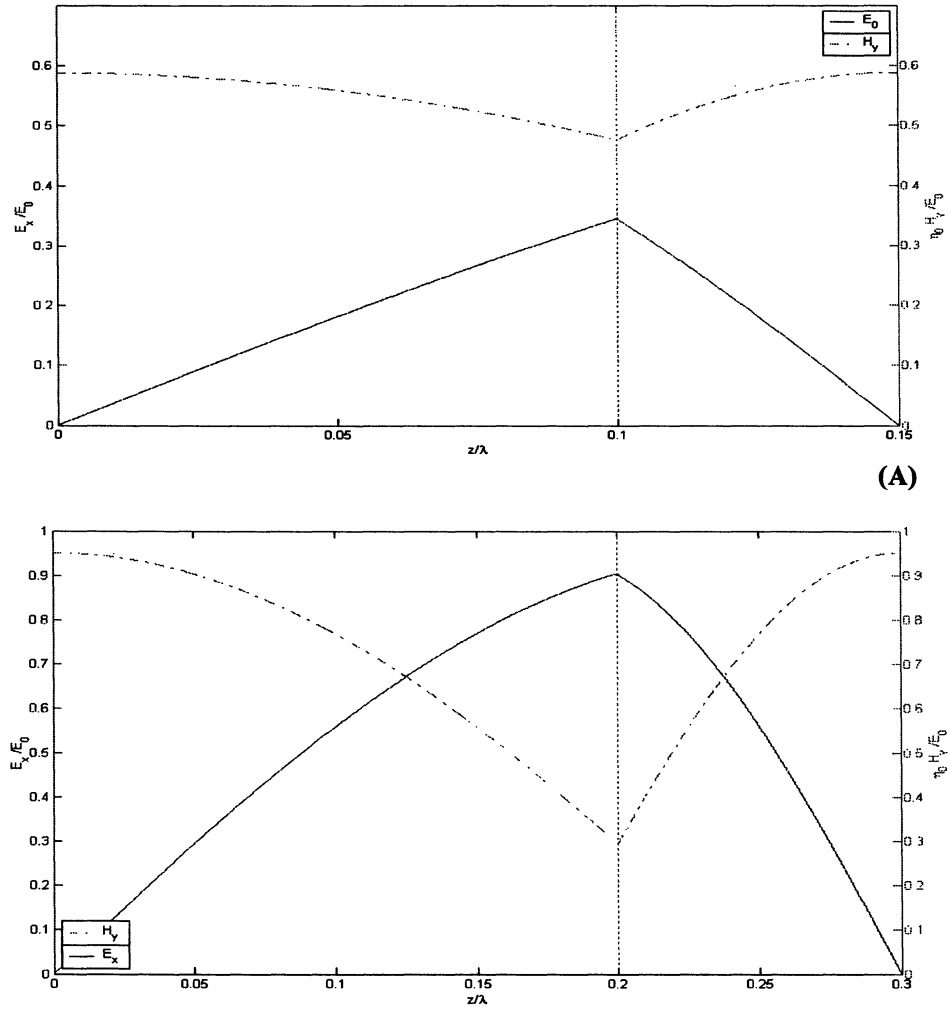

Figure 7. Sketch of the normalized magnitude of electric (E_x) and magnetic field (H_y) distribution as a function of z coordinate, given in Eqs. (9)-(12) for the 1-D cavity resonator described here. In the top Panel A, we assume $d_1/\lambda_o = 0.1$, $d_2/\lambda_o = 0.05$, $\varepsilon_1 = \varepsilon_o$, $\mu_1 = \mu_o$, $\varepsilon_2 = -2\varepsilon_o$, $\mu_2 = -2\mu_o$. In this case, the first slab occupies the region $0 < z/\lambda_o < 0.1$, while the second slab occupies $0.1 < z/\lambda_o < 0.15$. In the bottom Panel B, we take $d_1/\lambda_o = 0.2$, $d_2/\lambda_o = 0.1$, $\varepsilon_1 = \varepsilon_o$, $\mu_1 = \mu_o$, $\varepsilon_2 = -2\varepsilon_o$, $\mu_2 = -2\mu_o$. Here the first and second slabs are in regions $0 < z/\lambda_o < 0.2$ and $0.2 < z/\lambda_o < 0.3$, respectively.

Some other interesting features about this 1-D cavity resonator and the detailed analysis can be found in [10].

4. Waveguides Containing Paired DPS-DNG Structures

A natural extension to the idea of 1-D cavity resonators described in the previous section is the concept of guided-wave structures containing the paired DPS-DNG layers. We have studied this problem and presented some of our results in a recent conference [24]. Here we briefly mention one of the main findings in this problem. We return to the structure shown in Fig. 6, but this time we consider it as a parallel-plate waveguide with two perfectly conducting plates holding the two layers of DPS and DNG materials. Using the same Cartesian coordinate system (x,y,z) shown in Fig. 6, we express the electric field of the transverse electric (TE) mode as follows

$$E_{y1} = E_{o1}\sin\left(\sqrt{n_1^2k_o^2-\beta^2}\,z\right)e^{j\beta x} \qquad for \quad 0\le z\le d_1 \tag{13}$$

$$E_{y2} = E_{o2}\sin\left[\sqrt{n_2^2k_o^2-\beta^2}\,(d_1+d_2-z)\right]e^{j\beta x} \qquad for \quad d_1\le z\le d_1+d_2 \tag{14}$$

Similar to the analysis of the cavity resonator, following the source-free Maxwell equations and satisfying the boundary conditions, we obtain the following dispersion relation for the TE mode in this waveguide

$$\frac{\sqrt{n_2^2k_o^2-\beta^2}}{\mu_2}\tan\left(\sqrt{n_1^2k_o^2-\beta^2}\,d_1\right)+\frac{\sqrt{n_1^2k_o^2-\beta^2}}{\mu_1}\tan\left(\sqrt{n_2^2k_o^2-\beta^2}\,d_2\right)=0 \tag{15}$$

We note that when $\beta=0$, the above dispersion relation will reduce to the dispersion relation for the 1-D cavity resonator, given in Eq. (1), as expected. Since in this waveguide, $\mu_1>0$ and $\mu_2<0$, we can substitute $\mu_1=|\mu_1|$ and $\mu_2=-|\mu_2|$ in the above equation and obtain the following expression

$$\frac{\tan\left(\sqrt{n_1^2k_o^2-\beta^2}\,d_1\right)}{\tan\left(\sqrt{n_2^2k_o^2-\beta^2}\,d_2\right)}=\frac{\sqrt{n_1^2k_o^2-\beta^2}\,|\mu_2|}{\sqrt{n_2^2k_o^2-\beta^2}\,|\mu_1|} \tag{16}$$

As in the case of the 1-D cavity resonator, here also the *ratio* of the tangent of the thicknesses d_1 and d_2 (with some multiplicative constants) enters into the dispersion relations, and essentially no constraint on the *sum* of d_1 and d_2 is given here. Therefore, d_1 and d_2 can conceptually be chosen to be thin[1] or thick as long as the above ratio is satisfied. As we did in the case of the 1-D cavity, if we assume d_1 and d_2 to be chosen such that the small-argument approximation can be

used for the tangent function, Eq. (16) can be written approximately as

$$\frac{d_1}{d_2} \cong \frac{|\mu_2|}{|\mu_1|} \tag{17}$$

which is similar to the condition we obtained in Eq. (8) for the 1-D cavity. There is another interesting point about Eq. (17) for this case of parallel-plate waveguide: The approximate expression given in Eq. (17) does not depend on β. This implies that for this thin parallel-plate waveguide, one can, in principle, have a TE mode in which the longitudinal wavenumber (i.e., the waveguide wavenumber β) can be arbitrarily chosen to have any value between zero and $\min(n_1 k_o, n_2 k_o)$. In other words, in this peculiar case, the longitudinal wavenumber β would be independent of d_1 and d_2. This is one of the interesting characteristics of such a parallel-plate waveguide containing the paired DPS-DNG layers. Several features of this waveguide have been studied by Alu' and Engheta, and the results will be published in due time.

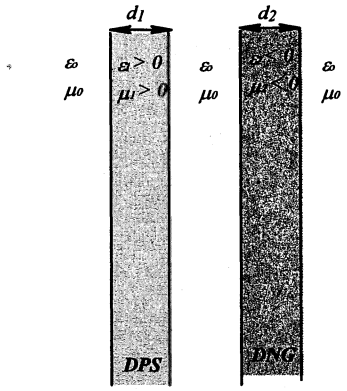

Figure 8. An idea for a mode coupler formed by the DPS and DNG slabs.

One of the interesting concepts related to waveguides with DNG materials is the property of anomalous mode coupling between an open dielectric slab and an open DNG slab. Figure 8 presents the sketch of a mode coupler formed by an open DPS slab parallel with an open DNG slab. The medium outside these slabs is assumed to be free space. Alu' and Engheta have studied the electromagnetic mode coupling between layers of DNG and DPS materials, and some of their findings have been presented in a conference [25]. This analysis has shown that the mode coupling between DNG and DPS layers exhibits anomalous characteristics for the direction of power coupling. This is due to the fact that in a DNG slab the direction of the real part of the Poynting vector of a guided mode is antiparallel with the direction of phase flow of that mode. Owing to the boundary conditions, the phase flow direction is the same in the two slabs, and thus when an open DNG slab is in

proximity of a parallel open DPS slab, the power coupling is anti-parallel [25].

Another interesting geometry for guided wave structures containing DNG materials is a stack of DPS-DNG layers in the form of slab waveguides, as sketched in Fig. 9.

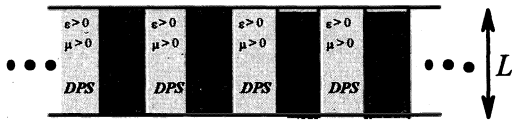

Figure 9. Stack of DPS-DNG paired structures in the form of slab waveguide.

Following the phase compensation properties of the paired DPS-DNG layers discussed earlier, it is anticipated that by choosing the relative thickness of the DPS and DNG layers phase variation for guided modes in such a complex slab waveguide will be affected notably, thus leading to interesting dispersion relations for the guided modes in this waveguide. This problem is currently under study.

5. Radiation in DNG Metamaterials

Radiation from electromagnetic sources in structures containing DNG metamaterials may possess interesting features due to the antiparallel nature of the Poyting vector and the phase velocity of a plane wave in such media. In order to understand source radiation in these media, we have studied the canonical problem of electromagnetic radiation from a traveling-wave thin current sheet located at the interface between a conventional DPS half space and a DNG half space [26]. Figure 10 presents the geometry of this problem.

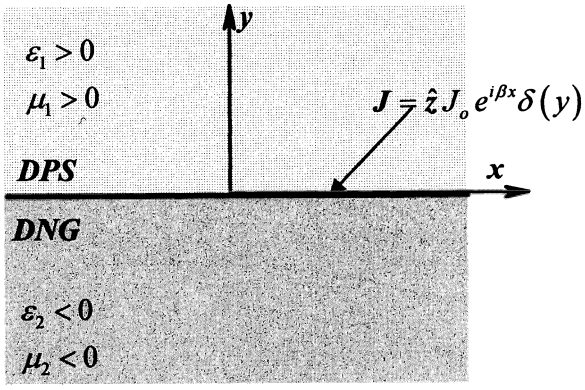

Figure 10. From Ref. [26]. An infinitely extent thin sheet of surface current is located at the interface between the DNG and DPS media.

In this problem, the current source is assumed to be

$$\boldsymbol{J} = \hat{z} J_o e^{i\beta x} \delta(y) \tag{18}$$

where J_o is the strength of the surface current density, β is the rate of the linear phase change in the x direction, $\delta(\cdot)$ is the Dirac delta function, and $\hat{z}$ is the unit vector in the z direction. In [26], we have considered both cases for the direction of the current flow; (1) the case in which the direction of current flow is along z, while the direction of phase variation of this traveling-wave current is along x; (2) the case in which the current flow and the direction of phase variation both being along the x direction. In [26], we have derived the expressions for the field distributions and the direction of the Poynting vectors in both half spaces, and have provided some physical remarks for the mathematical findings. In addition, we have also mentioned a brief note about launching Zenneck waves by a line current along this interface [26]. Here we only mention one of the interesting points about the direction of Poynting vectors in these two half spaces.

Figure 11 illustrates the relative direction of Poynting vectors and the wave vectors in the two half spaces. In the DPS half space ($y > 0$), the phase flow vector and the Poynting vector are parallel, and thus both the phase velocity and the Poynting vectors are propagating *away* from the source, when $\beta < \omega\sqrt{\varepsilon_1 \mu_1}$. In the DNG half-space ($y < 0$), however, the phase flow vector and the Poynting vector are antiparallel. As a result, when $\beta < \omega\sqrt{\varepsilon_2 \mu_2}$ while the Poynting vector should be pointed *away* from the source, the phase velocity vector should be pointed *towards* the source, as sketched in Fig. 11. It is also important to note that in the DNG half space the radiation power flows away from the source; however, unlike the case of DPS medium, here the x-component of the Poynting vector is pointed in the sense opposite to the direction of the current phase change along the x axis. The mathematical steps to arrive at these conclusions are described in [26]. Moreover, the case of $\beta > \omega\sqrt{\varepsilon_1 \mu_1}$ and/or $\beta > \omega\sqrt{\varepsilon_2 \mu_2}$ have also been discussed in [26].

One can speculate that such an interfacial source can provide us with possibility of launching waves in two directions shown in Fig. 11. This can provide an interesting potential possibility for the radome design, such as the one speculated in Fig. 12.

6. Summary

In this chapter, some of our ideas for potential applications of metamaterials with negative real permittivity and permeability have been presented. For some of these ideas, we have already shown mathematical analysis and physical explanations, and for some of others we have speculated about their characteristics and

electromagnetic properties. More research is currently under way to study some of these speculations.

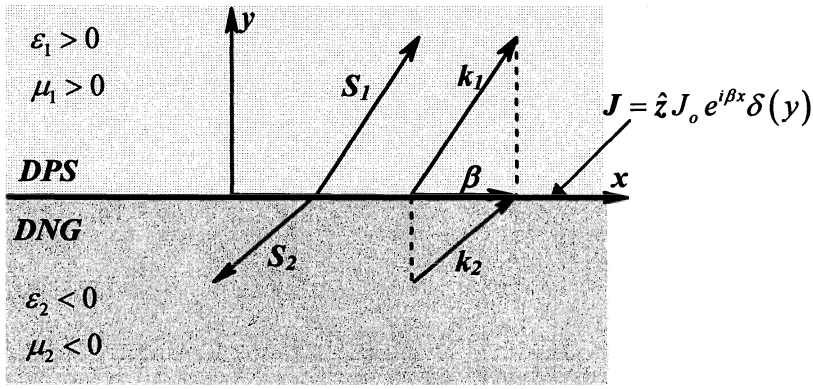

Figure 11. From Ref. [26]. Schematic representation of the directions of wave vectors k_1 and k_2, and the Poynting vectors S_1 and S_2. The directions of power flow of the electromagnetic radiation from the monochromatic traveling-wave current sheet J are shown as the vectors S_1 and S_2.

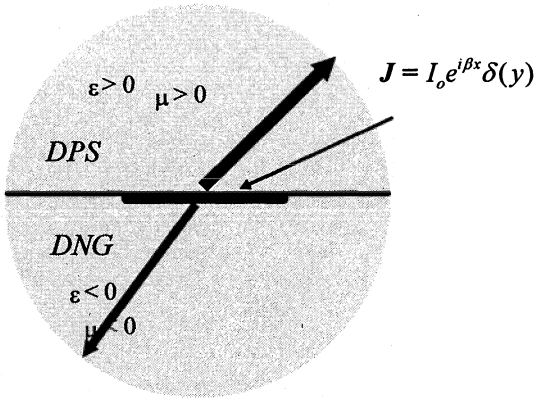

Figure 12. A speculative idea for a radome design. The upper half of such a radome would be made of a conventional DPS medium, while the lower half would be made of a DNG metamaterial. If the source is a traveling-wave interfacial antenna at the interface between the DPS and DNG media, the direction of main beams would be affected by the properties of the DNG and DPS media.

7. References

1. Shelby, R. A., Smith, D. R., and Schultz, S. (2001) Experimental verification of a negative index of refraction, *Science*, 292(5514), 77-79.
2. Smith, D. R., Padilla, W. J., Vier, D. C., Nemat-Nasser, S. C., and Schultz, S. (2000) Composite medium with simultaneously negative permeability and permittivity, *Physical Review Letters*, 84(18), 4184-4187.
3. Smith D. R., and Kroll, N. (2000) Negative refractive index in left-handed materials, *Physical Review Letters.*, **85**(14), 2933-2936.
4. Pendry, J. B., (2000) Negative refraction makes a perfect lens, *Physical Review Letters.*, 85(18), 3966-3969.
5. Shelby, R. A., Smith, D. R., Nemat-Nasser, S. C., and Schultz, S. (2001) Microwave transmission through a two-dimensional, isotropic, left-handed metamaterial, *Applied Physics Lett.*, **78**(4), 489-491.
6. Veselago, V. G. (1968) The electrodynamics of substances with simultaneously negative values of ε and μ, *Soviet Physics Uspekhi*, 10(4), 509-514. [in Russian (1967) *Usp. Fiz. Nauk*, **92**, 517-526.]
7. Lindell, I. V., Tretyakov, S. A., Nikoskinen, K. I., and Ilvonen, S. (2001) BW media – Media with negative parameters, capable of supporting backward waves, *Microwave and Optical Technology Letters*, **31**(2), 129-133.
8. Ziolkowski, R. W., and Heyman, E. (2001) Wave propagation in media having negative permittivity and permeability, *Physical Review E.*, **64**(5), 056625.
9. McCall, M. W., Lakhtakia, A., and Weiglhofer, W. S. (2002) The negative index of refraction demystified, *European Journal of Physics*, **23**, 353-359.
10. Engheta, N. (2002) An idea for thin subwavelength cavity resonators using metamaterials with negative permittivity and permeability, *IEEE Antennas and Wireless Propagation Letters*, **1**(1), 10-13, Digital Object Identifier: 10.1109/LAWP.2002.802576, on line at http://ieeexplore.ieee.org/Xplore/RecentIssue.jsp?Punumber=7727.
11. Garcia N. and Nieto-Vesperinas, M. (2002) Left-handed materials do not make a perfect lens, *Physical Review Letters*, **88**(20), 207403.
12. Marques, R., Medina, F., and Rafii-El-Idrissi, R. (2002) Role of bianisotropy in negative permeability and left-handed metamaterials, *Physical Review B*, **65**(14), 144440.
13. Valanju, P. M., Walser, R. M., and Valanju, A. P. (2002) Wave refraction in negative-index media: Always positive and very inhomogeneous, *Physical Review Letters*, **88**(18), 012220.
14. Kong, J. A., Wu, B.-I., and Zhang Y. (2002) A unique lateral displacement of a Gaussian beam transmitted through a slab with negative permittivity and permeability, *Microwave and Optical Technology Letters*, **33**(2), 136-139.
15. Silin R. A. and Chepurnykh, I. P. (2001) On media with negative dispersion, *Journal of Communication Technology and Electronics*, **46**(10), 1121-1125. (translated from Radiotekhnika (2001), **46**(10), 1212-1217.)
16. Saadoun, M. M. I., and Engheta, N. (1994) Theoretical study of electromagnetic properties of non-local omega media" in A. Priou (Guest ed.), *Progress in Electromagnetic Research (PIER) Monograph series*, **9**, ch. 15, pp. 351-397.
17. Collin, R. E. (1966) *Foundations for Microwave Engineering*, McGraw-Hill, New York.
18. Mayes, P. E., Deschamps, G. A., and Patton, W. T., (1961) Backward-wave radiation from periodic structures and application to the design of frequency independent antennas, *Proceedings of IRE*, **9**, 962-963.
19. Oliner, A. A., and Tamir, T., (1962) Backward wave on isotropic plasma slabs, *Journal of Applied Physics*, **33**, 231.
20. Gralak, B., Enoch, S., and Tayeb, G. (2000) Anomalous refractive properties of photonic crystals, *Journal of Optical Society of America, A.*, **17**(6), 1012-1020.

21. Notomi, M. (2000) Theory of light propagation in strongly modulated photonic crystals: Refractionlike behavior in the vicinity of the photonic bandgap, *Physical Review B*, **62**(16), 10696.
22. Kosaka, H., Kawashima, T., Tomita, A., Notomi, M, Tamamura, T., Sato, T., and Kawakami, S. (1999) Self-collimating phenomena in photonic crystals, *Applied Physics Letters*, **74**(9), 1212-1214.
23. Kosaka, H., Kawashima, T., Tomita, A., Notomi, M., Tamamura, T., Sato, T., and Kawakami, S. (1998) Superprism phenomena in photonic crystals, *Physical Review B*, **58**(16), 10096.
24. Engheta, N. (2002) Guided waves in paired dielectric-metamaterials with negative permittivity and permeability layers, a talk presented at the *National Radio Science Meeting (USNC-URSI)*, Boulder, Colorado, January 9-12, 2002, p. 66.
25. Alu', A. and Engheta, N. (2002) Anomalous mode coupling in guided-wave structures containing metamaterials with negative permittivity and permeability, presented at *the IEEE-Nanotechnology'2002 Conference*, Washington, DC, August 26-28, 2002.
26. Alu', A. and Engheta, N. (2002) Radiation from a traveling-wave current sheet at the interface between a conventional material and a metamaterial with negative permittivity and permeability, accepted for publication in *Microwave and Optical Technology Letters*, scheduled for December 20, 2002.

FREQUENCY RESPONSE ENGINEERING OF MAGNETIC COMPOSITE MATERIALS

Olivier ACHER
CEA Le Ripault,
Laboratoire Matériaux Magnétiques et Hyperfréquences
BP 16, F-37260 MONTS
acher@ripault.cea.fr

Abstract. Ferromagnetic metals have attractive microwave magnetic properties, but because of their conductivity, they can not be used under bulk form, and have to be made into composite materials. Ferromagnetic-based composites may be categorized into C2D, C1D and C0D depending on the number of macroscopic Conducting Dimensions they have. C2D and C1D composites are made from thin films and thin wires respectively. Considerable progress in the measurement techniques of the microwave properties of thin films, thin wires, and related composites are reported. Homogenization laws for C1D and C2D composites are well understood, and this establishes a duality between permeability measurements on the composite, and on the ferromagnetic constituent. Typical properties of the different categories of composites are illustrated. The permeability of the magnetic inclusions is often adequately described by a conventional uniform rotation model, but the existence of non uniform modes may provide further opportunities to synthesize other types of permeability response. Two theoretical guidelines for the frequency response engineering are presented. First, a definition of the effective permeability and permittivity is proposed. This definition is based on the fact that the quantities measured experimentally are the Fresnel Reflection and Transmission coefficients. It yields a simple expression for ε and μ related to a proper spatial averaging of the different fields. Some former definitions given in the literature are shown to yield improper results. Second, an integral quantity related to the imaginary permeability is shown to be bounded by the volume fraction of magnetic material in the composite, times the square of its saturation magnetization. This gives a criterion to assess whether a given spectral permeability response may be achieved or not through proper engineering of the composite response. It is also possible to tune the microwave properties of a magnetic material through an external action. The tuning of the permeability through a magnetic field or mechanical stress is presented. It is also indicated that the permittivity of a wire medium can be tuned by an external magnetic field.

1. Introduction

Magnetic materials are important for a variety of use at microwave frequencies. They are used as non reciprocal media, or to provide high impedance properties, or for Electro Magnetic Compatibility issues. Ferrites and Garnets have been the most used magnetic microwave materials up to now. However, ferromagnetic metals have better intrinsic magnetic properties, due to their high saturation magnetization, and they are already preferred to ferrites for a variety of use, such

S. Zouhdi et al. (eds.), Advances in Electromagnetics of Complex Media and Metamaterials, 39–59.

as inductors, or write heads for magnetic recording technology. However, the main limitation to the use of ferromagnetic materials at microwave frequencies is their conductivity. Because of their large conductivities, ferromagnetic metals can not be used in bulk form at microwave frequencies, since the waves penetrate only on a very small length. To overcome this limitation, ferromagnetic elements are mixed with an insulating matrix that provides the small permittivity that is necessary for a sufficient interaction with the incoming waves. A convenient classification of ferromagnetic-based microwave composites can be based on the number of macroscopic dimensions along which the composite is a conductor. Typical composite topologies based on ferromagnetic metals that are Conducting along 2 Dimensions (C2D), Conducting along 1 Dimension (C1D) and Conducting along 0 Dimension (C0D) are presented on Fig. 1.

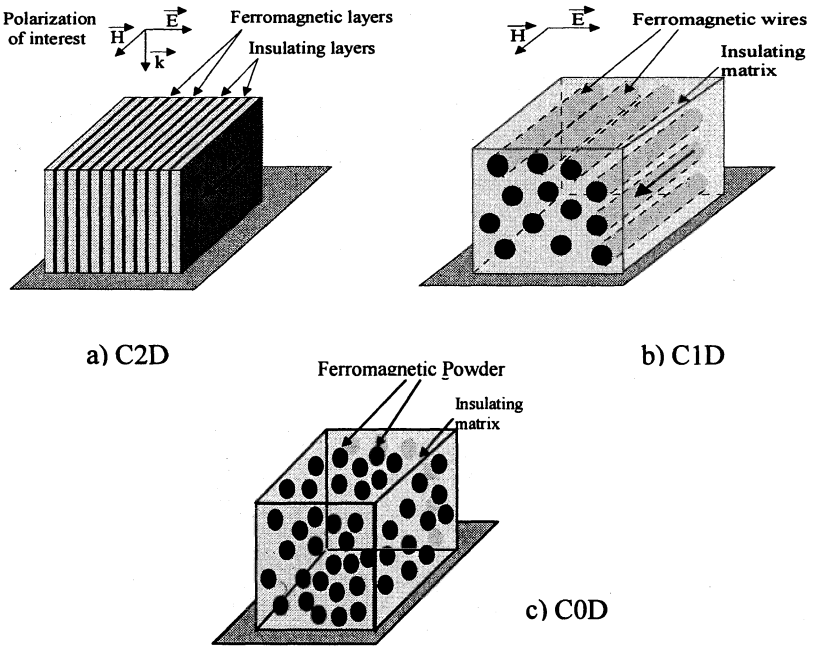

Figure 1. Ferromagnetic-based composite topologies ; a) composite Conducting along 2 Dimensions (C2D); b) composite Conducting along 1 dimension (C1D); c) composite Conducting along 0 Dimension (C0D).

Typical properties of these composites will be reviewed in this paper, and recent improvements in the characterization techniques will be presented. If the choice of a proper composite topology is of foremost importance to engineer microwave materials with a desired response, the optimization of the magnetic properties of

the individual inclusions is also a crucial parameter. It will be shown that the uniform gyromagnetic response of magnetic thin films and wires is well understood, but that it is also possible to take profit from non-uniform excitations in order to obtain different types of microwave responses.
Different definitions for the effective permeability and permittivity of a composite have been proposed, some of them incompatible. The proper definitions that should be used at microwave frequencies are reminded and illustrated. Besides, a sum rule has been recently derived, that gives some bounds of on the permeability levels as a function of the saturation magnetization of the composite constituents.

2. Engineering the microwave response of magnetic composites

The classification of ferromagnetic-based composites according to the number of macroscopic conducting dimensions is a natural approach. The demagnetizing coefficient is zero along a direction where the inclusion is very long, and this classification gives an indication of the number of space dimensions where the demagnetizing coefficients associated to the inclusion are zero. The demagnetizing effects have a strong influence on the effective properties of the composites, and on the microwave response of a ferromagnetic element. It is well known indeed that the gyromagnetic response of a magnetic element is dominated by its shape and the orientation of its magnetization. This classification is also useful, since the elaboration techniques of the different types of inclusions generally depend on their shape and dimensionality. The properties of the C2D, C1D and C0D composites are indeed associated to the properties of thin films, wires, and powders. It will be shown that for a given shape of a magnetic inclusion, the microwave properties can be very different depending on the magnetic domain topology inside the element.
The C2D and C1D composites are anisotropic. There is a very strong contrast in the eigen-values of the permittivity tensor, depending on the direction. The modulus of the permittivity along the conducting direction is typically 10^6 or larger, while it is only a few units normal to the elongated inclusions. As the percolation theory has been found useful to describe the properties of inhomogeneous media, these composites can be described as materials that are percolating or not depending on the direction under consideration. The C1D and C2D composites can be denominated "strongly anisotropic materials", to account for the very large contrast of permittivity and index depending on the direction in these materials. The analysis of the propagation of electromagnetic waves in a strongly anisotropic material is indeed simpler than for the general case of anisotropic materials [1]. In particular, the Poynting vector is channeled by the conducting laminations in a C2D.

2.1 PROGRESS IN MICROWAVE CHARACTERIZATION OF FERROMAGNETIC THIN FILMS, WIRES, AND RELATED COMPOSITES

A prerequisite to the development of C2D and C1D microwave composites is the availability of suitable microwave characterization techniques for the composites and the constitutive ferromagnetic elements. The development of microwave characterization techniques can be separated in two approaches.

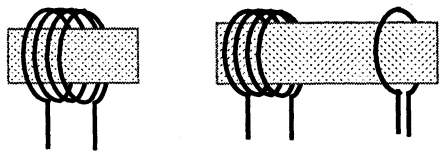

a) b)

Figure 2. Electrical engineering approach to the conception of permeameters : principle of a) single loop and b) two loops permeameters.

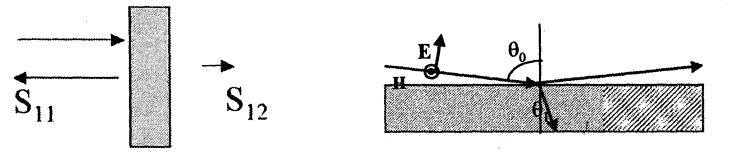

$R=(Z-1)/(Z+1)$ $(Z^2=\mu/\varepsilon)$

$\cos\theta_1 \cong 1$

$\Rightarrow R=(Z-\cos\theta_0)/(Z+\cos\theta_0)$

a) b)

Figure 3. Reflection-Transmission approach in the conception of permeameters : a) normal incidence approach ; b) grazing incidence configuration. The reflection coefficient is also indicated, for the air-medium interface (not for finite thickness layer).

The electrical-engineering approach has often been preferred to develop permeameters that measure the permeability of ferromagnetic thin films (fig. 2). In the single-coil approach, the sample is inserted in a coil, and the change in the inductance of the loaded coil is related to the permeance of the sample. The permeance is the product of the permeability of the sample by its thickness. In the two-coil approach, the sample is inserted inside two coils, generally named driving coil and pick-up coil. This behaves like a transformer, and a conventional electrical engineering approach allows the determination of the permeance from the characteristics of the transformer. These measurement setups are very efficient at low frequencies, but the measurement quality generally degrades when increasing the frequency. A reason is that propagation effects are generally neglected, but they may no longer be negligible when the sample size is not very small compared to the wavelength. One of the best two-coil setup is certainly that designed by

Yamaguchi [2], that allows measurements up to 3 GHz. It should be noted also that two-coil systems can measure off-diagonal elements of the permeability tensor [3]. Another approach to high frequency measurements is the transmission-line approach. The driving idea is to place a sample in a transmission line, and to measure the reflected and transmitted wave using a network analyzer (see fig. 3). Both the permeability and the permittivity can be deduced form the Fresnel reflection and transmission coefficients [4]. Different constraints on sample size, geometry, and bandwidth, are associated with the different types of guiding structures. The coaxial line is particularly convenient, as it is single mode over a wide frequency range. Using the APC-7 standard with 7 mm outer diameter, measurements can be performed from low frequencies up to 18 GHz. When dealing with thin ferromagnetic films, the problem is that for normal incidence (fig. 3a), the wave is completely reflected. The reflection coefficient at a boundary between air and a material is $R=(Z-1)/(Z+1)$ with $Z^2=\mu/\varepsilon$. The permittivities of ferromagnetic metals are given by $\varepsilon=-j\sigma/\varepsilon_0$, and they exceed $-j10^7$ at several GHz. As a result, $|Z|$ is very small compared to unity, and the reflection coefficient is very close to -1. The transmission coefficient is close to zero. As a consequence, the measurement of R and T under normal incidence reveals that the material is a good conductor, but does not carry significant information on the permeability. Let us now consider a wave arriving on the metal surface under oblique incidence at an angle θ_0 (cf. Fig. 3b), for a linear polarization with the E field in the incidence plane and H parallel to the interface. This is the polarization denominated "p" polarization in the vocabulary of spectroscopists, or "TM" polarization in the vocabulary of microwave engineers. The index of the metal is large, and according to Snell's law the angle of refraction is close to zero. The reflection coefficient writes :

$$R = (Z-\cos\theta_0)/(Z+\cos\theta_0) \qquad (1)$$

The key point is that at grazing incidence, $|\cos\theta_0|$ can be close to zero, like $|Z|$. This opens the possibility that non-trivial information on the permeability of strongly conducting materials may be obtained when measuring the reflection behavior for such incidence. And indeed, all the different thin film permeameters developed using transmission lines are with the propagation vector and H parallel to the film plane. We developed in the laboratory a technique that can be viewed either as a single coil technique, or as a shorted microstrip transmission line technique [5] (fig. 4a). It has been shown that this technique can be extended up to 6 GHz, by properly taking into account the propagative aspects. Inter-comparisons have been performed with the two-coil technique, which validates the approach [6]. A coaxial perturbation technique [7] has also been developed, which presents several advantages, in particular it does not require a reference sample with known permeability for calibration. However, it is restricted to flexible materials.
Microwave measurements under normal incidence on strongly anisotropic materials such as C1D and C2D can be performed, provided the electric field is

normal to the conducting direction(s). The coaxial line is a very attractive type of transmission line since it is single-mode up to elevated frequencies, and therefore it allows precise wide-band reflection-transmission measurement on small samples. We developed the wound torus method. It consists in manufacturing a torus suitable for coaxial line measurement, by winding a flexible ferromagnetic sheet deposited on a flexible insulator [8, 9], or winding an insulated wire [10] into such a torus (see fig. 4b and fig. 5).

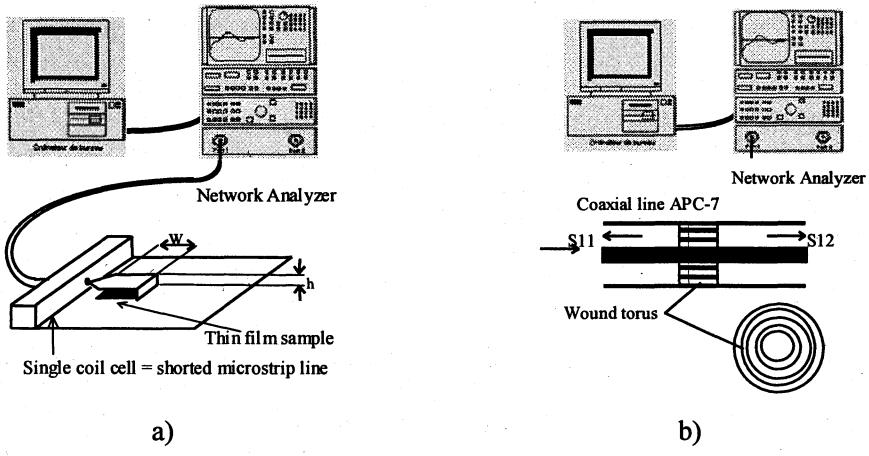

a) b)

Figure 4. Sketch of a) a single coil permeameter ; b) wound torus measurement set-up.

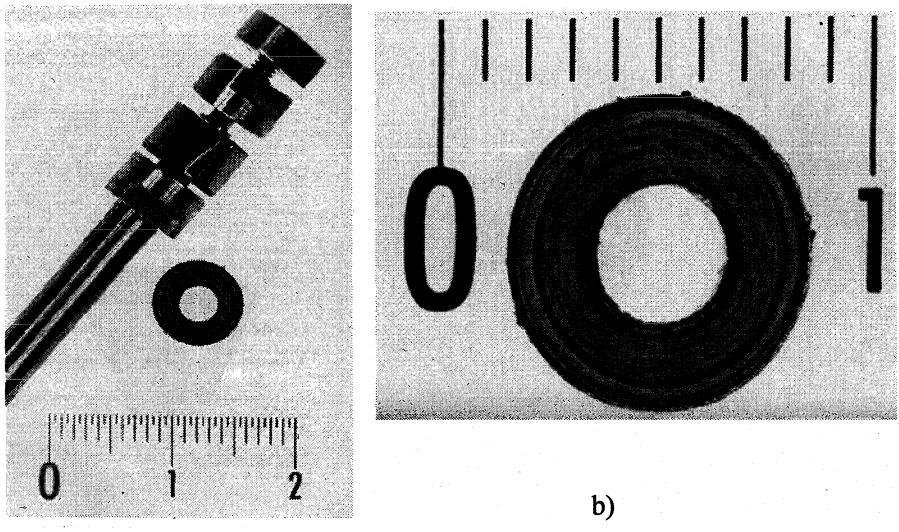

b)

Figure 5. a) Fabrication of a wound torus ; b) micrograph of a wound C2D torus. The ruler indicate the cm.

In this way, the elongated conducting elements are parallel to the magnetic field and normal to the electric field for the fundamental propagation mode. As a consequence, the reflection and transmission coefficients on this sample yield the permeability along the wires (or planes), and the permittivity normal to the conducting elements. These quantities are for the composite material. In the case of the permeability, there is a very simple relation between the parallel permeability μ_{ferro} of the constitutive elongated metallic elements and the permeability of the composite $\mu_{composite}$, as a function of the metal volume fraction f. It writes :

$$\mu_{composite} = f.A.\mu_{ferro}+(1-f) \qquad (2)$$

The factor A accounts for the skin effect. Its expression depends on the dimensionality of the inclusion. In the case of C2D materials, it writes :

$$A = tg(ka)/(ka) \qquad (3)$$

where 2a is the thickness of the metallic layer, and k the wave-vector in the ferromagnetic material.
In the case of C1D materials, it writes :

$$A = 2J_1(ka)/[kaJ_0(ka)] \qquad (4)$$

where 2a is the diameter of the metallic wire, and J_1, J_0 are Bessel functions.
It should be noted that the permeability measured directly on a thin film or wire using a permeameter is the quantity $A.\mu_{ferro}$. It is convenient to call it "apparent permeability", whereas μ_{ferro} is denominated "intrinsic permeability". The above relations express a straightforward duality between the properties of the C1D or C2D composites, and the apparent permeability of the elongated magnetic element. As a consequence, experimental results on wound torus can be either presented in the form of composite permeability, or apparent permeability. The wound torus method allows the determination of the permeability of thin films and wires up to 18 GHz, which is to our knowledge the highest frequency capability demonstrated by any type of permeameter [8]. Another advantage is that the wound torus method does not require a sample with known permeability for calibration. Several groups in the world are now using this technique [11, 12, 13]. However, this method is restricted to flexible wires and thin films.

2.2 C2D COMPOSITES

The Laminated Insulator Ferromagnetic on the Edge (LIFE) composites can be made from thin ferromagnetic layers deposited on thin flexible plastic sheets [9]. Mylar and kapton substrates with a thickness in the 3.5 μm to 12 μm range are convenient for that purpose. Figure 6a gives a micrograph of such a composite. Microwave measurements on C2D composites using the wound torus method

indicate that the permittivity is rather small as expected [9], and generally close to 4-j0. The permeability of a LIFE composite containing a volume fraction f=28% of ferromagnetic material is represented on figure 6b. Permeability levels at high frequencies are high. The product of the low frequency real susceptibility by the gyromagnetic resonance frequency F_r (defined by $\mu'(F_r)=1$) is found to exceed 200 GHz. For conventional spinnel ferrites, this product is bounded according to Snoek's law, and does not exceed 10 GHz. This LIFE material appears to have a figure of merit 20 times larger than any conventional ferrite.

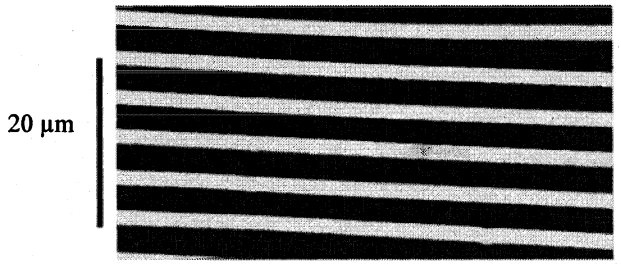

a)

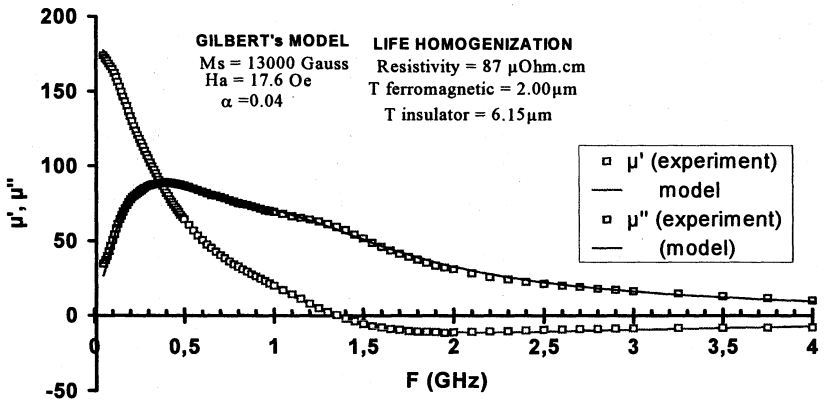

b)

Figure 6. a) Optical micrograph of a LIFE composite ; b) complex microwave permeability : experimental results obtained using the wound torus method (squares), and simulation (line).

The properties of LIFE materials have been investigated in several further works [14, 15, 16]. A straightforward way to engineer the frequency response of LIFE materials is to use ferromagnetic layers with specific magnetic response. The permeability response of a layer can be tuned trough the composition, the experimental deposition conditions, and further annealing procedure [17, 18]. The increase of the resonance frequency can also be achieved trough patterning [19].

2.3 C1D COMPOSITES

C1D composites were first made using varnished nickel or copper wires [10]. More recently, Amorphous Glass-Covered Wires (AGCW) turned out to be extremely attractive to make C1D composite materials [20, 21]. These wires have a ferromagnetic amorphous core surrounded by a glass shell [22]. The cross section of an amorphous glass-coated wire is sketched on figure 7.

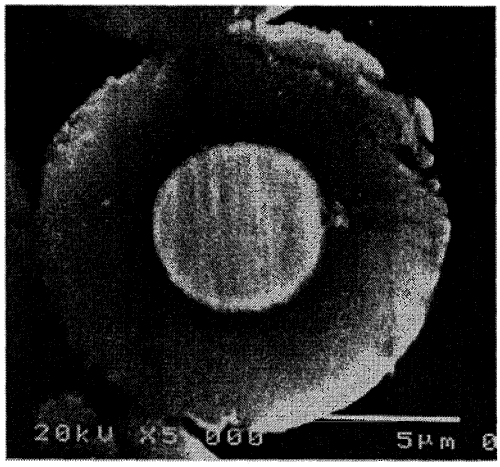

Figure 7. Optical micrograph of the cross section of an amorphous glass-coated microwire.

The glass shell brings an electrical insulation, that avoids short circuits between the wires in the C1D composite. The glass shell is also known to exert a large stress on the amorphous core, and it has been shown that the anisotropy inside the ferromagnetic core is dominated by magnetostrictive effects. For negative magnetostriction wires, the magnetization is expected to be essentially circumferential, as represented on figure 8b. Hysteresis measurements yield the anisotropy field that accounts for the stiffness in the circumferential direction (fig. 8a). This domain configuration is very similar to that of a soft thin film that would be curved into a torus around its hard axis direction. It has been shown that the microwave response of such a wire can be described by the conventional gyromagnetic equations, using the same demagnetizing coefficients as for a thin film [23].

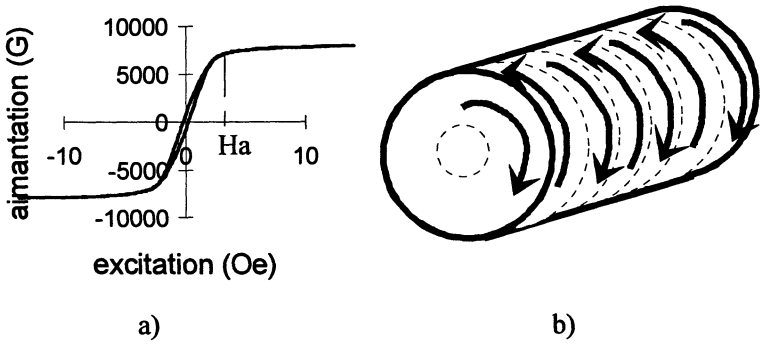

Figure 8. a) Typical hysteresis loop for an excitation along a negative magnetostriction AGCW ; b) sketch of the proposed magnetization configuration for a negative magnetostriction AGCW.

The apparent permeability computed from the experimental value of the anisotropy field and saturation magnetization, taking into account the skin effect through the factor A, is in good agreement with the measurement [24]. This is illustrated on figure 9. This holds especially for thin core diameter. The behavior of wires with core diameter larger than 12 μm is only qualitatively described by this model, as discussed in [24].

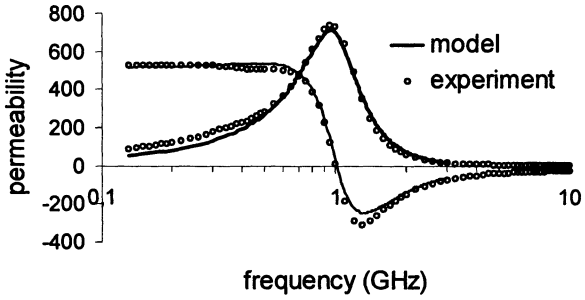

Figure 9. Apparent permeability of an AGCW measured using the wound torus method, and comparison with the apparent permeability computed from the gyromagnetic equations.

2.4 C0D COMPOSITES

Composites made of ferromagnetic powders diluted in an insulating matrix have been used for a variety of applications. A significant number of works have been dedicated to the understanding of the effective permeability and permittivity as a function of the volume fraction of the magnetic powders. The influence of the skin

effect has been observed and accounted for [25]. The extended Bruggeman model has been shown to give a fair account of the permeability of a C0D composite as a function of the filler volume fraction. C0D composites generally exhibit permeability levels that are significantly smaller than C1D and C2D composites. The advances in the field of C0D should now not so much be expected in term of composite topology or composite understanding, but rather in term of optimization of the ferromagnetic powder.
A significant advance has been the manufacturing of ferromagnetic powders in the FeCoNi system using the polyol process [26]. This chemical route leads to large collections of particles with spherical shape and very narrow size distribution, as illustrated on figure 10. The diameter can be adjusted from several nanometers up to a few microns, by properly adjusting the nucleation conditions [27].

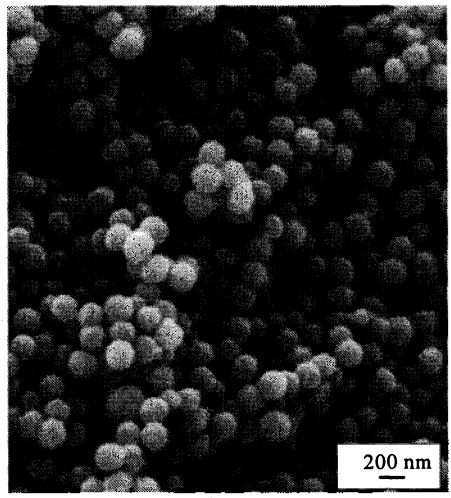

Figure 10. Scanning Electron Microscope image of Fe0.13-[Co80Ni20]0.87 particles obtained through the polyol process. Average diameter is 204 nm, standard deviation is as low as σ=25 nm.

It has been observed that composites obtained by dispersing these fine particles exhibit sharp imaginary permeability peaks [26], in contrast with conventional powders such as carbonyl iron powders that exhibit very broad beaks, as illustrated on figure 11.

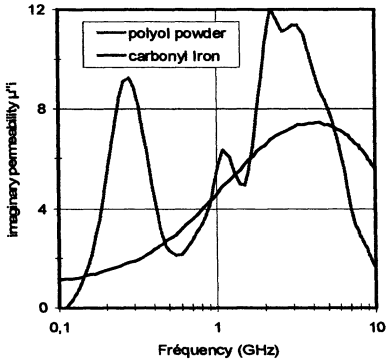

Figure 11. Intrinsic imaginary permeability of ferromagnetic powders deduced from experimental measurements on C0D composites, and inversion of Bruggeman law : comparison between conventional carbonyl iron powder (smooth curve) and submicronic polyol powder (curve with sharp peaks).

These sharp peaks have been shown to be due to exchange resonance modes [28, 29]. Further investigations have shown that 3 different regimes can be observed : for very small particles of the order of ten nanometers in diameter, a single sharp peak is observed, in association with the superparamagnetic behavior. For larger particles up to a fraction of μm in diameter, multiple sharp peaks are observed. For particles in the μm range, only a broad resonance is observed, and exchange resonance modes are no longer visible [30].

2.5 USING THE NON UNIFORM RESPONSE OF MAGNETIC INCLUSIONS

It has been shown [8, 9, 14, 20, 21] (see Eqs. 2-4, Fig. 6b and 9) that the microwave response of many C1D and C2D composites could be interpreted in term of uniform gyromagnetic resonance of the ferromagnetic element, plus skin effect, plus dilution. The skin effect factor A in Eq (2) does not change significantly the resonance frequency F_r (defined by $\mu'(F_r)=1$), but it broadens significantly the imaginary permeability peak. The dilution essentially impacts the magnitude of the effective permeability. As a consequence, the engineering of the microwave response of a C1D or C2D composite made of a ferromagnetic elongated element with uniform gyromagnetic response is rather straightforward. It basically consists in adjusting the resonance frequency through the material parameters of the inclusion [18, 19, 24], and tuning the broadening and the amplitude of the permeability through the thickness of the inclusion and the volume fraction.

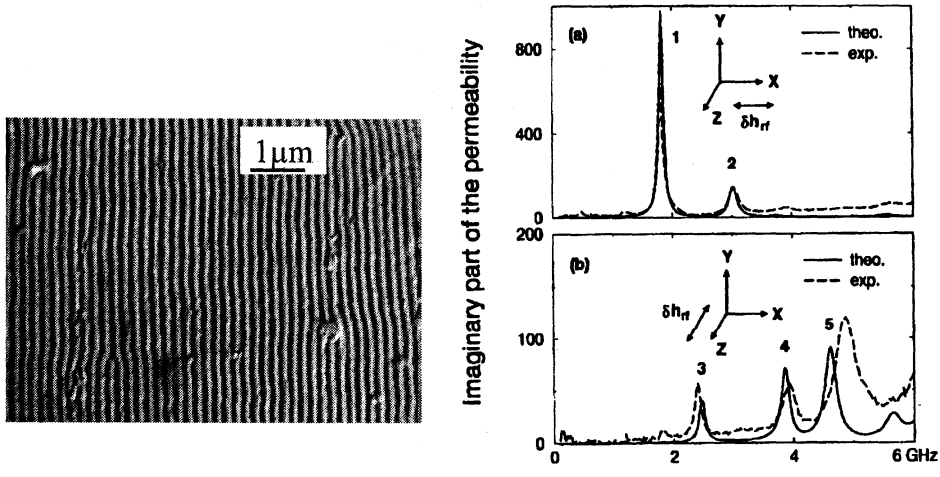

a) b)

Figure 12. a) Kerr Optical micrograph of the stripe domain structure of an amorphous CoFeZr layer; b) experimental (dashed curve) and theoretical response (full curve) of a CoFeZr with stripe domain structure, according to [31].

But in some cases, ferromagnetic elements can exhibit a response that is much richer than conventional gyromagnetic resonance. This is the case for example when a significant anisotropy normal to the film plane gives rise to a so-called stripe domain structure (Fig. 12a). Then, several narrow peaks can be observed on the permeability spectrum, in both direction of the film plane (Fig. 12b) [17]. The permeability exhibits a significant hysteresis, associated with the so-called rotatable anisotropy of the films. In a first approach, a film with stripe domain structure can be described as a system with two populations of domains in interaction, the magnetization precession being uniform within each population of domains. This description leads to an analytical expression of the first two resonance modes in the film plane, and accounts for the small linewidth of the peaks [32]. More recently, a numerical dynamic micromagnetic approach lead to an excellent agreement between the computed and the measured permeability [31]. Another example of non-uniform modes is observed in the small submicronic polyol made particles. It has been demonstrated that the sharp peaks observed in these materials are associated to non-uniform exchange-driven modes [29].

3. Guidelines for the design of microwave composites

3.1 CHOICE OF A PROPER DEFINITION FOR THE EFFECTIVE PERMEABILITY AND PERMITTIVITY

The notion of effective permeability and permittivity has been introduced above. It is a very usual approach to account for the properties of a composite through its effective properties. Significant efforts have been dedicated to the development of effective medium theories. However, very little attention has been paid until recently to the fact that no clear definition of the effective permeability and permittivity of a composite had been given. In fact, different approaches lead to incompatible values of effective parameters when skin effect is not negligible [13], because they rely on different definitions. As permeability and permittivity values are obtained through reflection – transmission measurements, it was found necessary to establish a definition of the effective quantities, so that the conventional expressions of the Fresnel coefficients using the effective quantities are valid. Using this approach, it has been shown that [33] :

$$\mu_{composite}=<B>/H_{insulator} \quad (5)$$

$$\varepsilon_{composite}=D_{insulator}/<E> \quad (6)$$

where the brackets correspond to the spatial average over the whole volume of a periodical cell in the composite, and $H_{insulator}$, $D_{insulator}$ are the fields in a plane containing no conductive element, and normal to the electric field. The hypothesis and approximations associated with these results are discussed in full detail in ref. 33.

An important consequence of this result is to provide a justification to Eqs 2 to 4. It allows the computation of the effective properties of C1D and C2D composites made of hollow inclusions [34]. In addition, the form of Eqs 5-6 is very convenient to deduce effective parameters from numerical resolution of Maxwell equations in an inhomogeneous material. This approach may be helpful in the development of metamaterials, which are sophisticated composites in which skin effect can not be neglected.

3.2 BOUNDS ON THE MICROWAVE PROPERTIES AND SUM RULES

The intuition suggests that there is a connection between the microwave permeability levels that can be attained, and the saturation magnetization. In the case of ferrite materials with cubic symmetry, Snoek's law [35] indicates that the product of the low frequency real permeability μ'_i by the gyromagnetic resonance frequency F_r is related to the saturation magnetization $4\pi M_s$ by :

$$\mu_i'.F_r = \frac{2}{3}(\gamma.4\pi M_s) \qquad (7)$$

In the case of a saturated thin film, it is easily shown that this law takes the form :

$$\mu_i'.F_r^2 = (\gamma.4\pi M_s)^2 \qquad (8)$$

However, Snoek's law gives no indication on the microwave permeability levels. In addition, it is not valid for composite or inhomogeneous materials. Recently, we derived a general sum rule, which is valid for a wide class of soft magnetic materials and composites [36] :

$$I_x = \int_0^{+\infty} F.\mu_x''(F)dF \le f\frac{\pi}{2d}(\gamma.4\pi M_s)^2 = \frac{I_{max}}{d} \qquad (9)$$

where F is the frequency, and f is the volume fraction of the ferromagnetic constituent in the composite (f=1 in the case of bulk magnetic material). d is the number of directions in space where the permeability is $\mu_x(F)$: d=3 in the case of an isotropic material, and d=1 in the case of a LIFE material made from films with uniaxial magnetization. This relation is valid in the case where skin effect is negligible. Exchange driven modes are not taken into account either.
In the relation (9), the left quantity I_x is related to the microwave losses. It is easily determined from permeability measurements performed with a network analyzer, and a proper measurement cell. The bound I_{max}/d is determined from static magnetic measurements, and from tabulated values of the gyromagnetic factor γ, that is close to 3 MHz/Oe for most ferromagnetic materials.
In the case of soft ferromagnetic films with well-defined in-plane magnetization and LIFE composites made from such films, it has been shown that the bound is attained [37] :

$$I_x = I_{max} \qquad (10)$$

The validity of Eqs 9-10 has been assessed by experimental results on a large variety of materials [38], either bulk or composite, with a large variety of dynamic response as reported on Fig. 13.
Hexagonal ferrites with in-plane anisotropy are an interesting class of microwave materials, but relation (9) does not apply as these materials exhibit very large out-of plane anisotropy fields, and hence the soft material hypothesis is not verified. But it has been shown that a sum rule can be derived, that takes into account this out of plane anisotropy, and that it is in excellent agreement with experimental results [39].

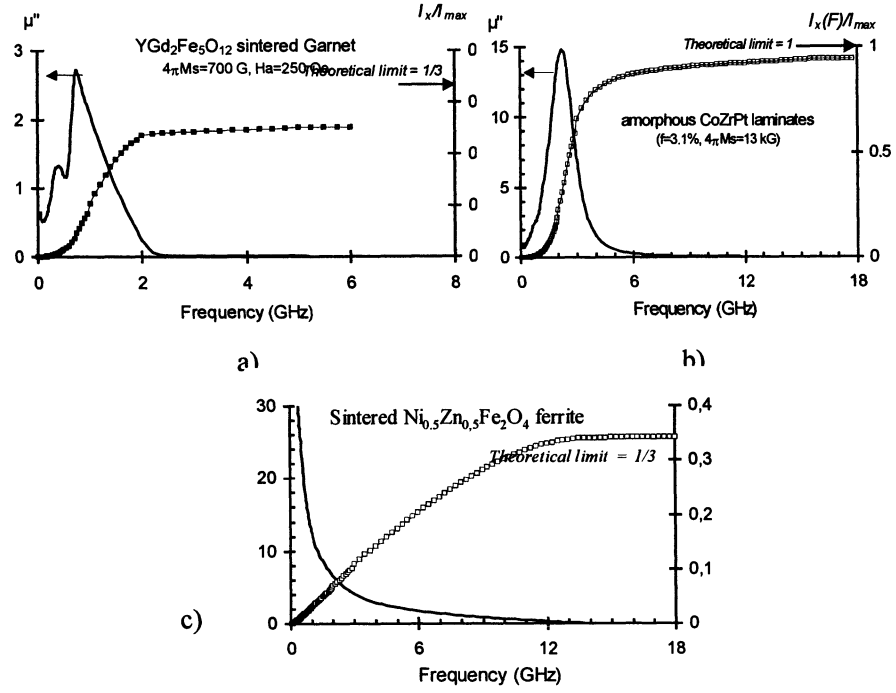

Figure 13. Imaginary permeability (left scale) and partial integral $I_x(F)/I_{max} = \left(\int_0^F \nu.\mu_x''(\nu)d\nu\right) / \left(\frac{\pi}{2} f(\chi.4\pi M_s)^2\right)$ (right scale) for a) a sintered garnet ; b) a LIFE composite ; c) a sintered ferrite.

This sum rule gives precise indications for engineering the response of magnetic materials. As an example, it gives a very straightforward indication on the minimal weight of thin magnetic absorbers [36]. It also opens significant possibilities in the field of instrumentation. In particular, it is useful to check the validity of high frequency measurements of permeameters [5].

4. Tuning the microwave response of a magnetic material

4.1 TUNING μ TROUGH AN EXTERNAL FIELD

A very straightforward way to tune the microwave response of a magnetic material is to apply an external static magnetic field. The evolution of the permeability with

the applied field is in most cases well understood from the gyromagnetic resonance equations [14].
A tunable microstrip filter has been manufactured using this principle [15, 40]. This filter is sketched on Fig. 14a), and the transmission coefficient is given on Fig. 14b and 14c. When the field is applied along the easy axis, the stopband shifts to higher frequencies, due to the shift in the gyromagnetic resonance frequency (Fig. 14b). In contrast, when a field is applied normal to the easy axis and is strong enough to change the orientation of the magnetization in the material, the permeability along the microwave H field is unity, and a flat transmission response is observed (Fig. 14c).

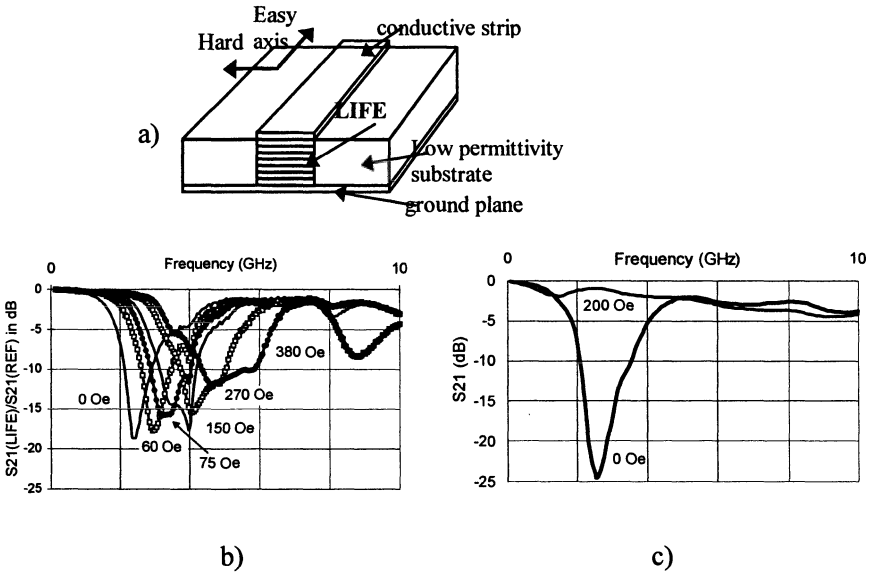

Figure 14. a) Sketch of a microwave filter consisting of a LIFE material inserted in a microstrip line ; b) operation with an external magnetic field along the microstrip line ; c) operation with an external magnetic field normal to the microstrip line and in the lamination plane.

4.2 TUNING μ TROUGH AN EXTERNAL STRESS

Another way to tune the microwave response of a material is to exert a significant stress. The effect of stress on the microwave properties of ferrites has been studied [41]. The evolution of the microwave permeability of ferromagnetic thin film when a parallel tensile stress is applied can be observed using a thin film permeameter [42]. A thin film deposited on a plastic substrate is preferred, because a large stress can be exerted using only moderate forces. The evolution with stress of the microwave permeability of an amorphous CoFeSiB material is presented on figure 15a). It can be seen that the square of the resonance frequency increases linearly with the stress, as predicted for a material with negative magnetostriction. The

saturation magnetostriction coefficient λ_s can be extracted from the slope of the variation [42], and is $-5.8\ 10^{-7}$ in the case of Fig. 15. Magnetostriction coefficients as low as $-0.5\ 10^{-7}$ can be measured using this method.

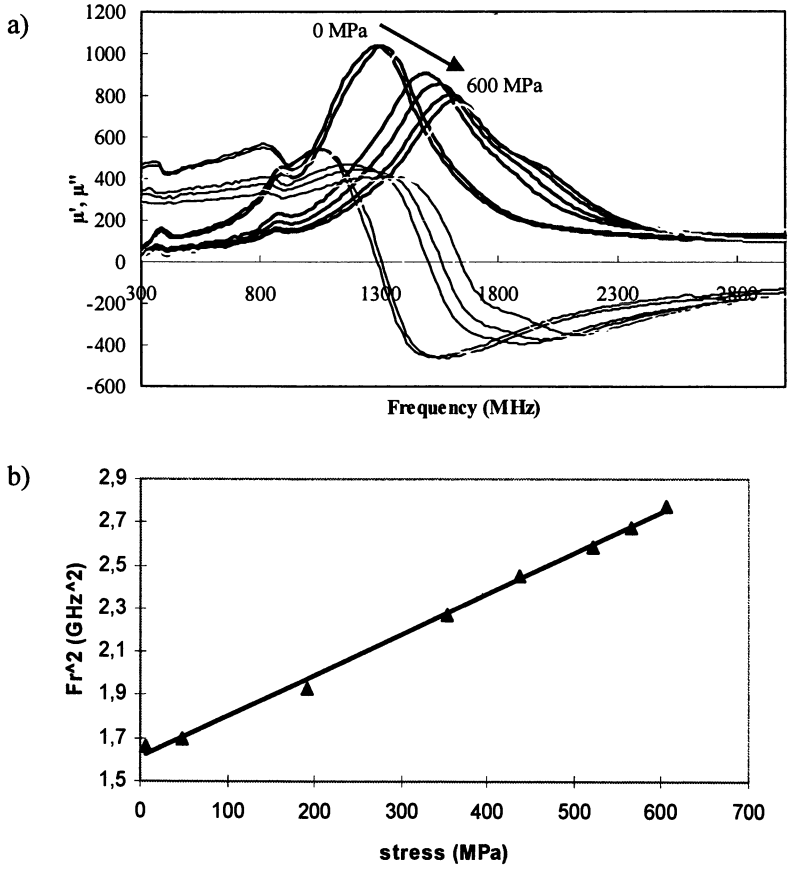

Figure 15. a) Evolution of the microwave permeability along the hard axis of a thin amorphous Co-based film deposited on a mylar substrate, for a tensile stress along the hard axis ; b) square of the gyromagnetic resonance frequency as a function of the applied stress (triangles) and best linear fit (line).

4.3 TUNING ε TROUGH AN EXTERNAL MAGNETIC FIELD

Recently, we have demonstrated that it is possible to tune not only the permeability of a magnetic-based composite, but also its permittivity. This result has been obtained on a wire medium consisting of parallel highly diluted amorphous glass-covered wires. The permittivity has been shown experimentally to be tunable using

an external magnetic field. At some frequencies, the sign of the real permittivity could be changed by increasing the external field [43].

5. Conclusion

Ferromagnetic materials now appear as extremely attractive microwave materials. Their conductivities used to be a strong limitation to their use at high frequencies, but thin films, microwires and small powders can be turned into composites with very attractive properties. The effective permeability of these composites can be related to the properties of the inclusions through accessible models, based on a proper definition of the effective properties of a composite. Significant progress has been made also in the field of microwave measurements of ferromagnetic constituents or composites. The properties of these materials can be engineered, in particular through the material parameters of the magnetic inclusions, but clear limits have been established that relate the microwave magnetic response to the saturation magnetization of the materials. The ferromagnetic-based composites are also attractive to make agile microwave devices. Not only the permeability, but also the permittivity of the composites can be tuned. If the application of an external field is a very simple way to tune the microwave response of a magnetic-based composite, it is also possible to use the stress dependence of most magnetic materials in order to control the response through the application of a stress.

6. Acknowledgements

I thank the researchers and Ph. D. students from the "Laboratoire Matériaux Magnétiques et Hyperfréquence" for their decisive contribution to the advanced microwave magnetic materials reviewed here, and in particular A.L. Adenot, S. Deprot, F. Duverger, P.-M. Jacquart, M. Ledieu and Ph. Toneguzzo.

7. References

1. Jacquart P.-M., Acher O. and Gadenne P. (1994) Reflection and transmission of an electromagnetic wave in a strongly anisotropic medium : application to polarizers and antireflection layers on a conductive plane, *Optics Com.* **108**, 355.
2. Yamaguchi M., Yabukami S., Arai K. I. (1997) A new 1MHz-2GHz permeance Meter for Metallic Thin Films, *IEEE Trans. Magn.* **33**, 2619.
3. Grimes C.A., Prodan J.V. (1993) Swept frequency permeameters for measuring the complex, off-diagonal permeability tensor components of anisotropic thin magnetic films, *J. Appl. Phys.* **73**, 6989.
4. Nicholson A.M. and Ross G.F. (1968) *IEEE Trans. Instrum. Meas* **17**, 395.
5. Pain D., Ledieu M., Acher O., Adenot A.-L. and Duverger F. (1999) An improved permeameter for thin film measurement up to 6 GHz, *J. Appl. Phys.* **85**, 5151.

6. Yamaguchi M., Acher O., Miyazawa Y., Arai K.I. and Ledieu M. (2002) Cross measurements of thin-film permeability up to UHF range, *J. Magn. Magn. Mater, accepted for publication.*
7. Adenot A.-L., Acher O., Pain D., Duverger F., Malliavin M.-J., Damiani D. and Taffary T. (2000) Broad band permeability measurment of ferromagnetic thin films or microwires by a coaxial line perturbation method, *J. Appl. Phys.* **87**, 5965.
8. Acher O., Vermeulen J.-L., Jacquart P.-M., Fontaine J.-M. and Baclet Ph. (1994) Permeability measurement on ferromagnetic thin films from 50 MHz up to 18 GHz, *J. Magn. Magn. Mater.* **136**, 269.
9. Acher O., Jacquart P.-M., Fontaine J.-M., Baclet Ph. and Perrin G. (1994) High impedance anisotropic composites manufactured from ferromagnetic thin films for microwave applications, *IEEE Trans. Magn.* **30**, 4533.
10. Jacquart P.-M. and Acher O. (1996) Permeability measurements on composites made of oriented metallic wires from 0.1 to 18 GHz, *IEEE Trans. Microwave Theory Tech.* **44**, 2116.
11. Mingzhong Wu, Zhao, Huahui He and Xi Yao (2001) Electromagnetic anisotropy of magnetic iron fibers at microwave frequencies, *J. Phys. D: Appl. Phys.* **34**, 1069.
12. Garcia-Miquel H., Esbri M.J., Andrés J.M., Garcia J.M., Garcia-Beneytez J.M. and Vazquez M. (2001) Power Absorption and Ferromagnetic Resonance in Co-Rich Metallic Glasses, *IEEE Trans. Magn.* **37**, 561.
13. Rozanov K.N., Simonov N.A. and Osipov A.V. (2002) Microwave Measurements of the Magnetic Film Permeability, *Journal of Communication Technology and Electronics* **47**, 210.
14 Acher O., Le Gourriérec P., Perrin G., Baclet Ph. and Roblin O. (1996) Demonstration of Anisotropic Composites with Tuneable Microwave Permeability Manufactured from Ferromagnetic Thin Films, *IEEE Trans. Microwave Theory Tech.* **44**, 674.
15. Adenot A.-L., Acher O., Taffary T., Quéffélec P. and Tanné G. (2000) Tuneable microstrip device controlled by a weak magnetic field using ferromagnetic laminations, *J. Appl. Phys.* **87**, 6914.
16. Lebourgeois R., Ganne J.P., Peyresoubes G., Rebernak W., Adenot. A.-L and Acher O. (2002) New ferromagnetic composites for radio-frequency applications, *J. Magn. Magn. Mater, accepted for publication.*
17. Suran G., Naili M., Niedoba H., Machizaud F., Acher O. and Pain D. (1999) Magnetic and structural properties of Co-rich CoFeZr amorphous thin films, *J. Magn. Magn. Mater.* **192**, 443.
18. Acher O., Boscher C., Le Guellec P., Baclet Ph and Perrin G. (1996) Investigation of the gyromagnetic permeability of amorphous CoFeNiMoSiB manufactured by different techniques, *IEEE Trans. Magn.* **32**, 4833.
19. Perrin G., Peuzin J.-C. and Acher O. (1997) Control of the resonance frequency of soft ferromagnetic amorphous thin films by strip patterning, *J. Appl. Phys.* **81**, 5166.
20. Malliavin M.-J., Acher O., Boscher C., Bertin F. and Larin V.S. (1999) High frequency permeability of thin amorphous wires with various anisotropic fields, *J. Magn. Magn. Mater.* **196-197**, 420.
21. Acher O., Adenot A.-L., and Deprot S. (2002) Parallel permeability of ferromagnetic wires up to GHz frequencies, *J. Magn. Magn. Mater, in press.*
22. Deprot S., Adenot A.-L., Bertin F., Hervé E. and Acher O. (2001) High frequency losses of ferromagnetic wires near the gyromagnetic resonance, *IEEE Trans. Magn.* **37**, 2404.
23. Acher O., Jacquart P.-M. and Boscher C. (1994) Investigation of high frequency permeability of thin amorphous wires, *IEEE Trans. Magn.* **30** 4542.
24. Deprot S., Adenot A.-L., Bertin F. and Acher O. (2002) Frequency response engineering of CoFeNiBSi microwires in the GHz range, *J. Magn. Magn. Mater, accepted for publication.*
25. Rousselle D., Berthault A., Acher O., Bouchaud J .-P. and Zérah P.G. (1993) Effective Medium at Finite frequency : Theory and experiment, *J. Appl. Phys.* **74**, 475.

26. Toneguzzo Ph., Acher O., Viau G., Fiévet-Vincent F. and Fiévet F. (1997), Observations of exchange resonance modes on submicrometer sized ferromagnetic particles, *J. Appl. Phys.* **81**, 5546.
27. Viau G., Toneguzzo Ph., Pierrard A., Acher O., Fiévet-Vincent F. and Fiévet F. (2001) Heterogeneous nucleation and growth of metal nanoparticles in polyols, *Scripta Mater.* **44**, 2263.
28. Toneguzzo Ph., Viau G., Acher O., Pierrard I., Rosenman I., Fiévet-Vincent F. and Fiévet F. (1999) Static and Dynamic Magnetic Properties of Fine CoNi and FeCoNi Particles Synthesized by the Polyol Process, *IEEE Trans. Magn.* **35**, 3469.
29. Mercier D., Lévy J.-C. S., Viau G., Fiévet-Vincent F., Fiévet F., Toneguzzo Ph. and Acher O. (2000) Magnetic resonance in spherical CoNi and FeCoNi particles, *Phys. Rev. B* **62**, 532.
30. Toneguzzo Ph., Viau G., Acher O., Guillet F., Bruneton E., Fiévet-Vincent F. and Fiévet F. (2000) CoNi and FeCoNi fine particles prepared by the polyol process : Physico-chemical characterization and dynamic magnetic properties, *J. Mat. Sci.* **35**, 3767.
31. Vukadinovic N., Vacus O., Labrune M., Acher O. and Pain D. (2000) Magnetic excitations in a weak-stripe domain structure : a 2-D dynamic micromagnetic approach, *Phys. Rev. Lett.* **85**, 2 817.
32. Acher O., Boscher C., Brulé B., Perrin G., Vukadinovic N., Suran G. and Joisten H. (1997) Microwave permeability of ferromagnetic thin films with stripe domain structure, *J. Appl. Phys.* **81**, 4057.
33. Acher O., Adenot A.-L., and F. Duverger F. (2000) Fresnel coefficients at an interface with a lamellar composite material, *Phys. Rev. B.* **62**, 13 748.
34. Acher O., Adenot A.-L., Lubrano F. and Duverger F. (1999) Low density artificial microwave magnetic composites, *J. Appl. Phys.* **85**, 4639.
35. J.L. Snoek (1948) *Physica* **XIV**, 207.
36. Acher O. and Adenot A.-L. (2000) Bounds on the dynamic properties of magnetic materials, *Phys. Rev. B.* **62**, 11 324.
37. Perrin G., Acher O., Peuzin J.-C. and Vukadinovic N. (1996) Sum rules for gyromagnetic permeability of ferromagnetic thin films : theoretical and experimental results, *J. Magn. Magn. Mater.* **157/158**, 289.
38. Acher O., Adenot A.-L and Duverger F. (2001) Sum rules on the dynamic permeability of magnetic materials and composites, *Materials Science Forum* **373-377**, 709.
39. Adenot A.-L., Acher O., Taffary T. and Longuet L. (2002) Sum rules on the dynamic permeability of hexagonal ferrites, *J. Appl. Phys.* **91**, 7 601.
40. Salahun E., Tanné G., Quéffélec P., Le Floc'h M., Adenot A.-L. and Acher O. (2001) Application of ferromagnetic composites in different planar tunable microwave devices, *Microwave Opt. Technol. Lett.* **30**, 272.
41. Ledieu M., Adenot A.-L., and Acher O. (2000) Permeability measurement of ferrite under stress up to 6 GHz, *IEEE Trans. Magn.* **36**, 3254.
42. Acher O., Vermeulen J.-L., Lucas A., Baclet Ph. and Kazandjoglou J. (1993) Direct measurement of permeability up to 3 GHz of Co-based alloys under tensile stress, *J. Appl. Phys.* **73**, 6162.
43. Reynet O., Acher O. and Latrach M., (2003) Tunable High Frequency Dielectric Response of Diluted Ferromagnetic Composites, *Electromagnetics*, to be published.

II.

METAMATERIALS WITH NEGATIVE PARAMETERS

A FLAVOUR OF CONSTITUTIVE RELATIONS: THE LINEAR REGIME

WERNER S WEIGLHOFER
Department of Mathematics, University of Glasgow
University Gardens, Glasgow G12 8QW, Great Britain

Abstract. Constitutive relations supplement the Maxwell equations to provide a selfconsistent and complete description of electromagnetic processes in materials. Some of the basic aspects relating to the characterization of different types of materials in terms of constitutive relations are reviewed in this contribution. Special emphasis is placed upon the different interpretations of time-domain and frequency-domain formulations. Some selected case studies show how nonlocality in time is equivalent to locality in frequency. The genesis of constitutive relations is exemplified through two mechanisms: a simple model for an electron plasma which leads to anisotropy and a homogenization technique from which a very general class of composite mediums, so-called Faraday chiral mediums, emerge. In the linear regime, the general bianisotropic medium, characterized by four constitutive dyadics (second-rank cartesian tensors) is the most general type of medium.

1. Introduction

The mathematical formalism developed by James Clerk Maxwell governs the description of all classical electromagnetic processes, be they propagation, radiation, scattering and the likes. All of those take place in a *medium* of some description. The mathematical characterization of mediums is therefore an important task that lies at the very basis of classical electromagnetic theory.

"What is a medium?" (Or "What is a *material*?", these two terms being used synonymously in this paper.) One can begin with the classical vacuum and ask if it can be called a medium after all, as it is devoid of any material interactions. More appropriately, therefore, the classical vacuum is a *reference* medium. Beyond the classical vacuum, in the realm of real physical materials one can further ask "What is a *complex* medium?" A question of that nature is very central to a whole series of specialist conferences, such as the *Bianisotropics* conferences, see for example [1, 2, 3], or the *Complex Mediums* conferences [4, 5, 6] as well as to recent books [7, 8, 9, 10]. Relating to the electromagnetic properties of a certain material,

S. Zouhdi et al. (eds.), Advances in Electromagnetics of Complex Media and Metamaterials, 61–80.

the term complex remains only very loosely defined and encompasses vastly different research topics. A sensible view and working hypothesis considers any bulk medium with an internal structure more complicated than that of a linear, homogeneous, isotropic dielectric–magnetic medium to be complex.

Whether a medium is *simple* or *complex*, constitutive relations must deliver a description of its electromagnetic properties. Therefore, they must provide a basis for a classification of mediums by certain criterions: distinctions on the basis of linearity versus nonlinearity, isotropy versus anisotropy/bianisotropy, homogeneity versus nonhomogeneity, spatial and/or temporal dispersion, and so on. A thorough study of constitutive relations will thus contribute towards a better understanding of electromagnetic complexity. The purpose of this contribution is to highlight some fundamental aspects associated with the delineation of constitutive relations, investigate their genesis in certain physical models of bulk matter or from homogenization formalisms. Furthermore, to study their mathematical structure as it is constrained by physical and mathematical conditions. The topic is vast and the author makes no claim to providing a comprehensive presentation in such a limited space; rather it is hoped that the selection of covered topics will whet to reader's appetite for further study of this interesting topic. The most significant restriction is that *linear* mediums shall be considered only; for constitutive relations pertaining to nonlinear electromagnetic response, the reader is referred to the literature [11, 12, 13].

In the following, Section 2 defines the two approaches to electromagnetic field analysis in the space–time and space–frequency domains, respectively. In Section 3, some fundamental comments of the role that constitutive relations play, are made. In Section 4, an exposition of constitutive relations for different types of mediums with increasing complexity is given before turning to bianisotropic mediums in Section 5 where such topics as symmetries, constraints and homogenization formalisms are covered.

The mathematical approach will be through the standard vector calculus of 3-vectors and 3×3-dyadics (second rank cartesian tensors). Alternative descriptions utilize the covariant tensor formalism [14] or the technique of 6-vectors and 6×6-dyadics [15, 16].

The following notational conventions are used: vectors are in bold face while dyadics/tensors of second rank are in normal face and underlined twice. Contraction of indexes is symbolized by a dot; that is, $\mathbf{a} \cdot \mathbf{b}$ stands for $\sum_i a_i b_i$, whereas $\underline{\underline{A}} = \mathbf{a}\,\mathbf{b}$ is a dyadic with elements $A_{ij} = a_i\, b_j$. The triplet of cartesian unit vectors is denoted by $(\mathbf{u}_x, \mathbf{u}_y, \mathbf{u}_z)$, and the position vector by $\mathbf{x} = x\mathbf{u}_x + y\mathbf{u}_y + z\mathbf{u}_z$. The unit dyadic is $\underline{\underline{I}} = \mathbf{u}_x\,\mathbf{u}_x + \mathbf{u}_y\,\mathbf{u}_y + \mathbf{u}_z\,\mathbf{u}_z$, and $\underline{\underline{0}}$ is the null dyadic. The superscript $^{-1}$ indicates inversion of a dyadic. Time-dependent quantities are distinguished by a tilde above their respective symbols.

2. The Maxwell Equations

2.1. THE SPACE–TIME DOMAIN

Classical electromagnetic theory is governed by the Maxwell equations. For fields depending on the spatial variable $\mathbf{x}$ and time t, they are given by

$$-\frac{\partial \tilde{\mathbf{D}}(\mathbf{x},t)}{\partial t} + \nabla \times \tilde{\mathbf{H}}(\mathbf{x},t) = \tilde{\mathbf{J}}_e(\mathbf{x},t)\,, \tag{1}$$

$$\nabla \times \tilde{\mathbf{E}}(\mathbf{x},t) + \frac{\partial \tilde{\mathbf{B}}(\mathbf{x},t)}{\partial t} = -\tilde{\mathbf{J}}_m(\mathbf{x},t)\,, \tag{2}$$

$$\nabla \cdot \tilde{\mathbf{D}}(\mathbf{x},t) = \tilde{\rho}_e(\mathbf{x},t)\,, \tag{3}$$

$$\nabla \cdot \tilde{\mathbf{B}}(\mathbf{x},t) = \tilde{\rho}_m(\mathbf{x},t)\,. \tag{4}$$

Therein, $\tilde{\mathbf{D}}(\mathbf{x},t)$ is the dielectric displacement, $\tilde{\mathbf{E}}(\mathbf{x},t)$ is the electric field, $\tilde{\mathbf{H}}(\mathbf{x},t)$ is the magnetic field and $\tilde{\mathbf{B}}(\mathbf{x},t)$ is the magnetic induction; whereas $\tilde{\mathbf{J}}_e(\mathbf{x},t)$, $\tilde{\mathbf{J}}_m(\mathbf{x},t)$, $\tilde{\rho}_e(\mathbf{x},t)$ and $\tilde{\rho}_m(\mathbf{x},t)$ are the electric and magnetic current and charge densities, respectively. Magnetic charge and magnetic current densities are fictitious quantities; however, their introduction into the Maxwell equations serves a dual purpose: the equations acquire a higher degree of symmetry (and show an associated invariance with respect to certain types of duality transformations [17]) and in some applications such usage leads to a simplified analysis, see the literature for more details [18, 19].

The two divergence relations (3) and (4) are generally viewed as consistency conditions in electromagnetics and not as independent differential equations. They will not play a role in the following. Indeed, they can be viewed as being implied by (1) and (2) provided it is assumed that the current and charge densities fulfil

$$\nabla \cdot \tilde{\mathbf{J}}_p(\mathbf{x},t) + \frac{\partial \tilde{\rho}_p(\mathbf{x},t)}{\partial t} = 0\,, \qquad p = e,m\,. \tag{5}$$

Henceforth, all sources are supposed to comply with the continuity equations (5).

2.2. THE SPACE–FREQUENCY DOMAIN

All the fields introduced previously are *real-valued* vector fields depending on position $\mathbf{x}$ and time t. A significant amount, probably the vast majority, of electromagnetics research dealing with simple and complex mediums alike is performed for frequency-dependent fields, however. One can apply

a Fourier transform with respect to time

$$\tilde{\mathcal{W}}(\mathbf{x},t) = \int \mathcal{W}(\mathbf{x},\omega)\, \exp(-i\omega t)\, d\omega\,, \quad \mathcal{W} = \mathbf{D}\,,\mathbf{E}\,,\mathbf{B}\,,\mathbf{H}\,,\mathbf{J}_e\,,\mathbf{J}_m\,,\rho_e\,,\rho_m\,, \tag{6}$$

which entails that (1)–(4) are transformed into

$$i\omega\mathbf{D}(\mathbf{x}\,,\omega) + \nabla \times \mathbf{H}(\mathbf{x}\,,\omega) = \mathbf{J}_e(\mathbf{x}\,,\omega)\,, \tag{7}$$

$$\nabla \times \mathbf{E}(\mathbf{x}\,,\omega) - i\omega\mathbf{B}(\mathbf{x}\,,\omega) = -\mathbf{J}_m(\mathbf{x}\,,\omega)\,, \tag{8}$$

$$\nabla \bullet \mathbf{D}(\mathbf{x}\,,\omega) = \rho_e(\mathbf{x}\,,\omega)\,, \tag{9}$$

$$\nabla \bullet \mathbf{B}(\mathbf{x}\,,\omega) = \rho_m(\mathbf{x}\,,\omega)\,, \tag{10}$$

whereas the continuity equations (5) turn into

$$\nabla \bullet \mathbf{J}_p(\mathbf{x},\omega) - i\omega\rho_p(\mathbf{x},\omega) = 0\,, \qquad p = e,m\,. \tag{11}$$

The two systems of vector partial differential equations (1)–(5) and (7)–(11) are equivalent starting points for electromagnetic field analysis. It must be appreciated, however, that there is a fundamental difference between these two systems: (1)–(5) contain real-valued (and thus measurable) field vectors depending on $\mathbf{x}$ and t, while in (7)–(11) the involved field quantities are *complex-valued field phasors*, depending on $\mathbf{x}$ and angular frequency ω. As such they are simply mathematical constructs and significant consequences of this distinction are discussed in more detail in a later section.

3. Why Constitutive Relations?

¿From the viewpoint of the previous section, where it was argued that the Maxwell 'divergence' equations are implied by the Maxwell 'curl' equations if only the continuity equations hold, the following *active* system of partial differential equations is at one's disposal. For fields depending on space–time:

$$-\frac{\partial\tilde{\mathbf{D}}(\mathbf{x}\,,t)}{\partial t} + \nabla \times \tilde{\mathbf{H}}(\mathbf{x}\,,t) = \tilde{\mathbf{J}}_e(\mathbf{x}\,,t)\,, \tag{12}$$

$$\nabla \times \tilde{\mathbf{E}}(\mathbf{x}\,,t) + \frac{\partial\tilde{\mathbf{B}}(\mathbf{x}\,,t)}{\partial t} = -\tilde{\mathbf{J}}_m(\mathbf{x}\,,t)\,; \tag{13}$$

while for field phasors depending on space–frequency:

$$i\omega\mathbf{D}(\mathbf{x}\,,\omega) + \nabla \times \mathbf{H}(\mathbf{x}\,,\omega) = \mathbf{J}_e(\mathbf{x}\,,\omega)\,, \tag{14}$$

$$\nabla \times \mathbf{E}(\mathbf{x}\,,\omega) - i\omega\mathbf{B}(\mathbf{x}\,,\omega) = -\mathbf{J}_m(\mathbf{x}\,,\omega)\,. \tag{15}$$

These two systems are repeated here such that one can see very clearly that (12), (13) and (14), (15), respectively, do not provide a sufficient number of differential equations to derive a solution for the fields or phasors. In both cases there are twelve unknown components: three each for the field vectors $\tilde{\mathbf{D}}(\mathbf{x},t)$, $\tilde{\mathbf{E}}(\mathbf{x},t)$, $\tilde{\mathbf{H}}(\mathbf{x},t)$, $\tilde{\mathbf{B}}(\mathbf{x},t)$ in the time-dependent case; and three each for the field phasors $\mathbf{D}(\mathbf{x},\omega)$, $\mathbf{E}(\mathbf{x},\omega)$, $\mathbf{H}(\mathbf{x},\omega)$, $\mathbf{B}(\mathbf{x},\omega)$ in the frequency-dependent case (the source terms on the respective right-hand sides are presumed to be prescribed), while the two systems only provide six partial differential equations each. As a consequence, six further relations (two vector equations) must be added in each case for a selfconsistent description of the electromagnetic field. Initially, we specify these relations in a very general form as the vector equations

$$\Pi_p \left\{\tilde{\mathbf{E}}(\mathbf{x},t),\tilde{\mathbf{D}}(\mathbf{x},t),\tilde{\mathbf{H}}(\mathbf{x},t),\tilde{\mathbf{B}}(\mathbf{x},t)\right\} = \mathbf{0}\,, \qquad p = e,m\,, \tag{16}$$

or

$$\Psi_p \left\{\mathbf{E}(\mathbf{x},\omega),\mathbf{D}(\mathbf{x},\omega),\mathbf{H}(\mathbf{x},\omega),\mathbf{B}(\mathbf{x},\omega)\right\} = \mathbf{0}\,, \qquad p = e,m\,. \tag{17}$$

Therein, $\Pi_{e,m}$ and $\Psi_{e,m}$, respectively, denote some general functional dependence between the involved fields and phasors. The relations (16) are the *constitutive relations* for space–time dependent fields, while (17) are the constitutive relations for space–frequency dependent field phasors. What specific functional dependence is present in (16) or (17) depends on a number of issues.

(i) In which kind of material(s) does the electromagnetic process take place: what is the *global* structure?
(ii) What constraints do physical conditions (such as symmetry requirements in crystals, for example, or reciprocity conditions) impose on the constitutive parameters: what are the *intrinsic* properties?
(iii) Are there structural conditions such as mathematical uniqueness requirements that constrain the constitutive properties further?

A selfconsistent problem is thus described by the Maxwell equations plus the constitutive relations that provide specific information about the material that is being considered. It is added parenthetically that the delineation of a complete electromagnetic problem further requires the specification of boundary and/or initial conditions, but that topic is not considered here.

Therefore, in a brief intermediate summary, electromagnetic field analysis requires

(A) the solution of (12), (13) and (16) for time-dependent fields, or
(B) the solution of (14), (15) and (17) for frequency-dependent field phasors.

4. Linear Constitutive Relations: A Flavour

4.1. THE CLASSICAL VACUUM OF ELECTROMAGNETICS

$$\tilde{\mathbf{D}}(\mathbf{x},t) = \epsilon_0\,\tilde{\mathbf{E}}(\mathbf{x},t)\,, \qquad \tilde{\mathbf{H}}(\mathbf{x},t) = \frac{1}{\mu_0}\,\tilde{\mathbf{B}}(\mathbf{x},t)\,, \tag{18}$$

provide the simplest implementation of constitutive relations and relate to the classical vacuum. As ϵ_0 and μ_0 are *true* constants (permittivity and permeability of vacuum, respectively, $\epsilon_0\mu_0 = 1/c^2$, where c is the speed of light in vacuum), the corresponding constitutive relations for the frequency-dependent field phasors, which follow from the inverse Fourier transform, are identical in appearance as per

$$\mathbf{D}(\mathbf{x},\omega) = \epsilon_0\,\mathbf{E}(\mathbf{x},\omega)\,, \qquad \mathbf{H}(\mathbf{x},\omega) = \frac{1}{\mu_0}\,\mathbf{B}(\mathbf{x},\omega)\,. \tag{19}$$

It is important to realize that the vacuum is the only 'medium' for which this equivalence holds. Its primary role is that of the reference medium of classical electromagnetism.

The constitutive relations of the vacuum also define a *minimum* mathematical structure for constitutive relations in general. When delineating general functional dependencies as in (16) or (17), one must aim to exclude pathological or contradictory, i.e., mathematically inconsistent, formulations. One can require that the constitutive relations of any material must be reducible to those of the classical vacuum when all material interactions are removed.

4.2. HOMOGENEOUS ISOTROPIC DIELECTRIC–MAGNETIC MEDIUMS

The linear, homogeneous, isotropic, dielectric–magnetic medium is the most widely employed material of electromagnetics research. Its frequency-domain constitutive relations are given by

$$\mathbf{D}(\mathbf{x},\omega) = \epsilon_0\epsilon(\omega)\,\mathbf{E}(\mathbf{x},\omega)\,, \qquad \mathbf{H}(\mathbf{x},\omega) = \frac{1}{\mu_0\mu(\omega)}\,\mathbf{B}(\mathbf{x},\omega)\,. \tag{20}$$

The true constants ϵ_0 and μ_0 are supplemented by two (dimensionless) constitutive parameters: relative permittivity $\epsilon(\omega)$ and relative permeability $\mu(\omega)$, both dependent on the circular frequency ω.

For this medium, one encounters for the first time the fundamental difference between constitutive relations in the frequency domain and in the time domain. For convenience, we first introduce an electric susceptibility χ_e and a magnetic susceptibility function χ_m as per

$$\epsilon(\omega) = 1 + \chi_e(\omega)\,, \qquad \mu^{-1}(\omega) = 1 - \chi_m(\omega)\,, \tag{21}$$

(note that χ_m was introduced for the benefit of the mathematical representation as in [20] and does not correspond to the standard definition of a magnetic susceptibility [21]). On using the Fourier transform (6) that connects the time and the frequency domains, it can be seen that (20) and (21) lead to

$$\tilde{\mathbf{D}}(\mathbf{x},t) = \epsilon_0\,\tilde{\mathbf{E}}(\mathbf{x},t) + \int_{-\infty}^{+\infty} \epsilon_0\,\tilde{\chi}_e(\tau)\,\tilde{\mathbf{E}}(\mathbf{x},t-\tau)\,d\tau\,, \tag{22}$$

$$\tilde{\mathbf{H}}(\mathbf{x},t) = \frac{1}{\mu_0}\,\tilde{\mathbf{B}}(\mathbf{x},t) - \int_{-\infty}^{+\infty} \frac{1}{\mu_0}\,\tilde{\chi}_m(\tau)\,\tilde{\mathbf{B}}(\mathbf{x},t-\tau)\,d\tau\,. \tag{23}$$

In these formulas, the electric and magnetic susceptibility kernels $\tilde{\chi}_e(t)$ and $\tilde{\chi}_m(t)$ are the Fourier transforms of the susceptibilities defined in (21):

$$\tilde{\chi}_p(t) = \int \chi_p(\omega)\,\exp(-i\omega t)\,d\omega\,, \qquad p = e,m\,. \tag{24}$$

The representation in (22) and (23) provides a very instructive interpretation in separating the material response of the medium into a contribution from the reference medium (the vacuum) and the actual material interaction. Indeed, it is motivated by the standard approach in describing the material properties of matter in the form

$$\tilde{\mathbf{D}}(\mathbf{x},t) = \epsilon_0\,\tilde{\mathbf{E}}(\mathbf{x},t) + \tilde{\mathbf{P}}(\mathbf{x},t)\,, \tag{25}$$

$$\tilde{\mathbf{H}}(\mathbf{x},t) = \frac{1}{\mu_0}\,\tilde{\mathbf{B}}(\mathbf{x},t) - \frac{1}{\mu_0}\,\tilde{\mathbf{M}}(\mathbf{x},t)\,, \tag{26}$$

in terms of an electric polarization $\tilde{\mathbf{P}}(\mathbf{x},t)$ and a magnetic polarization $\tilde{\mathbf{M}}(\mathbf{x},t)$. These terms can be clearly identified as the convolution integrals in (22) and (23), respectively.

To interpret the constitutive relations (22) and (23) correctly [20], one must first realize they are nonlocal with respect to time. Indeed, if one imposes the requirements that (i) no material medium can respond before it is stimulated and (ii) no material can have an instantaneous response (in other words, it must be *causal*), one is led to the conditions

$$\tilde{\chi}_e(t) \equiv 0\,, \qquad \tilde{\chi}_m(t) \equiv 0\,, \qquad t \le 0\,. \tag{27}$$

The constitutive relations (22) and (23), together with (27) provide the proper material description of a causal, linear, homogeneous, isotropic, dielectric–magnetic medium and we note that (27) is also in accordance with the Kramers–Kronig relations [18].

In fact, the use of constitutive relations that technically apply only for frequency-dependent field phasors to conduct a time-dependent field analysis remains an issue of considerable confusion in the research literature

to the present day, see, for example [22, 23, 24, 25, 26]. Such continuing practice is surprising in view of the observation that appropriate treatments through convolution integrals and causality conditions exist both in older [14, 18] and much more recent publications [27, 28, 20, 29].

4.3. BEYOND ISOTROPY

In all circumstances, at least from a principal perspective, the macroscopic formulation facilitated by the Maxwell equations plus constitutive relations must be based upon a microscopic model of electromagnetic (and possibly other) interactions. Because of the difficulty of solving truly atomistic problems involving bulk matter due to the large number of particles involved, exact representations must however be replaced by phenomenological or approximative models.

The example considered here is of a plasma of electrons in thermal motion. For simplicity, a homogeneous, collisionless, incompressible fluid model is employed [30]. The physical system comprises electrons in a classical vacuum, and we describe the state of the system with $\tilde{\mathbf{E}}(\mathbf{x},t)$, $\tilde{\mathbf{B}}(\mathbf{x},t)$ and an average electron velocity $\tilde{\mathbf{v}}(\mathbf{x},t)$. The Maxwell equations for vacuum are thus augmented by an electric current density due to the electrons' motion as per

$$-\epsilon_0 \frac{\partial \tilde{\mathbf{E}}(\mathbf{x},t)}{\partial t} + \nabla \times \tilde{\mathbf{H}}(\mathbf{x},t) + n_0\, q\, \tilde{\mathbf{v}}(\mathbf{x},t) = \mathbf{0}\,, \tag{28}$$

$$\nabla \times \tilde{\mathbf{E}}(\mathbf{x},t) + \mu_0 \frac{\partial \tilde{\mathbf{H}}(\mathbf{x},t)}{\partial t} = \mathbf{0}\,. \tag{29}$$

These equations are supplemented by the equation of motion for a charged, inviscid and incompressible fluid, given by

$$n_0\, q\, \tilde{\mathbf{E}}(\mathbf{x},t) + n_0 m \frac{\partial \tilde{\mathbf{v}}(\mathbf{x},t)}{\partial t} - n_0\, q\, B_0\, \mathbf{b}_0 \times \tilde{\mathbf{v}}(\mathbf{x},t) = \mathbf{0}\,. \tag{30}$$

Therein, $-n_0 q$ and $n_0 m$ are the background electron charge and mass densities, respectively. The model further contains a static magnetic field $\mathbf{B}_0 = B_0 \mathbf{b}_0$ of strength B_0 and fixed direction in space ($\mathbf{b}_0$ is a unit vector) that influences the electrons' motion. The Lorentz force density $-n_0 q \left(\tilde{\mathbf{E}} + \tilde{\mathbf{v}} \times \mathbf{B}_0\right)$ is clearly recognizable in (30). No externally prescribed source terms have been added to the system (28)–(30).

The aim is to obtain an effective electromagnetic formalism by elimination of the non-electromagnetic variable $\tilde{\mathbf{v}}(\mathbf{x},t)$. Straightforward manipulations permit recasting of (28)–(30) in the form (12) and (13) (setting $\tilde{\mathbf{J}}_e = \tilde{\mathbf{J}}_m = \mathbf{0}$ there), provided these two equations are supplemented by the

constitutive relations

$$\tilde{\mathbf{D}}(\mathbf{x},t) = \epsilon_0 \underline{\underline{\tilde{\epsilon}}} \star \tilde{\mathbf{E}}(\mathbf{x},t)\,, \qquad \tilde{\mathbf{H}}(\mathbf{x},t) = \frac{1}{\mu_0}\tilde{\mathbf{B}}(\mathbf{x},t)\,. \tag{31}$$

The effective electromagnetic medium has the same magnetic behaviour as the vacuum but the elimination of $\tilde{\mathbf{v}}(\mathbf{x},t)$ has manifested itself in a complicated constitutive relation linking $\tilde{\mathbf{D}}(\mathbf{x},t)$ and $\tilde{\mathbf{E}}(\mathbf{x},t)$. In (31), $\underline{\underline{\tilde{\epsilon}}}\star$ is a linear dyadic operator in space and time defined by

$$\underline{\underline{\tilde{\epsilon}}}\star = \underline{\underline{I}} + \omega_p^2 \left[\frac{\partial^2}{\partial t^2}\underline{\underline{I}} - \omega_c \left(\mathbf{b}_0 \times \underline{\underline{I}}\right)\frac{\partial}{\partial t}\right]^{-1}, \tag{32}$$

which be can be manipulated into

$$\begin{aligned}\underline{\underline{\tilde{\epsilon}}}\star \;=\; & \left(1 + \frac{\omega_p^2}{\omega_c^2 + \partial_{tt}}\right)\left(\underline{\underline{I}} - \mathbf{b}_0\,\mathbf{b}_0\right) + \frac{\omega_c\omega_p^2}{(\omega_c^2 + \partial_{tt})\,\partial_t}\,\mathbf{b}_0 \times \underline{\underline{I}} \\ & + \left(1 + \frac{\omega_p^2}{\partial_{tt}}\right)\mathbf{b}_0\,\mathbf{b}_0\,.\end{aligned} \tag{33}$$

The last expression was obtained by using simple dyadic manipulations [31]; $\omega_p^2 = n_0 q^2/m\epsilon_0$ is the plasma frequency while $\omega_c = qB_0/m$ is the gyro frequency ($\partial_t \equiv \partial/\partial t$, $\partial_{tt} \equiv \partial^2/\partial t^2$).

The operator representations in (32) and (33) are only formal ones but they exhibit a new feature not discussed before: $\tilde{\mathbf{D}}(\mathbf{x},t)$ and $\tilde{\mathbf{E}}(\mathbf{x},t)$ are not parallel anymore, and one is dealing with an *anisotropic* medium. Temporal dispersion is present by virtue of the presence of (inverse) time derivatives in the operator. Of course, one needs to clarify how to calculate inverses of composite operators containing temporal derivatives. One can assign the meaning

$$\left(\frac{\partial}{\partial t}\right)^{-1} f(t) \equiv \int_{-\infty}^{t} f(\tau)\,d\tau\,, \tag{34}$$

and

$$g(t) = \frac{1}{\alpha + \partial_{tt}}\,f(t) \;\Leftrightarrow\; (\alpha + \partial_{tt})\,g(t) = f(t)\,. \tag{35}$$

This interpretation is equivalent to the use of convolution integrals as in (22) and (23) in the previous section. Again, it is in the frequency domain, that a clearer interpretation of (31)–(33) emerges. By using the inverse Fourier transform, the frequency-domain constitutive relations

$$\mathbf{D}(\mathbf{x},\omega) = \epsilon_0 \underline{\underline{\epsilon}}(\omega)\;\cdot \mathbf{E}(\mathbf{x},\omega)\,, \qquad \mathbf{H}(\mathbf{x},\omega) = \frac{1}{\mu_0}\mathbf{B}(\mathbf{x},\omega)\,, \tag{36}$$

result, with

$$\underline{\underline{\epsilon}}(\omega) = \epsilon_1(\omega)\,\left(\underline{\underline{I}} - \mathbf{b}_0\,\mathbf{b}_0\right) + i\epsilon_2(\omega)\,\mathbf{b}_0 \times \underline{\underline{I}} + \epsilon(\omega)\,\mathbf{b}_0\,\mathbf{b}_0\,. \tag{37}$$

The constitutive parameters are

$$\epsilon_1(\omega) = 1 - \frac{\omega_p^2}{\omega^2 - \omega_c^2}\,, \qquad \epsilon_2(\omega) = -\frac{\omega_c\omega_p^2}{\omega\,(\omega^2 - \omega_c^2)}\,, \qquad \epsilon(\omega) = 1 - \frac{\omega_p^2}{\omega^2}\,. \tag{38}$$

It is easy to see that the transition from the operator $\tilde{\underline{\underline{\epsilon}}}\star$ to the dyadic $\underline{\underline{\epsilon}}(\omega)$ can be formally facilitated by the simple substitution $\partial/\partial t \to -i\omega$. These constitutive relations describe a *gyrotropic* medium of electric type. A similar dyadic structure for the magnetic properties describes a gyrotropic medium of magnetic type as exemplified by ferrites. Macroscopically, it is characterized by an anisotropy due to the presence of the distinguished direction $\mathbf{b}_0$ and three constitutive parameters ϵ_1, ϵ_2, ϵ. Beyond that, however, the physical model that was employed to study the electron plasma has also provided in (38) the exact (on the basis of the chosen model) dependence of those constitutive parameters on the circular frequency ω and on the fundamental plasma parameters, the plasma frequency ω_p and the gyro frequency ω_c.

The preceding derivation has shown that nonlocal behaviour in time is equivalent to local behaviour in frequency: the frequency-domain constitutive relations permit a local relation between $\mathbf{D}(\mathbf{x}\,,\omega)$ and $\mathbf{E}(\mathbf{x}\,,\omega)$ which is considerably easier to handle than the dependence of $\tilde{\mathbf{D}}(\mathbf{x}\,,t)$ on $\tilde{\mathbf{E}}(\mathbf{x}\,,t)$ via convolution integrals.

4.4. BEYOND HOMOGENEITY

Constitutive parameters that do not vary in space describe a homogeneous medium. While it is easy enough to postulate a nonhomogeneous medium by defining the constitutive parameters as arbitrary functions of position $\mathbf{x}$, actual field solutions can not be expected to emerge without specifying mathematical functions that detail such dependencies. Not surprisingly, the mathematical analysis becomes significantly more difficult when nonhomogeneous mediums are considered.

In the following we focus on a specific type of nonhomogeneity that manifests itself as periodicity. Well-studied examples are cholesteric liquid crystals (CLCs) with frequency-domain constitutive relations given by [32]

$$\mathbf{D}(\mathbf{x}\,,\omega) = \epsilon_0\,\underline{\underline{\epsilon}}(\mathbf{x},\omega)\;\cdot\mathbf{E}(\mathbf{x}\,,\omega)\,, \qquad \mathbf{H}(\mathbf{x}\,,\omega) = \frac{1}{\mu_0}\,\mathbf{B}(\mathbf{x}\,,\omega)\,, \tag{39}$$

where now

$$\underline{\underline{\epsilon}}(\mathbf{x},\omega) = \epsilon_a(\omega)\,\underline{\underline{I}} + [\epsilon_b(\omega) - \epsilon_a(\omega)]\;\mathbf{u}(z)\,\mathbf{u}(z)\,, \tag{40}$$

with

$$\mathbf{u}(z) = \mathbf{u}_x \cos\frac{\pi z}{\Omega} + \mathbf{u}_y \sin\frac{\pi z}{\Omega}\,. \tag{41}$$

This describes a helicoidal structure with periodicity along the z axis, with $\epsilon_a(\omega)$ and $\epsilon_b(\omega)$ as scalar parameters and $\mathbf{u}(z)$ as the local optical axis or director of the medium. The medium has a periodicity of Ω in the z-direction as per $\underline{\underline{\epsilon}}(z+\Omega,\omega) = \underline{\underline{\epsilon}}(z,\omega)$ and is technically a twisted, uniaxial, dielectric medium.

A speculative generalization of such a helicoidal structure led to the postulation of so-called *helicoidal bianisotropic mediums* [33] specified by

$$\mathbf{D}(\mathbf{x}\,,\omega) = \epsilon_0 \left[\underline{\underline{\alpha}}_{11}(z,\omega)\cdot\mathbf{E}(\mathbf{x}\,,\omega) + \underline{\underline{\alpha}}_{12}(z,\omega)\cdot\mathbf{H}(\mathbf{x}\,,\omega)\right]\,, \tag{42}$$

$$\mathbf{B}(\mathbf{x}\,,\omega) = \mu_0 \left[\underline{\underline{\alpha}}_{21}(z,\omega)\cdot\mathbf{E}(\mathbf{x}\,,\omega) + \underline{\underline{\alpha}}_{22}(z,\omega)\cdot\mathbf{H}(\mathbf{x}\,,\omega)\right]\,, \tag{43}$$

where the nonhomogeneous constitutive dyadics $\underline{\underline{\alpha}}_{\lambda\nu}(z,\omega)$ have the representations

$$\underline{\underline{\alpha}}_{\lambda\nu}(z,\omega) = \underline{\underline{S}}(z)\cdot\underline{\underline{\beta}}_{\lambda\nu}(\omega)\cdot\underline{\underline{S}}^{T}(z)\,, \quad \lambda = 1,2, \quad \nu = 1,2. \tag{44}$$

The unitary dyadic $\underline{\underline{S}}(z)$

$$\underline{\underline{S}}(z) = \cos\frac{\pi z}{\Omega}\,(\mathbf{u}_x\,\mathbf{u}_x + \mathbf{u}_y\,\mathbf{u}_y) + \sin\frac{\pi z}{\Omega}\,(\mathbf{u}_y\,\mathbf{u}_x - \mathbf{u}_x\,\mathbf{u}_y) + \mathbf{u}_z\,\mathbf{u}_z\,, \tag{45}$$

is responsible for the rotational nonhomogeneity of the helicoidal bianisotropic medium while the dyadics $\underline{\underline{\beta}}_{\lambda\nu}(\omega)$ must conform to the requirements of Lorentz covariance and obey the Post constraint (see (61) in Section 5) and be consistent with the Kramers–Kronig relations to be causal. Reciprocity and losslessness may impose additional requirements on the constitutive parameters [18, 14, 34, 35].

Since the original conceptualization of helicoidal bianisotropic mediums research has progressed rapidly, both theoretically and experimentally, towards sculptured thin films (STFs) which provide many interesting applications in optical and other technologies [36]. The constitutive characterization of STFs, in their various specifications, can exceed that of the helicoidal bianisotropic mediums even further in complexity; the unitary dyadic $\underline{\underline{S}}(z)$ may be a product of three different rotation dyadics because of the need to introduce as many as three rotation angles to describe the morphology of these highly complex mediums. A comprehensive review of STFs should be consulted for details [37]. Furthermore, the interested reader is directed to review presentations at previous *Bianisotropics* conferences [38, 39]. These and the many papers in the *Complex Mediums* conferences [4, 5, 6] and a predecessor conference [40] dealing with various aspects of STFs further exhibit the great significance of these nano-engineered materials.

5. Bianisotropic Mediums

5.1. GENERALITIES

We rewrite the very general constitutive relations (16) and (17) in the form

$$\tilde{\mathbf{D}}(\mathbf{x},t) = \tilde{\mathcal{L}}_D\left\{\tilde{\mathbf{E}}(\mathbf{x},t),\tilde{\mathbf{B}}(\mathbf{x},t)\right\}, \tag{46}$$

$$\tilde{\mathbf{H}}(\mathbf{x},t) = \tilde{\mathcal{L}}_H\left\{\tilde{\mathbf{E}}(\mathbf{x},t),\tilde{\mathbf{B}}(\mathbf{x},t)\right\}, \tag{47}$$

for time-dependent fields, and

$$\mathbf{D}(\mathbf{x},\omega) = \mathcal{L}_D\left\{\mathbf{E}(\mathbf{x},\omega),\mathbf{B}(\mathbf{x},\omega)\right\}, \tag{48}$$

$$\mathbf{H}(\mathbf{x},\omega) = \mathcal{L}_H\left\{\mathbf{E}(\mathbf{x},\omega),\mathbf{B}(\mathbf{x},\omega)\right\}, \tag{49}$$

for frequency-dependent field phasors, whereby $\tilde{\mathcal{L}}_{D,H}$ and $\mathcal{L}_{D,H}$ are certain *linear* operators. While these are still very general representations, they reflect the fact that for all practical purposes, constitutive relations are being substituted into the Maxwell equations, leading to an elimination of two of the unknown field vectors (or phasors). Implicit within such a procedure is a decision which two of the four field vectors are to be eliminated. In the time domain, a clear distinction is provided by the understanding that $\tilde{\mathbf{E}}(\mathbf{x},t)$ and $\tilde{\mathbf{B}}(\mathbf{x},t)$ emanate from the fundamental microscopic fields (and it is $\tilde{\mathbf{E}}(\mathbf{x},t)$ and $\tilde{\mathbf{B}}(\mathbf{x},t)$ that appear in the fundamental electromagnetic quantity, the Lorentz force), while $\tilde{\mathbf{D}}(\mathbf{x},t)$ and $\tilde{\mathbf{H}}(\mathbf{x},t)$ are macroscopic fields induced by the presence of material interactions [18, 14, 41]. As a consequence, (46) and (47), upon substitution into (12) and (13) lead to a field analysis in terms of $\tilde{\mathbf{E}}(\mathbf{x},t)$ and $\tilde{\mathbf{B}}(\mathbf{x},t)$. Once these are obtained, $\tilde{\mathbf{D}}(\mathbf{x},t)$ and $\tilde{\mathbf{H}}(\mathbf{x},t)$ can be calculated, if so desired, from (46) and (47).

Equivalently, (48) and (49) entail a field analysis in terms of $\mathbf{E}(\mathbf{x},\omega)$ and $\mathbf{B}(\mathbf{x},\omega)$. However, devoid of direct physical observability, field phasors are complex-valued quantities that can be used interchangeably. The bulk of all frequency-domain electromagnetics research is actually carried out in terms of $\mathbf{E}(\mathbf{x},\omega)$ and $\mathbf{H}(\mathbf{x},\omega)$, based on writing (48) and (49) in the alternative form

$$\mathbf{D}(\mathbf{x},\omega) = \mathcal{L}_{D'}\left\{\mathbf{E}(\mathbf{x},\omega),\mathbf{H}(\mathbf{x},\omega)\right\}, \tag{50}$$

$$\mathbf{B}(\mathbf{x},\omega) = \mathcal{L}_{B'}\left\{\mathbf{E}(\mathbf{x},\omega),\mathbf{H}(\mathbf{x},\omega)\right\}. \tag{51}$$

In the linear case considered here, a one-to-one correspondence between the $\mathbf{E},\mathbf{H}$ (often called the *Tellegen* representation) and the $\mathbf{E},\mathbf{B}$ formalism (often called the *Boys–Post* representation) can easily be facilitated for the general case of a bianisotropic medium [42, 43]. Inclination towards the use of $\mathbf{E}(\mathbf{x},\omega)$ and $\mathbf{H}(\mathbf{x},\omega)$ in frequency-domain analysis is based on the

conveniences (i) that substitution of (50) and (51) does not affect the terms involving spatial differentiation in (14) and (15); (ii) that boundary conditions on material interfaces are generally formulated in terms of $\mathbf{E}(\mathbf{x},\omega)$ and $\mathbf{H}(\mathbf{x},\omega)$ and (iii) that $\mathbf{E}(\mathbf{x},\omega)$ and $\mathbf{H}(\mathbf{x},\omega)$ define the Poynting vector (an issue that is of some importance in the engineering literature).

The previous discussion led to the impression that electromagnetic field analysis, whenever it involves complex mediums, is more complicated when pursued in the time domain than in the frequency domain. In addition to the necessity to take into proper account material responses that may be anisotropic or nonhomogeneous, time-domain formulations require complicated convolution integrals in their constitutive relations such that causality requirements are fulfilled. Therefore, a frequency-domain approach to a specific problem is often more feasible. Thus, the electromagnetic field analysis shall henceforth be performed in the frequency domain. The final results may, if so desired, be transferred into the time domain by the appropriate Fourier transforms.

The various operators $\mathcal{L}$, defined in (46)–(51) are linear for linear response properties. The most general type of linearity has been termed *bianisotropic*. A linear bianisotropic medium can thus be characterized by frequency-dependent constitutive relations given by

$$\mathbf{D}(\mathbf{x},\omega) = \underline{\underline{\epsilon}}(\mathbf{x},\omega) \cdot \mathbf{E}(\mathbf{x},\omega) + \underline{\underline{\alpha}}(\mathbf{x},\omega) \cdot \mathbf{B}(\mathbf{x},\omega)\,, \tag{52}$$

$$\mathbf{H}(\mathbf{x},\omega) = \underline{\underline{\beta}}(\mathbf{x},\omega) \cdot \mathbf{E}(\mathbf{x},\omega) + \underline{\underline{\mu}}^{-1}(\mathbf{x},\omega) \cdot \mathbf{B}(\mathbf{x},\omega)\,. \tag{53}$$

Therein, in the Boys–Post representation, $\underline{\underline{\epsilon}}(\mathbf{x},\omega)$ is the permittivity dyadic, $\underline{\underline{\mu}}(\mathbf{x},\omega)$ is the permeability dyadic, while $\underline{\underline{\alpha}}(\mathbf{x},\omega)$ and $\underline{\underline{\beta}}(\mathbf{x},\omega)$ are the two magnetoelectric dyadics. The dispersive nature of the medium is taken care of by their dependence on ω while the argument $\mathbf{x}$ indicates that the bianisotropic medium may also be nonhomogeneous. Alternatively,

$$\mathbf{D}(\mathbf{x},\omega) = \underline{\underline{\epsilon}}_T(\mathbf{x},\omega) \cdot \mathbf{E}(\mathbf{x},\omega) + \underline{\underline{\xi}}_T(\mathbf{x},\omega) \cdot \mathbf{H}(\mathbf{x},\omega)\,, \tag{54}$$

$$\mathbf{B}(\mathbf{x},\omega) = \underline{\underline{\zeta}}_T(\mathbf{x},\omega) \cdot \mathbf{E}(\mathbf{x},\omega) + \underline{\underline{\mu}}_T(\mathbf{x},\omega) \cdot \mathbf{H}(\mathbf{x},\omega)\,, \tag{55}$$

is called the Tellegen representation (hence the subscript $_T$); the terminology for the constitutive dyadics $\underline{\underline{\epsilon}}_T$, $\underline{\underline{\mu}}_T$, $\underline{\underline{\xi}}_T$ and $\underline{\underline{\zeta}}_T$ remains the same.

The two sets of constitutive relations (52), (53) and (54), (55) are linked through the identifications [42]

$$\underline{\underline{\epsilon}} = \underline{\underline{\epsilon}}_T - \underline{\underline{\xi}}_T \cdot \underline{\underline{\mu}}_T^{-1} \cdot \underline{\underline{\zeta}}_T\,, \qquad \underline{\underline{\alpha}} = \underline{\underline{\xi}}_T \cdot \underline{\underline{\mu}}_T^{-1}\,, \tag{56}$$

$$\underline{\underline{\beta}} = -\underline{\underline{\mu}}_T^{-1} \cdot \underline{\underline{\zeta}}_T\,, \qquad \underline{\underline{\mu}} = \underline{\underline{\mu}}_T\,; \tag{57}$$

or, vice versa,

$$\underline{\underline{\epsilon}}_T = \underline{\underline{\epsilon}} - \underline{\underline{\alpha}} \cdot \underline{\underline{\mu}} \cdot \underline{\underline{\beta}}\,, \qquad \underline{\underline{\xi}}_T = \underline{\underline{\alpha}} \cdot \underline{\underline{\mu}}\,, \tag{58}$$

$$\underline{\underline{\zeta}}_T = -\underline{\underline{\mu}} \cdot \underline{\underline{\beta}}, \qquad \underline{\underline{\mu}}_T = \underline{\underline{\mu}}. \tag{59}$$

Regardless which representation is chosen, the four constitutive dyadics contain the full information of the electromagnetic response of the bianisotropic medium. They provide a vast parameter space with a multitude of specializations relating to different types of mediums. Specific structures in the constitutive dyadics/tensors, or generally, operators, give rise to specific electromagnetic effects. And so, for many decades, a vast variety of different types of linear (and nonlinear), homogeneous and nonhomogeneous, isotropic, anisotropic and bianisotropic mediums have been studied.

There is consequently an extensive playground between the maximum of $4 \times 9 = 36$ complex-valued constitutive parameters and the greatest simplification to only two quantities. The latter arise when the reduction to a linear, homogeneous, isotropic, dielectric–magnetic medium is considered where $\underline{\underline{\epsilon}} = \epsilon_0 \epsilon \underline{\underline{I}}$, $\underline{\underline{\mu}} = \mu_0 \mu \underline{\underline{I}}$, $\underline{\underline{\alpha}} = \underline{\underline{\beta}} = \underline{\underline{0}}$. Many of the mediums thus obtained and characterized by certain properties have well-known names, such as chiral, uniaxial, biaxial, gyrotropic, and have been studied extensively in the literature. The reader is referred to a various attempts towards consistent classification schemes [42, 43, 9].

5.2. SYMMETRIES AND CONSTRAINTS

Theoretical exploration of the vast parameter space, spanned by the four constitutive dyadics can very quickly become very difficult and a reduction of the number of constitutive parameters is thus desirable. Needless to say, specializations and/or simplifications in general medium descriptions should be founded on two important principles: (i) they must be based on sound physical and mathematical considerations and (ii) they must contain, at least in the form of a principal mechanism, a scheme how such a medium, if it does not exist in natural form, can be manufactured.

A popular approach to the reduction of this large parameter space is the exploitation of symmetries. Symmetries in constitutive relations can occur because they appear intrinsically in the studied materials; well-known examples are provided by crystals. Furthermore, symmetries may be imposed, as one may demand, for example, that a specific medium should be Lorentz-reciprocal [44], for example in the Tellegen representation:

$$\underline{\underline{\epsilon}}_T = \underline{\underline{\epsilon}}_T^T, \qquad \underline{\underline{\xi}}_T = -\underline{\underline{\zeta}}_T^T, \qquad \underline{\underline{\mu}}_T = \underline{\underline{\mu}}_T^T, \tag{60}$$

(superscript ^{T} indicates transposition). Equally, there may be conditions based on appropriate approximations; for example, absence of dissipation.

In addition, one finds that a structural and uniqueness constraint, the Post constraint, must be fulfilled by any bianisotropic medium [14, 34]:

$$\text{Trace}\left[\underline{\underline{\alpha}}(\mathbf{x},\omega) - \underline{\underline{\beta}}(\mathbf{x},\omega)\right] \equiv 0\,, \tag{61}$$

for constitutive relations expressed in the Boys–Post form or

$$\text{Trace}\left[\underline{\underline{\mu}}_T^{-1}(\mathbf{x},\omega) \cdot \left(\underline{\underline{\xi}}_T(\mathbf{x},\omega) + \underline{\underline{\zeta}}_T(\mathbf{x},\omega)\right)\right] \equiv 0\,, \tag{62}$$

in the Tellegen form. The Post constraint is an algebraic condition, relevant whenever magnetoelectric coupling is present. All purely anisotropic mediums fulfil (61) identically, as can be seen by substituting $\underline{\underline{\alpha}}(\mathbf{x},\omega) = \underline{\underline{\beta}}(\mathbf{x},\omega) \equiv \underline{\underline{0}}$ into (61) or, equivalently, $\underline{\underline{\xi}}_T(\mathbf{x},\omega) = \underline{\underline{\zeta}}_T(\mathbf{x},\omega) \equiv \underline{\underline{0}}$ into (62), respectively. The Post constraint thus reduces the constitutive parameter space by one complex-valued quantity.

The above relations make it clear that the Post constraint is not a reciprocity condition, see (60). However, the Post constraint has its most important consequence for biisotropic materials in the observation that under the appropriate reductions of the dyadics in (61) and (62), the recognizable existence of *nonreciprocal* biisotropic mediums is negated. The repercussion is that the isotropic chiral medium is the most general isotropic medium that contains magnetoelectric coupling. For more details on this issue the reader is referred to a recent comprehensive review [34], that contains a literature survey, detailed evaluation of experimental and theoretical background as well as an analysis of opposing views that have been expressed on this subject.

5.2.1. *Biaxial bianisotropic mediums*

Biaxial bianisotropy provides an instructive example how a very specific structure in the constitutive relations arises from a simple symmetry requirement. In this instance we demand that the (homogeneous) bianisotropic medium as a whole is characterized by two distinct (crystallographic) axes. We then obtain the constitutive relations as [45]

$$\mathbf{D}(\mathbf{x},\omega) = \epsilon_0\, \underline{\underline{\epsilon}}_{bi}(\omega) \cdot \mathbf{E}(\mathbf{x},\omega) + (1/\eta_0)\, \underline{\underline{\alpha}}_{bi}(\omega) \cdot \mathbf{B}(\mathbf{x},\omega)\,, \tag{63}$$

$$\mathbf{H}(\mathbf{x},\omega) = (1/\eta_0)\, \underline{\underline{\beta}}_{bi}(\omega) \cdot \mathbf{E}(\mathbf{x},\omega) + (1/\mu_0)\, \underline{\underline{\mu}}_{bi}^{-1}(\omega) \cdot \mathbf{B}(\mathbf{x},\omega)\,, \tag{64}$$

($\eta_0 = \sqrt{\mu_0/\epsilon_0}$). The dimensionless constitutive dyadics are given by [45]

$$\underline{\underline{\epsilon}}_{bi}(\omega) = \epsilon_a(\omega)\, \underline{\underline{I}} + \epsilon_b(\omega)\, (\mathbf{u}_m\, \mathbf{u}_n + \mathbf{u}_n\, \mathbf{u}_m)\,, \tag{65}$$

$$\underline{\underline{\alpha}}_{bi}(\omega) = \alpha_a(\omega)\, \underline{\underline{I}} + \alpha_b(\omega)\, (\mathbf{u}_m\, \mathbf{u}_n + \mathbf{u}_n\, \mathbf{u}_m)\,, \tag{66}$$

$$\underline{\underline{\beta}}_{bi}(\omega) = \beta_a(\omega)\, \underline{\underline{I}} + \beta_b(\omega)\, (\mathbf{u}_m\, \mathbf{u}_n + \mathbf{u}_n\, \mathbf{u}_m)\,, \tag{67}$$

$$\underline{\underline{\mu}}_{bi}^{-1}(\omega) = \sigma_a(\omega)\, \underline{\underline{I}} + \sigma_b(\omega)\, (\mathbf{u}_m\, \mathbf{u}_n + \mathbf{u}_n\, \mathbf{u}_m)\,. \tag{68}$$

In the foregoing expressions, $\mathbf{u}_m$ and $\mathbf{u}_n$ are the two distinguished axes of the biaxial structure. The biaxial bianisotropic medium is a nonreciprocal medium. It is characterized by the eight complex-valued and frequency-dependent constitutive parameters ϵ_a, ϵ_b, α_a, α_b, β_a, β_b, σ_a, σ_b (the last two being essentially inverse permeability scalars), plus a real-valued angle ϕ, whereby $\cos\phi = \mathbf{u}_m \cdot \mathbf{u}_n$.

In a further illustration of previous developments, the Post constraint (61), for the biaxial bianisotropic medium simplifies to

$$3\,(\alpha_a - \beta_a) + 2\,(\alpha_b - \beta_b)\,\cos\phi = 0\,, \tag{69}$$

thus reducing the number of unconstrained medium parameters from $8\times2 + 1 = 17$ to 15 real-valued quantities.

The theoretical characterization of biaxial bianisotropic mediums as given in [45] provided the basis for detailed numerical homogenization studies [46, 47, 48] and a comprehensive review of these results can be found elsewhere in this book [49].

5.3. HOMOGENIZATION FORMALISMS

Previously, in Section 4.3, an instructive example detailed how constitutive relations emerge due to the coupling of the electromagnetic field vectors to a non-electromagnetic field. A different but exceedingly valuable approach to the delineation of constitutive relations is provided by different types of homogenization formalisms.

The aim of any homogenization formalism is to derive or at least provide solid estimates for the constitutive parameters of a homogenized composite medium based on a knowledge of the constitutive parameters and various geometrical/topological quantities pertaining to two or more constituent mediums. Homogenization formalisms operate within well defined limits of applicability. Best known among the various formalisms are those associated with the names of Maxwell Garnett and Bruggeman [50] and variations thereof [51]. A vast amount of literature on homogenization exists. We refer to it for introductory works [52] as well as detailed reviews [53, 54]. Very recent work has also provided significant progress with another homogenization formalism, the strong-property-fluctuation theory (SPFT) [55, 56, 57] (these references may also be consulted for historical background of the development of the SPFT).

5.3.1. *Faraday chiral mediums*

Let us, for illustrative purposes, homogenize a chiroferrite composite medium by following the given recipe. We take two component mediums, the

first one a magnetically biased ferrite characterized by [31]

$$\mathbf{D}(\mathbf{x},\omega) = \epsilon_0\,\epsilon^f(\omega)\,\mathbf{E}(\mathbf{x},\omega)\,, \tag{70}$$

$$\mathbf{B}(\mathbf{x},\omega) = \mu_0\left[\mu^f(\omega)\left(\underline{\underline{I}} - \mathbf{u}\,\mathbf{u}\right) + i\mu_g^f(\omega)\mathbf{u}\times\underline{\underline{I}} + \mu_u^f(\omega)\,\mathbf{u}\,\mathbf{u}\right]\cdot\mathbf{H}; \tag{71}$$

ϵ^f is the relative permittivity scalar, μ^f, μ_g^f and μ_u^f are relative permeability scalars. One may compare these constitutive relations of a gyrotropic medium of the magnetic type with (36) and (37) for a gyrotropic medium of the electric type. The second component is an isotropic chiral medium [58]:

$$\mathbf{D}(\mathbf{x},\omega) = \epsilon_0\,\epsilon^c(\omega)\,\mathbf{E}(\mathbf{x},\omega) + i\sqrt{\epsilon_0\mu_0}\,\xi^c(\omega)\,\mathbf{H}(\mathbf{x},\omega)\,, \tag{72}$$

$$\mathbf{B}(\mathbf{x},\omega) = -i\sqrt{\epsilon_0\mu_0}\,\xi^c(\omega)\,\mathbf{E}(\mathbf{x},\omega) + \mu_0\,\mu^c(\omega)\,\mathbf{H}(\mathbf{x},\omega)\,, \tag{73}$$

wherein ϵ^c, μ^c and ξ^c are the relative permittivity, relative permeability and the chirality parameter, respectively.

The ferrite medium and the isotropic chiral medium are then mixed in a certain volumetric proportion and the Bruggeman formalism [50], for example, can be successfully employed to extract the properties of the homogenized composite medium (HCM). Upon usage of the constitutive relations (70)–(73), this procedure yields

$$\mathbf{D}(\mathbf{x},\omega) = \epsilon_0\,\underline{\underline{\epsilon}}^{HCM}(\omega)\cdot\mathbf{E}(\mathbf{x},\omega) + i\sqrt{\epsilon_0\mu_0}\,\underline{\underline{\xi}}^{HCM}(\omega)\cdot\mathbf{H}(\mathbf{x},\omega)\,, \tag{74}$$

$$\mathbf{B}(\mathbf{x},\omega) = -i\sqrt{\epsilon_0\mu_0}\,\underline{\underline{\xi}}^{HCM}(\omega)\cdot\mathbf{E}(\mathbf{x},\omega) + \mu_0\underline{\underline{\mu}}^{HCM}(\omega)\cdot\mathbf{H}(\mathbf{x},\omega) \tag{75}$$

Each of the three constitutive dyadics $\underline{\underline{\epsilon}}^{HCM}$, $\underline{\underline{\mu}}^{HCM}$, $\underline{\underline{\xi}}^{HCM}$, is of the form:

$$\underline{\underline{\alpha}}^{HCM}(\omega) = \alpha^{HCM}(\omega)\,\left(\underline{\underline{I}} - \mathbf{u}\,\mathbf{u}\right) + i\alpha_g^{HCM}(\omega)\,\mathbf{u}\times\underline{\underline{I}} + \alpha_u^{HCM}(\omega)\,\mathbf{u}\,\mathbf{u}\,, \tag{76}$$

which can be recognized as of gyrotropic type again. A medium described by (74)–(76) is called a Faraday chiral medium; in this instance, a chiroferrite. The detailed numerical homogenization results given in [59] fully confirmed the correct characterization of chiroferrites on purely theoretical grounds [60]. By following a similar procedure, whereby the ferrite is replaced by a magnetically biased (cold) plasma (as described by (36) and (37)) leads to a Faraday chiral medium, again described by (74)–(76), this time termed chiroplasma; see [61] for comprehensive homogenization studies.

6. Conclusion

Theoretical, numerical and experimental investigations in the electromagnetics of complex mediums all require a clear understanding of constitutive relations. These supplement the Maxwell equations (together with boundary and/or initial conditions) to provide a complete specification of electromagnetic field problems. The more complex a medium is that requires

characterization, the more complex the constitutive relations which link the involved electromagnetic fields or phasors will be. Constitutive relations can be linear or nonlinear, homogeneous or nonhomogeneous, isotropic or anisotropic/bianisotropic, local or nonlocal in space and/or time; their mathematical expression can be in differential, integral or algebraic form.

Here, the focus was to provide a basic introduction into constitutive relations in the linear regime. For such a wide-ranging topic only a flavour of the many important issues could be addressed. Special emphasis was put on the important conceptual differences between the time domain and the frequency domain. A variety of different complex mediums that play an important role in electromagnetics and optics research were described with regard to their emergence from simple underlying physical models or as the outcome of different types of homogenization formalisms.

References

1. Weiglhofer, W.S., ed. (1997) *Proceedings of Bianisotropics'97, International Conference and Workshop on Electromagnetics of Complex Media*, Glasgow, UK.
2. Jacob, A.F. and Reinert, J., eds. (1998) *Proceedings of Bianisotropics '98, 7th International Conference on Complex Media*, Braunschweig, Germany.
3. Barbosa, A.M. and Topa, A.L., eds. (2000) *Proceedings of Bianisotropics 2000, 8th International Conference on Electromagnetics of Complex Media*, Lisbon, Portugal.
4. Lakhtakia, A., Weiglhofer, W.S. and Messier, R., eds. (2000) *Complex Mediums*, Proc. SPIE Vol. 4097, Bellingham, WA.
5. Lakhtakia, A., Weiglhofer, W.S. and Hodgkinson, I.J., eds. (2001) *Complex Mediums II: Beyond Linear Isotropic Dielectrics*, Proc. SPIE Vol. 4467, Bellingham, WA.
6. Lakhtakia, A., Dewar, G. and McCall, M.W., eds. (2002) *Complex Mediums III: Beyond Linear Isotropic Dielectrics*, Proc. SPIE Vol. 4806, Bellingham, WA.
7. Priou, A., Sihvola, A., Tretyakov, S. and Vinogradov, A. (1997) *Advances in Complex Electromagnetic Materials*, Kluwer, Dordrecht.
8. Singh, O.N. and Lakhtakia, A., eds. (2000) *Electromagnetic Fields in Unconventional Materials and Structures*, Wiley, New York.
9. Serdyukov, A., Semchenko, I., Tretyakov, S. and Sihvola, A. (2001) *Electromagnetics of Bi-anisotropic Materials*, Gordon and Breach, Amsterdam.
10. Weiglhofer, W.S. and Lakhtakia, A., eds. (2003) *Introduction to Complex Mediums for Optics and Electromagnetics*, SPIE Optical Engineering Press, Bellingham, WA.
11. Boyd, R.W. (1992) *Nonlinear Optics*, Academic Press, San Diego, CA.
12. Kobayashi, T. (1991) Introduction to nonlinear optical materials, *Nonlinear Optics*, **1**, pp. 91–117.
13. Weiglhofer, W.S. (2002) Constitutive relations, in [6], pp. 67–80.
14. Post, E.J. (1997) *Formal Structure of Electromagnetics*, Dover Press, New York (Reprinted from North-Holland, Amsterdam, 1962).
15. Altman, C. and Suchy, K. (1991) *Reciprocity, Spatial Mapping and Time Reversal in Electromagnetics*, Kluwer, Dordrecht.
16. Lindell, I.V., Sihvola, A.H. and Suchy, K. (1995) Six-vector formalism in electromagnetics of bianisotropic media, *J. Electrom. Waves Applic.*, **9**, pp. 887–903.

17. Lakhtakia, A. (1995) Covariances and invariances of the Maxwell postulates, in Barrett, T.W. and Grimes, D.M. (eds.), *Advanced Electromagnetism: Foundations, Theory and Applications*, World Scientific, Singapore, pp. 390–410.
18. Jackson, J.D. (1975) *Classical Electrodynamics*, Wiley, New York.
19. Kong, J.A. (2000) *Electromagnetic Wave Theory*, EMW Publishing, Cambridge, MA.
20. Weiglhofer, W.S. and Lakhtakia, A. (1996) On causality requirements for material media, *Arch. Elektron. Übertrag.*, **50**, pp. 389–391.
21. Van Bladel, J. (1985) *Electromagnetic Fields*, Hemisphere, New York.
22. Hillion, P. (1993) Electromagnetism in a moving chiral medium, *Phys. Rev. E*, **48**, pp. 3060–3065.
23. Ragusa, S. (1994) Electromagnetic first-order conservation laws in a chiral medium, *J. Phys. A: Math. Gen.*, **27**, pp. 2887–2890.
24. Flood, K.M. and Jaggard, D.L. (1995) Effective charge densities and current densities in isotropic chiral media, *J. Opt. Soc. Am. A*, **12**, pp. 177–183.
25. Hillion, P. (1995) Electromagnetic waves in linear media, *J. Phys. A: Math. Gen.*, **28**, pp. 2647–2659.
26. Weiglhofer, W.S. and Lakhtakia, A. (2001) Comment on 'Rigorous solution for transient propagation of electromagnetic waves through a medium: causality plus diffraction in time', *Opt. Lett.*, **26**, pp. 1218–1219.
27. Chew, W.C. (1990) *Waves and Fields in Inhomogeneous Media*, Van Nostrand-Reinhold, New York.
28. Karlsson, A. and Kristensson, G. (1992) Constitutive relations, dissipation, and reciprocity for the Maxwell equations in the time domain, *J. Electrom. Waves Applic.*, **6**, pp. 1517–1535.
29. Weiglhofer, W.S. and Lakhtakia, A. (1996) Causality and natural optical activity (chirality), *J. Opt. Soc. Am. A.*, **13**, pp. 385–386.
30. Felsen, L.B. and Marcuvitz, N. (1994) *Radiation and Scattering of Waves*, IEEE Press, Piscataway, NJ.
31. Chen, H.C. (1983) *Theory of Electromagnetic Waves*, McGraw-Hill, New York.
32. Chandrasekhar, S. (1977) *Liquid Crystals*, Cambridge University Press, Cambridge.
33. Lakhtakia, A. and Weiglhofer, W.S. (1995) On light propagation in helicoidal bianisotropic mediums, *Proc. Roy. Soc. Lon. A*, **448**, pp. 419–437; erratum (1998), **454**, p. 3275.
34. Weiglhofer, W.S. and Lakhtakia, A. (1998) The Post constraint revisited, *Arch. Elektron. Übertrag.*, **52**, pp. 276–279.
35. Kong, J.A. (1972) Theorems of bianisotropic media, *Proc. IEEE*, **60**, pp. 1036–1046.
36. Lakhtakia, A. (2002) Sculptured thin films: accomplishments and emerging uses, *Mater. Sci. Engg. C*, **19**, pp. 424–434.
37. Venugopal V.C. and Lakhtakia, A. (2000) Sculptured thin films: Conception, optical properties, and applications, in [8], pp. 151–216.
38. Lakhtakia, A. (1998) Batman presents: Applications of sculptured thin films with chiropterous flavor, in [2], pp. 297–300.
39. Lakhtakia, A. (2000) Filamentary, my dear Watson!, in [3], pp. 169–174.
40. Lakhtakia, A. and Messier, R., eds. (1999) *Engineered Nanostructural Films and Materials*, Proc. SPIE Vol. 3790, Bellingham, WA.
41. Lakhtakia, A. and Weiglhofer, W.S. (1996) Lorentz covariance, Occam's razor, and a constraint on linear constitutive relations, *Phys. Lett. A*, **213**, pp. 107–111; erratum (1996), **222**, p. 459.

42. Weiglhofer, W.S. (1998) A perspective on bianisotropy and *Bianisotropics'97*, *Int. J. Appl. Electromagn. Mech.*, **9**, pp. 93–101.
43. Weiglhofer, W.S. (1999) Electromagnetic theory of complex materials, in [40], pp. 66–76.
44. Krowne, C.M. (1984) Electromagnetic theorems for complex anisotropic media, *IEEE Trans. Antennas Propagat.*, **AP-32**, pp. 1224–1230.
45. Weiglhofer, W.S. and Lakhtakia, A. (1999) On electromagnetic waves in biaxial bianisotropic media, *Electromagnetics*, **19**, pp. 351–362.
46. Mackay, T.G. and Weiglhofer, W.S. (2001) Homogenization of biaxial composite materials: Nondissipative dielectric properties, *Electromagnetics*, **21**, pp. 15–26.
47. Mackay, T.G. and Weiglhofer, W.S. (2000) Homogenization of biaxial composite materials: Dissipative anisotropic properties, *J. Opt. A: Pure Appl. Opt.*, **2**, pp. 426–432.
48. Mackay, T.G. and Weiglhofer, W.S. (2001) Homogenization of biaxial composite materials: Bianisotropic properties, *J. Opt. A: Pure Appl. Opt.*, **3**, pp. 45–52.
49. Mackay, T.G. and Weiglhofer, W.S. (2002) A review of homogenization studies for biaxial bianisotropic materials, in Zouhdi, S., Sihvola, A., and Arsalane, M. (eds.), *Advances in Electromagnetics of Complex Media and Metamaterials*, Kluwer, Dordrecht, pp. 211–228.
50. Weiglhofer, W.S., Lakhtakia, A. and Michel, B. (1997) Maxwell Garnett and Bruggeman formalisms for a particulate composite with bianisotropic host medium, *Microw. Opt. Technol. Lett.*, **15**, pp. 263–266; erratum (1999), **22**, p. 221.
51. Michel, B., Lakhtakia, A., Weiglhofer, W.S. and Mackay, T.G. (2001) Incremental and differential Maxwell Garnett formalisms for bi-anisotropic composites, *Comp. Sci. Technol.*, **61**, pp. 13–18.
52. Lakhtakia, A., ed. (1996) *Selected Papers on Linear Optical Composite Materials*, SPIE Optical Engineering Press, Bellingham, WA.
53. Michel, B. (2000) Recent developments in the homogenization of linear bianisotropic composite materials, in [8], pp. 39–82.
54. Weiglhofer, W.S. (2000) Homogenization of particulate materials, in [4], pp. 146–154.
55. Mackay, T.G., Lakhtakia, A. and Weiglhofer, W.S. (2000) Strong-property-fluctuation theory for homogenization of bianisotropic composites: Formulation, *Phys. Rev. E*, **62**, pp. 6052–6064; erratum (2001), **63**, 049901.
56. Mackay, T.G., Lakhtakia, A. and Weiglhofer, W.S. (2000) Third-order implementation and convergence of the strong-property-fluctuation theory in electromagnetic homogenization, *Phys. Rev. E*, **64**, 066616.
57. Mackay, T.G., Lakhtakia, A. and Weiglhofer, W.S. (2001) The strong-property-fluctuation theory applied to the homogenisation of linear bianisotropic composites, in [5], pp. 243–255.
58. Lakhtakia, A. (1994) *Beltrami Fields in Chiral Media*, World Scientific, Singapore.
59. Weiglhofer, W.S., Lakhtakia, A. and Michel, B. (1998) On the constitutive parameters of a chiroferrite composite medium, *Microw. Opt. Technol. Lett.*, **18**, pp. 342–345.
60. Weiglhofer, W.S. and Lakhtakia, A. (1998) The correct constitutive relations of chiroplasmas and chiroferrites, *Microw. Opt. Technol. Lett.*, **17**, pp. 405–408.
61. Weiglhofer, W.S. and Mackay, T.G. (2000) Numerical studies on the constitutive parameters of a chiroplasma composite medium, *Arch. Elektron. Übertrag.*, **54**, pp. 259–264.

ELECTRODYNAMICS OF MEDIA WITH SIMULTANEOUSLY NEGATIVE ELECTRIC PERMITTIVITY AND MAGNETIC PERMEABILITY

V.G.VESELAGO
Moscow Institute of Physics and Technology
9 Institutski per. Dolgoprudny, Moscow district, 141700, Russia

Abstract. This chapter concentrates on basic properties of materials that can be characterised by having simultaneously negative permittivity and permeability. Poynting vector, Doppler effect, Cherenkov radiation, Snellius law, Fermat principle, possible devices, and experimental work on such materials are discussed.

1. INTRODUCTION

For the last two years we all became the observers of great interest to materials with simultaneously negative values of electric permittivity ε and magnetic permeability μ. It is necessary to note that highly interesting and unusual electrodynamic properties of such materials were considered in our old works [1-4]. However, these works did not get further development at that time, since neither us, nor other authors could manage to realize materials with simultaneously negative values of both ε and μ. Already in [1-4] it was shown that the main electrodynamic properties of such materials could be seen from the well-known equations changing the sign of the index of refraction n. Because of this fact, we introduced the concept of index of negative refraction [1]. It became also obvious that the class of "materials with negative n" is much broader than the class of "materials with simultaneously negative values of ε and μ. Materials with negative n are characterized by the opposite directions of the phase and group velocities. Such materials (or structures) are often called "materials with negative group velocity," and they are known for enough long time. As an example we can mention the backward-wave microwave tubes.

The materials, which exhibit negative refractions, were named in [1,2] as "left-handed materials". This term, well sounding in English, has no euphonic translation into Russian, and so we shall name materials with $n < 0$ "materials with negative refraction", or "negative-index media" - NIM. Accordingly, usual materials with $n > 0$ it is possible to mark as PIM.

S. Zouhdi et al. (eds.), Advances in Electromagnetics of Complex Media and Metamaterials, 83–97.

After appearance of papers [1-4] for a long time there were no publications on this problem until paper [5] appeared, followed by [6], in which R. Shelby, D. R. Smith, S. Schultz, et al. from the University of California at San Diego communicated on creation of artificial composite materials with negative values of ε and μ in the centimeter wave band. This composite material is a combination of small metallic wires and rings, positioned in space in a sort of lattice. As was reported in paper [6], direct experiments shown that such a structure can be really characterized by negative values of ε and μ, and, as a result, by a negative value of the refraction index $\mathbf{n}$.

2. MAIN ELECTROMAGNETIC PROPERTIES OF MATERIALS WITH NEGATIVE ε AND μ

In most equations of electrodynamics the values of ε and μ are present as a product $\varepsilon\mu$, for which a simultaneous change of the signs of both multiplicands is not essential. This completely pertains also to the value of the refractions index $\mathbf{n}$. However, from general considerations it is obvious that a simultaneous change of the signs of ε and μ must bring about some essential changes to electrodynamic characteristics of material. To find these changes, it is necessary to use equations of the 1-th order, in which ε and μ enter separately. Such equations are the Maxwell equations and material equations. Let us write them for a uniform plane wave, propagating in an isotropic material:[1]

$$[\mathbf{kE}] = \frac{\omega}{\mathbf{c}}\mu\mathbf{H} \tag{1}$$

$$[\mathbf{kE}] = -\frac{\omega}{\mathbf{c}}\varepsilon\mathbf{H} \tag{2}$$

$$\mathbf{D} = \varepsilon\mathbf{E} \tag{3}$$

$$\mathbf{B} = \mu\mathbf{H} \tag{4}$$

From equations (1-2) it is immediately seen that for positive ε and μ vectors $\mathbf{E}, \mathbf{H}$ and $\mathbf{k}$ form a right-hand system of orthogonal vectors, but for negative ε and μ the system becomes left-handed. At the same time the Poynting vector $\mathbf{S}$

$$\mathbf{S} = [\mathbf{EH}] \tag{5}$$

[1] Note that in the Russian literature, the vector (cross) product is often denoted by putting the two vectors inside square brackets. (editors)

always forms with vectors $\mathbf{E}$ and $\mathbf{H}$ a right-hand triple of vectors.
Now is important to remember that vector $\mathbf{k}$ is directed parallel to the phase velocity $\mathbf{v_{ph}}$, so, if ε and μ are negative, vector $\mathbf{v_{ph}}$ and vector $\mathbf{S}$ are oppositely directed. Usually in this case one speaks of "negative group velocity", but a more correct name is "negative phase velocity". Exactly, such terminology takes into account the fact that the group velocity corresponds to the direction of the energy flow from the source to the receiver. As to the phase velocity, that it not connected with the flow of energy, and can be directed toward the source if ε and μ are both negative, and as a result the refraction index $\mathbf{n}$ is negative too.
Here it is appropriate to remind that if only one of the values of ε and μ is negative, but the other is positive, equations in system (1-2) contradicts each other, and waves cannot propagate in such ambience. An example of such situation is the reflection of radio waves from the ionosphere.
Discussing possibilities of practical realization of materials with negative ε and μ, it is necessary to take into account that such materials must possess frequency dispersion. Really, in general, if dispersion absent, the field energy density in material can be written in the form

$$\mathbf{W} = \frac{1}{8\pi}\left(\varepsilon \mathbf{E}^2 + \mu \mathbf{H}^2\right) \tag{6}$$

For negative values of ε and μ (6) gives a negative density of energy that is undoubtedly wrong. If the frequency dispersion presents, expression (6), following [7] must be modified as

$$\mathbf{W} = \frac{1}{8\pi}\left(\frac{\partial(\varepsilon\omega)}{\partial\omega}\mathbf{E}^2 + \frac{\partial(\mu\omega)}{\partial\omega}\mathbf{H}^2\right) \tag{7}$$

As it is shown in [7], multipliers before $\mathbf{E}^2$ and $\mathbf{H}^2$ are positive even for negative ε and μ.
The fact that for negative ε and μ the phase and group velocities are oppositely directed, leads to a conclusion that some fundamental laws of electrodynamics and optics are expressed in an unusual way.

Among these laws we will discuss the Doppler and Cherenkov effects, Snellius law and Fermat's principle.

2.1. TRAVELING WAVES AND THE DOPPLER EFFECT

For usual materials with positive ε and μ, a traveling wave, radiated from an energy source, can be written in form, which is proportional to the value

$$e^{j(\omega t - kx)} \tag{8}$$

The wave vector in this expression is $\mathbf{k} = \frac{\omega}{c}\mathbf{n} = \frac{\omega}{c}\sqrt{\varepsilon\mu}$, and the value of the refraction index $\mathbf{n}$ is taken to be positive. This means that the phase velocity $\mathbf{v_{ph}} = \frac{\mathbf{c}}{\sqrt{\varepsilon\mu}}$ is also positive. If both ε and μ are negative, the index of refraction $\mathbf{n}$ also must be taken negative, and this brings about negative phase velocity.

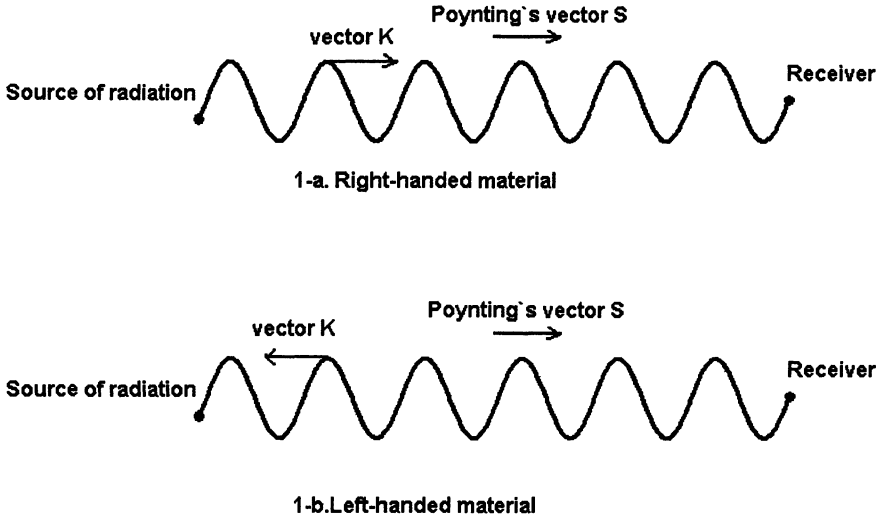

Figure 1. Poynting's vector $\mathbf{S}$ and the wave vector $\mathbf{k}$ for wave propagations in right-handed (PIM) and left-handed (NIM) materials.

In the case of $\mathbf{n} < \mathbf{0}$ (see Fig.1-b), a sinusoidal wave "is embroiled" in a source of energy, while the flow of energy always comes out of the source.
It is necessary to pay some special attention, if in the case when $\mathbf{n} < \mathbf{0}$ the medium possesses some, assume it to be small, absorption. For this case ε and μ are complex numbers and can be written as

$$\begin{aligned} \varepsilon &= \varepsilon' + j\varepsilon'' \\ \mu &= \mu' + j\mu'' \end{aligned} \tag{9}$$

which leads to the usual expression for the complex wave number $\mathbf{k}$:

$$\mathbf{k} = \mathbf{k}' + j\mathbf{k}'' \tag{10}$$

where

$$\begin{aligned} \mathbf{k}' &\approx \frac{\omega}{\mathbf{c}}\sqrt{\varepsilon'\mu'} \\ \mathbf{k}'' &\approx \frac{\mathbf{1}}{\mathbf{2}}\mathbf{k}'\left(\frac{\varepsilon''}{\varepsilon'} + \frac{\mu''}{\mu'}\right) \end{aligned} \tag{11}$$

For the usual media with positive ε' and μ' and negative imaginary parts (corresponding to lossy media), $\mathbf{k}''$ will also be negative, which brings about fading of the wave with growing x. If the real parts of ε and μ change sign, the value of $\mathbf{k}'$ changes its sign, but $\mathbf{k}''$ does not, as is seen from the second equation (11). So, for absorbing materials with negative refraction a wave becomes weaker with increasing the distance from the energy source, but the phase of a sinusoidal wave moves to the energy source.
The inverse motion of the sinusoidal wave for materials with negative refraction changes the sign of the Doppler effect, as it can be seen on Figure1. This becomes clear from the formula for the classical Doppler effect:

$$\omega = \omega_0\left(\mathbf{1} - \mathbf{n}\frac{\mathbf{v}}{\mathbf{c}}\right) \tag{12}$$

For the usual materials when the receiver moves to the source, the observed frequency increases, but for NIM materials it decreases.

2.2. CHERENKOV EFFECT

One more effect, whose realization greatly depends on simultaneous change of the signs of ε and μ, is the Cherenkov effect. In works under Pafomov [8] it was shown that an electron, passing through a medium with $n < 0$ radiates not onward, as in usual matter, but back. Corresponding pictures one can see on Figs. 2a and 2b. These pictures illustrate the well-known formula for the cone angle of the Cherenkov radiation:

$$\cos\theta = c / vn \qquad (13)$$

where c is the velocity of light, v is the velocity of an electron, and n is the index of refractions for the medium. If the index of refractions becomes negative, it is obvious that angle θ lies in the second quadrant, and, hereunder, the cone of the Cherenkov radiation is directed back.

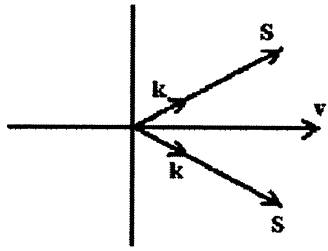

Figure 2a. Cherenkov effect in media with $n > 0$. Vector v is the electron velocity, S is the Poynting vector, and k is the wave vector.

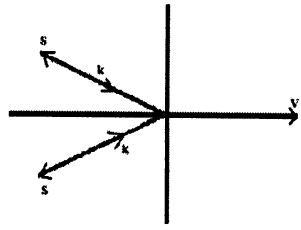

Figure 2b. Cherenkov effect in media with $n < 0$. The same notations as in Figure 2a.

2.3. SNELLIUS LAW

If we change, purely formally, in the formula of the Snellius law

$$\sin\varphi / \sin\psi = n \qquad (14)$$

the index of refraction n to $-n$, we will find that the refracted ray goes symmetrically to that direction, into which it goes in the custom case $n > 0$, as is shown on Fig. 3. Such a move of the ray always exists at refraction on a border between usual materials and materials with negative group velocity. On this circumstance for the first time pointed L.I. Mandelstam [9].

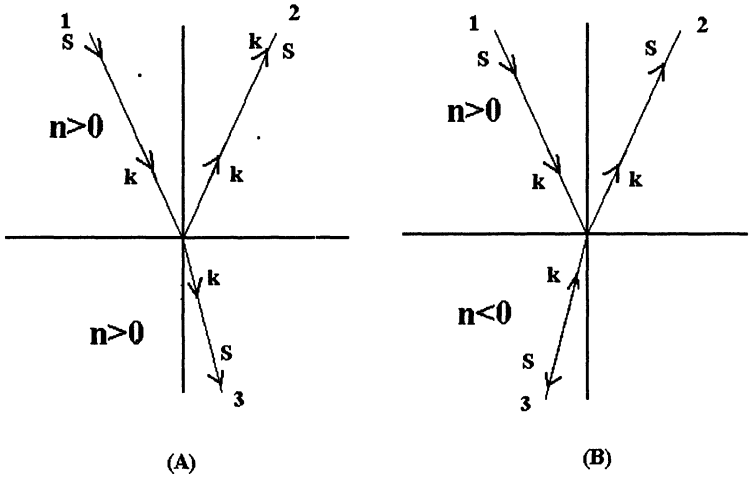

Figure 3. The beam path at refraction on the boundary of vacuum ($n > 0$) and material with positive refraction index ($n > 0$) (A) and negative one ($n < 0$) (B). 1-incident beams, 2-reflected beams, 3 –refracting beams. S - Poynting's vector, k - wave vector.

3. SOME DEVICES MADE OF MATERIALS WITH $n < 0$

It is very interesting to trace the beam path through lenses prepared by materials with $n < 0$. As Fig. 4 shows, for $n < 0$ the properties of lenses are exchanged, and a concave lens becomes convergent, but a convex lens becomes divergent.

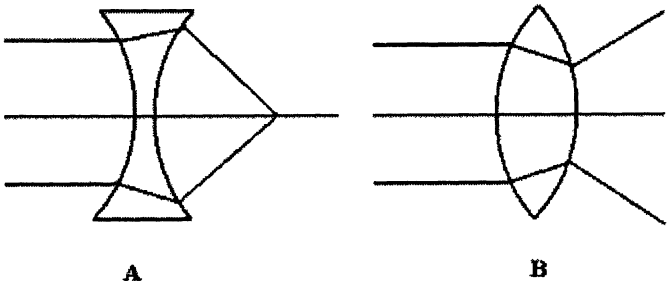

Figure 4. Paths of rays in lenses made of a material with $\mathbf{n < 0}$

However, probably the most interesting characteristics has a usual parallel-plane plate, prepared from a material with $\mathbf{n < 0}$. If on one side of such plate, shown on Fig. 5, is located a source of light **A**, its radiation will be focused into spot **B** on the opposite side of the device. However, this optical instrument is not a lens, since it does not collect at a point parallel beams of rays coming from infinity. But such plate is an ideal optical instrument, which without any distortion will convert a 3D object into its 3D image. Of course, this is true only if coefficient of refraction of the plate is exactly equal –1.

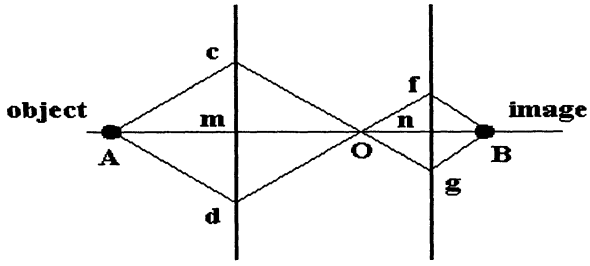

Figure 5. Beam path in a plane-parallel plate made of a material with $\mathbf{n = -1}$.

The detailed analysis of all characteristics of such "lenses" is made in papers [11,12]. It is important to note that in such "plane-parallel lens" light, going from an object to its image, spends on this way different time, depending on what exactly way it goes. One can see that, obviously, the propagation time on the way A-m-O-n-B is undoubtedly smaller than on the way A-c-O-g-B. This fact also

distinguishes this lens from the usual one, which in the ideal case is isochronic, since the light on its way from the subject to the image spends equal time, whatever path is taken. This lens has also a more paradoxical characteristic. This is because the length of the optical way from an object to its image is zero, independently on the real path of ray. This is explained by the fact, that the optical length for any optical ray, traveling in vacuum (n=1) is a equal to the length with the minus sign, if traveling in the lens with n=-1. Thus, the full length of the optical way is 0, for any ray connecting the object and its image. Such unusual situation raises the question about correct wording of Fermat's principle for light, propagating in materials with $\mathbf{n < 0}$.

3.1 ABOUT WORDING OF FERMAT'S PRINCIPLE FOR MATERIALS WITH $\mathbf{n < 0}$ [10]

The appearance of negative refraction materials, generally speaking, does not bring us any absolutely unusual phenomena, but as we made it clear above, some optical laws are realized in a different way than in the familiar for us case $\mathbf{n > 0}$. This pertains, in particular, to the Snellius law, to the Doppler and Cherenkov effects, as was discussed above. To the list of discussed phenomena and laws it is necessary to add one more important law, or more exactly, principle: Fermat's principle. Wording of this principle in literature exists in different variants, which possible reduce to the two main:

1.The light propagates from one point of space to another along the shortest path. Here, the term "the shortest" implies the minimum time spent for passing along this way.

2. The light propagates from one point of space to another along the paths, which correspond to the minimum of the optical length. Under the term "optical length" one understands the distance, which the light passes in vacuum for the time of propagation from one point of space to another, or the total number of wavelengthes along the given path.

As example of these different approaches, one can read the article "Fermat`s principle" from "British encyclopedia" (http://www.britannica.com/search?query=Fermat%60s%20principle&ct=&fuzzy=N): "Statement that light traveling between two points seeks a path such that the number of waves (the optical length between the points) is equal, in the first approximation, to that in neighbouring paths. Another way of stating this principle is that the path taken by a ray of light in traveling between two points requires either a minimum or a maximum time."

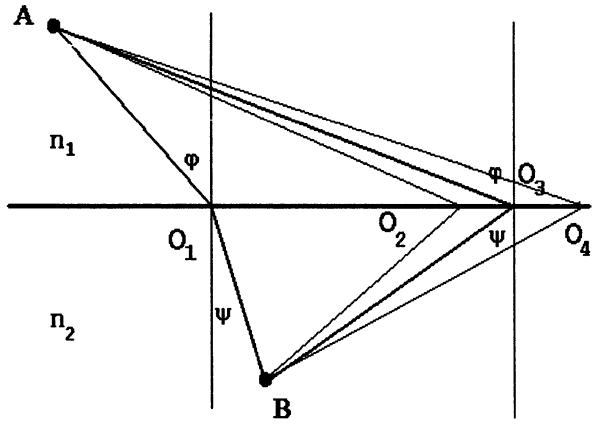

Figure 6. Passing of light from point A to point B through a planar border between two materials with indices of refraction $\mathbf{n_1}$ and $\mathbf{n_2}$.

Except these differences, it often becomes firmly established (absolutely correct) that the term "minimum length or time" in some cases must be replaced by the term "maximum" or even simply "extremum".

If we now return to the two wordings given above, it immediately becomes clear that they both are equally correct for light passing through media with $\mathbf{n > 0}$ or $\mathbf{n < 0}$ only, but not when on the way of propagation the light, at least partly, passes through materials with both signs of $\mathbf{n}$. This is easy confirmed on Fig. 6, where one can see possible ways of ray, crossing a flat surface, separating two media, having the index of refraction $\mathbf{n_1}$ and $\mathbf{n_2}$, respectively.

Let us discuss several cases possible in the situation depicted on Fig. 6.

1. Case $\mathbf{n=n_2/n_1>0}$. The light propagates along the way $\mathbf{AO_1B}$. The Snellius law

$$\mathbf{\sin\varphi / \sin\psi = n_2 / n_1 = n > 0} \qquad (15)$$

is fully correct for this way, and only for this way.

2. Case $\mathbf{n=n_2/n_1<0}$. The light spreads on way $\mathbf{AO_3B}$. The Snellius law

$$\mathbf{\sin\varphi / \sin\psi = n_2 / n_1 = n < 0} \qquad (16)$$

also is fully correct for this way, but with a negative value of $\mathbf{n=n_2/n_1}$.

It is easy to show that for both ways $\mathbf{AO_1B}$ and $\mathbf{AO_3B}$ the variations of the optical length

$$\begin{aligned}\delta L &= n_1(AO_1)+n_2(O_1B)\\ \delta L &= n_1(AO_3)+n_2(O_3B)\end{aligned} \qquad (17)$$

are zero, and for both ways the Snellius law is satisfied.

It is very important, that in the general case the optical length may be not only positive, but negative too, if a part of the way lies inside the materials with $n<0$.

As to ways $\mathbf{AO_2B}$ and $\mathbf{AO_4B}$, they are virtual ways from point $\mathbf{A}$ to point $\mathbf{B}$ for the case $\mathbf{n=n_2/n_1<0}$, but for both these ways equation

$$\delta L = 0 \qquad (18)$$

is not satisfied. Moreover, the time of light propagation from $\mathbf{A}$ to $\mathbf{B}$ along the way $\mathbf{AO_2B}$ is smaller, and along the way $\mathbf{AO_4B}$ is longer, than along the way $\mathbf{AO_3B}$, but the real path is only $\mathbf{AO_3B}$, because this is the path with an extremum of the optical length. Very important, that the type of extremum depends on the geometry of the problem and the actual values of $\mathbf{n_1}$ and $\mathbf{n_2}$.

Thereby, the wording of Fermat's principle as minima of time of light traveling is in general not correct. The correct wording is only the wording of this principle through extremum of the length of the optical path:

The actual path of light propagation corresponds to the local extremum of the optical path length, taking into account the negative sign for the optical length, where $\mathbf{n<0}$.

Using the term "local" takes into account the fact that in a problem there can be several possible optical ways, such that for them conditions (17) are satisfied. The full length of the optical way $\mathbf{L}$ between points $\mathbf{A}$ and $\mathbf{B}$ in the most common case, when the refraction index $\mathbf{n}$ changes from point to point, is defined by the integral

$$\mathbf{L}=\int_{\mathbf{A}}^{\mathbf{B}}\mathbf{ndl} \qquad (19)$$

Since the value of $\mathbf{n}$ in (19) can be negative, it is clear that the optical length L (in fact this value is an eiconal) can have any sign and any value. So, this length will

be negative if light passes through media with $n < 0$ only. In some cases the optical length of a path can be equal to zero. Exactly such is the length of the optical way between an object and its image in a "lens" made from a material with $n < 0$, as shown on Fig. 5 [13]. The notion of the optical length is connected with the total phase shift between an object and its image. This shift depends not only on the geometrical length, but also on the refraction index n, which defines the phase velocity of light, rather then the group velocity. Often used determination of the optical length through the propagation time in actually identifies the phase and group velocities, which is wrong in the general case, and in our particular case leads to serious mistakes.

4. EXPERIMENTAL REALIZATION OF NEGATIVE REFRACTION INDEX

As far back as in the beginning of our work on the problems of electrodynamics of materials with simultaneously negative ε and μ we tried to find such materials among magnetic semiconductors, that are materials, which are strong magnetics (for instance, ferromagnetics) and simultaneously have a semiconductive type of conductivity. Examples of such materials are the magnetic chalcogenides spinels, (for example $CdCr_2Se_4$), and exactly among them we searched for necessary materials [4]. Corresponding calculations were made, and the results showed that in principle magnetic semiconductors can have simultaneously negative ε and μ and, consequently, the negative index of refraction. However, practical attempts of realization of this sort of materials ended in failure, mostly because of large dissipation for penetrating waves.

The situation fundamentally changed, when a group of scientists from University of California at San Diego created a composite material, which had an effective negative value of the refraction index [5,6]. This material is a collection of thin metallic wires and open single rings. If one positions these elements in a certain order and on a determined distance, then such a medium can be described as a material with negative ε and μ.

On Fig. 7 the general view of the composite is shown, as suggested in [5,6].

The authors of work [6] have used a special installation (see Fig. 8), by means of which they could measure the angles of refraction at passing of rays through the border between two media.

In paper [6] a direct experimental validation of the Snellius law for materials with negative ε and μ was reported.

From Fig. 9 it is obviously seen that a ray, outgoing from a $n < 0$ material, is refracted from the vertical to the negative side, in full correspondence with Fig. 3. The ray, outgoing from teflon, is refracted to the positive side, and does not feel any anomaly.

4.1. WHAT CAN GIVE US MATERIALS WITH NEGATIVE REFRACTION?

First of all, it is necessary to take into account that materials with negative refraction present not only a very broad class of materials, but more exactly materials and devices.

Among them are:
1. Materials with simultaneously negative ε and μ.
2. Photonic Crystals.
3. Different sort of electronic devices using backward waves.

This list possibly continues. All that was be discussed in the present report, relates to the first item on this list. We do not discuss here characteristics of photonic crystals though they have characteristics very close to that of materials listed under item 1 of the above list, see, for example [13]. It is important to notice that our discussion concerns solely isotropic materials and, besides, we do not concern any question of frequency, and, more so, spatial dispersion, though these questions undoubtedly are very important for the whole class of these problems. The existence of composite materials with negative ε and μ has allowed for the present day to realize $\mathbf{n < 0}$ in the centimeter wave band. There is no doubt that reducing metallic elements opens a way to reduce the wavelength to millimeter, maybe close to the infrared region. However, penetration of such methods in the optical range is problematic. Nevertheless, it is possible to hope for creation of materials with $\mathbf{n < 0}$ in optical range on the base of photonic crystals.

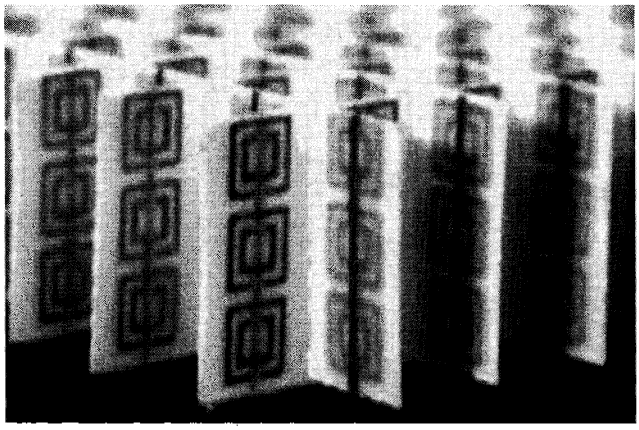

Figure 7. Construction of composite material with negative ε and μ (Reprinted with permission from [6]. Copyright [2001] American Association for the Advancement of Science.)

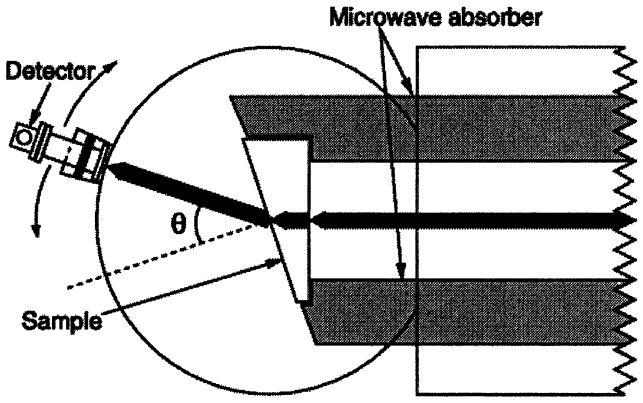

Figure 8. Special device for measurements of angles of refractions. (Reprinted with permission from [6]. Copyright [2001] American Association for the Advancement of Science.)

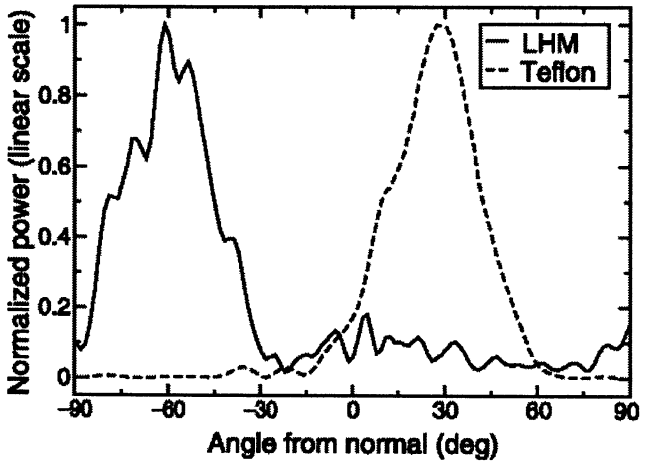

Figure 9. Angular dependencies of refraction for materials with negative index of refraction and for teflon. (Reprinted with permission from [6]. Copyright [2001] American Association for the Advancement of Science.)

At estimation of the role, which can play composites and photonic crystals in optics in general and in its practical exhibits, in particular, in the first place we call

attention to a possibility of manufacturing of material with negative refraction. This estimation, on our opinion, is correct, but unilateral. Indeed, the role of the composite, designed at San Diego, consists first of all in that we now can artificially create materials with any (in the known limits, certainly) values of ε and μ. But this in turn, allows not only to get materials with any ε and μ, but also with any values of wave impedance $z = \sqrt{\mu / \varepsilon}$. This is indeed important, since exactly the wave impedance defines the matching when radiation passes from one ambience into another. So under normal incidence of radiation to a border between two media reflection will be absent if the condition

$$z_1 = z_2 \tag{20}$$

is valid. Of course, now we are only at the beginning of a long way of studying materials with negative refraction. Now we need to investigate, both theoretically, but, *more important, experimentally*, all the properties of this new class of material. Of course, we will have on this way many difficulties, connected with remarkable amounts of dispersion and, possibly, anisotropy of these media. But, I am sure, history will meet our expectations.

5. References

1. Veselago V.G. (1967), About properties of substances with simultaneously negative values of dielectric and magnetic permeabilities, *Soviet Phys. Solid State* **8**, 2853
2. Veselago V.G. (1968) The electrodynamics of substances with simultaneously negative values of ε and μ, *Soviet Physics USPEKHI*, **10**, 509-514
3. Veselago V.G. (1967) The electromagnetic properties of a mixture of electric and magnetic charges, *Soviet Physics JETP*, **25**, 680
4. Veselago V.G. (1972) Electrodynamics of Substances with Simultaneously Negative Electrical and Magnetic Permeabilities, in E.Burstein and Francesco de Martini (eds.), POLARITONS, Proceedings of first Taormina research conference on the structure of matter, 2-6 October 1972, Taormina, Italy, Pergamon Press.
5. Smith D. R., Padilla W., Vier D. C., Nemat-Nasser S. C., Schultz S. (2000). A Composite medium with simultaneously negative permeability and permittivity, *Phys. Rev. Lett.*, **84**, 4184
6. Shelby R.A., Smith D.R., Shultz S., (2001) Experimental verification of a negative index of refraction, *Science*, **292**, 77
7. Landau L.D., Lifshitz E.M. (1984) *Electrodynamics of continuous media*, Pergamon Press, Oxford.
8. Pafomov V.E. (1959), Transition radiation and Cherenkov radiation, *Soviet. Phys. JETP*, **9**, 1321
9. Mandelstam L.I. (1945), Group velocity in crystal lattice (in Russian), *JETP*, **15**, 475
10. Veselago V.G.(2002) About the wording of Fermat's principle for light propagation in media with negative refraction index, http://xxx.lanl.gov/ftp/cond-mat/papers/0203/0203451.pdf
11. Pokrovsky A.L., Efros A.L.(2002) Diffraction in left-handed materials and theory of Veselago lens, http://xxx.lanl.gov/PS_cache/condmat/pdf/0202/0202078.pdf
12. Ziolkowski R.W., Heyman E. (2001)Wave propagation in media having negative permittivity and permeability, *Physical review E*, **64**, 056625
13. Notomi M. (2002) Negative refraction in photonic crystals, *Optical and Quantum Electronics* **34**, 133-143

MODELLING AND MICROWAVE PROPERTIES OF ARTIFICIAL MATERIALS WITH NEGATIVE PARAMETERS

S.A. TRETYAKOV, I.S. NEFEDOV[1], C.R. SIMOVSKI[2], S.I. MASLOVSKI
Radio Laboratory, Helsinki University of Technology
P.O. Box 3000, FIN-02015 HUT, Finland
[1] *On leave from Institute of Radio Engineering, Russian Academy of Sciences, Saratov Department*
[2] *On leave from State Institute of Fine Mechanics and Optics, St. Petersburg, Russia*

Abstract. In this review paper we discuss various possible physical realizations of artificial media with negative real parts of material parameters (wire media, split-ring resonators, omega and chiral particles, active composites). The physical phenomena behind the effect of negative parameters are explained, and analytical models for the material properties are given. Further, some simple electromagnetic systems which contain slabs of double-negative materials are studied: two-layer waveguides and one-dimensional electromagnetic crystals. Unusual properties of waves in these structures are discussed. The review describes results obtained mainly in the Radio Laboratory of the Helsinki University of Technology.

1. Introduction

In the recent literature, the first realization of artificial materials which can be described as a medium whose permittivity and permeability have negative real parts [1] was reported [2]. At the Advance Research Workshop *Bianisotropics'2002* held in Marrakech in May 2002, quite a number of new results in this research direction were reported, and a review presentation by V.G. Veselago, the originator of this field of electromagnetic research, was given. In this review paper we present a systematic overview of possible physical realizations of such materials followed by a discussion of simple waveguiding and periodical structures with double-negative slabs.

V.G. Veselago studied in sixties [1] the electromagnetic properties of materials whose permittivity and permeability simultaneously have negative real parts. He showed that these media exhibit unusual properties like

S. Zouhdi et al. (eds.), Advances in Electromagnetics of Complex Media and Metamaterials, 99–122.

support of backward waves (when the Poynting vector of a time-harmonic plane wave is directed opposite with respect to the wave vector) and anomalous negative refraction of plane monochromatic electromagnetic waves. This concept implies many other interesting features of wave propagation that were reviewed in [1]. We should note that in a very recent paper [3] claims are made that anomalous refraction is not possible, despite the known experimental evidence and numerical simulations. In fact, negative refraction of energy flow is not forbidden by causality [4]. Most new effects are consequences of the fact that this is a backward-wave material. We know, however, that backward waves can exist also for example in periodical structures. The fundamental difference between the *Veselago* medium and other backward-wave structures is that here we deal with a *medium,* whose microstructure can be averaged on the scale of the wavelength.

It appears that Veselago media do not exist in nature; earlier attempts to find realizations among magnetic semiconductors failed mainly due to high losses in that materials. The interest in creating such media artificially, for optical applications, was indicated by J. Pendry in [5]. This kind of medium can be obtained with arrays of conducting inclusions of a special shape. It is obvious that the response (at least, magnetic response) of these materials is resonant. Therefore, negative refraction and other new effects are possible only within a more or less narrow frequency band (or bands). This "negative" band is naturally a part of a resonant band of the inclusions that are used in the composite. This can be clearly illustrated by the Lorentz model of resonant dispersion.

Since it is easier to use resonant inclusions with millimeter-scale dimensions, it seems reasonable to focus on the realizations of Veselago media for the microwave region of the electromagnetic spectrum (optical composites will need very small particles) and to study their response experimentally. This work was recently started at the University of California at San Diego and the first positive experimental results published in [6] (transmission through slabs) and [2] (negative refraction). These experiments have been based on numerical simulations and a simple analytical model presented in [6] and [7]. It was a success despite that simulations seldom lead to discoveries, and the analytical model from [6] and [7] leaves many questions open. This fact influenced the contents of the present paper.

The composite proposed by scientists from the University of California at San Diego is a combination of two regular lattices: a lattice of vertical parallel wires which provide the desired electric properties and a lattice of the so-called *double split-ring resonators* (SRR) necessary to obtain resonant magnetic response of the medium.[1] A piece of this composite prepared

[1] In [6] and [7] it was maintained that SRR has only a resonant magnetic polarizability and no resonant electric one.

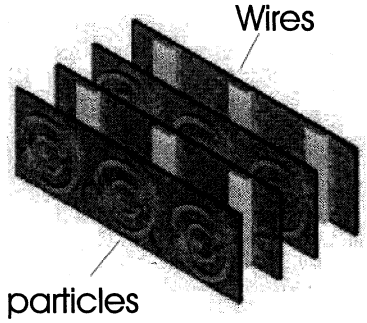

Figure 1. A piece of the composite invented at San Diego [6].

with the use of planar technology (SRR and strip wires on the surface of thin dielectric plates separated by air spacings) is shown in Fig. 1. Both components have been known before. Open loops and double open loops were used in the design of artificial magnetics for microwave absorbers [8, 9], and more recently analyzed in [7]. The wire medium was used as an artificial dielectric for many decades [10, 11], and, just like SRRs, recently brought to attention by Pendry et al. [12].[2]

At first glance, one can think, following [2, 6, 7], that at low frequencies (meaning that the distances between adjacent particles and wires are small compared to the wavelength) it is easy to estimate analytically the effective parameters of this medium. The effective medium made up by vertical wires can be described at low frequencies for electric fields polarized along the wires as a dielectric with the effective permittivity:

$$\epsilon_{\text{eff}} = 1 - \left(\frac{\omega_0}{\omega}\right)^2 \tag{1}$$

where parameter ω_0 is an analogue of the plasma frequency [10], and when $\omega < \omega_0$ the medium is opaque (for waves with the electric field polarized along the vertical axis). The magnetic response of this material is supposed to be the same as the vacuum response.

The permeability of the composite of SRR particles embedded into a wire medium matrix may then be found through the magnetic polarizability a_{mm} of an individual SRR particle, for example, within the frame of the Maxwell Garnett model (a_{mm} is assumed to be known from, say, from numerical modelling).

Though this way seems to be generally correct, there is a serious flaw in such speculations. Indeed, let us consider a composite formed by SRR

[2] It is a typical example showing that scientists working in different branches of physics often read different journals and use different terminology for the same things. *Artificial dielectric=metallic mesostructure*, *stop band=band gap*, etc.

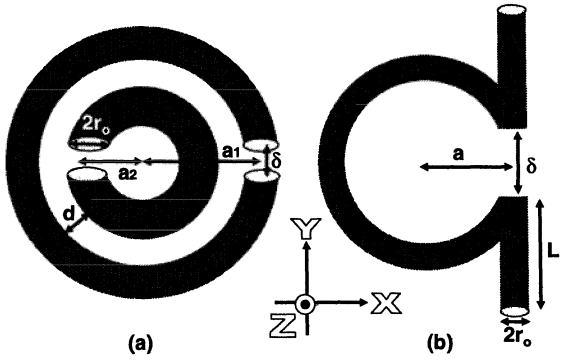

Figure 2. Geometry of prospective particles. (a) SRR particle (b) omega particle.

particles placed in a *homogeneous and continuous* medium with $\epsilon_{\text{eff}} < 0$. The resonant frequency of a particle is equal to $\omega_{\text{res}} = 1/\sqrt{LC}$, where L and C are particle effective inductance and capacitance. Because C is proportional to the permittivity of the matrix, ω_{res} is always imaginary and the particle resonance is impossible. One can extend this simple proof (see Section 2.5) and show that also lattices of wires cannot be described as media with negative permittivity if the wires are embedded into an isotropic and continuous matrix with a negative permeability. Therefore, only special arrangements of wires and SRR particles can lead to the desired pair of negative parameters of the composite. Analytical models of the constitutive parameters must take into account the periodicity of the structure.

Another deficiency of the previous work was treating the SRR particle as a scatterer with only magnetic response. In fact, SRR is a pair of mutually coupled resonators both possessing magnetic and electric resonances in the same range of frequencies. A more elaborate analytical model of an individual SRR particle has been recently developed and verified by numerical simulations in papers [13] and [14], and here we briefly reproduce the main results. It was also shown in [13] that SRR particles alone (without a wire lattice) allow to obtain simultaneously negative permeability and permittivity, if the particle geometry and their arrangement in space are properly chosen. Bianisotropic properties of double split-ring particles were studied also in [15].

Actually, it is known already for some time that double-negative material parameters can be realized also in systems containing inclusions of only one type. One example is the bianisotropic omega particle [16]: double-negative region was seen in simple model simulations (circuit model, losses ignored) in a paper published by Saadoun and Engheta in 1994 [17]. In paper [13] realizations of Veselago media with the use of omega inclusions

have been theoretically considered. These particles alone produce magnetic and electric responses of the same order of magnitude. Two particles: an SRR and an omega particle are shown in Fig. 2. In [13] we considered these particles made from wires of round cross section as in Fig. 2, and in [14] an analytical model has been developed for the planar variant of SRR. Analytical and numerical models of omega particles were developed in papers [17]–[20]. A reliable description of the omega particle electromagnetic response is available, and we do not discuss this question here.

Still another possibility is the use of racemic mixtures of chiral inclusions, for example canonical helices combining loops and straight-wire electric dipoles. In both omega and chiral realizations there is a possibility to design materials with equal permittivity and permeability in wide frequency ranges. This is because both types of polarizations are created by electric currents flowing along the same wire inclusion. A serious disadvantage, however, is a high level of resonant resistive losses in these composites. Finally, negative and *real* material parameters can be realized in composites with active inclusions [21], and we will briefly discuss this in the review.

Having described various physical realizations of Veselago media, we will move on to eigenwaves and dispersion properties of waveguides and periodical structures with Veselago slabs. These structures possess new and unique electromagnetic properties.

2. On possible realizations of media with negative parameters

A two-phase composite was used in the first reported realization of Veselago media, so that the electric and magnetic responses were provided by different sub-systems. Negative permittivity was due to a periodical array of thin parallel conducting wires. We will start our analysis from describing a simple analytical model of wire media and their electromagnetic properties.

2.1. WIRE MEDIA: NEGATIVE PERMITTIVITY COMPOSITES

This particular composite formed by a regular array of thin long metal wires has been known for a long time [10, 11] as an artificial dielectric with the effective permittivity being smaller than one or negative. Wire arrays (*wire media*) formed by long periodically cut wires were considered in [24], and the dynamic theory of waves in wire media is given in [25]. The generic plasmon frequency dependence

$$\epsilon = \epsilon_0 \left(1 - \frac{\omega_0^2}{\omega^2}\right) = \epsilon_0 \left(1 - \frac{\lambda^2}{\lambda_0^2}\right) \tag{2}$$

has been used for its effective permittivity, including papers on Veselago media [22]. Here, ω is the frequency, λ is the free-space wavelength cor-

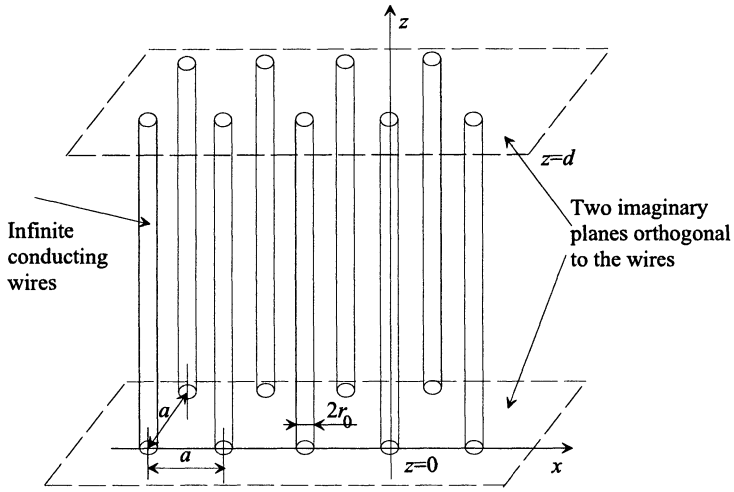

Figure 3. Geometry of the problem: an infinite periodical array of conducting wires.

responding to that frequency, and ω_0 and λ_0 are constants. In the known approach to the description of wire media [10, 11] it was assumed that between planar arrays of wires there were only travelling plane waves of the fundamental Floquet mode. However, this is true only when one of the periods is much smaller than the other one, and for arrays with square cells this assumption is not justified. We have shown in [23] that the estimation for λ_0 from [10]) leads to considerable errors if the wire radius is not very small. Furthermore, it appears, that only ideally conducting wires were considered before. In [23] we have analyzed the influence of resistive losses to the value λ_0. Here we review the quasi-static model of effective properties of wire media [23], which gives a simple and physically clear model of the effective permittivity. The model is easily extendable to more complicated situations, such as arrays of lossy wires or loaded wires.

2.1.1. *Estimation of effective permittivity*

The geometry of the problem is shown in Fig. 3. Consider a layer of a wire medium located between two imaginary planes orthogonal to the wires and positioned at $z = 0$ and $z = d$. Let us assume that the electric field in the medium is parallel to the wires (axis z), and the quasi-static conditions are satisfied. If distance d is much smaller than the wavelength λ, the space between the two cutting planes can be considered in the same way as plane capacitors, and the permittivity of the effective medium formed by conducting wires inside the layer can be found from simple quasi-static considerations. The result can be expressed in terms of the wire inductance

per unit length L:

$$\mathbf{D} = \left(\epsilon_0 \overline{\overline{I}} - \frac{\mathbf{z}_0 \mathbf{z}_0}{\omega^2 a^2 L}\right) \cdot \mathbf{E} \tag{3}$$

To find L we need to estimate the magnetic field distribution in the infinite array of wires. To do this, we note that due to the symmetry of the problem, magnetic field is zero at the middle points between wires. On the other hand, if the wires are thin, the main contribution into the flux comes from the area close to the wires. These observations bring us to the following estimation for the magnetic field in the space between two neighboring wires located at $x = 0$, $y = 0$ and $x = a$, $y = 0$:

$$H_y = \frac{I_w}{2\pi}\left(\frac{1}{x} - \frac{1}{a-x}\right) \tag{4}$$

This assumes the quasi-static formula for the magnetic field of the wires. Hence, for the inductance we obtain

$$L = \frac{\mu_0}{2\pi} \log \frac{a^2}{4r_0(a-r_0)} \tag{5}$$

and for the permittivity

$$\overline{\overline{\epsilon}} = \epsilon_0 \left(\overline{\overline{I}} - \frac{2\pi \mathbf{z}_0 \mathbf{z}_0}{(ka)^2 \log \frac{a^2}{4r_0(a-r_0)}} \right) \tag{6}$$

where $k = \omega\sqrt{\epsilon_0 \mu_0}$.

2.1.2. *Lossy and loaded wires*

The above result has been obtained for ideally conducting wires. If they can be described by some effective surface impedance Z_s additional to the inductance, the following formula for the permittivity can be obtained:

$$\overline{\overline{\epsilon}} = \epsilon_0 \left(\overline{\overline{I}} - \frac{2\pi \mathbf{z}_0 \mathbf{z}_0}{(ka)^2 \log \frac{a^2}{4r_0(a-r_0)} - jka\frac{a}{r_0}\frac{Z_s}{\eta}} \right) \tag{7}$$

where $\eta = \sqrt{\mu_0/\epsilon_0}$ is the free-space impedance. For example, for lossy wires (skin depth much smaller than the wire diameter) we see that the real part of the permittivity (which is negative) decreases in the absolute value (and the permittivity naturally becomes complex). Note that the loss effect increases at low frequencies.

More complicated and exotic behavior can be realized by loading wires by reactive impedances. For example, if we periodically cut the wires (and

possibly insert bulk capacitances into every cut), the effective permittivity becomes

$$\bar{\bar{\epsilon}} = \epsilon_0 \left[\bar{\bar{I}} + \frac{\mathbf{z}_0 \mathbf{z}_0}{j\omega\epsilon_0 a^2 \left(j\omega L + \frac{1}{j\omega C} \right)} \right] = \epsilon_0 \left[\bar{\bar{I}} + \frac{\mathbf{z}_0 \mathbf{z}_0 \, C}{\epsilon_0 a^2 (1 - \omega^2 LC)} \right] \tag{8}$$

Here, $1/(j\omega C)$ is the load impedance per unit length.

At low frequencies we have an effective medium with a positive permittivity defined by the capacitances of the gaps. Well above the resonance the material has a negative vertical component of the permittivity. Well below the resonance the material is a usual artificial dielectric with a positive effective permittivity.

2.2. SPLIT-RING RESONATORS

SRR particles are bianisotropic particles [15]–[20]. In other words, an external electric field produces a magnetic dipole in the particle and, at the same time, an external magnetic field induces an electric dipole. For SRR, this magnetoelectric effect is reduced by choosing the opposite positioning of the splits of both loops. However, it cannot cancel out exactly since the loops are of different sizes.

Consider the electromagnetic response of an individual SRR particle to local magnetic and electric fields. The polarizabilities of an SRR particle are dyadic coefficients relating the local electric and magnetic fields $\mathbf{E}^{\text{loc}}$, $\mathbf{H}^{\text{loc}}$ with the induced electric and magnetic dipole moments:

$$\mathbf{p} = \bar{\bar{a}}_{ee} \cdot \mathbf{E}^{\text{loc}} + \bar{\bar{a}}_{em} \cdot \mathbf{H}^{\text{loc}} \tag{9}$$

$$\mathbf{m} = \bar{\bar{a}}_{me} \cdot \mathbf{E}^{\text{loc}} + \bar{\bar{a}}_{mm} \cdot \mathbf{H}^{\text{loc}} \tag{10}$$

The electric and magnetic moments of the SRR as a whole are vector sums of the moments induced in the outer and inner loops (indices 1 and 2, respectively) :

$$\mathbf{p} = \mathbf{p}_1 + \mathbf{p}_2, \qquad \mathbf{m} = \mathbf{m}_1 + \mathbf{m}_2 \tag{11}$$

It allows to evaluate the polarizability of an SRR through those of the two loops taking into account their mutual coupling. It was done in [13], where approximate relations were obtained for the components of $\bar{\bar{a}}_{ee}$ and $\bar{\bar{a}}_{mm}$. In that model it was assumed that the inclusion is fabricated from a round wire of radius r_0 (see Fig. 2a). The section of the wire is small enough to satisfy the inequality $r_0 \ll a_{1,2}$, where $a_{1,2}$ are the averaged radii of rings 1 and 2. The distance δ between the broken ends of each ring is assumed to be small compared to $a_{1,2}$. Comparisons with numerical simulations have

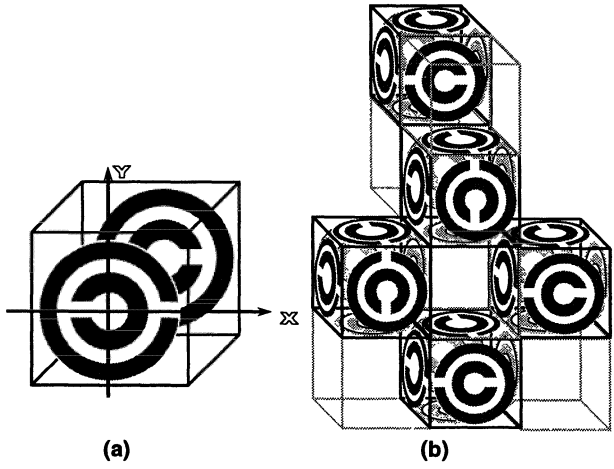

Figure 4. Preparing an isotropic group of SRR particles. (a) Particles located on the opposite sides of a cubic cell are rotated by 180°. (b) Composite can be prepared using the chessboard principle.

demonstrated a reasonable accuracy of the analytical model. Magnetoelectric polarizabilities $\overline{\overline{a}}_{em}, \overline{\overline{a}}_{me}$ have not been studied because in the composite structures of our present interest those are to be intentionally compensated.

2.3. CHESSBOARD COMPOSITES FROM SRR AND OMEGA PARTICLES (3D VESELAGO MEDIA)

There is a possibility to realize double negative materials using inclusions of only one type, which is possibly the only way to create isotropic materials with these properties. In this respect, two different kinds of particles arrangement were studied in [13]. The first one is a mixture with a random orientations of particles. The second one can be obtained by positioning the particles at the faces of a cubic unit cell, like it is shown in Figs. 4 and 5. Different inclusions and structures were finally compared.

We have found that the composite from cubic unit cells shown in Figs. 4 and 5 is more prospective (the resonance effect is more strong) than that with the random orientations of particles. This is because of the absence of scattering losses in dense regular arrays. Also this composite is easier to fabricate than the random one since it is possible to use planar technology.

2.3.1. *Effective polarizabilities of a cubic cell of SRR particles*

Consider a cubic cell of an array of SRR particles presented in Fig. 4. Electric field directed along an arbitrary edge of a cubic cell excites electric

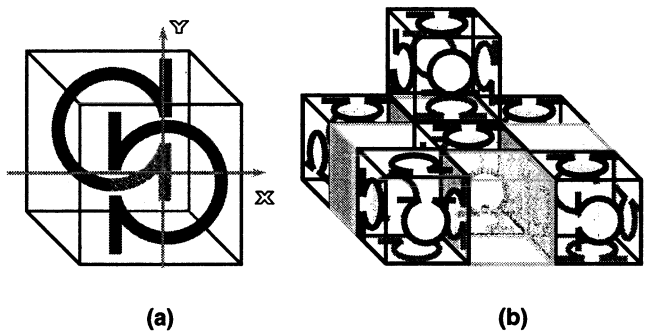

Figure 5. Isotropic arrangement of omega particles (the same method as in 4). (a) Omega particles are positioned at the sides of a cubic unit cells. (b) The arrangement of unit cells shown here allows to obtain an effectively isotropic medium.

dipoles in four SRR particles. For two particles $\mathbf{E}^{\text{loc}}$ is parallel to the line connecting the rings splits and corresponds to the polarizability a_{ee}^{xx}. For the other two particles $\mathbf{E}^{\text{loc}}$ is perpendicular to this line and corresponds to a_{ee}^{yy}. Consider now magnetic fields excite such cells. Magnetic field directed along an arbitrary edge of a cell induces two equivalent magnetic moments in two opposite particles. So, the magnetic polarizability of a unit cell turns out to be the double of a_{mm}^{zz}. To summarize, one cubic unit cell is approximately equivalent to an isotropic particle with the electric and magnetic polarizabilities given by

$$a'_{ee} = 2a_{ee}^{xx} + 2a_{ee}^{yy}, \qquad a'_{mm} = 2a_{mm}^{zz} \tag{12}$$

2.3.2. *Effective polarizabilities of a cubic cell of omega particles*
For a unit cubic cell of omega particles (see Fig. 5) the situation is quite different. Here the resonant excitation by electric fields directed along the arms of Ω (along the y-axis in the model of an individual particle) is mainly due to the presence of the arms [19]. Therefore, the total electric polarization of two opposite omega particles retains a resonant behavior. Within the resonant band the quasi-static component of the omega particle polarizability $a_{ee}^{xx\Omega}$ describing the response of a particle to the electric field applied normally to the arms (see Fig. 1) is small compared to $a_{ee}^{yy\Omega}$. Thus, one obtains for a unit cell from omega particles approximate relations

$$a'_{ee} \approx 2a_{ee}^{yy\Omega}, \qquad a'_{mm} = 2a_{mm}^{zz\Omega} \tag{13}$$

where $a_{ee}^{yy\Omega}$ and $a_{mm}^{zz\Omega}$ can be taken from [19].

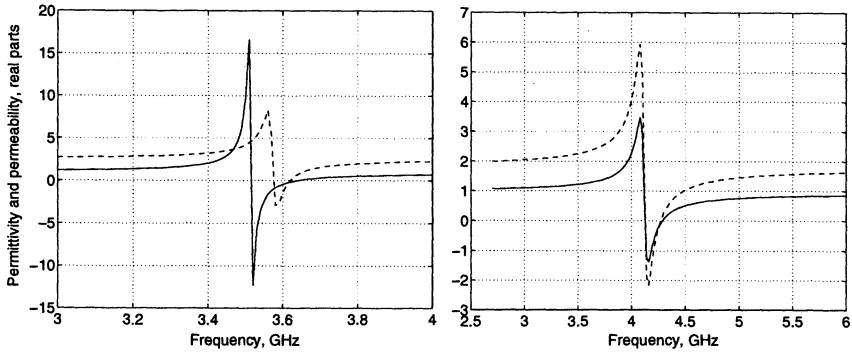

Figure 6. Left: Real parts of the permeability (solid) and permittivity (dashed) of the SRR composite from cubic cells versus frequency. Right: The same for an omega composite formed by cubic cells. The host relative permittivity equals 2.

2.3.3. *Maxwell Garnett modelling of SRR and omega composites*
With the calculated polarizabilities we have derived the material parameters through the well-known Maxwell Garnett model. If one supposes that the unit cells arrangement has a considerable dispersion of their sizes, one can apply the conventional Maxwell Garnett model for a random distribution of inclusions. In an example presented in Fig. 6 we plot the real parts of the permittivity and permeability for composites of SRR particles (Fig. 4) and omega particles (Fig. 5). For the case of SRR particles the averaged size of the cell is equal to $6 \times 6 \times 6 = 216$ mm^3 (the particle size was taken 5.8 mm), and the averaged distance between the centers of two adjacent cells is close to 11 mm which dramatically exceeds the size of the cell. This allows considering the composite as a mixture dilute enough to apply the Maxwell Garnett mixing rule. For the case of omega inclusions the averaged size of the unit cell was taken $6.5 \times 6.5 \times 6.5$ mm^3 (the omega particle largest dimension was 6.2 mm).

In Fig. 6 we can see that $\mathrm{Re}(\mu_{\mathrm{eff}})$ and $\mathrm{Re}(\epsilon_{\mathrm{eff}})$ are indeed negative simultaneously. The imaginary parts of $\mathrm{Re}(\mu_{\mathrm{eff}})$ and $\mathrm{Re}(\epsilon_{\mathrm{eff}})$ within the resonance band attain values -4 and -6, respectively. In the case under study the radiation losses dominate, and we can without additional errors assume the particles to be perfectly conducting.

2.3.4. *Maxwell Garnett model for regular arrays*
Now assume that the particle arrangement is regular (no dispersion in the sizes of the unit cells shown in Figs. 4 and 5), and the period is smaller than $\lambda/2$. Far from the particle resonance the Maxwell Garnett model is still valid for lattices (see, e.g. [26]–[28]). However, near the particle resonance the conventional variant of this model leads to serious errors. In regular arrays

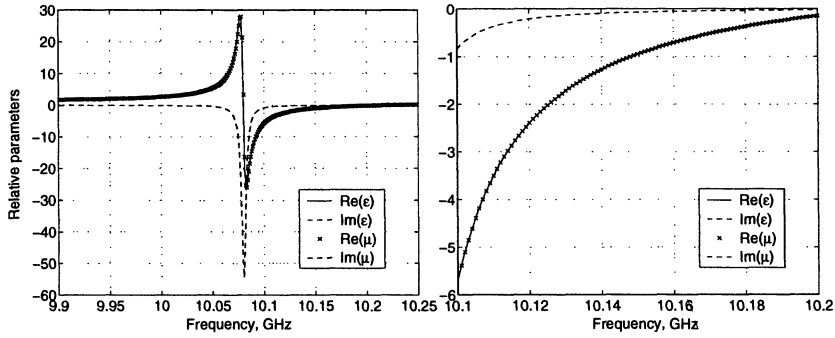

Figure 7. The material parameters of a racemic composite.

of scatterers excited by plane waves there are no radiation (scattering) losses at all, since the re-radiation of the lattice is a discrete series of spatial harmonics [29]. As it follows from the theory of resonant dielectrics [26] and of dipole lattices [29], the needed correction is a simple removal of the radiation resistance from the particle dipole polarizability. This rule remains valid for more general cases (particles possessing both electric and magnetic properties, lossy inclusions). Physically, this rule of damping the radiation resistance corresponds to the fact that in a lossless lattice of particles in which a plane wave propagates, the energy flow through any closed surface surrounding any particle is identically zero. This model in case of lossless inclusions leads to infinite values of permittivity and permeability at the resonance. When we introduce dissipation losses into the particle model (see the next paragraph) this singularity disappears. Notice, that in the realistic situation, the lattice cannot be ideally regular, so there are also small scattering losses.

2.4. REALIZATIONS AS COMPOSITES WITH RESONANT MAGNETOELECTRIC INCLUSIONS

In Fig. 7 an example for the material parameters of a racemic chiral composite medium are shown (a simplified analytical model). The left picture is for the total frequency range, and the right one is a blow-up in a narrower region where the real parts of the parameters are both negative. The inclusion dimensions and the concentration have been chosen so that the real parts of the permittivity and permeability are approximately equal. The medium inclusions are the canonical chiral particles [30, 31] resonating approximately at 10 GHz.

The metal inclusions are made of silver. Absorption in the particles leads to non-zero imaginary parts of the permittivity and permeability, see

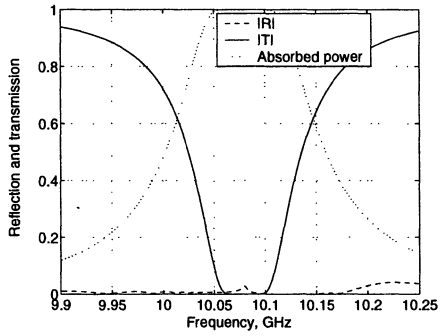

Figure 8. Slab reflection and transmission.

Fig. 7. The arrangement of inclusions is supposed to be regular and dense, so one can neglect the scattering losses in the composite.

Let us now consider the reflection and transmission for a slab of such material. These are presented on Fig. 8, for a 3 cm slab. We can see than in spite of the absence of scattering losses the resistive losses are high at the particle resonance. The wave impedance of the effective medium is nearly the same as that of free space and reflection is almost zero everywhere. The transmission coefficient turns out to be very small within the resonance band. However, the transmitted wave can be measured in the region of negative parameters. At 10.15 GHz the real parts of both the permittivity and permeability are close to -1, and the transmittance is about -3 dB[3].

2.5. WIRE MEDIA AND RESONANT MAGNETIC PARTICLES COMBINED

As it was shown above, the effective permittivity of a medium formed by long conducting cylinders can be found by a simple quasi-static approach. When we neglect losses, this approach leads to Eq. (6). That formula holds for cylinders separated by free space. If between cylinders there is a certain isotropic medium characterized by permittivity ϵ and permeability μ, one should replace ϵ_0 by $\epsilon\epsilon_0$ and μ_0 by $\mu\mu_0$ in (6):

$$\bar{\bar{\epsilon}}_{\text{mix}} = \epsilon_0 \left(\epsilon \bar{\bar{I}} - \frac{2\pi \mathbf{z}_0 \mathbf{z}_0}{\mu (k_0 a)^2 \log \dfrac{a^2}{4r_0(a - r_0)}} \right) \tag{14}$$

k_0 is still the free-space wavenumber here. One can see from (14) that if the filling medium has usual properties ($\mu > 0$, $\epsilon > 0$) the negative values of ϵ_{mix} are possible.

[3] It is possible that the Maxwell Garnett model overestimates the level of losses. Cancellation of the radiation resistance does not make this approximate model exact.

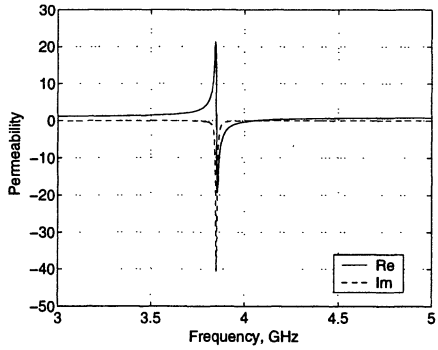

Figure 9. Effective permeability as a function of the frequency.

Let us suppose that the wires are immersed into a negative permeability medium, that is, $\epsilon > 0$ and $\mu < 0$. We obtain the result which has been already mentioned in the introductory section: now it is impossible to realize negative values of the mixture permittivity. This conclusion is quite general, assuming that there is indeed a *continuous medium* between the cylinders. A numerical example illustrating these concepts are given in Figs. 9–11.

We have considered a system composed of SRRs resonating at approximately 3.85 GHz. The resonators are placed inside a wire medium whose plasma-like frequency (at which the effective permittivity changes sign) is about 10 GHz. A simple *LC* model and the Maxwell Garnett mixing rule have been used to model the SRR subsystem. Scattering losses are assumed to be compensated by the particle interactions, as in regular crystals. The theory [23] (Section 2.1) has been used to model the cylinder array forming the wire-medium subsystem. In both calculations losses in the materials (copper wires, dielectric substrates) are taken into account. Fig. 9 represents the permeability of the SRR subsystem. The permeability of the entire system is the same. Fig. 10, left, shows the permittivity of the wire medium without magnetic inclusions. This result is well-known. The whole system (SRRs plus wire medium) has such permittivity when the SRRs are placed at the symmetry planes.

If the quasi-static interaction between SRRs and wires does not vanish, one should use modified formulas like Eq. (14). The medium permittivity for this case is represented on Fig. 10, right. It is seen that the real part of the medium permittivity becomes positive in the region of strong resonant behavior of the SRR subsystem.

Two plots on Fig. 11 show the transmission and reflection coefficients for a 2 cm slab of the material: the left plot is for the arrangement as in [2, 6], and the right one is for the case of strong interaction between the two subsystems. Also, the absorption power density in the slabs is depicted on

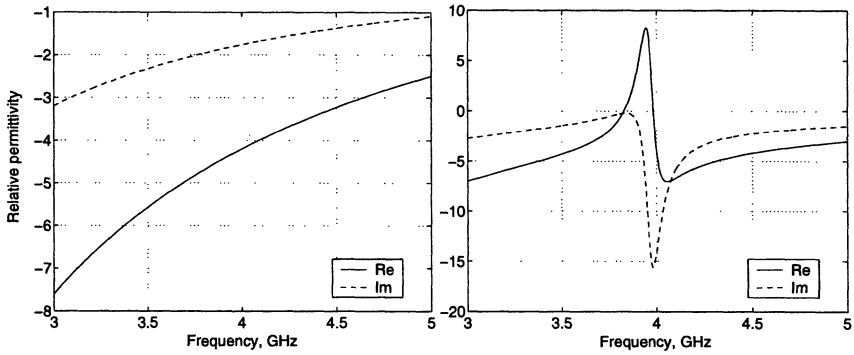

Figure 10. Effective permittivity as a function of the frequency.

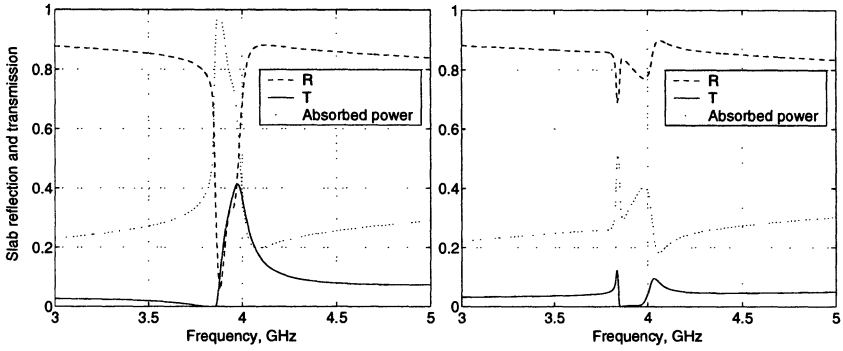

Figure 11. Slab reflection and transmission.

the plots by dotted lines. One can see that the transparency peak disappears on the second plot.

2.6. REALIZATIONS AS ACTIVE COMPOSITES: BROADBAND EFFECTS

Obviously, not all values of material parameters are realizable in composites with passive and linear inclusions, but many restrictions can be dropped if active inclusions are used in a composite metamaterial. In this case, we allow inclusions (artificial molecules) to contain electronic circuits, possibly with transistor amplifies etc., which also include local DC power supplies. This possibility was explored in [32]–[34] in view of other potential microwave applications. Also materials with real negative parameters can be realized in wide frequency ranges as synthetic materials with small inclusions (electric dipole and small loop antennas) loaded by simple impedance inverter circuits [21]. The geometry of the composite is shown in Fig. 12.

Let us assume that the density of the composite is very low, and the effective permittivity is approximately given by $\epsilon_{\text{eff}} = \epsilon_0 + N\alpha_{ee}$, where N

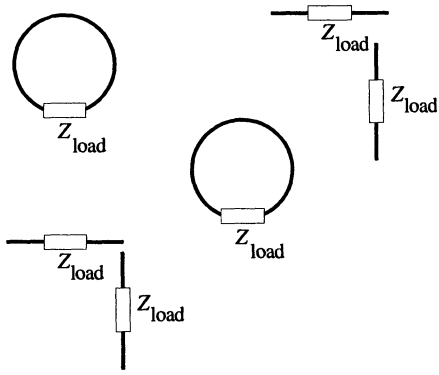

Figure 12. Composite made of short electric dipole antennas and small loop antennas loaded by bulk impedance circuits.

is the concentration of electric dipoles and α_{ee} is the particle polarizability.[4] Let us demand that $\epsilon_0 + N\alpha_{ee} = -|\epsilon_r|\epsilon_0$ and make use of the antenna model of small loaded electric dipole scatterers [31] to calculate the polarizability. This leads to the following condition for the load impedance [21]:

$$Z_{\text{load}} = \frac{-\frac{4}{3}\frac{Nl^2}{j\omega} - \epsilon_0(1+|\epsilon_r|)Z_{\text{inp}}}{\frac{Nl^2}{3j\omega Z_{\text{inp}}} + \epsilon_0(1+|\epsilon_r|)} \tag{15}$$

where $2l$ is the dipole antenna length, and Z_{inp} is its input impedance. For short wire dipole inclusions the input impedance is capacitive: $Z_{\text{inp}} = 1/(j\omega C)$, and we see that the required load is a negative capacitance

$$Z_{\text{load}} = -\frac{1}{j\omega}\left\{\frac{\frac{4}{3}Nl^2 + \frac{\epsilon_0(1+|\epsilon_r|)}{C}}{\frac{Nl^2C}{3} + \epsilon_0(1+|\epsilon_r|)}\right\} \tag{16}$$

In a similar way, for small wire loop inclusions

$$Z_{\text{load}} = -Z_{\text{inp}} + j\omega\frac{\mu_0 NS^2}{1+|\mu_r|} \tag{17}$$

the load should be inductive (positive or negative depending on the desired parameters). Such impedances can be (at least at moderate frequencies) realized by means of electronic feed-back circuits, so this realization appears to be in principle possible. In contrast to the previous examples, no resonators are needed, which means a possibility to provide negative and real effective parameters in a wide frequency range.

[4] This is of course a very crude approximation because in this particular case the particles are near the resonance and the polarizabilities are not very small.

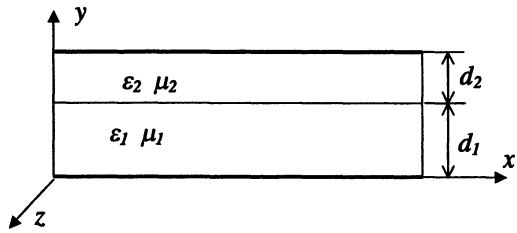

Figure 13. Two-layer planar waveguide. One of the layers is made of a material with negative parameters.

3. Waveguides with slabs of Veselago medium

Let us consider a plane two-layered waveguide, infinite along z and x directions and bounded by electric walls in the $x - z$ plane at distances d_1 and d_2 from the media interface [35] (see Fig. 13). The media are characterized by relative permittivities ε_1, ε_2 and permeabilities μ_1, μ_2. We will discuss eigenwaves propagating in z direction whose fields depend on time and the longitudinal coordinate as $\exp(\omega t - k_z z)$. There is no field dependence on coordinate x.

The dispersion equations for this waveguide can be found in the usual way, and they read

$$\frac{|\mu_1|}{k_{y1}} \tan k_{y1} d_1 - \frac{\mu_2}{k_{y2}} \tan k_{y2} d_2 = 0 \qquad \text{TE modes} \quad (E_z = E_y = 0) \tag{18}$$

$$\frac{k_{y1}}{|\varepsilon_1|} \tan k_{y1} d_1 - \frac{k_{y2}}{\varepsilon_2} \tan k_{y2} d_2 = 0 \qquad \text{TM modes} \quad (H_z = H_y = 0) \tag{19}$$

Here $k_{yi} = \sqrt{k^2 \varepsilon_i \mu_i - k_z^2}$ $(i = 1, 2)$, and k is the wavenumber in vacuum. Typical dispersion curves are shown in Fig. 14. In this example, the media parameters are the following: $\mu_1 = -2$, $\mu_2 = 1$, $\varepsilon_1 = -4$, $\varepsilon_2 = 1$, $d_1 = 0.5$ cm. The thicknesses of the second layer are: $d_2 = 1$ cm (dotted line), $d_2 = 1.1$ cm (solid line), $d_2 = 2$ cm (dashed line).

The dominant TM_0 mode has no cutoff and its slow-wave factor has the low-frequency limit

$$n_{TM_0} \to \sqrt{\frac{d_1\mu_1 + d_2\mu_2}{d_1/\varepsilon_1 + d_2/\varepsilon_2}} \tag{20}$$

If the media parameters are all positive, this value is always within the limits

$$\sqrt{\varepsilon_2\mu_2} \le \sqrt{\frac{d_1\mu_1 + d_2\mu_2}{d_1/\varepsilon_1 + d_2/\varepsilon_2}} \le \sqrt{\varepsilon_1\mu_1} \tag{21}$$

($\varepsilon_2\mu_2 < \varepsilon_1\mu_1$). However, if we allow negative values of the material parameters, there are no limits at all:

$$0 \leq \sqrt{\frac{d_1\mu_1 + d_2\mu_2}{d_1/\varepsilon_1 + d_2/\varepsilon_2}} \leq \infty \tag{22}$$

Very peculiar situations take place in the limiting cases. If

$$d_1/\varepsilon_1 + d_2/\varepsilon_2 \to 0 \tag{23}$$

we observe that the capacitance per unit length of our transmission line (we now consider the quasi-static limit) tends to infinity. This means that although the voltage drop between the plates tends to zero, the charge density on the plates remains finite. This can be understood from a simple observation that if we fix the charge densities (positive on one plate and negative on the other), the displacement vector is fixed and, in the quasi-static limit, it is constant across the cross section. However, the electric field vector is oppositely directed in the two slabs, if one of the permittivities is negative. In the limiting case (23) the total voltage tends to zero. Similarly, in the limiting case $d_1\mu_1 + d_2\mu_2 \to 0$, the inductance per unit lengths tends to zero. These conclusions should be taken with a grain of salt, because a capacitor filled by a material with negative permittivity is a source of energy (stored field energy is negative). Clearly, using passive components this is impossible, moreover, in the static limit there is no magnetic polarization in non-magnetic composites, so it is not possible to realize Veselago material at zero frequency with only passive inclusions.

Another interesting observation concerns the case when both layer thicknesses tend to infinity, that is, the case of waves travelling along a planar interface between two media. The dispersion equations reduce to

$$\frac{|\mu_1|}{k_{y1}} - \frac{\mu_2}{k_{y2}} = 0, \quad \text{TE modes}, \qquad \frac{k_{y1}}{|\varepsilon_1|} - \frac{k_{y2}}{\varepsilon_2} = 0, \quad \text{TM modes} \tag{24}$$

It is well known (and obvious from the above relations) that surface waves at an interface can exist only if at least one of the media parameters is negative, an obvious example is an interface with a free-electron plasma region. If both parameters are negative, both TE and TM surface waves can exist. A very special situation realizes if the parameters of the two media differ only by sign, that is, if $\varepsilon_1 = -\varepsilon_2$ and $\mu_1 = -\mu_2$. In this case the propagation factor cancels out from the dispersion relations, because $k_1 = k_2$. This means that waves with any *arbitrary* value of the propagation constant are all eigenwaves of the system at the frequency where this special relation between the media parameters is realized. A similar observation was made in [36] as an approximation in case of small heights $d_{1,2}$. For a

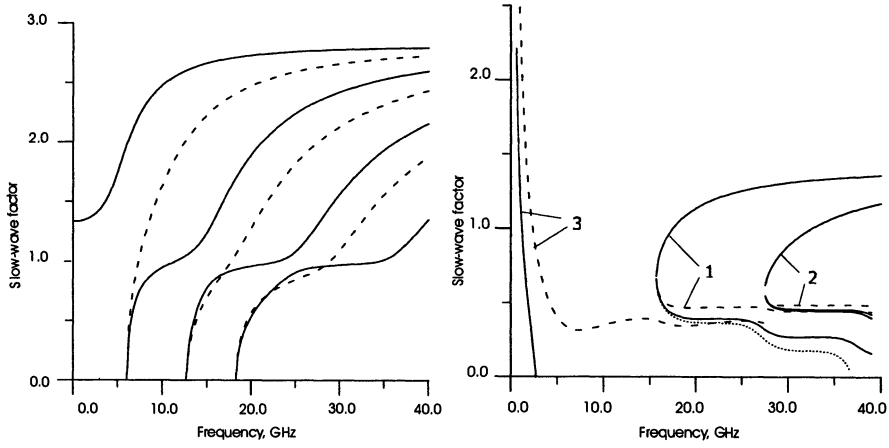

Figure 14. Dispersion curves for a two-layer planar waveguide. TM (solid) and TE (dashed) modes in a usual waveguide (left) and TE modes in a waveguide with a Veselago slab (right).

media interface this result is exact. More peculiar solutions of this basic waveguide problem were found and discussed in [35].

4. Electromagnetic crystals with double negative layers

Let us consider an inifinite periodic structure composed of alternating layers of two materials with different relative permittivities ε_1, ε_2 and permeabilities μ_1, μ_2 [37]. Focusing on the spatial resonances in the structure, we assume here that the material parameters do not depend on the frequency. As is shown in Fig. 15, one of the layers is a usual isotropic and lossless material ($\varepsilon_1 > 0$, $\mu_1 > 0$), but the other layer in every period is made of a Veselago medium ($\varepsilon_2 < 0$, $\mu_2 < 0$). The thicknesses of the two layers are $d_{1,2}$, respectively, and the period is denoted by $L = d_1 + d_2$. The propagation constant β of eigenwaves in this periodical structure can be found from the well-known eigenvalue equation, whose form is the same as for the corresponding structure made of usual materials:

$$\cos \beta L = \cos(k_1 d_1) \cos(k_2 d_2) - \frac{\eta_1^2 + \eta_2^2}{2\eta_1 \eta_2} \sin(k_1 d_1) \sin(\pm k_2 d_2). \qquad (25)$$

Here $\eta_i = \sqrt{\mu_i / \epsilon_i}$ $(i = 1, 2)$, $k_i = k n_i$, $n_i = \sqrt{\varepsilon_i \mu_i}$, are the absolute values of the refractive indices of the two layers forming every period, and k is the wavenumber in vacuum. The signs of the material parameters and of the refractive indices are explicitly included in this formula. The only difference in the derivation of (25) for the new structure is that in the slabs

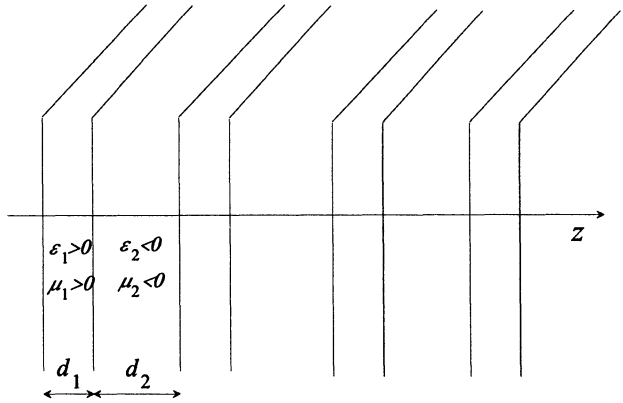

Figure 15. One-dimensional electromagnetic crystal with intermitting layers of a usual materials and a Veselago material.

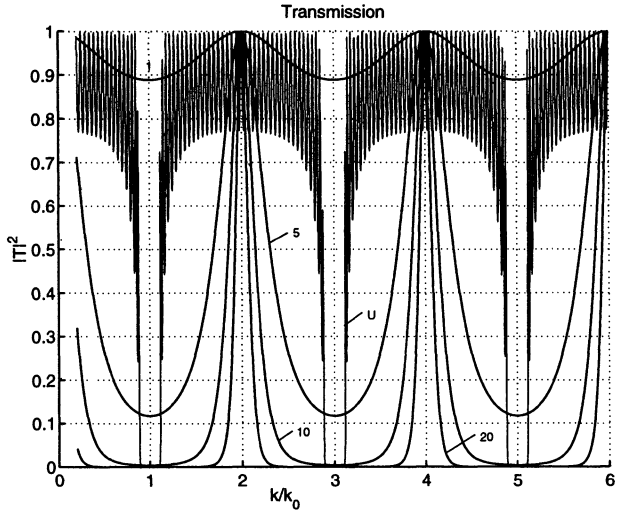

Figure 16. Transmission coefficient through a finite-length system (normal incidence). Crystal formed by two usual materials (curve marked by "U") and the new crystal compared. Note how the extremely wide band gaps are formed when the number of layers (shown by numbers) increases.

of negative materials the sign of the phase constant k_2 must be reversed. This corresponds to the lower sign in the last term of (25). The upper sign gives the equation for the usual case when $\varepsilon_2 > 0$, $\mu_2 > 0$.

If the thicknesses of the two layers forming each period are the same, the finite-period structure becomes transmittive with well-pronounced band gaps with the centers corresponding to the wavelengths satisfying the quarter-wave condition for the first band gap (and 3/4, 5/4, etc. for the other band

gaps), as also takes place in PBG structures composed of usual materials. Fig. 16 demonstrates the spectral transmission of such a structure for different numbers of periods. The transmittance of a usual 20-period structure is presented for comparison (marked by "U"). The results of our analysis show that the PBG structure composed of alternating normal and Veselago layers can be used as a narrow-band selective pass-band filter at wavelengths $2d_1n_1$, d_1n_1, etc., $(k/k_0 = 2, 4, \ldots)$. At other frequencies the structure acts as a reflector.

5. Conclusions

In this paper, we have reviewed various possible realizations of artificial media with negative material parameters. Both passive linear composites and active composites have been discussed. Simple analytical models developed for artificial wire media with negative effective permittivity and for split-ring resonators help to understand the physical phenomena in the composites and to design more complicated and advanced structures. The particle model in combination with the Maxwell Garnett mixing rule adapted for regular lattices gives a possibility to estimate the effective parameters. Finally, with the knowledge of the material parameters we can study reflection and transmission in slabs, waveguides, and electromagnetic crystals with novel composite insertions.

The quasi-static analytical model of wire media clearly explains the nature of their electromagnetic response and allows to take into account losses in the wires and the electromagnetic properties of the matrix material. Furthermore, extensions to more complicated systems, such as arrays of loaded wires, can be easily made.

The new analytical model of split-ring resonators explains the electromagnetic response of double split-ring resonators which have been used in the practical design of artificial composite materials with negative material parameters. We have shown that the system has two main resonances. One (the lower) resonance gives a strong magnetic response, such that in the resonance frequency range the real part of the polarizability is negative. The role of the second loop is twofold. First, the presence of the second loop reduces the resonance frequency because of magnetic coupling to the first loop and an additional load capacitance. The second loop should be also broken: although a closed second loop increases the load capacitance in the same way as an open one, the magnetic coupling between an open and broken loop leads to an increase of the resonance frequency and, more important, to a decrease of the total polarizability. The other role of the second loop is in reducing the magnetoelectric (bianisotropic) coupling effects. This can be seen from the fact that the sum of the two loop currents

is rather uniform around the loop, which is not so for an isolated broken loop.

We have discussed how the two subsystems, one providing electric and the other one providing magnetic response, interact in a composite. It was shown that it is most important that the coupling is minimized by proper positioning of loops in the symmetry planes of the wire array. Otherwise, only one of the effective parameters can be negative. With this respect, it is clear that the design of isotropic composites with negative parameters is not simple: interaction of wires and loops will be rather strong if the loop inclusions form an isotropic structure.

Other possible realizations can be based on the use of particles of only one type, for example omega or chiral inclusions. The advantage of this approach is that both parameters can have the same or very similar frequency dispersion, but on the other hand, the resonant losses become very high.

Our studies of two-layer planar waveguides with usual and Veselago layers lead to the following conclusions. Both TE and TM modes can change the dispersion sign. This is possible because the energy transport directions are opposite in the two layers, so there exists a spectral point, where the power flows in the two layers compensate each other. Under certain relations between the permeabilities and thicknesses of the layers there exists a non-dispersive TE mode without a low-frequency cutoff. Its slow-wave factor is constant and does not depend on the layer thicknesses. In contrast with the ordinary two-layered waveguide, where a dominant TM_0 mode has no low-frequency cutoff, in the new waveguide its analog disappears under certain conditions. In addition, such a wave can be non-dispersive under certain relations between the permittivities and thicknesses of the layers. Furthermore, this mode has a high-frequency cutoff under certain conditions. There exist both TE and TM super-slow waves, whose slow-wave factor is not restricted by the values of the permittivities and permeabilities of the layers. The fields of these waves decay exponentially in both layers from their interface in case of large propagation constants. It is remarkable, that such super-slow modes are caused not by large values of the permeability or permittivity, like it takes place near a resonance in ferrite or plasma, but by the layer thickness effects.

Novel metamaterials with negative parameters bring new design possibilities when included in one-dimensional regular lattices (PBG structures). The main conclusion is that these materials offer a possibility to design electromagnetic crystals with extremely wide stop bands. Although only one-dimensional structures have been considered, we expect that this conclusion can be valid for more general two- and three dimensional periodical media as well.

Obviously, in any practical realization of such waveguides and period-

ical media material losses and frequency dispersion of the parameters will essentially modify the system properties, so more studies of these effects are needed.

References

1. Veselago, V.G. (1968) The electrodynamics of substances with simultaneously negative values of ϵ and μ, *Soviet Physics Uspekhi* **10**, 509-514 (originally pubished in Russian in *Uspekhi Fizicheskikh Nauk* **92**, 1967, 517-526).
2. Shelby, R.A., Smith, D.R. and Schultz, S. (2001) Experimental verification of a negative index of refraction, *Science* **292**, 77-79.
3. Valanju, P.M., Walser, R.M. and Valanju, P.A. (2002) Wave refraction in negative-index media: always positive and very inhomogeneous, *Phys. Rev. Lett.* **88**, 187401(1-4).
4. Maslovski, S.I. (2002) On the problem of negative refraction, submitted to *Phys. Rev. Lett.*
5. Pendry, J.B., (2000) Negative refraction makes a perfect lens, *Phys. Rev. Lett.* **85**, 3966-3969.
6. Smith, D.R., Padilla, W.J., Vier, D.C., Nemat-Nasser S.C. and Schultz, S. (2000) Composite media with simultaneously negative permeability and permittivity, *Phys. Rev. Lett.* **84**, 4184-4187.
7. Pendry, J.B., Holden, A.J., Robbins D.J. and Stewart, W.J. (1999) Magnetism from conductors and enhanced nonlinear phenomena, *IEEE Trans. Microwave Theory Tech.* **47**, 2075-2084.
8. Kostin, M.V. and Shevchenko, V.V. (1993) Theory of artificial magnetic substances based on ring currents, *Sov. J. Communic. Technology and Electronics* **38**, 78-83.
9. Kostin, M.V. and Shevchenko, V.V. (1994) Artificial magnetics based on double circular elements, Proc. of *Bianisotropics'94,* Périgueux, France, 49-56.
10. Brown, J. (1960) *Artificial dielectrics,* in: Progress in dielectrics **2**, pp. 195-225.
11. King, R.J. , Thiel, D.V. and Park, K.S. (1983) The synthesis of surface reactance using an artificial dielectric, *IEEE Trans. Antennas and Propagat.* **31**, 471-476.
12. Pendry, J.B., Holden, A.J., Stewart, W.J. and Youngs, I. (1996) Extremely low frequency plasmons in metallic mesostructures, *Phys. Rev. Lett.* **76**, 4773-4776.
13. Simovski, C.R. and Sauviac, B. (2002) Toward creating the isotropic media with negative refraction, submitted to *Phys. Rev. B.*
14. Simovski, C.R., Sauviac, B. and Tretyakov, S.A. (2002) Double split-ring resonators: analytical and numerical modelling, submitted to *IEEE Trans. Antennas Propag.*
15. Marques, R., Medina, F. and El-Idrissi, R.R. (2002) Role of bianisotropy in negative permeability and left-handed metamaterials, *Phys. Rev. B* **65**, 14440(1-6).
16. Saadoum, M.M.I. and Engheta, N. (1992) A reciprocal phase shifter using novel pseudochiral or Omega medium, *Microwave and Optical Technology Lett.* **5**, 184-188.
17. Saadoun, M.M.I. and Engheta, N. (1994) Theoretical studies of electromagnetic properties of non-local Omega media, in *Progress in Electromagnetic Research* **PIER9**, pp. 351-397.
18. Mariotte, F., Sauviac, B. and Tretyakov, S.A. (2000) Artificial bianisotropic composites, Chapter 18 of the book *Frontiers of Mathematical Methods in Electromagnetics,* R. Mittra and D. Werner, Eds., IEEE Press.

19. Simovski, C.R., Tretyakov, S.A., Sochava, A.A., Sauviac, B. and Kharina, T.G. (1997) Antenna model for conductive omega particles, *J. of Electromagnetic Waves Applic.* **11**, 1509-1530.
20. Kharina, T.G., Tretyakov, S.A., Simovski, C.R., Sochava, A.A. and Bolioli, S. (1998) Experimental study of artificial Omega media, *Electromagnetics* **18**, 437-457.
21. Tretyakov, S.A. (2001) Meta-materials with wideband negative permittivity and permeability, *Microwave and Optics Technology Lett.* **31**, 163-165.
22. Smith, D.R. and Kroll, N. (2000) Negative refractive index in left-handed materials, *Phys. Rev. Lett.* **85**, 2933-2936.
23. Maslovski, S.I., Tretyakov, S.A. and Belov, P.A. (2002), Wire media with negative effective permittivity: a quasi-static model, *Microwave and Optical Technol. Lett.* **35**, 47-51.
24. Moses, C.A. and Engheta, N., (2001) Electromagnetic wave propagation in the wire medium: a complex medium with long thin inclusions, *Wave Motion* **34**, 301-317.
25. Belov, P.A., Tretyakov, S.A. and Viitanen, A.J. (2002) Dispersion and reflection properties of artificial media formed by regular lattices of ideally conducting wires, *J. Electromagnetic Waves and Applications* **16**, 1153-1170.
26. Sipe, J.E. and Van Kranendonk, J. (1974) Macroscopic electromagnetic theory of resonant dielectrics, *Phys. Rev. A* **9**, 1806-1822.
27. Simovski, C.R., He, S. and Popov, M., (2000), On the dielectric properties of thin molecular or composite layers, *Phys. Rev. B* **62**, 13718-13724.
28. Simovski, C.R. and Sauviac, B., (2002), On the bulk averaging approach for obtaining the effective parameters of thin magnetic granular films, *European Physical Journal: Applied Physics* **AP 17**, 11-20.
29. Tretyakov, S.A. and Viitanen, A.J. (2000) Plane waves in regular arrays of dipole scatterers and effective medium modelling, *J. Opt. Soc. Am.* **A 17**, 1791-1799.
30. Jaggard, D.L., Mickelson, A.R. and Papas, C.T. (1979) On electromagnetic waves in chiral media, *Appl. Phys.* **18**, 211-216.
31. Tretyakov, S.A., Mariotte, F., Simovski, C.R., Kharina, T.G. and Heliot, J.-P. (1996) Analytical antenna model for chiral scatterers: Comparison with numerical and experimental data, *IEEE Trans. Antennas Propag.* **44**, 1006-1014.
32. Auzanneau, F. and Ziolkowski, R.W. (1998) Theoretical study of synthetic bianisotropic materials, *J. Electromagn. Waves Applic.* **12**, 353-370.
33. Ziolkowski, R.W. (1997) The design of Maxwellian absorbers for numerical boundary conditions and for practical applications using engineered artificial materials, *IEEE Trans. Antennas Propag.* **45**, 656-671.
34. Tretyakov, S.A. and Kharina, T.G. (2000) The perfectly matched layer as a synthetic material with active inclusions, *Electromagnetics* **20**, 155-166.
35. Nefedov, I.S. and Tretyakov, S.A. (2002) Waveguide containing a backward-wave slab, submitted to *Radio Science.*
36. Engheta, N. (2002) Guided waves in paired dielectric-metamaterial with negative permittivity and permeability layers, in Proc. of *National Radio Science Meeting*, Boulder, Colorado, USA, p. 66.
37. Nefedov, I.S. and Tretyakov, S.A. (2002) Photonic band gap structure containing metamaterial with negative permittivity and permeability, to appear in *Phys. Rev. E.*

III.

PHOTONIC BAND GAP MATERIALS

ON THE ELECTROMAGNETIC MODELLING OF LEFT-HANDED METAMATERIALS

R. MARQUÉS and F. MEDINA
Departamento de Electricidad y Electrónica,
Universidad de Sevilla, Av. Reina Mercedes s/n, 41012 Sevilla, Spain

F. MESA
Departamento de Física Aplicada 1,
Universidad de Sevilla, Av. Reina Mercedes s/n, 41012 Sevilla, Spain

AND

J. MARTEL
Departamento de Física Aplicada 3,
Universidad de Sevilla, Av. Reina Mercedes s/n, 41012 Sevilla, Spain

Abstract. The electromagnetic modelling of discrete left-handed microwave metamaterials is discussed. A continuous-medium approach is proposed for the analysis of a wide class of left-handed and negative permeability media made by placing metallic inclusions in a host dielectric medium. This includes all artificial media made by the superposition of an artificial plasma and a negative magnetic permeability medium made of split ring resonators. The proposed model allows for the consideration of both edge- and broadside-coupled split rings resonators. It also allows for the use of wires and/or metallic plates in the plasma simulation. Other related physical effects that can appear in these artificial media, such as bianisotropy, are also taken into account. The numerical computations provided by the model are compared with full-wave numerical simulations and experimental results, showing a good agreement. The advantages and disadvantages of the different left-handed metamaterial designs considered along the text are also discussed.

1. Introduction

Media having dielectric permittivity, ϵ, and magnetic permeability, μ, both negatives were first proposed and analyzed in [1]. Since the **E**, **H** fields and the wavevector **k** form a left handed system in such media, Veselago named it as *Left-Handed Media* (LHM). This denomination will be used in the

S. Zouhdi et al. (eds.), Advances in Electromagnetics of Complex Media and Metamaterials, 123–140.

following, although other possibilities –such as double negative or negative refractive index media– are possible. Backward wave propagation, negative refractive index, inverse Doppler effect and anomalous Cerenkov radiation are other relevant effects in LHM [1]. Veselago focused his search for actual left-handed materials in hypothetical solid-state composites having "first, a sufficiently mobile charge carriers system, and, second, an interacting magnetic moments system" [1], i.e., a complex spin-plasma solid state material. Although Veselago's search was not successful, an alternative approach does success recently [2]. The LHM proposed in [2] was a composite material that behaves as a continuous media at microwave frequencies. It is built up as the superposition of an artificial plasma working below the plasma frequency and a regular array of high diamagnetic *particles*, which behave as an effective Negative Magnetic Permeability Media (NMPM). The artificial plasma is made by an infinite array of parallel wires [3] and the recently proposed Split Ring Resonators (SRRs) [4] are used as diamagnetic particles. The term *metamaterial* applied to this and other similar realizations, [5], comes from the fact that they are *artificial* media presenting electromagnetic properties which were not present in *nature*.

With regard to their architecture, the reported left-handed metamaterials belong to a wide class of artificial media which are used since long for electrical engineers. These artificial media include artificial dielectrics [6, 7], artificial plasmas [3], artificial diamagnetic materials and artificial chiral media [8]. All these materials are made by inserting electrically small metallic *particles* in a host dielectric medium and have been employed in the design of microwave lenses, coatings and other microwave devices [7, 8]. They are also useful in teaching since they allow for easy simulations of many optical properties of natural media at microwave frequencies. Moreover, the electromagnetic behavior of the reported diamagnetic particles for left-handed metamaterials –the SRRs [4]– resembles, in some aspects, that of the *chiral* and *pseudochiral* particles used in the design of bi-(iso/aniso)-tropic artificial media [9, 10, 11]. The above particles are always resonant, having their most useful properties near the resonance. In all these cases, the Kramers-Kronig relations impose a very similar behavior to the frequency dependence of all the constitutive parameters of the media [8, 12]. Therefore, regions of negative permeability and/or permittivity can be expected for chiral and pseudochiral particles (at least when losses are neglected) at those frequencies where cross-polarization effects are also present. Conversely, bi-(iso/anisotropic)-effects can be also expected in left-handed metamaterials [13].

A detailed electromagnetic analysis of all these artificial media, making use of the electromagnetic diffraction theory, will lead us to the theory of periodical structures [7] and photonic band-gap materials. However, as far

as the size of the metallic inclusions is much smaller than the free space wavelength, a continuous-medium approach will properly account for the main electromagnetic properties of the material. A great variety of homogeneization procedures [14] have been proposed to carry out the continuous-medium description of composite materials. Thus, two important questions can be posed: when the continuous-medium approach can be considered valid?, and which homogeneization procedure should be used?. The answer to these questions will mainly depend on the required accuracy. Usually, for most practical realizations of left-handed and chiral media, an inclusion size of a tenth of the free space wavelength is considered small enough for the application of the continuous-medium approach [2, 5, 15, 10, 11]. The well-known Lorentz local field theory [7] and Maxwell-Garnett formulas [11, 14] are usually considered appropriate for homogeneization. However, in some cases, the application of these formulas only implies a small correction to the simplest approximation for the susceptibilities of the medium: the particle polarizabilities multiplied by their volume density [13]. On the other hand, most experiments carried out with the aforementioned artificial media only involves the measurement of the absolute values of the transmission coefficients for the first diffraction lobe. Phase measurements, and/or the consideration of higher order lobes, will likely reveal the limitations of the continuous-medium approach (or would require smaller ratios between the particle size and the free space wavelength).

In this contribution, a continuous-medium model will be developed for the analysis of left-handed metamaterials composed of the superposition of an artificial plasma media and a NMPM medium made of a regular array of SRRs. This model includes most of the reported experimental realizations of left-handed metamaterials [2, 5, 16, 17] as well as many other related structures. 3-D artificial plasma made by wires [3] and 2-D artificial plasma made by wires and/or metallic plates [3] will be considered, as well as 1-D artificial plasma simulations by hollow metallic waveguides [17]. Two main designs for the SRRs will be analyzed: Edge-Coupled SRRs (EC - SRRs) [4] and Broadside-Coupled SRRs [13]. A comparative analysis of all the above alternatives will be carried out. Experimental results will be provided in order to validate the proposed model and to check its accuracy.

2. Artificial Plasma Media

As it is well known, a lossless plasma of *plasma frequency* ω_p can be characterized by an effective dielectric constant given by

$$\epsilon_{\text{eff}} = \epsilon_0 \left(1 - \frac{\omega_p^2}{\omega^2} \right). \tag{1}$$

Three- and two-dimensional arrangements of metallic wires and plates have been used since long by electrical engineers for simulating plasmas at microwave frequencies [3]. A 3-D simulation can be obtained by means of a 3-D grid of infinitely long metallic wires as is shown in Fig. 1a [3, 18]. For 2-D

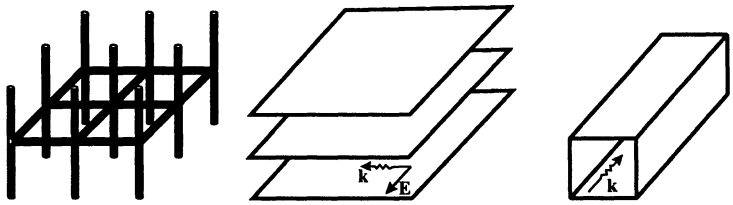

(a) (b) (c)

Figure 1. Artificial plasma media can be made of an array of wires, and/or metallic plates. Fig. 1a: 3-D artificial plasma made of a cubic array of metallic wires. Fig. 1b: 2-D artificial plasma made of an array of parallel metallic plates (the proper propagation direction and polarization are shown). Fig. 1c: 1-D simulation by a hollow metallic waveguide.

simulations, 2-D arrays or grids of infinitely long metallic wires also provide a good solution [3, 19]. However, a 2-D arrangement of metallic plates as that shown in Fig. 1b can provide an easier design in many cases [3, 16]. Finally, a hollow metallic waveguide (see Fig. 1c) simulates properly 1-D problems [17]. All these simulations provide artificial media with effective negative dielectric permittivity at frequencies below the plasma frequency of the considered medium.

As a first step, the array of parallel metallic plates shown in Fig. 1b will be analyzed. This design presents the obvious advantage that only one parallel-plate waveguide has to be considered for both the analysis and the experiment. However, plasma simulation is restricted to two dimensional problems. Consider a TE_{01} mode propagating along the parallel-plate waveguides of Fig. 1b. Neglecting losses, the phase constant of this mode is given by

$$k = \omega \sqrt{\mu_0 \epsilon_0 \left(1 - \frac{\omega_0^2}{\omega^2}\right)}, \tag{2}$$

where

$$\omega_0 = \frac{\pi}{a} \sqrt{\frac{1}{\mu_0 \epsilon_0}} \tag{3}$$

is the cutoff frequency of the waveguide (a is the distance between the plates). This phase constant is exactly the same as that for a TEM wave in a lossless plasma with plasma frequency $\omega_p = \omega_0$. Moreover, the mean electric

and magnetic fields in the waveguide cross-section are both perpendicular to the direction of propagation (the mean longitudinal magnetic field vanishes for TE modes), thus forming a "mean" TEM wave. In addition, the mean volume polarization in the array of Fig. 1.b (defined as $P = K/(j\omega a)$, where K is the surface current on the plates) is related to the mean electric field in the waveguide cross section by

$$P = -\epsilon_0 \frac{\omega_0^2}{\omega^2} \langle E \rangle \ , \tag{4}$$

where $\langle E \rangle$ is the mean electric field in the waveguide cross section. Thus, the considered TE_{01} mode exactly simulates the propagation of a TEM wave in a lossless plasma medium. Since the considered structure supports this mode for electric field polarization and wavevector both parallel to the plates, this simulation is restricted to this particular wave polarization and direction of propagation (for polarization perpendicular to the plates, the effective dielectric constant is ϵ_0).

A 3-D simulation, valid for any kind of wave polarization and direction of propagation, would require the 3-D grid of wires shown in Fig. 1a. The analysis of this configuration [3, 18] clearly becomes more involved than the 2-D simulation of Fig. 1b. In particular, the cutoff/plasma frequency of the medium is given by [18]

$$\omega_0 = \frac{\pi}{a} \sqrt{\frac{2}{\ln(a/r)}} \ , \tag{5}$$

where a is the lattice parameter and r the wire radius. Other wire configurations are useful for 2-D simulations [3],[19]. However, as was mentioned earlier, the parallel-plate configuration provides a simpler alternative in this case.

Finally, it can be easily realized that Eq. 2 remains valid for any type of hollow metallic waveguide. This fact suggest that a hollow metallic waveguide can simulate a lossless plasma in many one-dimensional problems [17]. In particular, a careful inspection of Fig. 1b shows that, for the considered TE_{01} mode propagation, there are many symmetry planes that can be substituted by additional metallic plates without affecting the field configuration. These planes are perpendicular to both the electric field and the plates (and then parallel to the direction of propagation). Therefore, these planes divide the whole structure in many shielded waveguides. One of these hollow metallic waveguides is shown in Fig. 1c. This waveguide supports the same TE_{01} mode considered for the parallel plate array of Fig. 1b, thus being a 1-D plasma simulation.

As our interest focuses in *transparent* left-handed media, and since almost-lossless metallic plates and wires are easily found at microwave

frequencies, lossless media have been specifically considered. The analysis of losses in plasma simulations and artificial plasma media can be found in [3, 18, 19] and references therein.

3. Artificial Negative Magnetic Permeability Media

Low-losses NMPM as those needed for building up left-handed media are not present in nature. Artificial NMPM made by inserting metallic inclusions in a dielectric medium were first proposed in [4]. These metallic inclusions are, in fact, small size resonators with a high quality factor working at microwave frequencies. In order to obtain an effective NMPM, the metallic inclusion must also show a strong diamagnetic behavior above the resonance. Thus, the composite media formed by these inclusions shows a region of negative effective permeability at frequencies above this resonance. The SRRs [4] fulfill all these requirements and can be easily manufactured by using the well-known and widespread planar technology. Therefore, they are at present the most extended alternative for building NMPM. Two kind of SRRs have been proposed, the Edge-Coupled SRR (EC-SRR) [4] and the Broadside-Coupled SRR (BC-SRR) [13]. Both kind of SRRs will be analyzed in the following.

3.1. ANALYSIS OF THE EDGE-COUPLED AND BROADSIDE-COUPLED SPLIT RING RESONATORS

The analyzed structures are shown in Figs.2a (EC-SRR) and 2b (BC-SRR). Both the EC-SRR and the BC-SRR show a very similar qualitative behavior when they are excited by an external time-harmonic varying magnetic field having a non-vanishing component perpendicular to the rings, B_z^{ext}. According to Faraday's law, this field induces an electromotive force around the rings. The electromotive force gives rise to current loops on the rings, which are closed through the capacitive gap between the rings, thus creating a strong electric field in the gap. Consequently, the whole structure behaves as an externally driven LC circuit. This circuit is formed by the series connection of two capacitances in parallel with an inductance (see Fig. 3). Each capacitance in Fig. 3 corresponds to the total capacitance between the rings in the upper and the lower half of the SRR. That is, $C \simeq \pi r_0 C_{\text{pul}}$, where C_{pul} is the per unit length capacitance in the gap between the rings. The inductance is the total inductance, L, of the rings. The resonance frequency is then given by

$$\omega_0^2 = \frac{2}{\pi r_0 C_{\text{pul}} L} \,. \tag{6}$$

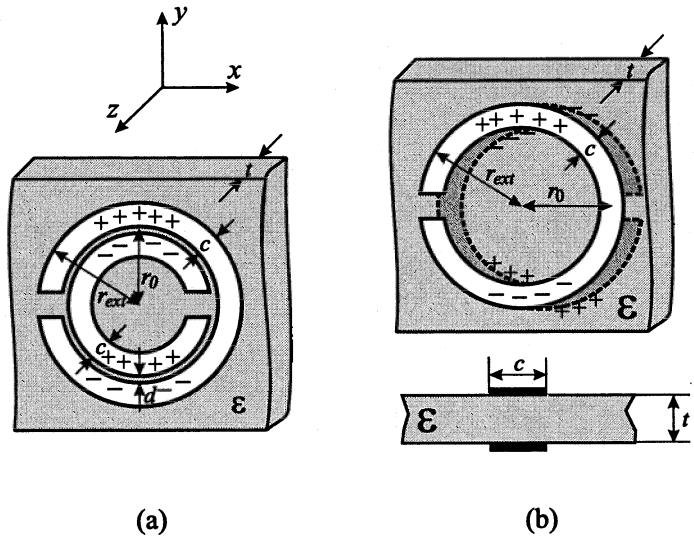

Figure 2. Split Ring Resonators (SRRs) for the design of NMPM. Fig. 2a: Edge-coupled SRR (EC-SRR). Fig. 2b: Broadside-coupled SRR (BC-SRR).

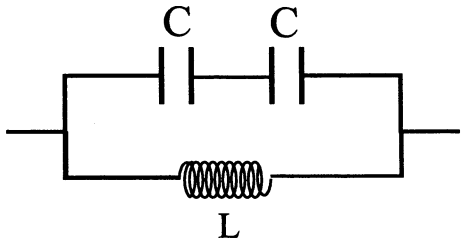

Figure 3. Equivalent circuit for both the EC-SRR and the BC-SRR of Fig. 2.

A more detailed analysis, which can be found in [13], also gives the following magnetic polarizability along the z-axis of the SRR:

$$m_z = \alpha_{zz}^{mm} B_z^{\text{ext}} \quad ; \quad \alpha_{zz}^{mm} = \frac{\pi^2 r_0^4}{L}\left(\frac{\omega_0^2}{\omega^2} - 1\right)^{-1} . \tag{7}$$

Notice that according to Eq. 7 the SRRs behave as highly diamagnetic particles above the resonance, as is required for NMPM design.

The two types of SRRs also show a quasi-static non-resonant electric polarizability along the x- and y-axis, which can be approximated by the polarizability of a metallic disk [7, 13]:

$$\alpha_{xx}^{ee} = \alpha_{yy}^{ee} = \epsilon_0 \frac{16}{3} r_{\text{ext}}^2 , \tag{8}$$

with r_{ext} being the external radius of the SRR.

Apart from cross-polarization effects, which will be accounted for in next section, equations 6 to 8 describe the behavior of both the BC-SRR and the EC-SRR provided L and C_{pul} are known. If the ring curvature is neglected, there are many design formulas for the calculation of C_{pul}. We have used those summarized in Tables 2.6 and 2.7 of [20] for the BC-SRR and the EC-SRR respectively –these expressions are, in turn, based on [21] and [22] respectively. The total inductance, L, has been approximated as that of a single ring of width c and average radius r_0. The suitability of this approximation for the BC-SRR is apparent. For the EC-SRR, this approximation is expected to work out properly considering that the total current around the SRR flows alternatively on the inner and the outer rings. This fact suggestes that an *equivalent* single ring of average radius r_0 and width c can model the actual configuration for the obtaining of L. In both cases L has been computed by using the variational formula: $L = 2U_m/I^2$, where U_m is the magnetostatic energy and I the total current on the ring. A uniform current distribution has been assumed for practical computations, which provides a reasonable accuracy because of the variational nature of the expression for L. Ohmic losses can be also accounted for by introducing a *complex* inductance $\hat{L} = L + R/(j\omega)$ instead of L into the above formulas, where R is the total resistance of the *equivalent* ring. If, as usual, the metallization thickness is larger than the skin depth, δ, at the operating frequency, this resistance can be approximated as

$$R = \frac{\pi r_0}{c\delta\sigma}\,, \tag{9}$$

where it has been assumed that the current flows on both sides of the rings (for the EC-SRR) or on the inner side of each ring (for the BC-SRR).

Following the reported model, a computer code has been developed for computing the SRR parameters. Computed results for the resonance frequency of some particular EC-SRR and an BC-SRR are shown in Figs. 4a and 4b respectively. Experimental results, obtained by placing the considered SRRs into a rectangular waveguide and measuring the *dip* in the $|S|_{12}$ coefficient, are also shown in the figures. The good agreement between theory and experiment evidences the accuracy of the model. A comparative analysis of the EC-SRR and the BC-SRR reveals that higher values for C_{pul} can be achieved in this latter configuration without affecting the total inductance, L. This increase can be achieved, for instance, by increasing the dielectric constant of the slab between the metallic strips, and/or decreasing the slab thickness. This increase in C_{pul} will lead to a considerable reduction in the frequency of resonance, thus allowing for a considerable reduction in the electrical size of the particle at resonance. This fact is of crucial

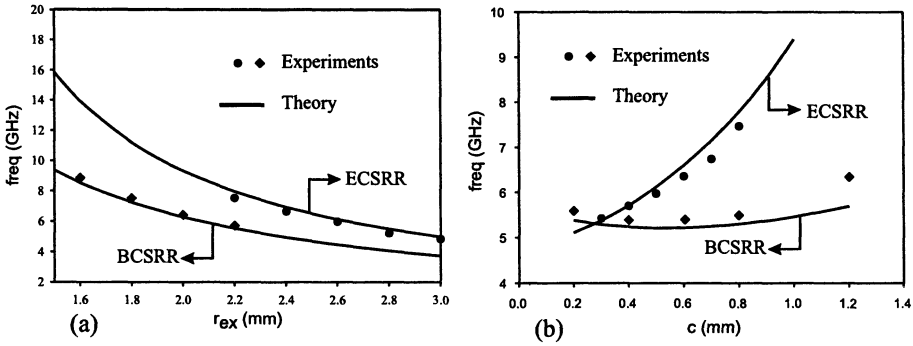

Figure 4. Computed and experimental results for the resonance frequency of the EC-SRR and the BC-SRR of Fig. 2, with $t = 0.49$ mm, $\epsilon = 2.43\epsilon_0$ and $d = 0.2$ mm (for the EC-SRR only). Fig. 4a: $c = 0.5$ mm and r_{ext} variable. Fig. 4b: $r_{\text{ext}} = 2.6$ mm for the EC-SRR, $r_{\text{ext}} = 2.3$ mm for the BC-SRR and c variable.

importance for the continuous media description of any discrete medium formed by SRRs.

3.2. CROSS-POLARIZATION EFFECTS IN EDGE-COUPLED SPLIT RING RESONATORS

A careful consideration of the behavior of the SRRs analyzed above shows that the closure of the current loops through the rings gap (by means of a field displacement current) must be associated with a non-vanishing per unit length polarization in the gap (see Figs. 2). This effect is present in both the EC-SRR and the BC-SRR. However, the polarization along the upper ($y > 0$) and lower ($y < 0$) halves mutually cancel out in the BC-SRR whereas they add up in the EC-SRR. Thus, when the EC-SRR is excited by an external magnetic field, a non-zero dipolar electric moment appears in addition to the magnetic moment given by Eq. 7. This electric dipole is directed along the y-axis and can be approximated by [13]

$$p_y = j\alpha_{yz}^{em} B_z^{\text{ext}} \;\; ; \;\; \alpha_{yz}^{em} = 2\omega_0 \pi r_0^3 C_{0,\text{pul}} d_{\text{eff}} \frac{\omega_0}{\omega} \left(\frac{\omega_0^2}{\omega^2} - 1 \right)^{-1} , \qquad (10)$$

where $C_{0,\text{pul}}$ is the free-space per unit length gap capacitance and d_{eff} is an effective distance that, in a first order approximation, can be taken as $d_{\text{eff}} = c + d$.

When the EC-SRR is excited by an external electric field with non-zero y-component, Onsager symmetry principle for the generalized susceptances [23] imposes that a magnetic dipole must be induced in the structure. This magnetic dipole must be directed along the z-axis and it is given by

$$m_z = -j\alpha_{yz}^{em} E_y^{\text{ext}} . \qquad (11)$$

Clearly, the presence of the above magnetic dipole must be associated with the appearance of an additional current on the EC-SRR. This current, in turn, will induce a non-zero y-directed electric dipole, as was shown in the previous paragraphs. Thus, the EC-SRR will present an additional resonant electric polarizability along the y-axis, which is found to be [13]

$$\alpha'^{ee}_{yy} = 4\omega_0^2 r_0^2 C_{0,\mathrm{pul}}^2 L d_{\mathrm{eff}}^2 \left(\frac{\omega_0^2}{\omega^2} - 1\right)^{-1} . \tag{12}$$

It is interesting to note that, near the resonance,

$$\alpha^{mm}_{zz}\alpha'^{ee}_{yy} \to |\alpha^{em}_{yz}|^2 . \tag{13}$$

This relation is usually found for metallic *particles* showing cross-polarization effects [12]. It suggests that artificial bi-(iso/aniso)-tropic media made of metallic inclusions satisfying Eq. 13 could also present regions of negative magnetic permeability and/or negative dielectric permittivity (at least, this must be true in the lossless limit).

3.3. HOMOGENEIZATION

In summary, both the EC-SRR and the BC-SRR are characterized by the following relations:

- EC-SRR:

$$p_x = \alpha^{ee}_{xx} E_x^{\mathrm{ext}} \tag{14}$$
$$p_y = (\alpha^{ee}_{yy} + \alpha'^{ee}_{yy}) E_y^{\mathrm{ext}} + \jmath\alpha^{em}_{yz} B_z^{\mathrm{ext}} \tag{15}$$
$$m_z = -\jmath\alpha^{em}_{yz} E_y^{\mathrm{ext}} + \alpha^{mm}_{zz} B_z^{\mathrm{ext}} \tag{16}$$

- BC-SRR:

$$p_x = \alpha^{ee}_{xx} E_x^{\mathrm{ext}} \tag{17}$$
$$p_y = \alpha^{ee}_{yy} E_y^{\mathrm{ext}} \tag{18}$$
$$m_z = \alpha^{mm}_{zz} B_z^{\mathrm{ext}} , \tag{19}$$

where the polarizabilities α are given in the preceding sections in terms of the total inductance, L, and the per unit length capacitances, C_{pul} and $C_{0,\mathrm{pul}}$, of each structure.

As far as the lattice parameter and the electrical size of the SRR can be considered small at the resonance frequency (Eq. 6), an arrangement of these *particles* can be viewed as an homogeneous medium. The constitutive

parameters of that homogeneous medium should be deduced from Eqs. 14–16 or Eqs. 17–19 by a suitable homogeneization procedure. In the most general case, these constitutive parameters will be given by

$$\mathbf{D} = \epsilon_0(\overline{\overline{1}} + \overline{\overline{\chi}}_e) \cdot \mathbf{E} - j\sqrt{\epsilon_0\mu_0}\ \overline{\overline{\kappa}} \cdot \mathbf{H} \tag{20}$$

$$\mathbf{B} = j\sqrt{\epsilon_0\mu_0}\ \overline{\overline{\kappa}}^{T} \cdot \mathbf{E} + \mu_0(\overline{\overline{1}} + \overline{\overline{\chi}}_m) \cdot \mathbf{H}\,, \tag{21}$$

where $\overline{\overline{\chi}}_e$, $\overline{\overline{\chi}}_m$ and $\overline{\overline{\kappa}}$ are the constitutive *macroscopic* tensor susceptibilities of the medium. The simplest approximation is to take $\chi_e = \alpha^{ee}/V$, $\chi_m = \mu_0\alpha^{mm}/V$ and $\kappa = -\sqrt{\mu_0/\epsilon_0}\,\alpha^{em}/V$, where V is the volume of the unit cell. This approximation neglects any difference between the *external* field acting on the SRR and the *average* field in the unit cell. However, in many cases, it may provide an useful approximation to the behavior of the medium. For cubic lattices, the well-known Maxwell-Garnett formulas, whose extension to bianisotropic media can be found in [11], can provide a more accurate alternative. Both approaches will be used in the following, and it will be shown that both lead to very similar results.

4. Composite Left-Handed Metamaterials

The usual way of building left-handed metamaterials consists in the superposition of two artificial composites of negative dielectric permittivity and negative magnetic permeability [2, 5, 16]. In [2] and [5], EC-SRRs and wires are used for providing negative dielectric permittivity and magnetic permeability respectively. In [16], BC-SRRs and parallel-plate waveguides are used for the same purpose. The first experimental realization of a left-handed metamaterial [2] only presents left-handed behavior for waves propagating in a given direction and for a given polarization, thus being a 1-D simulation. However, the experimental verification of many of the new physical effects present in left-handed media, such as negative refractive index [15] or planar lens behavior [24] needs of, at least, a 2-D realization. Metamaterials proposed in [5] and [13] provide this 2-D realization.

Usually, it is assumed that the electric and magnetic responses of the negative dielectric permittivity medium (NDPM) and the NMPM which compose the metamaterial are decoupled. Thus, the dielectric and magnetic susceptibilities of the resulting LHM are, in fact, the same as those of the aforementioned NDPM and NMPM respectively. However, this assumption is not always justified. For instance, the relative location and orientation of both the wires and the SRRs is crucial in forming the left-handed behavior for the metamaterial proposed in [2], as is reported in [25]. A similar observation can be made for the SRRs and plates in the medium proposed in [16]. As a general rule, the superposition of both the NDPM

and the NMPM should minimize the coupling between the constituents of both media, thus providing the aforementioned division between the electric and magnetic responses of the composite metamaterial [25]. This rule is, of course, only qualitative and should be verified by detailed full-wave numerical simulations and/or by experiment.

Assuming that the electric and magnetic responses of the constitutive NDPM and NMPM are decoupled, the determination of the macroscopic behavior of the composite LHM simply reduces to the computation of the susceptibilities of these two media. For both wires and plates artificial plasma media, the electric susceptibility (for the appropriate polarization and wave-propagation direction) can be written as

$$\chi_e = -\frac{\omega_p^2}{\omega^2} , \tag{22}$$

where ω_p is the *plasma frequency* of the medium. For a system of parallel plates, ω_p is simply the cutoff frequency (Eq. 3). For a system of wires, ω_p is approximately given by Eq. 5. Losses, if necessary, can be taken into account following the general procedures in [3] or [18]. However, it can be easily understood that, except for very thin wire media, losses in the composite LHM must be mainly associated with ohmic losses in the SRRs. The macroscopic susceptibilities of the SRR-made NMPM can be obtained from the polarizabilities of the corresponding EC-SRRs or BC-SRRs by means of the appropriate homogeneization procedure. A procedure for obtaining these polarizabilities, which includes ohmic losses in the SRRs, has been developed in the preceding sections.

Following the above schema, a computer code has been developed for the analysis of the aforementioned left-handed metamaterials. A first test for the reported method of analysis has been the computations of the phase constant, k, for the NMPM and the LHM reported in Figs. 2a and 2c of [2]. These media are sketched in Fig. 5 –see also [2] and [25]. Since the NMPM is made by a regular array of EC-SRR, the composite medium presents bianisotropic effects. For TEM waves with the considered polarization (E_y, B_z) and propagation direction (x), the phase constant is given by [13]

$$k_x = \omega\sqrt{\mu_{zz}\epsilon_{yy} - \mu_0\epsilon_0\kappa_{yz}^2} , \tag{23}$$

which differs from the usual expression for non bi-(iso/aniso)-tropic media by the presence of the magnetoelectric coupling term κ_{yz}. Fig. 6 shows the results for the phase constants of both the LHM and the NMPM (which is obtained when the wires are removed), computed using our numerical code. Two different procedures have been used for the NMPM homogeneization. The first one, whose results are marked as #1 in Fig. 6, simply takes $\chi_e =$

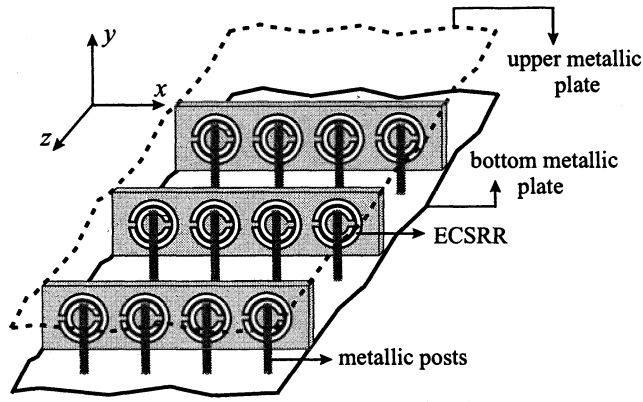

Figure 5. An sketch of the LHM analyzed in Fig. 6. Geometrical parameters for the EC-SRR are: $c = 0.8$ mm, $d = 0.2$ mm, $r_{\text{ext}} = 3.2$ mm, $t = 0.216$ mm and $\epsilon = 3.4\epsilon_0$. The lattice parameter is $a = 8$ mm and the plasma frequency for the wire media is 12 GHz.

α^{ee}/a^3, $\chi_m = \mu_0\alpha^{mm}/a^3$ and $\kappa = -\sqrt{\mu_0/\epsilon_0}\,\alpha^{em}/a^3$, with a^3 being the volume of the unit cell. The second one follows the Maxwell-Garnett schema for bianisotropic media [11] and is marked as #2 in the figure. The figure also shows the results of the full-wave numerical simulation reported in [2] as well as the measured 3 dB bandpass and stopband for the LHM and the NMPM respectively –which are obtained from Fig. 3 of [2]. The computed results reproduce qualitatively and quantitatively (with a reasonable degree of accuracy) both the experimental and the numerical results reported in [2]. It can be then deduced that the proposed model captures most of the physics of the studied phenomena, providing accurate results and physical insight. More accurate results can be expected from further improvements of the model, mainly in the computation of the L and C_{pul} parameters of the SRRs. Finally, from curves marked as #1 and #2, it can be deduced that the choice of the homogeneization procedure is not crucial for the validity of the model. However, this choice remains as an open question for future improvements. Of special relevance is the presence of a mismatch between the NMPM stopband and the LHM passband in the results computed using the proposed model. This mismatch appears as a direct consequence of the bianisotropy of the EC-SRRs [13] (clearly, it would not be present if bianisotropy was neglected). Since this mismatch also appears in both the experiments and the numerical simulations reported in [2], we can conclude that these results confirms the bianisotropy of the EC-SRR predicted by the model. Other qualitative and quantitative evidences of this bianisotropy are reported in [13].

The proposed model has been also applied to compute the *macroscopic* characteristics of other left-handed metamaterials designs. In particular a

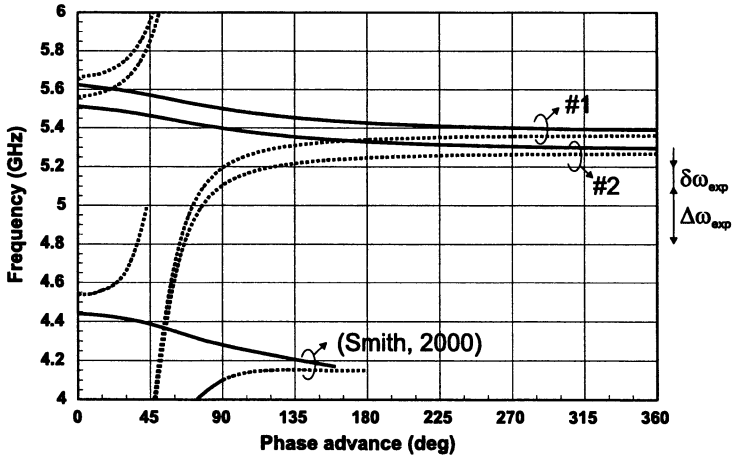

Figure 6. Numerical results for the phase advance ($k_x a$) for the LHM (solid lines) sketched in Fig. 5. The phase advance for the NMPM of Fig. 5 without the wires is also shown (dotted lines). The curves marked as #1 and #2 correspond to the different homogeneization procedures reported in the text. The results of the full-wave numerical simulation reported in (Smith, 2000) are also shown. The frequency band marked as $\Delta\omega_{\text{exp}}$ is the experimental frequency passband for the LHM (Smith, 2000). The experimental frequency stopband for the NMPM is the sum of $\Delta\omega_{\text{exp}}$ and the mismatch, $\delta\omega_{\text{exp}}$.

recently proposed 2-D isotropic metamaterial [16] has been analyzed. This design takes advantage of the aforementioned simulation of a 2-D plasma medium by a parallel-plate waveguide [3] and of the isotropic behavior of the reported BC-SRR. The proposed design is sketched in Fig. 7, for which left-handed wave propagation is expected for electric field polarization parallel to the plates. In fact, for this polarization, the parallel-plates simulates a plasma [3] and the magnetic field at the BC-SRRs location is maximum and directed perpendicular to the SRR-plane (i.e., along the direction of maximum polarizability). Notice that, since the BC-SRR does not show cross-polarization effects, the whole structure is isotropic for waves with the considered polarization and propagating in the plane of the structure. The device in Fig. 7 perfectly simulates the electromagnetic propagation along the bulk device formed by an infinite repetition of this design to the right and to the left of the figure. Therefore the NMPM to be considered in the model is a cubic array of BC-SRRs of lattice parameter a. Finally, the *plasma frequency* in Eq. 22 is given by Eq. 3. The computed results for the phase constant of electromagnetic waves with the considered polarization, propagating in the aforementioned LHM and NMPM are shown in Fig. 8. Only the simplest homogeneization procedure, referred as #1 in Fig. 6, has been used. The results obtained by using a Maxwell-Garnett approach are

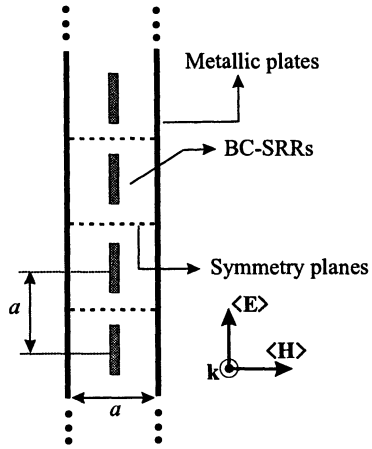

Figure 7. A 2-D left-handed metamaterial design formed by the superposition of a parallel-plate artificial plasma and a BC-SRR NMPM (front view). The polarization of the *macroscopic* mean fields is indicated (After [16]).

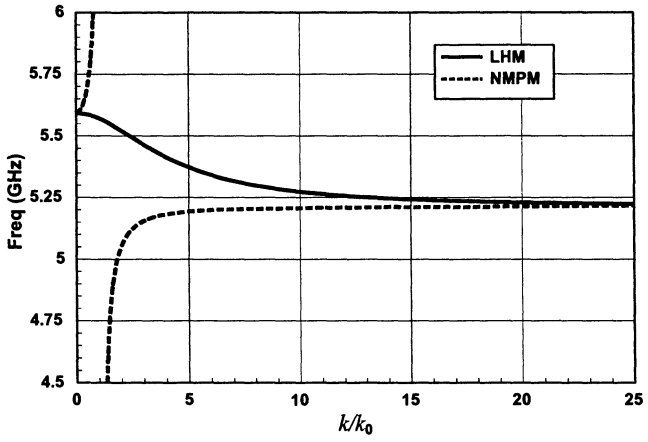

Figure 8. Computed results for the normalized (to the free space phase constant, k_0) phase constant, k_x/k_0, of the LHM sketched in Fig. 7 (solid line). The phase constant for the associated NMPM is also shown (dashed lines). Geometrical parameters are $a = 6$ mm, $r_{\text{ext}} = 2.3$ mm, $c = 0.5$ mm, $t = 0.49$ mm, $\epsilon = 2.43\epsilon_0$ (After [16]).

very similar. Since the BC-SRR does not show cross-polarization effects, there is not mismatch between the passband of the LHM and the stopband the NMPM. This 2-D LHM design can be applied in the experimental determination of negative refractive index an other LHM effects, as well as in the design of planar lenses.

An experimental verification of the results reported in Fig. 8 can be made by taking advantage of the symmetry of the structure under analysis.

In fact, it can be easily realized that the planes marked with dashed lines in Fig. 7 are symmetry planes of the structure and then perfect conducting plates can be placed at these planes without distorting the fields. Thus, the considered structure can be simulated by any of the SRR-loaded square waveguide limited by the plates and by two adjacent symmetry planes shown in Fig. 7. The experimental results for the $|S_{12}|$ transmission coefficient along one of such waveguides are shown in Fig. 9. As is predicted

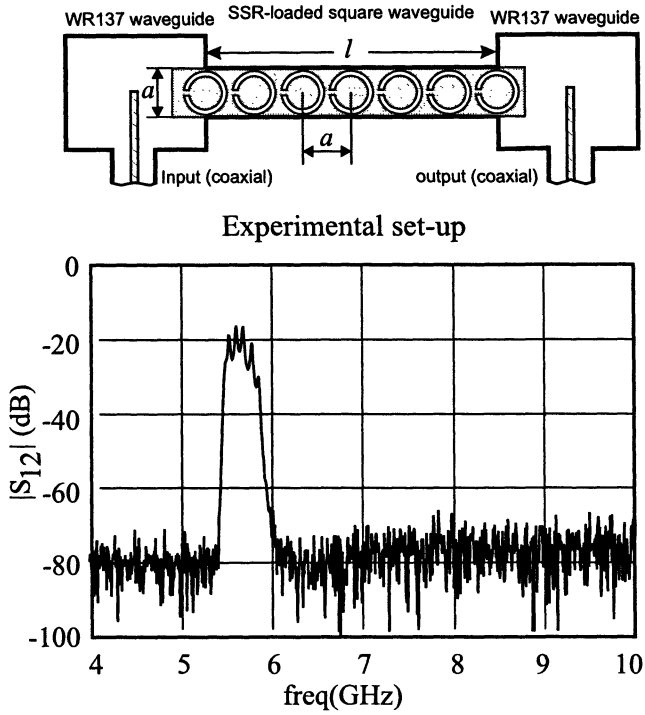

Figure 9. Experimental verification of the results shown in Fig. 8. The SRR-loaded square waveguide simulates the 2-D LHM of Fig. 7. The localization and width of the passband coincide approximately with the predictions of Fig. 8 (After [16]).

by computations, a passband appears just above the resonance frequency of the SRRs, with a bandwidth of several MHz. This results confirms the left-handed behavior of the structure as well as the suitability of the proposed model. Since the cutoff frequency of the hollow square waveguide (without the SRRs) is approximately 25 GHz, the reported transmission of electromagnetic waves through the SRR-loaded waveguide could be hardly justified by other mechanism than the here proposed. On the other hand, the transmission of electromagnetic waves through SRR-loaded metallic waveguides can be also regarded as a new one-dimensional LHM simulation

[17]. Experiments carried out with waveguides of different cross sections and lengths (and loaded with different types of SRRs) confirm this results: in all cases there appears a passband whose location and bandwidth is approximately predicted by the proposed LHM model. Moreover, neither the bandwidth nor the magnitude of the $|S_{12}|$ are substantially affected by the waveguide length and/or the number of SRRs inside the waveguide. This fact ratifies the interpretation of the electromagnetic wave transmission band in terms of an one-dimensional effective LHM. Posible applications of this effect can be in filtering and/or in the design of new small size transmission systems and other microwave devices.

5. Conclusions

It has been presented an electromagnetic model for the analysis of left-handed metamaterials composed by a regular array of edge-coupled or broadside-coupled split ring resonators (SRR) embedded in wires/plates artificial plasma media. This model, in spite of its simplicity, can be applied to a great variety of designs since it accounts for the most important physical effects of the artificial LHM, including a possible bianisotropy. A comparative analysis of the proposed edge-coupled and broadside-coupled SRRs have shown that the electrical size of the latter ones can be potentially much smaller than that of edge-coupled SSRs. This aspect becomes very important if metamaterials have to be characterized by means of a continuous-medium approach. Some designs for 1-D and 2-D left-handed metamaterials have been analyzed by using the reported model and their mutual advantages and disadvantages have been discussed.

Acknowledgements

This work has been supported by the Spanish Ministry of Science and Technology and FEDER funds (project number TIC2001-3163).

References

1. Veselago, V.G. (1968) Electrodynamics of substances with simultaneously negative electrical and magnetic permeabilities, *Soviet Phys. USPEKHI* **10**, pp. 509–514.
2. Smith, D.R., Padilla, W.J., Vier, D.C., Nemat-Nasser, S.C and Schultz, S. (2000) Composite medium with simultaneously negative permeability and permittivity, *Phys. Rev. Lett.* **84**, pp. 4184–4187.
3. Rotman, W. (1962) Plasma simulation by artificial dielectrics and parallel–plate media, *IRE Trans. on Antennas and Prop.* **AP-10**, pp. 82–95.
4. Pendry, J.B., Holden, A.J.,Robbins, D.J. and Stewart, W.J. (1999) Magnetism from conductors and enhanced nonlinear phenomena, *IEEE Trans. on Microwave Theory and Tech.*, **MTT-47**, pp. 2075–2084.

5. Shelby, R.A., Smith, D.R., Nemat-Nasser, S.C. and Schultz, S. (2001) Microwave transmission through a two-dimensional, isotropic, left-handed metamaterial, *Applied Phys. Lett.* **78**, pp. 489–491.
6. Koch, W.E. (1948) Metallic delay lenses, *Bell Syst. Tech. J.* **27**, pp. 58–82.
7. Collin, R.E. (1991) *Field theory of guided waves,* IEEE Press, N.Y.
8. Lindell, I.V., Sihvola, A,H., Tretyakov, S.A. and Viitanen, A.J. (1994) *Electromagnetic waves in chiral and bi-isotropic media.* Artech House, Boston and London.
9. Saadoun, M.M.I. and Engheta, N. (1992) A reciprocal phase shifter using novel preudochiral or Ω medium, *Microwave and Opt. Tech. Lett.* **5**, pp. 184–188.
10. Mariotte, F., Tretyakov, S.A., Sauviac, B. (1994) Isotropic chiral composite modeling: comparison between analytical, numerical, and experimental results, *Microwave and Opt. Tech. Lett* **7**, pp. 861–864.
11. Bahr, A.J. and Clausing, K.R. (1994) An approximate model for artificial chiral material, *IEEE Trans. on Antennas and Prop.* **AP-42**, pp. 1592–1599.
12. Tretyakov, S.A., Sochava, A.A., Simovski, C.R. (1996) Influence of chiral shapes of individual inclusions on the absorption in chiral composite materials, *Electromagnetics* **16**, pp. 113-127.
13. Marqués, R., Medina, F., Rafii-El-Idrissi, R. (2002) Role of bianisotropy in negative permeability and left-handed metamaterials, *Phys. Rev. B* **65** pp. 144440
14. Sihvola, A.H. (1999) *Electromagnetic mixing formulas and applications.* IEE, London.
15. Shelby, R.A., Smith, D.R., Schultz, S. (2001) Experimental verification of a negative index of refraction, *Science* **292**, pp. 77–79.
16. Marqués, R., Martel, J., Mesa, F. and Medina, F. (2002) A new 2-D isotropic left-handed metamaterial design: theory and experiment, *Microwave and Opt. Tech. Lett.* (in press).
17. Marqués, R., Martel, J., Mesa, F. and Medina, F. (2002) Left-handed media simulation and transmission of EM waves in sub-wavelength SRR-loaded metallic waveguides, *Phys. Rev. Lett.* (accepted for publication).
18. Pendry, J.B., Holden, A.J., Stewart, W.J. and Youngs, I. (1996) Extremely low frequency plasmons in metallic mesostructures, *Phys. Rev. Lett.* **76**, pp. 4773–4776.
19. Pitarke, J.M., García Vidal, F.J., Pendry, J.B. (1998) Effective electronic response of a system of metallic cilinders, *Pys. Rev. B* **57** pp. 15261–15266.
20. Bahl, I., Bhartia, P. (1998) *Microwave solid state circuit design*, Wiley, N.Y.
21. Wheeler, H.A. (1965) Transmission lines properties of parallel strips separated by a dielectric sheet, *IEEE Trans. Microwave Theory and Tech.* **MTT-13**, pp. 172–185.
22. Ghione, G., Naldi, C. (1984) Analytical formulas for coplanar lines and monolithic MICs, *Electronic Lett.*, **20**, pp. 179–181 .
23. Landau, L., Lifshitz, E. (1980) *Statistical Phys.*, Pergamonn Press, Oxford.
24. Pendry, J.B. (2000) Negative refraction makes a perfect lens, *Phys. Rev. Lett.* **85**, pp. 3966–3969.
25. Smith, D.R., Padilla, W.J., Vier, D.C., Shelby, R., Nemat-Nasser, S.C., Kroll, N. and Schultz, S. (2001) Left-handed metamaterials, in *Photonic crystals and light localization in the 21st century*, Proceedings of the NATO-ASI Conference on Photonic Crystals and Light Localization. Crete, June pp. 18–30, 2000, ed. by Costas M. Sokoulis (Kluwer Academic, Dordrecht), p. 351.

CONTROLLABLE SEMICONDUCTOR PHOTONIC BAND GAP STRUCTURES

IGOR NEFEDOV[1], VICTOR GUSYATNIKOV[2], EVGENII ALTSHULLER[2], AND YURII MOROZOV[1]
[1]*Radio Laboratory, Helsinki University of Technology, on leave from Institute of Radio Engineering and Electronics, Russian Academy of Sciences, Zelyonaya str. 38, Saratov, 410019, Russia*
[2]*Saratov State University, Astrakhanskaya str. 83, Saratov, Russia*

Abstract. The change in the refractive index of GaAs due to the light-induced generation of nonequilibrium charge carriers is shown to substantially change the transmission of a one-dimensional GaAs/GaAlAs photonic band-gap structure, allowing low-threshold optical switching. The transmission characteristics of this structure can be tuned not only by light, but also by electric field, which makes it possible to use the same structure as an electro-optical switch. We discuss also a possibility to change dramatically the refractive index of one of the layers, producing a peak inside the band gap. Such a change can be performed by injection of the carriers into one of the layers.

1. Introduction

Photonic band gap (PBG) structures, whose intensive investigations were started from the works by E. Yablonovitch [1] and S. John [2], continue to attract attention of the optical and microwave communities due to their possible applications in different areas of optics, photonics and microwave techniques. Special interest represent so-called controllable PBG structures whose parameters can be tuned by some external forces.

The possibility of shifting the edge of the photonic band gap (PBG) in one-dimensional PBG structures due to the nonlinear (intensity-dependent) additive to the refractive index of optical materials forming a PBG structure offers much promise for the creation of tunable optical switches, bistable devices, and logic gates. Such a shift can be performed dynamically [3] under intensive light power and can find applications in optical limiters.

S. Zouhdi et al. (eds.), Advances in Electromagnetics of Complex Media and Metamaterials, 143–156.

Recently we proposed another mechanism of optical control in semiconductor PBG structures (see Figure 1), when the wavelengths of the *controlling* and *controlled* light are different [4]. As a nonlinear effect changing the refractive index of the PBG material, we consider light-induced generation of non-equilibrium free charge carriers in a narrow-band semiconductor, namely, in GaAs.

We have studied also how the pulses of controlled light are formed by the controlling light pulses, whose duration is comparable with the lifetime of carriers. It was demonstrated that the minimal switching energy density does not depend on the lifetime and is equal to 0.0005 J/cm^2. Thus, the proposed mechanism of optical switching requires moderate energy densities and can be used in low-threshold all-optical devices.

Next we study electro-optical tuning of the same structure using Frantz-Keldysh effect, which allows to change the width of the electronic forbidden zone applying external electric bias field and in this way to change the concentration of light-induced carriers.

The light control mechanisms, mentioned above, are enough moderate and require the change of optical parameters of all GaAs layers along PBG structure in order to achieve effective light switching. Finally, we discuss another mechanism, where the permittivity of only one of the layer is changed dramatically, producing 'defect mode' and creating a transmission peak inside the photonic band gap. Such a change of permittivity is achieved due to injection of charge carriers through a p-n transition. In this case concentration of non-equilibrium carriers can be increased in two orders that gives a contribution to relative permittivity $\Delta\varepsilon \sim -0.6$.

2. Light-by-light control. Continuous regime of light transmission

The idea of optical switching is very simple. We take as a model a structure composed of M alternating GaAs-GaAlAs layers, see Figure 1. The absorbing layers are the GaAs layers as more narrow-band ones, and their intrinsic absorption edge corresponds to the width of the forbidden zone for the GaAs, which is equal approximately to $E_g = 1.4\,\mathrm{eV}$ corresponding to the wavelength $0.872\,\mu$m. In this section we discuss the light-by-light control and the lateral contacts for external bias electric field will be considered below. The spectrum of the transmission coefficient $|T|$ for the 40-period GaAs-$Al_{0.3}Ga_{0.7}As$ structure is presented in Figure 2 for the case of normal light incidence. The middle of the first band gap corresponds to $1.45\,\mu$m, satisfying the quarter-wave conditions for GaAs and $Al_{0.3}Ga_{0.7}As$ layers having thicknesses $d_1 = 0.1122\,\mu$m and $d_2 = 0.1242\,\mu$m, respectively. In this case the long-wavelength band edge coincides with $\lambda = 1.5\,\mu$m, which is widely used in the optical signal processing and is of specific interest.

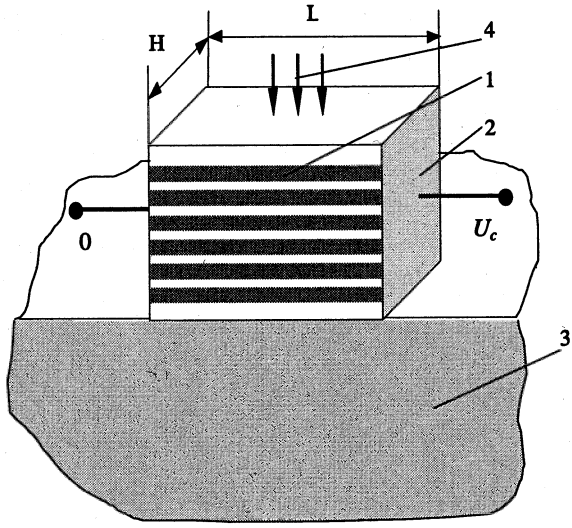

Figure 1. The structure under study. 1 - GaAs/GaAlAs Bragg superlattice; 2 - lateral contacts for bias electric field; 3 - GaAs substrate; 4 - the controlling and controlled light beams.

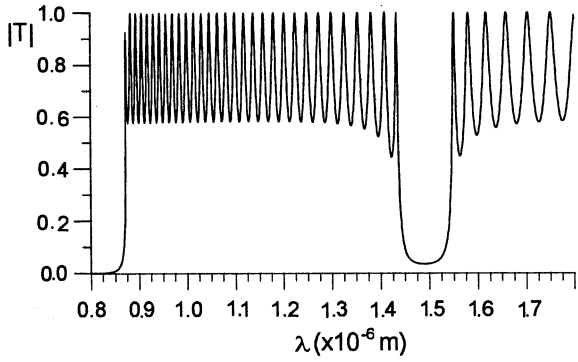

Figure 2. Transmission spectrum in the absence of the controlling light.

Other band gaps lie beyond the intrinsic absorption edge $\lambda_0 \simeq 0.8725\,\mu$m and are not seen at this plot. The refractive index of GaAs n_1 is larger, than for GaAlAs n_2. Light-induced charge carriers give a negative contribution to the refractive index of GaAs, the contrast between refractive indeces of material decreases, the band gap becomes narrower, and it follows, that the long-wavelength edge of the band gap shifts to shorter wavelengths. If the steepness of the band gap edge is enough high, a small shift of the band edge causes an essential influence on the transmission through the PBG structure.

2.1. ELECTRONIC PROCESSES IN GAAS UNDER LIGHT ILLUMINATION AND RESTRICTIONS OF THE MODEL

Let us consider electronic processes in GaAs which cause a change of the permittivity of this material. Controlling light, whose wavelength corresponds to the intrinsic absorption edge of GaAs, generates non-equilibrium free charge carriers, which contribute both to the real and imaginary parts of permittivity. The absorption coefficient α in GaAs layers at the wavelengths smaller than the intrinsic absorption edge, that corresponds to *controlling light*, is taken as $\alpha = B(h\nu - E_g)^{1/2}$, where h is the Plank constant, ν is the frequency of light. Proportionality coefficient B is taken from experimental work [7]. The index of absorption κ is connected with α as

$$\kappa = \alpha\lambda/(4\pi), \tag{1}$$

where λ is the wavelength of controlling light. Then, the permittivity is calculated as

$$\begin{aligned} \varepsilon' &= n_1^2 - \kappa^2, \\ \varepsilon'' &= 2n_1\kappa, \end{aligned} \tag{2}$$

where ε' and ε'' are the real and imaginary parts of permittivity, respectively. For our purposes we used such a spectral range, where this value changed from 100 cm^{-1} to 1000 cm^{-1}. Namely, this range of α is the most suitable for our investigation. If α >1000 cm^{-1}, the light power is absorbed within the first few layers of PBD structure and the tuning effect is small. If α <100 cm^{-1}, the controlling illumination causes too small influence on the optical parameters of the layers. That is why we did not take into account interband absorption beyond the intrinsic absorption edge, which is weak for pure GaAs. We did not take into account excitonic absorption because the range of room temperatures was considered. Thus, it was assumed, that the absorption beyond the intrinsic edge was caused only by free electrons.

Experimental data on light absorption by free carriers in GaAs within the spectral range 1 μm–4.5 μm are given in old and modern works [6]–[10]. It follows from them, that the absorption coefficient is proportional to the charge carriers concentration and does not depend on the wavelength within the range 1μm–4.5μm. That is why for the *controlled light* we assumed, that absorption in this spectral range is caused only by absorption on free electrons. We used for our calculations an approximation of the experimental results [9],[10]. Non-equilibrium holes recombine on deep trapping levels, they have much shorter lifetime and give a small contribution to the optical constants of materials. For example, concentration $N \sim 5{\cdot}10^{17}$ cm^{-3} corresponds to the absorption coefficient $\alpha \sim 5$ cm^{-1} at the wavelength 1.5 μm.

The contribution to the real part of the relative permittivity in the range considered is given by expression (Drude-Lorentz model) [5]

$$\Delta\varepsilon \cong -\frac{Ne^2}{m\varepsilon_0(2\pi\nu)^2}, \tag{3}$$

where N, e, and m are the concentration, charge and the effective electron mass, respectively, ε_0 is the permittivity of vacuum, and ν is the controlling light frequency. Applicability of such a model within the spectral range considered is confirmed by works [6]–[9].

The non-equilibrium charge carriers concentration was found from the the balance equation for the processes of generation and recombination of free charge carriers. We neglected the diffusion of the carriers and assumed that the quantum yield is close to unity: $N/\tau = P/h\nu$, where τ is the lifetime of the charge carriers and P is the radiation power, absorbed in the unit of the layer volume. Such an approximation is too rough in the general case, but it can be applied to the structures like GaAs-$Ga_xAl_{1-x}As$ because the non-equilibrium charge carriers will be grouped in the narrow-band GaAs layers due to the contravariant modulation of the zones edges. The modern technologies allow one to produce sufficiently perfect interfaces between the layers, which do not contribute to the increase of the recombination rate. The lifetime of the charge carriers τ was taken to be 10^{-7} s (τ changes from 10^{-7} to 10^{-9} s).

2.2. NUMERICAL SOLUTION

We use 2×2 transfer matrix method for the calculation of the transmission coefficient [11]. Let us consider the case of p-polarization.

Let E^i be the electric field of the incident wave, E^r and E^t be the fields of the reflected and transmitted wave, respectively. Using the relation $H_x = E_z/(\rho\cos\theta)$, omitting the subscript z and assuming that the surrounding medium is vacuum ($\varepsilon = \mu = 1$), one can write:

$$\begin{bmatrix} E^i + E^r \\ (E^i - E^r)/(\rho\cos\theta) \end{bmatrix} = [B] \begin{bmatrix} E^t \\ E^t/(\rho\cos\theta) \end{bmatrix}, \tag{4}$$

where $[B]$ is the transfer matrix of the multilayered structure, θ is the light incidence angle. The transmission $T = E^t/E^i$ and reflection $R = E^r/E^i$ coefficients are obtained from (4) as follows:

$$\begin{aligned} T &= 2/\left(B_{11} + B_{12}(\rho\cos\theta) + B_{21}\rho/\cos\theta + B_{22}\right) \\ R &= T(B_{11} + B_{12}(\rho\cos\theta)) - 1. \end{aligned} \tag{5}$$

The problem of the controlling light transmission through PBG structure is nonlinear, and the respective problem for the controlled light is

considered as a linear one. The nonlinear problem is solved in three stages. First we calculate the light propagation characteristics, neglecting the contribution of the generated charge carriers to the optical constants of the layers material. We took into account dispersion of the refractive indices of the GaAs and AlGaAs layers following [12].

At the second step we select the wavelength corresponding to the intrinsic absorption edge of GaAs. Next, the coordinate dependence of the Poynting vector is calculated, and the power absorbed by each layer is found.

At the third step we perform a self-consistent procedure of calculation of the PBG structure propagation characteristics obtained taking into account the contribution of carriers, generated by radiation, into the real and imaginary parts of the layer permittivity. As a convergence criterion we have used the convergence of the electric field distribution. It takes usually no more than 8-10 iterations for the convergence. At the third stage we calculate the spectral characteristics of the PBG structure with the parameters changed under illumination.

2.3. DISCUSSION OF THE RESULTS

In Figure 3 the shift of the band gap edge under illumination at $\lambda_0 = 0.8723\mu$m and for different values of the power density is presented. One can see from Figure 3, that the shift of the band gap edge increases with the power, but it is accompanied by the PBG resonant properties degradation, which is exhibited as a decrease of the transmission $|T|$ peak corresponding to the respective band edge as well as increasing of the transmission level within the band gap. One can achieve the amplitude modulation depth 94% at the wavelength $\lambda = 1.476\mu$m with the power density $P = 10.6\,\mathrm{kW\,cm^{-2}}$.

In Figure 4 the shift of the band gap edge for different values of the controlling light wavelengths is presented. Curve A corresponds to the non-perturbed case. One can see from Figure 4 that there is an optimal wavelength of the controlling light ($\lambda_0 = 0.8723\mu$m, curve D). For the wavelengths larger than the optimal one, the edge shift decreases (curves B,C), and at smaller wavelengths strong degradation of the pass band takes place (see curves E,F). The existence of the optimal wavelength is caused by the fact that the absorption is non-uniform in space and the most of radiation is absorbed in the first layers of PBG structure. At the same time, the absorption becomes very weak at larger wavelengths, that does not influence the PBG structure parameters. The power density of the controlling light is $5.9\,\mathrm{kW\,cm^{-2}}$. Thus, the optimal wavelength of the controlling light corresponds to the optimal power absorption along the PBG structure.

Considering the continuous regime of illumination, we have found that the power of the controlling radiation depends on the lifetime of the non-

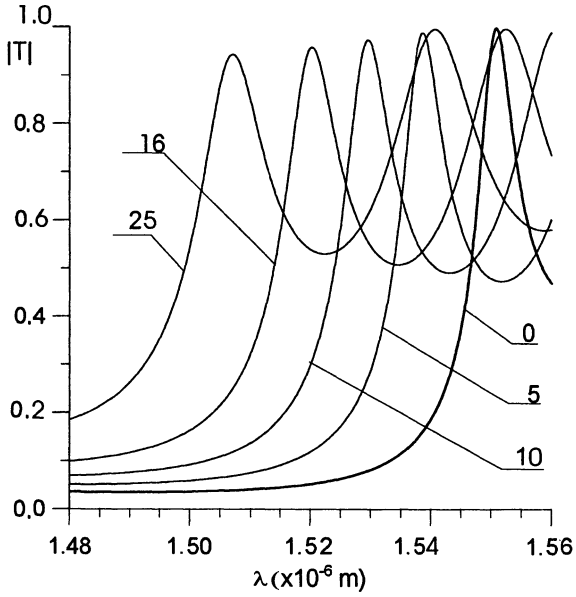

Figure 3. The transmission spectra for different energy flow densities of the controlling light P. The values of P in kW cm^{-2}) are pointed out at the corresponding curves.

equilibrium carriers. For a 40-period structure with the lifetime $\tau = 10^{-7}$ s the optimal switching power density is equal to 6 kW/cm^2. The response time of optical elements, which is generally determined by the inertia properties of optical nonlinearities employed in these elements, is a crucial parameter for all light-by-light-control devices, eventually characterizing the usefulness of PBG switches as short-pulse-control components. It is very important in this context to understand the basic features of transient processes accompanying the propagation of light pulses in PBG structures.

3. Formation of the controlled light pulses

Next we consider controlled pulse formation by pulses of controlling light. The concentration of non-equilibrium charge carriers N generated in GaAs is determined from the continuity equation written with the assumption that the concentration of light-induced non-equilibrium charge carriers is much higher than the equilibrium concentration of free carriers:

$$dN/dt = G - N/t, \tag{6}$$

where G is the generation rate of non-equilibrium charge carriers. The concentration of the carriers generated by a control light pulse with duration

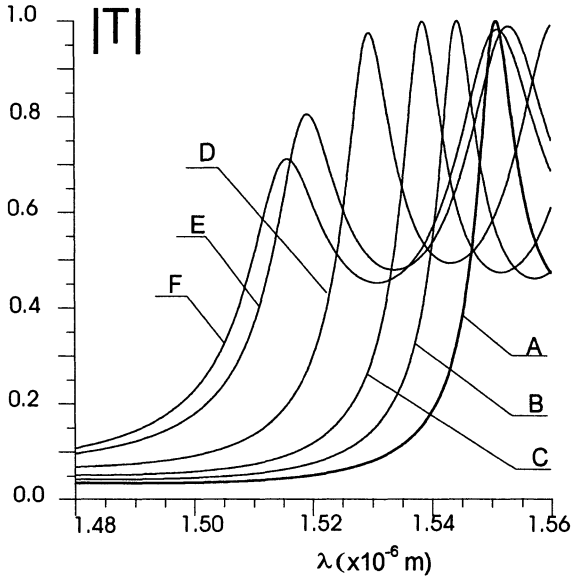

Figure 4. The transmission spectra for different wavelengths λ_0 of the controlling light: curve B corresponds to $\lambda_0 = 0.87253 \times 10^{-6}$ m, C – 0.87250×10^{-6} m, D – 0.8723×10^{-6} m, E – 0.8715×10^{-6} m, F – 0.871×10^{-6} m. Curve A corresponds to the absence of controlling light.

Δt is determined from the expression

$$n(t) = Gt(1 - \exp(-t/t)) \tag{7}$$

for $0 < t < \Delta t$ and

$$n(t) = n(\Delta t) \exp(-t/t) \tag{8}$$

for $t > \Delta t$. Assuming that the quantum yield of charge-carrier generation is equal to unity, we have $G = P/(h\nu)$, where P is the absorbed radiation power per unit volume. In the absence of control light, the transmission coefficient is at a maximum, since the wavelength of the probe light coincides with the edge of the photonic band gap of the PBG structure. As the control light pulse is switched on, shifting the PBG edge, the transmission coefficient starts to decrease, following the dynamics of the concentration of free charge carriers (Figures 5–6). Figure 5 shows the temporal evolution of the transmission coefficient at λ=1.508μm for the above-described PBG structure irradiated with a normal-incidence control pulse with the wavelength l0=0.8725μm, different pulses duration, and the same pulse energy, equal to 0.0005 joule/cm^2. The slope of the forward front is determined by the pulse duration. Figure 6 presents the time dependence of

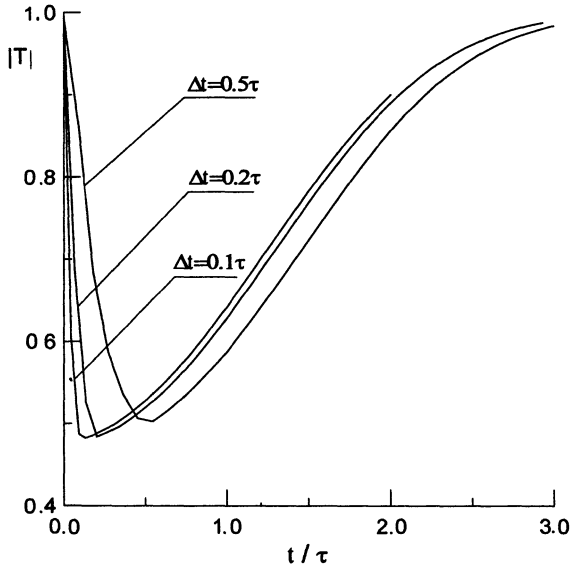

Figure 5. Time dependence of the transmission coefficient of the PBG structure irradiated with control light pulses with different pulse durations and the same pulse energy E=0.0005joule/cm^2.

the transmission coefficient for PBG structures of the above-described type with different lifetimes of carriers in the case when the energy density is constant E=0.0005 joule/cm^2, and the pulse duration $\Delta t = 2 \times 10^{-9}$ s. The slope of the back front is determined by the lifetime of carriers.

4. Electro-optical switching

We considered above the physical model of optical and electronic processes in GaAs/GaAlAs PBG structure under controlling light illumination. It was found that even a small deviation of the wavelength of controlling light from the optimal λ_0 causes an essential change of the light controlling action. In fact, any small change in electronic properties of semiconductor layers caused by some external action around λ_0 gives rise to similar effects.

In this section we consider a bias electric field as such an external action. The structure under study is the same. The long-wavelength edge of the photonic band gap corresponds to $\sim \lambda = 1.5\mu$m. Now we apply to the PBG structure a bias electric field using lateral contacts, see Figure 1. Such a bias dc electric field, applied to a semiconductor, reduces the effective width of the electronic band gap due to the Frantz-Keldish effect [5]. This reduction

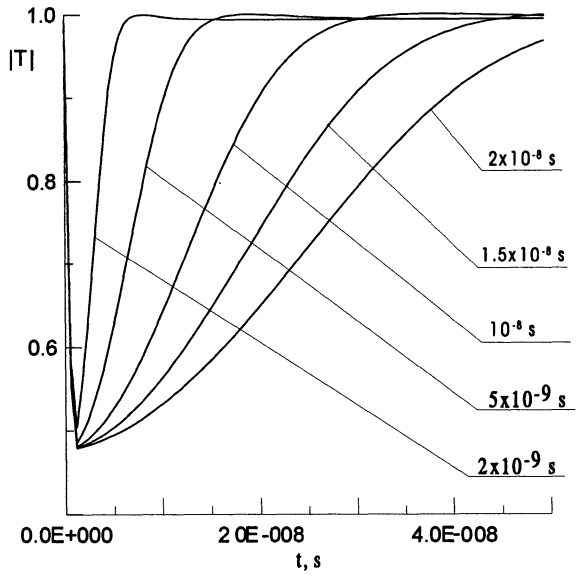

Figure 6. Time dependence of the transmission coefficient of the PBG structure irradiated with control light pulses with different lifetimes of carriers and the same pulse energy E=0.0005joule/cm^2 and pulse duration $\Delta t = 2 \times 10^{-9}$s.

$\Delta\varepsilon_g$ can be approximately expressed via the bias electric field strength E_c as

$$\Delta\varepsilon_g = \left(\frac{3|e|E_c h}{8\pi\sqrt{2m}}\right)^{2/3} \tag{9}$$

where e and m are the charge and the effective mass of electrons, respectively. Such a reduction of the electronic band gap changes the absorption coefficient of the controlling light. Hence, electric field may control the action of the controlling light. The transmission spectrum for a 40-period GaAs/GaAlAs structure near the long-wavelength band edge for different strengths of the electric field is presented in Figure 7. The lifetime of the non-equilibrium charge carriers τ is taken to be 10^{-8} s, and the energy flow density of the controlling light is P=40kW/cm^2. The structure with the sizes $H = L$=100μm was considered.

Figure 7 demonstrates that the spectral characteristics are identical for different wavelengths of the controlling light $\lambda_1 = 0.8727\mu$m and $\lambda_2 = 0.8730\mu$m, if some special values of the external bias electric field are chosen. If $E_c = 0$ (curve 1), the electric field does not influence the structure transmission, since λ_1=0.8727μm and λ_2=0.8730μm are beyond the intrinsic absorption edge of GaAs at room temperature, and the absorption coefficient of such a radiation is very small. As the applied electric field grows,

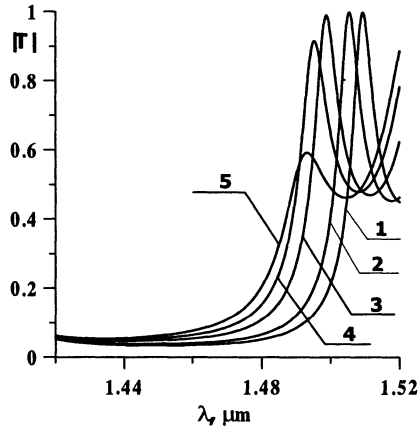

Figure 7. Transmission spectra for $\lambda_1 = 0.8727\mu$m: 1 - U_c=0; 2 - U_c=0.95V; 3 - U_c=1.0V; 4 - U_c=1.2V; 5 - U_c=3.0V and for $\lambda_2 = 0.8730\mu$m 1 - U_c=0; 2 - U_c=4.45V; 3 - U_c=4.5V; 4 - U_c=4.7V; 5 - U_c=6.5V.

the transmission of the structure lowers (curves 2,3,4). Since $\lambda_2 > \lambda_1$, and λ_2 lies farther from the electronic band edge, one should apply a larger external voltage to block the radiation at λ_2. There exists an optimum for the controlling value of U_c. A further increase in U_c decreases the steepness of the photonic band edge (curve 5). The optimal value of U_c depends on the wavelength of the controlling light.

5. The control of defect mode

In this section we discuss another way of tuning the optical characteristics of semiconductor PBG structure, based on the same mechanism. In difference with the above discussion, we consider here the case, when the optical characteristics are changed not of every layer, but only of one-three layers, and this change is achieved by injection of non-equilibrium carriers implemented by electric current through a heterotransition GaAlAs/GaAs.

The same 40-period PBG structure is considered. The thicknesses of the layers are taken in such a way, that the center of the band gap corresponds to the wavelength $\lambda_0 = 1.45\mu$m. The layers thicknesses in this case are d_{GaAs}=0.1122μm and d_{GaAlAs}=0.1242μm. We assume that there is a possibility of the current transmission between separate layers that causes injection of the carriers into GaAs layers. Figures 8-11 present the

transmission spectra of the PBG structure, where the dashed curve shows the initial characteristic, without injection.

Figure 8 demonstrates the change of transmission under a change of the electron concentration in the 20th period of a 40-period PBG structure. The presence of one layer with different parameters in the middle of the PBG structure causes a separate transmission peak within the photonic band gap. This is similar to the presence of a defect in the crystal lattice of a semiconductor, which creates a deep energy level in the electronic forbidden zone. Reduction of the concentration of the non-equilibrium carriers to 10^{19}cm^{-3} causes a shift of the peak toward the photonic band gap edge. On the other hand, the presence of one layer having a high concentration of carriers in the middle of the band gap can be interpreted as a system of two coupled resonators with an electrically tuned connection. Displacement of the controlled layer toward the edges of the PBG structure reduces the amplitude of the transmission peak inside the band gap, but a displacement toward the illuminated interface of the PBG structure influences the amplitude less than a displacement to the other interface (see Figure 9).

Presence of three controllable layers, repeated in the same number of periods, causes appearance of photonic minizones (Figure 10). There is a direct analogy with the minizone spectrum of the energy in semiconductor quantum superlattices.

6. Conclusion

In this paper we have demonstrated a possibility of creating low-threshold all-optical and electro-optical switches for near infrared, which can operate at room temperature. Their sizes may be of the order of several micrometers in total thickness. Inertia of the switching process is determined by the lifetime of carriers and was taken in our calculations from 10^{-7} to 10^{-9}s. In addition, the optical control mechanisms considered give the possibility of creating low-threshold all-optical and electrooptical logic gates [13].

References

1. Yablonovitch, E. (1987) Inhibited spontaneous emission in solid-state physics and electronics, *Phys. Rev. Lett.* **Vol. 58**, pp. 2059–2062
2. John, S. (1987) Strong localization of photons in certain disordered dielectric superlattices, *Phys. Rev. Lett.* **Vol. 58**, pp. 2486–2489
3. Scalora, M., Dowling, J.P., Bowden, C.M. and Bloemer, M.J. (1994) Optical limiting and switching of ultrashort pulses in nonlinear photonic band gap materials, *Phys. Rev. Lett.*, **Vol. 73**, pp. 1368–1371
4. Nefedov, I.S. and Gusyatnikov, V.N. (2000) Optically controlled GaAs-GaAlAs photonic band gap structure, *Journ. of Optics A: Pure and Applied Optics*, **no. 2**, pp. 344–347

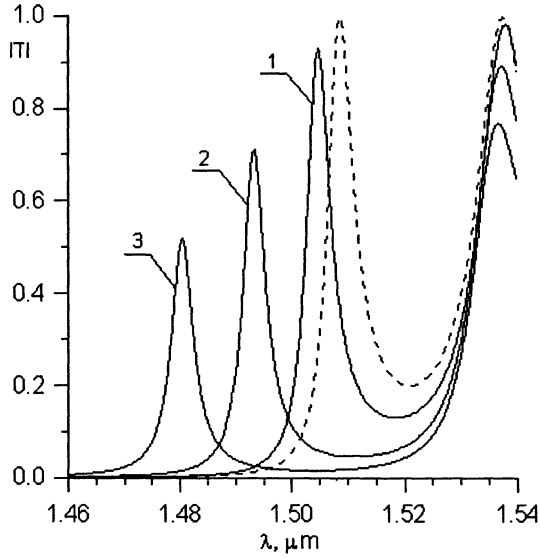

Figure 8. Transmission spectra for 40-period $GaAs/Ga_{0.7}Al_{0.3}As$ structure, where in the 20th period the electron concentration increases to: $1 \times 10^{19} cm^{-3}$ (curve 1); $3 \times 10^{19} cm^{-3}$ (curve 2), $5 \times 10^{19} cm^{-3}$ (curve 3).

5. Zeeger, K. (1973) *Semiconductor Physics*, Springer, Berlin
6. Sell, D.D., Casey, H.C., and Wecht, K.W. (1974) Concentration dependence of the refractive index for n- and p-type GaAs between 1,2 and 1,8 eV, *J. Appl.Phys.*, **Vol. 45 no. 2**, pp. 800-807
7. Casey, H. C., Sell, D. D., and Wecht, K. W. (1975) Concentration dependence of the absorption coefficient for n- and p-type GaAs between 1.3 and 1.6 eV, *J. Appl. Phys.*, **Vol. 46 no. 2**, pp. 250–257
8. Spitzer, W.G., and Whelan, J.M. (1959) Infrared absorption and electron effective mass in n-type gallium arsenide, *Phys. Rev.*, **Vol. 114 no. 1**, pp. 59–63
9. Balslev I. (1968) Optical absorption due to inter-conduction-minimum transitions in gallium arsenide, *Phys. Rev.*, **Vol. 173 no. 3**, pp. 762–766
10. Ganikhanov, F., Burr, K.C., Hilton, D.J., and Tang, C.L. (1999) Femtosecond optical-pulse-induced absorption and refractive-index changes in GaAs in the midinfrared, *Phys. Rev. B.*, **Vol. 173 no. 3**, pp. 8890–8896
11. Born, M. and Wolf, E. (1968) *Principles of optics*, Pergamon Press, Oxford-London-Edinburg-New York-Paris-Frankfurt
12. Casey, H.C. , and Panish, M.B. (1978) *Heterostructure lasers, Part A, Fundamental principles*, Academic Press, New York, San Francisco, London
13. Nefedov, I.S., Gusyatnikov, V. N., Kashkarov, P. K. and Zheltikov, A. M. (2000) Low-Threshold photonic band-Gap optical logic Gates, *Lasers Physics*, **no. 10**, pp. 640–643

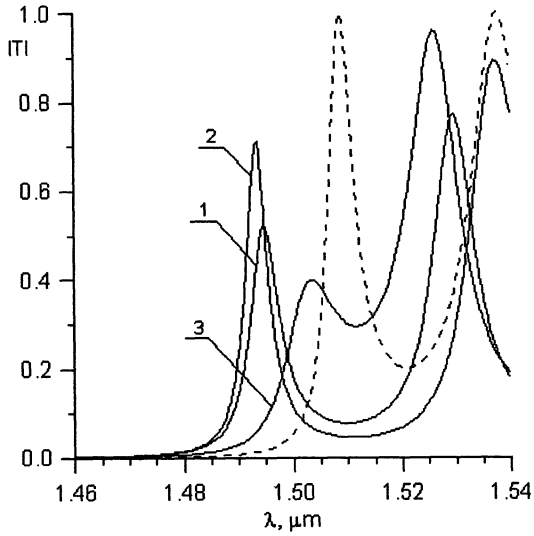

Figure 9. Transmission spectra for 40-period $GaAs/Ga_{0.7}Al_{0.3}As$ structure, where the electron concentration increases to $3 \times 10^{19} cm^{-3}$ in one GaAs layer, placed in the 10th period (curve 1), in the 20th period (curve 2), and in the 30th period (curve 3).

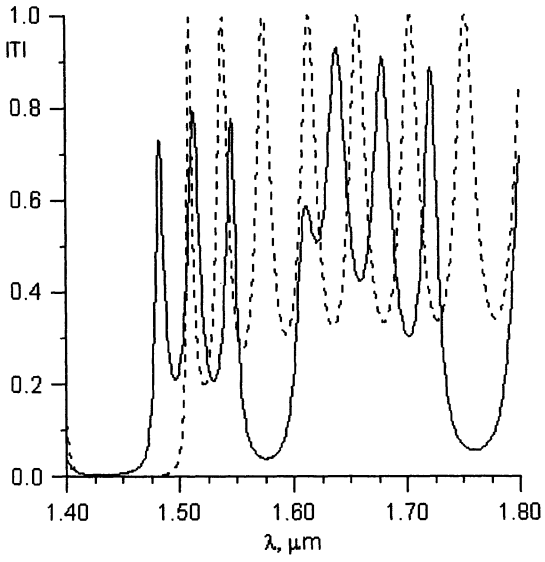

Figure 10. Transmission spectra for 40-period $GaAs/Ga_{0.7}Al_{0.3}As$ structure, where simultaneously in the 10th, 20th and 30th periods the electron concentration increases to the state with the electron concentration $3 \times 10^{19} cm^{-3}$.

PHOTONIC BAND GAP EFFECTS IN MAGNETIC FILM WITH PERIODICALLY STRIPED-DOMAIN STRUCTURE

I.L. LYUBCHANSKII, N.N. DADOENKOVA,
M.I. LYUBCHANSKII
Donetsk Physical & Technical Institute, National Academy of Sciences of Ukraine, 72, R. Lyuxemburg str., 83114, Donetsk, Ukraine

E. A. SHAPOVALOV
Department of Physics, Donetsk National University, 24, Universitetskaya str., 83055 Donetsk, Ukraine

TH. RASING
Research Institute for Materials, University of Nijmegen 6525 ED Nijmegen, The Netherlands

AND

A. LAKHTAKIA
Department of Engineering Science and Mechanics, Pennsylvania State University
University Park, PA 16802–6812, USA

Abstract. Photonic band gaps in magnetic films with periodically striped domains separated by Bloch-type domain walls are investigated. Calculations for yttrium iron garnet films are performed using the transfer matrix method. The dependence of forbidden gaps in the electromagnetic wave spectrum on the thicknesses of magnetic domains is numerically studied.

1. Introduction

Photonic band gap (PBG) materials — also called photonic crystals (PCs) — are currently the objects of intense theoretical and experimental research, because of promising applications in optoelectronics [1, 2]. These materials are one–, two–, and three–dimensional periodically ordered structures with periods comparable with the free–space wavelength of incident light.

S. Zouhdi et al. (eds.), Advances in Electromagnetics of Complex Media and Metamaterials, 157–174.

The major attraction of PCs is the existence of forbidden gaps in their transmittance spectrums.

Most publications on PCs are devoted to the theoretical and experimental investigations of dielectric and metallic materials. Although periodic magnetic structures also can be considered as PCs, less than forty papers appear to have been devoted to PBGs in magnetic materials. Following is a summary of published results known to us: The effect of magnetic permeability on PBGs was theoretically investigated by Sigalas *et al.* [3] and Kee *et al.* [4]. Theoretical investigations of magnonic band gaps in the spectrums of spin waves in one- and two-dimensional composite magnetic materials have also been reported [5]–[10]. External *dc* magnetic field tunability of microwave PBG effects in ferrite slabs with a two-dimensional ensemble of cylindrical holes has been observed [11, 12]. The magneto-optical properties of one-dimensional magnetic PCs were investigated theoretically and experimentally by Inoue *et al.* [13]–[17] and Levy *et al.* [18]–[21] for magnetic and nonmagnetic multilayers made of impurity-doped yttrium-iron garnet (YIG) films. Tanaka *et al.* [22, 23] fabricated magneto-photonic crystal structures with epitaxial nonmagnetic and ferromagnetic semiconductors. A multitude of theoretical investigations of light propagation in magnetic multilayers have been carried out [24]–[32]. The influence of an external magnetic field on PBG structures in one- and two-dimensional PCs was theoretically studied by several authors [33]–[35]. The effect of nonreciprocity in magnetic PCs was investigated theoretically by Figotin and Vitebsky [36]. The magneto-optic effects in a nonlinear PC were theoretically studied by Hu and Wang [37].

Nonuniform distributions of magnetization — i.e., the so–called magnetic domains (MDs) — exist in thin magnetic films [38]. These MDs can form labyrinth-domain structures as well as ordered periodic superstructures — which are either one-dimensional lattices of laminar domains or two-dimensional hexagonal lattices of magnetic bubbles (cylindrical magnetic domains) [38]. These periodically ordered domain structures can be analyzed as *magnetic PCs*. We note that guided electromagnetic wave propagation in magnetic films with striped-domain structure was theoretically studied by Sementsov [39]. Optical modes conversion in magneto-photonic crystal waveguides formed by one- and two-dimensional magnetic domain lattices was theoretically investigated in [40]. However, the presence of domain walls (DWs), which are inter-MD transition layers, has not been accounted for. Therefore, in this paper, we theoretically investigate PBG effects in thin magnetic films of YIG with periodically striped domains separated by Bloch-type DWs.

2. Permittivity tensor of a magneto-optical film

Let us consider a YIG film with cubic crystallographic symmetry and the laminar domain structure with the Bloch-type DWs shown in Figures 1 and 2. This film is supposedly of infinite dimensions in the XY plane with the Z axis parallel to the axis of periodic nonhomogeneity. The unit cell contains four layers: a domain of type $\uparrow$, another domain of type $\downarrow$, and two domain walls. The period $D = d_\uparrow + d_\downarrow + d_\odot + d_\otimes$, where $d_\uparrow$ and $d_\downarrow$ are the thicknesses of the domains with the magnetization vector $\mathbf{M}$ oriented upward and downward (along the X axis and in the opposite direction, respectively). The DW thicknesses d_{DW}, further classified as $d_\odot$ and $d_\otimes$, correspond to Bloch-type DWs with opposite orientation of magnetization (along $\pm Y$ axis) as shown on the Figures 1 and 2. We restrict our consideration to MDs with Bloch-type DWs, wherein $\mathbf{M}$ rotates in the XY plane. For simplicity's sake, we consider the DW as a thin magnetized layer between two MDs with magnetization orientation as shown in Figures 1 and 2. The chosen film with laminar magnetic domain structures can be considered as a 4–component superlattice with period D. We consider light propagation in either the XZ plane or the YZ plane, as depicted in Figures 1 and 2, respectively.

According to the usual approximation in magneto-optics [41, 42], we expand the permittivity tensor ε_{lm} with respect to the magnetization vector components M_k. Restricting this expansion by the quadratic on M_k terms, we represent ε_{lm} as

$$\varepsilon_{lm} = \varepsilon_{lm}^{(0)} + i \sum_{n=1}^{3} f_{lmn} \tilde{M}_n + \sum_{n,p=1}^{3} g_{lmnp} \tilde{M}_n \tilde{M}_p , \qquad l, m = 1, 2, 3 , \quad (1)$$

for each of the four layers in the unit cell. Here, $i = \sqrt{-1}$; $\varepsilon_{lm}^{(0)}$ is the magnetization–independent part of ε_{lm}; f_{lmn} and g_{lmnp} are the linear and quadratic magneto–optical tensors respectively, and $\tilde{\mathbf{M}} = \mathbf{M}/M_{sat}$ with the saturation magnetization denoted by M_{sat}.

The three tensors present on the right side of (1) have the following nonzero components for a YIG film with the crystallographic cubic symmetry [41]:

$$\begin{aligned}
&\varepsilon_{xx}^{(0)} = \varepsilon_{yy}^{(0)} = \varepsilon_{zz}^{(0)} = \varepsilon^{(0)}, \\
&f_{123} = f_{312} = f_{231} = -f_{132} = -f_{321} = -f_{213} = f, \\
&g_{xxxx} = g_{yyyy} = g_{zzzz} = g_{11}, \\
&g_{xxyy} = g_{xxzz} = g_{yyxx} = g_{yyzz} = g_{zzxx} = g_{zzyy} = g_{12}, \\
&g_{xyxy} = g_{xyyx} = g_{xzxz} = g_{xzzx} = \qquad (2)
\end{aligned}$$

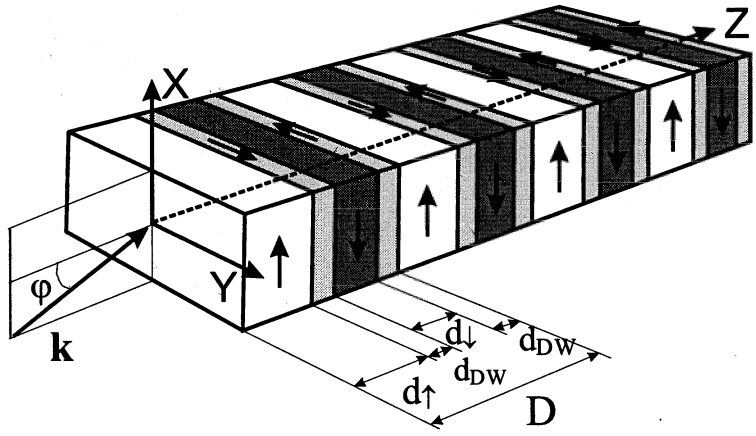

Figure 1. Schematic of a magnetic PC comprising many periods of thickness D. The directions of internal magnetization in the two types of MDs and the Bloch-type DWs are shown. Light propagates in the XZ plane.

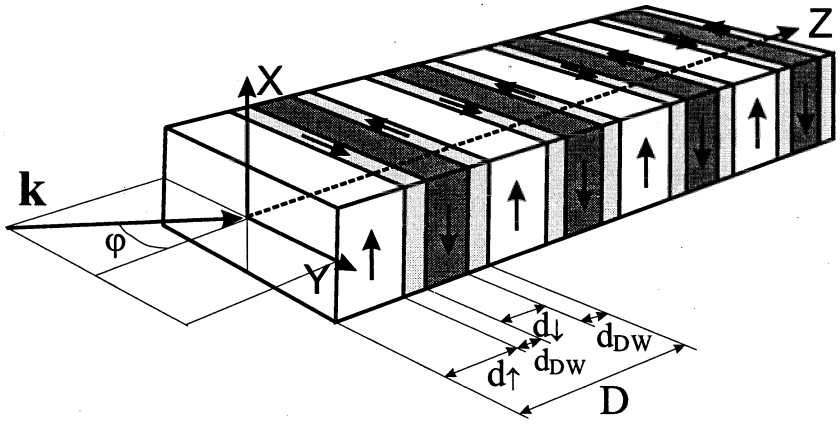

Figure 2. Same as Figure 1, except that light propagates in the YZ plane.

$$= g_{yxyx} = g_{yxxy} = g_{yzyz} = g_{yzzy} =$$
$$= g_{zxzx} = g_{zxxz} = g_{zyzy} = g_{zyyz} = g_{44}.$$

Accordingly, the permittivity tensors for the two MDs can be expressed as follows:

$$\varepsilon_{ij}^{(L)} = \begin{pmatrix} \varepsilon_{\parallel}^{(L)} & 0 & 0 \\ 0 & \varepsilon_{\perp}^{(L)} & \pm\varepsilon^{(L)\prime} \\ 0 & \mp\varepsilon^{(L)\prime} & \varepsilon_{\perp}^{(L)} \end{pmatrix}, \tag{3}$$

Here, $\varepsilon_{\parallel} = \varepsilon^{(0)} + g_{11}\tilde{M}^2$, $\varepsilon_{\perp} = \varepsilon^{(0)} + g_{12}\tilde{M}^2$ and $\varepsilon' = if\tilde{M}$. On the right side of (3), the upper signs hold for $L = \uparrow$, whereas the lower signs correspond to $L = \downarrow$. Similarly, we obtain

$$\varepsilon_{ij}^{(L)} = \begin{pmatrix} \varepsilon_{\perp}^{(L)} & 0 & \mp\varepsilon^{(L)\prime} \\ 0 & \varepsilon_{\parallel}^{(L)} & 0 \\ \pm\varepsilon^{(L)\prime} & 0 & \varepsilon_{\perp}^{(L)} \end{pmatrix}, \tag{4}$$

for DWs, wherein the upper and the lower signs, respectively, correspond to the $\odot$ and $\otimes$ magnetization orientations.

3. The 4 × 4 transfer matrix method

As magneto–optical films are anisotropic, optical propagation is best described using 4×4 matrixes [24]–[31], [43]. The transfer matrix method then yields the following two dispersion equations [24]:

$$\begin{cases} \cos(q_1 D) + \cos(q_2 D) = \frac{1}{2}\ \mathrm{Tr}\,(\hat{T}) \\ 1 + \cos(q_1 D)\cos(q_2 D) = \frac{1}{4}\left\{\left[\mathrm{Tr}(\hat{T})\right]^2 - \mathrm{Tr}(\hat{T}^2)\right\}, \end{cases} \tag{5}$$

Here, q_1 and q_2 are the wave numbers of the normal electromagnetic waves in the film, while $\hat{T}$ is the 4×4 transfer matrix.

For the four-component unit cell under consideration, we get

$$\hat{T} = \hat{E}_{\uparrow}\hat{S}_{\uparrow,\odot}\hat{E}_{\odot}\hat{S}_{\odot,\downarrow}\hat{E}_{\downarrow}\hat{S}_{\downarrow,\otimes}\hat{E}_{\otimes}\hat{S}_{\otimes,\uparrow}, \tag{6}$$

where $\hat{S}_{L,K}, (L, K = \uparrow, \downarrow, \odot, \otimes)$, connects electric and magnetic field amplitudes of light between an MD and a DW or *vice versa*. Matrixes $\hat{E}_L$ describe

a phase change inside a layer labelled L [24, 43]; thus,

$$\hat{E}_L = \begin{pmatrix} e^{ik^+_{z,L}d_L} & 0 & 0 & 0 \\ 0 & e^{-ik^+_{z,L}d_L} & 0 & 0 \\ 0 & 0 & e^{ik^-_{z,L}d_L} & 0 \\ 0 & 0 & 0 & e^{-ik^-_{z,L}d_L} \end{pmatrix}, \tag{7}$$

where $k^{\pm}_{z,L}$ are the z-components of the wave vectors of electromagnetic waves inside the layer L. The quantities $k^{\pm}_{z,L}$ depend on the mutual orientation of the wave vector and the magnetization direction inside the particular layer, as well as on the permittivity tensor.

The solution of the equations(5) can be presented as follows [24]:

$$\cos(q_1 D) = \frac{1}{4}\left[\mathrm{Tr}\,(\hat{T}) + \sqrt{2\mathrm{Tr}\,(\hat{T}^2) - \mathrm{Tr}^2\,(\hat{T}) + 8}\right], \tag{8}$$

$$\cos(q_2 D) = \frac{1}{4}\left[\mathrm{Tr}\,(\hat{T}) - \sqrt{2\mathrm{Tr}\,(\hat{T}^2) - \mathrm{Tr}^2\,(\hat{T}) + 8}\right]. \tag{9}$$

¿From the solutions of (8) and (9), we can determine the forbidden bands in the spectrums of normal electromagnetic waves.

Two configurations of light propagation are worthy of further consideration: (i) propagation in the XZ plane, and (ii) propagation in the YZ plane.

3.1. PROPAGATION IN XZ PLANE

Let us first consider light propagating in the XZ plane. Then, the longitudinal magneto-optical configuration (magnetization vector parallel to the incidence plane) is realized in both MDs ($\uparrow$ and $\downarrow$), whereas the transversal magneto-optical configuration (magnetization vector is perpendicular to the incidence plane) is realized in the Bloch-type DWs ($\odot$ and $\otimes$) .

For the longitudinal magneto-optical configuration, we get

$$(k^{\pm}_z)^2 = \frac{1}{2\varepsilon_\perp}\left[-(\varepsilon_\perp + \varepsilon_\parallel) + (\varepsilon_\perp\varepsilon_\parallel + \Delta\varepsilon) \pm \sqrt{D(k_x)}\right]. \tag{10}$$

Here,

$$\begin{aligned} D(k_x) &= (\varepsilon_\perp + \varepsilon_\parallel)^2 + \Omega^4(\Delta\varepsilon - \varepsilon_\perp\varepsilon_\parallel)^2 + 2\Omega^2 k_x^2 \times \\ &\quad \times \left[-\varepsilon_\perp(\varepsilon_\perp - \varepsilon_\parallel)^2 + (\varepsilon_\perp + \varepsilon_\parallel)(\varepsilon')^2\right], \\ \Delta\varepsilon &= \varepsilon_\perp^2 - (\varepsilon')^2, \end{aligned} \tag{11}$$

with $\Omega = \frac{\omega}{c}$, where ω is the angular frequency of light and c is the velocity of light in vacuum.

If the wave vector $\mathbf{k} = (k_x, 0, k_z)$ is perpendicular to the magnetization direction in the medium, then transverse electric (TE) and transverse magnetic (TM) modes are the normal electromagnetic waves with $(k_z^{\pm})^2$ determined as follows:

$$(k_z^+)^2 = k_{TM}^2 = -k_x^2 + \Omega^2 \frac{\Delta\varepsilon}{\varepsilon_\perp}, \quad (k_z^-)^2 = k_{TE}^2 = -k_x^2 + \Omega^2 \varepsilon_\parallel \tag{12}$$

For the boundary between the domain $\uparrow$ and the Bloch-type DW $\odot$, the components of the matrix $\hat{S}_{\uparrow,\odot}$ satisfy the following relationships:

$$\begin{aligned} &S_{11} = S_{22}, \quad S_{12} = S_{21}, \quad S_{31} = S_{42}, \quad S_{32} = S_{41}, \\ &S_{13}^* = S_{24}, \quad S_{14}^* = S_{23}, \quad S_{33}^* = S_{44}, \quad S_{34}^* = S_{43}. \end{aligned} \tag{13}$$

Explicit expressions for the components of $\hat{S}_{\uparrow,\odot}$ are as follows:

$$\begin{aligned} S_{11} &= \frac{1}{2ab}\left(a + \kappa^{TE}\kappa_\varepsilon^- b\right), \quad S_{12} = \frac{1}{2ab}\left(a - \kappa^{TE}\kappa_\varepsilon^- b\right), \\ S_{13} &= \frac{1}{2ab}\alpha\left(\frac{a}{\kappa^-} + \varrho^- b\right), \quad S_{14} = \frac{1}{2ab}\alpha\left(\frac{a}{\kappa^-} - \varrho^+ b\right), \\ S_{31} &= -\frac{1}{2ab}\beta\left(\frac{a}{\kappa_\varepsilon^+} + \kappa^{TE} b\right), \quad S_{32} = -\frac{1}{2ab}\beta\left(\frac{a}{\kappa_\varepsilon^+} - \kappa^{TE} b\right), \\ S_{33} &= \frac{1}{2ab}\left(a + \varrho^-\kappa^+ b\right), \quad S_{34} = \frac{1}{2ab}\left(a - \varrho^+\kappa^+ b\right). \end{aligned} \tag{14}$$

In the foregoing expressions,

$$a = \kappa^+\kappa_\varepsilon^- + \alpha\beta, \quad b = \kappa_-\kappa_\varepsilon^+ + \alpha\beta, \tag{15}$$

$$\alpha = -\frac{ik_x k_z^- \varepsilon'}{\Omega^2\Delta\varepsilon - \varepsilon_\perp (k^2)}, \quad \beta = -\frac{ik_x k_z^+ \varepsilon'}{\Omega^2\varepsilon_\parallel\varepsilon_\perp - \left(\varepsilon_\perp k_z^2 + \varepsilon_\parallel k_x^2\right)}, \tag{16}$$

and

$$\begin{aligned} \kappa^\pm &= \frac{k_z^\pm}{\Omega}, \quad \kappa_\varepsilon^\pm = \frac{k_z^\pm}{\Omega\varepsilon_\parallel}, \\ \kappa^{TM} &= \frac{k_z^{TM}}{\Omega}, \quad \kappa^{TE} = \frac{k_z^{TE}}{\Omega}, \\ \varrho^\pm &= \frac{\varepsilon_\perp k_z^{TM} \pm i\varepsilon' k_x}{\Omega\Delta\varepsilon}. \end{aligned} \tag{17}$$

The other $\hat{S}$ matrixes entering (6) can be easily constructed from $\hat{S}_{\uparrow,\odot}$. As an index exchange is equivalent to matrix inversion, we get

$$\hat{S}_{\odot,\uparrow} = \left(\hat{S}_{\uparrow,\odot}\right)^{-1}. \tag{18}$$

Denoting the index inversion operation which changes the direction of the arrows into the opposite one by tilde (for example, $\downarrow = \tilde{\uparrow}$, $\otimes = \tilde{\odot}$), we can express the other $\hat{S}$ matrixes in (6) as follows:

$$\hat{S}_{\odot,\downarrow} = \hat{S}_{\odot,\tilde{\uparrow}} = \left(\hat{S}_{\tilde{\uparrow},\odot}\right)^{-1}, \quad \hat{S}_{\otimes,\uparrow} = \hat{S}_{\tilde{\odot},\uparrow} = \left(\hat{S}_{\uparrow,\tilde{\odot}}\right)^{-1}, \tag{19}$$
$$\hat{S}_{\otimes,\uparrow} = \hat{S}_{\tilde{\odot},\uparrow} = \left(\hat{S}_{\uparrow,\tilde{\odot}}\right)^{-1}, \quad \hat{S}_{\downarrow,\otimes} = \hat{S}_{\tilde{\uparrow},\tilde{\odot}}.$$

Under the operation of index inversion, the components of $\hat{S}$ in (14) change according to the following rule: inversion of the indexes $\uparrow$ and $\downarrow$ involves the substitution $\alpha \Leftrightarrow -\alpha$ in (14); inversion of the indexes $\odot$ and $\otimes$ switches the replacement $\rho^{\pm} \Leftrightarrow \rho^{\mp}$ in (14).

3.2. PROPAGATION IN YZ PLANE

Let us now consider light propagation in the YZ plane, as shown on Figure (2). In contrast to the previous case, the longitudinal magneto-optical configuration is realized for DWs and the transversal magneto-optical configuration for MDs.

For the boundary between the Bloch-type DW $\odot$ and the domain $\uparrow$, the components of the matrix $\hat{S}_{\odot,\uparrow}$ satisfy the relationships

$$S_{11} = S_{22}^*, \quad S_{12} = S_{21}^*, \quad S_{31} = S_{42}^*, \quad S_{32} = S_{41}^*, \tag{20}$$
$$S_{13} = S_{24}, \quad S_{14} = S_{23}, \quad S_{33} = S_{44}, \quad S_{34} = S_{43},$$

and are given as follows:

$$S_{11} = \frac{1}{2ab}\left(a + \varrho^{+}\kappa^{-}b\right), \quad S_{12} = \frac{1}{2ab}\left(a - \varrho^{-}\kappa^{-}b\right), \tag{21}$$
$$S_{13} = -\frac{1}{2ab}\alpha\left(\frac{a}{\kappa_{\varepsilon}^{-}} + \kappa^{TE}\right), \quad S_{14} = -\frac{1}{2ab}\alpha\left(\frac{a}{\kappa_{\varepsilon}^{-}} - \kappa^{TE}\right),$$
$$S_{31} = \frac{1}{2ab}\beta\left(\frac{a}{\kappa^{+}} + \varrho^{+}b\right), \quad S_{32} = \frac{1}{2ab}\beta\left(\frac{a}{\kappa^{+}} - \varrho^{-}b\right),$$
$$S_{33} = \frac{1}{2ab}\left(a + \kappa^{TE}\kappa_{\varepsilon}^{+}b\right), \quad S_{34} = \frac{1}{2ab}\left(a - \kappa^{TE}\kappa_{\varepsilon}^{+}b\right).$$

In these equations, the quantities $a, b, \alpha, \beta, \varrho$ are determined as in (15)–(17) after replacing k_x by k_y. As in the previous case, we can construct all the necessary $\hat{S}$-matrixes entering (6) using (18) and (19).

4. Numerical Results

We solved (8) and (9) for a $Y_3Fe_5O_{12}$ film. The chosen YIG is transparent in the near–infrared regime; specifically, at the free–space (i.e., vacuum)

wavelength $\lambda_0 = 1150$ nm, we have $\varepsilon^{(0)} = 4.62$ and $f = 0.02$. These values were used for all spectral calculations presented here. Whereas the thicknesses of the magnetic domains depend on internal magnetization, the usual thickness d_{DW} of a domain wall in YIG films is just a small percentage of the lattice period D [38]. We set $d_{DW} = 0.05D$ for the numerical calculations.

The results of sample calculations are presented in Figures 3–10. We computed the normalized angular frequency $\Omega D/(2\pi)$ of light versus the normalized wave number $k_x D/(2\pi)$ corresponding to a particular eigenvalue inside the magnetic PC. Figures 3–6 represent the dispersion diagrams for electromagnetic wave propagation in the XZ plane, whereas Figures 7–10 hold for propagation in the YZ plane, normally to the magnetization direction inside the MDs. The dark curves and shaded areas correspond to the photonic band gaps. In these figures, PBGs are identified for both right– and left–elliptically polarized eigenwaves. The values of wave numbers $q_{1,2} = \pi/D$ and $q_{1,2} = 0$ correspond to the edges of the PBGs. From the presented results, we conclude that the widths and the number of the PBGs change not only with the frequency but also with the lattice period D and the ratio $d_\uparrow/d_\downarrow$ (which equals $1/8, 2/7, 1/2$ or 1 in Figures 3–10). The domain thicknesses depend on the external magnetic *dc* field applied normally to the magnetic field [38], which means that PBGs are magnetically tunable.

The spectrums of normal propagation exhibit a complex structure — new bands emerge as $k_{x(y)}$ increases. The positions and widths of these bands depend on the thicknesses of the MDs with the different magnetization orientations inside the domains. As equations (8) and (9) have complicated forms, their solutions naturally exhibit some peculiarities. Figures 3–10 show that PBGs can split with increase in $k_{x(y)}$ and new branches appear when the ratio $d_\uparrow/d_\downarrow$ changes. Band-splitting can even vanish for certain ranges of the ratio $d_\uparrow/d_\downarrow$. For instance, the modes labelled 1 and 2 in Figure 3 clearly split for $d_\uparrow/d_\downarrow = 1/8$ as k_x increases. But in Figure 4, with the ratio $d_\uparrow/d_\downarrow$ increased to $2/7$, the two branches of both modes are closer to each other. For $d_\uparrow/d_\downarrow = 1/2$ in Figure 5, mode 2 is barely split, while the splitting of mode 1 is actually eliminated. Also, as the ratio $d_\uparrow/d_\downarrow$ tends towards unity, additional modes are seen, for examples,

- the mode labelled 1 in the left box of Figure 5 and the modes labelled $1, 3, 5$ in the left box of Figure 6 which correspond to $q_{1,2}D = \pi$, as well as
- the modes labelled 2 and 4 on the right box of Figure 6, corresponding to $q_{1,2}D = 0$.

Some of these modes start at non-zero values of $k_{x(y)}$.

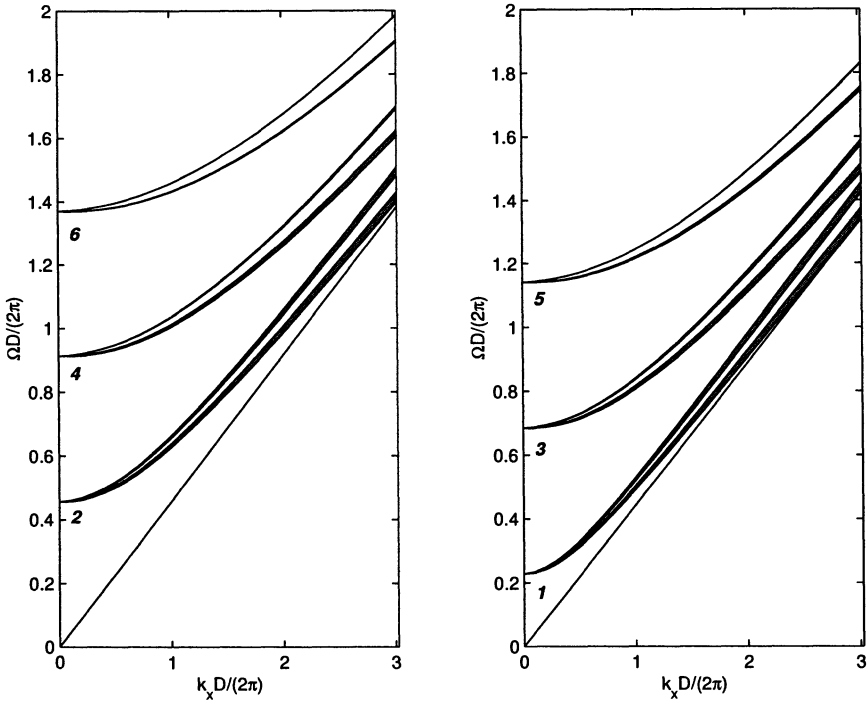

Figure 3. Normalized angular frequency $\Omega D/(2\pi)$ of light *versus* the normalized wave number $k_x D/(2\pi)$ of an eigenwave inside the magnetic photonic crystal when electromagnetic wave propagates in XZ plane. The domain thicknesses are $d_\uparrow = 0.1D$, $d_\downarrow = 0.8D$ and $d_{DW} = 0.05D$. The dark lines and the shaded regions present photonic band gaps. Left and right boxes correspond to the solutions of (8) and (9), respectively. The modes labelled as $1, 3, 5$ correspond to the values $q_{1,2}D = \pi$, whereas modes labelled as 2,4,6 refer to $q_{1,2}D = 0$

5. Conclusions

To conclude, we have shown that magnetic films with periodically striped domains can be considered as tunable PCs. The thicknesses of magnetic domains can be changed by applying a dc magnetic field, and the ratios of the thicknesses act as the *filling factors* of homogenization theories [44, 45].

Similar analysis can be accomplished for the striped-domain structure with the Néel-type DWs, wherein the magnetization vector rotates in the XZ plane. Then for the description of light propagation inside the DWs, we have to consider the polar magneto-optical configuration. Nonreciprocity

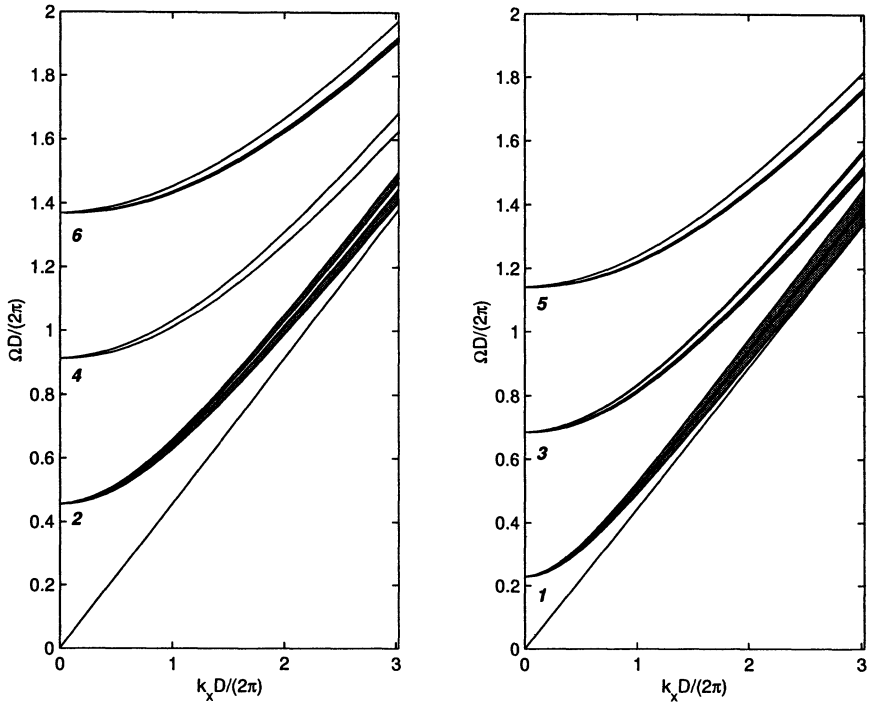

Figure 4. Same as Figure 3, except for $d_\uparrow = 0.2D$, $d_\downarrow = 0.7D$ and $d_{DW} = 0.05D$.

would occur in this configuration, as predicted by Figotin and Vitebsky [36]. Relevant calculations are in progress and will be published elsewhere.

The possibility of transforming a one-dimensional striped-domain structure to a two-dimensional lattice of magnetic bubbles under the increasing of *dc* magnetic field oriented normally to the film [38] is very interesting — thereby, in the same sample, we can effect transitions between PCs with different dimensionalities. Finally, let us indicate the possibility of investigating magnetic PCs with the nonlinear optical methods, e.g., nonlinear magneto-optical diffraction [46, 47].

Acknowledgement. This work was supported in part by a visitor's grant to Igor L. Lyubchanskii from the Dutch National Science Foundation (NWO).

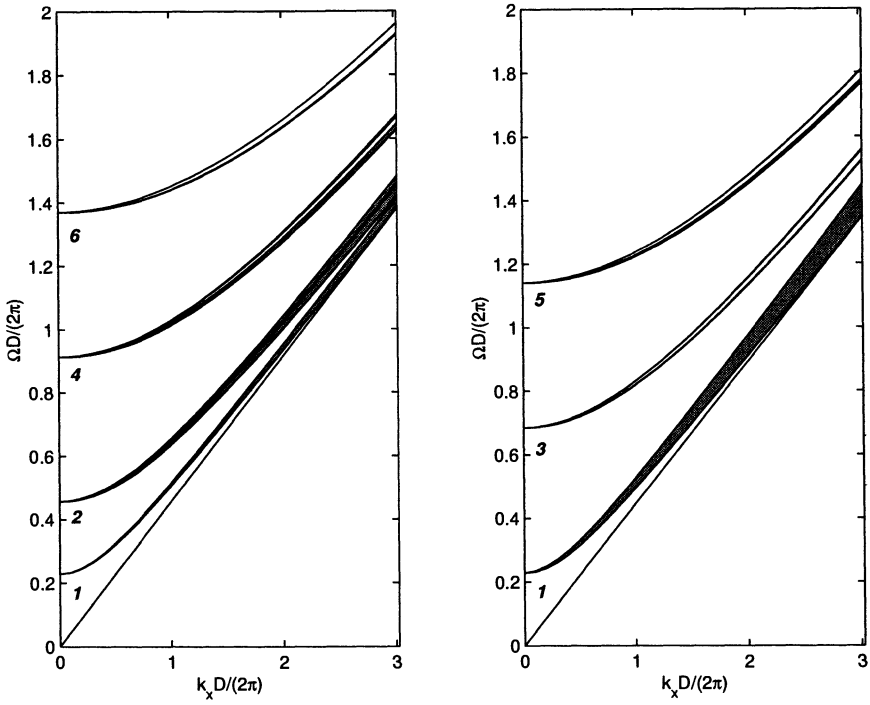

Figure 5. Same as Figure 3, except for $d_\uparrow = 0.3D$, $d_\downarrow = 0.6D$ and $d_{DW} = 0.05D$.

References

1. Joannopoulos, J.D., Meade, R.D. and Winn, J.N. (1995) *Photonic Crystals: Molding the Flow of Light*, Princeton University Press, Princeton, NJ, USA.
2. Sakoda, K. (2001) *Optical Properties of Photonic Crystals*, Springer, Berlin.
3. Sigalas, M.M., Soukoulis, C.M., Biswas, R. and Ho, K.M. (1997) Effect of the magnetic permeability on photonic band gaps, *Phys. Rev. B* **56**, pp. 959-962.
4. Kee, C.-S., Kim, J.-E., Park, H.-Y., Park, I. and Lim, H. (2000) Two-dimensional tunable magnetic photonic crystals, *Phys. Rev. B* **61**, pp. 15523-15525.
5. Vasseur, J.O., Dobrzynski, L., Djafari-Rouhani, B. and Puszkarski, H. (1996) Magnon band structure of periodic composites, *Phys. Rev. B* **54**, pp. 1043-1049.
6. Krawczyk, M., Lévy, J.-C., Mercier, D. and Puszkarski, H. (2001) Forbidden frequency gaps in magnonic spectra of ferromagnetic layered composites, *Phys. Lett. A* **282**, pp. 186-194.
7. Gulyaev, Yu.V. and Nikitov, S.A. (2001) Magnonic crystals and spin waves in periodic structures, *Dokl. Phys.* **46**, pp. 687–689.
8. Nikitov, S.A., Tailhades, Ph. and Tsai, C.S. (2001) Spin waves in periodic magnetic structures — magnonic crystals, *J. Magn. Magn. Mater.* **236**, pp. 320-330.
9. Al-Wahsh, H., Mir, A., Akjouj, A., Djafari-Rouhani, B. and Dobrzynski, L. (2001)

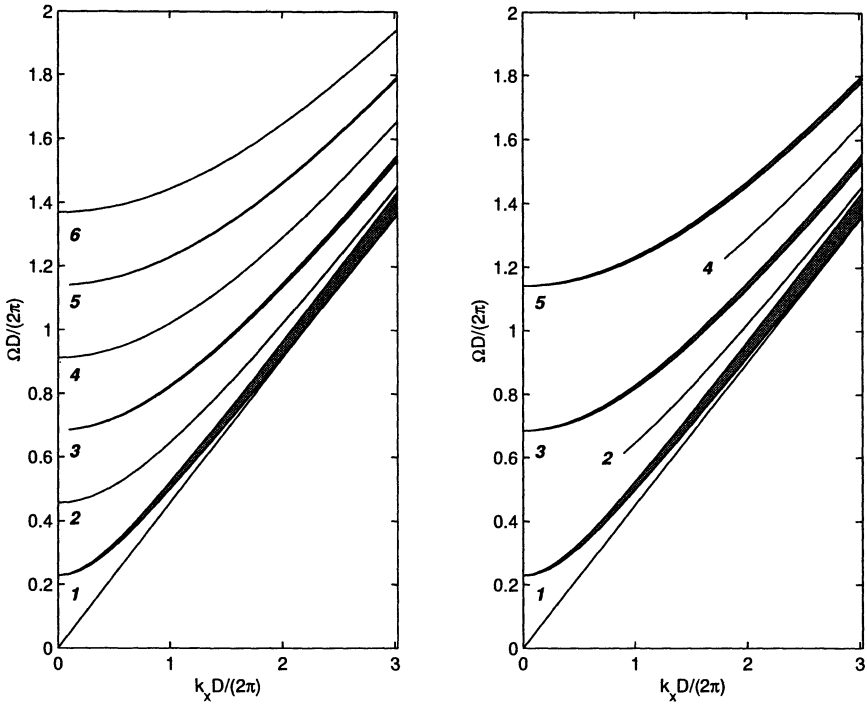

Figure 6. Same as Figure 3, except for $d_\uparrow = 0.45D$, $d_\downarrow = 0.45D$ and $d_{DW} = 0.05D$.

Magneto-transport in asymmetric serial loop structures, *Phys. Lett. A* **291**, pp. 333-337.

10. Mir, A., Al-Wahsh, H., Akjouj, A., Djafari-Rouhani, B., Dobrzynski, L. and Vasseur, J.O. (2002) Magnonic spectral gaps and discrete transmission in serial loop structures, *J. Phys.: Condens. Matter* **14**, pp. 637-655.
11. Kee, C.-S., Park, I., Lim, H. Kim, J.-E. and Park, H.–Y. (2001) Microwave photonic crystal multiplexer and its applications, *Current Appl. Phys.* **1**, pp. 84-87.
12. Kee, C.-S., Jang, M.-Y., Park, I., Lim, H., Kim, J.-E., Park, H.Y. and Lee, J.I. (2002) Photonic band gap formation by microstrip ring: A way to reduce the size of microwave photonic band gap structures, *Appl. Phys. Lett.* **80**, pp. 1520-1522.
13. Inoue, M. and Fujii, T. (1997) A theoretical analysis of magneto-optical Faraday effect of YIG films with random multilayer structures, *J. Appl. Phys.* **81**, pp. 5659-5661.
14. Inoue, M., Arai, K., Fujii, T. and Abe, M. (1998) Magneto-optical properties of one-dimensional photonic crystals composed of magnetic and dielectric layers, *J. Appl. Phys.* **83**, pp. 6768-6770.
15. Inoue, M., Arai, K., Fujii, T. and Abe, M. (1999) One-dimensional magnetophotonic crystals, *J. Appl. Phys.* **85**, pp. 5768-5770 .
16. Takeda, E., Todoroki, N., Kitamoto, Y., Abe, M., Inoue, M., Fujii, T. and Arai, K. (2000) Faraday effect enhancement in Co-ferrite layer incorporated into one-

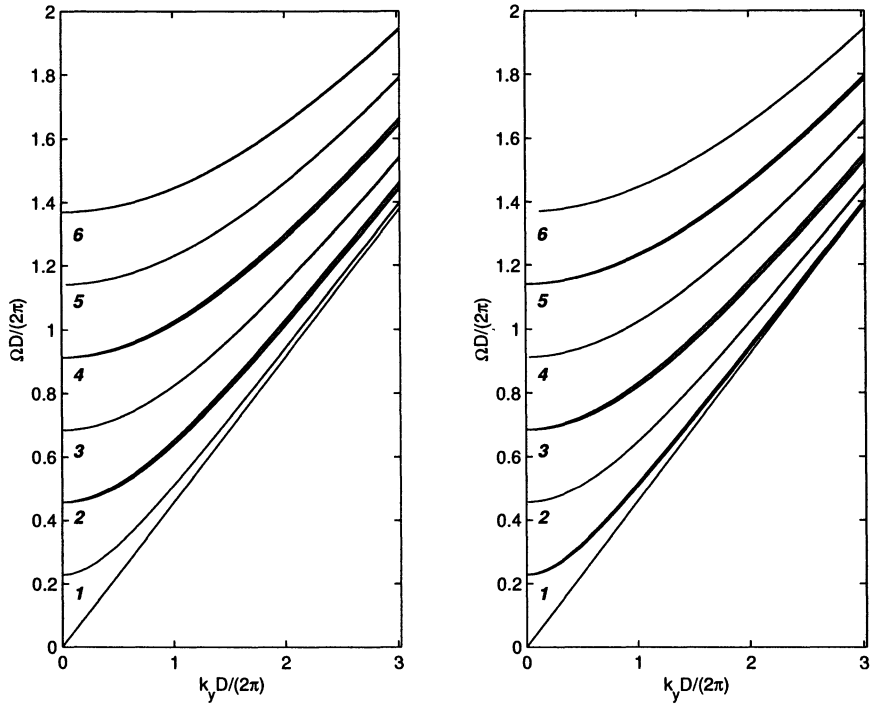

Figure 7. Normalized angular frequency $\Omega D/(2\pi)$ of light *versus* the normalized wave number $k_y D/(2\pi)$ of an eigenwave inside the magnetic photonic crystal when electromagnetic wave propagates in YZ plane. The domain thicknesses are $d_\uparrow = 0.1D$, $d_\downarrow = 0.8D$ and $d_{DW} = 0.05D$. The dark lines and the shaded regions present photonic band gaps. Left and right boxes correspond to the solutions of (8) and (9), respectively. The modes labelled as1, 3, 5 correspond to the values $q_{1,2}D = \pi$, whereas modes labelled as 2,4,6 refers to $q_{1,2}D = 0$

dimensional photonic crystal working as a Fabry-Pérot resonator, *J. Appl. Phys.* **87**, pp. 6782-6784.

17. Kato, H. and Inoue, M. (2002) Reflection-mode operation of one-dimensional magnetophotonic crystals for use in film-based magneto-optical isolator devices, *J. Appl. Phys.* **91**, pp. 7017-7019.
18. Steel, M.J., Levy, M. and Osgood, R.M. (2000) Large magneto-optical Kerr rotation with high reflectivity from photonic bandgap structures with defects, *J. Lightwave Technol.* **18**, pp. 1289-1296.
19. Steel, M.J., Levy, M. and Osgood, R.M. (2000) Photonic bandgaps with defects and the enhancement of Faraday rotation, *J. Lightwave Technol.* **18**, pp. 1297-1308.
20. Steel, M.J., Levy, M. and Osgood, R.M. (2000) High transmission enhanced Faraday rotation in one-dimensional photonic crystals with defects, *IEEE Photonics Technol. Lett.* **12**, pp. 1171-1173.

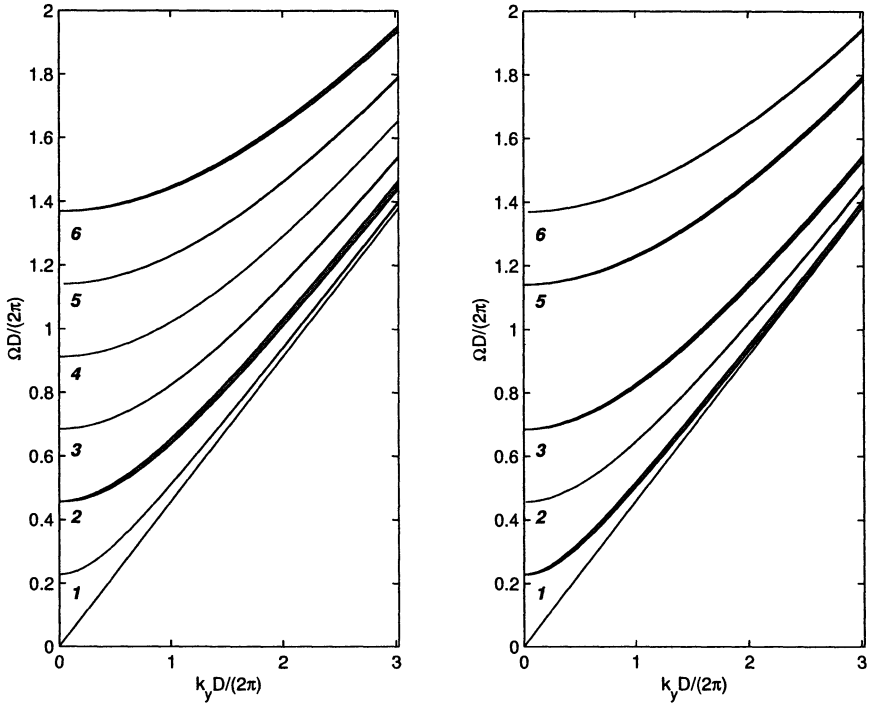

Figure 8. Same as Figure 7, except for $d_\uparrow = 0.2D$, $d_\downarrow = 0.7D$ and $d_{DW} = 0.05D$

21. Levy, M., Yang, H.C., Steel, M.J. and Fujita, J. (2001) Flat–top response in one-dimensional magnetic photonic bandgap structures with Faraday rotation enchancement, *J. Lightwave Technol.* **19**, pp. 1964-1969.
22. Shimizu, H., Miyamura, M. and Tanaka, M. (2001) Magneto-optical properties of a GaAs:MnAs hybrid structure sandwiched by GaAs/AlAs distributed Bragg reflectors: Enhanced magneto-optical effect and theoretical analysis, *Appl. Phys. Lett.* **78**, pp. 1523-1525.
23. Tanaka, M., Shimizu, H. and Miyamura, M. (2001) Enhancement of magneto-optical effect in GaAs:MnAs hybrid nanostructure sandwiched by GaAs/AlAs distributed Bragg reflectors: epitaxial semiconductor-based magneto-photonic crystal, *J. Cryst. Growth* **227**, pp. 839-846.
24. Borisov, S.B., Dadoenkova, N.N. and Lyubchanskii, I.L. (1993) Normal electromagnetic waves in bigyrotropic magnetooptic layered structures, *Opt. Spectrosc.* **74**, pp. 670-675.
25. Heim, K.R. and Scheinfein, M.R. (1996) An alternative approach for magneto-optic calculations involving layered media, *J. Magn. Magn. Mater.* **154**, pp. 141-152.
26. Ivanov, O.V. and Sementsov, D.I. (1997) Magneto-optical interaction of light with a periodic bi-gyrotropic structure, *Pure Appl. Opt.* **6**, pp. 455-464.
27. Sakaguchi, S. and Sugimoto, N. (1999) Multilayer films composed of periodic

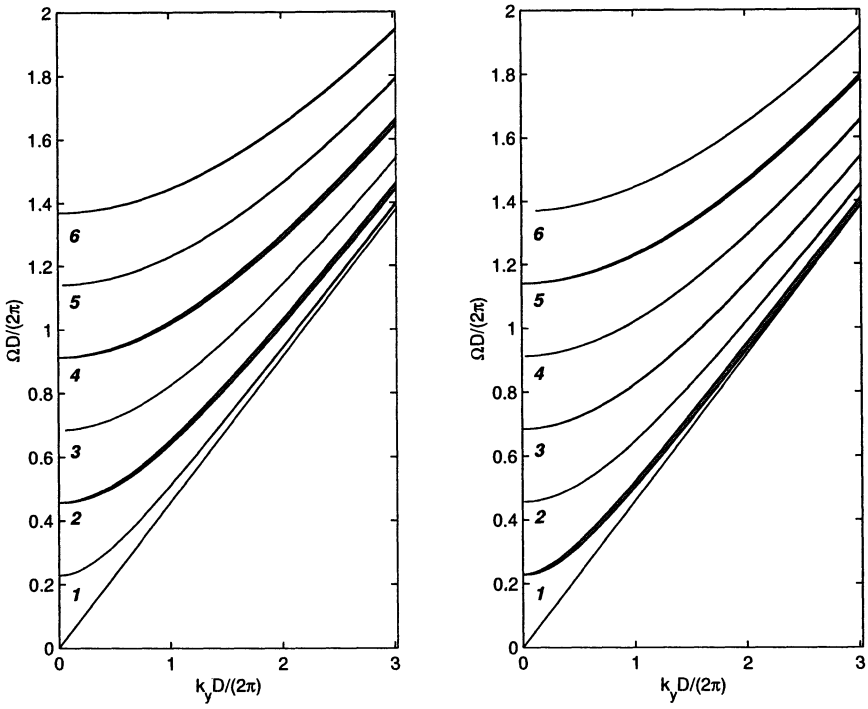

Figure 9. Same as Figure 7, except for $d_\uparrow = 0.3D$, $d_\downarrow = 0.6D$ and $d_{DW} = 0.05D$.

magneto-optical and dielectric layers for use as Faraday rotators, *Opt. Comm.* **162**, pp. 64-70.

28. Sakaguchi, S. and Sugimoto, N. (1999) Transmission properties of multilayer films composed of magneto-optical and dielectric materials, *J. Lightwave Technol.* **17**, pp. 1087-1092.
29. Schubert, M., Tiwald, T.E. and Woollam, J.A. (1999) Explicit solutions for the optical properties of arbitrary magneto-optic materials in generalized ellipsometry, *Appl. Opt.* **38**, pp. 177-187.
30. Abdulhalim, I. (2000) Analytic propagation matrix method for anisotropic magneto-optic layered media, *J. Opt. A: Pure Appl. Opt.* **2**, pp. 557-564.
31. Visnovsky, S., Postava, K. and Yamaguchi, T. (2001) Magneto-optic polar Kerr and Faraday effects in periodic multilayers, *Opt. Exp.* **9**, pp. 158-171.
32. Kim, K., Lim, H. and Lee, D.-H. (2001) Invariant imbedding equations for electomagnetic waves in stratified magnetic media: applications to one-dimensional photonic crystals, *J. Korean Phys. Soc.* **39**, pp. L956-L960.
33. Nishizawa, H. and Nakayama, T. (1997) Magneto–optic anisotropy effect on photonic band structure, *J. Phys. Soc. Jpn.* **66**, pp. 613–617.
34. Bulgakov, A.A. and Shramkova, O.V. (2001) Photonic band structure of a periodic semiconductor/dielectric multilayer in an external magnetic field, *J. Commun. Technol. Electron.* **46**, pp. 217-220.

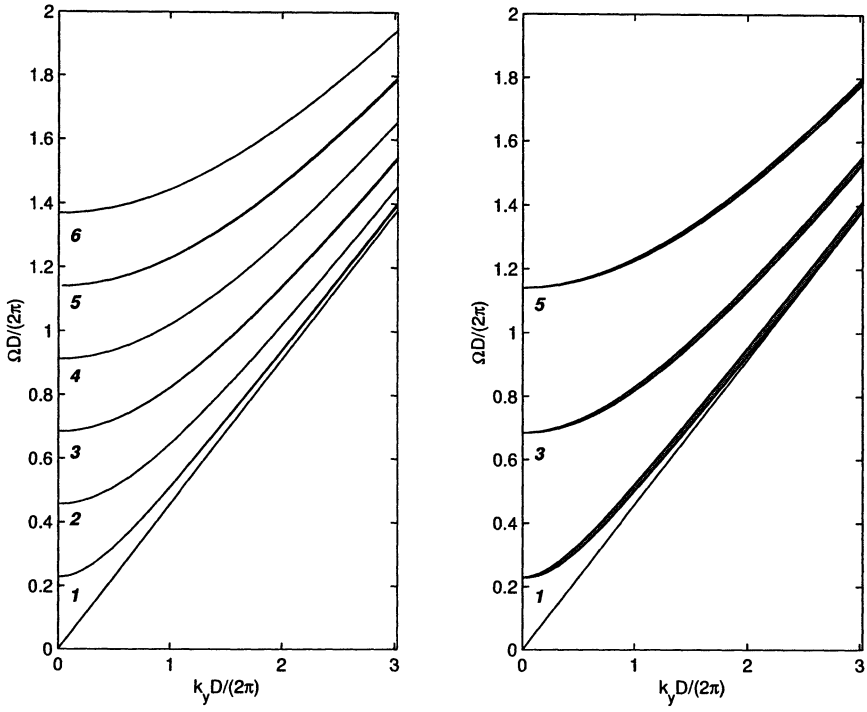

Figure 10. Same as Figure 7, except for $d_\uparrow = 0.45D$, $d_\downarrow = 0.45D$ and $d_{DW} = 0.05D$.

35. Kushwaha M.S. and Martinez, G. (2002) Magnetic-field-dependent band gaps in two-dimensional photonic crystals, *Phys. Rev. B* **65**, 153202.
36. Figotin, A. and Vitebsky, I. (2001) Nonreciprocal magnetic photonic crystals, *Phys. Rev. E* **63**, 066609.
37. Hu, B. and Wang, W.Z. (2002) Magneto-optic effects in a nonlinear photonic crystal, *Phys. Rev. B* **65**, 165207.
38. Hubert, A. and Schäfer, R. (1998) *Magnetic Domains: The Analysis of Magnetic Microstructures*, Springer, Berlin.
39. Sementsov, D.I. (1980) On the theory of optical waveguide modes in stripe domain structure, *Mikroelektronika* **9**, pp. 473-476.
40. Nikitov, S.A. and Tailhades, Ph. (2001) Optical modes conversion in magneto-photonic crystal waveguides, *Opt. Comm.* **199**, pp. 389-397.
41. Smolenskii, G.A. and Lemanov, V.V. (1975) *Ferrites and Their Technical Applications*, Nauka, Leningrad (in Russian).
42. Zvezdin, A.K. and Kotov, V.A. (1997) *Modern Magnetooptics and Magnetooptical Materials*, IoP, Bristol, UK.
43. Lakhtakia, A. (1993) Frequency–dependent continuum electromagnetic properties of a gas of scattering centers, *Adv. Chem. Phys.* **85** pt. 2, pp. 311–359.
44. Born, M. and Wolf, E. (1980) *Principles of Optics*, Pergamon, Oxford, UK.

45. Lakhtakia, A. (ed.) (1996) *Selected Papers on Linear Optical Composite Materials*, SPIE, Bellingham, WA, USA.
46. Dadoenkova, N.N., Lyubchanskii, I.L., Lyubchanskii and M.I., Rasing Th. (1999) Nonlinear magneto-optical diffraction from periodic domain structures in magnetic films, *Appl. Phys. Lett.* **74**, pp. 1880-1882.
47. Lyubchanskii, I.L., Dadoenkova, N.N., Lyubchanskii, M.I., Shapovalov, E.A., Zabolotin, A.E., Guslienko, K.Y. and Rasing Th. (2002) Nonlinear magneto-optical diffraction by two-dimensional magnetic superstructures, *Appl. Phys. B* **74**, pp. 711-714.

SIMULATION OF FINITE PHOTONIC CRYSTALS MADE OF BIISOTROPIC OR CHIRAL MATERIAL

Using the Method of Auxiliary Sources

D.D. KARKASHADZE[1], F.G. BOGDANOV[1,2], R.S. ZARIDZE[1],
A.Y. BIJAMOV[1], C. HAFNER[3], and D. ERNI[3]
[1]Tbilisi State University, Chavchavadze Ave., 380028 Tbilisi, Georgia
[2]Georgian Technical University, Kostava Str., 380075 Tbilisi, Georgia
[3]Swiss Federal Institute of Technology, CH-8092 Zurich, Switzerland

Abstract. This chapter proposes complex materials (anisotropic, chiral, Tellegen, and general biisotropic) as element base for Finite Photonic Crystal (FPC) devices, offers an effective method for their handling, illustrates possibilities of their numerical analysis and discusses results for FPC design. The approach is based on the Method of Auxiliary Sources (MAS) and its implementation to complex structures.

1. Introduction

Traditional Integrated Optics (IO) circuits are huge compared to the wavelength to avoid unacceptable high radiation losses on sharp bends in optical waveguides and undesired interaction between different components. Artificial Photonic Crystals (PCs) exhibit Photonic Band Gap (PBG), i.e. totally reflect the incident field in a certain frequency range. This is the key to new IO components based on the Finite Photonic Crystals (FPCs) with appropriate defects, where a distinct localization of the light field may occur [1]. For instance, a FPC defect waveguide is easily obtained from a line defect, represented by a column of missing elements in an underlying PC. Relying on such alternative wave-guiding scheme, more sophisticated IO components, such as sharp waveguide bends without radiation losses, couplers, splitters, resonators, filters, etc. can be designed. However, realization of such devices is rather demanding on accuracy because of coupling of thousands of resonating cells and needs thus development of high-efficient numerical methods.

In design of FPC devices, the following main steps are usually performed: 1) The PBG structure of an infinite, perfect PC is analyzed to find a PC with an according lattice structure providing sufficiently wide band gap (BG) that includes the operation wavelengths of the FPC device. This step requires solution of an eigenvalue problem for the perfect PC.

S. Zouhdi et al. (eds.), Advances in Electromagnetics of Complex Media and Metamaterials, 175–193.

2) The FPC defect modes are found for waveguides in PCs obtained from line defects breaking the symmetry of the perfect PC. This step requires solution of an eigenvalue problem for imperfect PC with broken periodicity.
3) The PC with additional defects, such as several waveguides of finite length, discontinuities along waveguides and so on, are analyzed to obtain defect modes in more complicated FPC devices (waveguide bends, filters, couplers, splitters, etc.).

This step requires solution of propagation, scattering and synthesis problems upon a huge number of cells with different material filling.

Up to now, various methods exist to analyze BG structure of PCs with different lattice structure [1]. The supercell method [2] is developed to analyze separate FPC defect modes. The Finite Differences Time Domain (FDTD) codes [3] and more accurate procedure based on the Multiple Multipole Program (MMP) [4-5] are usually used to analyze more complicated FPC devices. The software packages, such as MaX-1 [6] linking the solvers with optimizers for automatic FPC device design, are also created. However, drawback of these methods and codes is their restriction to the simple 2-parameter isotropic materials, whereas most of natural materials are complex, i.e. have additional material properties and arised from them interesting and useful properties, such as sensitivity to the polarization plane rotation direction, non-reciprocity, and so on. Moreover, most of complex materials, including 3-parameter chiral and Tellegen, were first discovered in optical range, in which their properties are manifested most intensively. Thus, we can expect that embedding complex materials in FPC device design might enlarge the chance to control their properties and be useful for design of tunable FPC devices and devices with additional functionalities.

The aim of this work is to propose the complex materials (anisotropic, chiral, Tellegen and general biisotropic) as element base of FPC and FPC devices, to offer the effective method for their handling, to illustrate the possibilities of computer code based on this method, and to present and discuss some numerical results of FPC design. To provide this aim, a new approach is suggested in this work which is based on the Method of Auxiliary Sources (MAS) [7-9] and its implementation [10-17] to the structures of complex (chiral and biisotropic) materials [18-22]. Note, that MAS is closely related to MMP: MAS mainly uses monopole solutions whereas MMP is based on more complicated multipole expansions.

The work is structured as follows. Chapter 2 is intended to adapt the MAS to FPC design and describe its stages. Section 2.1 gives a glance on physical essence of MAS and its main problems. Section 2.2 describes procedure of determining main singularities and optimal distributing auxiliary sources, which is the key problem for adapting MAS to particular problems. Section 2.3 gives a glance on mathematical aspects of applying MAS to particular boundary problems based on complex materials. Section 2.4 adapts the MAS to solution of eigenvalue problems for anisotropic, chiral and biisotropic media. Chapter 3 describes examples of simple FPC device simulation.

2. MAS solution of electromagnetic scattering problems

2.1. CONVENTIONAL MAS

To clarify the main idea of MAS, let us consider a simple scattering problem consisting of two domains D_1 and D_2 with different material properties (Figure 1), illuminated by the incident field $\{E^i, H^i\}$. Assume that the incident field has the point source S_1 that is located in the domain D_1.

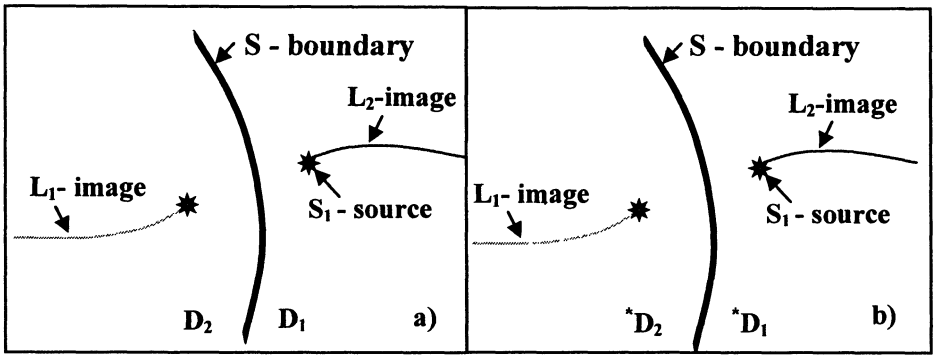

Figure 1. Boundary *(S)* between two different domains D_1 and D_2 (clear and the shaded region) from different viewpoints: a) The source S_1 and its two lines of images L_2 in D_1 and L_1 in D_2. b) The same treatment with exchanged material parameters defines the mirror domains ${}^*D_1$ and ${}^*D_2$.

Let $\{E_1,H_1\}$ and $\{E_2,H_2\}$ denote the scattered fields in D_1 and D_2 respectively. In Figure 1a, the line L_1 represents the image of the source S_1 in the domain D_1, whereas the line L_2 represents the image of S_1 in the domain D_2. In Figure 1b, the mirror domains ${}^*D_1$ and ${}^*D_2$ of the original domains are shown. The mirror domains are obtained simply by exchanging material parameters. These mirror domains are used for the continuation (with its derivatives) of the scattered fields beyond the border S. Let the continuations of $\{E_1,H_1\}$ and $\{E_2,H_2\}$ be $\{{}^*E_1, {}^*H_1\}$ and $\{{}^*E_2, {}^*H_2\}$, respectively. These fields are called image fields or fields of the mirror images. For a given source and boundary, the image fields are uniquely defined. It is important to know that the image fields have singularities in each of the "mirror" domains ${}^*D_1$ and ${}^*D_2$ along the lines of images L_1 and L_2. We call them Scattered Field's Main Singularities (SFMS) in the sense that their specification completely defines the scattered fields.

It is obvious that the total image fields $\{{}^*E_1+{}^*E^i, {}^*H_1+{}^*H^i\}$ and $\{{}^*E_2, {}^*H_2\}$ satisfy Maxwell's equations in the mirror domains ${}^*D_2$ and ${}^*D_1$, respectively. Moreover, these image fields also fulfill the continuity conditions along the boundary S. Now, we can repeat the procedure and determine the images of the image fields. These fields are nothing else than the original scattered fields. Thus,

determining 1) the lines images L_1 and L_2 and 2) the type of the singularities (the image source type) of the mirror fields on these lines leads to a very compact description of the scattered fields. These singularities can act as sources of this field (e.g. the simplest, zero order singularity corresponds to the well-known monopole field). For obtaining a numerical solution we must always work with a discrete approximation of these sources which were located along the lines of images, called auxiliary sources. Although these locations may be found in simple cases, it may be very time-consuming to find them for more complicated geometries. In such the cases we should then follow to the general recommendations outlined particularly in [15,23].

2.2. 2D SCATTERING AT A BOUNDARY BETWEEN TWO DOMAINS

Figure 2 depicts the geometry of a 2D scattering problem with an analytically defined boundary between two domains. For such cases, the procedure of an accurate localization of the SFMS has been elaborated in [24]. As mentioned before, this procedure becomes time-consuming for the complicated, multi-linked domains with boundaries that are only piecewise analytical. For such boundaries, it is reasonable find auxiliary lines that are between the boundaries and the lines of images. A major problem arises when one has to find the lines of images for complicated boundary shapes. This problem may be circumvented by the following procedure: Since we know that the start points of the lines of images are near the centers of principal curvatures of the boundary S, we can construct auxiliary lines that are between the boundaries and these centers.

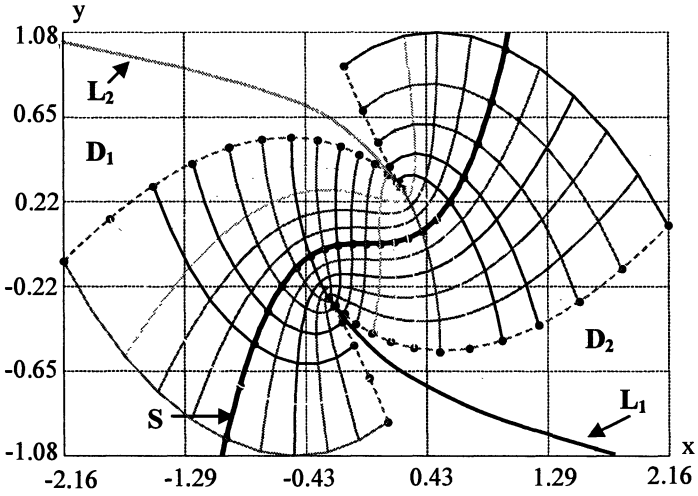

Figure 2. Geometry of a 2D scattering problem represented by an analytically defined boundary between two domains D_1 and D_2. The development towards two lines of images L_1 and L_2 are shown by auxiliary lines, each representing a different step in the underlying localization procedure of the SFMS.

In Figure 2, conformal mapping is used for constructing appropriate auxiliary lines. Note that this construction is not unique and that the conformal mapping easily allows one to find auxiliary lines at different distances from the boundaries. In general, we observe that the accuracy of the results increases with the distance of the auxiliary lines from the boundary. Since the auxiliary lines may not cross the lines of images, there are limit lines for the auxiliary lines. These limit lines are indicated in Figure 2 by dotted lines.

The next step is now to distribute auxiliary sources along the auxiliary lines and to construct appropriate matching points along the boundary. These matching points will be used later on to compute the amplitudes of the auxiliary sources. The simplest kind of auxiliary sources are monopole sources. In the following, we will focus on monopole sources. Note that a link to MMP [4-5] is easily obtained by using general multipole sources instead of monopoles. Figure 2 illustrates that both appropriate sets of auxiliary sources and matching points (circles on the boundary S) may be obtained from conformal mapping.

Assume that we have a set of N auxiliary sources on each side of the boundary, i.e., we have a total number of $2N$ unknown amplitudes for E and H waves and $4N$ unknowns for the general HE or EH waves. When imposing two continuity conditions according to the E and H wave case and 4 continuity conditions for the general case in each matching point, we immediately obtain a linear system of equations, which is characterized by a $2N$ by $2N$ matrix or a $4N$ by $4N$ matrix respectively. By solving this system, we obtain the amplitudes of the auxiliary sources. As alternatives, we can work with the Generalized Point Matching technique [25] that uses overdetermined systems of equations obtained by increasing the number of matching points, or Galerkin techniques that are well known from the Method of Moments (MoM) [26]. Corresponding examples and further descriptions of the mathematical background are given in [27-29]. It will be shown below, that this procedure is also efficient for the simulation of wave propagation in FPCs consisting of complex, composite materials.

FPCs usually consist of many bodies with specified geometry. However, the extension of the method described above to this more general case is straightforward and needs no further explanation. In the following subsection we will focus on the handling of complicated material properties that may offer new features for FPC devices because such media provide more degrees of freedom than conventional isotropic materials.

2.3 MAS COMPUTATION OF WAVES IN BIISOTROPIC MEDIA

In order to apply the MAS to biisotropic media, we must provide at least an explicit description for the simplest auxiliary sources, i.e., monopoles in such media. We assume that a four-parameter biisotropic medium [20-21] is present, which can be described by the constitutive relations

$$\vec{D}=\varepsilon\vec{E}+i\alpha\vec{B},\quad \vec{H}=i\beta\vec{E}+\mu^{-1}\vec{B} \tag{1}$$

Here ε, μ, α and β are the permittivity, the permeability, and the magnetoelectric admittances, respectively. Note that harmonic $e^{-i\omega t}$ time dependence is assumed and suppressed in the following. The constitutive relations include, as special cases, all other media with scalar parameters, such as chiral ($\alpha=\beta\neq 0$), Tellegen ($\alpha=-\beta$) and isotropic magneto-dielectric ($\alpha=\beta=0$) materials.

Biisotropic media are known to be sensitive to the direction of the polarization plane rotation. Therefore, it is very convenient to use the compact spinor notation for the electromagnetic field [30]:

$$\vec{F}=\begin{pmatrix}\vec{F}^{r}\\ \vec{F}^{\ell}\end{pmatrix}, \tag{2}$$

where $\vec{F}^{r}=\vec{E}+i\eta^{r}\vec{H}$ and $\vec{F}^{\ell}=\vec{E}-i\eta^{\ell}\vec{H}$ are the right-handed and left-handed components of the proposed spinor field. Here, η^{r}, η^{ℓ} are the corresponding components of the wave impedance matrix

$$\hat{\eta}=\begin{pmatrix}\eta^{r}\\ \eta^{\ell}\end{pmatrix},\quad \eta^{r,\ell}=\eta_0\cdot\left(\sqrt{\eta^{-2}+\frac{(\alpha+\beta)^2}{4}}\mp\frac{\alpha-\beta}{2}\right)^{-1},\quad \eta_0=\sqrt{\frac{\mu_0}{\varepsilon_0}},\quad \eta=\sqrt{\frac{\mu_r}{\varepsilon_r}}. \tag{3}$$

We now need to determine the electromagnetic spinor field (2) satisfying Maxwell's equations in Majorana-Dirac form:

$$\vec{\nabla}\times\vec{F}-\hat{k}\,\vec{F}=0. \tag{4}$$

The boundary conditions for the continuity of the tangential components of electromagnetic field at the boundary S of the domain D are:

$$\hat{W}\,\vec{F}(\vec{r})\Big|_{\vec{r}=\vec{r}^{\,s}}=\vec{f}(\vec{r}^{\,s}),\quad M(\vec{r}^{\,s})\in S. \tag{5}$$

Here $\hat{W}$ is the operator for the boundary conditions, and $\vec{f}(\vec{r}^{\,s})$ is a given function describing the excitation along the boundary. A standard procedure for constructing the solution of the given boundary problem (4)-(5) may be subdivided into the following six stages:

a) Near the boundary S, an auxiliary line S' is constructed as described in the previous subsection. Along the auxiliary line, we first uniformly distribute infinite set of auxiliary points $\{\vec{r}_n\}_{n=1}^{\infty}$. Note that for the numerical solution we will need

only a finite set of auxiliary points. The infinite set considered in the following, will allow us to construct different finite sets afterwards.
b) For a point $\vec{r}_n$, a spinor-vector basis is introduced as illustrated in Figure 3

$$\vec{\tau}_n = \begin{pmatrix} \vec{\tau}_n^{\,r} \\ \vec{\tau}_n^{\,\ell} \end{pmatrix} = \begin{pmatrix} \vec{\tau}_v + i\vec{\tau}_u \\ \vec{\tau}_v - i\vec{\tau}_u \end{pmatrix} \tag{6}$$

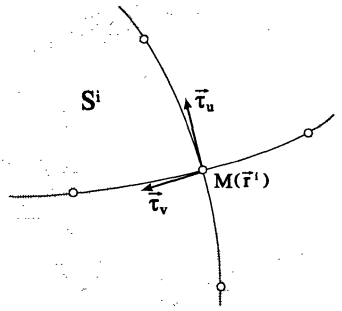

Figure 3: Spinor-vector basis on the auxiliary surface.

c) From the fundamental solutions of the Majorana-Dirac equations

$$\Delta \times \vec{\vec{F}}_n - \hat{k}\vec{\vec{F}}_n = \vec{\vec{\tau}}_n \cdot \delta(\vec{r} - \vec{r}_n) \tag{7}$$

for the auxiliary points, we obtain a set of functions given by

$$\left\{\vec{\vec{F}}_n(\vec{r},\vec{r}_n)\right\}_{n=1}^{\infty} \tag{8}$$

with radiation centers located at the auxiliary points $\{\vec{r}_n\}_{n=1}^{\infty}$. It has been shown in [10,15], that these functions may be expressed as follows

$$\vec{\vec{F}}_n^{\,r,\ell} = \vec{\nabla} \times \left(\hat{G}_n \cdot \vec{\vec{\tau}}_n\right) \pm \frac{1}{k^{r,\ell}} \vec{\nabla}\vec{\nabla}\left(\hat{G}_n \cdot \vec{\vec{\tau}}_n\right) \pm \hat{k} \cdot \left(\hat{G}_n \cdot \vec{\vec{\tau}}_n\right). \tag{9}$$

The corresponding matrices for the wave numbers and the Green's functions have the standard form [20,21]:

$$\hat{k}=\begin{pmatrix} k^r & 0 \\ 0 & -k^\ell \end{pmatrix}, \quad k^{r,\ell}=k\cdot\eta\cdot\left(\sqrt{\eta^{-2}+\frac{(\alpha+\beta)^2}{4}}\pm\frac{\alpha+\beta}{2}\right), \; k=k_0\sqrt{\varepsilon_r\mu_r} \tag{10}$$

$$\hat{G}_n=\begin{pmatrix} G_n^r & 0 \\ 0 & G_n^\ell \end{pmatrix}, \tag{11}$$

where

$$G_n{}^{r,\ell}(\vec{\rho},\vec{\rho}_n)=H_0^{(1)}(k^{r,\ell}|\vec{\rho}-\vec{\rho}_n|).$$

In addition to these monopole solutions, other singular solutions (namely, multipoles) of the wave equation exist.

d) Based of the set of functions (8), a new set of vector basis functions $\{\vec{\Phi}_n(\vec{r}^{\,s})\}_{n=1}^{\infty}$ valid on the surface S is obtained:

$$\vec{\Phi}_n(\vec{r}^{\,s})=\hat{W}\,\vec{F}_n(\vec{r},\vec{r}_n)\Big|_{\vec{r}=\vec{r}^{\,s}}, \quad \vec{r}^{\,s}\in S, \quad (n=1,2,...); \tag{12}$$

e) It has been proved [27-29] that the set (12) is complete and linearly independent in the functional space $\mathbf{L_2}$. This allows us to obtain an approximate solution of the considered boundary problem from the superposition of N basis functions of the truncated set given by the expression (8)

$$\vec{F}^{(N)}(\vec{r})=\sum_{n=1}^{N}\hat{a}_n\vec{F}_n(\vec{r},\vec{r}_n), \quad \vec{r}\in D, \qquad \hat{a}_n=\begin{pmatrix} a_n^r & 0 \\ 0 & a_n^\ell \end{pmatrix}, \tag{13}$$

where the expansion coefficients $\{\hat{a}_n\}_{n=1}^{N}$ define the unknown amplitudes of the auxiliary spinor sources. These coefficients can be determined using the point matching technique that was already outlined in the previous subsections.

f) Finally, using the electromagnetic spinor field $\vec{F}^{(N)}(\vec{r})$, the total (both right-hand and left-hand) components of the scattered electromagnetic field are derived from the simple relations linking the spinor representation to the vector representation of the electromagnetic field

$$\begin{aligned} \vec{E}^{sc}(\vec{r})&=\vec{E}_{sc}^{\,r}+\vec{E}_{sc}^{\,\ell}=\frac{\eta^r}{\eta^r+\eta^\ell}\sum_{n=1}^{N}a_n^\ell\vec{F}_n^{\,\ell}(\vec{r},\vec{r}_n)+\frac{\eta^\ell}{\eta^r+\eta^\ell}\sum_{n=1}^{N}a_n^r\vec{F}_n^{\,r}(\vec{r},\vec{r}_n) \\ \vec{H}^{sc}(\vec{r})&=\vec{H}_{sc}^{\,r}+\vec{H}_{sc}^{\,r}=\frac{i}{\eta^r}\vec{E}_{sc}^{\,r}-\frac{i}{\eta^\ell}\vec{E}_{sc}^{\,r} \end{aligned} \tag{14}$$

Accurate results are obtained efficiently when both the radiation centers $\{\vec{r}_n\}_{n=1}^{N}$ and

the types of auxiliary sources are selected according to the SFMS (See Section 2.2).

2.4. EIGENVALUE PROBLEMS

Eigenvalue problems in guided wave electromagnetics, e.g. calculation of the eigenvalues and eigenfields of cylindrical waveguides is usually reduced to the analysis of homogeneous systems of algebraic equations. Therefore, non-trivial solutions are only obtained if the matrix describing this system is singular i.e. the corresponding determinant is zero. This defines a highly nonlinear characteristic equation for the given eigenvalue problem. The same procedure may be used for the eigenvalue problems obtained in the analysis of resonators and photonic band gaps [31]. However, this procedure often exhibits severe numerical problems due to the large condition number of the matrix near the zeros of the determinant.

On the basis of MAS, a relatively simple method for eigenmode calculations was suggested in [7], based on the solution of an inhomogeneous system of linear algebraic equations. In order to obtain an inhomogeneous system, a fictitious excitation is introduced. This may be considered as a mathematical model of a real-world experiment, where one also needs an excitation for measuring the eigenvalues by finding the peak values of the field inside a resonator.

Let us consider a cylindrical waveguide with the cross-section D, bounded by the contour L. As before, the restriction to one single domain is for simplicity sake. However, the procedure can be easily extended to optical fibers with complicated cross sections, to more general composite waveguides, and to photonic crystals. Note that results for waveguides consisting of more than one single domain are also shown in this paper. Following the procedure proposed in [7], we examine the free space wavenumber k_0 dependence of the spinor field

$$\vec{F}\left(k_0,\vec{r}_p\right)=\sum_{n=1}^{N}\hat{b}_n\vec{F}_n\left(k_0,\vec{r}_p,\vec{r}_n\right)-\vec{f}\left(k_0,\vec{r}_p\right),\quad \vec{r}_p\in D\cdot \tag{15}$$

Again, the amplitudes of the auxiliary spinor sources $\{\hat{b}_n\}_{n=1}^{N}$ are obtained from the boundary conditions using the point matching technique. Equation (15) represents the expansion of the spinor field in the domain D in terms of the fundamental solutions $\vec{F}_n$ of the wave equation (7). The spinor field $\vec{f}$ imitates the excitation.

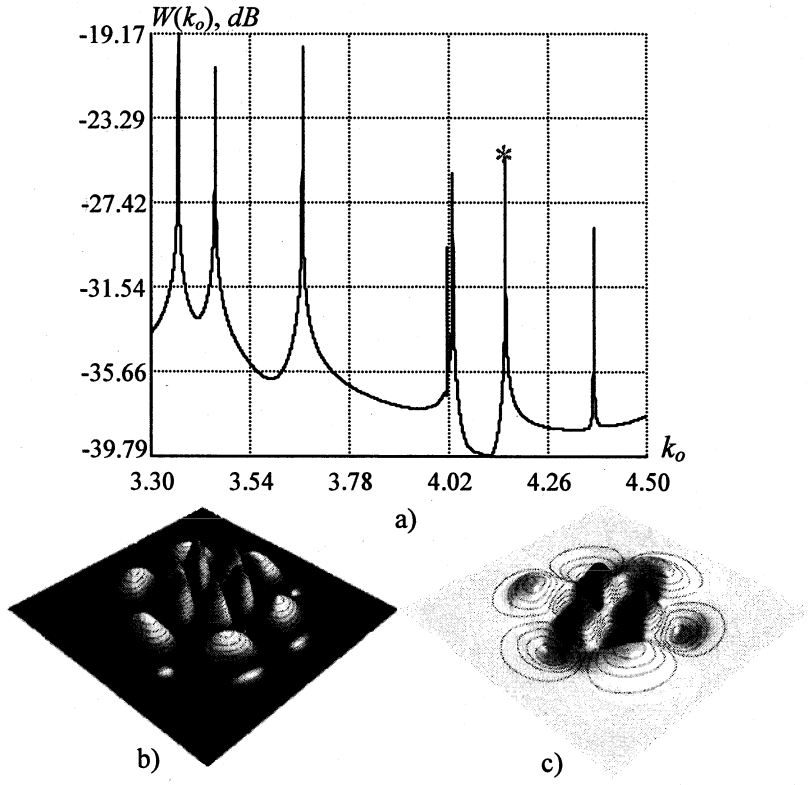

Figure 4: The total electromagnetic energy density $W(r_p)$ as a function of the free space wavenumber k_0, in a single test point within the core section of a linearly graded index fiber.

Note that this fictitious excitation is regular in D. When the wavenumber k_0 in (15) is sufficiently far away from resonance, the amplitudes of the spinor field are approximately zero:

$$\vec{F}\left(k_0, \vec{r}_p\right) \approx 0, \quad \vec{r}_p \in D \tag{16}$$

whereas the peaks in (15) represent distinct resonances (i.e. the eigenvalues). As in the real-world experiment, we do not want to check the entire field in all points of the domain D. Instead of this, we only inspect the total energy density in an appropriate test point. Choosing energy density as a test function guarantees a resonance peak with a one-to-one maximum value [7].

This is illustrated in Figure 4 for a linearly graded index fiber of radius R=1. The core of the fiber is isotropic but inhomogeneous with the dielectric constant

$$\varepsilon_r^D(r) = -8.0 \cdot r + 10.0,\ \mu_r^D = 1.0,\ r \in D. \tag{17}$$

The cladding of the fiber consists of a homogeneous anisotropic dielectric material with the following tensor description for the dielectric constant

$$\varepsilon_{0r} = \begin{pmatrix} 2.0 & 0 & 0 \\ 0 & 1.5 & 0 \\ 0 & 0 & 1.5 \end{pmatrix},\ \mu_{0r} = 1.0 \cdot \tag{18}$$

The maxims of the energy density in Figure 4a indicate the resonance wave numbers, i.e. the corresponding resonance frequencies. Since the corresponding peaks are very sharp, one can evaluate the resonance frequencies very accurately. From the sharpness of these peaks one also obtains information on the quality of the numerical model that was used The more accurate the numerical model, the sharper the peaks. Once the resonances have been found, one can easily plot all field components of the corresponding eigenmodes. To illustrate this, Figure 4b shows the amplitudes and Figure 4c shows values (at a certain time) of the longitudinal components of magnetic field for the eigenmode H_{32}.

This algorithm has been successfully applied to several eigenvalue problems with various geometries and materials. It is important to note that the number of auxiliary sources required for computing a mode with a given accuracy increases only very slowly with the frequency. Therefore, one can also compute higher order modes at high frequencies with a low numerical effort. Furthermore, the convergence is very rapid. Thus, one can easily obtain highly accurate results. As mentioned before, this is important for the FPC design and also for the analysis of fiber coupling that will be shown in the following section. We can also apply the method outlined above to the scattering problem with a real excitation and a lossy.

Figure 5a,b shows the absorption cross-sections of a multicore fiber consisting of a circular dielectric cylinder with 7 circular inclusions arranged as a centered hexagon. The distances between neighbor inclusions are d=1.5. The inclusions and made of chiral (Figure 5a) or biisotropic (Figure 5b) materials, respectively. The radii of cylinder and inclusions are R_d=2.5 and R=0.5, respectively. The permittivity and permeability of dielectric cylinder are $\varepsilon_{rd} = 1.5, \mu_{rd} = 1.0$. For inclusions: $\varepsilon_r = 10.0 + \mathrm{i}0.001, \mu_r = 1.0$, $\alpha = \beta = 0.0005$ (Figure 5a), $\alpha = 0.0005 + \mathrm{i}002$, $\beta = 0.0005 - \mathrm{i}0.002$ (Figure 5b).

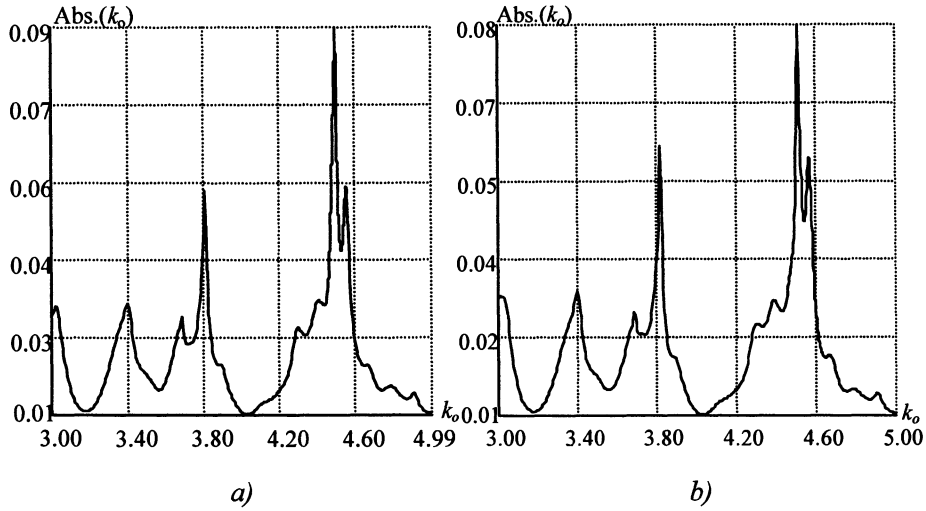

a) *b)*

Figure 5. Absorption cross-sections of biisotropic (a) and chiral (b) circular cylinder inclusions (centered hexagon) embedded in dielectric circular cylinder versus parameter k_0..

From Figures 5a,b we see that the absorption curves have sharp peaks near the resonance wave numbers. Furthermore, these peaks have a fine structure, i.e., they consist of a few closely located maxims corresponding to the interactions between the different inclusions.

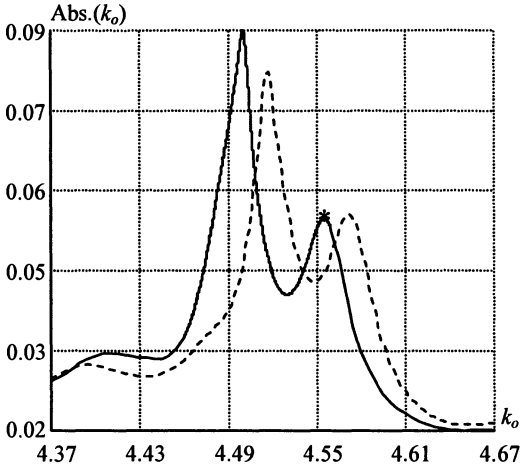

Figure 6. Resolution of curves in Figures 5a,b in narrow region. The dashed line depicts the chiral and the solid line stands for the biisotropic cases respectively.

To compare the absorption properties of FPC with chiral and biisotropic inclusions, Figure 6 resolves one of the closely located peaks in the absorption curves of Figures 5a,b. To investigate the nature of these peaks, we present the amplitudes of the magnetic field (Figure 7a) and of the electric field (Figure 7b) in the absorption peak marked in Figure 6 by a star. We see from Figures 7, that the maxims of absorption curve correspond to whispering gallery oscillations inside the inclusions. The fields related with these maxims are approximately the eigen fields of the considered multicore fiber.

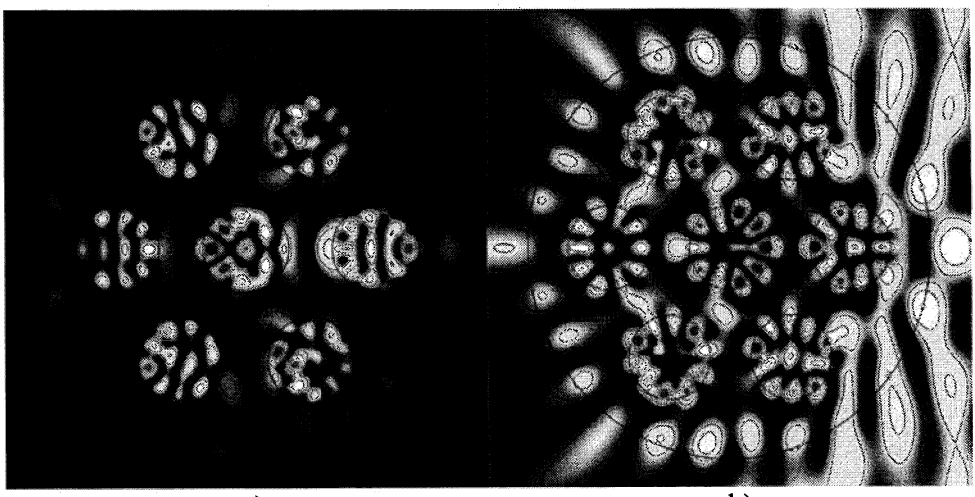

a) b)

Figure 7: Amplitudes of longitudinal components of the magnetic field (left) and of electric field (right) in biisotropic inclusions for k_0=4.5553 (TM-polarization, $\varepsilon_{dr}=1.5$, $\mu_{dr}=1.0$, $\varepsilon_r=10.0+\mathrm{i}0.001$, $\mu_r=1.0$, $\alpha=0.0005+i0.002$, $\beta=0.0005-\mathrm{i}0.002$, $k^r=15.2894$, $k^t=13.5720$, $n^r=3.3564$, $n^t=2.9794$).

Note that the longitudinal magnetic field component in Figure 7a is missing in the incident wave (plane wave excitation). The amplitude of this field is as large as the transverse magnetic field of the incident wave. Since the inclusions are made of biisotropic materials, this cross-polarization field is due to the chirality effect. Thus, adjusting the material properties of the inclusions allows one to control the polarization properties.

3. Simulation of Finite Photonic Crystals

FPC simulations based on MAS have been applied to analyze scattering and propagation processes in finite photonic crystals (and devices based on FPCs) with given crystallographic structure and involving certain defects, such as extrinsic cells, vacancies, dislocations, etc. Moreover, the method can be applied to

the analysis of small FPCs consisting only of a small number of primitive cells – the multicore fiber analyzed in the previous section may be considered as such a small FPC.

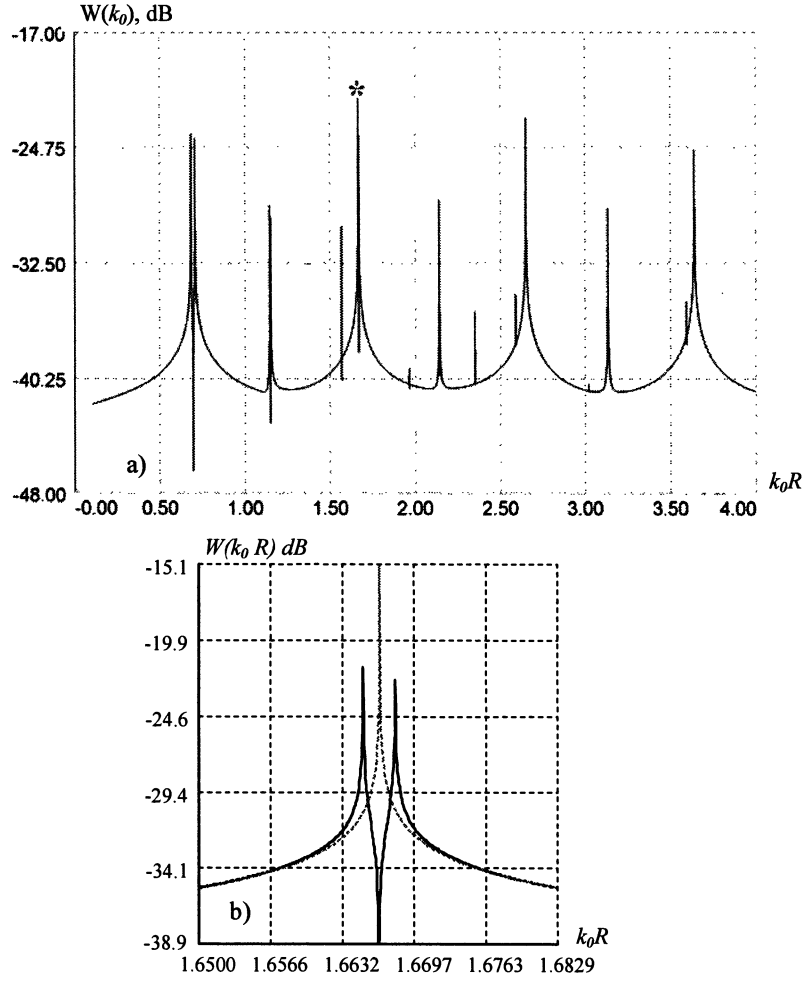

Figure 8: Spectral distribution of five circular cylinders placed in the form of a centralized square (a). Spectral line splitting caused by the inter-cell interactions *(b)*: $\varepsilon / \varepsilon_d = 10.0$ and R/d=0.25.

Various inter-cell interactions such as the shift of the resonance frequencies, the splitting of such spectral lines, and the alteration of the sensitivity to rotation directions of the primary field polarization plane may be observed. In order to analyze these interactions, we first consider a

simple example: An extremely small FPC consisting of a square-lattice with only five elements (a central element surrounded by four other elements) is depicted in Figure 8. Each element is represented by a dielectric circular cylinder embedded in air with radius $R/d = 0.25$ and with the relative permittivity according to $\varepsilon/\varepsilon_d = 10$, where d stands for the lattice constant. Figure 8a shows the electromagnetic field energy density at a certain internal point of the central element as a function of the free space wave number. From inspection of Figure 8a various resonances can be distinguished, some of them show a splitting into separate spectral lines due to the inter-cell interactions. This is illustrated in more detail in Figure 8b, which resolves the spectral lines in Figure 6a marked by a star. The dashed line in Figure 8b depicts the resonance behavior of one isolated element, whereas the solid line stands for the resonance behavior of the full FPC in which the splitting depends on the element's separation namely the lattice constant a.

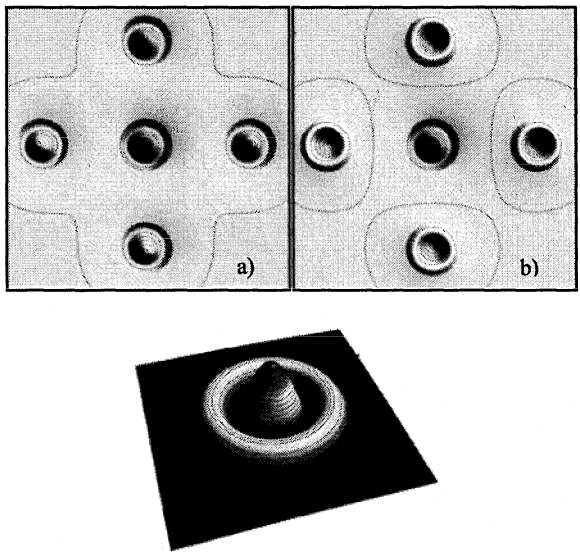

Figure 9. Eigenmodes H_{02} of five circular cylinders in the form of a centralized square on the splitted frequencies (a-b): $k_0R = 1.665102$ (even), $k_0R = 1.668076$ (odd); Eigenmode H_{02} *of* isolated cell (lines of equal - $|H_z|$) (c), $k_0R = 1.666650$.

The corresponding field profiles of eigenmodes at both splitting frequencies are given in Figure 9 as an intensity plot of the magnetic field strength: Figure 9a and 9b represent the two supermodes (i.e. even and odd mode, or phase and anti-phase type of the mode respectively) of the FPC, whereas Figure 9c represents the eigen field for one single element (i.e. the H_{02} mode). Both, supermode and eigenmode H_{02} are similar concerning the field distribution within

one element. In this configuration, the eigenmode spectrum of the FPC is essentially shaped by the eigenmode spectrum of the isolated element. In order to obtain the FPC's complete eigen solution, the corresponding band splitting has to be considered.

In a second example (Figure 10) we want to analyze the characteristic features of anisotropic materials when introduced into a FPC device. In standard FPC devices different types of defect waveguides are mainly used to control wave propagation at different frequencies. Anisotropic materials allow one to create FPC waveguides with separate waves with different rotation directions of the polarization plane.

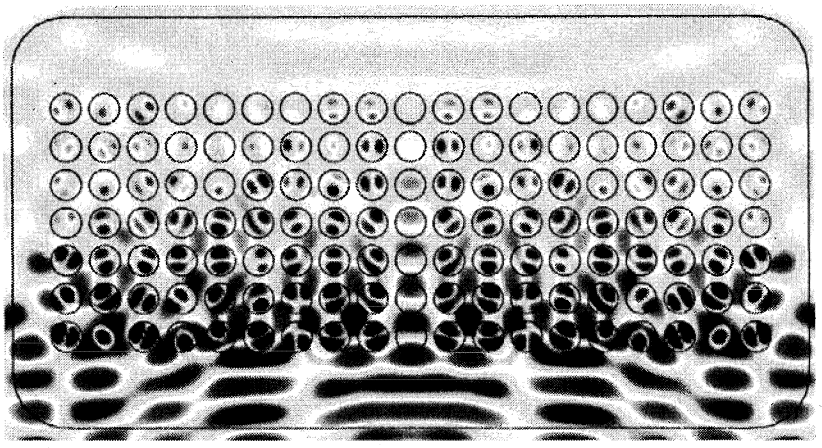

Figure 10. FPC of 1.04 × 0.54 consists of a square lattice embedded in the rectangular crystal made of anisotropic material. The square lattice is represented by $N = 133$ dielectric rods of circular cross-section with $\varepsilon_r = 10.0$ and radius $R = 0.02$, lattice spacing $d=0.05$. The rods of the FPC are arranged according to a 7×19 matrix. The crystal is being excited by the symmetrically placed dot source with $k_0 = 62.47$.

The underlying structure of the following example consists of a square lattice embedded in a rectangular crystal made of anisotropic material with

$$\hat{\varepsilon}_r = \begin{pmatrix} 2.0 & 0.0 & 0.0 \\ 0.0 & 1.5 & 0.0 \\ 0.0 & 0.0 & 1.5 \end{pmatrix}, \quad \mu_r = 1.0$$

Figure 11 shows a fragment of the waveguide channel obtained from vacancies in vertical direction. The material parameters, the distances between the elements, and the dimensions of the channel are adjusted in such a way that top-down wave

propagation is obtained, i.e., that the wave in the channel propagates towards the source.

Figure 11 clarifies the role of eigen-oscillations and their phases in the process of wave propagation along the waveguide channel. The rotation directions and the corresponding phases are adjusted in such a way that the energy from neighboring domains is transferred into the channel. Thus, the energy is forced to propagate mainly along this channel. As one can see, adjusting the geometry and material properties of the cells allows one to control the processes of wave propagation and energy transformation in a FPC, which might be very helpful for the design of FPC devices.

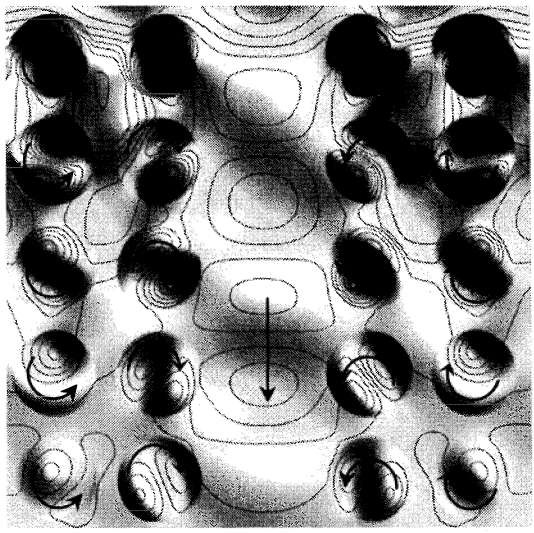

Figure 11. Lines of equal amplitudes of longitudinal component of magnetic field. The arrows show the directions of eigenmodes rotation. Fragment of the waveguide channel in the matrix 7x19 with vacancies along centerline: $R_i = 0.02;\ d = 0.05;\ \varepsilon_{rx}$=2.0, ε_{ry}=1.5, ε_{rz}=1.5, μ_r=1.0, $k_0 = 62.83;\ \mu_{ir} = 1.0, \varepsilon_{ir} = 10.0;$.

Due to the complexity of the field in the photonic crystals the calculations needed for design of the modern FPC based devices should be of very high accuracy about 0.05%.

4. Conclusion

An efficient MAS based code for analysis of FPC devices has been developed. This code can handle biisotropic, chiral, and other complex materials. Using this code, accurate solutions of wave propagation and scattering in the FPCs can been obtained. Moreover, eigenvalue problems such as waves propagation in

optical fibers can be analyzed. The MAS eigenvalue solver could be extended to the analysis of PBG structures and of infinite PC waveguides.

The MAS based program package allows one to easily investigate the electrodynamic behavior of various FPC devices and in order to simplify the synthesis of complicated FPC devices can be linked with appropriate optimization tools.

Acknowledgements

This work has been supported by the Swiss National Science Foundation (SCOPES project 7GEPJ065551).

5. References

1. Joannopoulos, J.D., Meade, R.D., Winn J.N. (1995) *Photonic Crystals: Molding the Flow of Light,* Princeton University Press, Singapore.
2. Yablonovitch, E., Gmitter, T.J., Meade, R.D., and Rappe, A.M., Brommer, K.D., and. Joannopoulos, J.D. (1991) Donor and acceptor modes in photonic band structures, *Phys. Rev. Lett.* **67 (24),** 3380-3383.
3. Mekis, Fan, A.S, and Joannopoulos, J.D. (1999). Absorbing boundary condition for finite-difference time-domain simulation of photonic crystal waveguides. *IEEE Microwave and Guided Wave Letters* **9**, 502.
4. Moreno, E. (2002) MMP Modeling and optimization of photonic crystals, optical devices, and nanostructures. *PhD Thesis ETH*, Zürich, N 14553.
5. Moreno, E., Erni, D., Hafner, Ch. (2002) Multiple multipole method with automatic multipole setting applied to the simulation of surface plasmons in metallic nanostructures, *J. Opt. Soc. Am.* **19**, No 1, 101-111.
6. Hafner, Ch. (1998/S) *MaX-1 A Visual Electromagnetics Platform for PCs*, John Wiley, Chichester.
7. Popovidi-Zaridze, R.S., Karkashadze, D.D., Akhvlediani, G.Z, Khatiashvili, J.H. (1981) Investigation of the possibilities of the method of auxiliary sources in solution of the two-dimensional electrodynamics problems. *Radiotekhnika i Elektronika*, **26**, N2, 254-262 (in Russian).
8. Zaridze, R., Karkashadze, D., Khatiashvili, J. (1985) *Method of auxiliary sources for investigation of along-regular waveguides*, Tbilisi State University Press, Tbilisi (in Russian).
9. Karkashadze, D., Zaridze, R.(1995) The method of auxiliary sources in applied electrodynamics, *Latsis Symposium on Computational Electromagnetics*, Zürich, Switzerland, pp. 163-180.
10. Bogdanov, F.G., Karkashadze, D.D. (1998) Conventional method of auxiliary sources in the problems of electromagnetic scattering by the bodies of complex materials. *Proc. Conf. on Electromagnetic and light scattering – Theory and applications*, Bremen, Germany, pp. 133-140.
11. Bogdanov, F.G., Karkashadze, D.D., Zaridze, R.S. (1998) Propagation in and scattering by biisotropic objects of complicated shape, in Arne F.Jacob and Jens Reinert (eds.), *Proceedings of 7th Interational Conference on Complex Media (Bianisotropic'98)*, Braunschweig, Germany, pp. 133-136.
12. Bogdanov, F.G., Karkashadze, D.D., Zaridze, R.S. (1998) New Materials Design: Scattering Problems and the Method of Auxiliary Sources, *Proceedings of III International*

Seminar/Workshop on Direct and Inverse Problems of Electromagnetic and Acoustic Wave Theory (DIPED-98), Lviv-Tbilisi, pp. 18-21.

13. Bogdanov, F.G., Karkashadze, D.D. (1998) Accumulating, directing and focusing properties of 2-D and 3-D objects of biisotropic materials, *Proceedings of III International Seminar/Workshop on Direct and Inverse Problems of Electromagnetic and Acoustic Wave Theory (DIPED-98)*, Lviv-Tbilisi, pp. 93-96.
14. Bogdanov, F.G., Karkashadze, D.D., Saparishvili, G.A., Zaridze, R.S. (1999) Computer simulation of high-frequency scattering by the bodies of composite materials, in *Proceedings of 4-th Conference on Electromagnetic and Light Scattering by Nonspherical Particles: Theory and Applications*, Vigo, Spain, pp. 295-302.
15. Bogdanov, F.G., Karkashadze, D.D., Zaridze, R.S. (1999) The method of auxiliary sources in electromagnetic scattering problems, in Th.Wriedt (eds.), *Generalized multipole techniques for electromagnetic and light scattering*, Elsevier Science B.V., pp. 143-172.
16. Bogdanov, F.G., Karkashadze, D.D., Zaridze, R.S., Bit-Babic, G.G., Tavzarashvili, K.N. (2000) About design of the adaptive antenna with chiral coating for portable cellular phones, in *Proceedings of V International Seminar/Workshop on Direct and Inverse Problems of Electromagnetic and Acoustic Wave Theory (DIPED-2000),* Lviv-Tbilisi, pp. 27-30.
17. Bogdanov, F.G., Karkashadze, D.D., Zaridze, R.S. (2000) Scattering and absorption problems solution upon the 3-D chiral and biisotropic objects, Proceedings of 8th International Conference on Electromagnetics of Complex media (BIANISOTROPICS 2000), Lisbon, pp. 233-236.
18. Bohren, C.F. (1974) Light scattering by an optically active sphere, *Chem. Phys. Lett.*. **29**, pp. 458-462.
19. Engheta, N. and Jaggard, D.L. (1988) Electromagnetic chirality and its applications, *IEEE Trans. Antennas Propagat. Soc. Newsletter,* **30,** 6-12.
20. Lakhtakia, A. (1994) *Beltrami fields in chiral media,* World Sci. Publ. Co., Singapore.
21. Lindell, I.V., Sihvola, A.H, Tretyakov, A.A., and Viitanen, A.J (1994) *Electromagnetic waves in chiral and bi-Isotropic media,* Artech House, Boston, London.
22. Cory, H. (1995) Chiral devices - an overview of canonical problems, Journ. Electromag. Waves and Applic., **9**, No. 5/6, 805-829.
23. Zaridze, R., Bit-Babik, G., Tavzarashvili, K., Uzunoglu, N., Economou, D. (2002) Wave Fields Singularity Aspects in Large-Size Scatterers and Inverse Problems, *IEEE Transactions on Antennas and Propagation*, **50**, N.1, 50-59.
24. Karkashadze, D.D. (2001) On status of main singularities in 3D scattering problems, in *Proceedings of VI International Seminar/Workshop on Direct and Inverse Problems of Electromagnetic and Acoustic Wave Theory (DIPED-2001),* Lviv, pp 81-84.
25. Hafner, Ch. (1999) *Post-modern Electromagnetics – Using intelligent Maxwell solvers,* Wiley, Chichester.
26. Harrington, R. F. (1993) Field Computation by Moment Methods, Wiley-IEEE Press.
27. Kupradze, V.D. (1967) About approximates mathematical physics problem, *Success of Mathematical Sciences, 22,* N2, 59-107. (in Russian).
28. Kupradze, V.D, Aleksidze, M.A. (1964) The method of functional equations for approximate solution of some boundary problems. Journal of Appl. Math. and Math. Physics, **4**, 683-715 (in Russian).
29. Aleksidze, M.A. (1991) *Fundamental functions in approximate solutions of the boundary problems,* Nauka, Moscow (in Russian).
30. Penrose, R., Ringler, W. (1986) *Spinors and space-time*, **1**, Cambridge University Press, Cambridge.
31. Moreno, E., Ern, D., and Hafner, Ch. (2002) Band structure computations of metallic photonic crystals with the multiple multipole method, *Phys. Rev. B*, **65**, No 15, 155120-1-155120-10.

IV.

ANALYSIS AND MODELLING OF BIANISOTROPIC STRUCTURES

PROPAGATION OF ELECTROMAGNETIC WAVES IN ARTIFICIAL ANISOTROPIC UNIFORM AND TWISTED OMEGA-STRUCTURES

S. A. KHAKHOMOV and I. V. SEMCHENKO
Department of General Physics, Gomel State University
Sovyetskaya Str. 104, 246019, Gomel, Belarus

Abstract. In this paper plane wave reflection and transmission phenomena in slabs of artificial bi-anisotropic uniform media are theoretically considered. The case of isotropic host medium having only dielectric properties is studied. Oblique incidence is assumed. The boundary-value problem for artificial omega structure is solved taking into account multiple reflections of electromagnetic waves from the sample's boundaries. The intensity of the reflected and transmitted waves is calculated, and the comparison with artificial uniaxial bi-anisotropic plate with microhelices is performed. The possibility of the design of twisted omega-structure whose microwave properties are similar to the optical properties of cholesteric liquid crystals is demonstrated. The modified formula de Vries for the rotation of the polarization plane of electromagnetic waves is found.

1. Introduction

In the last ten years, interest in complex artificial media having chiral and pseudochiral properties in the microwave region has been very high [1]-[3]. The main initial motivation was in the design of novel absorbing materials. As a result of very intensive investigations of chiral and, more generally, bi-anisotropic media, it has been found that more complicated properties of these materials can find many more potential applications than in microwave absorbers [4]-[7]. In this paper plane wave reflection and transmission phenomena in slabs of artificial bi-anisotropic uniform media are theoretically considered. The case of isotropic host medium having only dielectric properties is studied. After addition to host medium of Ω-shaped inclusions the artificial medium exhibits the pseudochiral and weak magnetic properties as well as anisotropy of dielectric properties. The concentration of Ω-shaped inclusions influences on magnetic, dielectric and pseudochiral properties simultaneously. The design of artificial media with requested characteristics, for example, impedance is possible. Oblique

S. Zouhdi et al. (eds.), Advances in Electromagnetics of Complex Media and Metamaterials, 197–210.

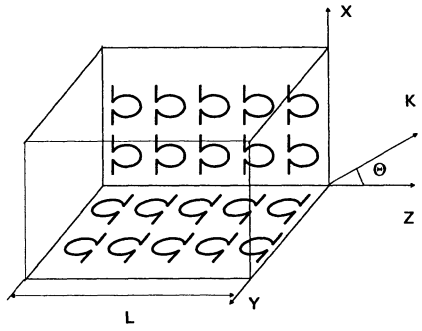

Figure 1. The geometry of the problem. The eigenwave in medium propagates along the **k** vector, which is oriented in the XOZ plane.

incidence is assumed. The boundary-value problem for artificial omega structure was solved taking into account multiple reflections of electromagnetic waves from the sample's boundaries. In article [8] normal incidence of waves on the slab with Ω-shaped inclusions was considered. In this paper, the analysis is extended to account for oblique incidence of waves (see Fig.1).

2. Theory

For time-harmonic fields with $\exp(j\omega t)$ the properties of bi-anisotropic media can be described by the following constitutive equations

$$\mathbf{D} = \varepsilon_0\varepsilon\mathbf{E} - j\sqrt{\varepsilon_0\mu_0}\alpha\mathbf{H} \tag{1}$$

$$\mathbf{B} = \mu_0\mu\mathbf{H} + j\sqrt{\varepsilon_0\mu_0}\widetilde{\alpha}\mathbf{E} \tag{2}$$

These material equations were proposed for bi-isotropic media in [9]-[11] and for natural crystals in [12, 13]. Here, $\mathbf{D}, \mathbf{B}, \mathbf{E}$, and $\mathbf{H}$ are the phasors of the usual field quantities, ε, μ, and α are the dyadics of the permittivity, permeability and of the coupling parameter, respectively, and the sign $\widetilde{\alpha}$ denotes the transpose operation. After substitution of (1), (2) into Maxwell's equations one can obtain the wave equation for the electric field vector $\mathbf{E}$

$$\mathrm{curl}(\mu^{-1}\mathrm{curl}\mathbf{E}) + (\varepsilon_0\mu_0(\varepsilon - \alpha\mu^{-1}\widetilde{\alpha}))\frac{\partial^2\mathbf{E}}{\partial t^2} + j\sqrt{\varepsilon_0\mu_0}(\mathrm{curl}(\mu^{-1}\widetilde{\alpha}\frac{\partial\mathbf{E}}{\partial t})) + \alpha\mu^{-1}\mathrm{curl}\frac{\partial\mathbf{E}}{\partial t} = 0 \tag{3}$$

For the considered uniform medium the dyadics of the permittivity, permeability and coupling parameter have the following form:

$$\varepsilon = \begin{pmatrix} \varepsilon_t & 0 & 0 \\ 0 & \varepsilon_t & 0 \\ 0 & 0 & \varepsilon_n \end{pmatrix}, \quad \mu = \begin{pmatrix} \mu_t & 0 & 0 \\ 0 & \mu_t & 0 \\ 0 & 0 & \mu_n \end{pmatrix}, \quad \alpha = \begin{pmatrix} 0 & \alpha & 0 \\ \alpha & 0 & 0 \\ 0 & 0 & 0 \end{pmatrix} \tag{4}$$

Taking into account the symmetry of the medium we can represent the wave equation (3) in the form as

$$\begin{aligned} &[k^2\mu_t^{-1}\cos^2\theta - \varepsilon_0\mu_0\omega^2(\varepsilon_t - \alpha^2\mu_t^{-1})]E_{ox} \\ &-[k^2\mu_t^{-1}\sin\theta(k\cos\theta + j\sqrt{\varepsilon_0\mu_0}\omega\alpha)]E_{oz} = 0 \end{aligned} \tag{5}$$

$$[k^2(\mu_t^{-1}\cos^2\theta + \mu_n^{-1}\sin^2\theta) - \varepsilon_0\mu_0\omega^2(\varepsilon_t - \alpha^2\mu_t^{-1}]E_{oy} = 0 \tag{6}$$

$$\begin{aligned} &[-k^2\mu_t^{-1}\sin\theta(k\cos\theta - j\sqrt{\varepsilon_0\mu_0}\omega\alpha)]E_{ox} \\ &+[k^2\mu_t^{-1}\sin^2\theta - \varepsilon_0\mu_0\omega^2\varepsilon_n]E_{oz} = 0 \end{aligned} \tag{7}$$

Here, ω is the angular frequency of the incident wave, ε_t and ε_n are the main values of the permittivity tensor, μ_t and μ_n are the main values of the permeability tensor, α is the main value of the coupling parameter tensor, and k is the wavenumber of the eigenmode, $c = (\sqrt{\varepsilon_0\mu_0})^{-1}$ is the speed of light in vacuum, θ is the angle between Z axis and vector k of an eigenmode in the medium.

¿From equations (5)-(7) can be obtained the dispersion equation, the solutions of which are the wavenumbers of the eigenmodes in the medium [4, 14, 15]:

$$k_{1,3} = \pm\omega\sqrt{\varepsilon_0\mu_0}\sqrt{\frac{\mu_n(\varepsilon_t\mu_t - \alpha^2)}{\mu_n\cos^2\theta + \mu_t\sin^2\theta}}, \tag{8}$$

$$k_{2,4} = \pm\omega\sqrt{\varepsilon_0\mu_0}\sqrt{\frac{\varepsilon_n(\varepsilon_t\mu_t - \alpha^2)}{\varepsilon_n\cos^2\theta + \varepsilon_t\sin^2\theta}} \tag{9}$$

¿From the equations (5), (7) the relations between the components of the electric field vector are found to be

$$\gamma_{2,4} = \frac{E_{oz}}{E_{ox}} = \frac{k_{2,4}^2\cos^2\theta - \varepsilon_0\mu_0\omega^2(\varepsilon_t\mu_t - \alpha^2)}{k_{2,4}^2\sin\theta(k_{2,4}\cos\theta + j\sqrt{\varepsilon_0\mu_0}\omega\alpha)} \tag{10}$$

The modes with wavenumbers $k_{1,3}$ are polarized along the Y axis, the modes with wavenumbers $k_{2,4}$ are polarized in the plane of incidence XOZ. The dependence of the wavenumbers of eigenmodes on the incidence angle is presented in Fig. 2. The dependences of the real and imaginary parts of γ on the incidence angle are presented in Figs. 3,4.

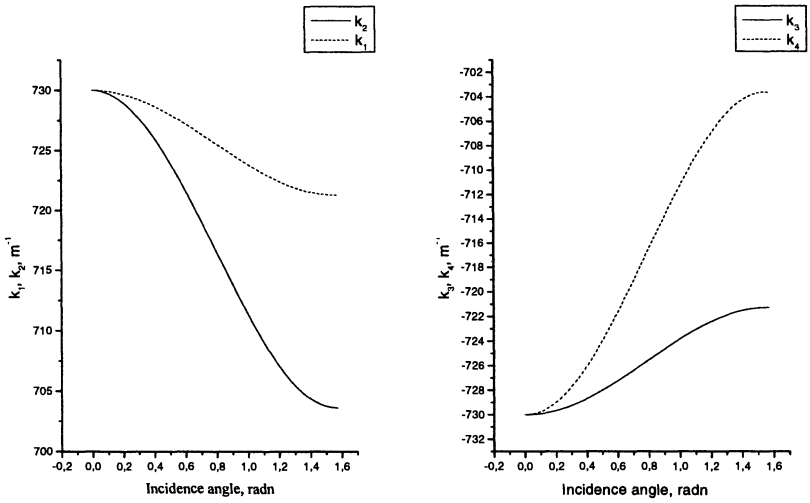

Figure 2. The dependence of the wavenumbers of eigenmodes on the incidence angle. $\omega/2\pi = 17$ GHz, $\varepsilon_t = 3.9$, $\varepsilon_n = 3$, $\mu_t = 1.1$, $\mu_n = 1$, $\alpha = 0.3$.

3. Reflection and transmission coefficients

¿From the continuity of the tangential components of the wave vectors at the boundaries of the medium the following equations are obtained:

$$k_0 \sin\theta_0 = k_1(\theta_1)\sin\theta_1 = k_2(\theta_2)\sin\theta_2 \tag{11}$$

where k_0 is the wavenumber of the incident wave. These equations allow to calculate the angles of refraction θ_1 and θ_2 for the first and the second mode as functions of incidence angle θ_0. For the third and fourth modes one obtains likewise:

$$k_0 \sin\theta_0 = k_3(\theta_3)\sin\theta_3 = k_4(\theta_4)\sin\theta_4. \tag{12}$$

The wavenumbers k_3 and k_4 have the negative values and correspond to the waves reflected from the back surface of plate. In this case also negative values of angles θ_3 and θ_4 follow from (12). The boundary conditions for the tangential components of $\mathbf{E}$ and $\mathbf{H}$ at $z = 0$ and $z = L$ (where L is the thickness of the plate) lead to the following system of eight algebraic equations:

$\underline{z = 0}$:

$$E^{\iota}_{ox} + E^{r}_{ox} = A_2 + A_4,$$

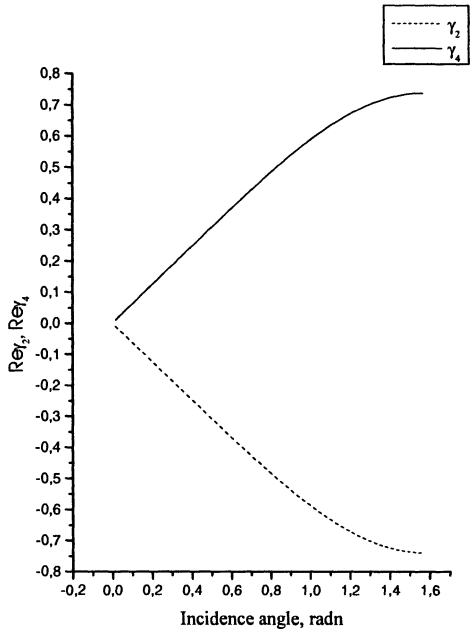

Figure 3. The dependence of the real part of γ on the incidence angle. $\omega/2\pi = 17$ GHz, $\varepsilon_t = 3.9$, $\varepsilon_n = 3$, $\mu_t = 1.1$, $\mu_n = 1$, $\alpha = 0.3$.

$$E^{\iota}_{oy} + E^{r}_{oy} = A_1 + A_3,$$

$$-\frac{k_0}{\omega}\cos\theta_0 E^{\iota}_{oy} + \frac{k_0}{\omega}\cos\theta_0 E^{r}_{oy} =$$

$$-\mu_t^{-1}\left\{\frac{k_1}{\omega}\cos\theta_1 + j\sqrt{\varepsilon_0\mu_0}\alpha\right\}A_1 - \mu_t^{-1}\left\{\frac{k_3}{\omega}\cos\theta_3 + j\sqrt{\varepsilon_0\mu_0}\alpha\right\}A_3,$$

$$\frac{k_0}{\omega}\cos\theta_0 E^{\iota}_{ox} + \frac{k_0}{\omega}\sin\theta_0 E^{\iota}_{oz} - \frac{k_0}{\omega}\cos\theta_0 E^{r}_{ox} - \frac{k_0}{\omega}\sin\theta_0 E^{r}_{oz} =$$

$$-\mu_t^{-1}\left\{\frac{k_2}{\omega}(-\cos\theta_2 + \gamma_2\sin\theta_2) + j\sqrt{\varepsilon_0\mu_0}\alpha\right\}A_2 -$$

$$\mu_t^{-1}\left\{\frac{k_4}{\omega}(-\cos\theta_4 + \gamma_4\sin\theta_4) + j\sqrt{\varepsilon_0\mu_0}\alpha\right\}A_4,$$

$\underline{z = L:}$

$$A_2\exp\{-jk_2\cos\theta_2 L\} + A_4\exp\{-jk_4\cos\theta_4 L\} = E^{\tau}_{ox}\exp\{-jk_0\cos\theta_0 L\},$$

$$A_1\exp\{-jk_1\cos\theta_1 L\} + A_3\exp\{-jk_3\cos\theta_3 L\} = E^{\tau}_{oy}\exp\{-jk_0\cos\theta_0 L\},$$

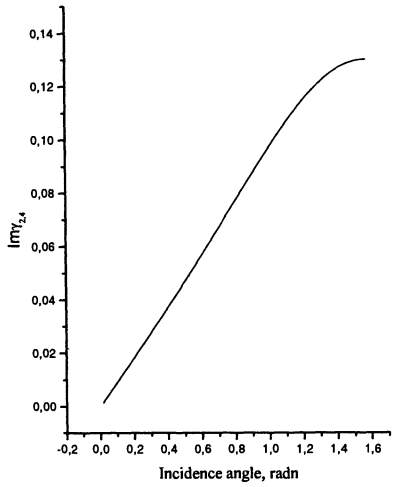

Figure 4. The dependence of the imaginary part of γ on the incidence angle. $\omega/2\pi = 17$ GHz, $\varepsilon_t = 3.9$, $\varepsilon_n = 3$, $\mu_t = 1.1$, $\mu_n = 1$, $\alpha = 0.3$.

$$
\begin{aligned}
-\mu_t^{-1}\left\{\frac{k_1}{\omega}\cos\theta_1 + j\sqrt{\varepsilon_0\mu_0}\alpha\right\} A_1 \exp\{-jk_1\cos\theta_1 L\} \\
-\mu_t^{-1}\left\{\frac{k_3}{\omega}\cos\theta_3 + j\sqrt{\varepsilon_0\mu_0}\alpha\right\} A_3 \exp\{-jk_3\cos\theta_3 L\} = \\
-\frac{k_0}{\omega}\cos\theta_0 E_{oy}^{\tau}\exp\{-jk_0\cos\theta_0 L\}, \\
-\mu_t^{-1}\left\{\frac{k_2}{\omega}(-\cos\theta_2 + \gamma_2\sin\theta_2) + j\sqrt{\varepsilon_0\mu_0}\alpha\right\} A_2 \exp\{-jk_2\cos\theta_2 L\} - \\
\mu_t^{-1}\left\{\frac{k_4}{\omega}(-\cos\theta_4 + \gamma_4\sin\theta_4) + j\sqrt{\varepsilon_0\mu_0}\alpha\right\} A_4 \exp\{-jk_4\cos\theta_4 L\} = \\
\frac{k_0}{\omega}(\cos\theta_0 E_{ox}^{\tau} - \sin\theta_0 E_{oz}^{\tau}\exp\{-jk_0\cos\theta_0 L\} \quad (13)
\end{aligned}
$$

Here, E_0^{ι}, E_0^{r} and E_0^{τ} are the phasors of the incident, the reflected and the transmitted waves; A_{1-4} are the phasors of the eigenmodes in the medium. For the incident wave the following relations hold:

$$E_{ox} = E_{op}\cos\theta_0, \quad E_{oz} = -E_{op}\sin\theta_0 \qquad (14)$$

where index p means a vector lying in the plane of incidence. For the

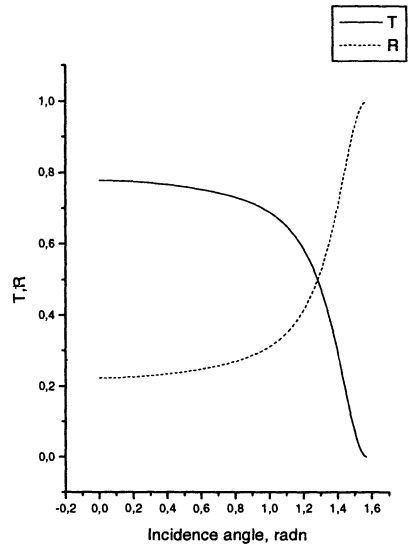

Figure 5. Transmission (T) and reflection (R) coefficients versus the angle of incidence for the perpendicular polarization. $L = 5.5$ mm, $\omega/2\pi = 17$ GHz, $\varepsilon_t = 3.9$, $\varepsilon_n = 3$, $\mu_t = 1.1$, $\mu_n = 1$, $\alpha = 0.3$.

transmitted and the reflected waves one can write:

$$E^{\tau}_{ox} = E^{\tau}_{p} \cos\theta_{\tau}, \quad E^{\tau}_{oz} = -E^{\tau}_{p} \sin\theta_{\tau} \tag{15}$$

$$E^{r}_{ox} = -E^{r}_{p} \cos\theta_{r}, \quad E^{r}_{oz} = -E^{r}_{p} \sin\theta_{r} \tag{16}$$

If at $z = 0$ and $z = L$ the slab interfaces the same medium (for instance air), then $\theta_0 = \theta_r = \theta_\tau$. Consequently, the number of unknowns (E^{τ}_{ox}, E^{τ}_{oz}, E^{r}_{ox}, E^{r}_{oz}) is reduced to two (E^{τ}_{p}, E^{r}_{p}). Then, we have obtained the system of eight equations with eight unknowns: A_{1-4}, $E^{\tau}_{oy} = E^{\tau}_{s}$, $E^{r}_{oy} = E^{r}_{s}$, E^{τ}_{p}, E^{r}_{p}. The system of equations allows to find the exact solutions of the boundary-value problem for uniform omega-structure at oblique incidence of electromagnetic waves. Although all the coefficients in the above system of eight linear equations are known explicitly, the analytical solution is still too involved to write it down. However, numerical solution is very simple and straightforward. The found solutions of the boundary-value problem for all frequencies obey the energy conservation law. The following parameters were chosen: the thickness of sample $L = 5.5$ mm; the incident wave frequency $\omega/2\pi = 17$ GHz; $\varepsilon_t = 3.9$; $\varepsilon_n = 3$; $\mu_t = 1.1$; $\mu_n = 1$; $\alpha = 0.3$. It is necessary to note that such problem was solved analytically in [4] using the vector transmission-line theory.

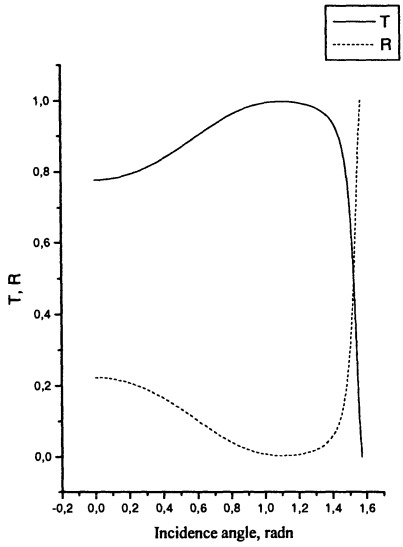

Figure 6. Transmission (T) and reflection (R) coefficients versus the angle of incidence for the parallel polarization. $L = 5.5$ mm, $\omega/2\pi = 17$ GHz, $\varepsilon_t = 3.9$, $\varepsilon_n = 3$, $\mu_t = 1.1$, $\mu_n = 1$, $\alpha = 0.3$.

The results of the numerical calculations are presented in Figs. 5,6. Figs. 5,6 show that the reflection coefficient has a non-monotonic dependence on the angle of incidence for both parallel and perpendicular polarization of the incident wave. For uniaxial bi-anisotropic slab with microhelices [7] on a certain angle, which depends on the incident wave polarization, intensity of the reflected wave is close to zero. It is an evidence of practically complete transmission of electromagnetic waves through the slab on these angles. These angles are different for various polarization of incident wave for anisotropic plate without chirality but chirality allows to draw together these angles for both polarizations [7]. For omega structure the situation is quite different. There is not angle, where intensity of the reflected wave is close to zero for both polarizations simultaneously.

4. Macroscopic helical structure

In paper [16] was shown a possibility of the design of a twisted structure whose microwave properties are similar to the optical properties of cholesteric liquid crystals. This structure also exhibits local chirality. Analogical structure can be designed for media with Ω-inclusions. Such a struc-

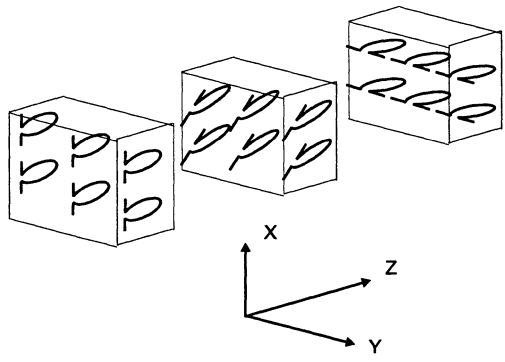

Figure 7. The geometry of the problem.

ture can be a multilayer anisotropic chiral sample. When the number of layers increases, the Ω-inclusions turn at a constant angle around the z axis which is perpendicular to the planar (see Fig. 7). As a result the sample as a whole acquires a helical structure which is analogical to the structure of cholesteric liquid crystals. The thickness of every layer is about 0.5–1 mm. This allows to provide the period of the macrohelical structure close to the wavelength in the microwave region. Some earlier results on plane waves in helicoidal media of various physical nature have been published in [17, 18, 19]. For a review of other papers in this area see [20].

For the considered twisted medium the local dyadics of the permittivity, permeability and coupling parameter have the following form:

$$\varepsilon = \begin{pmatrix} \varepsilon_{11} & 0 & 0 \\ 0 & \varepsilon_{22} & 0 \\ 0 & 0 & \varepsilon_{33} \end{pmatrix}, \quad \mu = \begin{pmatrix} 1 & 0 & 0 \\ 0 & \mu_{22} & 0 \\ 0 & 0 & 1 \end{pmatrix}, \quad \alpha = \begin{pmatrix} 0 & \alpha_{12} & 0 \\ 0 & 0 & 0 \\ 0 & 0 & 0 \end{pmatrix} \tag{17}$$

where $\varepsilon_{11} = \varepsilon_{host} + \varepsilon_{11(omega)}$, $\varepsilon_{22} = \varepsilon_{host}$, $\varepsilon_{33} = \varepsilon_{host} + \varepsilon_{33(omega)}$. It is assumed that host medium has not magnetic properties. The constitutive relations (1),(2) take the form

$$\mathbf{D} = \varepsilon_0 \varepsilon(z)\mathbf{E} - j\sqrt{\varepsilon_0 \mu_0}\alpha(z)\mathbf{H} \tag{18}$$

$$\mathbf{B} = \mu_0 \mu(z)\mathbf{H} + j\sqrt{\varepsilon_0 \mu_0}\widetilde{\alpha}(z)\mathbf{E} \tag{19}$$

where

$$\varepsilon(z) = U(z)\varepsilon\widetilde{U}(z), \quad \mu(z) = U(z)\mu\widetilde{U}(z), \quad \alpha(z) = U(z)\alpha\widetilde{U}(z) \tag{20}$$

and $U(z)$ is the rotation dyadic (around the unit vector $\mathbf{c}$). In the matrix form we can write

$$U(z) = \begin{pmatrix} \cos(qz) & -\sin(qz) & 0 \\ \sin(qz) & \cos(qz) & 0 \\ 0 & 0 & 1 \end{pmatrix} \tag{21}$$

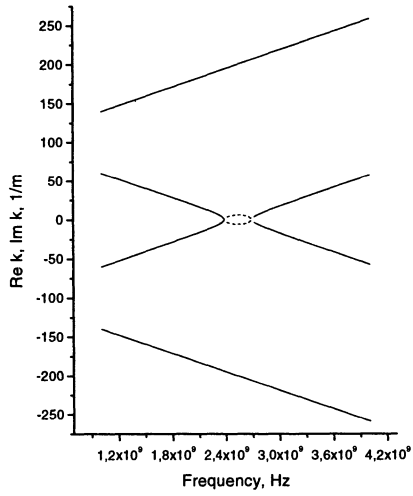

Figure 8. The solutions of the dispersion equation as functions of the frequency. Solid line corresponds to the real part of the wavenumbers, and dashed line corresponds to the imaginary part. $\varepsilon_{11} = 3.9$, $\varepsilon_{22} = 3$, $\mu_{11} = 1$, $\mu_{22} = 1.1$, $\alpha = 0.3$, and $q = 100$ radn/m.

Parameter q depends only on the geometry of the structure: it is determined by the pitch P of the rotation along the axis z ($|q| = \frac{2\pi}{P}$). Here we assume that the pitch of the helix along z is much larger than the thickness of individual layers. In that case the local properties are homogeneous in the transverse direction with respect to the local direction of vector **a**.

The wave equation (3) take the form

$$\begin{aligned}\mathrm{curl}(\mu^{-1}(z)\mathrm{curl}\mathbf{E}) + (\varepsilon_0\mu_0(\varepsilon(z) - \alpha(z)\mu^{-1}(z)\widetilde{\alpha}(z)))\frac{\partial^2\mathbf{E}}{\partial t^2} + \\ j\sqrt{\varepsilon_0\mu_0}(\mathrm{curl}(\mu^{-1}(z)\widetilde{\alpha}(z)\frac{\partial\mathbf{E}}{\partial t})) + \alpha(z)\mu^{-1}(z)\mathrm{curl}\frac{\partial\mathbf{E}}{\partial t} = 0 \qquad (22)\end{aligned}$$

¿From wawe equation (22) can be obtained the dispersion equation

$$\begin{aligned}k^4\mu_{22}^{-1} - k^2[2q^2\mu_{22}^{-1} + \omega^2\varepsilon_0\mu_0(\varepsilon_{11} + \varepsilon_{22}\mu_{22}^{-1} - \alpha_{12}^2\mu_{22}^{-1})] + \\ q^4\mu_{22}^{-1} - q^2\omega^2\varepsilon_0\mu_0(\varepsilon_{11}\mu_{22}^{-1} + \varepsilon_{22} - 2\alpha_{12}^2\mu_{22}^{-1}) + \\ \omega^4\varepsilon_0\mu_0(\varepsilon_{11} - \alpha_{12}^2\mu_{22}^{-1})\varepsilon_{22} = 0 \qquad (23)\end{aligned}$$

Using the twisted coordinat system, we have found explicit solutions for the wave numbers k_m and ellipticities γ_m of the eigenmodes of electromagnetic

field for such a medium with helical structure:

$$k_{1,2} = k_0 \left[\frac{1}{2}(\varepsilon_{11}\mu_{22} + \varepsilon_{22} - \alpha_{12}^2) + \frac{q^2}{k_0^2} \pm \sqrt{\frac{1}{4}(\varepsilon_{11}\mu_{22} - \varepsilon_{22} - \alpha_{12}^2)^2 + \frac{q^2}{k_0^2}[(\varepsilon_{11} + \varepsilon_{22})(\mu_{22} + 1) - \alpha_{12}^2(1 + 2\mu_{22}^{-1})]} \right]^{\frac{1}{2}} \quad (24)$$

$$k_{3,4} = -k_{1,2} \quad (25)$$

where $k_0 = \omega\sqrt{\varepsilon_0\mu_0}$ is the vacuum wave number,

$$\gamma_m = -\frac{q^2 + k_m^2\mu_{22}^{-1} - \omega^2\varepsilon_0\mu_0(\varepsilon_{11} - \alpha_{12}^2\mu_{22}^{-1})}{q(k_m(1 + \mu_{22}^{-1}) + \omega\sqrt{\varepsilon_0\mu_0}\alpha_{12}\mu_{22}^{-1}} \quad (26)$$

It is necessary to note that such problem for cholesteric liquid crystals with local chirality was solved analytically in [21]. The frequency dependence of the wavenumbers in the twisted coordinat system is presented in Fig. 8. Such kind of frequency dependence is well known in cholesteric liquid crystals optics [22].

Let us consider the influence of local coupling parameter on the Bragg reflection of electromagnetic waves in the medium with helical structure. Equating to zero wave number k_2 in (24) we can obtain the following values of the frequency boundaries of the Bragg reflection region:

$$\omega_1 \approx \frac{q}{\sqrt{\varepsilon_0\mu_0}\sqrt{\varepsilon_{22}\mu_{22}}}\left[1 - \frac{\alpha_{12}^2\mu_{22}^{-1}(2\varepsilon_{11} - \varepsilon_{22}\mu_{22})}{2\varepsilon_{11}(\varepsilon_{11} - \varepsilon_{22}\mu_{22})}\right] \quad (27)$$

$$\omega_2 \approx \frac{q}{\sqrt{\varepsilon_0\mu_0}\sqrt{\varepsilon_{11}}}\left[1 + \frac{\alpha_{12}^2\mu_{22}^{-1}}{2(\varepsilon_{11} - \varepsilon_{22}\mu_{22})}\right] \quad (28)$$

As we can see from (27), (28) the local coupling parameter can cause shifts of the frequency boundaries of the region of the Bragg reflection. Naturally, also the influence of the local chirality is exhibited as a change of the width of the Bragg diffraction region. The shift of the boundaries of the region of the Bragg reflection is proportional to α_{12}^2. In the case when $\varepsilon_{22} \ll \varepsilon_{11}$ and $\mu_{22} \to 1$ from (27), (28) can be obtained the following expressions

$$\omega_1 \approx \frac{q}{\sqrt{\varepsilon_0\mu_0}\sqrt{\varepsilon_{22}\mu_{22}}}\left[1 - \frac{\alpha_{12}^2}{\varepsilon_{11}}\right], \quad \omega_2 \approx \frac{q}{\sqrt{\varepsilon_0\mu_0}\sqrt{\varepsilon_{11}}}\left[1 + \frac{\alpha_{12}^2}{2\varepsilon_{11}}\right] \quad (29)$$

The expressions for k_1 and k_2 (24) represent the wave numbers in the twisted coordinat system which accompanies the rotation of macroscopic helical structure. Therefore in the usual laboratory coordinat system the

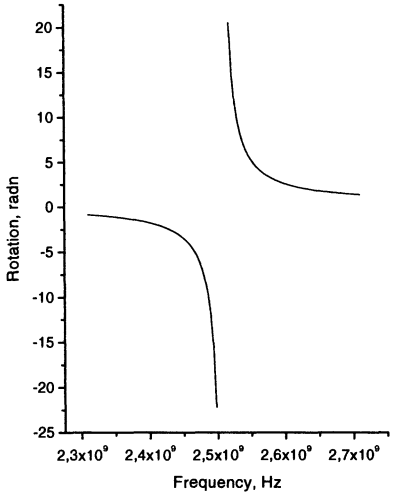

Figure 9. Rotation of the polarization plane of the transmitted wave as a function of the frequency. $\varepsilon_{11} = 3.9$, $\varepsilon_{22} = 3$, $\mu_{11} = 1$, $\mu_{22} = 1.1$, $\alpha = 0.3$, $q = 100$ radn/m and $L = 0.155$ m.

specific rotation of polarization plane of electromagnetic wave (for unit thickness of the sample) can be found as

$$v = \frac{1}{2}[(k_1 - q) - (k_2 + q)] \tag{30}$$

We have found the modified De Vries formula [23] for the rotation of the polarization plane:

$$v = \frac{k_0^2}{2(k_0^2\overline{\varepsilon}\overline{\mu} - q^2)}\left[q(\Delta\varepsilon\Delta\mu + \frac{\alpha_{12}^2}{4}(1 - 2\mu_{22}^{-1})) + \frac{k_0^2}{4q}(\overline{\varepsilon}\Delta\mu - \overline{\mu}\Delta\varepsilon + \frac{\alpha_{12}^2}{2})^2\right] \tag{31}$$

Here the following notations for the mean values and the anisotropy characteristics of the material parameters have been introduced:

$$\overline{\varepsilon} = \frac{\varepsilon_{11} + \varepsilon_{22}}{2}, \qquad \Delta\varepsilon = \frac{\varepsilon_{11} - \varepsilon_{22}}{2}, \qquad \overline{\mu} = \frac{\mu_{22} + 1}{2}, \qquad \Delta\mu = \frac{1 - \mu_{22}}{2}.$$

The dependence of the rotation of the polarization plane of the transmitted wave on the frequency is presented in Fig. 9. The peaks of the curves can be explained by the peculiarities of the De Vries formula: this formula gives infinity in the center of the region of the Bragg diffraction.

In [24], a design of isotropic polarizers formed by two lattices with wire helices was proposed. Our present results demonstrate another possibility of the design of a structure for transformations of the polarization state of electromagnetic waves. In contrast to the earlier proposed device [24], this structure can operate in a wide frequency range, because its operation is not based on the thickness resonance phenomena.

5. Conclusion

In this paper plane wave reflection and transmission phenomena in slabs of artificial bi-anisotropic uniform media are theoretically considered. The case of isotropic host medium having only dielectric properties is studied. Oblique incidence is assumed. The boundary-value problem for artificial uniform omega structure is solved taking into account multiple reflections of electromagnetic waves from the sample's boundaries. The intensity of the reflected and transmitted waves is calculated, and the comparison with artificial uniaxial bi-anisotropic plate with microhelices is performed. The possibility of the design a twisted omega-structure whose microwave properties are similar to the optical properties of cholesteric liquid crystals is demonstrated. The influence of the coupling parameter on the Bragg diffraction of electromagnetic waves in omega-medium with macrohelical structure is investigated. The modified formula de Vries for the rotation of the polarization plane of electromagnetic waves is found.

References

1. M.M.I Saadoun and N. Engheta, (1992), A reciprocal phase shifter using novel pseudochiral or Ω medium, *Microw. and Opt. Technol. Lett.*, **vol. 5**, pp. 184-188.
2. A.L. Topa, C.R. Paiva, and A.M. Barbosa, (1998), Hybrid-mode propagation in pseudochiral uniaxial waveguides with restangular cross section, *Bianisotropics'98*, Braunschweig, Germany, June 3-6, pp. 151-154.
3. A.A. Sochava, C.R. Simovski, S.A. Tretyakov, (1997), Chiral effects and eigenwaves in bi-anisotropic omega structures, in *Advances in Complex Electromagnetic Materials* (Ed. by A. Priou, A. Sihvola, S. Tretyakov, and A. Vinogradov), pp. 85-102.
4. A.N. Serdyukov, I.V. Semchenko, S.A. Tretyakov, and A.H. Sihvola, (2001), *Electromagnetics of bi-anisotropic materials*, Gordon and Breach Sciense Publishers.
5. Book of Abstracts, *Int. Conf. "Problems of Interaction of Radiation with Matter"*, Ed. by I.V.Semchenko and S.A. Khakhomov, Gomel State University, 30 Oct.-1 Nov. 2001.
6. I.V. Semchenko, S.A. Khakhomov, S.A. Tretyakov, and A.H. Sihvola, Elrectromagnetics waves in artificial chiral structures with dielectric and magnetic properties, (2001), *Electromagnetics*, **vol. 21, no. 5**, pp. 401-414.
7. I.V. Semchenko, S.A. Khakhomov, (2002), Artificial uniaxial bi-anisotropic media at oblique incidence of electromagnetic waves, *Electromagnetics*, **vol. 22, no. 1**, pp. 71-84.

8. I.V. Semchenko, S.A. Khakhomov, (2001), Reflection and transmission of electromagnetic waves at the normal incidence on the bi-anisotropic omega structure, *Proceedings of the Gomel State University*,**no. 6,** (in Russian).
9. A.H. Sihvola, I.V. Lindell, (1991), Bi-isotropic constitutive relations, *Microwave and Opt. Tech. Lett.*, **vol. 4, no.8**, pp.195-297.
10. J.A. Kong, (1986), *Electromagnetic Wave Theory*, Willey, New York.
11. J.C. Monzon, (1990), Radiation and scattering in homogeneous general bi-isotropic region, *IEEE Trans. Ant. Propagat.*, **vol. 38, no.2**, pp.227-235.
12. F.I. Fedorov, (1976), *Theory of gyrotropy*, Nauka i tekhnika, Minsk (in Russian).
13. B.V. Bokut, and A.N. Serdyukov, (1971), To phenomenological theory of natural optical activity, *Zhurnal Eksperiment. i Teor. Fiziki*, **vol. 61, no.5**, pp. 1808 - 1813,(in Russian).
14. S.A. Tretyakov and A.A. Sochava, (1993), Proposed composite material for non-reflecting shields and antenna radomes, *Electron. Lett.*, **vol. 29**, pp. 1048-1049.
15. S.A. Tretyakov and A.A. Sochava, (1994), Novel uniaxial bianisotropic materials: reflection and transmission in planar structures, in *Progress in Electromagnetic Research,* **vol. 9**, pp. 157-179.
16. I.V. Semchenko, S.A. Khakhomov, S.A. Tretyakov, and A.H. Sihvola, (1999), Microwave analogy of optical properties of cholesteric liquid crystals with local chirality under normal incidence of waves, *J. Phys. D: Appl. Phys.* **vol.32**, pp. 3222-3226.
17. V.V. Varadan, A. Lakhtakia, and V.K. Varadan, (1988), Reflection and transmission characteristics of a structurally chiral slab: Intrinsic anisotropy and form chirality, *Optik,* **vol. 80**, pp. 27-32.
18. A. Lakhtakia and W. S. Weiglhofer, (1995), On light propagation in helicoidal bianisotropic mediums, *Proc. R. Soc. Lond.,* **vol. A 448**, pp. 419-437.
19. A. Lakhtakia, (1998), Anomalous axial propagation in helicoidal bianisotropic media, *Optics Communications,* **vol. 157**, pp. 193-201.
20. I. Abdulhaim, (1987), Light propagation along the helix of chiral smectics and twisted nematics, *Opt. Commun.*, **vol. 64**, pp. 443-448.
21. I.V. Semchenko and A.N. Serdyukov, (1982), Influence of molecular gyrotropy on the light propagation in cholesteric liquid crystals, *Reports of Academy of Sciences of BSSR,* **vol. 26, no. 3**, pp. 235-237, (in Russian).
22. V.A. Belyakov and A.S. Sonin, (1982), *Cholesteric liquid crystals optics*, Nauka, Moscow, (in Russian).
23. H. De Vries,(1951), Rotatory power and optical properties of certain liquid crystals, *Acta Cristallogr.*, **vol. 4**, pp. 219-226.
24. E.N. Korshunova, A.N. Sivov, and A.D. Shatrov, (1997), The isotropic turn polarizer of transmitted type formed by two lattices with wire helices, *Radiotekhnika i elektronika,* **vol. 42, no. 10**, pp. 1157-1160, (in Russian).

A REVIEW OF HOMOGENIZATION STUDIES FOR BIAXIAL BIANISOTROPIC MATERIALS

TOM G. MACKAY
School of Mathematics
University of Edinburgh
The King's Buildings, Edinburgh EH9 3JZ, United Kingdom
AND
WERNER S. WEIGLHOFER
Department of Mathematics, University of Glasgow
University Gardens, Glasgow G12 8QW, United Kingdom

Abstract. Biaxial mediums in the form of naturally occurring orthorhombic, monoclinic and triclinic crystals are of long-standing scientific and technological importance. We consider the conceptualization of artificial biaxial mediums, through the homogenization of simple component mediums. Biaxiality in homogenized composite mediums originates from two noncollinear distinguished axes presented by the component mediums; these distinguished axes can have either an electromagnetic or topological origin. The relationship between the biaxial composite structure and the geometry, orientation and composition of the component mediums is explored for the nondissipative dielectric case. Extending these studies to include the effects of dissipation in dielectric–magnetic materials, a generalized biaxial composite structure is revealed for which the principal axes of real and imaginary parts of the permittivity and permeability constitutive dyadics do not coincide. Furthermore, in the bianisotropic regime, yet more general HCM structures arise; in particular, complex symmetries are presented in the constitutive dyadics which would not be anticipated from a familiarity with the dielectric or dielectric–magnetic case.

1. Introduction

Since the earliest days of electromagnetics, the naturally occurring biaxiality of certain mediums has been much exploited for scientific and technological purposes [1]. In crystallography such mediums provide the orthorhombic, monoclinic and triclinic classifications [2]. Aspects of electromagnetic biaxiality which have been scrutinized in the recent research literature include Green functions [3]–[5], depolarization dyadics [6, 7] and wave propagation [8].

S. Zouhdi et al. (eds.), Advances in Electromagnetics of Complex Media and Metamaterials, 211–228.

Our focus here is on the manifestation of biaxiality through the homogenization of composite mediums. A composite medium may be regarded as effectively homogeneous provided that the structural length scales of its component mediums are sufficiently small compared with electromagnetic wavelengths [9, 10]. Such a homogenized composite medium (HCM) is typically characterized by electromagnetic properties which are more complex than those of its component mediums. For example, *Faraday chiral mediums* [11] in the form of *chiroferrites* [12] and *chiroplasmas* [13] arise from the homogenization of an isotropic chiral component medium with either a magnetically biased ferrite or a magnetically biased plasma component medium, respectively. In the present chapter we consider biaxial HCMs originating from simple component mediums; i.e., components mediums which are either isotropic or uniaxial with respect to their electromagnetic and topological properties.

The development of effectively biaxial composites through the homogenization of assemblies of parallel ellipsoidal inclusions is well-documented for the purely dielectric regime [14, 15]. Of particular historical interest is Wiener's pioneering analysis of parallel dielectric ellipsoids [16] (reproduced in [9]). Recent reports have dealt with the percolation phenomenon associated with the homogenization of metallic ellipsoids [17, 18]. We present here a review of detailed parametric studies of the conceptualization of biaxial HCMs, relating both the intrinsic electromagnetic properties and the topological structure of the component mediums to the HCM form. The numerical results presented provide an overview of results available elsewhere [19]–[21]. Specifically, two-phase homogenization scenarios are considered where neither component medium is in itself biaxial. However, the component mediums collectively present two noncollinear distinguished axes. Each distinguished axis arises from either uniaxial electromagnetic constitutive properties or spheroidal particulate topology. The distinguished axes of the component phases do not bear an obvious relation to the optical axes of the HCM [21]. In Section 2 preliminaries relating to the characterization of biaxiality and to homogenization formalisms are described. Illustrative numerical results pertaining to nondissipative biaxial dielectric HCMs [19] are presented in Section 3. The consequences of dissipation [20] are explored in Section 4, and this is followed by a consideration of the most general case of biaxiality, namely bianisotropic biaxiality [21], in Section 5. We conclude in Section 6 with some closing remarks.

In the notational convention adopted, vectors are in boldface. Dyadics are double underlined: 3×3 dyadics are in normal face whereas 6×6 dyadics are in boldface. The 3×3 (6×6) unit dyadic is denoted by $\underline{\underline{I}}$ ($\underline{\underline{\mathbf{I}}}$) while the triad of cartesian unit vectors is represented as ($\mathbf{u}_x$, $\mathbf{u}_y$, $\mathbf{u}_z$). The permittivity and permeability of free space are given by ϵ_0 and μ_0, respectively.

2. Preliminaries

2.1. CHARACTERIZATIONS OF BIAXIALITY

The relative permittivity dyadic of a nondissipative biaxial dielectric medium may be represented by [22] (see also [23, 5, 19])

$$\underline{\underline{\epsilon}}_{bi} = p_\epsilon \underline{\underline{I}} + q_\epsilon(\mathbf{u}_m\mathbf{u}_n + \mathbf{u}_n\mathbf{u}_m)\,, \tag{1}$$

where p_ϵ and q_ϵ are dimensionless real-valued permittivity scalars. The real-valued unit vectors $\mathbf{u}_m$ and $\mathbf{u}_n$ lie along along the directions of the *optic ray axes* [1]; i.e., they give the two privileged directions in which monochromatic plane waves propagate with only one permissible group velocity. The advantage of (1) over the widely-used diagonal dyadic representation of biaxial permittivity (see, for example, [24])

$$\underline{\underline{\tilde{\epsilon}}}_{bi} = \epsilon_x\mathbf{u}_x\mathbf{u}_x + \epsilon_y\mathbf{u}_y\mathbf{u}_y + \epsilon_z\mathbf{u}_z\mathbf{u}_z\,, \tag{2}$$

is that the representation (1) affords an immediate crystallographic interpretation. Matters pertaining to biaxial representations are further discussed elsewhere [22].

In order to accommodate dissipative mechanisms, representation (1) generalizes to [20]

$$\underline{\underline{\epsilon}}_{bi} = \underline{\underline{\epsilon}}^{r}_{bi} + i\,\underline{\underline{\epsilon}}^{i}_{bi}\,, \quad \underline{\underline{\epsilon}}^{\chi}_{bi} = p^{\chi}_{\epsilon}\underline{\underline{I}} + q^{\chi}_{\epsilon}(\mathbf{u}^{\chi}_{m\epsilon}\mathbf{u}^{\chi}_{n\epsilon} + \mathbf{u}^{\chi}_{n\epsilon}\mathbf{u}^{\chi}_{m\epsilon})\,, \quad (\chi = r, i), \tag{3}$$

where p^{χ}_{ϵ} and q^{χ}_{ϵ} are real-valued scalars, and $\mathbf{u}^{\chi}_{m\epsilon}$ and $\mathbf{u}^{\chi}_{n\epsilon}$ are real-valued unit vectors. Similarly, the diagonal representation (2) generalizes to [25]

$$\underline{\underline{\tilde{\epsilon}}}_{bi} = \underline{\underline{\tilde{\epsilon}}}^{r}_{bi} + i\underline{\underline{\tilde{\epsilon}}}^{i}_{bi}\,, \quad \underline{\underline{\tilde{\epsilon}}}^{\chi}_{bi} = \epsilon^{\chi}_{x}\mathbf{u}^{\chi}_{x}\mathbf{u}^{\chi}_{x} + \epsilon^{\chi}_{y}\mathbf{u}^{\chi}_{y}\mathbf{u}^{\chi}_{y} + \epsilon^{\chi}_{z}\mathbf{u}^{\chi}_{z}\mathbf{u}^{\chi}_{z}\,, \quad (\chi = r, i), \tag{4}$$

where, as with (3), all dyadic entries and unit vectors are real-valued, and the triads $(\mathbf{u}^r_x, \mathbf{u}^r_y, \mathbf{u}^r_z)$ and $(\mathbf{u}^i_x, \mathbf{u}^i_y, \mathbf{u}^i_z)$ specify different cartesian frames, in general. The equivalence of representations (3) and (4) is straightforwardly revealed through diagonalizing the real symmetric dyadic $\underline{\underline{\epsilon}}^{\chi}_{bi}$ in (3).

Biaxial crystal structures are classified via the relative orientations of their three basis vectors which form the primitive unit cell of the Bravais lattice [26]. For the *orthorhombic* class, the three basis vectors are mutually perpendicular and the identity

$$(\mathbf{u}^r_x, \mathbf{u}^r_y, \mathbf{u}^r_z) \equiv (\mathbf{u}^i_x, \mathbf{u}^i_y, \mathbf{u}^i_z), \tag{5}$$

between triads of cartesian unit vectors in (4) holds. Expressed in terms of representation (3), the orthorhombic condition (5) is equivalent to the situation in which the unit vector pairs $\mathbf{u}^r_m$, $\mathbf{u}^r_n$ and $\mathbf{u}^i_m$, $\mathbf{u}^i_n$ lie in the same

plane with a common plane bisecting the pair $\mathbf{u}_m^r$, $\mathbf{u}_n^r$ and the pair $\mathbf{u}_m^i$, $\mathbf{u}_n^i$ [20]. More general biaxial categories, namely the *monoclinic* and *triclinic* classes, are associated with nonperpendicular basis vectors and for these classes (5) does not hold [25]. Thus, for the most general dissipative biaxial dielectric structure, nine real-valued parameters are required to characterize the permittivity: three scalars for each of the diagonal forms of $\underline{\underline{\tilde{\epsilon}}}_{bi}^r$ and $\underline{\underline{\tilde{\epsilon}}}_{bi}^i$ and a further three Eulerian angles relating $(\mathbf{u}_x^r, \mathbf{u}_y^r, \mathbf{u}_z^r)$ to $(\mathbf{u}_x^i, \mathbf{u}_y^i, \mathbf{u}_z^i)$.

We see that (1) and (3) provide a convenient and physically-insightful characterization of biaxial mediums. Thus far, we have limited our consideration to biaxial dielectric mediums, characterized by the relative permittivity dyadic $\underline{\underline{\epsilon}}_{bi}$. Broadening our discussion, biaxial dielectric–magnetic mediums [20] may be specified with the relative permittivity dyadic (3) together with the analogous relative permeability dyadic

$$\underline{\underline{\mu}}_{bi} = \underline{\underline{\mu}}_{bi}^r + i\,\underline{\underline{\mu}}_{bi}^i\,, \quad \underline{\underline{\mu}}_{bi}^\chi = p_\mu^\chi\,\underline{\underline{I}} + q_\mu^\chi(\mathbf{u}_{m\mu}^\chi\mathbf{u}_{n\mu}^\chi + \mathbf{u}_{n\mu}^\chi\mathbf{u}_{m\mu}^\chi)\,, \quad (\chi = r, i), \tag{6}$$

where p_μ^χ and q_μ^χ are real-valued scalars, and $\mathbf{u}_{m\mu}^\chi$ and $\mathbf{u}_{n\mu}^\chi$ are real-valued unit vectors. Furthermore, the most general biaxial class in the linear regime, namely that of the biaxial bianisotropic medium [21], may be described in terms of the relative permittivity dyadic (3) and relative permeability dyadic (6), combined with the biaxial magnetoelectric dyadics

$$\begin{aligned} \underline{\underline{\xi}}_{bi} &= \underline{\underline{\xi}}_{bi}^r + i\,\underline{\underline{\xi}}_{bi}^i\,, & \underline{\underline{\xi}}_{bi}^\chi &= p_\xi^\chi\,\underline{\underline{I}} + q_\xi^\chi(\mathbf{u}_{m\xi}^\chi\mathbf{u}_{n\xi}^\chi + \mathbf{u}_{n\xi}^\chi\mathbf{u}_{m\xi}^\chi) \\ \underline{\underline{\zeta}}_{bi} &= \underline{\underline{\zeta}}_{bi}^r + i\,\underline{\underline{\zeta}}_{bi}^i\,, & \underline{\underline{\zeta}}_{bi}^\chi &= p_\zeta^\chi\,\underline{\underline{I}} + q_\zeta^\chi(\mathbf{u}_{m\zeta}^\chi\mathbf{u}_{n\zeta}^\chi + \mathbf{u}_{n\zeta}^\chi\mathbf{u}_{m\zeta}^\chi) \end{aligned} \quad (\chi = r, i), \tag{7}$$

wherein all scalars and unit vectors are real-valued. Biaxial HCMs of the dielectric, dielectric–magnetic and bianisotropic types are explored in Sections 3, 4 and 5, respectively.

2.2. HOMOGENIZATION FORMALISM

We consider HCMs developing from only two (distinct) component mediums: an inclusion medium which is labelled a, and a host medium which is labelled b. Each component medium is envisioned in particulate form. The component particles are assumed to be randomly distributed but similarly oriented, with surfaces parameterized as [29]

$$\mathbf{R}_s(\theta, \phi) = s\,\underline{\underline{U}} \cdot \hat{\mathbf{R}}(\theta, \phi)\,, \tag{8}$$

where $\hat{\mathbf{R}}(\theta, \phi)$ is the radial unit vector depending on the spherical polar coordinates θ and ϕ, $\underline{\underline{U}}$ is a real-valued symmetric *shape* dyadic, and s is a linear measure.

Let

$$\underline{\underline{\mathbf{K}}}_{\nu} = \begin{pmatrix} \epsilon_0 \underline{\underline{\xi}}_{\nu} & i\sqrt{\epsilon_0\mu_0}\,\underline{\underline{\xi}}_{\nu} \\ i\sqrt{\epsilon_0\mu_0}\,\underline{\underline{\zeta}}_{\nu} & \mu_0 \underline{\underline{\mu}}_{\nu} \end{pmatrix}, \qquad (\nu = a, b, HCM), \tag{9}$$

denote the constitutive dyadics of the component mediums a and b, and of the HCM, respectively. These are defined by the corresponding constitutive relations [27, 28]

$$\begin{aligned} \mathbf{D}(\mathbf{x}) &= \epsilon_0 \underline{\underline{\xi}}_{\nu} \cdot \mathbf{E}(\mathbf{x}) + i\sqrt{\epsilon_0\mu_0}\,\underline{\underline{\xi}}_{\nu} \cdot \mathbf{H}(\mathbf{x}) \\ \mathbf{B}(\mathbf{x}) &= i\sqrt{\epsilon_0\mu_0}\,\underline{\underline{\zeta}}_{\nu} \cdot \mathbf{E}(\mathbf{x}) + \mu_0 \underline{\underline{\mu}}_{\nu} \cdot \mathbf{H}(\mathbf{x}) \end{aligned} \qquad (\nu = a, b, HCM). \tag{10}$$

In the following sections we describe parametric numerical studies [19]–[21] in which $\underline{\underline{\mathbf{K}}}_{HCM}$ is estimated from $\underline{\underline{\mathbf{K}}}_{a}$ and $\underline{\underline{\mathbf{K}}}_{b}$ together with their associated shape dyadics. Since we are dealing with biaxial HCMs, all 3×3 HCM constitutive dyadics are symmetric. Furthermore, all component mediums considered here are reciprocal. Consequently, we have $\underline{\underline{\zeta}}_{HCM} = -\underline{\underline{\xi}}_{HCM}$ and $\underline{\underline{\zeta}}_{HCM}$ need not be further mentioned.

A considerable number of formalisms have been developed in order to estimate the constitutive parameters of HCMs [9, 15, 29]. The Maxwell Garnett formalism [30], including its incremental and differential variants [31], has gained particular prominence in recent years. For the present studies, the Bruggeman homogenization formalism is adopted as it permits the particulate topology of both component mediums to be varied independently. The Bruggeman formalism, especially in its application to anisotropic and bianisotropic HCMs, has been well established in the recent research literature [29]–[32]. The Bruggeman estimate of $\underline{\underline{\mathbf{K}}}_{HCM}$ is obtained by solving the nonlinear equation

$$f_a \underline{\underline{\boldsymbol{\alpha}}}^{a/HCM} + f_b \underline{\underline{\boldsymbol{\alpha}}}^{b/HCM} = \underline{\underline{\mathbf{0}}}. \tag{11}$$

In (11), the generalized polarizability of component medium ℓ ($\ell = a, b$) is given by

$$\underline{\underline{\boldsymbol{\alpha}}}^{\ell/HCM} = \left(\underline{\underline{\mathbf{K}}}_{\ell} - \underline{\underline{\mathbf{K}}}_{HCM}\right) \cdot \left[\underline{\underline{\mathbf{I}}} + i\omega \underline{\underline{\mathbf{D}}}^{U^{\ell}/HCM} \cdot \left(\underline{\underline{\mathbf{K}}}_{\ell} - \underline{\underline{\mathbf{K}}}_{HCM}\right)\right]^{-1}, \tag{12}$$

where $\underline{\underline{\mathbf{D}}}^{U^{\ell}/HCM}$ is the *depolarization dyadic* of a $\underline{U}$-shaped exclusion volume of component medium ℓ, immersed in the HCM. The depolarization dyadic is essentially the singularity of the corresponding free-space dyadic Green function [33, 34]. For biaxial mediums, the depolarization dyadic may be expressed explicitly in terms of elliptic functions [6]. An iterative solution to (11) is developed as

$$\underline{\underline{\mathbf{K}}}_{HCM}[n] = \mathcal{T}\left(\underline{\underline{\mathbf{K}}}_{HCM}[n-1]\right), \qquad (n = 1, 2, \ldots), \tag{13}$$

where the operator $\mathcal{T}$ defined as

$$\begin{aligned}\mathcal{T}(\underline{\underline{\mathbf{K}}}_{HCM}) = & \left\{ f_a \underline{\underline{\mathbf{K}}}_a \cdot \left[\underline{\underline{\mathbf{I}}} + i\omega \underline{\underline{\mathbf{D}}}^{U^a/HCM} \cdot \left(\underline{\underline{\mathbf{K}}}_a - \underline{\underline{\mathbf{K}}}_{HCM} \right) \right]^{-1} + \right. \\ & \left. f_b \underline{\underline{\mathbf{K}}}_b \cdot \left[\underline{\underline{\mathbf{I}}} + i\omega \underline{\underline{\mathbf{D}}}^{U^b/HCM} \cdot \left(\underline{\underline{\mathbf{K}}}_b - \underline{\underline{\mathbf{K}}}_{HCM} \right) \right]^{-1} \right\} \\ & \cdot \left\{ f_a \left[\underline{\underline{\mathbf{I}}} + i\omega \underline{\underline{\mathbf{D}}}^{U^a/HCM} \cdot \left(\underline{\underline{\mathbf{K}}}_a - \underline{\underline{\mathbf{K}}}_{HCM} \right) \right]^{-1} + \right. \\ & \left. f_b \left[\underline{\underline{\mathbf{I}}} + i\omega \underline{\underline{\mathbf{D}}}^{U^b/HCM} \cdot \left(\underline{\underline{\mathbf{K}}}_b - \underline{\underline{\mathbf{K}}}_{HCM} \right) \right]^{-1} \right\}^{-1}, \end{aligned} \tag{14}$$

and the initial value $\underline{\underline{\mathbf{K}}}_{HCM}[0]$ is provided by the Maxwell Garnett homogenization formalism [29, 32]. A characteristic of the Bruggeman formalism is that the two component mediums are treated symmetrically. Notwithstanding, it is convenient and conventional to refer to them as the *host* medium and the *inclusion* medium.

The estimate of $\underline{\underline{\mathbf{K}}}_{HCM}$ depends crucially on the volumetric proportion of inclusion medium to host medium, namely f_a. Clearly, $\underline{\underline{\mathbf{K}}}_{HCM} \to \underline{\underline{\mathbf{K}}}_a$ as $f_a \to 1$ and $\underline{\underline{\mathbf{K}}}_{HCM} \to \underline{\underline{\mathbf{K}}}_b$ as $f_a \to 0$. For illustrative purposes, we choose $f_a = 0.3$ for all numerical calculations presented here.

3. Nondissipative dielectric properties

We begin our study of biaxial HCMs by considering nondissipative dielectric HCMs [19] with relative permittivity dyadics of the form

$$\underline{\underline{\epsilon}}_{HCM} = p_\epsilon \underline{\underline{I}} + q_\epsilon (\mathbf{u}_m \mathbf{u}_n + \mathbf{u}_n \mathbf{u}_m) , \tag{15}$$

where p_ϵ, $q_\epsilon \in \mathbb{R}$. We explore biaxiality arising from two distinct origins: firstly from the shapes of the constituent particles and secondly from the intrinsic electromagnetic properties of the component mediums. Notice that the distinguished axes presented by the component mediums lie in a plane perpendicular to the plane containing $\mathbf{u}_m$ and $\mathbf{u}_n$; furthermore, the plane of the distinguished axes bisects the angle between $\mathbf{u}_m$ and $\mathbf{u}_n$ [19]. In the numerical examples presented here, the distinguished axes presented by the component mediums are chosen to lie in the xy plane. Consequently, we have

$$\mathbf{u}_m = \sin\theta \cos\phi \, \mathbf{u}_x + \sin\theta \sin\phi \, \mathbf{u}_y + \cos\theta \, \mathbf{u}_z , \tag{16}$$

$$\mathbf{u}_n = \sin\theta \cos\phi \, \mathbf{u}_x + \sin\theta \sin\phi \, \mathbf{u}_y - \cos\theta \, \mathbf{u}_z . \tag{17}$$

3.1. TOPOLOGICAL BIAXIALITY

We homogenize two isotropic dielectric component mediums: medium a with relative permittivity $\epsilon_a = 3.5$ and medium b with relative permittivity $\epsilon_b = 1.2$. The same spheroidal particulate shape is chosen for both component mediums, but the spheroid axis of medium a is orientated at an angle ψ_a in the xy plane with respect to the spheroid axis of medium b. Thus, we have that corresponding shape dyadics for mediums a and b are given as [29, 30]

$$\underline{\underline{U}}_\ell = \begin{pmatrix} 2\cos^2\psi_\ell + \sin^2\psi_\ell & \sin\psi_\ell\cos\psi_\ell & 0 \\ \sin\psi_\ell\cos\psi_\ell & 2\sin^2\psi_\ell + \cos^2\psi_\ell & 0 \\ 0 & 0 & 1 \end{pmatrix}, \qquad (\ell = a, b), \quad (18)$$

with $\psi_b = 0$.

Estimates of the HCM parameters p_ϵ, q_ϵ, θ and ϕ for $\psi_a \in [0, \pi]$ are plotted in Figure 1. The plane in which $\mathbf{u}_m$ and $\mathbf{u}_n$ lie, as given by ϕ, rotates about the z axis as ψ_a increases, whereas the angle between $\mathbf{u}_m$ and $\mathbf{u}_n$, as given by $2(\theta - \pi/2)$, increases to a maximum at $\psi_a = \pi/2$ and falls to 0 as ψ_a tends to 0 and π. At $\psi_a = 0$ and π, the spheroid axes of the host and inclusion mediums are parallel and anti-parallel, respectively; therefore the constituent mediums together present only one distinguished axis and the resulting HCM is accordingly uniaxial. The scalars p_ϵ and q_ϵ are not greatly influenced by ψ_a.

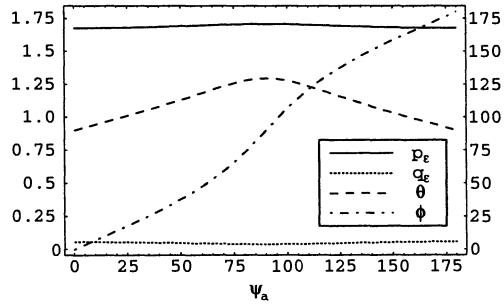

Figure 1. Isotropic spheroidal inclusions with isotropic spheroidal host. Relative permittivity scalars p_ϵ and q_ϵ (left scale) and angles θ and ϕ (in degrees, right scale) of the HCM plotted against inclusion spheroid axis angle ψ_a. (Reproduced from [19]).

3.2. ELECTROMAGNETIC BIAXIALITY

We now turn our attention to the case where both host and inclusion mediums comprise spherical particles of uniaxial permittivity. Analogously to Section 3.1, the permittivity axis of medium a is taken to be orientated at an angle λ_a in the xy plane with respect to the permittivity axis of medium b. That is, we select the relative permittivity dyadics $\underline{\underline{\epsilon}}_\ell = \underline{\underline{Y}}_\ell$ where

$$\underline{\underline{Y}}_\ell = \begin{pmatrix} 3\cos^2\lambda_\ell + \sin^2\lambda_\ell & 2\sin\lambda_\ell\cos\lambda_\ell & 0 \\ 2\sin\lambda_\ell\cos\lambda_\ell & 3\sin^2\lambda_\ell + \cos^2\lambda_\ell & 0 \\ 0 & 0 & 1 \end{pmatrix}, \qquad (\ell = a, b), \quad (19)$$

for mediums a and b, with $\lambda_b = 0$.

The corresponding HCM constitutive parameters are plotted for $\lambda_a \in [0, \pi]$ in Figure 2. The scalar permittivity parameters p_ϵ and q_ϵ are considerably more orientationally dependent than they are in Section 3.1. As $\lambda_a \to 0$ and π, we see that $\theta \to \pi/2$ and the scalars $p_\epsilon \to 1$ and $q_\epsilon \to 1$ and thus the HCM permittivity dyadic acquires the uniaxial form. Unlike the situation in which the distinguished axes arise from the shape of the constituent particles, the orientation of the plane containing $\mathbf{u}_m$ and $\mathbf{u}_n$ does not follow the angle of the distinguished permittivity axis λ_a, rather it oscillates about the x axis.

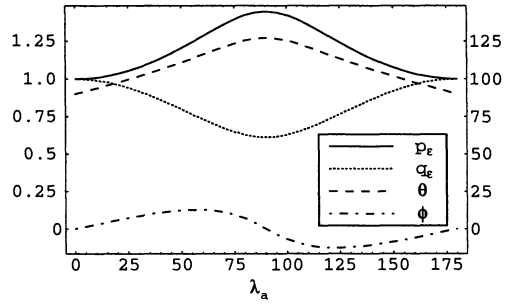

Figure 2. As for Figure 1 but for uniaxial spherical inclusions with uniaxial spherical host. Constitutive parameters of the HCM plotted against inclusion permittivity axis angle λ_a. (Reproduced from [19]).

4. Dissipative anisotropic properties

We now broaden our investigation of biaxial HCMs, firstly by introducing the effects of dissipation in Section 4.1, and secondly by considering

dielectric–magnetic mediums in Section 4.2 [20]. For all calculations described in Section 4.1, the HCM relative permittivity dyadics have the general biaxial form

$$\underline{\underline{\epsilon}}_{HCM} = p^r_\epsilon \underline{\underline{I}} + q^r_\epsilon(\mathbf{u}^r_{m\epsilon}\mathbf{u}^r_{n\epsilon} + \mathbf{u}^r_{n\epsilon}\mathbf{u}^r_{m\epsilon}) + i\left[p^i_\epsilon \underline{\underline{I}} + q^i_\epsilon(\mathbf{u}^i_{m\epsilon}\mathbf{u}^i_{n\epsilon} + \mathbf{u}^i_{n\epsilon}\mathbf{u}^i_{m\epsilon})\right], \tag{20}$$

while in Section 4.2 the corresponding HCM relative permeability dyadic

$$\begin{aligned}\underline{\underline{\mu}}_{HCM} = {} & p^r_\mu \underline{\underline{I}} + q^r_\mu(\mathbf{u}^r_{m\mu}\mathbf{u}^r_{n\mu} + \mathbf{u}^r_{n\mu}\mathbf{u}^r_{m\mu}) + \\ & i\left[p^i_\mu \underline{\underline{I}} + q^i_\mu(\mathbf{u}^i_{m\mu}\mathbf{u}^i_{n\mu} + \mathbf{u}^i_{n\mu}\mathbf{u}^i_{m\mu})\right],\end{aligned} \tag{21}$$

arises. In (20) and (21), $p^{r,i}_{\epsilon,\mu}$ and $q^{r,i}_{\epsilon,\mu}$ are real-valued scalars and

$$\begin{aligned}\mathbf{u}^\chi_{\kappa c} = {} & \sin\theta^\chi_{\kappa c}\cos\phi^\chi_{\kappa c}\,\mathbf{u}_x + \sin\theta^\chi_{\kappa c}\sin\phi^\chi_{\kappa c}\,\mathbf{u}_y + \cos\theta^\chi_{\kappa c}\,\mathbf{u}_z\,, \\ & (\chi = r,i;\ \ \kappa = m,n;\ \ c = \epsilon,\mu).\end{aligned} \tag{22}$$

The biaxiality of the HCM arises from the fact that the constituent mediums collectively possess two noncollinear distinguished axes. These axes originate from either the particulate topologies of the component mediums or from uniaxiality in their electromagnetic constitutive properties. In Sections 4.1 and 4.2 we consider only constituent mediums with distinguished axes lying in the xy plane. As a consequence, the HCM unit vector pairs $\mathbf{u}^\chi_{mc}$ and $\mathbf{u}^\chi_{nc}$ always lie in planes perpendicular to the xy plane with the xy plane bisecting the angle between $\mathbf{u}^\chi_{mc}$ and $\mathbf{u}^\chi_{nc}$. Therefore, we have the following identities

$$\theta^\chi_{mc} = \pi - \theta^\chi_{nc} = \theta^\chi_c, \qquad \phi^\chi_{mc} = \phi^\chi_{nc} = \phi^\chi_c, \qquad (\chi = r,i;\ \ c = \epsilon,\mu). \tag{23}$$

All graphs displayed in Sections 4 and 5 are presented with reference to the key given in Table 1.

Table 1: Key for Figures 3–8. $X = \theta$, ϕ, p or q.

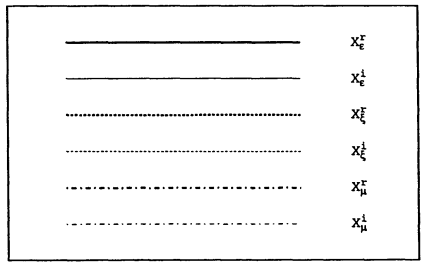

4.1. TOPOLOGICAL BIAXIALITY

Consider the homogenization of inclusion and host mediums which are both isotropic dielectric. We choose a host medium of relative permittivity $\epsilon_b = 1.2$ and homogenize with inclusions of dissipative relative permittivity $\epsilon_a = 3(1+i)$. Directional effects are introduced via the topologies of the component mediums a and b which are described by the shape dyadics (18) with $\psi_b = 0$.

The defining angles $\theta_\epsilon^{r,i}$ and $\phi_\epsilon^{r,i}$ for the HCM unit vectors $\mathbf{u}_{m\epsilon,n\epsilon}^{r,i}$ are plotted as functions of the spheroid axis angle ψ_a in Figure 3. The HCM scalar permittivities $p_\epsilon^{r,i}$ and $q_\epsilon^{r,i}$ vary little with ψ_a and are not displayed. The variation of θ_ϵ^r and ϕ_ϵ^r (and p_ϵ^r and q_ϵ^r) with ψ_a is similar to that found for the nondissipative dielectric case in Section 3, and the quantities arising from dissipative processes (θ_ϵ^i, ϕ_ϵ^i, p_ϵ^i and q_ϵ^i) behave in an analogous manner. At the endpoints $\psi_a = 0, \pi$, the unit vectors $\mathbf{u}_{m\epsilon,n\epsilon}^{r,i}$ all lie on a common line (the x axis) and the HCM has a uniaxial structure. At the midpoint $\psi_a = \pi/2$, we have $\phi_\epsilon^{r,i} = \pi/2$ and therefore $\underline{\underline{\epsilon}}_{HCM}$ has a diagonal form and the HCM is orthorhombic biaxial. The orthorhombic case arises in this instance when the distinguished axes of the constituent mediums are orthogonal. Aside from these special cases, we observe $\theta_\epsilon^r \neq \theta_\epsilon^i \neq \phi_\epsilon^r \neq \phi_\epsilon^i$ and the biaxial HCM is of the monoclinic/triclinic type, in spite of the fact that the chosen values were such that $\mathrm{Re}\,\epsilon_a = \mathrm{Im}\,\epsilon_a$ (where $\epsilon_a = \mathrm{Re}\,\epsilon_a + i\,\mathrm{Im}\,\epsilon_a$, and $\mathrm{Re}\,\epsilon_a$, $\mathrm{Im}\,\epsilon_a$ are real-valued).

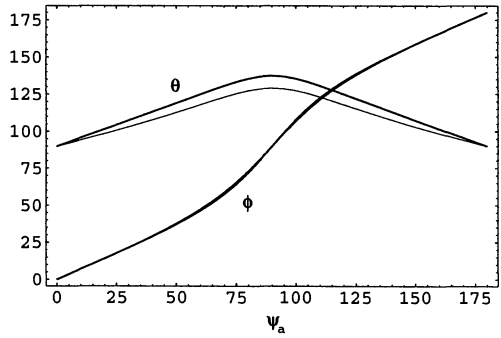

Figure 3. Dissipative spheroidal inclusion medium with nondissipative spheroidal host medium (both mediums isotropic dielectric). HCM unit vector angles $\theta_\epsilon^{r,i}$ and $\phi_\epsilon^{r,i}$ plotted against inclusion spheroid orientation angle ψ_a. (Key: $X = \theta$, ϕ in Table 1). (Reproduced from [20]).

Greater differences between θ_ϵ^r and θ_ϵ^i, and between ϕ_ϵ^r and ϕ_ϵ^i, than those displayed in Figure 3 can be achieved by choosing $\mathrm{Re}\,\epsilon_a \neq \mathrm{Im}\,\epsilon_a$. We

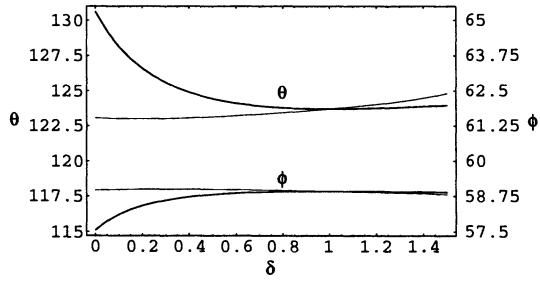

Figure 4. As for Figure 3 but with dissipative host medium. HCM unit vector angles $\theta_\epsilon^{r,i}$ and $\phi_\epsilon^{r,i}$ plotted against degree of host medium dissipation δ. (Key: $X = \theta, \phi$ in Table 1). (Reproduced from [20]).

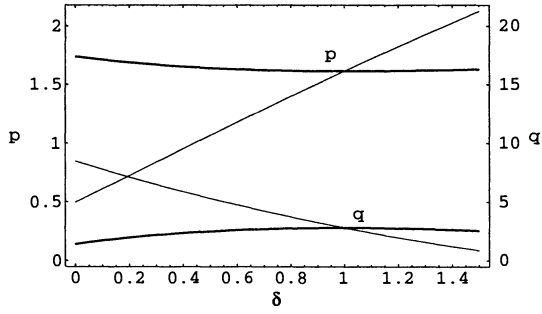

Figure 5. As for Figure 4 but with HCM scalar permittivities $p_\epsilon^{r,i}$ and $q_\epsilon^{r,i}$ plotted against degree of host medium dissipation δ. (Key: $X = p, q$ in Table 1). (Reproduced from [20]).

explore this matter further by repeating the homogenization of Figure 3 but with an allowance made for dissipation in the host medium by taking $\epsilon_b = 1.2(1 + i\delta)$. For a spheroid inclusion angle of $\psi_a = 70°$, the HCM unit vector angles $\theta_\epsilon^{r,i}$ and $\phi_\epsilon^{r,i}$ and scalar permittivities $p_\epsilon^{r,i}$ and $q_\epsilon^{r,i}$ are plotted against δ in Figures 4 and 5 respectively. The point of interest occurs at $\delta = 1$ and we find,

$$\begin{aligned} &\mathrm{Re}\,\underline{\underline{\epsilon}}_b = \rho\,\mathrm{Im}\,\underline{\underline{\epsilon}}_b\,, \quad \mathrm{Re}\,\underline{\underline{\epsilon}}_a = \rho\,\mathrm{Im}\,\underline{\underline{\epsilon}}_a \\ &\Rightarrow \quad \theta_\epsilon^r = \theta_\epsilon^i\,, \quad \phi_\epsilon^r = \phi_\epsilon^i\,, \quad p_\epsilon^r = p_\epsilon^i\,, \quad q_\epsilon^r = q_\epsilon^i\,, \end{aligned} \tag{24}$$

where ρ is a proportionality constant. At $\delta = 1$ the HCM is orthorhombic biaxial (since $\phi_\epsilon^r = \phi_\epsilon^i$), despite the distinguished axes of the constituent medium spheroids not being perpendicular. Furthermore, the structure at

this point is a highly specialized form of orthorhombic for which $\underline{\underline{\epsilon}}_{HCM}$ is specified by only four real-valued parameters (θ_ϵ^r, ϕ_ϵ^r, p_ϵ^r and q_ϵ^r), although the HCM is both biaxial and dissipative.

4.2. ELECTROMAGNETIC BIAXIALITY

We now extend our investigations to the case of dielectric–magnetic materials. Unlike the previous example in Section 4.1, here we consider constituents in which the distinguished axes have an electromagnetic, rather than topological, origin. We explore the homogenization of a dissipative uniaxial host medium with relative constitutive dyadics $\underline{\underline{\epsilon}}_b = \underline{\underline{\mu}}_b = (1+i\,\delta)\underline{\underline{Y}}_b$ and $\lambda_b = 0$, with a dissipative inclusion medium with relative constitutive dyadics $\underline{\underline{\epsilon}}_a = (1+i)\underline{\underline{Y}}_a$, $\underline{\underline{\mu}}_a = (2+i)\underline{\underline{Y}}_a$ and $\lambda_a = 50°$. Both host and inclusion mediums are based on spherical topology. Notice that the distinguished axes for the inclusion permittivity and permeability dyadics are parallel and lie at angle λ_a in the xy plane to the distinguished axes of the corresponding host medium, which are also parallel.

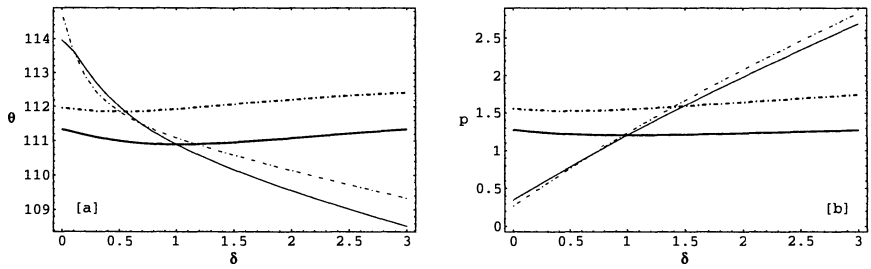

Figure 6. Dissipative inclusion medium with dissipative host medium (both mediums uniaxial dielectric–magnetic). HCM unit vector (a) polar angles $\theta_{\epsilon,\mu}^{r,i}$ and (b) scalar permittivities and permeabilities $p_{\epsilon,\mu}^{r,i}$ plotted against degree of host medium dissipation δ. (Key in Table 1: $X = \theta$ for (a), $X = p$ for (b)). (Reproduced from [20]).

The calculated angles $\theta_{\epsilon,\mu}^{r,i}$ and scalars $p_{\epsilon,\mu}^{r,i}$ are plotted against δ in Figure 6. (The equivalent graphs for $\phi_{\epsilon,\mu}^{r,i}$ and $q_{\epsilon,\mu}^{r,i}$ show analogous behaviour to Figures 6 and are not displayed). The key features of these two figures (and the corresponding graphs for $\phi_{\epsilon,\mu}^{r,i}$ and $q_{\epsilon,\mu}^{r,i}$ which are not displayed) may be summarized by

$$\mathrm{Re}\,\underline{\underline{\epsilon}}_b = \rho\,\mathrm{Im}\,\underline{\underline{\epsilon}}_b\,, \quad \mathrm{Re}\,\underline{\underline{\epsilon}}_a = \rho\,\mathrm{Im}\,\underline{\underline{\epsilon}}_a \quad \Rightarrow \quad \theta_\epsilon^r = \theta_\epsilon^i\,, \quad \phi_\epsilon^r = \phi_\epsilon^i\,, \quad p_\epsilon^r = p_\epsilon^i\,, \quad q_\epsilon^r = q_\epsilon^i\,; \tag{25}$$

$$\mathrm{Re}\,\underline{\underline{\mu}}_b = \sigma\,\mathrm{Im}\,\underline{\underline{\mu}}_b\,, \quad \mathrm{Re}\,\underline{\underline{\mu}}_a = \sigma\,\mathrm{Im}\,\underline{\underline{\mu}}_a \quad \Rightarrow \quad \theta_\mu^r = \theta_\mu^i\,, \quad \phi_\mu^r = \phi_\mu^i\,, \tag{26}$$

where ρ and σ are proportionality scalars. Observe that the biaxial structure of the HCM is orthorhombic with respect to permittivity at $\delta = 1$ and orthorhombic with respect to permeability at $\delta = 0.5$. The biaxial HCM structure becomes orthorhombic with respect to permittivity when ratios of real and imaginary parts of $\underline{\underline{\epsilon}}_b$ and $\underline{\underline{\epsilon}}_a$ are equal. Furthermore, it is an especially symmetric form of biaxiality involving equalities between the scalar permittivities $p_\epsilon^{r,i}$ and $q_\epsilon^{r,i}$. An orthorhombic state with respect to permeability occurs when ratios of real and imaginary parts of $\underline{\underline{\mu}}_b$ and $\underline{\underline{\mu}}_a$ are equal; however, at this point $p_\mu^r \neq p_\mu^i$ and $q_\mu^r \neq q_\mu^i$. The graphs of p_μ^r and p_μ^i do intersect but not at $\delta = 0.5$ and not at the point where q_μ^r and q_μ^i intersect. The discrepancy between the dielectric orthorhombic state and the magnetic orthorhombic state arises from the fact that $\underline{\underline{\epsilon}}_a$ and $\underline{\underline{\epsilon}}_b$ are isomorphic up to a rotation of basis vectors in the xy plane, whereas $\underline{\underline{\mu}}_a$ and $\underline{\underline{\mu}}_b$ are not.

5. Bianisotropic properties

Finally, in this section we explore the conceptualization of biaxial bianisotropic mediums through the process of homogenization [21]. Biaxial bianisotropy is found to arise when (i) the component mediums undergoing homogenization present two noncollinear distinguished axes and (ii) the most basic form of magnetoelectric coupling in the form of isotropic chirality is present in at least one of the component mediums. For illustrative purpose, we consider here the case where directionality arises from the intrinsic electromagnetic properties of the component mediums.

Three constitutive dyadics are required to describe the reciprocal biaxial bianisotropic HCMs arising in this section: $\underline{\underline{\epsilon}}_{HCM}$ and $\underline{\underline{\mu}}_{HCM}$ as specified in (20) and (21), respectively, along with the analogous magnetoelectric dyadic

$$\underline{\underline{\xi}}_{HCM} = p_\xi^r \underline{\underline{I}} + q_\xi^r (\mathbf{u}_{m\xi}^r \mathbf{u}_{n\xi}^r + \mathbf{u}_{n\xi}^r \mathbf{u}_{m\xi}^r) + i \left[p_\xi^i \underline{\underline{I}} + q_\xi^i (\mathbf{u}_{m\xi}^i \mathbf{u}_{n\xi}^i + \mathbf{u}_{n\xi}^i \mathbf{u}_{m\xi}^i) \right]. \tag{27}$$

The associated real-valued unit vectors are specified as in (22) but with $c = \epsilon, \xi$ and μ. Observe that a total of 33 real-valued parameters is required to specify the general biaxial bianisotropic structure given by (20), (21) and (27); i.e., 12 parameters for each independent constitutive dyadic (2 each for p_c^χ and q_c^χ and 4 each for $\theta_{\kappa c}^\chi$ and $\phi_{\kappa c}^\chi$ where $\chi = r, i$; $\kappa = m, n$; $c = \epsilon, \xi, \mu$) less by 3 through the choice of coordinate frame. For the numerical studies described in Section 5.1, the choice of coordinate system is such that we consider only constituent mediums with distinguished axes lying in the xy

plane. Accordingly, the HCM unit vector pairs $\mathbf{u}_{m\tau}^{\chi}$ and $\mathbf{u}_{n\tau}^{\chi}$ always lie in planes perpendicular to the xy plane with the xy plane bisecting the angle between $\mathbf{u}_{m\tau}^{\chi}$ and $\mathbf{u}_{n\tau}^{\chi}$. Therefore, the identities (23) hold with $c = \epsilon, \xi$ and μ.

5.1. ELECTROMAGNETIC BIAXIALITY

We consider the homogenization of dissipative uniaxial bianisotropic mediums based on spherical topology. We take an inclusion medium specified by the relative constitutive dyadics $\underline{\underline{\epsilon}}_a = 2(1+i)\,\underline{\underline{Y}}_a$, $\underline{\underline{\xi}}_a = -\underline{\underline{\zeta}}_a = (1+i)\,\underline{\underline{Y}}_a$ and $\underline{\underline{\mu}}_a = 1.5(1+i)\,\underline{\underline{Y}}_a$; and a host medium given by $\underline{\underline{\epsilon}}_b = \underline{\underline{\xi}}_b = -\underline{\underline{\zeta}}_b = \underline{\underline{\mu}}_b = (1+i\delta)\,\underline{\underline{Y}}_b$ with $\lambda_b = 0$. The angle λ_a represents the angle by which the distinguished axes of the inclusion medium are rotated in the xy plane with respect to the host medium distinguished axes (the distinguished axes of each constitutive dyadic all being parallel for both component mediums). For the dissipation parameter $\delta = 2.5$, the corresponding HCM polar and azimuthal unit vector angles $\theta_{\epsilon,\xi,\mu}^{r,i}$ and $\phi_{\epsilon,\xi,\mu}^{r,i}$ and parameters $p_{\epsilon,\xi,\mu}^{r,i}$ and $q_{\epsilon,\xi,\mu}^{r,i}$ are displayed as functions of λ_a in Figure 7(a)–(d), respectively. When the distinguished axes of the uniaxial component mediums are aligned parallel or anti-parallel (i.e., $\lambda_a = 0$ or π), then we have $\theta_{\epsilon,\xi,\mu}^{r,i} = \phi_{\epsilon,\xi,\mu}^{r,i} = 0$ and the HCM acquires a uniaxial bianisotropic form. Also, when the distinguished axis of the host medium is perpendicular to that of the inclusion medium (i.e., $\lambda_a = \pi/2$), we see that $\phi_{\epsilon,\xi,\mu}^{r,i} = 0$ and a biaxial bianisotropic HCM structure which is orthorhombic with respect to all four of its constitutive dyadics emerges. In general, however, the computed biaxial HCM structure represented in Figure 7 is of the generalized monoclinic/triclinic type with angles $\theta_{\epsilon,\xi,\mu}^{r,i}$ and $\phi_{\epsilon,\xi,\mu}^{r,i}$, and scalars $p_{\epsilon,\xi,\mu}^{r,i}$ and $q_{\epsilon,\xi,\mu}^{r,i}$, all taking distinct values. This most general biaxial form arises in spite of the high degree of symmetry which is present between the various constitutive dyadics of the component mediums specified.

It was shown in Section 4 for biaxial dielectric–magnetic HCMs arising from uniaxial components that an orthorhombic HCM structure results when the ratios of the real and imaginary components of the host and inclusion medium constitutive dyadics are equal, despite the distinguished axes of the constituents being nonperpendicular. We investigate the generalization of this result to bianisotropic HCMs by repeating the homogenization of Figure 7 with the orientation angle λ_a fixed at 50° and allowing the dissipation parameter δ to vary. The resulting HCM constitutive parameters are plotted as functions of δ in Figure 8. At the point $\delta = 1$ we have $\mathrm{Re}\,\underline{\underline{c}}_\ell = \mathrm{Im}\,\underline{\underline{c}}_\ell$ $(\ell = a, b;\ c = \epsilon, \xi, \mu\ )$ and, from Figure 8(b), we observe $\phi_c^r = \phi_c^i$ $(c = \epsilon, \xi, \mu)$; i.e., the HCM is orthorhombic biaxial with respect to all four constitutive dyadics. We emphasize that this orthorhombic state

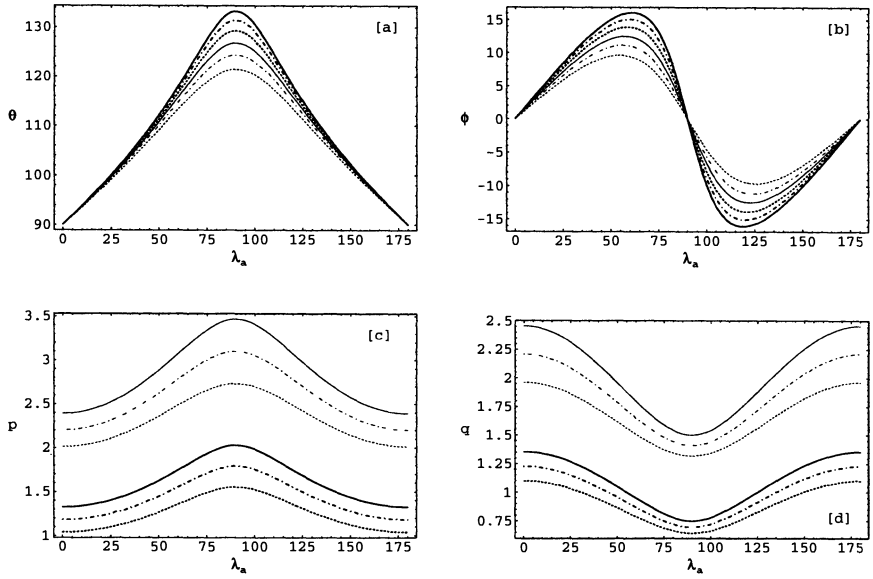

Figure 7. Uniaxial bianisotropic spherical inclusions homogenized with uniaxial bianisotropic spherical host medium. HCM unit vector (a) polar angles $\theta^{r,i}_{\epsilon,\xi,\mu}$ (degrees) and (b) azimuthal angles $\phi^{r,i}_{\epsilon,\xi,\mu}$ (degrees), and parameters (c) $p^{r,i}_{\epsilon,\xi,\mu}$ and (d) $q^{r,i}_{\epsilon,\xi,\mu}$ plotted against inclusion orientation angle λ_a. (Key in Table 1: $X = \theta$ for (a), $X = \phi$ for (b), $X = p$ for (c), $X = q$ for (d)). (Reproduced from [21]).

is *not* associated with perpendicularity of the distinguished axes in the component mediums (i.e., $\lambda_a \neq \pi/2$). An equivalent orthorhombic state does not arise in the case of the homogenization of Figure 7 since $\delta \neq 1$ in this instance. Furthermore, inspecting Figure 8(a), (b) and (c), we see that this is an especially symmetric orthorhombic state for which $\theta^r_c = \theta^i_c$, $p^r_c = p^i_c$, and $q^r_c = q^i_c$ $(c = \epsilon, \xi, \mu)$.

A significant difference between the biaxial bianisotropic HCM represented by Figure 8, and the analogous biaxial dielectric–magnetic HCM reported in Section 4.2 (see Figure 6), is that in the present example the orthorhombic structure does not emerge if the ratios of real and imaginary parts of only one of the component constitutive dyadic-types are equal. That is, for example, here we have

$$\mathrm{Re}\,\underline{\underline{\epsilon}}_b = \mathrm{Im}\,\underline{\underline{\epsilon}}_b\,, \qquad \mathrm{Re}\,\underline{\underline{\epsilon}}_a = \mathrm{Im}\,\underline{\underline{\epsilon}}_a \qquad \not\Rightarrow \qquad \phi^r_\epsilon = \phi^i_\epsilon\,, \tag{28}$$

in general.

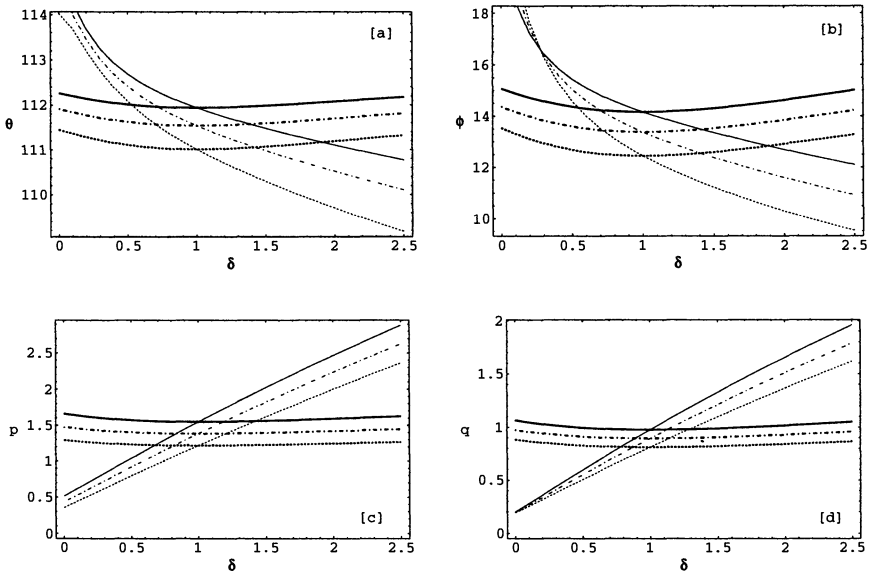

Figure 8. As for Figure 7 but with HCM constitutive parameters plotted against dissipation parameter δ. (Key in Table 1: $X = \theta$ for (a), $X = \phi$ for (b), $X = p$ for (c), $X = q$ for (d)). (Reproduced from [21]).

6. Concluding remarks

For dielectric mediums it is well established in Sections 3 and 4 that, through the process of homogenization, an effective medium biaxial with respect to permittivity arises provided the component mediums present two noncollinear distinguished axes. If the distinguished axes of the component mediums are perpendicular, or alternatively if the ratios of real and imaginary parts of the permittivity dyadics of the host and inclusion mediums are equal, then an orthorhombic biaxial structure results, for which the complex HCM permittivity dyadic can be diagonalized. Otherwise, the biaxial dielectric HCMs have a monoclinic/triclinic structure — a structure characterized as having a complex permittivity dyadic with principal axes of real and imaginary parts which do not coincide. The generalization of these results to the homogenization of dielectric–magnetic mediums gives rise to richer HCM structures in which orthorhombic dielectric and magnetic forms may be realized independently of one another. Generalizing further — through the introduction of magnetoelectric coupling — vastly increases the range and complexity of HCM structures which may be conceptualized from relatively simple component mediums. Even with the restriction to

reciprocal mediums, a generalized biaxial bianisotropic HCM form emerges which requires 33 real-valued parameters in order to completely specify its constitutive dyadics. With such a large parameter space, only illustrative examples giving insights into the structure and symmetries of the constitutive properties are practicably presented. A highly symmetric biaxial bianisotropic HCM, orthorhombic with respect to all of its constitutive dyadics, is achievable through balancing real and imaginary components of the component medium constitutive dyadics, even though the distinguished axes presented by constituents are not orthogonal.

Acknowledgment: For financial assistance towards attendance at the NATO Advanced Research Workshop, *Bianisotropics 2002*, Marrakech, Morroco, 2002: TGM thanks the *Centre for Materials Science and Engineering* (University of Edinburgh) and WSW thanks the Organizing Committee.

References

1. Born, M, and Wolf, E. (1997) *Principles of Optics*, Cambridge University Press, Cambridge, UK.
2. Nye, J.F. (1957) *Physical Properties of Crystals*, Cambridge University Press, Cambridge, UK.
3. Cottis, P.G. and Kondylis, G.D. (1995) Properties of the dyadic Green's function for an unbounded anisotropic medium, *IEEE Trans. Antennas Propagat.*, **43**, pp. 154–161.
4. Cottis, P.G., Vazouras, C.N. and Spyrou, C. (1999) Green's function for an unbounded biaxial medium in cylindrical coordinates, *IEEE Trans. Antennas Propagat.*, **47**, pp. 195–199.
5. Weiglhofer, W.S. and Lakhtakia, A. (1995) On singularities of dyadic Green functions and long–wavelength scattering, *Electromagnetics*, **15**, pp. 209–222.
6. Weiglhofer, W.S. (1998) Electromagnetic depolarization dyadics and elliptic integrals, *J. Phys. A: Math. Gen.*, **31**, pp. 7191–7196.
7. Weiglhofer, W.S. and Mackay, T.G. (2002) Needles and pillboxes in anisotropic mediums, *IEEE Trans. Antennas Propagat.*, **50**, pp. 85–86.
8. Abdulhalim, I. (1999) Analytic propagation matrix method for linear optics of arbitrary biaxial layered media, *J. Opt. A.: Pure Appl. Opt.*, **1**, pp. 646–53.
9. Lakhtakia, A., ed. (1996) *Selected Papers on Linear Optical Composite Materials*, SPIE Optical Engineering Press, Bellingham, WA.
10. Lakhtakia, A. (2000) On direct and indirect scattering approaches for homogenization of particulate composites, *Microw. Opt. Technol. Lett.*, **25**, pp. 53–56.
11. Weiglhofer, W.S. and Lakhtakia, A. (1998) The correct constitutive relations of chiroplasmas and chiroferrites, *Microw. Opt. Technol. Lett.*, **17**, pp. 405–408.
12. Weiglhofer, W.S., Lakhtakia, A. and Michel, B. (1998) On the constitutive parameters of a chiroferrite composite medium, *Microwave Opt. Technol. Lett.* **18**, pp. 342–345.
13. Weiglhofer, W.S. and Mackay, T.G. (2000) Numerical studies on the constitutive parameters of a chiroplasma composite medium, *Arch. Elektron. Übertrag.*, **54**, pp. 259–265.

14. Ward, L. (1980) *The Optical Constants of Bulk Materials and Films*, Adam Hilger, Bristol, UK.
15. Sihvola, A. (1999) *Electromagnetic Mixing Formulas and Applications*, The Institution of Electrical Engineers, London, UK.
16. Wiener, O. (1912) Die Theorie des Mischkörpers für das Feld der Stationären Strömung, *Abh. Math.-Phys. Kl. Sächs.*, **32**, pp. 507–604.
17. Sherwin, J.A., Lakhtakia, A. and Michel, B. (2000) Homogenization of similarly oriented, metallic, ellipsoidal inclusions using the Bruggeman formalism, *Opt. Comm.*, **178**, pp. 267–273.
18. Mackay, T.G., Lakhtakia, A. and Weiglhofer, W.S. (2001) Homogenisation of similarly oriented, metallic, ellipsoidal inclusions using the bilocal–approximated strong–property–fluctuation theory, *Opt. Comm.*, **197**, pp. 89–95.
19. Mackay, T.G. and Weiglhofer,W.S. (2001) Homogenization of biaxial composite materials: nondissipative dielectric properties, *Electromagnetics*, **21**, pp. 15–26.
20. Mackay, T.G. and Weiglhofer, W.S. (2000) Homogenization of biaxial composite materials: dissipative anisotropic properties, *J. Opt. A: Pure Appl. Opt.*, **2**, pp. 426–432.
21. Mackay, T.G. and Weiglhofer, W.S. (2001) Homogenization of biaxial composite materials: bianisotropic properties, *J. Opt. A: Pure Appl. Opt.*, **3**, pp. 45–52.
22. Weiglhofer, W.S. and Lakhtakia, A. (1999) On electromagnetic waves in biaxial bianisotropic media, *Electromagnetics*, **19**, pp. 351–362.
23. Chen, H.C. (1993) *Theory of Electromagnetic Waves*, TechBooks, Fairfax, VA.
24. Kong, J.A. (1986) *Electromagnetic Wave Theory* Wiley, New York.
25. Bohren, C.F. and Huffman, D.R. (1983) *Absorption and Scattering of Light by Small Particles*, Wiley, New York.
26. Ashcroft, N.W. and Mermin, N.D. (1976) *Solid State Physics*, Saunders College, Philadelphia, PA.
27. W.S. Weiglhofer, (1998) A perspective of bianisotropy and Bianisotropics'97, *Int. J. Appl. Electromag. Mech.*, **9**, pp. 93–101.
28. Weiglhofer, W.S. (2002) A flavour of constitutive relations: the linear regime, in Zouhdi, S., Sihvola, A., and Arsalane, M. (eds.), *Advances in Electromagnetics of Complex Media and Metamaterials*, Kluwer, Dordrecht, pp. 61–80.
29. Michel, B. (2000) Recent developments in the homogenization of linear bianisotropic composite materials, in Singh, O.N. and Lakhtakia, A. (eds.), *Electromagnetic Fields in Unconventional Structures*, Wiley, New York, pp. 39–82.
30. Weiglhofer, W.S., Lakhtakia, A. and Michel, B. (1997) Maxwell Garnett and Bruggeman formalisms for a particulate composite with bianisotropic host medium, *Microwave Opt. Technol. Lett.*, **15**, pp. 263–266; erratum (1999), **22**, p. 221.
31. Michel, B., Lakhtakia, A. Weiglhofer, W.S. and Mackay, T.G. (2001) Incremental and differential Maxwell Garnett formalisms for bi-anisotropic composites, *Compos. Sci. Technol.*, **61**, pp. 13–18.
32. Michel, B., Lakhtakia, A. and Weiglhofer, W.S. (1998) Homogenization of linear bianisotropic particulate composite media — Numerical studies, *Int. J. Appl. Electromag. Mech.*, **9**, pp. 167–78; erratum (1999), **10**, pp. 537–538.
33. Michel, B. and Weiglhofer, W.S. (1997) Pointwise singularity of dyadic Green function in a general bianisotropic medium, *Arch. Elektron. Übertrag.*, **51**, pp. 219–232; erratum (1998), **52**, p. 31.
34. Michel, B. (1997) A Fourier space approach to the pointwise singularity of an anisotropic dielectric medium, *Int. J. Appl. Electromag. Mech.*, **8**, pp. 219–227.

DISPERSION PROPERTIES OF STOP-BAND STRUCTURES FROM THIN METALLIC SPIRALS

CONSTANTIN R. SIMOVSKI
Physics Dept., St. Petersburg State Institute of Fine Mechanics and Optics
Sablinskaya, 14, 197101, St. Petersburg, Russia.
Temporary: Radio Lab., Helsinki University of Technology
P.O. Box 3000, FIN-02015, Espoo, Finland

Abstract. Novel photonic crystals for the microwave regime are under study: lattices from infinitely long spirals and lattices from canonical chiral particles. Many interesting dispersion properties are revealed, which make such structures prospective for technical applications: rejector and band frequency filtering including the high-selectivity filtering, polarization filtering and transformation, etc. Dispersion characteristics can be easily adjusted mechanically tuning the spiral step.

1. Introduction

Photonic crystals (PC) or photonic band gap (PBG) structures are extensively used nowadays for both fundamental research and applications in the optical range as well as at microwaves (see e.g. in [1], [2], etc.). The role of PC for optical science and engineering is very important, and the optical studies in this domain are more advanced. PBG structures in the microwave range (in this regime the name *stop-band structures* is more suitable) are widely applied in antenna systems with the aim to increase the antenna gain and improve the pattern. Stop-band structures (SBS) are also prospective at microwaves for frequency and polarization filtering and for the polarization transformations. Nevertheless, the applications of SBS in the microwave regime are in the present time more modest than the applications of PC in optics.

However, it is interesting to study SBS in the microwave regime where the analytical methods are possible to develop for them. In the optical range it is difficult to obtain high-contrast and lossless inclusions, and the PC for optical applications are usually prepared from dielectric inclusions or polymer molecules whose size is comparable with the wavelength λ in

S. Zouhdi et al. (eds.), Advances in Electromagnetics of Complex Media and Metamaterials, 229–244.

the background medium and with the lattice period. On the contrary, at microwaves, it is possible to consider metallic inclusions as perfectly electrically conducting (PEC) ones. The high contrast between the materials of the inclusion and the host (dielectric) matrix allows obtain lossless SBS even at frequencies where a characteristic size of the inclusion is small compared to λ. The inclusion smallness allows apply models of dipole-dipole interaction for lattices from electrically small PEC particles or small ferrite spheres [3, 4] and a model of line currents interaction for lattices of infinitely long metallic cylinders [5].

It is not surprising that the photonic crystals from spirals were first studied in the spectrum of visible light [7]. The purpose of the cited work was to protect the band-gap structure of a PC from the destruction due to the defects[1]. The spirals of the PC in [7] were closely packed polymer chain molecules whose spiral step and diameter were of the order of λ. Optical activity and other properties of conventional chiral media were not discovered in this work. Paper [7] gave a pulse to the present study of SBS from PEC spirals in the microwave range. Such the structure can be interesting for microwave applications. It it clear that the lossless[2] polarization filters and transformers can be obtained with them. Let us assume that in a SBS the eigenwaves have elliptic polarization as it must be in chiral structures. Let the eigenwave with right-handed polarization is allowed whereas a left-handed one is forbidden at the reference frequency. If a stochastically or linearly polarized electromagnetic wave illuminates a layer (thick enough, of course) of such the medium the left-handed polarized component will be completely (or almost completely) reflected whereas the right-handed one will be transmitted without losses. This novel feature and other similar features are studied and discussed in the present paper.

2. Objects of study and problem formulation

We study three kinds of a rectangular lattice: a chiral lattice of infinitely long spirals (shown in Fig. 1), a pseudo-chiral lattice of infinitely long spirals (shown in Fig. 2, on the bottom) and a lattice of canonical chiral particles (shown in Fig. 3). All the lattices are assumed to be PEC and prepared from thin wires. The first one is a doubly periodic lattice of identical parallel spirals. The lattice can be realized as a set of parallel grids of parallel spirals with the step d along the z-axis and the grid period b (see Fig. 1) .

The spiral step a and the radius r are assumed be small enough compared to the wavelength in free space. The spiral geometry is not helicoidal.

[1] The diamond-like PBG structures (for example the famous Yablonovite) are sensitive to the defects which can squeeze or even destroy their band-gap.

[2] The main principle of PC and SBS is the energy conservation (at least approximate).

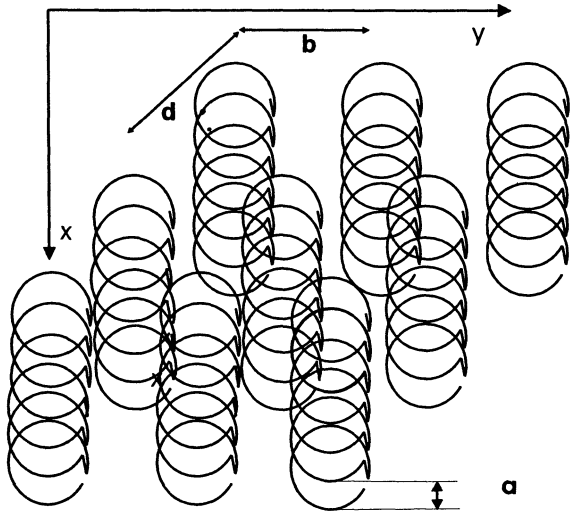

Figure 1. Chiral lattice from parallel spirals.

Spirals are formed by plane broken loops (the split width and the wire cross section radius ρ are much smaller than the loop radius r). Loops are connected by short straight wires as it is shown in Fig. 1. An analytical model of the reflection and transmission properties of a single-layer grid from such parallel spirals has been recently developed in [6]. Below we use the results from [6] and restrict our theory by the case of normal propagation: the eigenwave wave-vector β is directed along the $z-$axis (see Fig. 2). We consider the wave propagation in both chiral and pseudochiral structures as the propagation in a periodical quasi-stratified medium. In [8] it was indicated that two planar dyadics of reflection $\overline{\overline{R}}_+$ (the reflection from the left side of the single layer) and $\overline{\overline{R}}_-$ (the reflection from its right side) and two planar dyadics of transmission $\overline{\overline{T}}_+$ (the transmission from the left interface to the right one) and $\overline{\overline{T}}_-$ (the transmission from the right to the left) completely determine the propagation factor of the eigenwaves in a periodical structure of layers. These four dyadics also allow find the eigenpolarizations. So, the eigenwaves of the periodic structure of arbitrary layers (with never mind which inner structure of the layer) can be found through the reflection and transmission characteristics of a single layer in free space.

In this approximation we neglect the quasi-static interaction between the layers. However, it has been known since long ago that the quasi-static contribution into interaction of two parallel meshes is negligible compared to the contribution of their plane-wave interaction [9] under the condition

that the mesh period is not much larger than the distance d between two meshes. We assume that the same law is correct for the grids of spirals. Therefore, the approximation of wave interaction of parallel grids adopted in [8] is also adopted in the present paper. Correspondingly, in our studies the period b does not exceed d.

The model from [6] from which we take the explicit expression for all these dyadics uses the theory of loop antenna arrays. This model satisfies to the conditions of the energy conservation and reciprocity. The first of these conditions can be written as two independent equations

$$|R_{xx}|^2 + |T_{xx}|^2 + |R_{xy}|^2 + |T_{xy}|^2 = 1, \quad |R_{yy}|^2 + |T_{yy}|^2 + |R_{yx}|^2 + |T_{yx}|^2 = 1. \tag{1}$$

The reciprocity principle requires the symmetry of both of two reflection dyadics $\overline{\overline{R}}_{\pm} = \overline{\overline{R}}_{\pm}^{T}$, and relates two transmission ones $\overline{\overline{T}}_{+} = \overline{\overline{T}}_{-}^{T}$ (index T denotes a transposal dyadic).

Due to chirality two reflection coefficients of the grid from parallel spirals $\overline{\overline{R}}_{+}$ and $\overline{\overline{R}}_{-}$ are not the same and $\overline{\overline{T}}_{+}$ and $\overline{\overline{T}}_{-}$ are dyadics of general kind. Only the xx-components of $\overline{\overline{R}}_{+}$ and $\overline{\overline{R}}_{-}$ are the same [6]:

$$R_{\pm}^{xx} = -\frac{1}{1 + j\alpha + \chi^2 + \frac{2jbX_l}{a\eta}} \tag{2}$$

and $xy-$components have opposite signs

$$R_{+}^{xy} = \frac{\pm j\chi}{1 + j\alpha + \chi^2 + \frac{2jbX_l}{a\eta}} = -R_{-}^{xy}, \tag{3}$$

where sign plus corresponds to the right-handed spirals and minus corresponds to the left-handed ones. Here $\alpha = kb\log(b/2\pi\rho)/\pi$, $\chi = k\pi r^2/a$, $\eta = \sqrt{\mu_0/\epsilon_0}$. X_l denotes the loop input reactance (referred to its split) which is calculated taking into account the electromagnetic interaction of loops. The series representation for X_l we do not reproduce here is given in [6][3]. The $yy-$components of $\overline{\overline{R}}_{+}$ and $\overline{\overline{R}}_{-}$ also have opposite signs:

$$R_{\pm}^{yy} = \mp\frac{\chi^2}{1 + j\alpha + \chi^2 + \frac{2jbX_l}{a\eta}} \tag{4}$$

and also one has

$$T_{\pm}^{yy} = 1 - R_{\pm}^{yy}, \qquad T_{\pm}^{xx} = 1 + R_{\pm}^{xx}, \quad T_{\pm}^{xy} = R_{\pm}^{xy} = -T_{\pm}^{yx}.$$

All these coefficients are referred to the plane in which the spiral axes are located.

[3] The radiation resistances of loops and of straight wire pieces cancel out in the grid due to the regular arrangement of these elements.

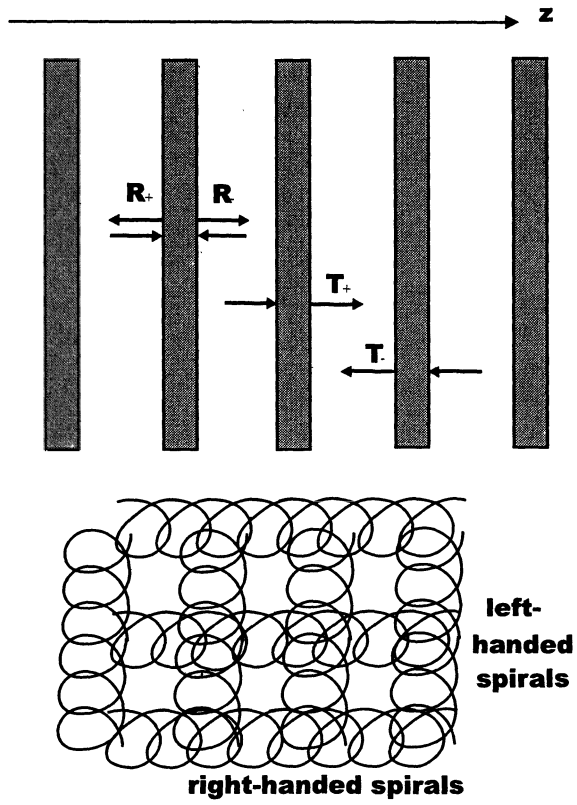

Figure 2. Pseudo-chiral grid from spirals with opposite handedness and propagation of eigenwaves in a layered structure

Now consider an infinite set of pseudo-chiral grids. Such the grid can be realized as two orthogonal arrays of parallel spirals: one array of right-handed spirals and one array of left-handed ones with the same parameters of spirals and same grid period b positioned in two parallel planes very closely. Of course, two mutually orthogonal spirals will interact with one another. However, in our model we do not take into account this interaction and consider the reflection and transmission coefficients of such a pseudo-chiral grid as a simple superposition of the corresponding coefficients of two chiral arrays (see Fig. 2). Though this model is not strict it is much simpler than the chiral SBS and it is useful to start with its study. Reflection coefficients $\overline{\overline{R}}_+$ and $\overline{\overline{R}}_-$ turns out to be equal and also $\overline{\overline{T}}_+ = \overline{\overline{T}}_-$. Elementary consideration allows express components of $\overline{\overline{R}}$ and $\overline{\overline{T}}$ of a pseudochiral grid

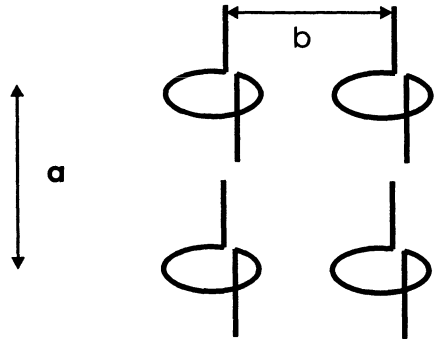

Figure 3. Chiral grid from canonical chiral particles

through $\overline{\overline{R}}$ and $\overline{\overline{T}}$ of a chiral one:

$$R^{xx}_{\text{pseudo}} = R^{yy}_{\text{pseudo}} = R^{xx}_{+} - R^{yy}_{+}, \quad R^{xy}_{\text{pseudo}} = R^{yx}_{\text{pseudo}} = 2R^{xy}_{+} \tag{5}$$

and

$$T^{xx}_{\text{pseudo}} = T^{yy}_{\text{pseudo}} = 1 + R^{xx}_{+} + R^{yy}_{+}, \quad T^{xy}_{\text{pseudo}} = T^{yx}_{\text{pseudo}} = 0. \tag{6}$$

No rotation of the polarization plane occurs in the transmitted wave. In the reflected wave the polarization rotates. However, when vectors $-E$ and $\mathbf{H}$ of the incident wave make the angle 45° with the spiral axes no polarization occurs also in the reflected wave. In the coordinates $OX'Y'$ turned by $\pi/4$ with respect to the $OXY-$system the reflection dyadic is also diagonal: $R^{x'x'}_{\text{pseudo}} = R^{y'y'}_{\text{pseudo}} = R_1 - jR_2$, where

$$R_1 = \frac{\chi^2 - 1}{1 + j\alpha + \chi^2 + \frac{2jbX_l}{a\eta}}, \quad R_2 = \frac{2\chi}{1 + j\alpha + \chi^2 + \frac{2jbX_l}{a\eta}}, \tag{7}$$

Relations (7) satisfy the energy conservation conditions as well as (5) and (6).

We also study below an infinite set of rectangular arrays of finite spirals whose length (and diameter) is small compared to λ. General formulas we obtain for this case keep valid for arbitrary shape of such spirals, however the numerical examples correspond to the so-called canonical chiral particles, widely studied in the theory of chiral composites, e.g. in [10]. A grid from such particles is shown in Fig. 3.

3. Pseudo-chiral SBS

In this case the dispersion equation takes the classical form of that of a periodically loaded transmission line [11]:

$$\cos \beta d = \cos kd + \frac{j}{2Z} \sin kd, \tag{8}$$

where Z is the sheet impedance of a single pseudo-chiral mesh referred to its central plane and normalized to the impedance of the free space η. Relating Z with the reflection and transmission coefficients as Eq. (9) from [8] allows one can then express Z through the parameters of a spiral:

$$Z = j \frac{X_l/\eta + \alpha}{1 + \chi^2}.$$

Eigenwaves in this case have linear polarization and the polarization plane makes the angle 45° with the axes of spirals.

In Fig. 4 we present an example of a dispersion plot of the pseudo-chiral SBS, where the frequency of eigenwave is given in GHz and the propagation factor (horizontal axis) is normalized (multiplied by d/π). The geometrical parameters of the structure are following: $\rho = 0.2$ mm, $r = 1.5$ mm, $a = 4$ mm, $b = d = 8$ mm. The first pass-band corresponds to the resonance of Z which is the parallel-circuit one. The straight line is the dispersion plot of free space, and the crossing of the lower dispersion branch with this line indicates the resonance of Z when the currents in spirals are exactly equal to zero.

The second dispersion branch practically repeats that of a lattice of straight wires (when $r = 0$ and the other parameters are the same). This fact reflects a common law for pseudo-chiral and chiral lattices from long spirals: the presence of loops influences only to the frequency region around the resonance of the sheet impedance. In practical cases this band is $0 < \omega \leq \omega_1$, where $\omega_1 = \pi c/d$. Dispersion plot in the high-frequency regions does not differ from the plot of a conventional wire medium.

In the example illustrated by Fig. 4 the effective inductance L per unit length of a spiral is high due to the mutual coupling of loops. By varying the spiral step one can tune the shape of the first dispersion branch so that it repeats the second one, and one obtains two identical dispersions in two different frequency bands.

If one increases a the resonance pass-band becomes narrower. In Fig. 5 the case $\rho = 0.2$ mm, $r = 1.5$ mm, $a = 50$ mm, $b = d = 5$ mm is presented, when the relative width of the mini-band is 2%. If $a > 50$ mm the mini-band stops to shrink since the inductance L attains its minimum (the self-inductance of a single loop).

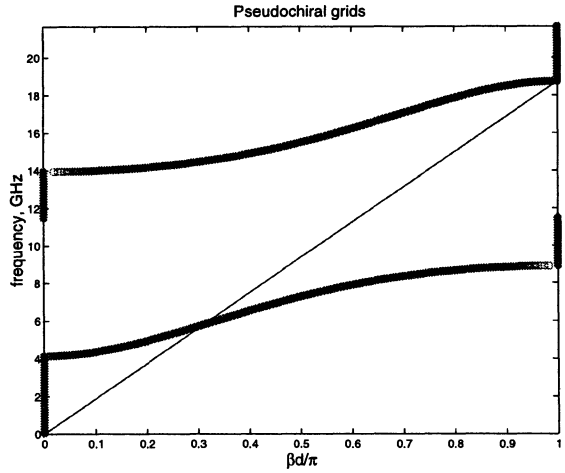

Figure 4. Dispersion plot for normal propagation through a pseudo-chiral lattice with parameters of a spiral $\rho = 0.2$ mm, $r = 1.5$ mm, $a = 4$ mm, $b = d = 8$ mm.

One also can reveal interesting effects when decreasing the spiral step. The case $\rho = 0.2$ mm, $r = 1.5$ mm, $a = 0.5$ mm, $b = d = 5$ mm is illustrated by Fig. 6. The inductance L here is very high (and is close to that of a perfect solenoid) and the capacitance between adjacent loops is also very high. As a result, the resonant frequency attains the value 51 MHz. At this frequency the lattice periods are smaller than $10^{-3}\lambda$. It is known, that the surface of the half-space filled by SBS of arbitrary kind behaves as a magnetic wall at the upper edge of the low-frequency stop-band. In our case this upper edge is 51 MHz. Positioning the lattice of finite thickness over the ground plane we can expect that at the frequencies between $40 - 50$ MHz (near the edge of lower stop-band) the reflection properties of the whole structure will be close to those of a half-space if the lattice contains, for example, $10 - 20$ periods. Therefore, the reflection coefficient must be close to $+1$ at these frequencies. However, the thickness of the structure is of the order $\lambda/100$. This is an exciting result[4]. Another interesting feature of the same plot is the very narrow mini-band at 30 GHz. In the case under consideration the magnetic currents in the loops dominate in the range $0 - 30$ GHz, and it leads to the dramatic transformation of the second ("wire-medium") dispersion branch. Within the band $25 - 30$ GHz the reflection coefficient of a single grid is close to -1. One can conclude that this dispersion branch corresponds to the Fabry-Pérot resonance. In

[4] For comparison: the usual thickness of a structure modelling the magnetic wall over the ground plane is $\lambda/4$.

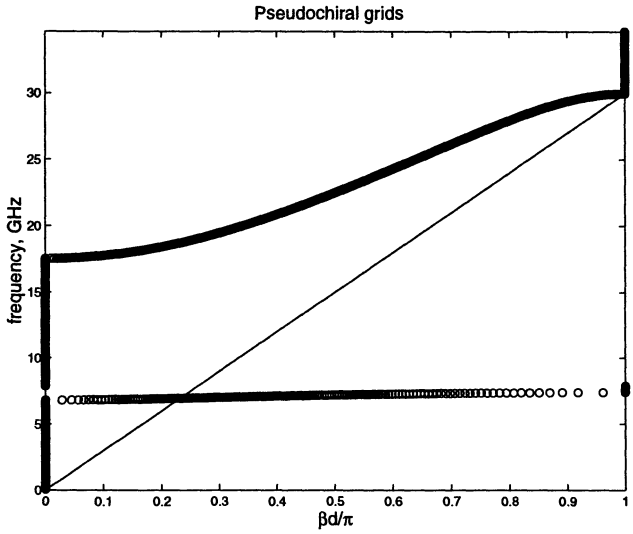

Figure 5. Dispersion plot for normal propagation through a pseudo-chiral lattice with parameters of a spiral $\rho = 0.2$ mm, $r = 1.5$ mm, $a = 50$ mm, $b = d = 5$ mm.

this way one can obtain the very high selectivity of the frequency filtering. The case from Fig. 6 corresponds to the relative bandwidth of transmission 0.0012.

4. SBS from small chiral particles

In order to understand better the behavior of chiral SBS from infinite spirals let us first consider the lattices from small uniaxial chiral particles. Let the particles be identical and oriented in parallel along the y-axis. Periods in the plane $(x - y)$ are $a \times b$ as it is shown in Fig. 3. Then any reference particle has electric and magnetic dipole moments $\mathbf{p} = p\mathbf{y}_0$ and $\mathbf{m} = m\mathbf{y}_0$. These can be expressed through the y-component of the local field:

$$p = a_{ee}E_y^{\mathrm{loc}} + a_{em}H_y^{\mathrm{loc}}, \tag{9}$$

$$m = a_{me}E_y^{\mathrm{loc}} + a_{mm}\mathbf{H}_y^{\mathrm{loc}}. \tag{10}$$

Local field is that produced by all other particles but the reference one at the phase center of the reference particle. Electric dipoles in the chosen geometry of the lattice do not contribute into H_y^{loc} and magnetic dipoles do not contribute into E_y^{loc}. Then the local field can be expressed through the known interaction factor C of the rectangular dipole lattice that has

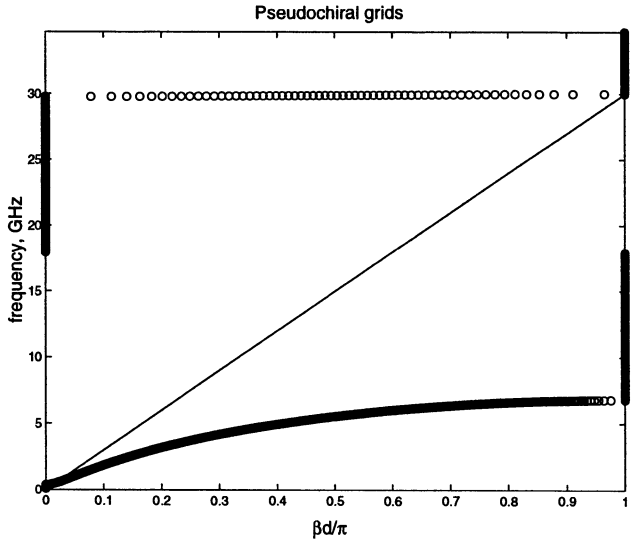

Figure 6. Dispersion plot for normal propagation through a pseudo-chiral lattice with parameters of a spiral $\rho = 0.2$ mm, $r = 1.5$ mm, $a = 0.5$ mm, $b = d = 5$ mm.

been calculated in [3]:

$$E_y^{\text{loc}} = Cp, \qquad H_y^{\text{loc}} = \frac{Cm}{\eta^2}, \tag{11}$$

where

$$C = \alpha + j\frac{k^3}{6\pi\epsilon_0} + \frac{\eta\omega}{2ab}\frac{\sin kd}{\cos kd - \cos \beta d}. \tag{12}$$

Here α is a real value, which can be evaluated explicitly as a series sum [4]. For this parameter a good closed-form approximation has been obtained for the case $a = b$ in [3]

$$\alpha = \frac{\eta\omega}{4a^2}\left[\frac{\cos\left(\frac{ka}{1.438}\right)}{\left(\frac{ka}{1.438}\right)} - \sin\left(\frac{ka}{1.438}\right)\right].$$

Substituting (11) into (9),(10) and taking into account an important identity derived for chiral particles in [10]

$$a_{ee}a_{mm} = a_{em}a_{me} = -a_{em}^2, \tag{13}$$

we obtain the dispersion equation in a form

$$1 - C\left(a_{ee} + \frac{a_{mm}}{\eta^2}\right) = 0.$$

Substituting (12) into this equation and taking into account another important relation [12]:

$$\mathrm{Im}\left(\frac{1}{a_{ee}+\frac{a_{mm}}{\eta^2}}\right)=\frac{k^3}{6\pi\epsilon_0},$$

we obtain the following dispersion equation in form

$$\cos\beta d=\cos kd+\frac{1}{2\gamma}\sin kd. \tag{14}$$

Here we have denoted

$$\gamma=4ab\frac{\mathrm{Re}\left(\frac{1}{a_{ee}+\frac{a_{mm}}{\eta^2}}\right)-\alpha}{\eta\omega}.$$

Equation (14) is again a classical form of dispersion equation, and it looks like strange for chiral lattices. It is well-known that uniaxial chiral media possess two elliptically polarized eigenwaves with different propagation factors [13], and there is no physical reason for the mode degeneration appearing in our case. At low frequencies our model must match with the theory of a continuous chiral medium. Let us consider the predictions of this theory.

The constitutive equations for a reciprocal uniaxial chiral medium are given by [13]:

$$\mathbf{D} = \epsilon_0\bar{\bar{\epsilon}}\cdot\mathbf{E}+j\sqrt{\epsilon_0\mu_0}\bar{\bar{\xi}}\cdot\mathbf{H}, \tag{15}$$

$$\mathbf{B} = \mu_0\bar{\bar{\mu}}\cdot\mathbf{H}-j\sqrt{\epsilon_0\mu_0}\bar{\bar{\xi}}\cdot\mathbf{E}. \tag{16}$$

If the host matrix is free space the material parameters are following dyadics $\bar{\bar{\epsilon}}=\mathbf{x}_0\mathbf{x}_0+\mathbf{z}_0\mathbf{z}_0+\epsilon_y\mathbf{y}_0\mathbf{y}_0$, $\bar{\bar{\mu}}=\mathbf{x}_0\mathbf{x}_0+\mathbf{z}_0\mathbf{z}_0+\mu_y\mathbf{y}_0\mathbf{y}_0$ and $\bar{\bar{\xi}}=\mathbf{x}_0\mathbf{x}_0+\mathbf{z}_0\mathbf{z}_0+\xi_y\mathbf{y}_0\mathbf{y}_0$, where for lossless case ϵ_y,μ_y and ξ_y are real values. The Maxwell Garnett model has been developed for this medium in [14]. It allows express ϵ_y,μ_y and ξ_y through individual particle polarizabilities and particles concentration N:

$$\epsilon_y=1+\frac{Na_{ee}-3N^2\epsilon_0F}{\epsilon_0D},\qquad \mu_y=1+\frac{Na_{mm}-3N^2\mu_0F}{\mu_0D},$$

$$\xi_y=\pm\frac{N|a_{em}|}{\sqrt{\epsilon_0\mu_0}D}. \tag{17}$$

In the last equation signs + and − correspond to right and left helices, respectively. In (17) we have denoted

$$D=1-\frac{N}{3}\left(\frac{a_{ee}}{\epsilon_0}+\frac{a_{mm}}{\mu_0}\right)+N^2F,\quad F=\frac{1}{9}\frac{a_{ee}a_{mm}-a_{em}a_{me}}{\epsilon_0\mu_0}.$$

Relation (13) means that $F = 0$ that simplifies (17).

In [13] it was shown that the propagation factor of both eigenwaves in uniaxial chiral medium is determined by two parameters $A_{\pm}$:

$$A_{\pm} = \frac{1}{2} \pm \sqrt{\frac{1}{4}(\mu_z - \epsilon_z)^2 - \xi^2} \tag{18}$$

The same parameters determine also the axial admittance and the ellipse of polarization of eigenwaves. For eigenwaves propagating along the z-axis one has from [13]

$$Y_{\pm}^{\text{axial}} = \frac{H_{y\pm}}{E_{y\pm}} = \frac{j\xi}{\eta}(A_{\pm} - \epsilon_y), \tag{19}$$

$$\mathbf{E}_{\pm} = G\left[\sqrt{A_{\pm}}(A_{\pm} - \epsilon_y)\mathbf{x}_0 + jP\mathbf{y}_0)\right], \tag{20}$$

where G is an arbitrary scalar value and $P = \xi_y$. From (17) one has $P = |\xi_y|$ or $P = -|\xi_y|$ for right-handed or left-handed chiral media, respectively. Now let us prove that one of the eigenwaves has the propagation factor which equals simply to the free space wave-number k, and this is the wave of left-polarization for the case of right-handed spirals (and vice versa).

Substituting relations (17) into (18) we easily obtain $A_- = 1$ that proves the first assertion. From (20) we have

$$\mathbf{E}_- \sim (E_x^- \mathbf{x}_0 + jE_y^- \mathbf{y}_0),$$

where $E_x^- = (1 - \epsilon_y) < 0$ and $E_y^- = |\xi| > 0$ that proves the second assertion. For the other eigenwave one has

$$\mathbf{E}_+ \sim (E_x^+ \mathbf{x}_0 + jE_y^+ \mathbf{y}_0),$$

where $E_x^- = \sqrt{\epsilon_y + \mu_y - 1}(\mu_y - 1) > 0$ and $E_y^+ = |\xi| > 0$, so, its polarization is right-handed. This eigenwave interacts with the right-handed chiral particles, whereas the left-handed eigenwave does not. The strange absence of interaction can be explained in the following way: the particle polarization by local field consists of two parts: that due to E_y^{loc} and that due to H_y^{loc}. For eigenwave with left-handed polarization the phase relations between E_y^{loc} and H_y^{loc} are so that these two parts cancel out. To prove it mathematically one can use the Clausius-Mossotti equations to find the relation between local electric and magnetic fields:

$$Z_{\text{loc}}^- = \frac{E_{y-}^{\text{loc}}}{H_{y-}^{\text{loc}}} = \frac{E_{y-} + \frac{P_{y-}}{3\epsilon_0}}{H_{y-} + \frac{M_{y-}}{3\mu_0}}, \tag{21}$$

together with the substitutions

$$P_{y-} = (\epsilon_y - 1)E_{y-} + j\xi_y H_{y-}, \qquad M_{y-} = (\mu_y - 1)H_{y-} - j\xi_y E_{y-}.$$

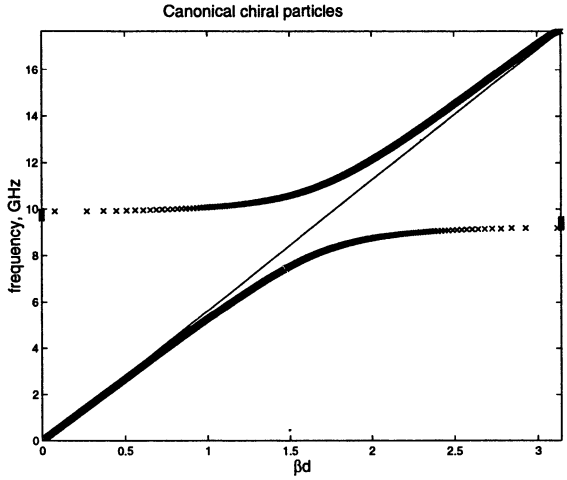

Figure 7. Dispersion plot for normal propagation through a chiral lattice from small particles. Case $l = 2r = 2$ mm, $\rho = 0.2$ mm, $a = b = d = 6$ mm.

Then one can substitute (19) into (21) (taking into account that $A_- = 1$) and check that two expressions in prances in both equations (following from (9) and (10))

$$p = \left(a_{ee} Z_{\text{loc}}^- + a_{em}\right) H_y^{\text{loc}}, \tag{22}$$

$$m = \left(-a_{em} Z_{\text{loc}}^- + a_{mm}\right) H_y^{\text{loc}} \tag{23}$$

are identical zeros. So the particles are not excited by this wave in a continuous chiral medium. The same situation is hold for chiral lattices.

In our numerical examples we used the model of a canonical chiral particle developed in [10], which can be approximately considered as a uniaxial particle if the length of an arm l exceeds the radius of a loop r. We have found that the influence of chiral lattice from small particles depends on the relation between the edge of the first pass-band $\omega_1 = c\pi/d$ and the frequency of particle resonance ω_0. If $\omega_0 < \omega_1$ as in Fig. 7 (main particle parameters are $l = 2r = 2$ mm, $\rho = 0.2$ mm, lattice parameters are $a = b = d = 6$ mm) one obtains a narrow stop-band at low frequencies, and the lattice behaves as a rejecting filter. If $\omega_0 > \omega_1$ as in Fig. 8 (main particle parameters are $l = 2r = 1$ mm, $\rho = 0.1$ mm, lattice parameters are $a = b = 4$ mm, $d = 12$ mm) one obtains a very narrow mini-band within the stop-band, when the lattice behaves as a high-quality transmitting filter. The mini-band belongs to the resonant band of particles and corresponds to the Fabry-Pérot resonance.

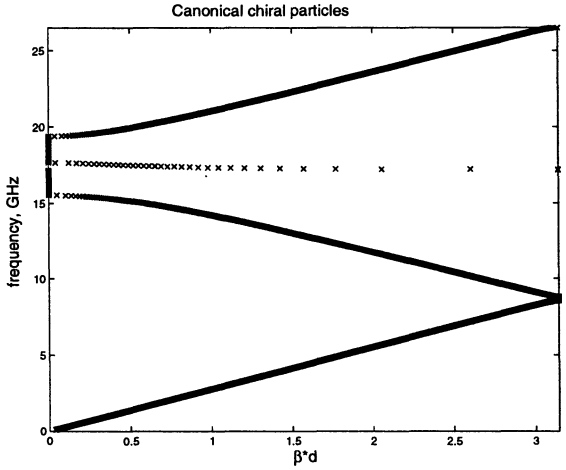

Figure 8. Dispersion plot for normal propagation through a chiral lattice from small particles. Case $l = 2r = 1$ mm, $\rho = 0.1$ mm, $d = 2a = 2b = 12$ mm.

5. Chiral SBS from infinite spirals

Let us now discuss the results obtained for chiral lattices of long spirals (see Fig. 1). In this case the theory from [8] gives two following equations for two coupled modes (notations $\mathbf{A}_{\pm}$ refer to the complex amplitudes of modes with forward and backward propagation, respectively):

$$\left(\overline{\overline{I}} - \overline{\overline{T}}_{-} e^{-j(k-\beta)d}\right) \cdot \mathbf{A}_{+} - e^{-jkd} \overline{\overline{R}}_{+} \cdot \mathbf{A}_{-} = 0, \tag{24}$$

$$\left(\overline{\overline{I}} - \overline{\overline{T}}_{+} e^{-j(k+\beta)d}\right) \cdot \mathbf{A}_{-} - e^{-jkd} \overline{\overline{R}}_{-} \cdot \mathbf{A}_{+} = 0 \tag{25}$$

Equating the determinant of the system (24)-(25) (which is a set of four scalar equations) to zero we obtain a complex dispersion equation. Its solution allows find the eigenpolarizations taking into account that $\mathbf{A}_{+} \to \mathbf{A}_{-}$ when the sign of β is inverted.

The dispersion equation at each frequency has two different roots. It is not surprising that one of them turns out to be trivial $\beta = k$ at every frequency. Corresponding eigenpolarization is the left-handed elliptical one for right-handed spirals, the wave does not interact with the lattice. Another root turns out to be equal to the root of the dispersion equation (8) obtained for a pseudo-chiral lattice. Now, the frequency selectivity revealed in pseudo-chiral lattices is combined with the polarization selectivity, and the polarization filter-transformer mentioned above can be fulfilled in the needed frequency bands. Note, that the lattice from small chiral particles allows realize such the polarization transformation, too. However, the struc-

ture with long spirals is preferable (the resonance of a small chiral particle is a series resonance and corresponds to the high level of resistive losses which are negligible in long spirals from copper or silver). The part of the incident wave field which corresponds to the eigenwave with no interaction will, probably pass through the lattice of small spirals without losses. However, the other part which corresponds to the interacting wave will be reflected with big losses. Meanwhile, the stop-band in the medium from long spirals is the usual low-frequency stop-band of wire media, when the currents in the wires are not very high, and the losses should be insignificant. This structure is more adequate to a lossless photonic crystal. When the radius of the spiral is getting small (practically, smaller than ρ) the dispersion plot of a chiral lattice transits into corresponding plot for a wire medium at all frequencies. The eigenpolarizations degenerate in this case into linear ones: the right-handed transforms to the $x-$polarization (parallel to the wires), and the left-handed transits to the $y-$polarization (orthogonal to the wires).

6. Conclusion

In the present paper one has developed explicit analytical models for lattices from pseudo-chiral grids and small chiral particles and also a semi-analytical model for a lattice from grids of parallel spirals. As a conclusion one can simply list the main properties of these structures:

- In uniaxial chiral lattices from infinitely long and from very short perfectly conducting spirals one eigenmode propagates as in free space. If the spirals are right-handed the polarization of this mode is left-handed and vice versa;
- Dispersion of another (interacting) eigenmode in chiral lattice from infinitely long spirals does not differ from dispersion of an eigenwave in the corresponding pseudo-chiral lattice;
- Filtering with extremely narrow frequency band is possible due to Fabry-Pérot resonance which can be obtained in all the structures considered above;
- The interface of a lattice from infinite spirals whose step is small with respect to its radius behaves as a magnetic wall at very low frequencies (lattice period is $100 - 1000$ times smaller than the wavelength in free space);
- If the plane wave illuminates the interfaces of a chiral lattice, and the frequency belongs to the stop-band of the interacting mode, the incident wave splits onto two parts with different elliptic polarizations. The component left-handed polarization (in the case of right-handed

spirals) propagates in the lattice without losses, whereas the right-handed one is totally reflected.
- The structures from infinite spirals are very sensitive to small deviations of the spiral step. It allows to control their dispersion properties mechanically (pulling and squeezing the spirals).

7. Acknowledgement

This work has been supported by Nokia Fellowship grant. Author is grateful also to S.L. Prosvirnin for a fruitful discussion.

References

1. Joannopoulos, J., Mead, R. and Winn, J. (1995) *Photonic Crystals*, Princeton Univ., Princeton.
2. Soukoulis, C. (ed.), (1996) *Photonic Band Gap Materials*, Kluwer Academy Publisher, Dordrecht.
3. Tretyakov, S.A. and Viitanen, A.J. (2000) Plane waves in regular arrays of dipole scatterers and effective medium modelling, *J. Opt. Soc. Am.*, A **17**, pp. 1791-1799.
4. Belov, P.A., Tretyakov,S.A., and Viitanen, A.J. (2002) Non-reciprocal microwave band-gap structures, *Phys. Rev.*, E, in print.
5. Belov, P.A. , Tretyakov, S.A. and Viitanen, A.J. (2002) Dispersion and reflection properties of artificial media formed by regular lattices of ideally conducting wires, *J. of Electromagn. Waves and Applic.*, in print.
6. Yatsenko V.V. and Tretyakov, S.A. (1998) Reflection of electromagnetic waves from dense arrays of thin long spirals, *Int. J. of Applied Electromagn. and Mechanics*, **9**, No 2, 191-200.
7. Toader, O. , John, S. (2001) Proposed square spiral microfabrication architecture for large 3D photonic band gap crystals, *Science,* **292**, May 11, pp. 1484-1492.
8. Prosvirnin, S.L. and Vasilyeva, T.D. (2000) Eigen waves of periodic layered structure of complex arrays, in *Proc. Bianisotropics'2000*, 8-th Int. Conf. on Electromagn. Complex Media, Lisbon, Portugal, Sept., pp. 283-287.
9. Kontorovich, M.I., Akimov, V. P., Astrakhan, M.I., and Fersman, G.A. (1983) *Electrodynamics of mesh structures*, Moscow, Radio i Sviaz (in Russian).
10. Tretyakov, S.A., Mariotte, F., Simovski, C.R., Kharina T.G. and Héliot J.-Ph. (1996) Analytical antenna model of small chiral scatterers: comparison with numerical and experimental data, *IEEE Trans. Antennas Prop.*, **AP-44**, No 7, pp.1006-1015.
11. Collin, R.E. (2001) *Foundations of microwave engineering*, IEEE Press, NY.
12. Tretyakov, S.A. and Viitanen, A.J. (2000) Electromagnetic properties of periodical arrays with small non-reciprocal inclusions, *J. Electromagn. Waves Applic.*, **14**, No 8, pp. 1159-1177.
13. Lindell, I.V., Sihvola, A.H., Tretyakov,S.A. and Viitanen, A.J. (1994) *Electromagnetic waves in chiral and bi-isotropic media*, Artech House, London.
14. Tretyakov, S.A. and Mariotte, F. (1995) Maxwell Garnett modelling of uniaxial chiral composites with bianisotropic inclusions, *J. of Electromagn. Waves and Applic.*, **9**, No 7/8, pp. 1011-1025.

V.

ADVANCED COMPUTATIONAL METHODS FOR ELECTROMAGNETIC WAVES INTERACTION WITH METAMATERIALS

EFFECTIVE ELECTRON MODEL OF THE WIRE HELIX EXCITATION AT MICROWAVES: FIRST STEP TO OPTIMIZATION OF PITCH ANGLE OF HELIX

I.V. SEMCHENKO, S.A. KHAKHOMOV,
and E.A. FEDOSENKO
Department of General Physics, Gomel State University
Sovyetskaya Str. 104, 246019, Gomel, Belarus

Abstract. A possibility to use the helical model of molecules for the description of interaction of electromagnetic waves with the artificial chiral media is shown. An analytical model, allowing to calculate electric dipole moment and magnetic moment, induced in the helix under the action of the incident electromagnetic wave, is formed. On the base of present model the evaluation of effective parameter of magneto-electric coupling for single helix is performed. The optimal pitch angle of loops of helix elements of artificial composite media is calculated, which ensures the maximum values of average chirality parameter. It is shown, that optimal pitch angle strongly depends on the number of loops of helix. For example, if the helix consists of a few loops, the optimal pitch angle is close to 2-5 degrees with respect to plane which is perpendicular to axis of helix.

1. Introduction

At present time various methods for description of interaction of electromagnetic waves with artificial chiral media are used. One of the primary tasks is to calculate the effective parameters of artificial composite structure, taking into account electric and magnetic properties of host media and chiral properties of metallic helical inclusions.

The first possible method is based on using of the integral equations of electromagnetics. This method allows to calculate distribution of current in the single helix and to find the radiated fields [1]-[4]. Advantage of this method is accuracy, however this method is sufficiently complex even in the case of the single helix. It is necessary to take into account that in artificial chiral media the helix concentration of about $70/\text{cm}^3$ is achieved [5]. To use the method of integral equations in this case is much difficult.

Second possible method is based on using of mathematical model, according to which the metallic helix can be considered as a combination

S. Zouhdi et al. (eds.), Advances in Electromagnetics of Complex Media and Metamaterials, 245–256.

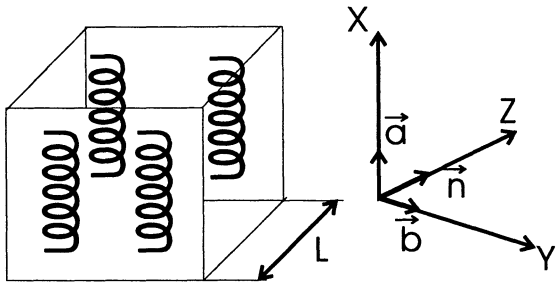

Figure 1. Orientation of axes of microhelices in anisotropic chiral media.

of the rectilinear conductor and flat round loop (so called "wire and loop model") [3, 4, 6]. The approximate calculation of components of a polarizability tensor of single helix in electric and magnetic fields of incident wave are possible. After an averaging procedure in the volume we can determine the effective parameters of artificial chiral media. Defect of this method is not taking into account a pitch angle of the helix (or angle of winding of loops), because the helix is considered as a flat loops.

In our paper a possibility to use the helical model of molecules [7] for the description of interaction of electromagnetic waves with the artificial chiral media is shown. An analytical model, allowing to calculate electric dipole moment and magnetic moment, induced in the helix under the action of the incident electromagnetic wave, is formed. On the base of present model the evaluation of effective parameter of magneto-electric coupling for single helix is performed. The optimal pitch angle of loops of helix elements of artificial composite media is calculated, which ensures the maximum values of average chirality parameter. It is shown, that optimal pitch angle strongly depends on the number of loops of helix. For example, if the helix consists of a few loops, the optimal pitch angle is close to 2-5 degrees with respect to plane which is perpendicular to axis of helix.

The obtained optimal pitch angle of helix has been compared with same parameter of helices which were used in experimens in Technical University of Braunschweig, Germany [10] and University of Stellenbosch, South Africa [5].

2. Theory

Methods to design and manufacture artificial chiral media with uniaxial structure were recently described in [5]. It was proposed to wind thin wires around Nylon threads, to align these microhelices and then to cast them into epoxy resin. In this case the permittivity and chirality of the effective

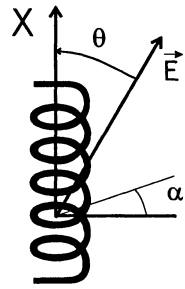

Figure 2. Orientation of **E** vector relatively to axis of microhelix.

medium are characterized by uniaxial tensors, the axis of which is oriented along the direction of the parallel Nylon threads (see Fig.1).

The electomagnetic field of incident wave influences on electrons of metallic helices. The electric dipole moments which caused by magnetic field and magnetic dipole moments which caused by electric field can be explained by classical electron theory and helical model of molecules [7]. The equation of electron motion in this case has the form:

$$m\dot{v} = -ks + \gamma\ddot{v} - eE\cos\theta\sin\alpha \tag{1}$$

where s is displacement of electron along helix, $v = \dot{s}$ is velosity of electron along helix, m is electron mass, e is elementary electrical charge, k is effective coefficient describing a quasi-elastic force which effects on electrons in the opposite direction of their displacement,

$$\gamma = \frac{e^2}{6\pi\varepsilon_0 c^3} \tag{2}$$

is coefficient characterising the dissipative forces caused by radiation of helix (radiation losses), ε_0 is electric constant, c is speed of light in vacuum. Here we consider the helix as perfectly conducting chiral particle and the dissipative force is mainly due to radiation losses.[1]

The angle between a vector **E** of electric field of wave and axis of helix is θ (see Fig.2). Therefore the component of electric field along helix element in any it's point is equal to

$$E_s = E\cos\theta\sin\alpha, \tag{3}$$

[1] In [8] the Lorentz electron theory has been modified and term $f_{dis} = \gamma\ddot{v}$ for dissipative force has been introduced instead of term $f_{dis} = -\gamma_1 v$ with other effective coefficient γ_1. The basic condition which the polarizabilities of all bi-anisotropic particles must satisfy to has been obtained in the work [9]. This condition implies the lossy term in the Landau form, too.

where α is angle of helix rise relatively to plane which is perpendicular to axis of helix.

For time-harmonic fields with

$$\mathbf{E} = \mathbf{E}_0 e^{-j\omega t} \tag{4}$$

the solution of equation (1) has the general form

$$s = s_0 e^{-j\omega t} \tag{5}$$

The displacement of electron along helix is

$$s = \frac{-eE_0 \cos\theta \left(\omega_0^2 - \omega^2 + j\omega^3\Gamma\right) \sin\alpha}{m\left(\left(\omega_0^2 - \omega^2\right)^2 + \omega^6\Gamma^2\right)} e^{-j\omega t} \tag{6}$$

where ω_0 is resonance frequency and

$$\frac{k}{m} = \omega_0^2, \quad \frac{\gamma}{m} = \Gamma. \tag{7}$$

The current density can be represented in the the form

$$\mathbf{J} = \rho\mathbf{v} = -eN\mathbf{v} \tag{8}$$

where $\rho = -e\delta(\mathbf{r})$ is volume density of charge in the case of single electron, δ is Dirac delta function, N is effective concentration of electrons of conductivity which move along helix trajectories. The component of current density which oriented perpendicularly to helix axis is

$$J_\perp = \rho v_\perp = \rho v_s \cos\alpha \tag{9}$$

$$v_s = \frac{ds}{dt} = \sin\alpha \frac{j\omega eE_0 \cos\theta \left(\omega_0^2 - \omega^2 + j\omega^3\Gamma\right)}{m\left(\left(\omega_0^2 - \omega^2\right)^2 + \omega^6\Gamma^2\right)} e^{-j\omega t} \tag{10}$$

is electron velosity along helix,

$$v_\perp = v_s \cos\alpha = v_s \frac{rq}{\sqrt{r^2q^2 + 1}} \tag{11}$$

is component of velosity which is perpendicular to axis of helix, r is radius of loop of helix. Parameter q depends only on the geometry of the helix: it is determined by the pitch P of the rotation along the Z axis

$$|q| = \frac{2\pi}{P}. \tag{12}$$

Magnetic moment for single electron which is caused by electric field along X axis of helix is

$$m_x = -\frac{1}{2} \int\limits_{(\mathrm{V})} re\delta(r) v_s \cos\alpha d\mathrm{V} = -\frac{1}{2} erv_\perp \tag{13}$$

Taking into account (10),(11) for single electron we obtaine

$$m_x = -\frac{e^2}{2m}\frac{r^2 q}{r^2 q^2 + 1}\frac{j\omega\left(\omega_0^2 - \omega^2 + j\omega^3\Gamma\right)}{\left(\omega_0^2 - \omega^2\right) + \omega^6\Gamma^2}E_0 \cos\theta e^{-j\omega t}. \tag{14}$$

The electric dipole moment induced by the electric field is equal

$$p_x = -es\sin\alpha = \frac{e^2}{m}\frac{1}{r^2 q^2 + 1}\frac{\omega_0^2 - \omega^2 + j\omega^3\Gamma}{\left(\omega_0^2 - \omega^2\right) + \omega^6\Gamma^2}E_0 \cos\theta e^{-j\omega t}. \tag{15}$$

Let us consider the influence of magnetic field on electron motion into helix. From Maxwell's equation

$$\oint_{(l)} \mathbf{E}d\mathbf{l} = -\frac{\partial}{\partial t}\int_{(S)} \mathbf{B}d\mathbf{S} \tag{16}$$

taking into account that $\mathbf{E}$ vector should form with $\frac{\partial \mathbf{B}}{\partial t}$ vector left-handed system and magnetic field is time-harmonic $\mathbf{H} = \mathbf{H}_0 e^{-j\omega t}$ we obtaine the following expression

$$E_{az} = \frac{1}{2}j\omega r\mu_0 H_0 \cos\beta e^{-j\omega t} \tag{17}$$

where β is angle between $\mathbf{H}$ vector and helix axis, E_{az} is azimuth component of $\mathbf{E}$.

After solving the electron motion equation

$$m\dot{v} = -ks + \gamma\ddot{v} - eE_{az}\cos\alpha \tag{18}$$

the displacement of electron along the helix under magnetic field influence can be found:

$$s = -\frac{er}{2m}j\omega\frac{\omega_0^2 - \omega^2 + j\omega^3\Gamma}{\left(\omega_0^2 - \omega^2\right)^2 + \omega^6\Gamma^2}\mu_0 H_0 cos\alpha \cos\beta e^{-j\omega t} \tag{19}$$

The electric dipole moment for single electron excited along helix axis under magnetic field influence has the form

$$p_x = -es\sin\alpha =$$
$$\frac{e^2}{2m}\frac{r^2 q}{r^2 q^2 + 1}j\omega\frac{\omega_0^2 - \omega^2 + j\omega^3\Gamma}{\left(\omega_0^2 - \omega^2\right)^2 + \omega^6\Gamma^2}\mu_0 H_0 \cos\beta e^{-j\omega t} \tag{20}$$

The magnetic moment induced by the magnetic field along helix axis

$$m_x = -\frac{1}{2}erv_x\cos\alpha =$$
$$\frac{e^2}{4m}r^2\frac{r^2 q^2}{r^2 q^2 + 1}\omega^2\frac{\omega_0^2 - \omega^2 + j\omega^3\Gamma}{\left(\omega_0^2 - \omega^2\right)^2 + \omega^6\Gamma^2}\mu_0 H_0 \cos\beta e^{-j\omega t} \tag{21}$$

The X axis projections of electric and magnetic moments of single microhelix can be represented in the following form

$$p_x^s = \frac{1}{2} N p_x \mathrm{V}^s, \tag{22}$$

$$m_x^s = \frac{1}{2} N m_x \mathrm{V}^s \tag{23}$$

where N is effective concentration of electrons of conductivity which move along helix trajectories, V^s is volume of single microhelix. The effective concentration will be determined below. Factor $\frac{1}{2}$ takes into account, that the current distribution in microhelix is close to a linear function, vanishing at the wire ends.

The single microhelix as small particles of complex shapes can be characterized in the bi-anisotropic approximation by dyadic electric and magnetic polarizabilities, which define the bi-anisotropic relations between induced electric and magnetic dipole moments $\mathbf{p}^s$, $\mathbf{m}^s$ and external electric and magnetic fields $\mathbf{E}$, $\mathbf{H}$ [10]-[13]:

$$\mathbf{p}^s = \overline{\overline{\alpha}}_{ee} \cdot \mathbf{E} + \overline{\overline{\alpha}}_{em} \cdot \mathbf{H} \tag{24}$$

$$\mathbf{m}^s = \overline{\overline{\alpha}}_{me} \cdot \mathbf{E} + \overline{\overline{\alpha}}_{mm} \cdot \mathbf{H} \tag{25}$$

Due to the reciprocity principle, the cross-coupling coefficients $\overline{\overline{\alpha}}_{em}$ and $\overline{\overline{\alpha}}_{me}$ are related to each other as:

$$\mu_0^{-1} \overline{\overline{\alpha}}_{em} = -\overline{\overline{\alpha}}_{me}^T \tag{26}$$

This relation is coupled with the determination of magnetic moment which is used above (see Equation (13)). Also, the dyadics $\overline{\overline{\alpha}}_{ee}$ and $\overline{\overline{\alpha}}_{mm}$ are symmetrical:

$$\overline{\overline{\alpha}}_{ee} = \overline{\overline{\alpha}}_{ee}^T, \qquad \overline{\overline{\alpha}}_{mm} = \overline{\overline{\alpha}}_{mm}^T \tag{27}$$

The described model allows to calculate electric and magnetic moments of single helix.

Let us consider, for example, dielectric material consists of 5-turn Copper wire helices [10], concentration of which in a sample is $n_s = 4 \cdot 10^6$ m^{-3}. The helices have a nominal radius $r = 0.92$ mm and pitch $P = 0.37$ mm. The parameter $q = \frac{2\pi}{P} = 16.97 \cdot 10^3$ radn/m. The length of 5-turn helix is

$$L^s = 5P\sqrt{r^2 q^2 + 1}. \tag{28}$$

In considered case $L^s = 28.93$ mm.

The resonance exitation of current in helix takes place in case when length of helix is approximately equal to half of wavelength of electromagnetic field in medium

$$L^s = \frac{\pi c}{\omega_0 \sqrt{\varepsilon}} \tag{29}$$

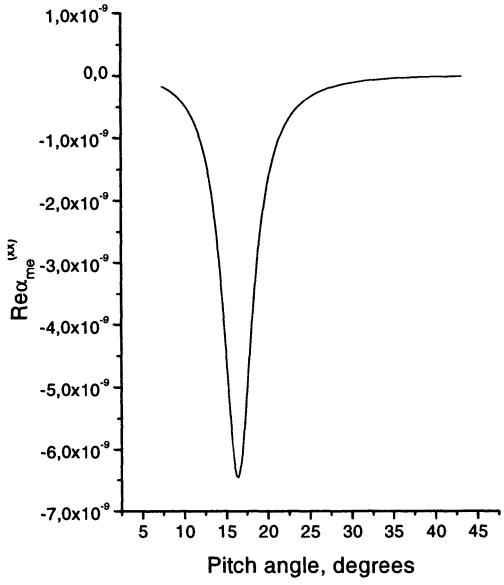

Figure 3. The real part of $\alpha_{me}^{(xx)}$ as function of pitch angle (number of loops $n = 1$)

Here ε is mean value of permittivity of chiral medium, ω_0 is resonance frequency of electromagnetic waves and c is speed of light in the vacuum. The expression (29) allows to represent a resonance frequency as function of helix length. For material which was investigated in [10] the resonance frequency is equal $\omega_0 = 2.64 \cdot 10^{10}$ radn/s, that corresponds to the mean value of permittivity $\varepsilon = 1.52$.

3. Analytical results

The current in the center of helix we can find as follows [15]

$$I = \frac{\mathcal{E}_E}{(Z_1 + Z_w)n}. \tag{30}$$

Here

$$\mathcal{E}_E = \frac{1}{2} E_x H \tag{31}$$

is the electromotive force generated by the incident electric field at the center of helix,

$$H^s = L^s \sin\alpha \tag{32}$$

is full height of helix, Z_{l} and Z_{w} are loop and wire antennas input impedances for canonical helix [12]-[15], n is number of loops of helix.

If terms of the order $(kl)^5$ and higher-order terms are neglected, the input admittance of a linear wire antenna can be expressed as [14]

$$Y_{\mathrm{w}} = -2\pi j \frac{kl}{\eta \Psi_{dr}} \left[1 + k^2 l^2 \frac{F}{3} + j k^3 l^3 \frac{1}{3(\Omega - 3)}\right] \tag{33}$$

where the parameters are

$$F = 1 + \frac{1.08}{\Omega - 3}, \quad \Omega = 2\log\frac{2l}{r_0} \tag{34}$$

$$\Psi_{dr} = 2\log\frac{l}{r_0} - 2, \quad \eta = \sqrt{\frac{\mu}{\varepsilon}} \tag{35}$$

Here the current distribution function has been approximated by a second-order polynomial. Approximate formula for the input admittance [14]:

$$Y_{\mathrm{l}} = \frac{j}{\pi\eta}\left[\frac{1}{A_0} + \frac{2}{A_1} + \frac{2}{A_2}\right] \tag{36}$$

with the first three Fourier coefficients

$$A_0 = \frac{ka}{\pi}\left[\log\frac{8a}{r_0} - 2\right] + \frac{1}{\pi}\left[0.667(ka)^3 - 0.267(ka)^5\right]$$
$$+ j\left[0.167(ka)^4 - 0.033(ka)^6\right]$$
$$A_1 = \left(ka - \frac{1}{ka}\right)\frac{1}{\pi}\left[\log\frac{8a}{r_0} - 2\right] + \frac{1}{\pi}\left[-0.667(ka)^3 + 0.207(ka)^5\right]$$
$$+ j\left[0.333(ka)^2 - 0.133(ka)^4 + 0.026(ka)^6\right]$$
$$A_2 = \left(ka - \frac{4}{ka}\right)\frac{1}{\pi}\left[\log\frac{8a}{r_0} - 2.667\right]$$
$$+ \frac{1}{\pi}\left[-0.4ka + 0.21(ka)^3 - 0.086(ka)^5\right] + j\left[0.05(ka)^4 - 0.012(ka)^6\right] \tag{37}$$

where $k = \omega\sqrt{\varepsilon\mu}$ is the wave number in the background medium, $l = \frac{P}{2}$ is a half of length of canonical helix wire, r_0 is a radius of wire. The wire and loop antennas input impedances are inverses of the admittances: $Z_{\mathrm{l}} = 1/Y_{\mathrm{l}}$, $Z_{\mathrm{w}} = 1/Y_{\mathrm{w}}$.

The comparison of relations (8) , (23) and (30) allows us to obtaine the effective concentation of electrons of conductivity which move along the helix trajectories.

The following relation for magnetic moment caused by electric field in single helix is obtained

$$m_x^s = -\frac{\pi r^2 L^s}{4(Z_l + Z_w)\sqrt{r^2 q^2 + 1}} E_x \tag{38}$$

where X axis is oriented along axis of helix, r is radius of loop, L^s is full length of helix.

In proposed model is assumed that the current in helix decreases from center to ends as linear function (vanishing at the wire ends). The following supposition is used also: the full length of helix is approximately equal to $\lambda/2$, where λ is wave length of electromagnetic field in this medium. This assumption allows to express the radius of canonical helix a with the help of parameter q:

$$a = \frac{1}{2\pi}\left[\frac{\lambda}{2n} - \frac{2\pi}{|q|}\right] \tag{39}$$

where n is number of loops of helix and values of q satisfy to following inequality

$$|q| > \frac{4\pi n}{\lambda} \tag{40}$$

4. Calculation according obtained effective electron model

The parameter of magneto-electric coupling $\overline{\overline{\alpha}}_{me}$ in the general case can be described as dyadic. The dependences of real and imaginary parts of component α_{me}^{xx} on pitch angle are presented in Figs. 3,4. In this case the helix consists of one loop only.

From the analysis of figures we can conclude that the dependence of imaginary part of α_{me}^{xx} on pitch angle is nonmonotonic. We can see also that at the pitch angle which is close to 18 degrees the imaginary part of parameter α_{me}^{xx} changes the sign and reaches the minimal and maximal value. The imaginary part of parameter α_{me}^{xx} is responsible for the turn of polarization plane of electromagnetic waves in artificial chiral medium. The dependence of real part of α_{me}^{xx} on pitch angle is also nonmonotonic but has the same sign for all values of pitch angle. The maximal value of the real part corresponds to the pitch angle nearly to 18 degrees. The real part of parameter α_{me}^{xx} is responsible for circular dichroism of electromagnetic waves in artificial chiral medium. We have obtained that optimal parameters of helices considerably depend on the number of loops of helix. The results of analitical calculations are presented in Table 1.

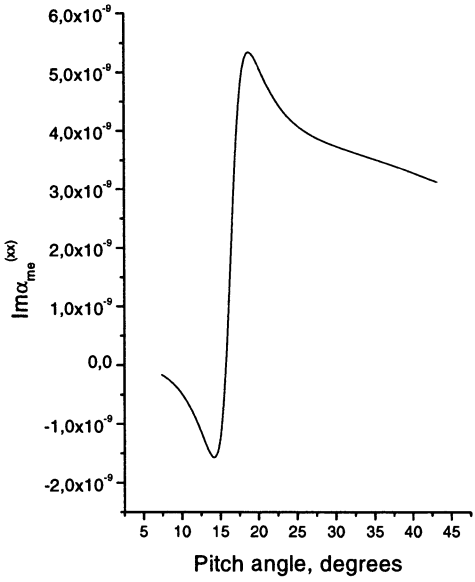

Figure 4. The imaginary part of $\alpha_{me}^{(xx)}$ as function of pitch angle (number of loops $n = 1$)

In previous experimental investigations which were performed in Technical University of Braunschweig, Germany [10], were used the 5-loop microhelices with pitch angle nearly to 4 degrees which is close to optimal values calculated accordingly our model.

For other hand, in experimental researshes which were performed in University of Stellenbosch, South Africa [5] were used, for example, the 2-loop microhelices with pitch angle nearly to 20 degrees, radius of loop about 0.6 mm, radius of Cooper wire about 20 micron, pitch about 1.5 mm and full length of helix about 8.47 mm. However, the optimal pitch angle for such helix according to our model is equal 8.6 degrees. This pitch angle is far from angle which was used in experiments [5]. The value of $\mathrm{Im}\alpha_{me}^{xx}$ according to our model is equal $5.17 \cdot 10^{-12} \frac{\mathrm{m}^3}{Ohm}$ for pitch angle 20 degrees, and optimal value is equal $-4.49 \cdot 10^{-10} \frac{\mathrm{m}^3}{Ohm}$ for pitch angle 8.6 degrees.

TABLE I. Helices with various number of loops and constant $L^s = \frac{\lambda}{2} = 28.93$ mm

Number of loops	Optimal pitch angle α, degrees	Radius of loop, mm	Height of helix $H^s = L^s \sin\alpha$, mm	Value of $\mathrm{Im}\alpha_{me}^{xx}$, $\frac{m^3}{Ohm}$
1	18.7	4.36	9.28	$5.34 \cdot 10^{-9}$
2	1.7	2.3	0.85	$1.44 \cdot 10^{-9}$
3	2.4	1.53	1.24	$-6.6 \cdot 10^{-9}$
4	3.2	1.15	1.61	$5.59 \cdot 10^{-9}$
5	4	0.92	2.02	$-4.29 \cdot 10^{-9}$
6	4.8	0.76	2.42	$-7.04 \cdot 10^{-9}$

5. Conclusion

A possibility to use the helical model of molecules for the description of interaction of electromagnetic waves with the artificial chiral media is shown. An analytical model, allowing to calculate electric dipole moment and magnetic moment, induced in the helix under the action of the incident electromagnetic wave, is formed. On the base of present model the evaluation of effective parameter of magneto-electric coupling for single helix is performed. The optimal pitch angle of loops of helix elements of artificial composite media is calculated, which ensures the maximum values of average chirality parameter. It is shown, that optimal pitch angle strongly depends on the number of loops of helix. For example, if the helix consists of a few loops, the optimal pitch angle is close to 2-5 degrees with respect to plane which is perpendicular to axis of helix.

6. Acknowledgments

The authors are grateful to Professor Constantin Simovski of St. Petersburg Institute of Fine Mechanics and Optics, Russia for many useful remarks and for many discussions on this topic.

References

1. *Antennas*, Ed. by A.I. Shpuntov, (1951), Moscow, Sov. radio, 292 p. (in Russian)
2. Samusenko A.I., (1993), Mathematical modeling of radiators from ultrathin conductors, *Izvestiya vuzov. Radioelektronika*, **vol. 36, no. 7**, p. 64-69. (in Russian)
3. Demidchik V.I.,Kornev R.V., (2001), Antenna model of chiral scatterers, *Vestnik Belorusskogo gosudarstvennogo universiteta*, **Ser.1, no. 2**, p.14-16. (in Russian)
4. Demidchik V.I., Kukharchik P.D., Kornev R.V., (2001), Analysis of chiral scatterers by the method of integral equations, *Izvestiya Gomelskogo gosudarstvennogo universiteta*, **no. 5**, p.63-66. (in Russian)
5. Kuehl S.A., Grove S.S, Kuehl E., Bingle M., Cloete J.H., (1997), Manufacture of microwave chiral materials and their electromagnetic properties. *Advances in Complex Electromagnetic Materials*, ed. by A. Priou, Kluwer Academic Publishers, 317-332.
6. Marriotte F., Tretyakov S. A., Sauviac B., (1996), Modeling effective properties of chiral composites, *IEEE Antennas and Propagation Magazin*, **vol.38, no. 2**, p.22-32.
7. Kauzmann W., (1957), *Quantum chemistry. An introduction*, New York, Academic Press.
8. Landau L.D. and Lifshits E.M., (1973), *Theory of field*, Moscow, Nauka, (in Russian).
9. Tretyakov S.A. and Viitanen A.J., (2000), Electromagnetic properties of periodical arrays with small non-reciprocal inclusions, *J. Electromagn. Waves Applic.*, V. 14, No 8, pp. 1159-1177.
10. J. Psilopoulos, J. Reinert, and A.F. Jacob, (2000), Fabrication effects on the resonance bandwidth of chiral materials, *Proceedings of Bianisotropics 2000*, 27-29 September 2000, Lisbon, Portugal, 313-316.
11. I.E. Tamm, (1976), *Basis of electricity theory*, Moscow, Nauka, 616 p, (in Russian).
12. *Antenna Handbook: Theory, Applications, and Design*, ed. by Y.T. Lo and S.W. Lee, (1988), New York: Van Nostrand Reinold Co., Chapter 7.
13. R.W.P. King and G.S. Smith, with M. Owens and T.T. Wu, (1981), *Antennas in Matter: Fundamentals, Theory, and Applications*, Cambridge, MA, and London, England: The MIT Press.
14. R.W.P. King and C.W. Harrison, (1969), *Antennas and Waves: A Modern Approach*, Cambridge, MA, and London, England: The MIT Press.
15. A.N. Serdyukov, I.V. Semchenko, S.A. Tretyakov, and A.H. Sihvola, (2001), *Electromagnetics of bi-anisotropic materials*, Gordon and Breach Sciense Publishers.

TRANSMISSION AND REFLECTION OF ELECTROMAGNETIC WAVES BY THE PLANE STRATIFIED STRUCTURES POSSESSING GYROTROPIC PROPERTIES

A. N. BORZDOV
Department of Theoretical Physics,
Belarussian State University
Fr. Skaryny avenue 4, 220050 Minsk, Belarus
Fax: + 375-17-226 05 30; email: boralex@bsu.by

Abstract. An approach to introduction of effective constitutive tensors of the periodic layered systems, based on the approximate calculation of the characteristic matrix of the unit cell with the help of Campbell–Hausdorff series [1], is used for analysis of the plane stratified bianisotropic structures. These structures can possess gyrotropic (bianisotropic) properties even in a case, when layers are nongyrotropic (form gyrotropy). It is shown that by using the presented approach, the effects of form gyrotropy (bianisotropy) can be explained in terms of the theory of effective parameters. The possibilities of introduction of effective material tensors not dependent on the parameters of incident wave, and also the accuracy of different approximations will be discussed. Previously obtained theoretical results are verified by means of extensive computations of transmission and reflection of plane electromagnetic waves by systems at hand for different planes and angles of incidence.

1. Introduction

One of the most fruitful approaches in the theory of propagation of waves in multilayered media is the operator formalism based on the use of intrinsic representation of vectors and operators. It enables one to find compact coordinate-free formulae for very complex systems and to avoid the cumbersome calculations required by usual components techniques and caused mainly by the necessity of adopting a different coordinate system for each different layer.

In this paper we use this formalism to find the effective material tensors of the medium formed by a periodic set of plane bianisotropic layers with different thicknesses l_n ($n = 1, 2, \ldots N$, where N is the number of the layers which constitute the unit cell). These tensors are similar to the effective

S. Zouhdi et al. (eds.), Advances in Electromagnetics of Complex Media and Metamaterials, 259–269.

tensors of permittivity ϵ, permeability μ and pseudotensors of gyrotropy α, β of homogeneous medium, and coincide with them in the long wavelength approximation. The effective tensors introduced in this paper can be very handy, for example, for analysis transmission and reflection of electromagnetic waves by multilayered bianisotropic systems, especially periodic ones. In general, these tensors destine more for describing properties of systems as a whole, rather than for analysis of propagation of waves inside the systems.

In recent years attention has been frequently focused on the study of the effective properties of plane stratified periodic media. In doing so most often a long wavelength approximation is used. For example, in [2] the coordinate-free formulae for the effective tensors of permittivity ϵ, permeability μ and pseudotensors of gyrotropy α, β of the plane stratified periodic bianisotropic systems of the most general type were obtained. But it is well known [3], [4] that some systems composed from nongyrotropic layers can possess gyrotropic (bianisotropic) properties due to their specific structure (i.e. possess form gyrotropy). Phenomena of this kind cannot be explained in the framework of a long wavelength approximation. To treat such problems it is necessary to extend the wave band, in which the effective tensors can be used: One way of doing this is to employ an approach [5], based on the approximate calculation of the characteristic matrix of the unit cell with the help of Campbell–Hausdorff series (section 2). Recently it was shown that by using this approach the effects of form gyrotropy (bianisotropy) can be really explained in terms of the theory of effective parameters (see [6]–[8], for example).

The main purpose of this paper is to introduce the above mentioned effective material tensors of the medium, feasible for the use in the wide wave band. By means of numerical calculations for the transmission and reflection tensors we also show that form bianisotropy can be really explained in terms of the theory of effective parameters.

In what follows we assume for materials of the layers the following constitutive relations, written in matrix form

$$\begin{pmatrix} \mathbf{D}_n \\ \mathbf{B}_n \end{pmatrix} = \mathcal{R}_n \begin{pmatrix} \mathbf{E}_n \\ \mathbf{H}_n \end{pmatrix}, \quad \mathcal{R}_n = \begin{pmatrix} \varepsilon_n & \alpha_n \\ \beta_n & \mu_n \end{pmatrix}, \tag{1}$$

where ε_n, μ_n and α_n, β_n are the dielectric permittivity, the magnetic permeability tensors and the pseudotensors of gyrotropy, respectively. If ε_n, μ_n, α_n, β_n $(n = 1, 2, \ldots N)$ are complex nonsymmetric tensors, then equation (1) describe an absorbing anisotropic and gyrotropic medium, subject to the influence of external electric and magnetic fields and elastic deformations.

2. Effective Material Tensors Of Bianisotropic Multilayered Systems

A great variety of methods is used to introduce the effective material tensors of one-dimensional structures. For example, approaches originating from experimental methods of measurement of effective material parameters are discussed in [9]. The characteristic matrix technique employed here is based totally on the use of exact solutions of Maxwell equations.

The characteristic matrix $P = \exp(ik_0 l M)$ of a layer with thickness l relates the six-vectors $(\mathbf{E}, \mathbf{H})^T$ at the layer boundaries ($k_0 = \omega/c$). The matrix M can be written in the form [10]

$$M = \mathcal{T}_q Q_\times (\mathcal{R} - \mathcal{B}_\times) \mathcal{T}_q, \tag{2}$$

$$Q_\times = \begin{pmatrix} \mathbf{0} & -\mathbf{q}^\times \\ \mathbf{q}^\times & \mathbf{0} \end{pmatrix}, \ \mathcal{B}_\times = \begin{pmatrix} \mathbf{0} & -\mathbf{b}^\times \\ \mathbf{b}^\times & \mathbf{0} \end{pmatrix}, \tag{3}$$

$$\mathcal{T}_q = \mathcal{E} - \mathcal{N}_q, \ \mathcal{E} = \begin{pmatrix} 1 & 0 \\ 0 & 1 \end{pmatrix}, \ \mathcal{N}_q = \mathcal{R}_q^{-1} Q (\mathcal{R} - \mathcal{B}_\times), \ Q = \begin{pmatrix} \mathbf{q} \otimes \mathbf{q} & \mathbf{0} \\ \mathbf{0} & \mathbf{q} \otimes \mathbf{q} \end{pmatrix}, \tag{4}$$

where the operator $\mathcal{R}_q^{-1}$ is the inverse to the operator

$$\mathcal{R}_q = \begin{pmatrix} \varepsilon_q \mathbf{1} & \alpha_q \mathbf{1} \\ \beta_q \mathbf{1} & \mu_q \mathbf{1} \end{pmatrix}, \tag{5}$$

$$\varepsilon_q = \mathbf{q}\varepsilon\mathbf{q}, \mu_q = \mathbf{q}\mu\mathbf{q}, \alpha_q = \mathbf{q}\alpha\mathbf{q}, \beta_q = \mathbf{q}\beta\mathbf{q}.$$

Here, $\mathbf{q}^\times$ is the antisymmetric dyadic dual to the unit normal of the boundaries of $\mathbf{q}$, $\mathbf{b}$ is the tangential component of refraction vector $\mathbf{m}$ [12],[11], and $\mathbf{q} \otimes \mathbf{q}$ is the dyad (defined by the dyadic product $\otimes$) and $\mathbf{1}$ is the unit dyadic.

In the case of a strcture formed by two alternate layers with different thicknesses l_n and different sets of tensor constants $\varepsilon_n, \mu_n, \alpha_n, \beta_n$ ($n = 1, 2$), the characteristic matrix of the unit cell has the form

$$P = \exp(ik_0 L M) = \exp(ik_0 l_2 M_2) \exp(ik_0 l_1 M_1), \tag{6}$$

where $L = l_1 + l_2$ is the system period and M is matrix, defining effective material tensors.

Note, that matrices $\exp(ik_0 l_2 M_2)$ and $\exp(ik_0 l_1 M_1)$ in general case do not commute. As a consequence for the left-incident and right-incident waves we must use different material parameters. Of course, in the long wavelength approximation, characteristic matrices commute and (6) defines the usual constitutive tensors, the same, as obtained in [2], for example.

The matrix (6) can be expressed in terms of the layers parameters with the help of Campbell–Hausdorff series [1] as follows

$$M = \begin{pmatrix} A & B \\ C & D \end{pmatrix} = f_1 M_1 + f_2 M_2 + i f_1 \frac{\pi l_2}{\lambda} [M_2, M_1] - \frac{\pi^2 l_1 l_2}{3\lambda^2} \{ f_1 [[M_2, M_1], M_1] + f_2 [[M_1, M_2], M_2] \} + \cdots \tag{7}$$

where $f_n = l_n/L$ is the relative thickness of the n-th layer, $\sum_{n=1}^{N} f_n = 1$, and $[M_2, M_1] = M_2 M_1 - M_1 M_2$. If $\pi l_n/\lambda \ll 1$, then the series (7) converges rapidly and one can drop the remainder of it after the k–th term. Here for the sake of simplicity we have limited our consideration by three terms of series. The first and the second terms correspond to the long wavelength limit.

The tensor parameters A, B, C, D can be directly used for the analysis of the wave propagation in the considered system, for example for finding the reflection and transmission tensors [11] (see section 3).

For the sake of simplicity we assume $\mathbf{q}$ to be the left and the right eigenvector of each of the tensors $\varepsilon_n, \mu_n, \alpha_n, \beta_n$ $(\varepsilon_n \mathbf{q} = \mathbf{q}\varepsilon_n \equiv \varepsilon_{nq}\mathbf{q}, \cdots)$. Besides, we shall use in (6)–(7) the matrices M_I, M_{1I}, M_{2I}, describing the transformation of the tangential components of the field vectors, instead of M, M_1, M_2, describing the transformation of the full six-vectors. In the majority of applications this is permissible. Under above–mentioned conditions we have:

$$M_{nI} = Q_\times \left[\mathcal{R}_n - \frac{1}{\delta_n} \mathcal{R}_{nq}^T \begin{pmatrix} \mathbf{a}\otimes\mathbf{a} & \mathbf{0} \\ \mathbf{0} & \mathbf{a}\otimes\mathbf{a} \end{pmatrix} \right] \mathcal{T}, \tag{8}$$

$$\mathcal{T} = \begin{pmatrix} I & 0 \\ 0 & I \end{pmatrix}, \; I = \mathbf{1} - \mathbf{q}\otimes\mathbf{q}, \tag{9}$$

where $\mathcal{R}_{nq}^T$ is the transpose operator, and $\mathbf{a} = \mathbf{b}\mathbf{q}^\times$,

$$[M_{2I}, M_{1I}] = Q_\times [\mathcal{R}_{21} - \Delta(\mathbf{a})] \mathcal{T}, \tag{10}$$

$$\mathcal{R}_{21} = \mathcal{R}_2 Q_\times \mathcal{R}_1 - \mathcal{R}_1 Q_\times \mathcal{R}_2, \tag{11}$$

$$\Delta(\mathbf{a}) = \Delta_L \begin{pmatrix} \mathbf{a}\otimes\mathbf{a} & \mathbf{0} \\ \mathbf{0} & \mathbf{a}\otimes\mathbf{a} \end{pmatrix} + \begin{pmatrix} \mathbf{a}\otimes\mathbf{a} & \mathbf{0} \\ \mathbf{0} & \mathbf{a}\otimes\mathbf{a} \end{pmatrix} \Delta_R, \tag{12}$$

where

$$\Delta_L = \left[\mathcal{R}_{2I} Q_\times \frac{\mathcal{R}_{1q}^T}{\delta_1} - \mathcal{R}_{1I} Q_\times \frac{\mathcal{R}_{2q}^T}{\delta_2} \right], \; \Delta_R = \left[\frac{\mathcal{R}_{2q}^T}{\delta_2} Q_\times \mathcal{R}_{1I} - \frac{\mathcal{R}_{1q}^T}{\delta_1} Q_\times \mathcal{R}_{2I} \right], \tag{13}$$

and $\mathcal{R}_{nI} = \mathcal{T}\mathcal{R}_n\mathcal{T}, n = 1, 2.$

In the same way one can derive formulae for the systems comprising more than two layers in the unit cell.

2.1. CORRECT INTRODUCTION OF EFFECTIVE MATERIAL TENSORS

Though effective material tensors generally are not constitutive tensors, we shall denote them as ε, μ and α, β.

For the correct introduction of material tensors of the medium equivalent in the considered approximation to the system at hand, the matrix M_I is bound to depend on the effective tensors, angle and plane of incidence in the same way as in the homogeneous medium. From (7)–(12) it follows that these conditions are met if $\Delta(\mathbf{a}) = 0$. In this case we can find the effective material tensors in the same way as in [6]

$$\mathcal{R} = \begin{pmatrix} \varepsilon & \alpha \\ \beta & \mu \end{pmatrix} = \mathcal{T}\left(f_1\mathcal{R}_1 + f_2\mathcal{R}_2 + if_1\frac{\pi l_2}{\lambda}\mathcal{R}_{21}\right)\mathcal{T} + \mathcal{R}_q Q, \qquad (14)$$

with

$$\mathcal{R}_q = \left(f_1\mathcal{R}_{1q}^{-1} + f_2\mathcal{R}_{2q}^{-1}\right)^{-1}. \qquad (15)$$

For example, $\Delta(\mathbf{a}) = 0$ if $\Delta_L = \Delta_R = 0$. That takes place provided [6]

$$\mathcal{R}_{2I}\mathcal{R}_{2q} = \mathcal{R}_{1I}\mathcal{R}_{1q}, \ \mathcal{R}_{2q}\mathcal{R}_{2I} = \mathcal{R}_{1q}\mathcal{R}_{1I}, \qquad (16)$$

Note that both relations (16) are equivalent if $\alpha_i = \beta_i = 0$. Even so it is rigid enough requirement, signifying that tensors ε_{1I} and ε_{2I}, μ_{1I} and μ_{2I} are bound to have the same eigenvectors.

Of course, the above mentioned conditions need not be met exactly with regard to approximate nature of method. We can find estimates $\|\Delta_L\|$ and $\|\mathcal{R}_{21}\|$ instead. It should be more than sufficient if $\|\Delta_L\|, \|\Delta_R\|$ are far less than $\|\mathcal{R}_{21}\|$. In what follows we shall use Euclidean norm

$$\|X\| = \left[(XX^\dagger)_t\right]^{\frac{1}{2}}, \qquad (17)$$

where $X^\dagger$ is Hermitian transposed tensor and $(XX^\dagger)_t$ is a trace of tensor $XX^\dagger$.

By way of an example let us consider nongyrotropic, nonmagnetic layers with real symmetric tensors ε_i. In this case

$$\|\Delta_L\|^2 = \left(\frac{\varepsilon_{2+}}{\varepsilon_{1q}} - \frac{\varepsilon_{1+}}{\varepsilon_{2q}}\right)^2 + \left(\frac{\varepsilon_{2-}}{\varepsilon_{1q}} - \frac{\varepsilon_{1-}}{\varepsilon_{2q}}\right)^2 + 2\sin\phi^2\left(\frac{\varepsilon_{1+}}{\varepsilon_{1q}} - \frac{\varepsilon_{1-}}{\varepsilon_{1q}}\right)\left(\frac{\varepsilon_{2+}}{\varepsilon_{2q}} - \frac{\varepsilon_{2-}}{\varepsilon_{2q}}\right), \qquad (18)$$

$$\|\mathcal{R}_{21}\|^2 = 2\left[(\varepsilon_{2+} - \varepsilon_{1+})^2 + (\varepsilon_{2-} - \varepsilon_{1-})^2 + 2\sin\phi^2(\varepsilon_{1+} - \varepsilon_{1-})(\varepsilon_{2+} - \varepsilon_{2-})\right], \qquad (19)$$

where ϕ is the angle between the preferred axes of crystals, $\varepsilon_{i+}, \varepsilon_{i-} (i = 1, 2)$ are the eigenvalues of tensors $\varepsilon_{iI} = I\varepsilon_i I$. Formulae for magnetic crystals are similar to (18),(19). Since usually $\|\alpha_i\|, \|\beta_i\| \ll \|\varepsilon_i\|, \|\mu_i\|$, corresponding formulas are valid also for analysis of the gyrotropic layers.

Inasmuch $\mathbf{a}^2 \sim \varepsilon_{iq}$, from (18), (19), (12) it follows that for identical layers ($\varepsilon_{1+} = \varepsilon_{2+}, \varepsilon_{1-} = \varepsilon_{2-}$) values $\|\Delta(\mathbf{a})\|$ and $\|\mathcal{R}_{21}\|$ are approximately equal. The situation changes in the case of different parameters of the layers. In this case it is possible to choose parameters of the crystals provided that the following condition is fulfilled:

$$\|\Delta(\mathbf{a})\| \ll \|\mathcal{R}_{21}\|. \tag{20}$$

Relation (20) can be provided much easier for structures comprising, for example, three layers in the unit cell. Then we have

$$\begin{aligned} M &= f_1 M_1 + f_2 M_2 + f_3 M_3 + \\ &\frac{i\pi}{\lambda} \{f_3 l_2 [M_3, M_2] + f_3 l_1 [M_3, M_1] + f_1 l_2 [M_2, M_1]\} + \ldots, \end{aligned} \tag{21}$$

and instead of $\|\Delta(\mathbf{a})\|$, $\|\mathcal{R}_{21}\|$ (11)–(13) we shall have more complicated but more versatile expressions, which can be changed by varying thicknesses of the layers. It should be noted that sometimes the "wide wave band approximation" reduces to the long wavelength approximation. In particular, if $\mathcal{R}_1 = \mathcal{R}_3$, $l_1 = l_2 = l_3$, then $[M_3, M_1] = 0$, $[M_3, M_2] = -[M_2, M_1]$ and the structure do not possess properties of form gyrotropy [6].

Obviously, conditions (16) and (20) can be met only for some particular systems. On the other hand, formulas (14), (8)–(11) are valid for arbitrary material parameters of the layers in the case of normal incidence ($\mathbf{a} = \mathbf{0}$) and for a small enough angles of incidence. Therefore, it is worthwhile to calculate terms, corresponding to the long wavelength limit, with taking into account $\mathbf{a}$, but to take $\mathbf{a} = \mathbf{0}$ when calculating commutators. This approach applies to the systems of general type.

2.2. CONVERGENCE OF CAMPBELL–HAUSDORFF SERIES

To compare the accuracy of different approximations, namely, long wavelength approximation and approximations, using three and five terms of Campbell–Hausdorff series, let us consider the most simple case of normal incidence onto the nongyrotropic nonabsorbing layers of the same thickness $l_1 = l_2 = l$. As this takes place we have

$$M_I = \frac{1}{2}(M_{1I} + M_{2I}) + i\frac{\pi l}{2\lambda}\{[M_{2I}, M_{1I}] + i\frac{\pi l}{3\lambda}[[M_{2I}, M_{1I}], M_{1I} - M_{2I}]\} + \cdots \tag{22}$$

Generally speaking, the Campbell–Hausdorff series

$$Z = X + Y + \frac{1}{2}[X,Y] + \frac{1}{12}[X,[X,Y]] + \frac{1}{12}[Y,[Y,X]] + \cdots \tag{23}$$

converges provided $\|X\| < \frac{ln2}{2}, \|Y\| < \frac{ln2}{2}$, where $\|X\| = \left[\text{trace}\left(XX^{\dagger}\right)\right]^{\frac{1}{2}}$ is Euclidean valuation of X. In our case series converges if

$$\frac{\pi \max(l_1, l_2)}{\lambda} \leq \frac{ln2}{4\ \max(\|M_{1I}\|, \|M_{2I}\|)} \tag{24}$$

For example, in the case of nonmagnetic crystals with $\|\varepsilon_I\| \sim 4.5$ (eigenvalues of $\varepsilon_I \sim 3.0$) we have $\frac{\pi l}{\lambda} \leq 0.039$.

After simple calculations we find the effective material tensors of the system at hand

$$\alpha_I = \beta_I^{\dagger} = i\frac{\pi l}{2\lambda} R_\alpha,\ R_\alpha = \left(\varepsilon_{1I}\mathbf{q}^{\times}\Delta\mu_I - \Delta\varepsilon_I\mathbf{q}^{\times}\mu_{1I}\right), \tag{25}$$

$$\varepsilon_I = \frac{1}{2}\left(\varepsilon_{1I} + \varepsilon_{2I}\right) + \varepsilon',\ \mu_I = \frac{1}{2}\left(\mu_{1I} + \mu_{2I}\right) + \mu', \tag{26}$$

$$\varepsilon' = i\frac{\pi l}{2\lambda}\left(i\frac{\pi l}{3\lambda}\right) R'_\varepsilon,\ R'_\varepsilon = -R_\alpha\mathbf{q}^{\times}\Delta\varepsilon_I - \Delta\varepsilon_I\mathbf{q}^{\times}R_\beta, \tag{27}$$

$$\mu' = i\frac{\pi l}{2\lambda}\left(i\frac{\pi l}{3\lambda}\right) R'_\mu,\ R'_\mu = R_\beta\mathbf{q}^{\times}\Delta\mu_I + \Delta\mu_I\mathbf{q}^{\times}R_\alpha, \tag{28}$$

where $\Delta\varepsilon_I = \varepsilon_{2I} - \varepsilon_{1I}$, and $\Delta\mu_I = \mu_{2I} - \mu_{1I}$.

It is worth noting that third term of Campbell–Hausdorff series give rise to the effective "tensors of gyrotropy" α_I, β_I while the fourth and fifth terms contribute only in the effective permittivity and permeability tensors (terms ε', μ' in (26)).

From (25),(27), (28) it follows that

$$\|R_\alpha\| \leq 2\left(\|\varepsilon_{1I}\|\ \|\Delta\mu_I\| + \|\Delta\varepsilon_I\|\ \|\mu_{1I}\|\right), \tag{29}$$

$$\|R_\beta\| \leq 2\left(\|\varepsilon_{1I}\|\ \|\Delta\mu_I\| + \|\Delta\varepsilon_I\|\ \|\mu_{1I}\|\right), \tag{30}$$

$$\|R'_\varepsilon\| \leq 2\ \|\Delta\varepsilon_I\|\left(\|R_\alpha\| + \|R_\beta\|\right), \tag{31}$$

$$\|R'_\mu\| \leq 2\ \|\Delta\mu_I\|\left(\|R_\alpha\| + \|R_\beta\|\right). \tag{32}$$

From above estimations and formulae (25)–(28) it is clear that in the convergence range the contribution of the fourth and fifth terms of Campbell–Hausdorff series in effective tensors is far less than the contribution of third term, and usually may be thought of as negligibly small if compared with the contribution of the first and second terms.

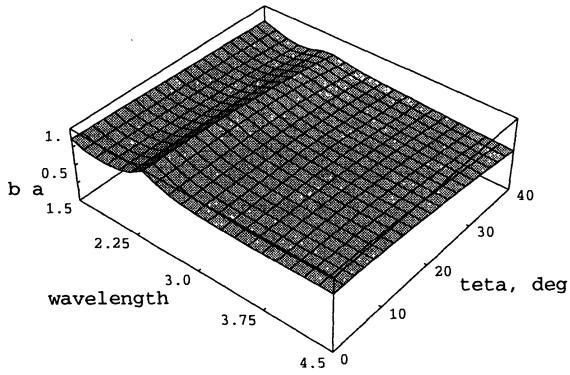

Figure 1. Ratio b/a of a short to long axis of the vibrational ellipse for one of the eigenwaves of transmission tensor as a function of ratio $\frac{\lambda}{2L}$ wavelength to the total thickness of system and angle of incidence θ. Azimuth of incident wave $\psi = 45^o$. 6-layers periodic systems. $N = 3$. Exact computation by means of characteristic matrices.

3. Transmission and reflection of elecromagnetic waves by the multilayered systems possessing gyrotropic properties

To verify the presented approximate method of introduction of effective tensor parameters, extensive computations were carried out, both with the use of approximate and exact formulae. To calculate transmission and reflection tensors we employed an approach based on the characteristic matrices and operators of impedance technique (see, for example [11]). By means of this technique for the operators d_E and r_E, describing transmission and reflection of the tangential components of vector E, we obtain

$$d_E = -2\mathbf{q}^{\times} \left[(\gamma_0, I)\, P^{-} \begin{pmatrix} \gamma_N^{-} \\ I \end{pmatrix} \right]^{-} \mathbf{q}^{\times} \tag{33}$$

$$r_E = \mathbf{q}^{\times} \left[(\gamma_0, -I)\, P^{-} \begin{pmatrix} \gamma_N^{-} \\ I \end{pmatrix} \right] \left[(\gamma_0, I)\, P^{-} \begin{pmatrix} \gamma_N^{-} \\ I \end{pmatrix} \right]^{-} \mathbf{q}^{\times}, \tag{34}$$

where the operator P^{-} is the pseudoinverse [14],[11] to the characteristic matrix P, and γ_0 and γ_N are the surface impedances of incident and transmitted waves [11].

Our prime interest here is with gyrotropic properties of the systems formed by the periodic set of identical anisotropic nongyrotropic layers rotated at a uniform rate across the period. It is well known that such systems possess chiral properties (see, for example, [4],[3]). In the optical region they are used as optical filters [13].

For the sake of simplicity we analyze the systems with the unit cell composed of three layers. This facilitates a comparison of exact and ap-

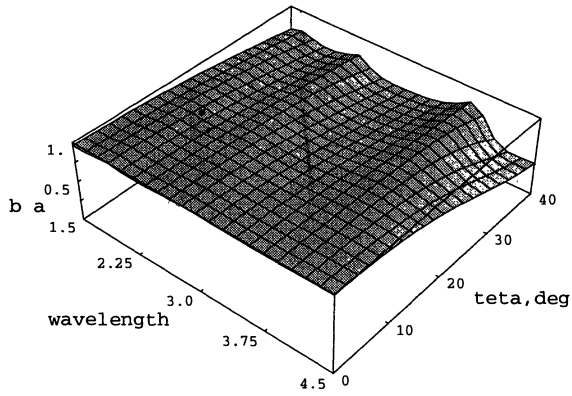

Figure 2. Ratio b/a of a short to long axis of the vibrational ellipse for one of the eigenwaves of transmission tensor as a function of ratio $\frac{\lambda}{2L}$ wavelength to the total thickness of system and angle of incidence θ. Azimuth of incident wave $\psi = 45°$. 6-layers periodic systems. $N = 3$. Approximate calculation of characteristic matrices with the help of Campbell–Hausdorff series. $\mathbf{a} \neq 0$

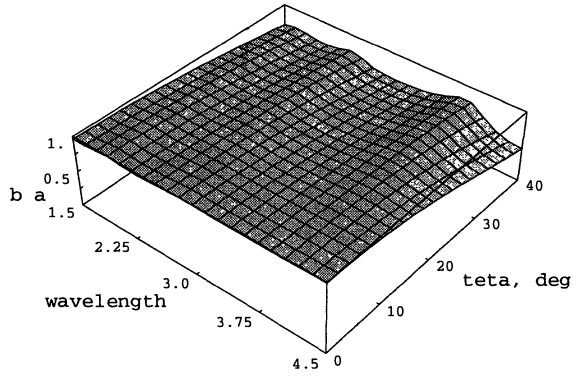

Figure 3. Ratio b/a of a short to long axis of the vibrational ellipse for one of the eigenwaves of transmission tensor as a function of ratio $\frac{\lambda}{2L}$ wavelength to the total thickness of system and angle of incidence θ. Azimuth of incident wave $\psi = 45°$. 6-layers periodic systems. $N = 3$. Approximate calculation of characteristic matrices with the help of Campbell–Hausdorff series. $\mathbf{a} = 0$ for commutators.

proximate formulae. The latter can be easily derived from the formula (21) in the same manner as it was done in section 2.

It is necessary to differentiate the rotation of the vibration ellipse of the propagating wave due to the permittivity (permeability) being tensors and rotation due to the nonzero magneto–electric tensors (gyrotropy, chirality) while discussing the form bianisotropy. Manifestations of gyrotropy are often suppressed due to the permeability (permittivity) being tensors,

especially in the optical wave region [12]. It is known that by varying the relative thicknesses and mutual orientation of the layers one can form medium with transversely isotropic effective tensors ε, μ (see [2]). In transversely isotropic medium one can easily observe manifestations of form gyrotropy (form chirality, in particular).

If $l_1 = l_2 = l_3$, then medium is transversely isotropic provided that each of the identical plates rotates through a constant angle 60^o with respect to previous one over unit normal to interfaces. We computed the systems with the following values of material constants: $\varepsilon_x = 5, \varepsilon_y = \varepsilon_z = 3.5, \mu_x = 4.0, \mu_y = \mu_z = 3.0$ (here $\varepsilon_x, \varepsilon_y, \varepsilon_z$ and μ_x, μ_y, μ_z are the eigenvalues of ε, μ, one of their eigenvectors is set along z-axis).

Figures 1–3 show the computed ratio b/a of a short to long axis of the vibrational ellipse for one of the eigenwaves of transmission tensor. In all three cases eigenwaves have circular polarization, i.e., the system under consideration can be viewed as a homogeneous bianisotropic media at a short enough wavelength.

Besides, the figures illustrate very good agreement between the exact (Figure 1) and approximate solutions (Figures 2–3) in a wide range of angles of incidence. The same good agreement takes place for computed eigenvalues of transmission and reflection tensors.

4. Conclusion

In this paper, an operator formalism is employed for the introduction of effective material tensors of bianisotropic multilayered periodic structures in a wide wave band. It is based on the approximate calculation of the characteristic matrix of the unit cell of the system with the help of Campbell–Hausdorff series. For a great variety of systems, the series converges quickly.

We show that effective material tensors, not dependent on the parameters of incident wave, can be introduced for media of general type in the wide wave band. That makes it possible to explain effects of form gyrotropy (bianisotropy) in terms of the theory of effective material parameters of multilayered anisotropic systems. By means of computations, both exact and those based on the proposed approximate method, it was demonstrated that some systems, composed from nongyrotropic layers, display gyrotropic properties due to their specific structure.

Computations of parameters of the systems under consideration, carried out by means of characteristic matrices technique, are in good agreement with the approximate results obtained with the use of Campbell–Hausdorff series.

References

1. Serre, J.P. (1965) *Lie Algebras Lie Groups*, Benjamin, New York–Amsterdam
2. Borzdov, A.N. (1997) Effective material parameters of plane stratified bianisotropic superlattices, in A.Priou et al. (eds), *Advances in Complex Electromagnetic Materials, NATO ASI Series, 3* , **vol. 28** , Kluwer Academic Publishers, Dordrecht, pp. 145–154.
3. Gerritsen, H.J. and Yamaguchi, R.T. (1971) A microwave analog of optical rotation in cholesteric liquid crystals, *Am. J. Phys.*, **vol. 39**, pp. 920–923
4. Varadan, V.V., Lakhtakia, A. and Varadan, V.K. (1988) Reflection and transmission characteristics of a structurally chiral slab: Intrinsic anisotropy and form chirality, *Optik*, **vol. 80, no. 1**, pp. 27–32
5. Borzdov, A.N. (1997) Effective properties of plane stratified bianisotropic systems, in W.S. Weiglhofer (ed), *Proc. Bianisotropics'97*, University of Glasgow, Great Britain, pp. 145–148
6. Borzdov, A.N. (1999) Operator formalism in the theory of effective parameters of plane stratified bianisotropic structures, *Electromagnetics*, **vol. 19, no. 6**, pp. 501–512
7. Borzdov, A.N. (2000) Effective constitutive tensors of bianisotropic multilayered mediums, in A.M.Barbosa and A.L.Topa (eds), *Proc. Bianisotropics'2000*, Technical University of Lisbon, Portugal, pp. 131–134
8. Borzdov, A.N. (2000) Effective properties of multilayered bianisotropic systems, in A.M.Barbosa and A.L.Topa (eds), *Proc. Bianisotropics'2000*, Technical University of Lisbon, Portugal, pp. 135–138
9. Vinogradov, A.P., Merzlikin, A.M. (2002) On homogenization of one-dimentional systems, *JETP*, **vol. 121**, pp. 1–8
10. Borzdov, G.N. (1990) Evolution operators of electromagnetic waves in crystals, *Sov. Phys. Cryst.*, **vol. 35, no. 3**, pp. 535–551
11. Barkovskii, L.M., Borzdov G.N. and Lavrinenko, A.V. (1987) Fresnel's reflection and transmission operators for stratified gyroanisotropic media, *J. Phys. A: Math.Gen.*, **vol. 20**, pp. 1095–1106
12. Fedorov, F.I. (1976) *Theory of Gyrotropy*, Nauka i Tekhnika, Minsk
13. Title, A.M. and Rosenberg, W.J. (1981) Tunable birefringent filters, *Optical Engineering* **20**, 815-823.
14. Gantmacher, F.R. (1988) *Theory of Matrices*, Nauka, Moscow.

SELECTIVE REFLECTION AT AN OBLIQUE INCIDENCE OF ELECTROMAGNETIC WAVES ONTO STRATIFIED PERIODIC GYROTROPIC STRUCTURES

I.V. SEMCHENKO and V. E. KAGANOVICH
Department of General Physics, Gomel State University
Sovyetskaya Street 104, 246019 Gomel, Belarus
Fax: + 3-75-232-572412; email: isemchenko@gsu.unibel.by

Abstract. Oblique incidence of electromagnetic waves onto stratified periodic gyrotropic structures is considered. Gyrotropic properties of this multilayered medium are stipulated by the effect of an external magnetic field. By means of the matrix method the dependence of intensity of reflected and transmitted waves on the angle of incidence, number of cells and strength of external magnetic field are obtained. Such a structure, exhibiting the selective reflection of electromagnetic waves, can be used as the polarization converter controlled by a magnetic field.

1. Introduction

Multilayer composite materials have been of great interest for many years in the scientific community dealing with the electromagnetic properties of materials [1]-[11]. Works [1]-[3] describe magneto-optics in a unique framework. It is shown that in the thin-film limit, the Kerr effect obeys an additivity law for a system consisting of any number of magnetic films. The prediction is verified experimentally and in numerical calculations on an Fe/Cu/Fe 3-layer stack grown on a Pb-substrate. An elementary formula is derived for the magneto-optic Kerr effect from model superlattices. The features of interaction of light with the periodic bigyrotropic media are researched in the work [4]. Coefficients of reflection and transmition, ellipticity and turn angle of a polarization plane of a light wave in resonance and nonresonance frequency bands are obtained. Method of 4×4 matrixes is offered to use in paper [5] for the description of propagation of electromagnetic waves in bianisotropic chiral stratified structures. The dependences of amplitudes and polarization characteristics of reflected and transmitted waves from the angle of incidence of a wave are investigated. The reflection and

S. Zouhdi et al. (eds.), Advances in Electromagnetics of Complex Media and Metamaterials, 271–280.

transmission of light in stratified anisotropic structures containing layers which interact in coherent and incoherent modes with a transmitted light wave is considered in paper [6]. In paper [7] the formulas of intensity and polarization of a reflected and transmitted light for a case of the three-layered system are obtained. The system consists of a ferromagnetic film and nonmagnetic layers, bounding with it. The effects of an interference and attenuation of light are taken into account. In paper [8] the expression of the Fresnel coefficients for a wave incident on a semi-infinite composite are derived. In papers [9]-[11] the properties of lamellar insulator ferromagnetic on the edge material in a microwave device under a static field are studied.

2. Theory

One of the possibilities of creation of controlled converters of electromagnetic waves polarization is the use of stratified periodic structures, combining the properties of their components.

The additional control of an electromagnetic wave at an oblique incidence on the boundary of stratified periodic structure is possible. The wave intensity and polarization depend on the angle of wave propagation in the multilayered structure. We take into account that the eigenmodes propagate in gyrotropic layer at different angles with respect to boundary.

We consider a stratified periodic structure, consisting of any quantity of elementary cells, placed in an external magnetic field. It is supposed, that the first layer of such a cell is isotropic, and does not possess the gyrotropic properties. The second layer is also isotropic, however it possesses the gyrotropic properties, that leads to circular birefringence of waves inside the layer (see fig. 1).

For a gyrotropic layer of such a structure the constitutive equations have the form [12, 13]

$$\begin{cases} \vec{D} = \varepsilon_0 \varepsilon \vec{E} + i\varepsilon_0 \vec{g} \times \vec{E} \\ \vec{B} = \mu_0 \mu \vec{H} \end{cases} \tag{1}$$

where ε and μ are relative permittivity and relative permeability, $\vec{g}$ is the vector of gyrotropy, dependent on crystallographic symmetry of a medium and vector of strength of an external magnetic field.

The continuity of tangential components of electric and magnetic field strength vector on the boundary of layers can be described by means of 4×4 matrix which connects the incident wave with transmitted and reflected waves. Elements of such a matrix I_{ij} $(i, j = 1, 2, 3, 4)$, connecting an incident wave to transmitted and reflected waves on the boundary of nongyrotropic

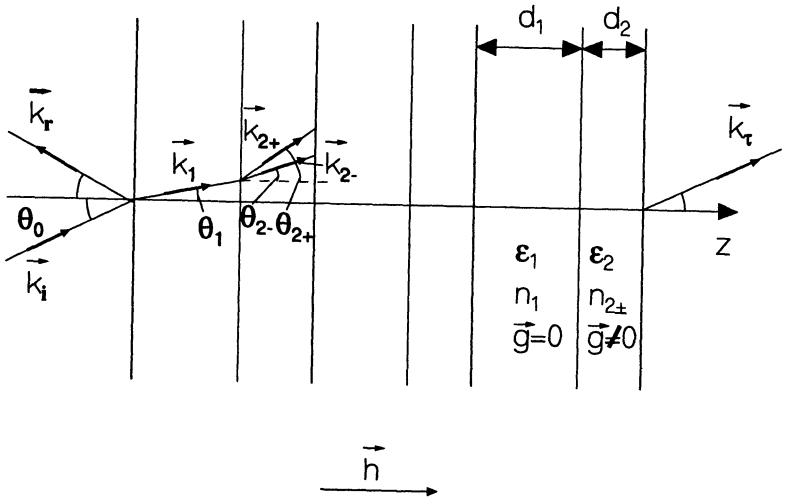

Figure 1. Schematic representation of a gyrotropic stratified periodic medium.

and gyrotropic media, are following:

$$
\begin{aligned}
\mathrm{I}_{11} &= A_{+}^{(2)} & \mathrm{I}_{12} &= \alpha_{-}\cos(\theta_{-})A_{-}^{(2)} \\
\mathrm{I}_{13} &= -A_{+}^{(1)} & \mathrm{I}_{14} &= \alpha_{-}\cos(\theta_{-})A_{-}^{(1)} \\
\mathrm{I}_{21} &= \frac{B_{+}^{(2)}}{\alpha_{+}\cos(\theta_{+})} & \mathrm{I}_{22} &= B_{-}^{(2)} \\
\mathrm{I}_{23} &= \frac{-B_{+}^{(1)}}{\alpha_{+}\cos(\theta_{+})} & \mathrm{I}_{24} &= B_{-}^{(1)} \\
\mathrm{I}_{31} &= \mathrm{I}_{13} & \mathrm{I}_{32} &= -\mathrm{I}_{14} \\
\mathrm{I}_{33} &= \mathrm{I}_{11} & \mathrm{I}_{34} &= -\mathrm{I}_{12} \\
\mathrm{I}_{41} &= -\mathrm{I}_{23} & \mathrm{I}_{42} &= \mathrm{I}_{24} \\
\mathrm{I}_{43} &= -\mathrm{I}_{21} & \mathrm{I}_{44} &= \mathrm{I}_{22}
\end{aligned}
\tag{2}
$$

where

$$
A_{\pm}^{(p)} = \frac{\mu_2 n_1 \cos(\theta_1) + (-1)^p \mu_1 n_{\pm} \cos(\theta_{\pm})}{2\mu_2 n_1 \cos(\theta_1)}
$$

$$B_{\pm}^{(p)} = \frac{\mu_2 n_1 \cos(\theta_{\pm}) + (-1)^p \mu_1 n_{\pm} \cos(\theta_1)}{2\mu_2 n_1 \cos(\theta_1)}$$

$$\alpha_{\pm} = \frac{i\mu_2 g_z}{(n_{\pm})^2 - \mu_2 \varepsilon_2}$$

$p = 1, 2$, indexes $+$ and $-$ specify membership of parameters to left and right circular component of waves; θ_+ and θ_- are angles between an axis z and wave vectors of left and right circular component of a wave in a gyrotropic layer; θ_1 is an angle between an axis z and a wave vector of a wave in a nongyrotropic layer; μ_1, ε_1, $n_1 = \sqrt{\varepsilon_1 \mu_1}$ are relative permeability, relative permittivity and refraction factor of a layer, not possessing the gyrotropic properties; μ_2, ε_2 are relative permeability and relative permittivity of gyrotropic layer. Refraction factor of gyrotropic layer equals

$$n_{\pm} = \sqrt{\frac{2\mu_2\varepsilon_2^2 - \mu_2 g_z^2 \sin^2(\theta_{\pm}) \mp \sqrt{\mu_2^2 g_z^4 \sin^4(\theta_{\pm}) + 4\mu_2^2 \varepsilon_2^2 g_z^2 \cos^2(\theta_{\pm})}}{2\varepsilon_2}}$$

where g_z is z-component of a vector of gyrotropy.

Elements of matrix J_{ij} (i, j = 1, 2, 3, 4), connecting an incident wave to transmitted and reflected waves on the boundary of gyrotropic and nongyrotropic media can be expressed in a similar way:

$$\begin{aligned}
\mathrm{J}_{11} &= -D_+ - C_+ \cos(\theta_1) & \mathrm{J}_{12} &= D_+\alpha_- \cos(\theta_1) + C_+ \cos^2(\theta_-)\alpha_- \\
\mathrm{J}_{13} &= D_+ - C_+ \cos(\theta_1) & \mathrm{J}_{14} &= D_+\alpha_- \cos(\theta_1) - C_+ \cos^2(\theta_-)\alpha_- \\
\mathrm{J}_{21} &= \frac{D_- + C_- \cos(\theta_1)}{\alpha_- \cos(\theta_-)} & \mathrm{J}_{22} &= \frac{-D_+\alpha_- \cos(\theta_1) - C_- \cos^2(\theta_+)\alpha_+}{\alpha_- \cos(\theta_-)} \\
\mathrm{J}_{23} &= \frac{-D_- + C_- \cos(\theta_1)}{\alpha_- \cos(\theta_-)} & \mathrm{J}_{24} &= \frac{-D_+\alpha_- \cos(\theta_1) + C_- \cos^2(\theta_+)\alpha_+}{\alpha_- \cos(\theta_-)} \\
\mathrm{J}_{31} &= \mathrm{J}_{13} & \mathrm{J}_{32} &= -\mathrm{J}_{14} \\
\mathrm{J}_{33} &= \mathrm{J}_{11} & \mathrm{J}_{34} &= -\mathrm{J}_{12} \\
\mathrm{J}_{41} &= -\mathrm{J}_{23} & \mathrm{J}_{42} &= \mathrm{J}_{24} \\
\mathrm{J}_{43} &= -\mathrm{J}_{21} & \mathrm{J}_{44} &= \mathrm{J}_{22}
\end{aligned} \tag{3}$$

where

$$D_{\pm} = \frac{1}{2}\frac{\alpha_{\pm}}{\alpha_- - \alpha_+}, \; C_{\pm} = \frac{1}{2}\frac{\mu_2}{n_{\pm}}\frac{n_1}{\mu_1}\frac{\cos(\theta_{\pm})\alpha_{\pm}}{\cos^2(\theta_-)\alpha_- - \cos^2(\theta_+)\alpha_+}$$

The matrix, describing wave propagation in a medium, D_j has a standard diagonal view [14]:

$$D_j = \begin{pmatrix} e^{i\vec{k}_{j+}(\vec{r}_a-\vec{r}_b)} & 0 & 0 & 0 \\ 0 & e^{i\vec{k}_{j-}(\vec{r}_a-\vec{r}_b)} & 0 & 0 \\ 0 & 0 & e^{i\vec{k'}_{j+}(\vec{r}_a-\vec{r}_b)} & 0 \\ 0 & 0 & 0 & e^{i\vec{k'}_{j-}(\vec{r}_a-\vec{r}_b)} \end{pmatrix} \quad (4)$$

where $\vec{k}_{j\pm}$ are wave vectors of left- or righthanded circularly polarized waves in a j-th layer, propagating with the z-direction, $\vec{k'}_{j\pm}$ are wave vectors of left- or righthanded circularly polarized waves in a j-th layer, propagating opposite to the z-direction, $\vec{r}_a$ and $\vec{r}_b$ are radius-vectors of boundary of a j-th layer.

Using boundary conditions for waves in each layer, we have calculated the matrix M, which connects the incident wave with transmitted and reflected waves [14, 15]

$$M = JD_1ID_2 \quad (5)$$

If the stratified periodic structure consists of N elementary cells, we have to raise the matrix M to power N. The matrix M^{eff} for the whole stratified periodic structure can be written down as product

$$M^{eff} = I_a M^N I_b \quad (6)$$

where I_a and I_b are matrixes of transmission of an electromagnetic wave through the boundaries between air and structure.

To obtain the maximum of reflection by each cell at an oblique incidence of waves, the thickness of layers has to satisfy to following relations

$$2k_1d_1\cos(\theta_1) = (2m_1+1)\pi,\ 2k_2d_2\cos(\theta_2) = (2m_2+1)\pi \quad (7)$$

where m_1 and m_2 are integer numbers, k_1 and k_2 are wave numbers of right- or lefthanded circularly polarized waves in the first and the second layer, θ_1 and θ_2 are angles between an axis z and wave vectors of left and right circular component wave in the first and second layer.

Selecting the thickness of a gyrotropic layer, depending on frequency of electromagnetic waves and strength of a magnetic field we can obtain the maximum reflection for one circularly polarized wave and simultaneously minimum for opposite polarization. If we increase the number of cells of structure the intensity of one reflected circularly polarized wave monotonously increases and reaches the saturation. Intensity of another circularly polarized reflected wave oscillates, periodically accepting close to

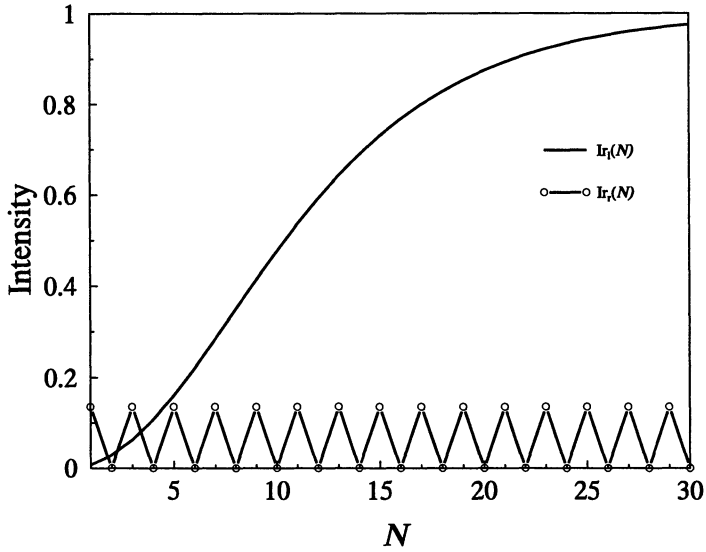

Figure 2. Dependence of normalized intensity of a reflected wave on the number of cells in case of incidence of lefthanded and righthanded circularly polarized waves.

the zero value (see fig. 2). It enables to obtain the polarization of a reflected wave close to circular.

3. Numerical calculation

We calculate the intensity and polarization of transmitted and reflected waves with the help of matrix elements.

Figures 3 and 4 show the dependence of the normalized intensities of reflected and transmitted waves on the angle incidence in case of incidence of lefthanded wave. Figures 5 and 6 present the similar dependence in case of incidence on a stratified periodic structure of righthanded wave.

It is visible from figures 3 and 4 that at the estimated value of an angle of incidence (15°) for a lefthanded polarized wave the local maximum of intensity of a reflected wave is observed and, consequently, minimum for a transmitted wave. At the same time for an incident righthanded wave (see figures 5 and 6) the maximum of reflection takes place under another angle of incidences.

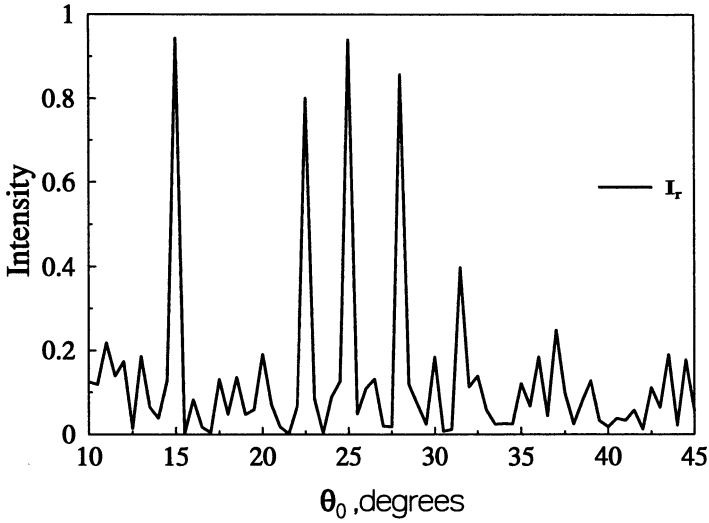

Figure 3. Dependence of normalized intensity of a reflected wave on the angle of incidence in case of incidence of lefthanded circularly polarized wave.

As you can see from the figure 7, the intensity of a reflected wave has the maximum value in case of incidence of a lefthanded polarized wave and intensity is close to zero in case of incidence of a righthanded wave.

The polarization selectivity as well as frequency selectivity are possible at wave reflection from the gyrotropic stratified periodic structure in an external magnetic field. If we change an angle of incidence or an external magnetic field or the frequency of electromagnetic waves both transmitted and reflected waves change their polarization properties. This allows to use this structure, exhibiting selective reflection of electromagnetic waves, as the polarization converter controlled by a magnetic field.

4. Conclusion

We have considered oblique incidence of electromagnetic waves onto stratified periodic gyrotropic structures. Gyrotropic properties of this multilayered medium are stipulated by the effect of an external magnetic field. By means of the matrix method the dependence of intensity of reflected and transmitted waves on the angle of incidence, number of cells and strength of external magnetic field are obtained. The additional control of an electromagnetic wave at an oblique incidence on the boundary of a stratified periodic structure is possible.

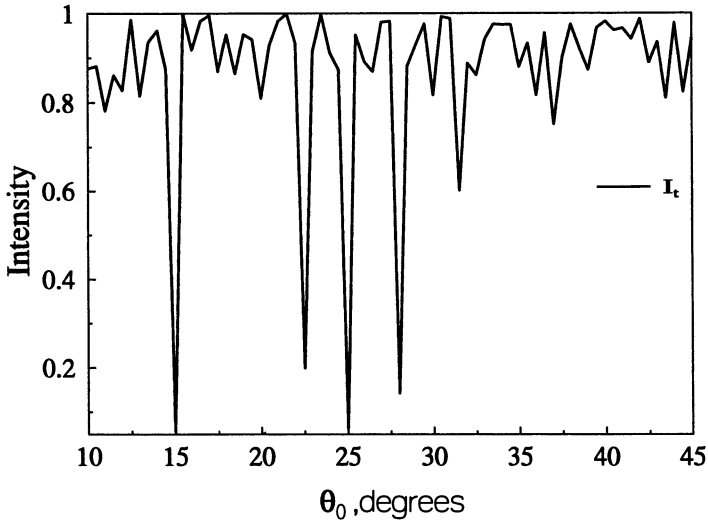

Figure 4. Dependence of normalized intensity of a transmitted wave on the angle of incidence in case of incidence of lefthanded circularly polarized wave.

References

1. Zak, J., Moog, E.R., Liu, C. and Bader, S.D. (1990) Additivity of the Kerr effect in thin-film magnetic systems, *J. Magn. Magn. Mat.*, **Vol. 88**, pp. L261–L266
2. Zak, J., Moog, E.R., Liu, C. and Bader, S.D. (1990) Universal approach to magneto-optics, *J. Magn. Magn. Mat.*, **Vol. 89**, pp. 107–123
3. Zak, J., Moog, E.R., Liu, C. and Bader, S.D. (1991) Elementary formula for the magneto-optic Kerr effect from model superlattices, *Appl. Phys. Lett.*, **Vol. 58 no. 11**, pp. 1214–1216
4. Ivanov, O.V., Sementsov, D.I. (1996) Magneto-optical interaction of light with the periodic bigyrotropic medium, *Crystallography*, **Vol. 41 no. 5**, pp. 791–797 (in Russian)
5. Ivanov, O.V., Sementsov, D.I. (2000) Propagation of light in chiral stratified media. A method of 4×4 matrixes, *Crystallography*, **Vol. 45 no. 3**, pp. 534–540 (in Russian)
6. Ivanov, O.V., Sementsov, D.I. (2000) Coherent and incoherent reflection and transmission of light through anisotropic stratified structures, *Crystallography*, **Vol. 45 no. 5**, pp. 899–904 (in Russian)
7. Maevski, V.M. (1985) The theory of magneto-optical effects in multilayered systems with arbitrary orientation of magnetization, *Physics of metals and physical metallurgy*, **Vol. 59 no. 2**, pp. 213–219 (in Russian)
8. Acher, O., Adenot, A.L. and Duverger, F. (2000) Fresnel coefficients at an interface with a lamellar composite material, *Phys. Rev. B*, **Vol. 62 no. 20**, pp. 13748–13756
9. Olivier Acher, Pierre Le Gourriérec, Géraldine Perrin, Philippe Baclet and Olivier Roblin (1996) Demonstration of anisotropic composites with tuneable microwave

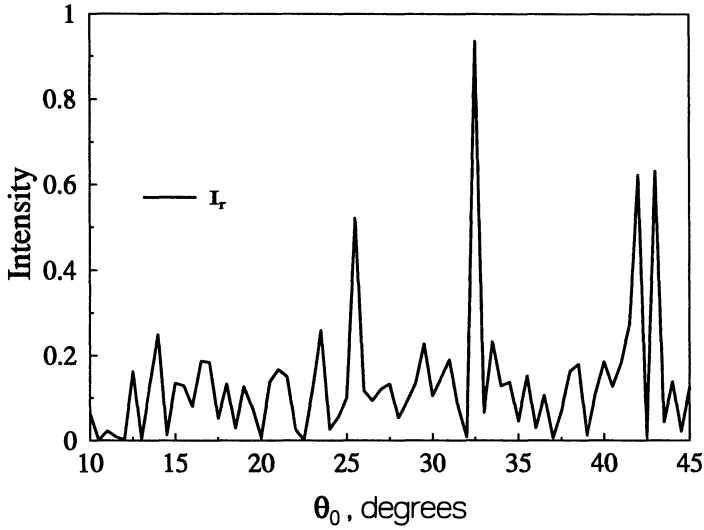

Figure 5. Dependence of normalized intensity of a reflected wave on the angle of incidence in case of incidence of righthanded circularly polarized wave.

permeability manufactured from ferromagnetic thin films, *IEEE Trans. Microwave Theory Tech.*, **Vol. 44 no. 5**, pp. 674–684

10. Acher, O., Baclet, P., Perrin, G., Roblin, O., Le Gourriérec, P. (1996) Investigation of the microwave permeability of ferromagnetic film laminations under a magnetic field, *J. Magn. Magn. Mater.*, **Vol. 157/158**, pp. 480–481
11. Adenot, A.L., Acher, O., Taffary, T., Quéffélec, P. and Tanné, G. (2000) Tuneable microstrip device controlled by a weak magnetic field using ferromagnetic laminations, *J. Appl. Phys.*, **Vol. 87 no. 9**, pp. 6914–6916
12. Fedorov, F.I. (1976) *Theory of gyrotropy.* Science and Technics, Minsk, (in Russian).
13. Konstantinova, A.F., Grechuschnikov, B.N., Bokut', B. V., Valyaschko, E.G. (1995) *Optical properties of crystals.* Science and Technics, Minsk, (in Russian).
14. Azzam, R.M.A., Bashara, N. M. (1977) *Ellipsometry and polarized light.* North-Holland Publishing Company.
15. Amnon Yariv, Pochi Yeh. (1984) *Optical waves in crystals.* A Wiley-Interscience Publication, John Wiley and Sons.

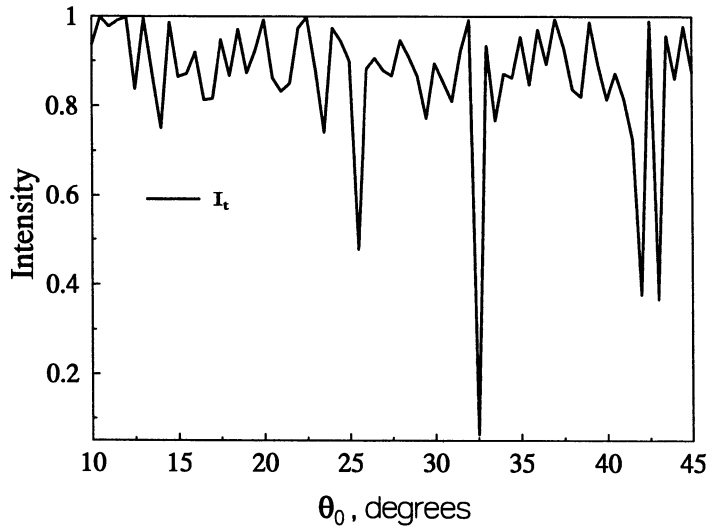

Figure 6. Dependence of normalized intensity of a transmitted waves on the angle of incidence in case of incidence of righthanded circularly polarized wave.

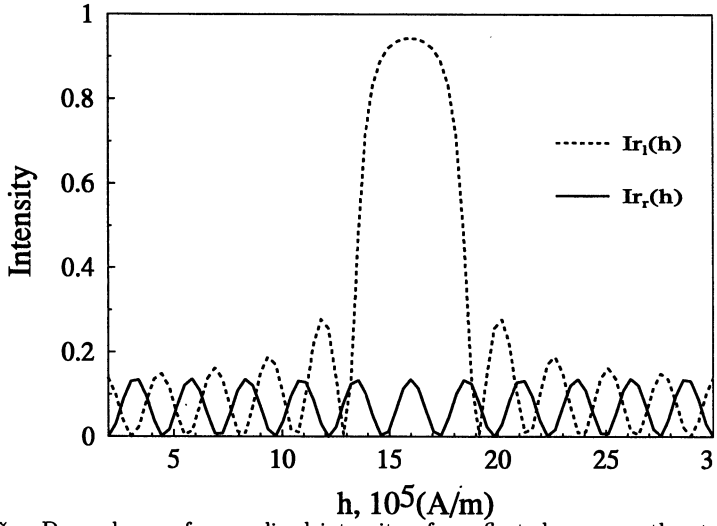

Figure 7. Dependence of normalized intensity of a reflected wave on the strength of an external magnetic field in case of incidence of lefthanded and righthanded circularly polarized waves.

RESONANCES OF CLOSED MODES IN THIN ARRAYS OF COMPLEX PARTICLES

SERGEY PROSVIRNIN
Institute of Radio Astronomy
Krasnoznamennaya Street 4, Kharkov 61002, Ukraine
AND
SAID ZOUHDI
Laboratoire de Génie Électrique de Paris LGEP–Supélec
Plateau de Moulon, 91192 GIF–SUR–YVETTE Cedex, France

Abstract. Numerical analysis of the reflection properties of double-periodic thin arrays is carried out. This analysis indicates the presence of extremely high quality band stop and band pass resonances due to the excitation of non-symmetric current mode.

1. Introduction

Controlling the reflection and/or the transmission frequency properties of surfaces is an important problem of applied electromagnetics. For various microwave applications, there is a need to use active material layers with thicknesses extremely small in comparison to the wavelength. These frequency selective surfaces (FSS) are boundary surfaces consisting of some metal or dielectric bodies or the surfaces separated volumes in which there is a need to obtain electromagnetic fields possessing radical different characteristics.

There are several well known periodic arrays of different shapes (rectangular, circular) metal patches (e.g. [3], [4]) and the self-resonant grids such as grids of Jerusalem conducting crosses [1] which are used as FSS. Practically, the first low frequency resonance of such structure appears for a wavelength a bit greater than the array period. As a consequence of this, the transversal size of the whole FSS must be larger in comparison to the wavelength. The quality factor of such structures resonances is not high.

However, the situation is different with the arrays of complex shape resonating particles in that the array resonance is practically the same as the resonance of an individual particle. Conducting particles with resonant

S. Zouhdi et al. (eds.), Advances in Electromagnetics of Complex Media and Metamaterials, 281–290.

size of the order $\lambda/10$ are well known. So the total size of the array may be approximately the same as a wavelength. Recently, great attention has been paid to the study of frequency selective properties of complex shaped particles arrays, such as for example a bianisotropic Ω-shaped planar conducting particle [7], [12], a plano-chiral S-shaped particle [8] and C-shaped particle [10]. The properties of arrays of Ω, S, C-shaped particles and some other ones are well known now. In short, they have simple resonance characteristics and low quality factors.

If we want to design very thin structures having resonant band reflecting or transmitting characteristics with a high quality factor, the next step is to focus on the way of the structure complexity. Multi-particle arrays have these desired properties.

The problems of producing artificial dielectric possessing higher values of effective permittivity and photonic band gap structures are very close to the FSS problem mentioned above.

Commonly, complex materials are fabricated by randomly embedding most often simple metal inclusions like disks, spheres, ellipsoids or needles into a dielectric matrix. These particles have small sizes compared to the wavelength in the host medium and are located so that the distance between them is also small with respect to λ. Such materials possess an effective permittivity of a small value of the order of few units within a wide frequency band. In some applications, however, one needs very high values of effective permittivity at least within a narrow frequency band [2]. The introduction of high quality factor resonating particles in the layer is only one of the ways allowing to solve the problem.

Besides, the required curing process of the host materials and the fixed shape, size, and concentration of the samples are disadvantages. To avoid these difficulties, one can use layered materials with planar periodic arrays of conducting particles on the surface of each layer produced by inexpensive lithography process. Thus, the main purpose of this work is the study of resonance properties of multi-particle arrays which can possess band pass or band stop frequency characteristics with high quality factors.

2. Resonances of Closed Modes

Generally speaking, the resonance high quality factor and the layer small thickness are contradictory requirements. Actually, very thin open structure usually cannot have inner resonating volumes and on the other hand, resonating inclusions are strongly coupled with free space. Consequently, their resonance quality factor is low.

Nevertheless, there are ways to produce thin structures showing high quality frequency resonances thanks to the use of both the field excitation

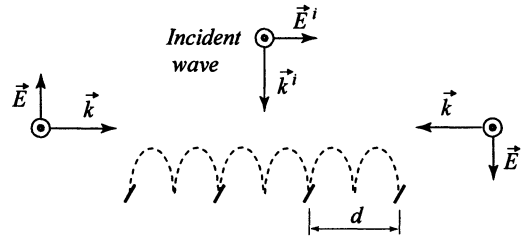

Figure 1. A grating of narrow inclined strips.

in large resonance volume and extremely reducing the coupling between resonating inclusions and free space. This has been achieved by a resonance regime of a so-called *closed modes.*

2.1. FULL REFLECTION FROM THIN STRIP GRATING DUE TO LARGE RESONANCE VOLUME

As an example of a very thin structure with *large resonance volume*, let us consider one-periodic planar grating of very thin narrow infinitely long metal strips (see Figure 1). Let us firstly consider the case of strips placed in grating so that their planes are orthogonal to the grating plane. If a normally incident plane wave polarized orthogonally impinges on the strips, the reflection coefficient of such a knife grating is equal to zero for any frequency.

Let us now incline the strip planes with regard to their plane in the knife grating. The strip width is much smaller than the wavelength. There is now weak interaction between the incident wave and the grating. If the wavelength value is close to the grating period but the shade is larger than it $\lambda \gtrsim d$, a sharp resonance of full reflection occurs. The reason behind the resonance reflection is an indication of a standing wave along the grating plane. The nodes of standing waves are placed in the strip positions. The field of the standing wave occupies a large volume and it is weakly coupled to the field of the incident wave. If the strip width or the strip plane inclination angle decrease, the resonance quality factor of rises.

This full reflection effect was analyzed in [11]. Normal incidence is a requirement for full reflection. Resonance reflection takes place in the case of inclined incidence also but the value of the reflection coefficient is less than one in this case. If we increase the angle of incidence, the first spatial partial wave appears and the resonance reflection vanishes.

The disadvantage for a practical use of this effect is the nearness of resonance frequency of the full reflection to the frequency of the grating first partial waves producing side lobes.

2.2. EIGEN MODES OF TWO-ELEMENT PARTICLES

Resonance regime of closed modes in double periodic arrays of multi-element plane particles is more convenient for microwave applications.

There is a well known the work which analyzed resonance properties of two-element bi-helix particle [6]. Let us mention also the work [5] which is very close to this subject and which studied two-slot waveguide diaphragms.

A two-element particle may be considered as a reciprocal two-port network. The properties of particle consisting of coupled elements are determined by a matrix of complex impedances

$$\mathbf{Z} = \begin{pmatrix} Z_1 & Z_c \\ Z_c & Z_2 \end{pmatrix} \tag{1}$$

where Z_1 and Z_2 are proper impedances of first and second element respectively, Z_c is a mutual coupling impedance. These impedances are frequency dependent values. Eigenfrequencies of two element particles can be found by solving the following equation,

$$\det(\mathbf{Z}) = 0. \tag{2}$$

If the elements of particle are different and have different values of proper impedances

$$Z_2 = Z_1 + \zeta \tag{3}$$

The solution of equation (2) can be found in the form

$$Z_1 = -\zeta/2 \pm \sqrt{(\zeta/2)^2 + Z_c^2}. \tag{4}$$

Thus, two element particle has two lower eigenfrequencies as follows from (4).

Eigen currents in elements of particle are satisfying the set of equations

$$Z_1 I_1 + Z_c I_2 = 0 \tag{5}$$

$$Z_c I_1 + Z_2 I_2 = 0. \tag{6}$$

Two eigenmodes have currents

$$I_2 = -I_1 \left(\sqrt{1 + \eta^2} - \eta \right) \tag{7}$$

$$I_2 = I_1 \left(\sqrt{1 + \eta^2} + \eta \right) \tag{8}$$

corresponding to upper and lower sign in expression (4). Here $\eta = \zeta/(2Z_c)$.

If elements of particle are identical, an exact solution of equation (2) can be obtained

$$Z_1 = \pm Z_c. \tag{9}$$

Eigenmodes have currents $I_2 = -I_1$ and $I_2 = I_1$ respectively.

In the case ζ has a small value, the particle has eigenfrequencies and eigenmodes close to those of particle of identical elements. The difference between the resonant frequencies of particles consisting of two identical elements and the resonant frequency of the same single element resides in the fact that the latter one corresponds to the greatest value of the mutual coupling impedance. If the coupling of identical elements is small, the resonant frequency as for the symmetric current distribution so as for the non-symmetric one (closed mode resonance) is approximately the same as the resonant frequency of the single element of particle.

3. Two-Element Arrays of Complex Shaped Particles

Very sharp resonances of reflection from infinitely thin double-periodic *multi-element* FSS can appear due to resonant properties of strip particles of periodic cell. *Multi-particle* structure of array cell is essential to existence of higher quality resonance of closed mode. For the sake of simplicity we restrict ourselves only to the case of array of two-element particles.

The method of moments is used to solve the problem of electromagnetic scattering by arrays of thin narrow curvilinear strips.

3.1. TWO-ELEMENT ARRAY WITH IDENTICAL ELEMENTS

For example let us consider first a double-periodic two-element array. Each cell of this array contains two identical strip elements opposite one to another. The left split between the strips is a little different from the right split, so that the unit cell is dissymmetric with regards to Oy axis (see Figure 2). The frequency dependence of the reflection coefficients magnitudes are shown in Figure 2. In the same figure the reflection coefficients magnitudes corresponding to an array of one-element C-shaped particles are shown for comparison.

If a normal incident wave is polarized in y direction, a sharp reflection resonance occurs (see curve 4). This resonance corresponds to a closed mode (non-symmetric current mode in two-element particle) because equal and opposite directed currents in the two elements complex particle radiate a little in free space. If the incident is x-polarized wave, a symmetric current mode is exited only. The corresponding resonance has low quality factor. The mutual coupling between the particle elements is not large so closed mode resonance and resonance of symmetric current distribution exited by

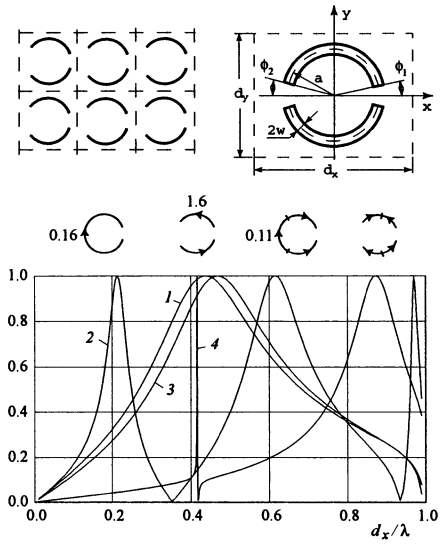

Figure 2. Absolute values of the reflection coefficients of arrays without substrate : $d_x = d_y = 3$ mm, $a = 1.25$ mm, $\phi_1 = 10°$, $2w = 0.1$ mm, r_{xx} (curve 1) and r_{yy} (curve 2) of an array of C-shaped particles ($\phi_2 = 0°$); r_{xx} (curve 3) and r_{yy} (curve 4) of a two-element particles array: the elements of the unit particle are identical, ($\phi_2 = 15°$: the unit cell is dissymmetric with regards to Oy axis).

x-polarized incident wave have approximately equal frequencies. However, the quality factors of these resonances are essentially different. Current distributions and maximum conventional values of current are shown above in Figure 2. They are concerned with resonance frequencies in the case of incident wave polarized along Oy axis. The current maximum value corresponding to the closed mode resonant frequency largely exceeds the current values at usual resonances.

If non-symmetry encreases, the quality factor of the closed mode resonance decreases (see Figure 3).

Reflection characteristics of an array placed on a substrate are similar. Resonant frequencies are shifted to low values. In general the level of reflection is higher in comparison to the one corresponding to an array without substrate (see Figure 4).

3.2. TWO-ELEMENT ARRAY WITH DIFFERENT ELEMENTS

Let us now consider reflection by an array of two different length elements in each cell. They are placed symmetrically to Oy axis as shown in Figure 5. The properties of an array with symmetrically placed different length elements are qualitativly quite different from the array with identical

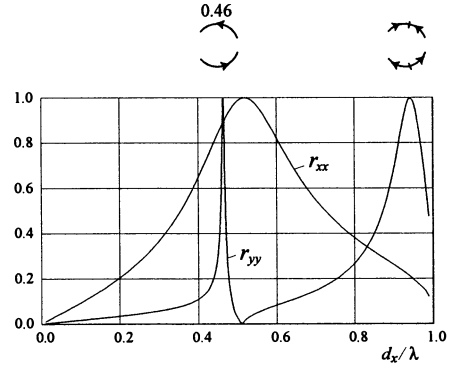

Figure 3. Absolute values of the reflection coefficients of an array without substrate: the elements of the unit particle are identical, $d_x = d_y = 3$ mm, $a = 1.25$ mm, $2w = 0.1$ mm, $\phi_1 = 10°$, $\phi_2 = 30°$ (the unit cell is dissymmetric with regards to Oy axis).

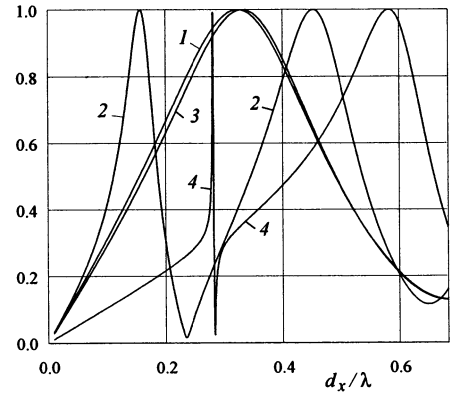

Figure 4. Absolute values of the reflection coefficients of arrays on substrate: $d_x = d_y = 3$ mm, $a = 1.25$ mm, $\phi_1 = 10°$, $2w = 0.1$ mm, $\varepsilon = 3$, $h = 0.25$ mm, r_{xx} (curve 1) and r_{yy} (curve 2) of an array of C-shaped particles ($\phi_2 = 0°$); r_{xx} (curve 3) and r_{yy} (curve 4) of a two-element particles array: the elements of the unit particle are identical, ($\phi_2 = 2.5°$: the unit cell is dissymmetric with regards to Oy axis).

elements. In these arrays non-symmetric high quality current mode can appear against the excitation of the usual symmetric mode.

There are two closely located reflection maxima and a very sharp resonance of full transmittance between frequencies of full reflection. Each reflection resonance appears, roughly speaking, due to the excitation of one of the elements of complex particle. A full transmittance resonance appears due to non-symmetric current mode in the two-element particle. It is a high quality closed mode resonance. Current amplitudes in the case of non-symmetric current mode are approximately equal in each part of

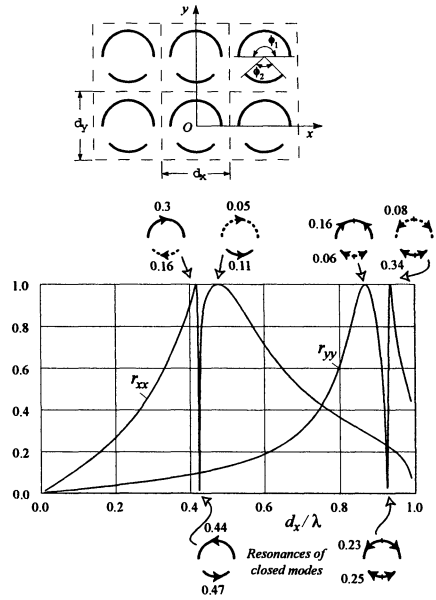

Figure 5. Absolute values of the reflection coefficients of an array without substrate: the elements of the unit particle have different lengths, $d_x = d_y = 3$ mm, $a = 1.25$ mm, $2w = 0.1$ mm, $\phi_1 = 160°$, $\phi_2 = 148°$, (the unit cell is symmetric with regards to Oy axis).

the two-element particle. In Figure 5, resonant and non-resonant current distributions are shown respectively by solid and dashed lines.

So one can obtain thin narrow-band filter of full transmittance. The narrow-band transparent properties of the array of different-element particles are quite similar to the rejection properties of a two-aperture iris in a rectangular waveguide studied in [5].

3.3. CLOSED MODES OF THE GRATING OF WAVY STRIPS

The next example of structures showing closed mode resonance is a grating of wavy strips (see Figure 6). The scattering of electromagnetic waves by gratings of wavy strips was analyzed in [9].

Let us note that the grating of narrow straight strips is approximately fully transparent for incident wave orthogonally polarized with respect to strips. In the case of gratings of wavy strips and the same y-polarization of incident wave, the currents on the two halves of the strip in the boundaries of the grating cell are equal in values but oppositely directed along the Ox axis (see Figure 7) owing to the symmetry of the grating. We can consider the grating of wavy strips as a two-element array. Actually, a current on

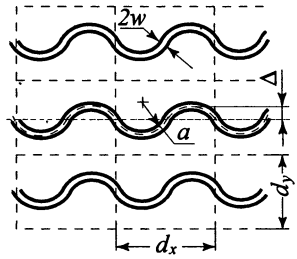

Figure 6. A grating of wavy strips.

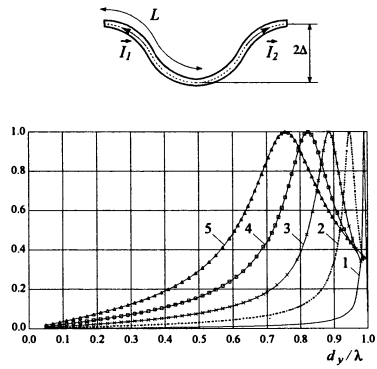

Figure 7. Absolute values of the reflection coefficients: grating of wavy strips without substrate, $d_x = d_y$, $2w/d_y = 0.05$, $\Delta/d_y = 0.05$ (curve 1), 0.1 (curve 2), 0.15 (curve 3), 0.2 (curve 4), 0.25 (curve 5).

the strip has zero values for such excitation in the points where a tangent to the strip is parallel to Ox axis. We can imagine strips cut in these points. Now the grating may be considered as a two-element array of curvilinear dipoles. Thus, such a two-element array consists of identical elements but placed at different locations and its reflection properties are similar to the properties of the array considered in Section 3.1.

If half of length of stretched strip placed in the period cell of the grating is approximately equal to half of wavelength $L = \lambda/2$ a resonance reflection appears. The set of dependencies magnitude of reflection coefficient r_{yy} versus normalized frequency is shown in Figure 7 for different values of amplitude of wavy strip Δ/d_y. If the amplitude of the wavy strip decreases the quality factor of reflection resonance increases.

4. Conclusions

Thus, two-element arrays of strip particles are very thin structures which can possess extremely high quality reflection or transmission resonances

due to the excitation of non-symmetric current mode. Because such current mode weakly couples with free space, these resonances are similar to resonances of closed modes in finite widening extension of single-mode waveguide. If elements of stretched lengths placed in one array cell are different from each other, very sharp transmission resonances can appear in the rejection frequency band.

One can expect to obtain more complex resonance frequency characteristics due to use of multi-element arrays.

Electron devices such as photo diodes and *p-i-n* diodes may be used for the array properties control. Due to switching diodes one can modify a geometry of array particle from one-element to two-element by connecting or disconnecting elements in complex particles of array.

References

1. Anderson, I.: 1975, 'On the theory of self-resonant grids'. *The Bell system technical journal* **55**, 1725–1731.
2. Chang, W.: 1966, 'Infinite phased bipole arrays'. *Proc. IEEE* **56**, 1892–1900.
3. Chen, C. C.: 1970, 'Scattering by a two-dimensional periodic array of conducting plates'. *IEEE Trans. Antennas Propagat.* **AP–18**(9), 660–665.
4. Cwik, T. A. and R. Mittra: 1987, 'Scattering from a periodic array of free-standing arbitrarily shaped perfectly conducting or resistive patches'. *IEEE Trans. Antennas Propogat.* **35**(11), 1226–1234.
5. Kirilenko, A. A. and L. P. Mospan: 2000, 'Reflection resonances and natural oscillations of two-aperture iris in rectangular waveguide'. *IEEE Trans. Microwave Theory Tech.* **48**(8), 1419–1421.
6. Lagarkov, A., V. Semenenko, V. Chistyaev, D. Ryabov, S. Tretyakov, and C. Simovski: 1997, 'Resonance properties of bi-helix media at microwaves'. *Electromagnetics* **17**(3), 213–237.
7. Norgren, M. and S. He: 1994, 'Electromagnetic reflection and transmission for a dielectric-omega interface and an omega-slab'. *Int. J. Infrared Millim. Waves* **15**, 1537–1554.
8. Prosvirnin, S.: 1998, 'Analysis of electromagnetic wave scattering by plane periodical array of chiral strip elements'. In: *Proc. of 7-th Intern. Conf. on Complex Media "Bianisotropics-98"*. Braunschweig, Germany, pp. 185–188.
9. Prosvirnin, S., S. Tretyakov, and P. Mladyonov: 2002, 'Electromagnetic wave diffraction by planar periodic gratings of wavy metal strips'. *J. Electromagnetic Waves and Applications* **16**(3), 421–435.
10. Prosvirnin, S., S. Tretyakov, T. Vasilyeva, A. Fourrier-Lamer, and S. Zouhdi: 2000, 'Analysis of reflection and transmission of electromagnetic waves in complex layered arrays'. *Journal of Electromagnetic Waves and Applications* **14**(6), 807–826.
11. Vorob'ev, S. N. and S. L. Prosvirnin: 1988, 'Total reflection of electromagnetic waves from a widely spaced grating formed by tilted metal strips'. *Sov. Phys.-Tech. Phys. (USA)* **33**(3), 276–281.
12. Zouhdi, S., G. E. Couenon, and A. Fourrier-Lamer: 1999, 'Scattering from a periodic array of thin planar chiral structures - calculation and measurements'. *IEEE Trans. Antennas Propagat.* **47**(6), 1061–1065.

SURFACE AND LEAKY MODES OF MULTILAYERED OMEGA STRUCTURES

A.L. TOPA, C.R. PAIVA and A.M. BARBOSA
Instituto de Telecomunicações
Instituto Superior Técnico
Av. Rovisco Pais, 1
1049-001 Lisboa, Portugal

Abstract. We investigate the discrete real and complex solutions of the modal equation of an asymmetric pseudochiral slab waveguide, in which both the film and the substrate are pseudochiral media. When the pseudochiral parameter exceeds a certain transition value, power leakage occurs since one of the characteristic waves ceases to be internally reflected at the film-substrate interface. The analysis includes a parametric study of the effect of the media on the propagation characteristics of multilayered omega structures. The dependence of the propagation characteristics on the frequency is also addressed.

1. Introduction

The pseudochiral or omega medium is an artificial complex medium, which is obtained by doping a host isotropic medium with Ω–shaped conducting microstructures [1]. An external electric or magnetic field induces both electric and magnetic polarizations, which are perpendicular to each other. The electromagnetic properties of these media suggest its application in the design of reciprocal devices and components for the microwave and millimeter wave regimes [2]–[4].

The surface modes of a grounded pseudochiral slab have been analyzed in [5]. In this paper, we investigate the discrete real and complex solutions of the modal equation of an asymmetric pseudochiral slab waveguide, in which both the film and the substrate are pseudochiral media with an isotropic superstrate. The case in which both media have the same pseudochiral parameter has been considered in [6] while, in this paper, a more general structure where the film and the substrate have different omega parameters is analyzed. Moreover, the dependence of the propagation characteristics on frequency is addressed. This analysis can be extended to general *open* multi-

S. Zouhdi et al. (eds.), Advances in Electromagnetics of Complex Media and Metamaterials, 291–305.

layered omega structures, consisting of several stacked layers (pseudochiral or not) above an omega substrate, where the upper medium is the air.

While the surface guided modes are completely bounded by the film, the complex eigenmodes radiate energy into the substrate. These modes may propagate in the waveguide provided that the constitutive parameters are properly chosen. They cannot be found in common isotropic waveguides, where only leaky unguided modes may exist, and are well known for their role in several devices such as beam couplers that convert the energy of a beam to the guided modes of a thin–film dielectric slab waveguide [7]. Power leaks into the substrate because one of the two constituent characteristic waves ceases to be totally internal reflected at the film–substrate interface. These complex waves are usually termed semileaky waves [8] or leaky guided modes [9], since one of the two characteristic waves still remains completely guided by the film layer.

For the spatial orientation considered in this paper only hybrid modes propagate in the waveguide. Each hybrid mode is a weighted combination of two characteristic waves. Leakage occurs under the form of an exiting wave, when one of the two composite characteristic waves ceases to be totally reflected. In this case, the longitudinal wavenumber becomes complex, as two real roots of the modal equation collide over the real axis and originate a pair of conjugate complex roots. Therefore, the complete discrete spectrum of this waveguide includes a set of complex solutions in addition to the real guided modes. The present analysis is mainly focused on the leakage effect and includes a parametric study of the effect of the media on the propagation characteristics of multilayered omega structures.

2. Open Multilayered Omega Waveguides

2.1. PROBLEM FORMULATION

For the sake of generality, let us consider a multilayered omega structure, made of an arbitrary number of layers over a semi-infinite substrate and having the air as the upper medium. The structure is assumed to be uniform in the transverse direction and built with spatially nondispersive and lossless homogeneous Ω layers. In this section, field expressions in a general layer and in the substrate are derived.

For a bianisotropic Ω–medium the constitutive relations may be written as [10]

$$\begin{aligned} \mathcal{D} &= \overline{\epsilon} \cdot \boldsymbol{E} + \overline{\xi} \cdot \mathcal{H} \\ \mathcal{B} &= \overline{\zeta} \cdot \boldsymbol{E} + \overline{\mu} \cdot \mathcal{H} \end{aligned}, \tag{1}$$

where $\mathcal{H} = Z_0 \boldsymbol{H}$, $\mathcal{D} = \boldsymbol{D}/\epsilon_0$ and $\mathcal{B} = Z_0 \boldsymbol{B}/\mu_0$ are normalized field vectors. In this case, $\overline{\epsilon}$ and $\overline{\mu}$ are dimensionless relative dielectric permittivity

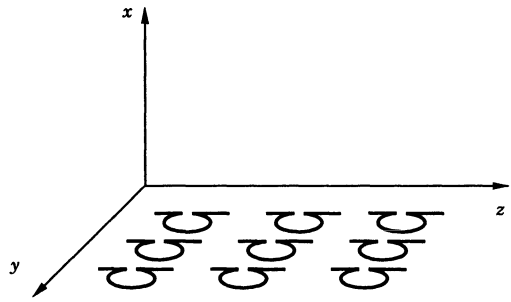

Figure 1. Spatial orientation of the planar Ω–shaped perfectly conducting microstructures in the hosting isotropic medium.

and relative magnetic permeability tensors, and $\overline{\xi}$ and $\overline{\zeta}$ are dimensionless magnetoelectric coupling tensors. As the medium is assumed to be spatially nondispersive, these relations are local.

We consider time-harmonic field variation of the form $\exp(j\omega t)$, and forward plane wave propagation of the form $\exp(-jkz)$, where k is the longitudinal wavenumber given by $k = (\beta - j\alpha)k_0$ with β being the normalized phase constant and α the normalized attenuation constant.

The Ω–shaped microstructures doped in the isotropic host material are oriented as depicted in Fig. 1. The normal to the plane of the loops points in the x–direction while the stems are aligned along z and the loops are oriented in the y–direction. Therefore tensors $\overline{\epsilon}$, $\overline{\mu}$, $\overline{\xi}$ and $\overline{\zeta}$ have the following dyadic representation [5]:

$$\begin{aligned} \overline{\epsilon} &= \epsilon_{xx}\hat{\boldsymbol{x}}\hat{\boldsymbol{x}} + \epsilon_{yy}\hat{\boldsymbol{y}}\hat{\boldsymbol{y}} + \epsilon_{zz}\hat{\boldsymbol{z}}\hat{\boldsymbol{z}} \\ \overline{\mu} &= \mu_{xx}\hat{\boldsymbol{x}}\hat{\boldsymbol{x}} + \mu_{yy}\hat{\boldsymbol{y}}\hat{\boldsymbol{y}} + \mu_{zz}\hat{\boldsymbol{z}}\hat{\boldsymbol{z}} \\ \overline{\xi} &= j\Omega\hat{\boldsymbol{z}}\hat{\boldsymbol{x}} \\ \overline{\zeta} &= -j\Omega\hat{\boldsymbol{x}}\hat{\boldsymbol{z}} \end{aligned} \quad , \tag{2}$$

where Ω is the dimensionless pseudochiral parameter here assumed to be positive. This parameter would be negative if the loops were oriented in the negative y–direction. Moreover, all the constitutive parameters are real since the media are assumed lossless.

With the spatial orientation depicted in Fig. 1, all the propagating modes in the waveguide are hybrid, since the two characteristic waves propagate coupled. When $\Omega = 0$ the hybrid modes degenerate into TE and TM surface modes of the common biaxial anisotropic waveguides.

Choosing E_z and $\mathcal{H}_x$ as the field supporting components, all the other field components may be expressed as [5]

$$\mathcal{H}_y = -j\frac{1}{\mu_{yy} - \dfrac{\beta^2}{\epsilon_{xx}}}\partial_{x'}E_z \tag{3}$$

$$E_y = -\frac{1}{\beta}(\mu_{xx}\mathcal{H}_x - j\Omega E_z) \tag{4}$$

$$\mathcal{H}_z = j\frac{1}{\mu_{zz}}\partial_{x'}E_y \tag{5}$$

where a normalized transverse distance $x' = k_0 x$ has been introduced, and $\partial_{x'}$ stands for $\partial/\partial x'$.

Moreover, the transverse wavenumbers of the two characteristic waves h_a and h_b can be written as

$$h_r^2 = \frac{(R_{11} + R_{22}) \mp \sqrt{(R_{11} + R_{22})^2 - 4(R_{11}R_{22} - R_{12}R_{21})}}{2} \tag{6}$$

with $r = a, b$ and where

$$R_{11} = \epsilon_{zz}\left(\mu_{yy} - \frac{\beta^2}{\epsilon_{xx}}\right) \tag{7}$$

$$R_{12} = j\Omega\left(\mu_{yy} - \frac{\beta^2}{\epsilon_{xx}}\right) \tag{8}$$

$$R_{21} = j\Omega\frac{\epsilon_{zz}}{\mu_{xx}}\left(\mu_{yy} - \frac{\beta^2}{\epsilon_{xx}}\right) - j\Omega\epsilon_{yy}\frac{\mu_{zz}}{\mu_{xx}} \tag{9}$$

$$R_{22} = \mu_{zz}\left(\epsilon_{yy} - \frac{\beta^2}{\mu_{xx}}\right) - \frac{\Omega^2}{\mu_{xx}}\left(\mu_{yy} - \frac{\beta^2}{\epsilon_{xx}}\right) \tag{10}$$

Therefore, in (6) one has

$$\begin{aligned} R_{11} + R_{22} \;=\; & \tfrac{1}{\mu_{xx}}\left\{\left[\mu_{yy}(\epsilon_{zz}\mu_{xx} - \Omega^2) + \mu_{zz}\epsilon_{yy}\mu_{xx}\right]\right. \\ & \left. -\beta^2\left[\tfrac{1}{\epsilon_{xx}}(\epsilon_{zz}\mu_{xx} - \Omega^2) + \mu_{zz}\right]\right\} \end{aligned} \tag{11}$$

and

$$R_{11}R_{22} - R_{12}R_{21} = \epsilon_{zz}\mu_{zz}\left(\mu_{yy} - \frac{\beta^2}{\epsilon_{xx}}\right)\frac{1}{\mu_{xx}}\left[\epsilon_{yy}\left(\mu_{xx} - \frac{\Omega^2}{\epsilon_{zz}}\right) - \beta^2\right] \tag{12}$$

The field supporting components of the surface modes in the air, i.e., for $x' > t'$ where $t' = k_0 t$ is the normalized total layer thickness, may be expressed as

$$\begin{cases} E_z &= D\exp[-jh_d(x' - t')] \\ \mathcal{H}_x &= E\exp[-jh_d(x' - t')] \end{cases}, \tag{13}$$

where $h_d^2 = 1 - \beta^2$.

In each omega layer, the support field components can be written as

$$\begin{cases} E_z = \Psi_a + \Psi_b \\ \mu_{xx}\mathcal{H}_x = \tau_a\Psi_a + \tau_b\Psi_b \end{cases}, \tag{14}$$

where

$$\tau_r = \frac{h_r^2 - R_{11}}{R_{12}} = \frac{R_{21}}{h_r^2 - R_{22}} \tag{15}$$

with $r = a, b$ representing the two characteristic waves of the unbounded omega medium.

In the substrate, *i.e.*, for $x' < 0$, one has

$$\begin{cases} \Psi_a^s = C_a \exp(jq_a x') \\ \Psi_b^s = C_b \exp(jq_b x') \end{cases}, \tag{16}$$

where superscript s stands for *substrate*, and q_a and q_b are the transverse wavenumbers in the substrate.

2.2. SEMI-LEAKY MODES

If one considers separately the contribution of the two characteristic waves propagating in the film, one can easily see that both waves will be totally reflected at $x' = 0$ as long as $\beta > \gamma_a$ and $\beta > \gamma_b$, where γ_r with $r = a, b$ is such that $q_r = 0$ for $\beta = \gamma_r$. From (12), one can easily see that

$$\gamma_a = \sqrt{\epsilon_{yy}^s(\mu_{xx}^s - \frac{\Omega_s^2}{\epsilon_{zz}^s})} \tag{17}$$

and

$$\gamma_b = \sqrt{\epsilon_{xx}^s \mu_{yy}^s} \tag{18}$$

Therefore, if $\beta < \gamma_a$ or $\beta < \gamma_b$, semileaky modes will occur as long as one of the two characteristic waves is not totally internally reflected at the substrate interface. These modes correspond to a coupled mode in which one of the characteristic waves is bounded by the waveguide while the other is radiating energy into the substrate, thereby forcing the longitudinal propagation constant to become complex.

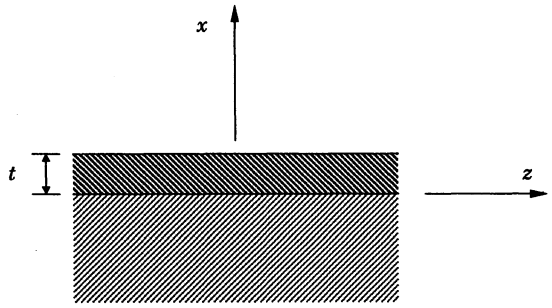

Figure 2. Asymmetric pseudochiral slab waveguide: Both the film and the substrate are made of Ω–media and the upper medium is the air.

3. Asymmetric Omega Slab

3.1. MODAL EQUATION

In this section, the analysis is focused on an asymmetric omega slab waveguide as depicted in Fig. 2. In the film, *i.e.*, for $0 < x' < t'$, one has in (14)

$$\begin{cases} \Psi_a^f &= A_a \sin(h_a x') + B_a \cos(h_a x') \\ \Psi_b^f &= A_b \sin(h_b x') + B_b \cos(h_b x') \end{cases} . \tag{19}$$

where superscript f stands for *film*. Hence, in addition to the longitudinal normalized wavenumber β, there are eight unknowns to be determined in this problem: A_a, A_b, B_a, B_b, C_a, C_b, D and E.

Enforcing the boundary conditions at $x' = 0$ and $x' = t'$, some of these unknowns are easily determined while the others can be obtained through the following linear system

$$\begin{bmatrix} P_a & P_b & Q_a & Q_b \\ R_a & R_b & S_a & S_b \\ T_a & T_b & U_a & U_b \\ V_a & V_b & X_a & X_b \end{bmatrix} \cdot \begin{bmatrix} A_a \\ A_b \\ B_a \\ B_b \end{bmatrix} = \begin{bmatrix} 0 \\ 0 \\ 0 \\ 0 \end{bmatrix} , \tag{20}$$

where

$$P_r = (\mu_{yy}^s - \frac{\beta^2}{\epsilon_{xx}^s})(\tau_b^s - \tau_a^s)h_r \tag{21}$$

$$\begin{aligned} Q_r = -(\mu_{yy}^f - \frac{\beta^2}{\epsilon_{xx}^f})[&jq_a(\tau_b^s - \tau_r^f) - jq_b(\tau_a^s - \tau_r^f) \\ &-(\Omega_f - \Omega_s)(q_a - q_b)] \end{aligned} \tag{22}$$

$$R_r = \eta_{zz}^s h_r(\tau_b^s - \tau_a^s)(\tau_r^f - j\Omega_f) \tag{23}$$

$$S_r = -\mu_{zz}^f \Big\{ jq_a(\tau_a^s - j\Omega_s)(\tau_b^s - \tau_r^f) - jq_b(\tau_b^s - j\Omega_s)(\tau_a^s - \tau_r^f) \\ -[q_a(\tau_a^s - j\Omega_s) - q_b(\tau_b^s - j\Omega_s)](\Omega_f - \Omega_s)\} \tag{24}$$

$$T_r = jh_d h_r \cos(h_r t') - (\mu_{yy}^f - \frac{\beta^2}{\epsilon_{xx}^f}) \sin(h_r t') \tag{25}$$

$$U_r = -jh_d h_r \sin(h_r t') - (\mu_{yy}^f - \frac{\beta^2}{\epsilon_{xx}^f}) \cos(h_r t') \tag{26}$$

$$V_r = (\tau_r^f - j\Omega_f)[h_r \cos(h_r t') + jh_d \mu_{zz}^f \sin(h_r t')] \tag{27}$$

$$X_r = -(\tau_r^f - j\Omega_f)[h_r \sin(h_r t') - jh_d \mu_{zz}^f \cos(h_r t')] \quad , \tag{28}$$

with $r = a, b$, and f stands for *film*.

The modal equation for the hybrid modes for this waveguide can be derived by setting to zero the determinant of the 4×4 matrix in (20).

3.2. CUTOFF OF THE SURFACE MODES

Henceforth, without loss of generality, we will assume that $\epsilon_{xx}^s \mu_{yy}^s > \epsilon_{yy}^s \mu_{xx}^s$, *i.e.*, that $\gamma_b > \gamma_a$, with γ_a and γ_b given by (17) and (18), respectively. In this case, the cutoff of the surface guided modes is reached whenever $q_b = 0$, or from (7) and (8), whenever

$$R_{11}^s = R_{12}^s = 0 \, , \tag{29}$$

which means that $\beta = \gamma_b$. In this case, $q_a = \sqrt{R_{22}^s}$ with

$$R_{22}^s = \mu_{zz}^s \left(\epsilon_{yy}^s - \frac{\epsilon_{xx}^s \mu_{yy}^s}{\mu_{xx}^s} \right) \tag{30}$$

real and negative. Moreover, one has

$$R_{21}^s = -j\Omega_s \epsilon_{yy}^s \frac{\mu_{zz}^s}{\mu_{xx}^s} \, , \tag{31}$$

and, therefore, from (15)

$$\tau_a^s \to \infty \tag{32}$$

and

$$\tau_b^s = j \frac{\Omega_s \epsilon_{yy}^s}{\epsilon_{yy}^s \mu_{xx}^s - \epsilon_{xx}^s \mu_{yy}^s} \, . \tag{33}$$

In this case, the modal equation at cutoff can be written as

$$(T_a R_b - R_a T_b)(X_a - X_b) - (R_a V_b - V_a R_b)(U_a - U_b) \\ +(V_a T_b - T_a V_b)(S_a - S_b) = 0 \tag{34}$$

One should note that

$$S_a - S_b = -\mu_{zz}^s q_a(\tau_a^f - \tau_b^f) \tag{35}$$

so that the cutoff only depends on Ω_f, which means that it is independent from the value of Ω_s.

Below this point, all hybrid modes, with the exception of the fundamental H_1 mode, turn into semi-leaky modes.

3.3. CUTOFF OF THE SEMI–LEAKY MODES

Rigorously speaking, the cutoff of each semi–leaky mode is only reached whenever $\Im\{q_a\} = 0$. However, it was seen that the odd–order semi–leaky modes never reach cutoff. Below the cutoff of the odd–order surface modes, the semi–leaky modes exhibit a singular behavior, never becoming improper leaky modes. This result will be clarified in a forthcoming publication.

For the even–order semi-leaky modes, the exact cutoff condition, which is hardly analytically implemented, can be reasonably approximated by $q_a = 0$. In this case, from (7)–(10), one has

$$R_{11}^s R_{22}^s = R_{12}^s R_{21}^s \tag{36}$$

which means that at cutoff, one may take $\beta = \gamma_a$. In the approximation β is taken real at cutoff. In this case,

$$q_b = \sqrt{R_{11}^s + R_{22}^s} \tag{37}$$

with $R_{11}^s + R_{22}^s$, real and positive. Moreover, one has

$$\tau_a^s = -\frac{R_{11}^s}{R_{12}^s} = -\frac{R_{21}^s}{R_{22}^s} \tag{38}$$

and

$$\tau_b^s = \frac{R_{22}^s}{R_{12}^s} = \frac{R_{21}^s}{R_{11}^s} \,. \tag{39}$$

Hence, for the even–order semi–leaky modes an approximate cutoff condition can be obtained by taking $q_a = 0$ in the modal equation, in which case, very approximate results are obtained.

One should stress the fact that the same procedure is not applicable to the odd–order semi–leaky modes, as far as these modes never reach cutoff.

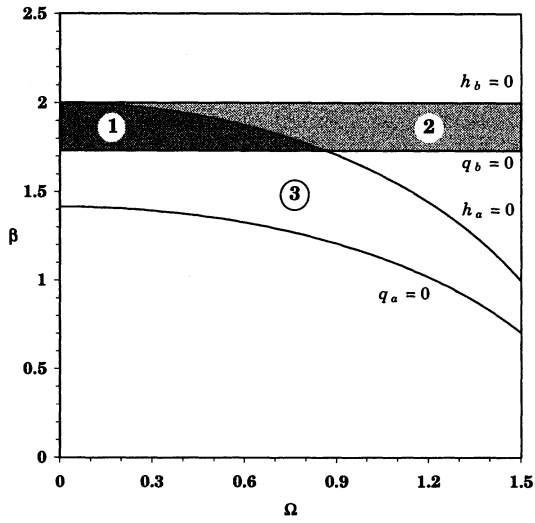

Figure 3. The three ranges for the normalized phase constant β as a function of the pseudochiral parameter Ω, for the hybrid modes of the pseudochiral planar waveguide depicted in Fig. 2: (1) Homogeneous surface modes; (2) Inhomogeneous surface modes; (3) Semileaky modes.

3.4. NUMERICAL RESULTS

In the numerical simulation the following values for the dimensionless constitutive parameters are assumed: $\epsilon^f_{xx} = \epsilon^s_{yy} = 2$, $\epsilon^f_{yy} = 4$, $\epsilon^f_{zz} = \epsilon^s_{zz} = 3$, $\epsilon^s_{xx} = 1$, $\mu^f_{xx} = \mu^s_{xx} = 1$, $\mu^f_{yy} = \mu^s_{zz} = 2$ and $\mu^f_{zz} = \mu^s_{yy} = 3$. For the time being, we will assume that $\Omega_f = \Omega_s = \Omega$.

In Fig. 3, we show the three ranges for the normalized phase constant, as a function of the pseudochiral parameter Ω. Considering separately the contribution of the two characteristic waves propagating in the film, one has $\beta_b > \beta > \gamma_b$ for one of the waves, where

$$\beta_b = \sqrt{\epsilon^f_{xx}\mu^f_{yy}} \tag{40}$$

is such that $h_b = 0$ for $\beta = \beta_b$ while γ_b is given by (18). For the other characteristic wave, one has $\beta_a > \beta > \gamma_a$, where

$$\beta_a = \sqrt{\epsilon^f_{yy}\left(\mu^f_{xx} - \frac{\Omega_f^2}{\epsilon^f_{zz}}\right)} \tag{41}$$

is such that $h_a = 0$ for $\beta = \beta_a$ while γ_a is given by (17).

Once again, without loss of generality, we have assumed that $\epsilon^f_{xx}\mu^f_{yy} > \epsilon^f_{yy}\mu^f_{xx}$, *i.e.*, that $\beta_b > \beta_a$. From Fig. 3, one can easily see that both waves

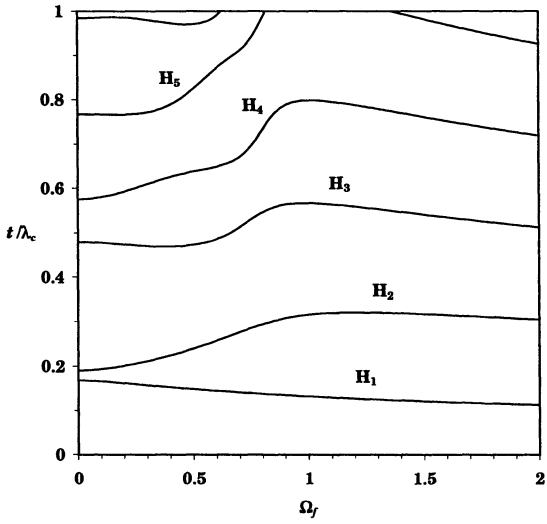

Figure 4. Operational diagram: Variation of the cutoff parameter t/λ_c with the pseudochiral parameter Ω_f for the first hybrid modes.

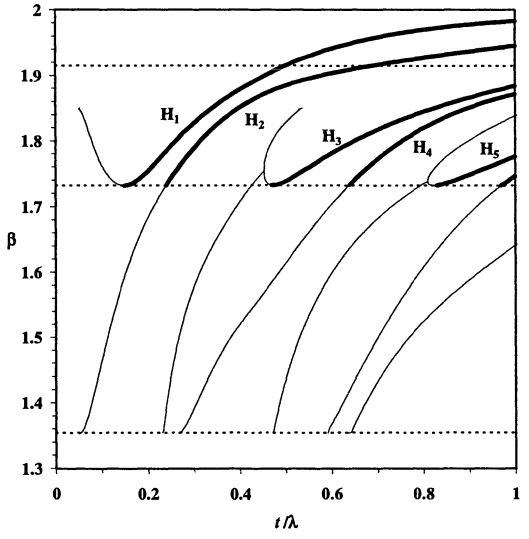

Figure 5. Dispersion diagram: Variation of the normalized longitudinal wavenumber β with t/λ for the first propagating hybrid modes, when $\Omega = 0.5$. The thick lines correspond to the surface modes while the thin lines correspond to the leaky improper and semi-leaky modes. The even–order semi-leaky modes cutoff at the lower dashed line while the odd-order modes continue beyond that line (not represented) as they never cutoff.

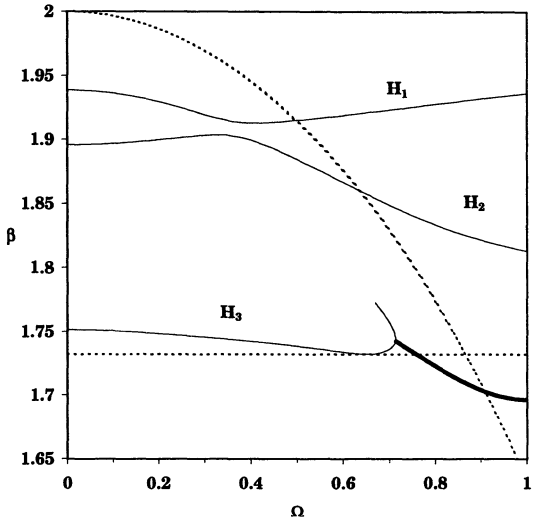

Figure 6. Variation of the normalized phase constant β with Ω for the first propagating hybrid modes of an asymmetric slab waveguide with $t/\lambda = 0.5$. The thick line represents the semileaky mode while the curved dashed line corresponds to $h_a = 0$ and the horizontal to $q_b = 0$.

propagate with total internal reflection at $x = 0$ whenever $\beta > \gamma_b$. Within this range, region (1) corresponds to homogeneous surface modes, while region (2) corresponds to inhomogeneous surface modes.

If $\beta < \gamma_b$, *i.e.* in region (3), semileaky modes will occur since one of the two characteristic waves is not totally internally reflected from the film–substrate interface. These modes correspond to a coupled mode in which one of the characteristic waves is guided in the film while the other is radiating energy into the substrate, thereby forcing the longitudinal propagation constant to become complex.

In Fig. 4, the variation of t/λ_c with Ω_f — where λ_c denotes the cutoff wavelength — is presented. These curves are independent of the value of Ω_s and were calculated using Eq. (34). For a given value of t', where $t' = 2\pi t/\lambda$, one can easily obtain from Fig. 4 the number of propagating modes. Hereafter, the descriptor H_p will represent each hybrid mode, where the subscript p, with $p \geq 1$, indicates the order of the mode and all the modes are ordered after increasing cutoff frequencies.

In Fig. 5, the variation of β with t/λ is presented for $\Omega = 0.5$. The thick lines correspond to the surface guided modes while the thin lines correspond to the leaky improper and semi-leaky modes. In the high–frequency regime, *i.e.* when $t/\lambda \rightarrow \infty$, there is an aymptotic value for β, which corresponds to $h_b = 0$. For all modes, the dispersion curve always converges to β_b [5].

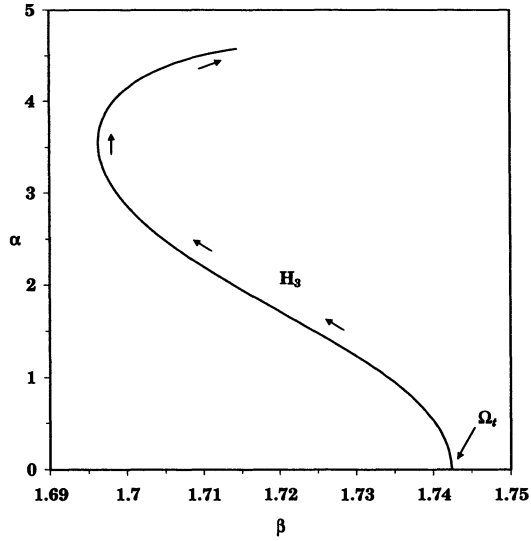

Figure 7. Root locus in the complex plane of the normalized longitudinal wavenumber for the third hybrid mode, which becomes complex when Ω exceeds the transition value $\Omega_t = 0.71475$. Arrows indicate Ω increasing between Ω_t and 1.2.

When $\Omega_f = \Omega_s = 0$ the hybrid modes degenerate into the common TE and TM surface modes of the biaxial anisotropic case, with the dispersion curves crossing each other instead of displaying coupling points.

Moreover, one should stress that the fundamental surface mode H_1 never leaks into the substrate, while the odd–order semi–leaky modes continue beyond the lower horizontal dashed line since they never reach cutoff, as explained in section 3.3.

In Fig. 6 the variation of the normalized phase constant β with the pseudochiral parameter Ω is depicted for the first propagating hybrid modes of an asymmetric slab waveguide with $t/\lambda = 0.5$. The curved dashed line corresponds to the asymptotic value $h_a = 0$ while the horizontal one corresponds to $q_b = 0$. The semileaky mode (thick line) starts propagating for Ω above some transition value Ω_t, after the collision of two leaky unguided modes.

In Fig. 7 we show the *root locus* in the complex plane of the normalized longitudinal wavenumber for the same semileaky mode of Fig. 6. The leakage starts occurring for Ω above the transition value Ω_t, roughly corresponding to $\beta = \gamma_b$.

Figure 8 shows the variation of the leakage constant α with Ω for the second even–order semileaky mode.

The variation of the leakage constant α, in dB/λ, with the normalized

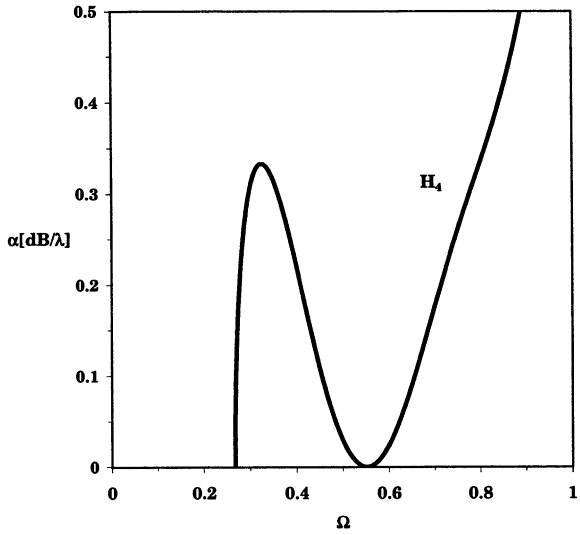

Figure 8. Leakage constant α in dB/λ versus the pseudochiral parameter Ω for the fourth propagating hybrid mode of Fig. 8, which becomes a semileaky mode for increasing Ω. The leakage starts occurring for Ω above some transition value corresponding to $\beta = \beta_b$ given by (40) for which $q_b = 0$.

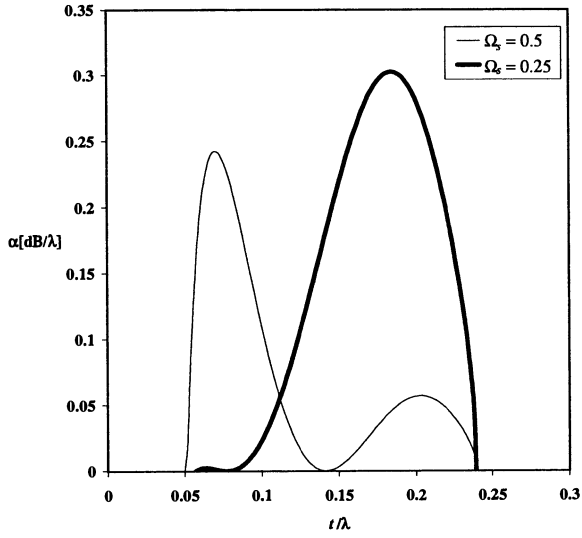

Figure 9. Leakage constant α in dB/λ versus the normalized slab thickness t/λ for the second propagating hybrid mode, for $\Omega_f = 0.5$ and for two different values of Ω_s.

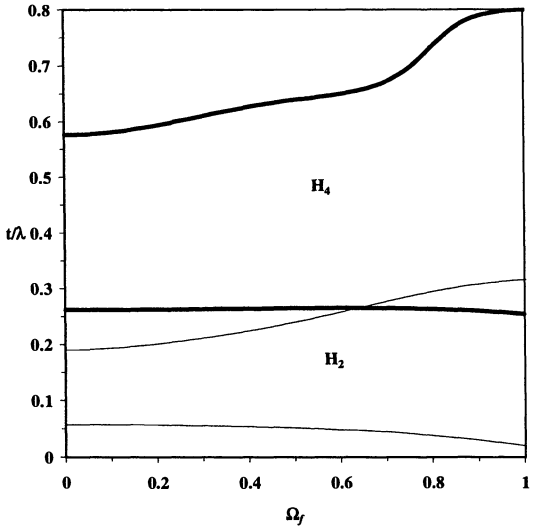

Figure 10. Allowed band for the semi-leaky H_2 and H_4 hybrid modes, as a function of Ω_f, when $\Omega_s = 0.5$. The thick lines are for the H_4 semi-leaky mode and the thin lines for H_2.

slab thickness t/λ is depicted in Fig. 9 for the second propagating hybrid mode, when $\Omega_f = 0.5$ and for two different values of Ω_s. Significant changes are observed when a different pseudochiral Ω parameter in considered in the two regions.

Finally, Fig. 10 shows the allowed bands for the first two even–order semi-leaky hybrid modes H_2 and H_4, as a function of Ω_f, when $\Omega_s = 0.5$. An overlapping region is obtained, which means that, for a convenient set of parameters, both modes will propagate as semi–leaky modes in the same structure. For the odd-order semi–leaky modes it is not possible to define a lower bound corresponding to the cutoff since, as seen, this modes never reach cutoff.

4. Conclusions

The discrete complex spectrum of an asymmetric pseudochiral slab waveguide was explored. It was shown that an asymmetric pseudochiral slab waveguide, where both the film and the substrate are made of pseudochiral Ω–media, can support semileaky modes radiating energy into the substrate. Leakage may occur, as far as the pseudochiral parameter Ω is raised above a certain transition value. The propagation characteristics dependence on the frequency was analyzed. The analysis herein presented can be easily generalized to open multilayered omega structures.

5. Acknowledgment

This work was partially supported by FCT, under project POSI/CPS/39589 – 2001.

References

1. Saadoun, M.M.I. and Engheta, N. (1992) Pseudochiral Ω–medium and guided–wave structures: Theory and principles, *Proc. URSI Int. Symp. Electromag. Theory*, Sydney, 17–20.
2. Saadoun, M.M.I. and Engheta, N. (1992) A reciprocal phase shifter using novel pseudochiral or Ω–medium, *Microwave Opt. Technol. Lett.* **5**, 184–188.
3. Mazur, J. and Pietrzak, D. (1996) Field displacement phenomenon in a rectangular waveguide containing a thin plate of an Ω–medium, *IEEE Microwave Guided Wave Lett.* **6**, 34–36.
4. Topa, A.L., Paiva, C.R., and Barbosa, A.M. (1998) Full–wave analysis of a non-radiative dielectric waveguide with a pseudochiral Ω–slab, *IEEE Trans. Microwave Theory Tech.* **46**, 1263–1269.
5. Topa, A.L., Paiva, C.R., and Barbosa, A.M. (1998) Complete spectral representation for the electromagnetic field of planar multilayered waveguides containing pseudochiral Ω–media, *Progress in Electromagnetics Research* **18**, Ch. 5, 85–104, EMW Publishing, Cambridge.
6. Topa, A.L., Paiva, C.R., and Barbosa, A.M. (2001) Complex eigenmodes in planar waveguides with pseudochiral omega media, *Izvestiya Gomel'skogo Gosundarstvennogo Universiteta* **9**, No. 6, 84–88.
7. Tamir, T. (Ed.,1979) *Integrated Optics*, Springer-Verlag, New York, Ch. 3.
8. Paiva, C.R., Topa, A.L., and Barbosa, A.M. (1992) Semileaky waves in dielectric chirowaveguides," *Optics Lett.* **17**, No. 23, 1670–1672.
9. Knoesen, A., Gaylord, T.K., and Moharam, M.G. (1988) Hybrid guided modes in uniaxial dielectric planar waveguides, *IEEE J. Lightwave Technol.* **6**, No. 6, 1083–1104.
10. Paiva, C.R. and Barbosa, A.M. (1992) A linear–operator formalism for the analysis of inhomogeneous biisotropic planar waveguides, *IEEE Trans. Microwave Theory Tech.* **40**, pp. 672–678.

THE COMPETITION OF BRAGG REFLECTION AND FRESNEL'S REFLECTION OF ELECTROMAGNETIC WAVES IN THE ARTIFICIAL HELICOIDAL BIANISOTROPIC MEDIA WITH LOCAL CHIRALITY

I. V. SEMCHENKO and S. A. KHAKHOMOV
Department of General Physics, Gomel State University
Sovyetskaya Str. 104, 246019, Gomel, Belarus

Abstract. On the base of the exact solution of the boundary-value problem for artificial helicoidal media with local chirality we describe the reflection of electromagnetic waves on the periodic structure of medium as well as Fresnel's reflection from sample's boundaries. It allows to model the transmission and reflection of electromagnetic waves in dependence on the obtained parameters of artificial helicoidal medium and to design the device for polarization transformation. A possibility of the minimizing of size of a structure for transformations of the polarization state of electromagnetic waves is shown.

1. Introduction

In paper [1] was shown a possibility of the design of a structure whose microwave properties are similar to the optical properties of cholesteric liquid crystals. This structure also exhibits local chirality because it contains the small wire helices. Such a structure can be a multilayer anisotropic chiral sample. When the number of layers increases, the helices turn at a constant angle around the axis which is perpendicular to the planar (see Fig. 1).

As a result the sample as a whole acquires a macroscopic helicoidal structure which is analogical to the structure of cholesteric liquid crystals. Methods to design and manufacture artificial chiral media with uniaxial homogeneous structure were described in [2]. It was proposed to wind thin wires around Nylon threads, to align these helices and then to cast them into epoxy resin. In this case the permittivity and chirality of the effective medium are characterized by uniaxial tensors, the axis of which is oriented along the direction of the parallel Nylon threads. The axis of the macroscopic helicoidal structure is orthogonal to both the boundaries of the layers and the Nylon lines (see Fig. 1), i.e., to the local optical axes of layers.

S. Zouhdi et al. (eds.), Advances in Electromagnetics of Complex Media and Metamaterials, 307–318.

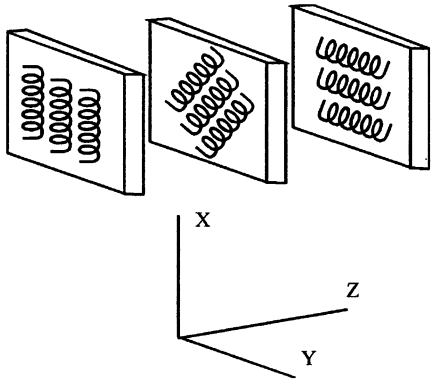

Figure 1. Geometry of the medium

The thickness of every layer is about 0.5–1 mm. This allows to provide the period of the macroscopic helicoidal structure close to the wavelength in the microwave region.

Here we assume that the pitch of the macroscopic helicoidal structure along z is much larger than the thickness of individual layers. In that case the local properties are homogeneous in the transverse direction with respect to the local direction of vector $\mathbf{a}$. In other words, the pitch and diameter of the wire helices in every layer are much smaller than the pitch of macroscopic helicoidal structure along z. If the signal frequency corresponds to resonant effects at the scale of the macroscopic helicoidal structure along z, than the local chirality effects are weak for the case of "infinite" wire helices in individual layers. However, these local chirality effects can be large if the wire helices are cut into sections so that every section resonates at a frequency close to that of the resonance of the main crystal structure (macroscopic helicoidal structure).

Vector $\mathbf{a}$ rotates around the helicoidal structure axis as

$$\mathbf{a}(z) = \overline{\overline{U}}(z) \cdot \mathbf{a}(0) \tag{1}$$

where

$$\overline{\overline{U}}(z) = \exp[qz\mathbf{c} \times \overline{\overline{I}}] = \begin{pmatrix} \cos(qz) & -\sin(qz) & 0 \\ \sin(qz) & \cos(qz) & 0 \\ 0 & 0 & 1 \end{pmatrix} \tag{2}$$

is the rotation dyadic (around the unit vector $\mathbf{c}$). $\overline{\overline{I}}$ is the unit dyadic. Here $\mathbf{c}$ is unit vector along z axis, $\mathbf{a}(0)$ is unit vector along x axis. Parameter q depends only on the geometry of the macroscopic helicoidal structure: it is determined by the pitch P of the rotation along the axis z ($|q| = \frac{2\pi}{P}$).

The solution of the boundary-value problem [1] allows to describe both reflection of electromagnetic waves on the macroscopic periodic structure of

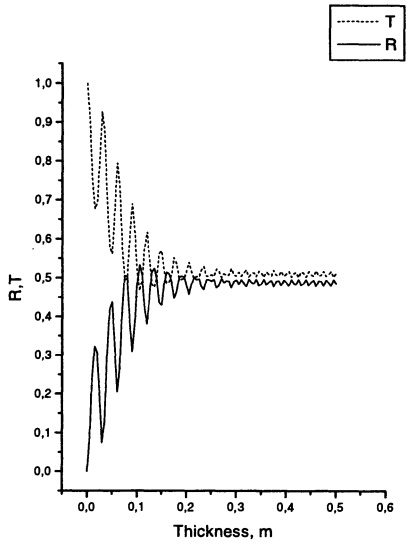

Figure 2. Transmission (T) and reflection (R) coefficients as functions of the sample thickness. $\bar{\epsilon} = 3.45$, $\Delta\epsilon = 0.45$, $\kappa_a = 0.3$, $q = 100$ radn/m, $\omega = 18.6$ GHz.

the medium (Bragg reflection) and wave reflection from the boundaries of the sample (Fresnel's reflection). Such reflection of electromagnetic waves on the macroscopic periodic structure of the medium is possible when the frequency of the incident wave satisfies to so called "Bragg condition". This kind of reflection of light on the macroscopic periodic structure of the medium is well known in the optics of cholesteric liquid crystals and is named "Bragg reflection" [3]. The other kind of interaction of electromagnetic wave with artificial structure is the reflection from the boundaries of the sample (so called Fresnel's reflection).

Linearly polarized wave can be represented as a sum of two circularly polarized waves with opposite direction of rotation of the electric field strength vector **E** in space. Two different ways of propagation for circularly polarized waves in helicoidal medium in Bragg region exist. For example, circularly polarized wave has the direction of rotation of vector **E** in space, which coincides with the direction of rotation of local axis of helicoidal medium, i.e. vector **a**. This wave feels the significant reflection in Bragg region and practically full reflection of wave from thick sample takes place. The circular wave with the opposite direction of rotation of vector **E** does not interact with the periodic helicoidal structure. Only Fresnel's reflection of this wave from boundaries of sample is possible.

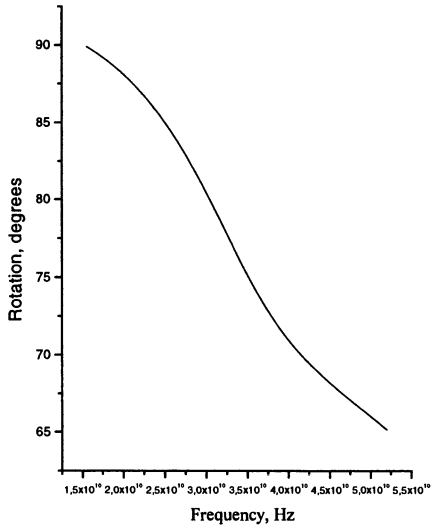

Figure 3. Rotation of the polarization plane of the transmitted wave as a function of the frequency. $\bar{\epsilon} = 3.45$, $\Delta\epsilon = 0.45$, $\kappa_a = 0.3$, $q = 100$ radn/m,$L = 0.015$ m.

Some earlier results on plane waves in helicoidal media of various physical nature have been published in [4]-[8]. For a review of other papers in this area see [6, 9].

This study is motivated by the possibility to decrease the size of the sample for transformations of the polarization state of electromagnetic waves which was proposed in [1]. In contrast to the earlier proposed device [1], this sample can have a minimal size, because its operation is based on the phenomenon of the competition of Bragg reflection of electromagnetic waves on the periodic helicoidal structure of medium and Fresnel's reflection from boundaries of sample.

2. Theory

On the level of constitutive relations, this medium has locally uniaxial permittivity and permeability dyadics, and also uniaxial reciprocal magnetoelectric (chirality) dyadics.

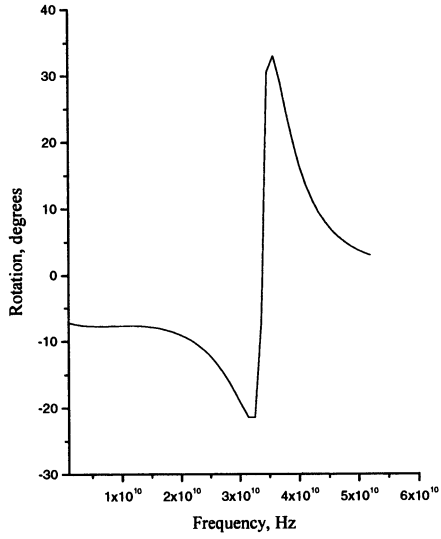

Figure 4. Rotation of the polarization plane of the reflected wave as a function of the frequency. $\bar{\epsilon} = 3.45$, $\Delta\epsilon = 0.45$, $\kappa_a = 0.3$, $q = 100$ radn/m, $L = 0.015$ m.

All the helices at given z have the same direction along vector $\mathbf{a}(z)$, thus $\kappa_t = 0$. The constitutive relations take the form

$$\mathbf{D} = \epsilon_0(\epsilon_t \overline{\overline{I}}_t + \epsilon_a \mathbf{a}(z)\mathbf{a}(z)) \cdot \mathbf{E} + j\sqrt{\epsilon_0\mu_0}\,\kappa_a \mathbf{a}(z)\mathbf{a}(z) \cdot \mathbf{H} \tag{3}$$

$$\mathbf{B} = \mu_0(\mu_t \overline{\overline{I}}_t + \mu_a \mathbf{a}(z)\mathbf{a}(z)) \cdot \mathbf{H} - j\sqrt{\epsilon_0\mu_0}\,\kappa_a \mathbf{a}(z)\mathbf{a}(z) \cdot \mathbf{E} \tag{4}$$

for this specific geometry. Incident wave propagates along z axis. The transverse unit dyadic is denoted by $\overline{\overline{I}}_t = \overline{\overline{I}} - \mathbf{a}(z)\mathbf{a}(z)$. The analysis is restricted to the case when the magnetic effects can be neglected and set $\mu_a = \mu_t = 1$.

The field in the multilayer anisotropic chiral sample is excited by a plane electromagnetic wave

$$\mathbf{E}_e = (A_{1e}\mathbf{b}(0) + A_{2e}\mathbf{a}(0))e^{jk_0 z - j\omega t} \tag{5}$$

$$\mathbf{H}_e = \frac{1}{\eta_0}(A_{2e}\mathbf{b}(0) - A_{1e}\mathbf{a}(0))e^{jk_0 z - j\omega t} \tag{6}$$

where $k_0 = \omega\sqrt{\epsilon_0\mu_0}$ is the vacuum wavenumber, $\eta_0 = \sqrt{\mu_0/\epsilon_0}$ is the free-space wave impeadance and $\mathbf{b}(0)$ is unit vector along y axis.

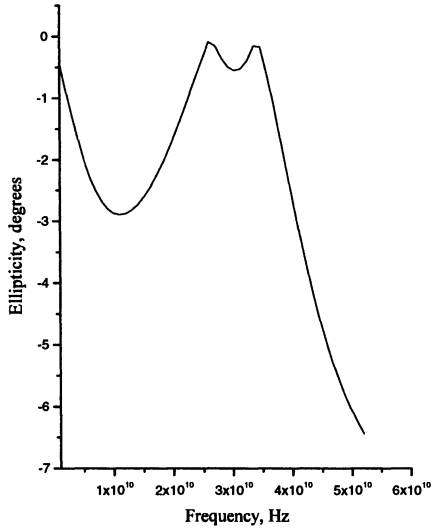

Figure 5. Ellipticity of the transmitted wave as a function of the frequency $\bar{\epsilon} = 3.45$, $\Delta\epsilon = 0.45$, $\kappa_a = 0.3$, $q = 100$ radn/m, $L = 0.015$ m.

A reflected wave

$$\mathbf{E}_r = (A_{1r}\mathbf{b}(0) + A_{2r}\mathbf{a}(0))e^{-jk_0z-j\omega t} \tag{7}$$

$$\mathbf{H}_r = \frac{1}{\eta_0}(A_{1r}\mathbf{a}(0) - A_{2r}\mathbf{b}(0))e^{-jk_0z-j\omega t} \tag{8}$$

and a transmitted wave

$$\mathbf{E}_\tau = (A_{1\tau}\mathbf{b}(L) + A_{2\tau}\mathbf{a}(L))e^{jk_0z-j\omega t} \tag{9}$$

$$\mathbf{H}_\tau = \frac{1}{\eta_0}(A_{2\tau}\mathbf{b}(L) - A_{1\tau}\mathbf{a}(L))e^{jk_0z-j\omega t} \tag{10}$$

also exist outside of the sample.

Here $\mathbf{a}(L)$ and $\mathbf{b}(L)$ are the unit vectors which have turned on the angle qL:

$$\mathbf{b}(L) = \overline{\overline{U}}(L) \cdot \mathbf{b}(0) \tag{11}$$

$$\mathbf{a}(L) = \overline{\overline{U}}(L) \cdot \mathbf{a}(0) \tag{12}$$

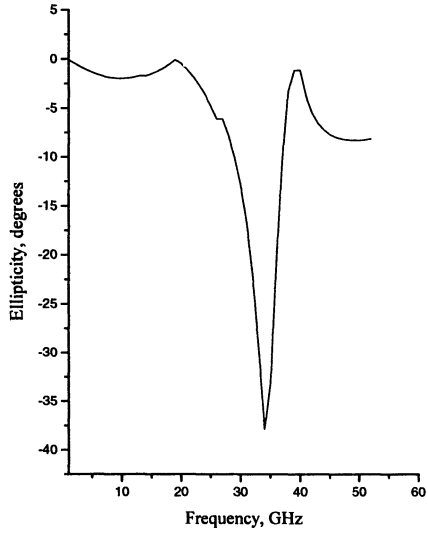

Figure 6. Ellipticity of the reflected wave as a function of the frequency. $\bar{\epsilon} = 3.45$, $\Delta\epsilon = 0.45$, $\kappa_a = 0.3$, $q = 100$ radn/m, $L = 0.015$ m.

where L is thickness of sample,

$$\overline{\overline{U}}(L) = \exp[qL\mathbf{c} \times \overline{\overline{I}}] \tag{13}$$

is the dyadic of rotation on the angle qL.

The electric field strength vector in the sample is the sum of four plane waves

$$\mathbf{E} = \sum_{m=1}^{4} A_m \overline{\overline{U}}(z) \cdot \frac{\mathbf{a}(0) + j\rho_m \mathbf{b}(0)}{\sqrt{1+\rho_m^2}} e^{jk_m z - j\omega t} \tag{14}$$

where k_m and ρ_m are wavenumbers and ellipticities of eigenmodes in the twisted coordinate system. The magnetic field strength vector is

$$\mathbf{H} = \frac{-j}{\omega\mu_0}\mathbf{c} \times \overline{\overline{I}} \cdot \frac{d}{dz}\mathbf{E} + \frac{j}{\eta_0}\kappa_a \mathbf{a}(z)\mathbf{a}(z) \cdot \mathbf{E} \tag{15}$$

The wavenumbers of eigenmodes of electromagnetic field in the twisted coordinate system for such a helicoidal medium taking into account the

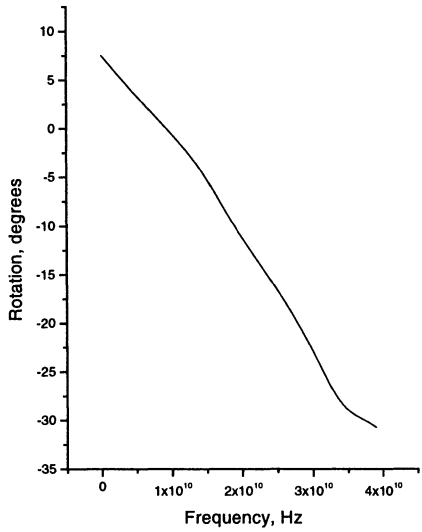

Figure 7. Rotation of the polarization plane of the transmitted wave as a function of the frequency. $\bar{\epsilon} = 3.45$, $\Delta\epsilon = 0.45$, $\kappa_a = 0.3$, $q = 100$ radn/m, $L = 0.0301$ m.

local chiral properties have been obtained [1]:

$$k_{1,2} = k_0\sqrt{\bar{\epsilon} - \frac{\kappa_a^2}{4} + \eta^2 \pm \sqrt{4\eta^2(\bar{\epsilon} - \frac{\kappa_a^2}{4}) + (\Delta\epsilon + \eta\kappa_a)^2}} \tag{16}$$

$$k_{1,2} = -k_{3,4} \tag{17}$$

The following notations for mean values and the anisotropy characteristics of the material parameters have been introduced: $\bar{\epsilon} = \frac{1}{2}(\epsilon_t + \epsilon_a)$, $\Delta\epsilon = \frac{1}{2}(\epsilon_t - \epsilon_a)$, $\eta = \frac{\kappa_a}{2} + \frac{q}{k_0}$

The system of eight algebraic linear equations was obtained from the condition of continuity of the tangential components of electric and magnetic field strength vectors on the interfaces where $z = 0$ and $z = L$ [1]. All characteristics of reflected and transmitted waves near the frequency region of Bragg reflection for various polarizations of the incident wave were determined in [1].

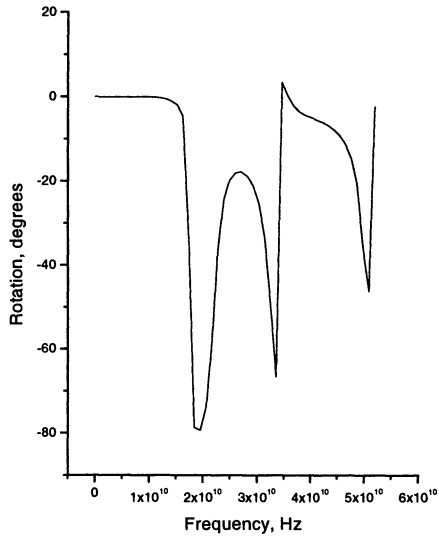

Figure 8. Rotation of the polarization plane of the reflected wave as a function of the frequency. $\overline{\epsilon} = 3.45$, $\Delta\epsilon = 0.45$, $\kappa_a = 0.3$, $q = 100$ radn/m, $L = 0.0301$ m.

3. Numerical results and Discussions

The solutions of the system of equations allow to describe both reflection of electromagnetic waves on the macroscopic helicoidal structure of the medium and wave reflection from the boundaries of sample. Calculations have been performed for linearly polarized incident wave with polarization along wire helices on the first boundary of the sample (along vector $\mathbf{a}(0)$). The following values of parameters have been chosen: $\overline{\epsilon} = 3.45$, $\Delta\epsilon = 0.45$, $\kappa_a = 0.3$, $q = 100$ radn/m, $\omega = 18.6$ GHz. In all cases the permeability was assumed to be equal to μ_0. The dependence of the intensity of the transmitted and reflected wave on the sample thickness is presented in Fig. 2.

Two different ways of propagation for circularly polarized waves in helicoidal medium in Bragg frequency region exist. For example, the right-handed circular wave has the direction of rotation of vector $\mathbf{E}$, which coincides with the direction of rotation of local axis of helicoidal medium, i.e. vector $\mathbf{a}$. This wave feels the significant reflection in Bragg frequency region and practically full reflection of wave from thick sample takes place.

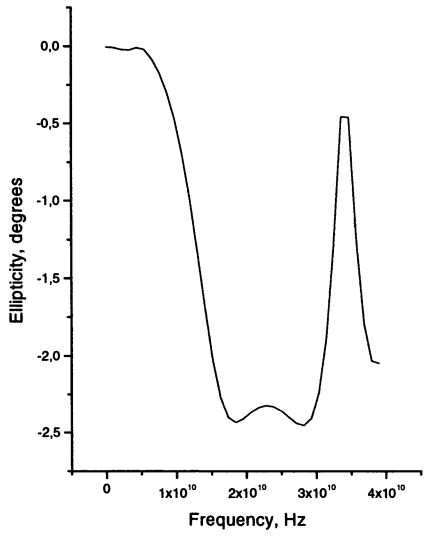

Figure 9. Ellipticity of the transmitted wave as a function of the frequency. $\bar{\epsilon} = 3.45$, $\Delta\epsilon = 0.45$, $\kappa_a = 0.3$, $q = 100$ radn/m, $L = 0.0301$ m.

The circular wave with the opposite sign of polarization does not interact with the periodic helicoidal structure. Only Fresnel's reflection of this wave from boundaries of sample is possible. So, we can conclude that the Bragg reflection in the macroscopic helicoidal structure is selective with respect both to frequency and polarization of electromagnetic wave. As a result the reflection and transmission coefficients for linearly polarized incident wave have the behavior, which is shown in Fig. 2.

In paper [1] the intensities of reflected and transmitted waves for sample thickness $L = 0.155$ m were investigated. As we can see from Fig. 2 the reflection and transmission coefficients at this thickness are close to saturation. Using competition of Bragg reflection of electromagnetic waves on the macroscopic helicoidal structure of medium and Fresnel's reflection from boundaries of sample can give a possibility to minimize the thickness of sample for transformation of the polarization state of waves.

The dependence of the rotation of the polarization plane of the transmitted and reflected wave on the frequency is presented in Figs. 3 and 4. The dependence of the ellipticity of the transmitted and reflected wave on the frequency is presented in Figs. 5 and 6. All figures are plotted for linearly

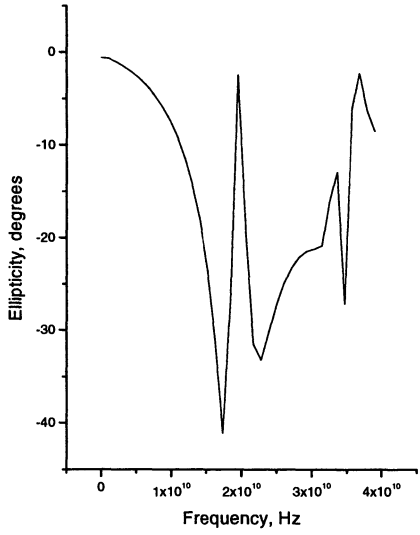

Figure 10. Ellipticity of the reflected wave as a function of the frequency. $\bar{\epsilon} = 3.45$, $\Delta\epsilon = 0.45$, $\kappa_a = 0.3$, $q = 100$ radn/m, $L = 0.0301$ m.

polarized incident wave with polarization along wire helices on the first boundary of the sample (along vector $\mathbf{a}(0)$). The rotation of polarization plane and ellipticity were calculated for the thickness $L = 0.015$ m which corresponds to the first maximum on the Fig. 2. The change of the sign of rotation of polarization plane for reflected wave is possible when the frequency changes (see Fig. 3). In the narrow frequency region near to the resonance the reflected wave has polarization which is close to circular polarization (see Fig. 6). The transmitted wave polarization is close to linear in all region of investigated frequencies (for this thickness of the sample).

In view of possible comparisons with previous results we have calculated characteristics of the transmitted and reflected wave for the thickness $L = 0.0301$ m which corresponds to the first minimum on the Fig. 2.

The dependence of the rotation of the polarization plane of the transmitted and reflected wave on the frequency and the dependence of the ellipticity of the transmitted and reflected wave on the frequency in this case are presented in Figs. 7-10.

4. Conclusion

On the base of the exact solution of the boundary-value problem for helicoidal medium with local chirality we describe the Bragg reflection of electromagnetic waves on the periodic structure of medium as well as Fresnel's reflection from sample's boundaries. It allows to model the transmission and reflection of electromagnetic waves in dependence on the obtained parameters of artificial helicoidal medium and to design the device for polarization transformation. Our present results demonstrate possibility of the minimizing of thickness of sample for transformation of the polarization state of electromagnetic waves. In contrast to the earlier proposed device [1], this structure can have a minimal size, because its operation is based on the phenomenon of the competition of Bragg reflection of electromagnetic waves on the macroscopic helicoidal structure of medium and Fresnel's reflection from boundaries of sample.

5. Acknowledgments

The authors are grateful to Professor Constantin Simovski of St. Petersburg Institute of Fine Mechanics and Optics, Russia for many useful remarks and for many discussions on this topic.

References

1. I.V. Semchenko, S.A. Khakhomov, S.A. Tretyakov, and A.H. Sihvola, (1999), Microwave analogy of optical properties of cholesteric liquid crystals with local chirality under normal incidence of waves, *J. Phys. D: Appl. Phys.* **vol.32**, pp. 3222-3226.
2. S.A. Kuehl, S.S. Grove, E. Kuehl, M. Bingle, J.H. Cloete, (1997), Manufacture of microwave chiral materials and their electromagnetic properties, in *Advances in Complex Electromagnetic Materials,* ed. by A. Priou et al., Kluwer Academic Publishers, NATO ASI Series 3, Vol. 28, pp. 317-332.
3. V.A. Belyakov and A.S. Sonin, (1982), *Cholesteric liquid crystals optics*, Nauka, Moscow (in Russian).
4. V.V. Varadan, A. Lakhtakia, and V.K. Varadan, (1988), Reflection and transmission characteristics of a structurally chiral slab: Intrinsic anisotropy and form chirality, *Optik,* **vol. 80**, pp. 27-32.
5. A. Lakhtakia and W. S. Weiglhofer, (1995), On light propagation in helicoidal bianisotropic mediums, *Proc. R. Soc. Lond.,* **vol. A 448**, pp. 419-437.
6. I. Abdulhaim, (1987), Light propagation along the helix of chiral smectics and twisted nematics, *Opt. Commun.*, **vol. 64**, pp. 443-448.
7. I.V. Semchenko and A.N. Serdyukov, (1982), Influence of molecular gyrotropy on the light propagation in cholesteric liquid crystals, *Reports of Academy of Sciences of BSSR,* **vol. 26, no. 3**, pp. 235-237. (in Russian).
8. A. Lakhtakia, (1998), Anomalous axial propagation in helicoidal bianisotropic media, *Optics Communications,* **vol. 157**, pp. 193-201.
9. A.N. Serdyukov, I.V. Semchenko, S.A. Tretyakov, and A.H. Sihvola, (2001), *Electromagnetics of bi-anisotropic materials.* Gordon and Breach.

USE OF CONTEMPORARY MATHEMATICAL APPLICATIONS FOR EXACT SOLUTION OF LIGHT PROPAGATION PROBLEM IN LAYERED MEDIA

Propagation and Scattering

A. F. KONSTANTINOVA, K. K. KONSTANTINOV,
B. V. NABATOV, AND E. A. EVDISHCHENKO
Shubnikov Institute of Crystallography, Russian Academy of Sciences, Leninskii pr. 59, Moscow, 117333 Russia.
E-mail: AFKonst@USA.NET

Abstract. This chapter discusses optical effects in layered anisotropic systems and illustrates their response with use of Mathematica software.

1. Introduction

The solution of the boundary problems of light propagation through crystalline plates and layered media with due regard of its multiple reflection is considered in a large number of works. In optically active media, these problems become rather complicated, and the corresponding calculations and the analytical expressions are rather cumbersome. These problems are solved by different methods. Thus, F.I. Fedorov suggested the covariant method, which provided rather a compact solution of this complex problem [1]. This method allowed one to solve many boundary problems in crystal optics [2–6]. Nevertheless, in complicated cases, one has to use computers.

Berreman [7] suggested the method of 4 x 4 matrices for studying reflection and transmission of the polarized light incident onto planar layered anisotropic media at a certain angle. The method is considered in detail elsewhere [8]. However, Berreman's method did not find extensive application for solving various problems of crystal optics. Possibly, this is partly associated with the fact that most of the problems of crystal optics have already been solved, and, in many practically important instances, very convenient analytical expressions have already been derived.

At present, any problem of light propagation in plates and layered systems with an arbitrary set of optical properties, including anisotropy, absorption, and optical activity, can be solved by the Berreman method with the aid of the system of computer mathematics – the application package Mathematica-4.1 or any other

S. Zouhdi et al. (eds.), Advances in Electromagnetics of Complex Media and Metamaterials, 319–338.

similar software package. Below, we consider just such a method for solving the boundary problems of crystal optics.

2. Berreman's Method

First, let us formulate the problem to be solved. Let a plane monochromatic wave with the wavelength λ be incident from isotropic medium I with the refractive index n_i onto an anisotropic optically active (gyrotropic) absorbing crystal at an angle ϕ_i (Fig. 1). Upon the wave refraction by medium II, two waves propagate from the upper face of the plate toward its lower face and two waves propagate in the backward direction from the upper and lower faces and undergo numerous reflection processes. The light exits to medium III at an angle ϕ_t with the refractive index n_t.

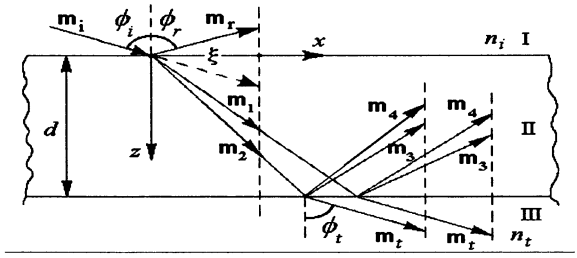

Figure 1. Reflection and transmission of a plane wave with due regard for multiple reflection at the oblique incidence of light onto the system: (I) isotropic ambient medium, (II) anisotropic plate; (III) isotropic substrate. The *y*-axis is normal to the drawing plane; $\mathbf{m}_j = n_j \mathbf{n}_j$ are the refraction vectors of the incident (*i*) and reflected (*r*) waves, the waves refracted in the forward (*1*, *2*) and backward (*3*, *4*) directions, and the transmitted (*t*) waves, where n_j are the corresponding refractive indices and $\mathbf{n}_j$ are the corresponding wave normals.

The transition matrix of system of the principal axes of tensors that describe the properties of the anisotropic medium to the Cartesian coordinate system *xyz* can be written with the aid of the Eulerian angles φ, θ, and ψ. In a package "Mathematica-4.1" the transition from one system of coordinates to another is carried out by three consecutive turns: on an angle φ around of an axis *z*, on an angle θ around of an axis *x* and on an angle ψ around of an axis *z*. The Maxwell equations for the fields in a medium can be written in the Cartesian coordinate system as a single matrix equation. The relationships between the intensity vectors of electric and magnetic fields **E**, **H** and electric and magnetic induction vectors **D**, **B** are set by the constitutive relations:

$$\begin{bmatrix} \mathbf{D} \\ \mathbf{B} \end{bmatrix} = \mathbf{M} \begin{bmatrix} \mathbf{E} \\ \mathbf{H} \end{bmatrix}, \qquad \mathbf{M} = \begin{pmatrix} \varepsilon & \rho \\ \rho' & \mu \end{pmatrix}, \tag{1}$$

where the block matrix **M** is called the optical matrix; ε and μ are the tensors of dielectric permittivity and magnetic permeability and ρ and ρ' are the tensors which describe the optical activity of crystals.

In Berreman's method the solution of a problem on definition of fields of the reflected and transmitted waves is reduced to the solution of system of four linear differential equations:

$$\frac{\partial}{\partial z}\psi = i\,\omega\,\Delta\,\psi, \tag{2}$$

where $\psi = [E_x, H_y, E_y, -H_x]$ is the generalized vector-column of the field, Δ is the differential 4 x 4 propagation matrix for the given medium. Obviously, the elements of the matrix Δ are the functions of the elements of the optical matrix **M** and the direction of the wave normal of the incident wave, i.e., $\Delta = f(\varepsilon, \mu, \rho, \rho', \varphi, \theta, \psi, \phi_i, n_i)$. Equation (2) is the wave equation of the generalized field vector ψ.

3. The Various Constitutive Relations at the Description of Optical Activity of Crystals

The elements of a matrix Δ essentially depend on the constitutive relations. Let us consider in more details how different authors write down the constitutive relations, which include optical activity. In the most general case, all tensors, which appear in the constitutive relations, have 9 components.

It was shown in [1], what type of constitutive relations give the correct description of optical activity. The same constitutive relations were received in [9]. They are used in many works [10 – 21]. We shall name them as Condon–Fedorov relations:

$$D_j = \varepsilon_{jk} E_k + i\,\alpha_{jk} H_k, \quad B_j = \mu_{jk} H_k - i\,\tilde{\alpha}_{jk} E_k \tag{3}$$

In [22, 23] the following constitutive relations were used

$$D_j = (\varepsilon_{jk} + i\,e_{jkl}\,g_{lm}\,n_m)\,E_k\,, \quad B_j = \mu_{jk} H_k\,, \tag{4}$$

where e_{jkl} is Levi-Civita tensor, n_m are directing cosines of wave normals. We will name (4) as Born-Landau relations.

In [24] the following constitutive relations (Drude's relations) were introduced

$$D_j = \varepsilon_{jk} E_k + i\,\gamma_{jk} H_k\,, \quad B_j = \mu_{jk} H_k \tag{5}$$

In the given constitutive relations pseudotensors of the second rank g_{lm}, γ_{jk}, α_{jk} are used and differently describe optical activity. They are even named differently in different works. As it is used to in crystal optics we will name them as gyration tensors. These constitutive relations were also used in works [7, 8, 25].

In a general case, the constitutive relations (3) – (5) for optically active crystals can be written as [7, 8]:

$$\mathbf{D} = \varepsilon\mathbf{E} + \rho\,\mathbf{H}, \quad \mathbf{B} = \mu\mathbf{H} + \rho'\,\mathbf{E} \tag{6}$$

In [1] it was shown, that the law of preservation of energy is violated, if the equations (4), (5) are used for solving boundary problems. Therefore theory of optical activity based on the constitutive relations (4), (5), is called approximate, and theory based on the constitutive relations (3) is called exact. Despite of this fact, the constitutive relations (4), (5) are used in many works for the description of optical activity.

In addition, in experimental research of optically active crystals, results for calculation of gyration tensor components g_{jk} are treated with using equations (4). If equations (3) are used, the same experimental results are described in different way, and this difference is substantial. Let us have a look on the interrelation of components of gyration tensors α_{jk} , g_{jk} and γ_{jk}, included in constitutive relations (3) – (5).

4. Physical Meaning of Eigenvalues and Eigenvectors of a Matrix Δ

We received the characteristic equation of matrix Δ for uniaxial optically active crystals using constitutive relations (3). Comparing it with the exact equation of normals in [1] it turned out, that the coefficients of both equations of the fourth degree completely coincide. Hence, eigenvalues η_j of a matrix Δ are solutions of equation of normals. At oblique incidence of light the value η_j is projection of refraction vectors of waves on a normal direction z to a plate. They are related with refraction indices n_j of eigenwaves by the equation

$$\eta_j^2 = n_j^2 - \xi^2, \tag{7}$$

where $\xi = n_i \sin\phi_i$. It is obvious that at normal incidence of light on a crystal ($\xi = 0$) the eigenvalues of matrix Δ completely determine refraction indices of waves propagating through a crystal. The positive values of η_j correspond to all waves of a "direct course", i.e. waves going from the top side to bottom, and negative values correspond to all waves of a "return course ".

Eigenvectors $\psi_j = [E_{xj}, H_{yj}, E_{yj}, -H_{xj}]$ of matrix Δ are the generalized vectors of fields of eigenwaves (refracted and reflected). The polarization of eigenwaves is determined by mutual spatial orientation of the crystal and refraction vector of the incident wave. At normal incidence and coincidence of axes of the chosen system of coordinates to the main axes of tensor ε_{jk}, α_{jk}, g_{jk} and γ_{jk} and relations

$$k_E = E_{yj} / E_{xj} \text{ and } k_H = H_{yj} / H_{xj} \tag{8}$$

determine the state of polarization of fields $\boldsymbol{E}_j$ and $\boldsymbol{H}_j$ of j-th eigenwave in the crystal corresponding to refraction index n_j (see (7)). At oblique incidence the specified relations determine projections of ellipses of polarization of eigenwaves to the surface of the crystal plate. Thus it is obvious, that the information on optical properties of medium, including polarization of eigenwaves and their indices of refraction is carried by matrix Δ.

5. Comparison of Refraction Indices and Polarization of Eigenwaves Obtained Using Various Constitutive Relations

5.1. CRYSTALS OF CLASSES OF SYMMETRY *32, 422, 622*

At first we shall consider optically active crystals, in which the tensor of dielectric permittivity ε_{jk}, and gyration tensors α_{jk} , g_{jk} and γ_{jk}, describing optical activity in the different constitutive relations (3) – (5), all have identical diagonal type. Only the crystals of classes *32, 422, 622* ($\varepsilon_{11} = \varepsilon_{22} \neq \varepsilon_{33}$, $\alpha_{11} = \alpha_{22} \neq \alpha_{33}$, $g_{11} = g_{22} \neq g_{33}$, $\gamma_{11} = \gamma_{22} \neq \gamma_{33}$) or crystals of cubic classes *23, 432* ($\varepsilon_{11} = \varepsilon_{22} = \varepsilon_{33}$, $\alpha_{11} = \alpha_{22} = \alpha_{33}$, $g_{11} = g_{22} = g_{33}$, $\gamma_{11} = \gamma_{22} = \gamma_{33}$) possess these properties.

In the majority of experimental works refraction indices n_1, n_2 are calculated using constitutive relations (4) and the solution of this equation is:

$$n_{1,2}^2 = \{(n_{01}^2 + n_{02}^2) \pm [(n_{01}^2 - n_{02}^2)^2 + 4\,G^2\,]^{1/2}\} / 2, \qquad (9)$$

$$\text{where} \quad n_{01}^2 = \varepsilon_{11}, \quad n_{02}^2 = \varepsilon_{11}\,\varepsilon_{33} / (\varepsilon_{11}\sin^2\theta + \varepsilon_{33}\cos^2\theta), \qquad (10)$$

n_{01}, n_{02} are refraction indices of eigenwaves in the crystal without the account of optical activity; G is scalar parameter of gyration:

$$G = g_{ik}\, n_k\, n_i \qquad (11)$$

In uniaxial crystals $g_{22} = g_{11}$, and equation (11) can be written as:

$$G = g_{11}\sin^2\theta + g_{33}\cos^2\theta\,, \qquad (12)$$

where θ is the angle between wave normal and optical axis, and thus the angle between an optical axis and normal to the surface of a plate for a normal incidence of light.

Now, we will compare expressions for refraction indices n_1, n_2 received using constitutive relations (3), (4) and (5) for two most important cases of normal incidence of light, along optical axis and perpendicular to it. Let us consider at the beginning the case of propagation of light along optical axis. The results are

presented in the table below. It should be noticed that in results below, the expressions of the components of eigenvectors appear without constant multiplier.

Also, it is necessary to notice, that when constitutive relations (4) are used, tensor g_{jk} is written down differently, than when equations (3) are used and it looks like:

$$\varepsilon = \begin{pmatrix} \varepsilon_{11} & -ig_{33} & 0 \\ ig_{33} & \varepsilon_{11} & 0 \\ 0 & 0 & \varepsilon_{33} \end{pmatrix}, \tag{13}$$

TABLE. The constitutive relations offered by the different authors, refraction indices $n_{1,2}$, generalized vectors $\psi_{1,2}$ of fields of eigenwaves and kind of matrix Δ at normal incidence of light in optically active crystals of classes *32*, *422*, *622* in the direction of optical axis ($\theta = 0°$) and of classes *23*, *432*

Authors, the constitutive relations, $n_{1,2}$, $\psi_{1,2}$	Matrix Δ
Condon, Fedorov [9, 1] $D_j = \varepsilon_{jk} E_k + i\alpha_{jk} H_k$, $B_j = \mu_{jk} H_k - i\,\tilde{\alpha}_{jk} E_k$ $n_{1,2} = \sqrt{\varepsilon_{11}} \mp \alpha_{11}$ $\psi_{1,2} = [\pm i / \sqrt{\varepsilon_{11}},\ \pm i,\ 1 / \sqrt{\varepsilon_{11}},\ 1]$	$\begin{pmatrix} 0 & 1 & -i\alpha_{11} & 0 \\ \varepsilon_{11} & 0 & 0 & -i\alpha_{11} \\ i\alpha_{11} & 0 & 0 & 1 \\ 0 & i\alpha_{11} & \varepsilon_{11} & 0 \end{pmatrix}$
Born, Landau [22, 23] $D_j = (\varepsilon_{jk} + i\, e_{jkl}\, g_{lm}\, n_m)\, E_k$, $B_j = \mu_{jk} H_k$ $n_{1,2} = \sqrt{\varepsilon_{11} \mp g_{33}}$ $\psi_{1,2} = [\pm i / \sqrt{\varepsilon_{11} \mp g_{33}},\ \pm i,\ 1/\sqrt{\varepsilon_{11} \mp g_{33}},\ 1]$	$\begin{pmatrix} 0 & 1 & 0 & 0 \\ \varepsilon_{11} & 0 & ig_{33} & 0 \\ 0 & 0 & 0 & 1 \\ -ig_{33} & 0 & \varepsilon_{11} & 0 \end{pmatrix}$
Drude, Berreman [24, 7] $D_j = \varepsilon_{jk} E_k + i\,\gamma_{jk} H_k$, $B_j = \mu_{jk} H_k$ $n_{1,2} = \sqrt{\varepsilon_{11} + \gamma^2_{11}/4} \mp \gamma_{11}/2$ $\psi_{1,2} = [i\,(\pm\sqrt{\varepsilon_{11} + \gamma^2_{11}/4} + \gamma_{11})/\varepsilon_{11},\ \pm i,\ 1/(\sqrt{\varepsilon_{11} + \gamma^2_{11}/4} \mp \gamma_{11}),\ 1]$	$\begin{pmatrix} 0 & 1 & 0 & 0 \\ \varepsilon_{11} & 0 & 0 & -i\gamma_{11} \\ 0 & 0 & 0 & 1 \\ 0 & i\gamma_{11} & \varepsilon_{11} & 0 \end{pmatrix}$

One can see that expressions for refraction indices obtained using different constitutive relations are different even for light propagating along optical axis and the expressions for them can be written down as:

$$n_{1,2} = \sqrt{\varepsilon_{11}} \mp \alpha_{11} \approx \sqrt{\varepsilon_{11}} \mp g_{33} / (2\sqrt{\varepsilon_{11}}) \approx \sqrt{\varepsilon_{11}} \mp \gamma_{11} / 2 \tag{14}$$

Let us note, that using the equations (3) $n_{1,2}$ are calculated precisely, and using the equations (4), (5) expressions given for $n_{1,2}$ are the result of the approximate extraction of the square root. From (14) the relation between components of gyration tensors α_{11}, g_{33} ,γ_{11} follows as:

$$\alpha_{11} = g_{33} / (2\sqrt{\varepsilon_{11}}) = \gamma_{11} / 2 \qquad (15)$$

Let us note, that for any of the equations (3) – (5) ellipticity of eigenwaves $k_E = E_{yj}/E_{xj} = \pm i$ and thus eigenwaves are circularly polarized.

Now, let us consider the expressions for refraction indices obtained using only equations (3) and (4), for the plate cut parallel to optical axis ($\theta = 90°$), i.e. for light propagating perpendicular to the optical axis:

$$n_{1,2}^2 = (\varepsilon_{11} + \varepsilon_{33} + 2\alpha_{11}\alpha_{33} \pm \sqrt{(\varepsilon_{33} - \varepsilon_{11})^2 + 4(\alpha_{11} + \alpha_{33})(\alpha_{11}\varepsilon_{33} + \alpha_{33}\varepsilon_{11})})/2, \quad (16)$$

$$n_{1,2}^2 = (\varepsilon_{11} + \varepsilon_{33} \pm \sqrt{(\varepsilon_{33} - \varepsilon_{11})^2 + 4g_{11}^2}) / 2. \qquad (17)$$

As well as in the previous case, the distinction in the description of optical activity is well visible.

As it was shown [26], the constitutive relations (4) describe the phenomenon of optical activity within the product of parameters of anisotropy with parameters of gyrotropy. The expression in (16) (exact theory) passes into expression in (17) (approximate theory) if we set:

$$g_{11} = \sqrt{\bar{\varepsilon}}(\alpha_{11} + \alpha_{33}), \qquad (18)$$

where $\varepsilon_{11,33} = \bar{\varepsilon} \mp \Delta\varepsilon$, $\bar{\varepsilon} = (\varepsilon_{11} + \varepsilon_{33}) / 2$, $\Delta\varepsilon = (\varepsilon_{33} - \varepsilon_{11}) / 2$ and neglect in (16) terms $(2\alpha_{11}\alpha_{33})$ in comparison with $(\varepsilon_{11} + \varepsilon_{33})$.

However, the most important question is the basic distinction in the description of optical activity obtained using the different constitutive relations. The rotation of plane of polarization for light propagating along the axis is determined by different components of gyration tensor if different constitutive relations are used, namely:

$$\chi = \pi d (n_2 - n_1) / \lambda = \pi d\, 2\alpha_{11} / \lambda = \pi d\, g_{33} / (\lambda\sqrt{\varepsilon_{11}}) = \pi d\, \gamma_{11} / \lambda \qquad (19)$$

If constitutive relations (4) are used for light propagating along an optical axis, the distinction in refraction indices, and correspondingly the rotation of plane of polarization, is determined by component g_{33}, which is different from the two other identical components. If constitutive relations (3) are used for the description of optical activity, the rotation of plane of polarization is determined by two

identical components g_{11}. In case of light propagating in the direction, perpendicular to the optical axis, all optical parameters, including of refraction indices of eigenwaves, are determined by two identical components of gyration tensor $g_{11} = g_{22}$ if equations (4) are used. If equations (3) are used the same optical parameters are determined by the sum of components $(g_{11} + g_{33})$. This is the basic distinction in the description of optical activity by the different the constitutive relations. It should be considered by experimental and theoretical consideration of the phenomenon of optical activity.

Let us consider some basic features of calculation of refraction indices obtained using the various constitutive relations for crystals of different classes of symmetry.

5.2. CRYSTALS OF CLASSES OF SYMMETRY *3*, *4*, *6* AND *3m*, *4mm*, *6mm*

There are antisymmetric components $\alpha_{21} = -\alpha_{12}$ besides diagonal components of gyration tensor in crystals of classes *3*, *4*, *6* [1, 27]. Using constitutive relations (4) it was assumed that the gyration tensor is completely symmetric. The same was assumed in [22, 23, 28–31]. Therefore crystals of classes *32*, *422*, *622* and *3*, *4*, *6* were described by identical diagonal gyration tensors and components $\alpha_{21} = -\alpha_{12}$ were set equal to zero. The matrixes Δ are suitable for crystals of classes *32*, *422*, *622* at $\alpha_{12} = \alpha_{21} = 0$, classes *3m*, *4mm*, *6mm* at $\alpha_{11} = \alpha_{22} = \alpha_{33} = 0$ and classes *23*, *432* at $\alpha_{11} = \alpha_{22} = \alpha_{33}$, $\alpha_{12} = \alpha_{21} = 0$.

The matrix Δ for crystals of these classes for oblique incidence of light and $\theta = 0°$ (optical axis is perpendicular to plane of the plate), $\psi = 0°$ and any angle φ can be written as:

$$\Delta = \begin{pmatrix} -i\alpha_{12} & \dfrac{\varepsilon_{33} - \alpha_{33}^2 - \xi^2}{\varepsilon_{33} - \alpha_{33}^2} & -\dfrac{i(\alpha_{11}(\varepsilon_{33} - \alpha_{33}^2) + \alpha_{33}\xi^2)}{\varepsilon_{33} - \alpha_{33}^2} & 0 \\ \varepsilon_{11} & i\alpha_{12} & 0 & -i\alpha_{11} \\ i\alpha_{11} & 0 & -i\alpha_{12} & 1 \\ 0 & \dfrac{i(\alpha_{11}(\varepsilon_{33} - \alpha_{33}^2) + \alpha_{33}\xi^2)}{\varepsilon_{33} - \alpha_{33}^2} & \dfrac{\varepsilon_{11}(\varepsilon_{33} - \alpha_{33}^2) - \varepsilon_{33}\xi^2}{\varepsilon_{33} - \alpha_{33}^2} & i\alpha_{12} \end{pmatrix} \quad (20)$$

In crystals of classes of symmetry *3*, *4*, *6* the component α_{12} appear in expressions for refraction indices (expressions are done for $\theta = 0°$ and $\theta = 90°$, accordingly):

$$n_{1,2} = \sqrt{\varepsilon_{11} - \alpha_{12}^2} \pm \alpha_{11}; \quad (21)$$

$$n_{1,2}^2 = \frac{\varepsilon_{11} - \alpha_{11}^2 - \alpha_{12}^2}{\varepsilon_{11} - \alpha_{11}^2}(\varepsilon_{11} + \varepsilon_{33} + 2\alpha_{11}\alpha_{33} \pm \sqrt{(\varepsilon_{33} - \varepsilon_{11})^2 + 4(\alpha_{11} + \alpha_{33})(\alpha_{11}\varepsilon_{33} + \alpha_{33}\varepsilon_{11})})/2. \quad (22)$$

For a long time crystals of classes *3m*, *4mm*, *6mm* were considered as inactive, since their gyration tensor is antisymmetric: $\alpha_{21} = -\alpha_{12}$ and $\alpha_{11} = \alpha_{22} = \alpha_{33} = 0$. It was shown in [32] that in these crystals optical activity is manifested only at oblique incidence of light (ellipticity of eigenwaves is distinct from zero only in this case). However, from expressions (21) and (22) one can see that even for normal incidence the refraction indices depend on components α_{12}.

5.3. CRYSTALS OF CLASSES OF SYMMETRY $\bar{4}$, $\bar{4}2m$

In crystals of class $\bar{4}$ the components are $\alpha_{22} = -\alpha_{11}$, $\alpha_{33} = 0$, $\alpha_{21} = \alpha_{12}$. In addition in crystals of class $\bar{4}2m$ components $\alpha_{12} = \alpha_{21} = 0$. The type of gyration tensor in crystals of these classes essentially differs from the type of tensor in crystals of others uniaxial classes. This difference is that only one axis of gyration tensor α coincides with one axis of tensor ε, and they both coincide with a direction of the optical axis of a crystal. If the direction of this axis coincides with an axis z of laboratory system of coordinates, two other main axes of tensor ε are directed along axes x and y, and two other main axes of tensor α are rotated by some angle in relation to axes x and y. For calculation of refraction indices of these crystals it is necessary to rotate the system of main axes of gyration tensor α and tensor ε around axis z on an angle φ. Let us emphasize, that in uniaxial crystals of other classes both for normal, and oblique incidence of light such rotation does not change the type of tensors α and ε at $\theta = 0°$ and $\theta = 90°$, whereas in crystals of classes, $\bar{4}$, $\bar{4}2m$ even for normal incidence the rotation on an angle φ, while not changing tensor ε, plays determining role in calculation of refraction indices for $\theta = 90°$.

The matrix Δ for crystals of these classes for normal incidence at $\theta = \psi = 0°$ and any value of angle φ is:

$$\Delta = \begin{pmatrix} -i\alpha_{12} & 1 & i\alpha_{11} & 0 \\ \varepsilon_{11} & i\alpha_{12} & 0 & -i\alpha_{11} \\ i\alpha_{11} & 0 & i\alpha_{12} & 1 \\ 0 & -i\alpha_{11} & \varepsilon_{11} & -i\alpha_{12} \end{pmatrix} \qquad (23)$$

Refraction indices calculated from these matrixes are:

$$\text{for } \theta = 0° \quad n_{1,2}^2 = \varepsilon_{11} - \alpha_{11}^2 - \alpha_{12}^2, \qquad (24a)$$

$$\text{for } \theta = 90° \quad n_{1,2}^2 = \frac{\varepsilon_{11} - \alpha_{11}^2 - \alpha_{12}^2}{2(\varepsilon_{11} - [\cos(2\varphi)\alpha_{11} + \sin(2\varphi)\alpha_{12}]^2)} \text{ x}$$

$$x\,(\varepsilon_{11}+\varepsilon_{33}\pm\sqrt{(\varepsilon_{33}-\varepsilon_{11})^2+4[\cos(2\varphi)\alpha_{11}+\sin(2\varphi)\alpha_{12}]^2\varepsilon_{33}}\,) \qquad (24b)$$

Using constitutive relations (4) expressions for $n_{1,2}$ at $\theta = 90°$ can be written as:

$$n_{1,2}{}^2=(\varepsilon_{11}+\varepsilon_{33}\pm\sqrt{(\varepsilon_{33}-\varepsilon_{11})^2+4[\cos(2\varphi)g_{11}+\sin(2\varphi)g_{12}]^2}\,)/2 \qquad (25)$$

Comparing expressions (24) and (25) one can see which approximations are made in this case and the relations between components in the exact and approximate theories are clearly visible:

$$g_{11}=\alpha_{11}\,\bar{n}\,,\quad g_{12}=\alpha_{12}\,\bar{n} \qquad (26)$$

5.4. CRYSTALS OF ORTHORHOMBIC CLASS OF SYMMETRY *222*

In the most common case in biaxial crystals all components of tensors ε and α are distinct from zero. Thus tensor ε is symmetric, and tensor α is tensor of any type. With the help of a package "Mathematica-4.1" the matrix Δ can be written in the general form. However, it looks too cumbersome and does not have much practical use to be presented here. To obtain correct dependence of refraction indices of eigenwaves for an angle φ for crystals of classes *1*, *2*, *m* and *mm2*, it is necessary to perform the calculations similarly to case of crystals of classes $\bar{4}$, $\bar{4}2m$. It is clear that the expressions will turn out very cumbersome, therefore we will not present them here.

Let us consider in details crystals of an orthorhombic class *222*. In these crystals the main axes of tensors ε and α coincide with the axes of symmetry *2*. In laboratory system of coordinates these tensors are diagonal ($\varepsilon_{jk}=0$, $\alpha_{jk}=0, j\neq k$). For normal incidence the refraction indices are equal:

$$n_{1,2}{}^2=(\varepsilon_{11}+\varepsilon_{22}+2\,\alpha_{11}\,\alpha_{22}\pm\sqrt{(\varepsilon_{22}-\varepsilon_{11})^2+4(\alpha_{11}+\alpha_{22})(\alpha_{11}\varepsilon_{22}+\alpha_{22}\varepsilon_{11})}\,)/2 \qquad (27)$$

The matrix Δ in case $\varphi=\theta=\psi=0°$ for oblique incidence is:

$$\Delta=\begin{pmatrix} 0 & \dfrac{\varepsilon_{33}-\alpha_{33}^2-\xi^2}{\varepsilon_{33}-\alpha_{33}^2} & -\dfrac{i(\alpha_{22}(\varepsilon_{33}-\alpha_{33}^2)+\alpha_{33}\xi^2)}{\varepsilon_{33}-\alpha_{33}^2} & 0 \\ \varepsilon_{11} & 0 & 0 & -i\alpha_{11} \\ i\alpha_{11} & 0 & 0 & 1 \\ 0 & \dfrac{i(\alpha_{22}(\varepsilon_{33}-\alpha_{33}^2)+\alpha_{33}\xi^2)}{\varepsilon_{33}-\alpha_{33}^2} & \dfrac{\varepsilon_{22}(\varepsilon_{33}-\alpha_{33}^2)-\varepsilon_{33}\xi^2}{\varepsilon_{33}-\alpha_{33}^2} & 0 \end{pmatrix} \qquad (28)$$

Analogous matrixes are obtained at $\varphi = 0°$, $\theta = \psi = 90°$, and $\varphi = \theta = 90°$, $\psi = 0°$. With this consideration the approximated connection between components of gyration tensors g_{ii} and α_{jj} can be written as:

$$g_{11} \approx (\alpha_{22} + \alpha_{33})\sqrt{\frac{\varepsilon_{22} + \varepsilon_{33}}{2}}, \quad g_{22} \approx (\alpha_{11} + \alpha_{33})\sqrt{\frac{\varepsilon_{11} + \varepsilon_{33}}{2}}, \quad g_{33} \approx (\alpha_{11} + \alpha_{22})\sqrt{\frac{\varepsilon_{11} + \varepsilon_{22}}{2}}. \tag{29}$$

One can see that in the given expressions relation between components of g_{ii} and α_{ij} is similar to relation revealed for crystals of classes *32*, *422*, *622* (15), and is true with the same approximation.

6. Solution of Boundary Problems in Crystal Optics

Once matrix Δ is determined, one can use it to solve the boundary problem of light propagation in a layered system. In [7, 8], it was suggested to integrate Eq. (2) by dividing the anisotropic medium of thickness d into layers of small thicknesses so that within each such layers the elements of the matrix Δ are independent of z. As a result, for a layer of thickness h, the solution has the form

$$\psi(z + h) = \exp(i\,\omega h\,\Delta)\,\psi(z) = \mathbf{L}(h)\,\psi(z) \tag{30}$$

The matrix $\mathbf{L}(h) = \exp(i\omega h\Delta)$, which describes the transformation of the field of the light wave during its propagation through a plate, is called the layer matrix. Further solution of the problem reduces to the determination of the layer matrix $\mathbf{L}(h)$. It was suggested [7, 8] to expand the function $\mathbf{L}(h)$ into a series in powers of Δ. Obviously, this expansion is approximate. In [33], layer matrix $\mathbf{L}(h)$ is determined with the use of the similarity transformation. With this aim, one has to determine numerically the eigenvalues and eigenvectors of matrix Δ for each layer. This method is rather cumbersome and requires considerable computational resources. In [34] the exact calculation of the layer matrix $\mathbf{L}(h)$ is obtained with the invocation of the Sylvester theorem.

Now, we pass on to the direct description of the ways of solving the formulated problem. First, the form of all the tensors ε, μ, α should be set in the principal coordinate system defined by the triad of the Eulerian angles φ, θ, ψ ($\varphi = 0°$, $\theta = 0°$, $\psi = 0°$). Thanks to the interface used in the Mathematica-4.1 system and convenient representation of input data, all the tensors can be set in a very clear symbolic and numerical form and can be readily modified. Thus, the block optical matrix $\mathbf{M}$ is readily determined. The built-in function sets the rotation matrix for the transition from the principal coordinate system of the tensor to new coordinates chosen in the formulation of the specific problem. Then, the form of each tensor is determined in the new coordinate system, and the matrix $\mathbf{M}$ is formed.

The next stage of the solution following the determination of all of the tensors ε, μ and α is the determination of the matrix Δ. In all the studies we are aware of the matrices Δ are determined with the use of the relationships indicated in [7, 8]. Using the package Mathematica-4.1, one can readily obtain the expression for the layer matrix **L**(*h*) with the aid of the built-in function called the "matrix exponent":

$$\mathbf{L}(h) = MatrixExp(i\,2\,\pi\,h\,\Delta\,/\,\lambda) \tag{31}$$

As was indicated in [7, 8], the matrix **L**(*h*) relates the fields at the entrance and exit surfaces of the plate (for each layer, $h = d$):

$$\psi_t\,(d) = \mathbf{L}(d)\,(\psi_i\,(0) + \psi_r\,(0)), \tag{32}$$

where the subscripts *i*, *r* and *t* indicate the incident, reflected, and transmitted waves, respectively, whereas, similar to [7, 8], the generalized fields are written as

$$\psi_i = \begin{bmatrix} E_{ip}\cos\phi_i \\ n_i E_{ip} \\ E_{is} \\ n_i E_{is}\cos\phi_i \end{bmatrix},\quad \psi_r = \begin{bmatrix} -E_{rp}\cos\phi_r \\ n_i E_{rp} \\ E_{rs} \\ -n_i E_{rs}\cos\phi_r \end{bmatrix},\quad \psi_t = \begin{bmatrix} E_{tp}\cos\phi_t \\ n_t E_{tp} \\ E_{ts} \\ n_t E_{ts}\cos\phi_t \end{bmatrix}, \tag{33}$$

where E_{ip} and E_{is} are the known components of the electric field of the incident wave of any polarization (linear, circular, or elliptic) and E_{rp}, E_{rs}, E_{tp} and E_{ts} are the components of the electric fields of the reflected and transmitted waves. Here the subscript 'p' indicates the wave polarization parallel to the incidence plane (the *p*-polarization) and the subscript 's' indicates the polarization normal to the incidence plane (the *s*-polarization).

Thus, for the linearly polarized incident wave with the azimuth β_P, the components E_{ip}, E_{is} are

$$E_{ip} = \cos\beta_P,\quad E_{is} = \sin\beta_P\,, \tag{34}$$

where $\beta_P = 0°$ corresponds to the *p*-polarization of the incident light and $\beta_P = 90°$, to the *s*-polarization. For the circularly polarized light we have

$$E_{ip} = \mp\, i\,\sqrt{2}\,/\,2,\quad E_{is} = \sqrt{2}\,/\,2\,, \tag{35}$$

where the upper sign corresponds to the right-hand circular polarization.

When writing Eq. (33), we took into account that in the optically isotropic and nonmagnetic ambient media, the components of the magnetic field are proportional to the corresponding orthogonal components of the electric field with the proportionality coefficient being equal to the refractive index of the medium.

Writing the generalized vectors of the fields of the incident, reflected, and the transmitted waves ψ_j ($j = i, r, t$) as is suggested in [7, 8], we can solve the system of linear algebraic equations (32) with respect to the unknown components of the fields of the reflected and transmitted waves. To solve the boundary problem, we introduce a new generalized field vector **Q** which includes the components of the electric fields of the transmitted and reflected waves,

$$\mathbf{Q} = \{E_{tp}, E_{ts}, E_{rp}, E_{rs}\} \tag{36}$$

related to the generalized vectors of the fields of the transmitted ψ_t and reflected ψ_r waves by the relationships

$$\psi_t = T_m \mathbf{Q}\,; \quad \psi_r = R_m \mathbf{Q}\,, \tag{37}$$

where

$$T_m = \begin{pmatrix} \cos\phi_t & 0 & 0 & 0 \\ n_t & 0 & 0 & 0 \\ 0 & 1 & 0 & 0 \\ 0 & n_t \cos\phi_t & 0 & 0 \end{pmatrix}, \quad R_m = \begin{pmatrix} 0 & 0 & -\cos\phi_i & 0 \\ 0 & 0 & n_i & 0 \\ 0 & 0 & 0 & 1 \\ 0 & 0 & 0 & -n_i \cos\phi_i \end{pmatrix}.$$

Then Eq. (32) can be rewritten as:

$$T_m \mathbf{Q} = \mathbf{L}\,\psi_i + \mathbf{L}\,R_m \mathbf{Q}\,, \tag{38}$$

therefore the vector introduced earlier is determined as

$$\mathbf{Q} = (T_m - \mathbf{L}\,R_m)^{-1}\,\mathbf{L}\,\psi_i\,. \tag{39}$$

Calculating the vector **Q**, we can directly determine the components of the fields of the reflected and transmitted waves. Knowing these components, we can write the reflection and transmission matrices for the plate in the form [8]

$$\mathbf{E}_r = \begin{bmatrix} E_{rp} \\ E_{rs} \end{bmatrix} = \mathbf{R}\,\mathbf{E}_i = \begin{pmatrix} r_{pp} & r_{ps} \\ r_{sp} & r_{ss} \end{pmatrix} \begin{bmatrix} E_{ip} \\ E_{is} \end{bmatrix}, \tag{40a}$$

$$\mathbf{E}_t = \begin{bmatrix} E_{tp} \\ E_{ts} \end{bmatrix} = \mathbf{T}\,\mathbf{E}_i = \begin{pmatrix} t_{pp} & t_{ps} \\ t_{sp} & t_{ss} \end{pmatrix} \begin{bmatrix} E_{ip} \\ E_{is} \end{bmatrix} \tag{40b}$$

The matrices **R** and **T** are the complex amplitude reflection and transmission matrices, respectively. Once the reflection and transmission

coefficients are determined, one can calculate the reflection and transmission coefficients for the intensities,

$$R_{ij} = (\mathrm{Re}\, r_{ij})^2 + (\mathrm{Im}\, r_{ij})^2, \tag{41}$$

and also the reflectance and transmittance (the amplitude of the incident wave is assumed to be unity)

$$R = |\, E_{rp} \,|^2 + |\, E_{rs} \,|^2, \quad T = (\, |\, E_{tp} \,|^2 + |\, E_{ts} \,|^2\,)\, n_t \cos\phi_t / n_i \cos\phi_i \tag{42}$$

One should pay attention to the factor ($n_t \cos\phi_t / n_i \cos\phi_i$) in Eq. (42). If the refractive indices of the ambient media are equal, $n_t = n_i$, this factor is unity and, thus, is omitted in the formulas. If $n_t \neq n_i$, the law of energy conservation R + T = 1 [35] is fulfilled only if this factor is also taken into account, which can be considered as a certain criterion of the validity of the computation.

The components of the reflection and transmission matrices (40) thus determined allow one to calculate the characteristics of the polarizations of the reflected and transmitted waves, i. e., the azimuths χ_r and the ellipticities $k_{r,t}$ = tg $\gamma_{r,t}$ written in the form:

$$\begin{aligned} \mathrm{tg}\, 2\chi_{r,t} &= 2\, \mathrm{Re}\, (E_{rs,\,ts} / E_{rp,\,tp}) / (1 - |\, E_{rs,\,ts} / E_{rp,\,tp} \,|^2) \\ \sin 2\gamma_{r,t} &= 2\, \mathrm{Im}\, (E_{rs,\,ts} / E_{rp,\,tp}) / (1 + |\, E_{rs,\,ts} / E_{rp,\,tp} \,|^2) \end{aligned} \tag{43}$$

In crystal optics, one has often to study the variation in the intensity of the light transmitted in the direction normal to the plate located between arbitrarily oriented polarizer (β_P) and analyzer (β_A). In this case, the light intensity can be written in different ways, in particular, as

$$J = T\,(1 + \cos 2\gamma_t \cos(2\beta_A - 2\chi_t)) / 2 \tag{44}$$

Thus, the use of Berreman's method and the package Mathematica-4.1 allows one to solve any problems of light propagation through crystalline plates with arbitrary sets of optical properties such as birefringence, absorption, and optical activity. No limitations are imposed on the presence or absence of magnetic properties. Thus, there is a possibility not only to obtain the numerical results by a comparatively simple and clear way, but also to derive the analytical expressions that describe various optical characteristics. It should be emphasized once again that Berreman's method is still not widely used in crystal optics.

7. Some Examples of Solving Boundary Problems in Crystal Optics. Discussion of the Results

Using all the above stated material allowed us to write an original program and calculate, with the aid of the built-in functions of the package Mathematica-4.1, the characteristics of the reflected and transmitted light for crystals of any class by

setting the tensors ε and α in their general, including complex, forms, and construct the dependences of these characteristics on all the parameters of the media for which the calculations are made. Since the present study is aimed at the investigation of insufficiently studied optical properties of some specific classes of crystals, we consider here only some purely illustrative examples. The detailed study of some interesting characteristics of the light propagation in crystals will be considered later.

It should be indicated that all the calculations were made for $\lambda = 0.6328$ μm, $n_i = 1$, and $n_t = 1$ if not specified otherwise. These curves are also constructed using the package "Mathematica-4.1".

Figure 2 shows the change in the polarization azimuth χ_t (a) and ellipticity k_t (b) of the transmitted light as a function of the orientation angle of the optical axis, θ, for the normal incidence of the *p*-polarized light onto the optically active plate. If the light propagates along the optical axis (θ = 0°), the angle χ_t corresponds to the rotation value of the polarization plane of the incident light. If the optical axis deviates from the normal the change of the value χ_t has an oscillating character. The oscillating amplitude first drastically decreases, then becomes zero, at θ ≈ 52°, and, finally increases again up to a certain value. The ellipticity value of the transmitted light k_t also shimmies. Thus up to the value of θ ≈ 52° the ellipticity sign is positive, and after this value of θ the ellipticity sign becomes negative. This behavior of χ_t and k_t is associated with the fact that the components α_{11} and α_{33} of the gyration tensor have different signs. All crystals, which have the gyration tensor components of opposite signs, exhibit the same feature, when at the certain value of θ the plate behaves as inactive ($\chi_t = 0$, $k_t = 0$).

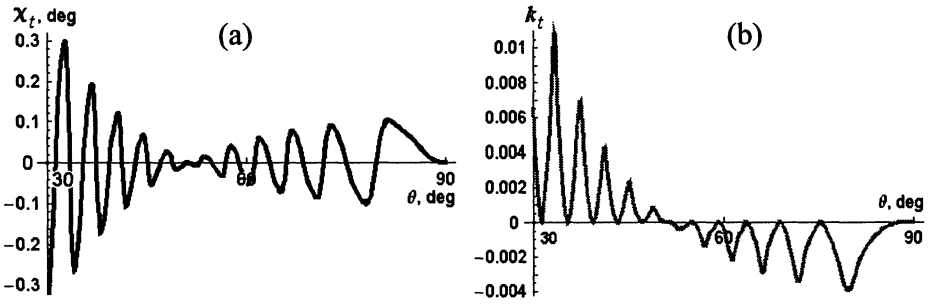

Figure 2. Polarization azimuth χ_t (a) and ellipticity k_t (b) of the light wave transmitted through the optically active crystalline plate normally to its surface ($\phi_i = 0$) as a function of angle θ of the deviation of the optical axis from the surface normal: $n_1 = n_2 = 1.97$, $n_3 = 1.99$, $\alpha_{11} = \alpha_{22} = -5.2 \cdot 10^{-5}$, $\alpha_{33} = 12 \cdot 10^{-5}$, $\varphi = \psi = 0°$, $d = 300$ μm, $\lambda = 0.4$ μm.

Figure 3 shows the intensity of reflectivity as a function of the angle of light incidence for the plates prepared from absorbing biaxial (Fig. 3a) and isotropic (Fig. 3b) crystals. One can clearly see the considerable difference between the light reflection from the anisotropic and isotropic plates at small incidence angles: the coefficients R_{pp} and R_{ss} the isotropic plate have the same values, whereas in the biaxial crystals, R_{pp} and R_{ss} values are different, which is the distinguishing sign of crystal anisotropy.

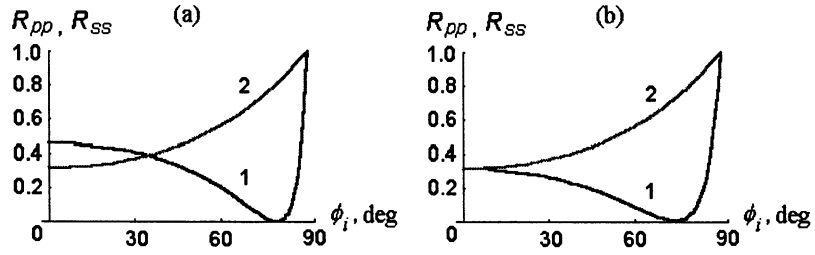

Figure 3. Reflectivity R_{jj} as a function of the angle of light incidence, ϕ_i, for an absorbing 2-μm-thick plate (1) R_{pp}, the *p*-polarized incident light; (2) R_{ss}, the *s*-polarized incident light. (a) biaxial crystal, $n_1 = 5.12 + i\,0.635$, $n_2 = 4.37 + i\,0.817$, $n_3 = 3.41 + i\,0.723$ (the refractive indices are equal to those of antimony glance, class *222*), $\theta = 90°$, $\varphi = \psi = 0°$; (b) isotropic crystal; $n_1 = n_2 = n_3 = 3.41 + i\,0.723$.

Figure 4 compares the influence of the optical activity and the magnetic properties on the intensity of the light transmitted by the plate of a uniaxial crystal located between the crossed polarizer and analyzer normally to its surface for some orientations of the optical axis. Figure 4a illustrates an increase in the intensity with an increase in the angle of the deviation of the optic axis from the surface normal of the plate, θ.

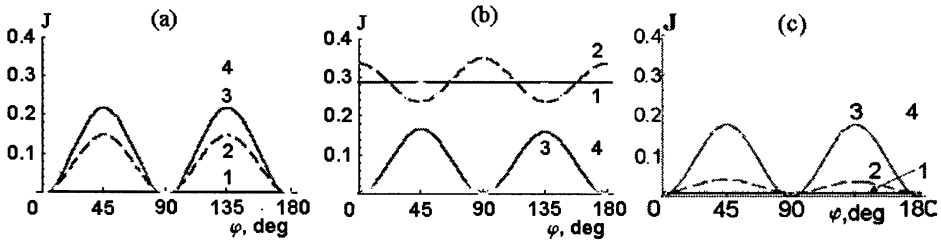

Figure 4. Intensity of the light transmitted through 1-mm-thick plate prepared from a uniaxial crystal normally to its surface ($\phi_i = 0°$) placed between the crossed polarizer and analyzer as a function of the angle φ of the plate rotation about the surface normal: $n_1 = n_2 = 1.5$, $n_3 = 1.51$, $\psi = 0°$; (1) $\theta = 0°$, (2) $\theta = 5°$, (3) $\theta = 20°$, (4) $\theta = 90°$; (a) optically inactive nonmagnetic crystal ($\alpha_{jj} = 0$, $\mu_{jj} = 1$), (b) optically active nonmagnetic crystal ($\alpha_{11} = \alpha_{22} = -10^{-5}$, $\alpha_{33} = 5 \cdot 10^{-5}$, $\mu_{jj} = 1$); (c) optically active magnetic crystal ($\alpha_{11} = \alpha_{22} = -10^{-5}$, $\alpha_{33} = 5 \cdot 10^{-5}$, $\mu_{11} = \mu_{22} = 1.01$, $\mu_{33} = 1.03$).

It is clearly seen that if the light propagates along the optical axis ($\theta = 0°$, lines 1) in an optically active crystal, the intensity of the transmitted light has a nonzero value (Fig. 4b, c). At small angles θ ($\theta = 5°$, curves 2) one can notice the simultaneous influence of birefringence (because the intensity curve oscillates) and the optical activity (because the intensity curve is above the abscissa in the whole range of the rotation angles of the specimen). In magnetic crystals (Fig. 4c), with an increase of the angle θ, the variation in the light intensity considerably increases in comparison with the intensity in nonmagnetic crystals (Fig. 4a).

Figure 5 shows the influence of the type of polarization (circular or linear) of the incident light on the characteristics of the reflected light. For the incident p-polarized light, the dependence of R on the incidence angle has the minimum in the vicinity of the Brewster angle (Fig. 5a), whereas for the circularly polarized incident light no such minimum is observed, and the reflectivity R is much higher (Fig. 5b).

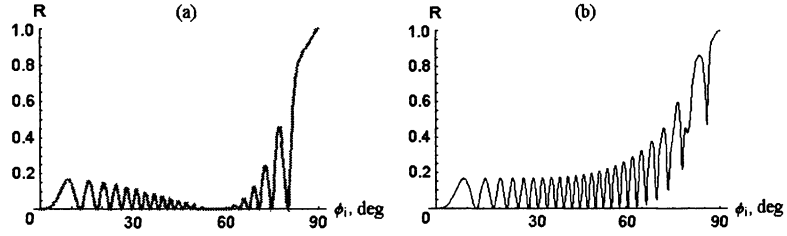

Figure 5. Reflectivity, R, as a function of the angle of light incidence ϕ_i for a plate prepared from an optically active uniaxial crystal; (a) the incident light has the p-polarization, (b) the incident light has the right-hand circular polarization, $n_1 = n_2 = 1.55$, $n_3 = 1.56$, $\alpha_{11} = \alpha_{22} = -10 \cdot 10^{-5}$, $\alpha_{33} = 3 \cdot 10^{-5}$. $\varphi = \theta = \psi = 0°$, $d = 20$ μm.

The use of three dimensional figures allows to present complex dependencies in easy to understand form. For example, Fig. 6 shows the dependence of reflection coefficient for the intensities R_{pp} and R_{sp} on the angle of light incidence ϕ_1 and simultaneously on the angle φ of the plate rotation around the surface normal plate which is prepared from optically active uniaxial crystal. One can clearly see the region of the Brewster angle on the dependence of diagonal reflection coefficient R_{pp} on the angle ϕ_i and on the angle φ (Fig. 6a). The Fig. 6b illustrates the influence of optical activity parameters on off–diagonal reflection coefficient R_{sp}. It is seen, that at the angle $\varphi = 0°$ the value of $R_{sp} \neq 0$ at any value of the angle of incidence ϕ_i except for $\phi_i = 0°$. The dependence $R_{sp}(\phi_i)$ is asymmetric relatively to the plane $\varphi = 180°$ unlike in optically inactive crystal.

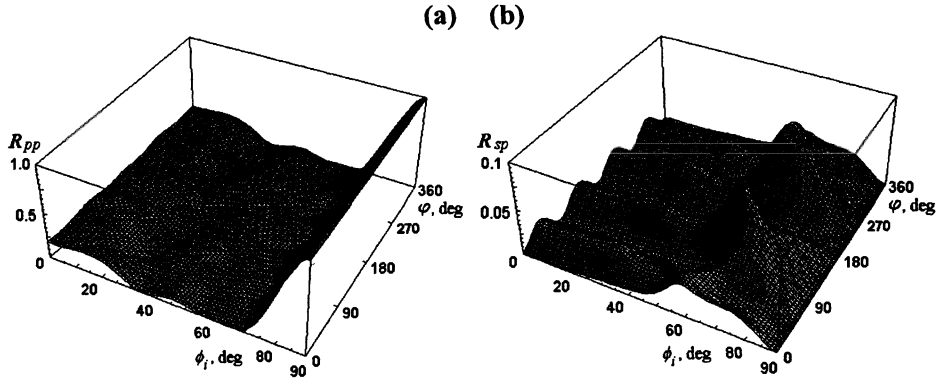

Figure 6. Reflection coefficients from the intensities, R_{pp} (a) and R_{sp} (b), as a function of the angle of light incidence ϕ_i and the angle φ of the plate rotation about the surface normal. The optical parameters are: $n_1 = n_2 = 1.65$, $n_3 = 1.7$, $\alpha_{11} = \alpha_{22} = -0.02$, $\alpha_{33} = 0.005$, $\theta = 60°$, $\psi = 0°$, $d = 2$ μm.

8. Conclusion

In this work Berreman's method and package "Mathematica-4.1" is used, with help of which analytical form for the matrix Δ is derived and its features for optically active crystals of various classes of symmetry are considered. It is shown that matrix Δ represents independent interest in research of crystals, as its eigenvalues are refraction indices, and the eigenvectors determine the condition of polarization of waves, propagating through crystal.

The connection between components of gyration tensors, used for the description of optical activity in some standard theories is established. It is shown that the exact constitutive relations of Condon–Fedorov, more often used in theoretical works, essentially differently describe the phenomenon of optical activity in comparison with the approximate relations of Born–Landau, used in experimental works. The expressions for refraction indices obtained using different constitutive relations allow one to determine boundaries of applicability of the approximate theory.

Thus, it is shown that the combined use of Berreman's method and the package Mathematica-4.1 opens new opportunities for solving the problems of crystal optics and studying any characteristics of the light propagation in crystals with various optical properties. The method can be used for obtaining exact solution of problems of light propagation in various layered media, including anisotropic, absorbing, gyrotropic, magnetic, multilayer media and any arbitrary combination of such media. The dependences considered above clearly demonstrate the universal nature of this approach, namely, the possibility of constructing any necessary dependences of the reflected and transmitted light with due regard for the optical activity and the magnetic properties and absorption in the

plate and the substrate. Moreover, it is also possible to set the functional dependences of the optical properties of crystals (e.g., on the wavelength or the temperature) to set any polarization of the incident light, and to consider the dependence of the intensity and polarization of the light transmitted through the plate placed between the arbitrarily oriented polarizer and analyzer. A more detailed review of the problems described in the current article is done in [36].

9. References

1. Fedorov, F.I. (1976) *Theory of Gyrotropy,* Nauka i Tekhnika, Minsk.
2. Konstantinova, A.F., Grechuchnikov, B.N., Bokut', B.V., and Valyachko, E.G. (1995) *Optical Properties of Crystals,* Nauka i Tekhnika, Minsk.
3. Bokut', B.V., Konstantinova, A.F., and Serdyukov, A.N. (1972) Propagation of light in optically active uniaxial crystals, *Sov. Phys. Cryst.* **17** (4), 711 – 714.
4. Filippov, V.V. (1983) Method of obtaining dispersion equation for normal and surface waves in layered anisotropic systems, *Sov. Phys. Cryst.* **28** (2), 136 – 139.
5. Konstantinova, A.F., Tronin, A.Yu., Nabatov, B.V., and Evdishchenko, E.A. (1999) Propagation of light in a biaxial crystalline film under oblique incidence of light, *Crystallogr. Rep.* **44**, 140 – 148.
6. Konstantinova, A.F., Nabatov, B.V., Tronin, A.Yu., and Evdishchenko, E.A. (2000) Gyrotropy parameters influence on characteristics of light transmitted and reflected from uniaxial gyrotropic film, *Poverkhnost'* **10**, 65 – 73.
7. Berreman, D.W. (1972) Optics in stratified and anisotropic media: 4x4-matrix formulation, *J. Opt. Soc. Am.* **62**, 502 – 510.
8. Azzam, R.M. and Bashara, N.M. (1977) *Ellipsometry and Polarized Light,* North-Holland, Amsterdam.
9. Condon, E.U. (1937) Theories of optical rotatory power, *Rev. Mod. Phys.* **9**, 432 – 457.
10. Aleksandrov, V.N. (1970) Energy conservation in the theory of optical activity, *Sov. Phys. Cryst.* **15** (6), 867 – 870.
11. Bokut', B.V., Serdyukov, A.N., and Fedorov, F.I. (1970) The phenomenological theory of optically active crystals, *Sov. Phys. Cryst.* **15** (6), 871 – 875.
12. Barkovskiy, L.M. (1977) Parametric transformation of light in the crystals, *Kristallografiya* **22**, 21 – 26.
13. Georgieva, E. (1995) Reflection and refraction at the surface of an isotropic chiral medium: eigenvalue–eigenvectors solution using a 4x4 matrix method, *J. Opt. Soc. Am. A.* **12**, 2203 – 2211.
14. Silverman, M.P. and Badoz, J. (1990) Light reflection from a naturally optically active birefringent medium, *J.Opt.Soc.Am. A.* 7, 1163 – 1173.
15. Bassiri, S., Papas, C.H., and Engheta, N. (1988) Electromagnetic wave propagation through a dielectric-chiral interface and through a chiral slab, *J.Opt.Soc.Am. A.* **5**, 1450–1459.
16. Lakhtakia, A., Varadan, V.V., and Varadan, V.K. (1988) *J.Opt.Soc.Am. A.* **5** (2) 175.
17. Sihvola, A.H. and Lindell, I.V. (1991) *Microwave and Opt. Tech. Lett.* **4**, 295.
18. Weiglhofer, W.S. and Lakhtakia, A. (1993) *J.Phys. D: Appl. Phys.* **26**, 2117.
19. Lindell, I.V., Sihvola, A.H., Tretyakov, S.A., and Viitanen, A.J. (1994) *Electromagnetic Waves in Bi-Isotropic and Chiral Media.* Boston, Artech House.
20. Gevorgyan, A.A. (2001) Reflection and transmission of light through one layer of naturally gyrotropic medium with external magnetic field, *Optica i Spectroscopya* **91**, 812 – 818.
21. Lalov, I.J. and Kojouharova, N.A. (2000) Reflection of electromagnetic waves at the boundary of optically active media, *Bulgarian Journal of Physics* **27**, 66 – 71.
22. Born, M. (1937) *Optics,* Khar'kov, Kiev, GNTIU.
23. Landau, L.D. and Lifshits, E.M. (1982) *Elektrodinamika sploshnykh sred,* Nauka, Moscow.

24. Drude, P. (1922) *The Theory of Optics,* Longmans, Green, New York.
25. Sah, Yuvaraj and Krishna, J.Gowri (2001) Optical properties of an isotropic optically active medium at oblique incidence, *J.Opt.Soc.Am. A.* **18**, 1388 – 1392.
26. Evdishchenko, E.A., Konstantinova, A.F., and Grechushnikov, B.N. (1991) Accuracy of calculation of refractive indices and ellipticities of natural waves in optically active crystals, *Sov. Phys. Cryst.* **36** (4), 470 – 473.
27. Voigt, W. (1903) Zur theorie des lichtes fur active krystalle, *Nachriechten.* **1**, 156 – 202.
28. Nye, G.F. (1957) *Physical Properties of Crystals,* Oxford at the Clarendon Press.
29. Yariv, A. and Yeh, P. (1984) *Optical Waves in Crystals: Propagation and Control of Laser Radiation* Wiley, New York.
30. Sirotin, Yu.I. and Shaskolskaya, M.P. (1975) *Fundamentals of Crystal Physics,* Nauka, Moscow.
31. Shubnikov, A.V. (1958) *Fundamentals of optical crystallography.* AN SSSR, Moscow.
32. Konstantinova, A.F. and Nabatov, B.V. (1995) Manifestation of the optical activity in uniaxial crystals of the mirror-reflection classes, *Crystallography Reports*, **40** (2), 197 – 200.
33. Yakovlev, D.A. (1998) *Opt. Spectrosc.* **84**, 748.
34. Palto, S.P. (2001) *J.Exp.Theor.Phys.* **92**, 552.
35. Born, M. and Wolf, E. (1969) *Principles of Optics*, Pergamon, Oxford.
36. Konstantinova, A.F., Konstantinov, K.K., Nabatov, B.V., and Evdishchenko, E.A. (2002) Use of contemporary mathematical applications for exact solution of problems of light propagation in anisotropic layered media. I.General solution of boundary problems in crystal optics, *Crystallography Reports*, **47** (4), 00.

VI.

HETEROGENEOUS MATERIALS AND WAVE LOCALIZATION

ON ELECTRODYNAMICS OF ONE-DIMENSIONAL HETEROGENEOUS SYSTEM BEYOND HOMOGENIZATION APPROXIMATION

A. P. VINOGRADOV and A. M. MERZLIKIN
Institute of Theoretical and Applied Electromagnetism (ITAE), JIHT
Russian Academy of Sciences
Izhorskaya 13/19, Moscow, 127412, Russia

Abstract. This chapter discusses electromagnetic modelling of one-dimensionally inhomogeneous materials. Different spatial scales are taken into account and the analysis is extended beyond the basic homogenization approximation. The wave localization is related to the total increase of band gaps with the infinite growth of the size and structural complexity of the cell.

1. Introduction

It is the multi-scale nature of the problem that is at the bottom of numerous effects observed at electromagnetic waves transport in inhomogeneous media. The basic yardstick is the wavelength λ. The mutual relation of this scale with other scales determines the phenomena that should be taken into account.

As a rule one considers two additional relevant scales. The first scale is the inclusion size d or the correlation length ξ and the second scale is the sample size L. Each of the scales is responsible for its own feature of the wave transport.

Since we are going to deal with phenomenon of localization, which was firstly predicted and studied in quantum mechanics, it is necessary to make some remarks concerning the relation of electromagnetic and quantum theories. First of all they have a common feature because the electromagnetic fields and the wave function are governed by wave equations. These are the Maxwell and Schrödinger equations. In the simplest case these equations reduce to the Helmholtz equation

$$\nabla^2\psi + k^2\psi = 0, \tag{1}$$

An important for us difference between quantum and classical cases is that in the quantum problem the disturbance of k^2 comes additively into equation (1)

$$k_0^2 = \frac{2m(E-V_0)}{\hbar^2}, \qquad \delta k^2 = \frac{2mV(r)}{\hbar^2}$$

whereas in the classical case it does it multiplicatively

$$k_0^2 = \frac{\varepsilon_0\omega^2}{c^2}, \qquad \delta k^2 = \frac{\delta\varepsilon}{\varepsilon_0}k_0^2,$$

S. Zouhdi et al. (eds.), Advances in Electromagnetics of Complex Media and Metamaterials, 341–361.

As a consequence, at low frequencies the role of scattering of electromagnetic waves is of no importance. This is the reason why the quasi-static approach is so popular in electromagnetism, begetting the whole branch of the investigations, so-called homogenization problem. It is commonly assumed that if $d \ll \lambda$ one can solve the Laplace equation instead of the Maxwell ones. Being dimensionless the Laplace equation makes the analysis easier. Namely, since there remain only two relevant scales (d and L) any quantity may depend on their ratio only. It permits to consider unbounded systems because tending the system size to infinity is just the same as tending the inclusion size to zero: $d/L \to 0$. Such a sight is good to some extent only. The growth of L brings back into the problem the wavelength because even weak effects depending on the ratio d/λ may cause qualitative changes of the actual picture of phenomena. As an example one can consider the process of radiation by inclusions. For perfect crystals this process results in cancellation of the incident wave and generation of the refracted one [1] the wave number of which can be calculated in neglecting the radiation process. If there are fluctuations in distribution of the scatterers we should take into account the additional polarization of the volume with fluctuation ΔN of inclusion concentration. The random nature of fluctuations results in non-coherent (diffuse) character of the waves radiated by these fluctuations. As long as fluctuations are small, one introduces for description of the diffuse scattering the imaginary part ε''_{eff} of the effective permittivity [2][1]. But at distances greater than $\lambda/\sqrt{\varepsilon''_{eff}}$ almost all of electromagnetic energy is transferred by diffusively scattered waves. This makes senseless the description of the energy transfer in terms of the material (macroscopic) Maxwell equations. Thus, the increase of L carries us from homogenization range where the constitutive parameters do not depend on the system size to mesoscopic range where a new constitutive parameter, the diffusion coefficient may depend on system size. In particular, it can exponentially tend to zero with increase of the system size. This phenomenon is called localization. And the scale that characterizes the tendency is called localization length.

Surprisingly, to observe the latter phenomena the existence of a scale that is small in terms of the wavelength is demanded. This scale is the thickness of the transition layer between adjacent volumes with different permittivity values. If the scale becomes greater than the wavelength (smooth disturbance) the role of scattering becomes smaller. We pass to the range of quasi-classical description or geometrical optics. Unlike the diffusion range where $L_{loc} \approx \lambda\left(\lambda/d\right)$ in this range the localization length grows with frequency increase. The waves become extended. Most strikingly these three ranges (the range of homogenization, the range of localization, the range of geometrical optics) manifest themselves in one-

---

[1] The quantity ε'' is proportional to the damping factor $(\Delta N/N)^2 \beta$ of the dipole moment induced in the volume with fluctuation ΔN of inclusion concentration. Here $\beta \sim \omega^3$ is the dipole moment damping factor of a single inclusion [3].

dimensional systems. Firstly, the homogenization range shrinks down to zero frequency. It turns out that the introduction of the effective permittivity is justified in the static case only. An attempt to take into account the effects of retardation leads to strong dependence of the effective permittivity upon the system size.

2. Size dependence of effective parameters

Let us consider a finite laminated system. The parameters of layers are chosen to satisfy the long wavelength approximation and to exclude any mesoscopic effects [4] connected with resonances on a separate layer or period: $k_0 d << 1$. Moreover, in the case of random system the sample thickness L is chosen to be much smaller than the localization length. The latter condition does not significantly restrict our consideration because in the long wavelength approximation the inequalities $\lambda << L << L_{loc}$ are fulfilled for a wide interval of L-values.

For a periodic one-dimensional system the exact solution of the electrostatic problem is well known (see review in [5]). Indeed, if the external field is applied parallel to the layers, then the electric field is the same in all the layers due to continuity of its tangential component. Averaging the constitutive relation $D = \varepsilon E$, we obtain, that the average field and averaged displacement are connected by the same relation, but with effective permittivity $\varepsilon_{eff} = <\varepsilon>$, where the brackets denote volume averaging. Corrections to the static solution were found by Rytov [6, 7]. Rytov exactly solved the infinite ($L = \infty$) problem for the one-dimensional system with periodically alternating permittivity. Now this work has become classical, begetting a sequence of followers who apply the Rytov method to various systems [8 – 11]. Nevertheless, some of Rytov's results look unphysical.

For the periodic system with two homogeneous layers of different substances in the period cell Rytov derived dispersion equation (2) for the effective wavenumber $k_{eff} = k_0 n_{eff}$

$$\cos\left(k_0 n_{eff}^{Ryt} 2d\right) = \cos\left(k_0\sqrt{\varepsilon_1}d\right)\cos\left(k_0\sqrt{\varepsilon_2}d\right) - \left(\sqrt{\frac{\varepsilon_1}{\varepsilon_2}} + \sqrt{\frac{\varepsilon_2}{\varepsilon_1}}\right)\frac{\sin\left(k_0\sqrt{\varepsilon_1}d\right)\sin\left(k_0\sqrt{\varepsilon_2}d\right)}{2} \quad (2)$$

and introduced the concept of the characteristic impedance Z_{eff}, which was given by the ratio $<E>/<H>$. Here ε_1 and ε_2 are the values of the permittivity of the substances and the brackets denote averaging over the cell period. Ultimately, using the common relations $k_{eff} = k_0\sqrt{\varepsilon_{eff}\mu_{eff}}$ and $Z_{eff} = \sqrt{\mu_{eff}/\varepsilon_{eff}}$ one can retrieve the effective parameters. At first sight this approach seems to be physically sound. However, "something is rotten in the state of Denmark". Indeed, since Rytov [6] dealt with an infinite system, he considered solutions only with a perfectly real wavenumber. As a consequence he restricted himself to the real values of the

permittivity. However, even in the long wavelength approximation the ε_{eff} and μ_{eff} turn out to be complex quantities:

$$\varepsilon_{eff} = \langle\varepsilon\rangle\left[1 + i(k_0 d/8)(\varepsilon_2 - \varepsilon_1)/\sqrt{\langle\varepsilon\rangle}\right], \quad \mu_{eff} = \left[1 - i(k_0 d/8)(\varepsilon_2 - \varepsilon_1)/\sqrt{\langle\varepsilon\rangle}\right] \qquad (3)$$

Moreover, either ε_{eff} or μ_{eff} has a negative imaginary part. To attribute to these imaginary parts a physical sense one has to consider the situation where only one of them is essential. For example, only if the whole system is placed in a loop of magnetic field where the value of the electric field and the energy dissipation caused by the electric field can be neglected can one definitely talk about connection of the energy generation with a negative imaginary part of μ_{eff}. This situation is absolutely impossible for unbounded systems where each of the imaginary parts cannot be separately connected by itself with the energy dissipation/generation. It seems that this strange result (3) is due to consideration of the infinite system.

Really we always deal with bounded systems and the present communication is devoted to the analysis of the constitutive parameters of a bounded system. Since any bounded system is not translation-invariant, Rytov's approach cannot be directly applied here. In particular, Rytov's definition of the impedance is useless for bounded systems because there exist simultaneously two waves propagating inside the sample in the opposite directions. These waves have the ratio $< E >/< H >$ of the opposite sign. Thus, the characteristic impedance introduced by Rytov depends not only on the material properties but also on the relation between the amplitudes of just mentioned waves.

Let us consider another definition of the constitutive parameters. Our approach is based on the usual experimental method of ε_{eff} and μ_{eff} measurement where the parameters are obtained from the measured values of the reflectivity r and transmittance t [12]. First, to introduce the effective parameters we consider an inhomogeneous sample under investigation as a uniform one made of a material with ε_{eff} and μ_{eff}. Further, we attribute to this auxiliary sample the same values of reflectivity and transmittance as the initial composite system has. Employing well-known expressions for r and t for a homogeneous layer [7, 13] we arrive at the expressions for k_{eff} and Z_{eff}:

$$Z_{eff} = \sqrt{\left[(1-r)^2 - t^2\right]/\left[(1+r)^2 - t^2\right]}, \quad \exp(ik_{eff}L) = t(1+Z_{eff})/\left[1 + r + (1-r)Z_{eff}\right]$$

and, ultimately, to the expressions $\varepsilon_{eff} = k_{eff}/(k_0 Z_{eff})$, $\mu_{eff} = k_{eff} Z_{eff}/k_0$.

In our computer simulations we have found the values of r and t by exactly solving the microscopic problem of propagation of an electromagnetic wave within the bounded system. As $\varepsilon(x)$ is a piecewise constant function, it is possible to write down the solutions in each layer and then to sew them together employing the ordinary Maxwell boundary conditions [13, p. 55]. Really, the algorithm reduces to

multiplication of T-matrices of the layers. To unify the speculations it is convenient to put in between the adjacent layers an auxiliary vacuum layer of zero width. Such a consideration allows us to speak about the T-matrix of a separate layer. This matrix links amplitude of waves in vacuum layers located on the right and left sides of the layer. It is obvious, that the T-matrix of the entire system is a product of such T-matrices of separate layers: $T = T_N T_{N-1} \ldots T_1 T_0$.

The results of the computer simulations are represented in Figures 1-4. The behavior of all quantities depends upon the parity of the number of layers N. We shall distinguish two cases. The first is the "even-layer-system" when the system consists of an integer number of periods or an even number of layers. The second case is the "odd-layer-system" when the number of layers is odd and the system includes a half-integer number of periods. The difference in behavior is observed already in the static case. The permittivity of the even-layer-system achieves its bulk value $\langle\varepsilon\rangle$ already at the first period, whereas the permittivity of the odd-layer-system slowly tends to this value with the thickness increase: $\varepsilon_{eff} = \langle\varepsilon\rangle + 0.5(\varepsilon_2 - \varepsilon_1)(d/L)$.

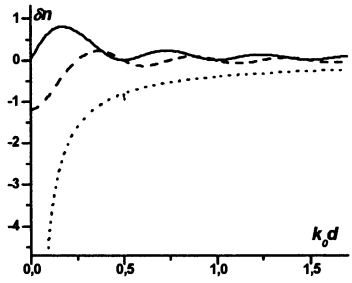

Figure 1. $\delta n = \left(n_{eff} - n_{eff}^{Ryt}\right)10^3$ as a function of L/λ_{eff}, $\varepsilon_1 = 2$, $\varepsilon_2 = 3$, $k_0 d = 0.01$. The dotted line represents the odd-layer-case. In the even-layer-case the solid line represents $\mathrm{Re}\,\delta n$, the dashed line represents $\mathrm{Im}\,\delta n$.

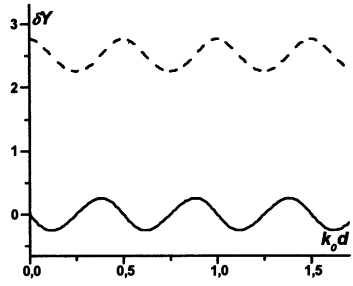

Figure 2. The even-layer-system. $\delta Y = \left(\sqrt{\varepsilon_{eff}/\mu_{eff}} - Y_{eff}^{Ryt}\right)10^3$ against L/λ_{eff}. The solid line represents $\mathrm{Re}\,\delta Y$, the dashed line presents $\mathrm{Im}\,\delta Y$. For the same system parameters as in Fig. 1.

For time-varying fields one may expect a more serious discrepancy between the even-layer- and odd-layer-systems. The reason is that the odd-layer-system is symmetric with respect to reversal of the direction of the wave incidence whereas the even-layer-system is not. In particular, the reflectivity of the odd-layer-system does not depend on the direction of the wave propagation. The even-layer-system has reflectivity dependent on the direction of wave incidence. Reversing the direction of incidence the situation with the even-layer-system becomes equivalent to the primary one only with a change in the order of the layers inside the period.

The behavior of the even-layer-system qualitatively differs both from that in the static case where the bulk values are achieved at the first period and from Rytov's

one. Despite that the effective refractive index $n_{eff} = k_{eff} / k_0$ slowly approaches its Rytov's value it is a complex quantity (see Fig. 1). The non-zero imaginary part does not mean that there is any energy dissipation. During our computer simulation we controlled the energy conservation law $|R|^2 + |T|^2 = 1.0 \pm 10^{-14}$. The non-zero imaginary part of k_{eff} is compensated by the non-zero imaginary part of the effective admittance Y_{eff}. The effective admittance, permittivity and permeability do not tend to any limit but oscillate around certain values. Y_{eff} exhibits a perfectly periodic dependence upon the sample thickness L (see Fig. 2). The real part of the admittance oscillates around Rytov's value. The imaginary part of the admittance oscillates around the quantity that differs from Rytov's value. The effective parameters, being functions both of the wavenumber and of the admittance, tend to a periodic behavior.

In the odd-layer-case the symmetry of the systems allows to introduce effective parameters and at first sight nothing causes worry (see Fig. 1). Indeed, the wavenumber is real and its behavior looks like one of the permittivity in the static case. Namely, the effective wavenumber slowly tends to its bulk value k_{eff}^{Ryt} predicted by Rytov. However, the admittance (see Fig. 3) is a purely real quantity what differs this case from Rytov's solution. The admittance as a function of the sample thickness L exhibits periodic cusps of different intensity. What is important is that this intensity does not decay.

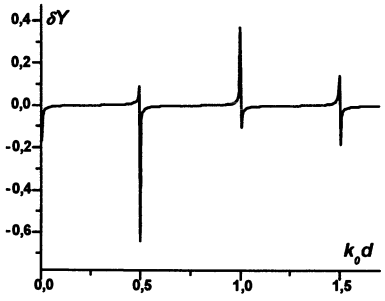

Figure 3. The odd-layer-system. The dependence of $\delta Y = \sqrt{\varepsilon_{eff} / \mu_{eff}} - Y_{eff}^{Ryt}$ against L / λ_{eff}. For the same parameters as in Fig. 1.

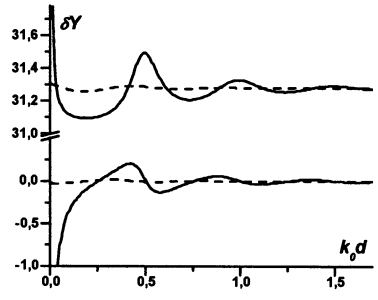

Figure 4. $\delta Y = \left(\sqrt{\varepsilon_{eff} / \mu_{eff}} - Y_{eff}^{Ryt}\right) 10^2$ for dissipative systems. The solid line represents the odd-layer, dashed line the even-layer-case. The upper couple of curves present the imaginary parts of admittance while the lower curves pictures the real ones. The parameters of the system are $\varepsilon_1 = 2 + i$, $\varepsilon_2 = 3 + i$, $k_0 d = 0.01$.

These cusps are observed where the sample thickness approximately equals to the thickness of antireflective sample (the thickness of the antireflective sample is equal to an integer number of half-wavelengths. The observed behavior can be

estimated in the following way. Let us represent the odd-number system as one composed of two subsystems: the first subsystem consists of the first layer with permittivity, say ε_1, the second subsystem is replaced by a homogeneous system with permittivity $\varepsilon_3 = (\varepsilon_1 + \varepsilon_2)/2$, which with a good accuracy describes the effective permittivity of an even-layer-system. Since $k_o d\sqrt{\varepsilon_1} << 1$ and $k_o L\sqrt{\varepsilon_3} - \pi << 1$ (antireflective sample) it is easy to get the following estimation of the effective admittance $\sqrt{\varepsilon_{eff}/\mu_{eff}}$:

$$\varepsilon_{eff}/\mu_{eff} = \langle\varepsilon\rangle + 0.5(\varepsilon_1 - \varepsilon_2)/\left[1 - \pi/\left(k_0 d\sqrt{\langle\varepsilon\rangle}\right)\right]$$

Formally, for L_{odd} approaching $\pi/k_0\sqrt{\langle\varepsilon\rangle}$ the admittance tends to infinity. The values obtained during computer simulation are finite due to discreteness of the system. The incommensurability between the effective wavelength and period results in a random character of the maximum values. The constitutive parameters being functions of k_{eff} and Z_{eff} exhibit a combination behavior. They tend to a periodic behavior.

It is worth emphasizing that the exact values of reflectivity and transmittance slightly differ from that calculated employing Rytov's solution. The difference is $O(k_{eff}d)$. Nevertheless, this small difference results in a large difference in the constitutive parameters if we try to retrieve them for antireflective sample.

The appearance of dissipation decreases the effects. The oscillations of admittance are attenuated as the system becomes opaque. Though we cannot directly determine the value of the wavenumber in this limit case we can still define this value as the limit $k_{eff}(L)$ at $L \to \infty$. Nevertheless the values of ε_{eff} and μ_{eff} differ from the Rytov ones. We think that this is due to the existence of a transition layer where the solution still feels the boundary. It is this transition layer that is responsible for the input admittance of the opaque system (Fig. 4).

To conclude, we have to note that randomization of the system does not lead to disappearance of the effects too (see Fig 5).

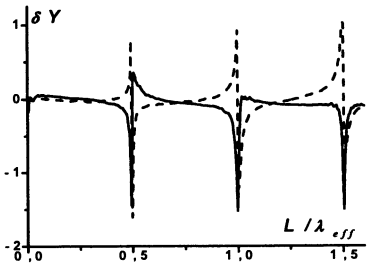

Figure 5. Effective admittance of the random system

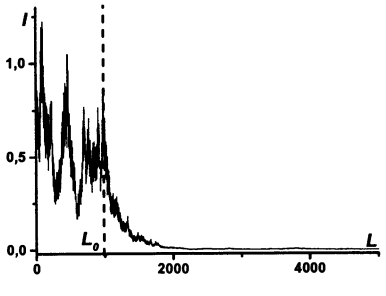

Figure 6. A typical distribution of field in one-dimensional random medium

3. Frequency dependence of the localization length

The effect of localization of both quantum and classical waves has been intensively studied throughout the last decade. All this time the apparent simplicity of one-dimensional systems attracts the researchers but does not give simple answers. This concerns, for example, the frequency dependence of the localization length $L_{loc}(\omega)$, where $L_{loc}(\omega)$ a typical distance at which the fields or wave function fall down. On the one hand it seems that there are strong theoretical results. In the frame of the scaling it is proved that the localization of waves is observed in any one-dimensional random system and that at high frequencies $L_{loc}(\omega) \sim \omega^{-2}$. The Herbert-Jones-Thouless theorem [4, 14, 15] states that the high frequency limit is equal either to infinity (the waves are delocalized) or to a constant. On the other hand, there are random systems in which there is neither the high frequency limit nor even localization [4, 16].

At present there exists a detailed theoretical investigation of the localization effect in approximation of a delta-correlated-process only [17-19]. The obtained results are in agreement with predictions of the scaling hypothesis [4]. Application of the approximation to the one-dimensional electromagnetic problem means that the values of permittivity at different points are independent. In other words, the medium consists of layers of infinitesimal thickness. It is noteworthy that the existence of a scale (in the previous example this is a layer thickness) that is much less than the wavelength is not only a condition that makes the theoretical consideration easy but also the key issue causing the localization. Indeed, if all the scales including the thickness of a transition layer between layers are greater than the wavelength (the variation of permittivity $\varepsilon(x)$ is smooth) the wave scattering is small and the localization length tends to infinity as the frequency increases.

Below we consider an intermediate case. The layers building up the system are of a finite thickness that differs the system from one begot by delta-correlated process. But the thickness of the transition layer between layers is zero. It means that we deal with sharp interfaces between layers. It is shown that in such systems the behavior of localization length $L_{loc}(k_0)$ at high frequencies is determined by the number of different types of layers building up the system. In particular, in case of a binary system composed of two types of layers there is no high frequency limit. Moreover, it is shown that the localization length has a high frequency limit in the case of infinite number of different types of layers only.

The object of the present investigation is a one-dimensional, random, lossless system. We confine our consideration to electromagnetic waves. The electromagnetic problem differs from the quantum one [17]. This difference does not consist only in the methods of consideration: in the quantum problem one is usually interested in the eigenvalue problem, whereas in electromagnetics (and acoustics) one deals with the problem of scattering. The most important difference for us is that in the quantum mechanics there is only one random quantity, the

potential $U(x)$, whereas in electrodynamics there are two independent functions that describe the properties of the medium and can independently fluctuate. These are the pair, permittivity $\varepsilon(x)$ and permeability $\mu(x)$, or, what is equivalent, a pair of the wavenumber k and characteristic impedance ζ. The first pair of functions is convenient for description of smooth, continuous in space distribution of parameters, and the second one is useful at study of the piecewise continuous system (e.g. a system of homogeneous layers). Below we shall consider the latter case, describing the properties of the j-th layer by the pair (k_j,ζ_j), more exact by the pair $(k_j d_j,\zeta_j)$, where d_j is the thickness of j-th layer and $k_j d_j$ is the optical path over the layer.

In terms of the scattering problem localization of electromagnetic waves denotes total reflection. It is supposed that in the case of a one-dimensional random system the module of the reflection coefficient tends to unity and the transmission coefficient exponentially vanishes with the sample thickness growth [17]. In this connection the localization length is defined as

$$L_{loc} = \gamma_{loc}^{-1} = -L/\langle \ln|t| \rangle \tag{4}$$

where γ_{loc} is the Lyapunov index.

We calculate the transmittance coefficient t by a semi-analytical solution of the Maxwell equations employing the method of T-matrix. Because we consider a normal incidence of the wave, the field in each layer is the sum of left-going and right-going waves. The amplitudes A_{j+1}, B_{j+1} and A_{j-1}, B_{j-1} of such waves in the layers, which are adjacent to the j-th layer, can be related by application of the conditions of continuity of the tangential components of electrical and magnetic fields at the interface surfaces. To unify the speculations it is convenient to put in between the adjacent layers an auxiliary vacuum layer of zero width. Such a consideration allows us to speak about the T-matrix of a separate layer. This matrix links amplitude of waves in vacuum layers located on the right and left sides of the layer. It is obvious, that the T-matrix of the entire system is a product of such T-matrixes of separate layers [13]: $T = T_N T_{N-1} \ldots T_1 T_0$, where

$$T_j = \begin{pmatrix} \cos(k_j d) + i\dfrac{\left(1+Y_j^2\right)}{2Y_j}\sin(k_j d) & i\dfrac{\left(Y_j^2-1\right)}{2Y_j}\sin(k_j d) \\ i\dfrac{\left(1-Y_j^2\right)}{2Y_j}\sin(k_j d) & \cos(k_j d) - i\dfrac{\left(1+Y_j^2\right)}{2Y_j}\sin(k_j d) \end{pmatrix} \tag{5}$$

Here, $(k_j d)$ and Y_j are the optical path through and the admittance of *j-th* layer.

Below we need an expression for the condition of the layer's transparency in terms of the T-matrix. For this purpose the T-matrix of any sample can be

expressed through the reflection coefficients r_R and r_L, corresponding to right-incident and left-incident waves, as well as through the transmittance coefficient t (since $\det T = 1$, the value of t is independent of the direction of incidence [20]):

$$M = \begin{pmatrix} t - r_L r_R / t & -r_L / t \\ r_R / t & 1/t \end{pmatrix} \tag{6}$$

Thus, Eq. (5) with the condition of layer transparency ($|t| = 1$) reads $T = \pm I$, where I is the unit diagonal matrix. For any uniform layer with $Y_j \neq 1$ this condition is satisfied if and only if $k_j d = \pi n, n \in Z$.

The simplest random system is a random mixture of layers of two different types. Below we confine ourselves to the case $d_1 = d_2 = d$, $\mu_1 = \mu_2 = 1$, $\varepsilon_1 \neq \varepsilon_2$. For this case our computer simulations show that as frequency increases the localization length does not tend to any limit (Fig. 7) because there exist frequencies at which the localization length tends to infinity with the system size growth. Until we deal with a certain finite realization of the system that is consisted of N elementary layers it is well-known that there are $O(N)$ resonant frequencies at which the transmittance coefficient t is about unity. However the values of these frequencies depend on realization and N. In accordance with the Herbert-Jones-Thouless theorem t should only on the average tend to zero at any frequency. Nevertheless, the smooth curve obtained after averaging of $\gamma_{loc} = 1/L_{loc}$ over 1000 realizations (Fig. 7) points out at existence of the frequencies where even after averaging $\gamma_{loc} = 0$, that means absence of localization.

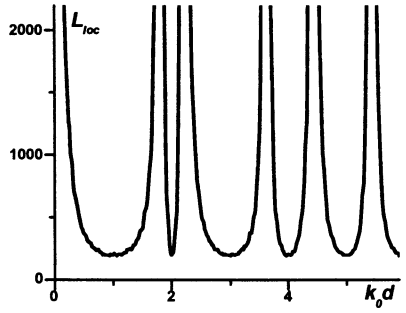

Figure 7. The frequency dependence of $L_{loc}(k_0)/d$ for random binary mixture of layers with permittivity $\varepsilon_1 = 2.0$ and $\varepsilon_2 = 3.0$, $L = 5000d$. The concentrations of layers of different types are: $p_1 = p_2 = 1/2$

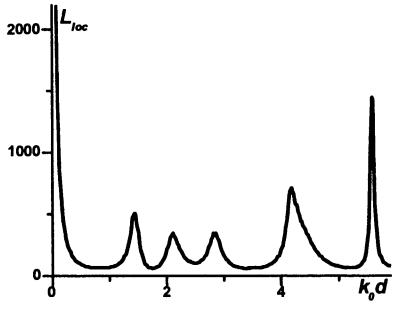

Figure 8. The frequency dependence of $L_{loc}(k_0)/d$ for a random triple mixture of layers with permittivity $\varepsilon_1 = 2.0$, $\varepsilon_2 = 3.0$ and $\varepsilon_2 = 5.0$, $L = 5000d$. ($p_1 = p_2 = p_3 = 1/3$).

These frequencies could be found without computer simulation. Indeed, any sample of a binary mixture is transparent (there is no localization) at a set of frequencies k_0, at which one of the elementary layers is transparent. For example if the layer of the first kind is transparent, i.e. $k_0 d\sqrt{\varepsilon_1} = n\pi,\ n = 1,2,...$ (in this case the T-matrix of this layer equals $\pm I$), then the T-matrix of the entire sample is equal $\pm$ product of the T-matrixes of layers of the second type. This product is equal to $\pm T$ matrix of a uniform sample consisting of the layers of the second type only. These frequencies are defined by the parameters of the elementary layers only; they depend on neither the entire sample thickness nor the realization of a given stochastic process. Because these sets of frequencies are unbounded there is no high frequency limit $\lim_{\omega\to\infty} L_{loc}(\omega)$.

The next step of our consideration is the triple-component system $d_1 = d_2 = d_3 = d$, $\mu_1 = \mu_2 = \mu_3 = 1$. To make the consideration non-trivial we demand fulfillment of two conditions. First, the optical paths of any two elementary layers of different types are incommensurable in pairs. Second, all the components are to have different impedance. Under fulfillment of these conditions the dependence $L_{loc}(k_0)$ (Fig. 8) qualitatively differs from one of a binary system (see Fig. 7).

The violation of the first condition (the optical paths of two different elementary layers are commensurable) means that there are frequencies at which two elementary layers are transparent. In this case the T-matrix of the total sample is equal to $\pm T$-matrix of the homogeneous layer consisting of layers of the third type. It is obvious that there is no localization in this case. In violation of the second condition (necessity of impedance dispersion) there are no reflections on interfaces and we deal with the homogenization regime. In terms of T-matrices delocalization of waves in systems with fixed characteristic impedance is a consequence of T-matrix commutation. The latter fact becomes evident after presentation the T-matrix (5) of an elementary layer in the Jordan form

$$T_j = SJS^{-1} = \begin{pmatrix} \frac{1+Y_j}{2Y_j} & \frac{Y_j-1}{2Y_j} \\ \frac{Y_j-1}{2Y_j} & \frac{1+Y_j}{2Y_j} \end{pmatrix} \begin{pmatrix} \exp(ik_j d) & 0 \\ 0 & \exp(-ik_j d) \end{pmatrix} \begin{pmatrix} \frac{1+Y_j}{2Y_j} & \frac{Y_j-1}{2Y_j} \\ \frac{Y_j-1}{2Y_j} & \frac{1+Y_j}{2Y_j} \end{pmatrix}^{-1} \qquad (7)$$

Since the S-matrix depends on the admittance only and the admittance is the same in any layer, all the layers have the same S-matrices. The J-matrices are always commutative $J_1 J_2 = J_2 J_1$. Hence the T-matrices of adjacent layers are commutative too: $T_1 T_2 = SJ_1 J_2 S^{-1} = SJ_2 J_1 S^{-1} = T_2 T_1$. As a consequence the random system is equivalent to the system consisted of three uniform layers. Our conditions are necessary conditions for absence of frequencies when L_{loc} diverges.

Unfortunately, we have no rigorously proof of the sufficiency of there conditions. Nevertheless, keeping the sufficiency as a hypothesis which is

confirmed by our computer simulation, we can estimate the value of the localization length $L_{loc}^{(123)}(k_0)$ of a triple system employing the frequency dependence of the localization length $L_{loc}^{(12)}(k_0)$ of a binary system, which results by removing layers of any type, e. g. of the third type, from the triple system. At frequency $k_0^{(3)}$ where the elementary layer of the removed component is transparent the T-matrix of the whole sample is equal to $\pm T$-matrix of the binary system. Tending the thickness of the whole sample to infinity we find $L_{loc}^{(123)}\left(k_0^{(3)}\right) = L_{loc}^{(12)}\left(k_0^{(3)}\right)/(1-p_3)$. Thought, the optical paths of the elementary layers are incommensurable in pairs, the frequencies $k_0^{(3)}$ can be as close as one likes to the frequencies, at which $L_{loc}^{(12)}(k_0)$ is infinitely large. Therefore, $L_{loc}^{(123)}(k_0)$ can reach very high values. More precisely $\forall A > 0$ and $\forall \Omega > 0$ there is a frequency $k_0^A > \Omega$ such, that $L_{loc}^{(123)}\left(k_0^A\right) > A$. From above it follows that there is no high frequency limit $\lim\limits_{k_0 \to \infty} L_{loc}(k_0)$ in the triple system too. Carrying out similar speculations on induction one can deduce that for any N-component mixture ($N < \infty$) there is no high frequency limit $\lim\limits_{k_0 \to \infty} L^{(1,\ldots,N)}{}_{loc}(k_0)$. Nevertheless, since $L^{(1,\ldots,N)}{}_{loc}(k_0)$ is strongly majorized by $L^{(1,\ldots,N-1)}{}_{loc}(k_0)/(1-p(N))$ the incommensurability of optical paths provides a decrease of the summit heights and the localization length should tend to some limit as $N \to \infty$.

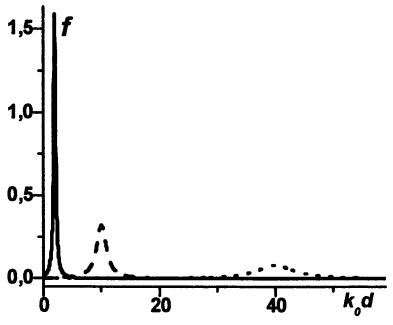

Figure 11. The distribution function

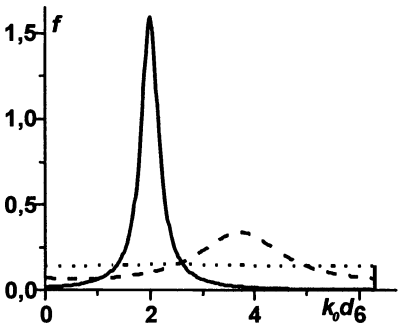

Figure 12. The reduced distribution function

To give a more rigorous prove of this statement consider a continuous distribution of the elementary layers with respect to their optical paths $l_{opt} = kd$. Given the corresponding distribution function $f(l_{opt})$ at any frequency it is easy to find it at any other frequency. An increase of the frequency results in a shift of the frequency where the maximum of $f(l_{opt})$ is observed and in a decrease of the value

of this maximum (see Figures 11-12). It is obvious that the optical paths, which are different by the value of $2\pi n$, are absolutely equivalent in the T-matrix language. Hence we can consider only optical paths that are smaller than 2π and deal with reduced distribution function obtained by summing the corresponding values of $f(l_{opt})$: $\hat{f}(l_{opt}) = \sum_n f(l_{opt} + 2\pi n)$. If the measure of commensurable paths is zero the reduced distribution function $\hat{f}(l_{opt})$ tends to $1/2\pi$ as $k_0 \to \infty$ (Fig. 12). Thus we arrive at a situation where the optical paths distribution is independent on the frequency. It is worth emphasizing that the T-matrix depends on the frequency through the corresponding dependence of the optical path only. As a consequence, if localization is observed then the localization length is independent on the frequency. Certainly this constant value is proportional to the mean thickness of the elementary layers and depends on the impedance distribution. In particular, this constant value is equal to infinity if the standard deviation of the impedance distribution is equal to zero.

If the refractive index can take any value in the interval $[0, \infty]$ and the layer thickness is fixed the reduced distribution of the optical paths is independent of the frequency. Hence the localization length should take a constant value at any frequency.

For any finite-component system the reduced distribution function is a sum of δ-functions. A frequency increase results in unlimited motion of these δ-functions in the interval $[0, 2\pi]$. As a consequence there is no high frequency limit of the localization length.

It is worth emphasizing that simultaneously with continuous distribution of the optical paths of the elementary layers the impedance has to be continuously distributed too. To prove this statement let us consider the system of layers made of two different materials (see [4]). If the thickness of the elementary layers made of the first material is fixed [16], and the thickness of the elementary layers made of the second material is continuously distributed, there are still frequencies, at which the waves are delocalized. These frequencies are determined by transparency of the layers of the first type.

4. Localization of the electromagnetic waves in one-dimensional system

The main troubles in the physical interpretation of localization are caused by non-Gaussian nature of fluctuations experienced by quantities (wave amplitude, transmittance, reflection etc.) commonly used in wave physics. The disengagement of these concepts from the effects observed by localization invalidates developing a harmonious view on the problem. Recently localization has been connected with the effect of coherent backscattering [4]. The latter should be destroyed in the presence of magnetic field because the system becomes nonreciprocal [4]. Unfortunately, consideration of ferrite layers placed in magnetic field that is perpendicular to them shows that the mathematical formulation of the problem

coincides with one for dielectric layers but employing circular polarization instead of linear polarization. In other words magnetic field does not destroy localization of electromagnetic waves. Thus, one needs developing a language for speculations. We think that the band theory may fit this purpose. The reason is alike behavior of waves both in random media and in regular systems if the frequency lies in a band gap. It seems that the Bragg scattering rather than the coherent backscattering suites to make an adequate base for comprehensive understanding of one-dimensional localization.

To attribute to any finite realization of a random system (below called a primitive cell) a band structure it is reasonable to consider a periodic system built up by duplicating the primitive cell. The dispersion equation has the form (9) where T is the T-matrix of the primitive cell and J is the Jordan form of the matrix.

Below, to simplify the discussion, we assume all the elementary layers to be of identical thickness, say d. Then the total thickness L of the primitive cell is proportional to the number N of elementary layers it consists of. As L tends to infinity we arrive at an absolutely irregular system.

The simplest non-trivial primitive cell is built up of two different elementary layers of the total thickness $L = d_1 + d_2$. The Jordan form of the T-matrix of this primitive cell looks as

$$T = S \begin{Vmatrix} \exp\left(ik_0 n_{eff}^{Ryt} L\right) & 0 \\ 0 & \exp\left(-ik_0 n_{eff}^{Ryt} L\right) \end{Vmatrix} S^{-1} \tag{8}$$

with n_{eff}^{Ryt} from (2). Eq. (2) may be written in the form

$$2\cos\left(k_{eff} L\right) = Sp(T) = Sp(J) \tag{9}$$

This is the general form of the dispersion equation. Eq. (2) predicts the existence of frequency gaps where the wave number is a perfectly imaginary quantity and $|Sp(T)| > 2$ (see. Fig. 12). The wave with the frequency belonging to a frequency gap is evanescent with the Lyapunov index $\gamma^{Sp} = k_0 n_{eff}^{Ryt} = \mathrm{Im}\arccos\left[0.5\mathrm{Sp}(T)\right]/L$. Fulfillment of the condition $\gamma^{Sp} = 0$ means that the waves are delocalized.

Now consider the evolution of the band structure as the period construction becomes more complicated. Complication of the period structure implies an increase of the amount of elementary layers included in the primitive cell. A complication can be achieved by various methods. We can introduce new types of elementary layers having different values of permittivity or simply join together several periods and arbitrary mix the existing elementary layers. To have a possibility to compare systems with different L we follow the second way. Really, a plane join of the neighborhood cells of regular system cannot lead to any new physical consequences. The situation changes after mixing the order of layers in a new joint cell (see. Fig. 13). There appear new frequency gaps where $|Sp(T)|$

exceeds 2. Thus, the complication of the period leads to the birth of new band gaps (see Figs. 9-10). For sufficiently thick systems almost all frequencies lie in the frequency gaps. It is reasonable to consider this fact as localization identifying $1/\gamma^{Sp}$ with localization length.

In the case of the binary random system considered in the previous chapter each realization of a sample built up of N elementary layers has $O(N)$ band gaps where the Lyapunov index is greater than zero[2]. However, the positions of these frequency gaps depend on realization and N (see Figures 9, 10). With an increase of N the envelope of frequency dependence of the Lyapunov index averaged over an ensemble is clearly seen (Fig 10). This envelope corresponds to the frequency dependence of the localization length obtained after averaging expression (4) over an ensemble. Hence, the entire frequency range turns in to the band gaps separated by countable number of frequencies where the binary system is transparent.

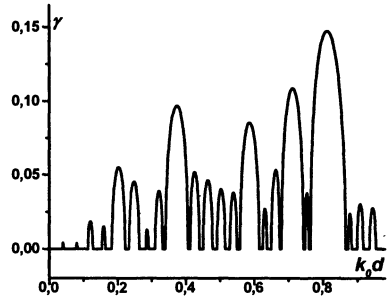

a

Figure 9. The gap structure of a particular realization of a binary system($\varepsilon_1 = 2, \varepsilon_2 = 10$) with L=40

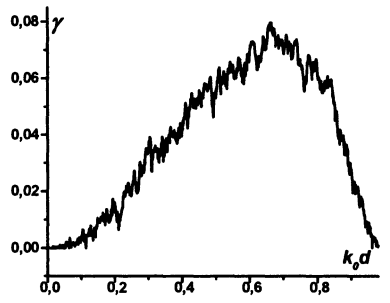

b

Figure 10. The gap structure of the sequel of the realization in Fig. 9, L=1000

It is easy to show that this definition of the localization length coincides with the common one in the limit $L \to \infty$. Indeed, it follows from (6) that $Sp(T) = t + (1 - r_L r_R)/t$. Taking into account that $Sp(T) = 2\cos\left(i\gamma^{Sp} L\right)$ we arrive at

$$\gamma^{Sp} = k_0 \operatorname{Im}\left(n_{eff}\right) = \left\{\ln(t) + \ln\left[1 - r_L r_R + t^2 + \sqrt{\left(1 - r_L r_R + t^2\right)^2 - 4t^2}\right]\right\}/(L) \qquad (10)$$

If localization happens in a given realization then at $L \to \infty$ we have $|t| << |r_L| \sim |r_R| \sim 1$ but $|1 - r_L r_R| \sim 1$ [19]. This means that the γ^{Sp} tends to γ_{loc} from (4).

---

[2] The graphical abilities do not permit to image the true dependence of γ on the frequency in Fig. 10. Almost all minima have zero value. In the domain $k_0 d \in [0, 0.8]$ there are more than 500 minima.

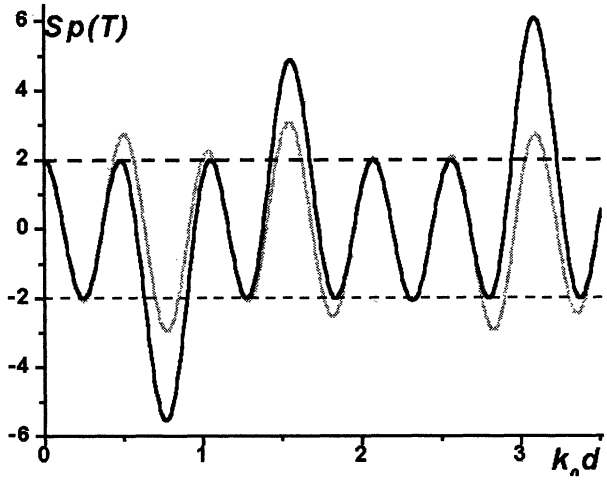

Figure 13. The behavior of Sp(t) of the six-layer cells. In the first cell (black line) ε takes values 2,7,2,7,2,7, in the second cell (gray line) ε takes values 2,7,7,2,7,2.

It is a common place that frequency gaps exist due to the Bragg reflection [20]. Since we have connected localization in one-dimensional systems with formation of frequency gaps it is reasonable to consider the Bragg reflection as a physical mechanism of localization. Early the influence of the frequency gaps on the value of the localization length in a system that is periodic on the average was noted in [21], but the frequency gaps were not identified as a reason of localization. Moreover, in [22] the Bragg reflection and Anderson localization due to disorder are considered as competition mechanisms of wave localization.

To verify our hypothesis we consider a system consisting of a majority of randomly situated Bragg-reflectors. As Bragg-reflectors we employ two samples. The first sample consists of five layers of identical thickness d and with permittivity values equal 2, 10, 4, 20, 6, respectively. The second sample is built up of elementary layers of the same thickness but with the permittivity values 4, 5, 7, 10, 4. The band structure of these Bragg-reflectors is shown in Fig. 14. For further study we chose frequency $k_0 d = 0.244$ that belongs to both band gaps. Next, we construct three random samples. The first sample is built up by the Bragg-reflectors of the first type randomly distributed in vacuum. The second sample differs from the first one by the type of the Bragg reflectors and realization. The third sample is built up by interpenetration of the above samples. These samples have the same thickness of $100d$. It is seen (Fig. 15) that the weakening of the field happens inside the Bragg-reflectors while in between the Bragg-reflectors the strength of fields may achieve high values due to resonance. It seems that usually these regions are usually associated with localized states.

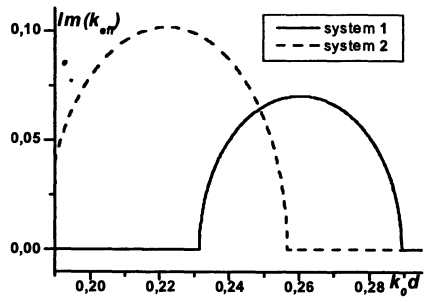

Figure 14. The band structure of the periodic systems employing the five-layer Bragg-reflectors as cells.

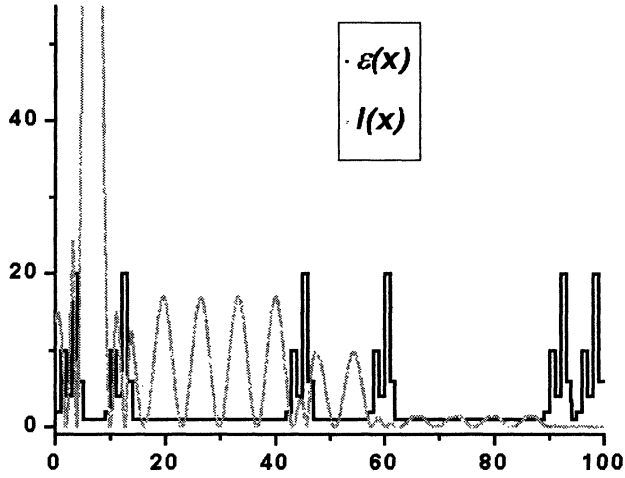

Figure 15. The distribution of intensity of left-to-right incident wave (dotted line) in the second random sample. The solid line represents the permittivity distribution.

The band structures of periodic systems, which have these samples as elementary cells, are shown in Fig. 16. Comparing Fig. 14 and Fig. 18 we can see that though the band structures become more complicated (there appear new bands) the quote of band gaps increases making a free propagation of waves to be improbable. Thus the complication of the cell structure leads to the localization of waves. Unfortunately, the band structure does not exhibit a superposition. Inside the common band gap of two first systems there exist frequencies at which the third system is transparent. The frequency $k_0 d = 0.244$ is purposely chosen to illustrate this fact. In spite of that the two first systems still have a positive Lyapunov index (the waves are localized) their plane sum is transparent. This situation is illustrated in Figs. 17-19. To make it pictorially we consider samples consisting of two elementary cells. It is seen that the wave is explicitly localized in the first two cases

and delocalized in the third one. It seems that it is the absence of the band gap superposition that makes one resort to vague explanations though the picture of wave localization has long been known in regular systems.

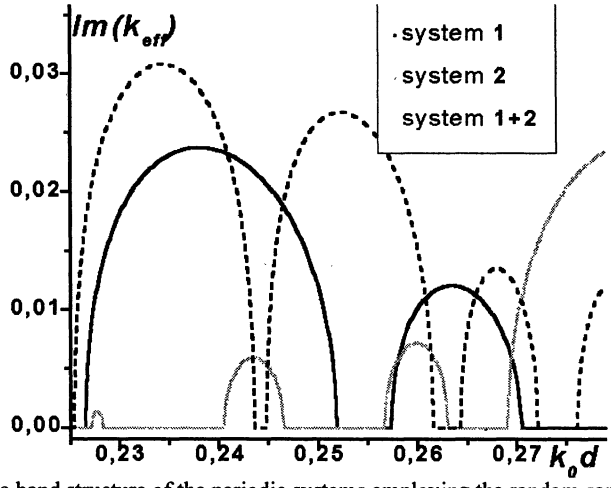

Figure 16. The band structure of the periodic systems employing the random samples as cells

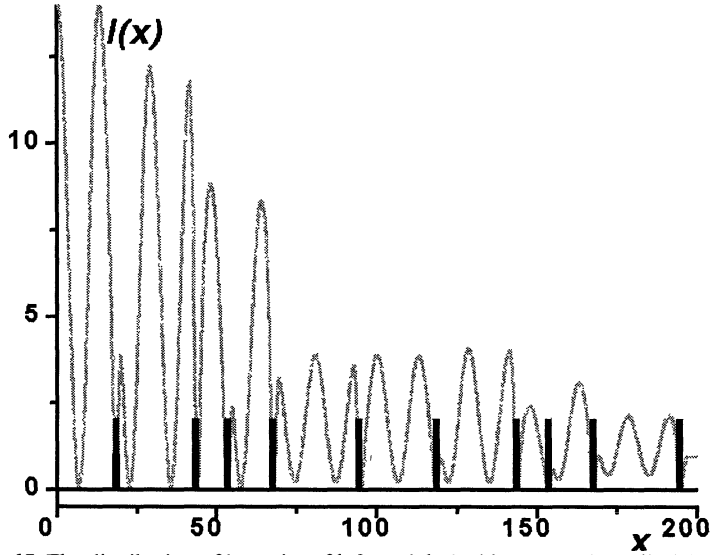

Figure 17. The distribution of intensity of left-to-right incident wave (gray line) in the first random sample. The vertical columns mark the positions of the Bragg reflectors.

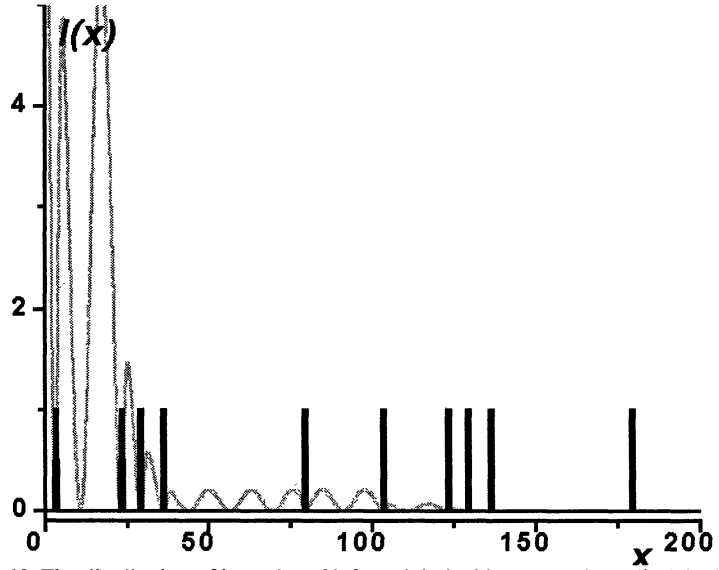

Figure 18. The distribution of intensity of left-to-right incident wave (gray line) in the second random sample. The vertical columns mark the positions of the Bragg reflectors.

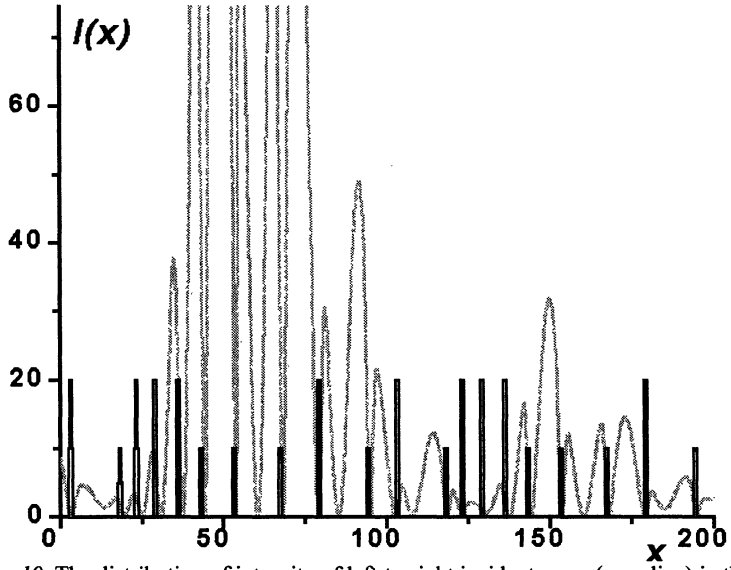

Figure 19. The distribution of intensity of left-to-right incident wave (gray line) in the third sample. The short vertical columns mark the positions of the first Bragg reflectors and the high columns mark the second ones.

5. Conclusions

It is shown that the interplay of different space scales (wavelength λ, system size L, the mean size of inhomogeneity a, etc.) in a one-dimensional problem can drastically change the regime of wave propagation in heterogeneous media. At $L \sim \lambda$, the propagation is of mesoscopic character even if $d << \lambda$ and the homogenization regime could be expected. At $d \sim \lambda$, the anticipated localization of waves may not happen even if $L >> \lambda$. The cause is the existence of a non-zero portion of layers with commensurable optical paths. It is the Bragg reflection rather than coherent backscattering that determines the localization in one-dimensional electromagnetic problems. We relate localization to the total increase of band gaps with the infinite growth of the size and structure complexity of the cell.

ACKNOWLEDGMENTS

This work was partly supported by the Russian Foundation for Basic Research under the Contracts 00-15-96570 and No 01-02-17962.

REFERENCES

1. Born M. and Huang Kun (1954), *Dynamical theory of crystal lattices*, The Clarendon Press, Oxford
2. BrekhovskikhV. L.. (1985) The effective permittivity of a random medium by accounting the second moments of fields, *JETP*, **89**, 2013-2020. (in Russian)
3. Sobel'man I. I. (2002) On the theory of light scattering in gases, *Physics Uspekhi* **245**, 75-80
4. Sheng P. (1995) *Introduction to wave scattering, localization, and mesoscopic phenomena*, Academic Press, London.
5. Sanchez-Palensia E. (1980) *Non-homogeneous media and vibration theory*, Springer-Verlag, New York.
6. Rytov S. M, (1956) Acoustic properties of a finely layered medium, *Akust. Zh.* **11**, 71-83
7. Brekhovskikh L. M. (1960) *Waves in Layered Media*, Academic, New York
8. Djafari Rouhani B. and Sapriel J. (1986) Effective dielectric and photoelastic tensors of superlattices in the long wave regime, *Phys. Rev. B* **34**, 7114-7117.
9. Akcakaya E. and Farnell G. W. (1988) Effective elastic and piezoelectric constant of superlattices, *J. Appl. Phys.* **64**, 4469-4473.
10. Slepyan G. Ya., Gurevich A. V., and Maximenko S. A. (1995) Floquet-Bloch waves in periodic chiral media, *Phys. Rev. E*, **51**, 2543-2549.
11. Semchenko I. V. (1990) Gyrotropic properties of superlattices in the long wavelength approximation, *Kristallografiya*, **35**, 1047-1050 (in Russian).
12. Francsechetti G.(1967) A complete analysis of the reflection and transmission methods for measuring the complex permeability and permittivity of materials at microwaves, *Acta frequenza*, **36**, 757-764.
13. Born M. and Wolf E. (1980) *Principles of optics*, sixth ed. Pergamon Press, Oxford
14. Thouless D. J. (1972) A relation between the density of state and range of localization for one dimensional random systems, *J. Phys. C.*, **5**, 77-81
15. Herbert D. C., Jones R. (1971) Localized states in disordered systems, *J. Phys. C*, **4**, 1145-1161
16. Pi-Gang Luan and Zhen Ye (2001) Acoustic wave propagation in a one-dimensional layered system, *Phys Rev E*, **63**, 066611-1 – 066611-8

17. Klyatskin V. and Saichev A. (1992) Static and dynamic localization of plane waves in disordered laminar media, *Uspehki Fiz. Nauk*, **162,** 16-193 (in Russian)
18. Freilikher V., Pustilnik M. and Yurkevich I. (1994) Wave transmission through lossy media in the strong-localization regime, *Phys. Rev. B,* **50**, 6017-6022
19. Kim K. (1998) Reflection coefficient and localization length of waves in one-dimensional random media, *Phys. Rev. B*, **58**, 6153-6160
20. Vinogradov A. and Merzlikin A. (2002) On the problem of homogenization of one-dimensional systems, *JETP* **121**, 1-8 (in Russian)
21. McGurn A. R., Maradudin A. A. (1993) Anderson localization in one-dimensional randomly disordered optical systems that are periodic on average, *Phys. Rev. B*, **47**, 13120-13125
22. Bulgakov S. A., Nieto-Vasperinas M. (1997) Frequency properties of random photonic lattices, *Waves in Random Media*, **7**, 183-192

LOCALIZED ELECTROMAGNETIC AND ELASTIC FIELDS WITH APPLICATIONS TO CONTROL LASER RADIATION

G.N. BORZDOV
Department of Theoretical Physics
Belarusian State University
Fr. Skaryny avenue 4
220050 Minsk, Belarus

Abstract. The localized electromagnetic and elastic fields, defined by the spherical harmonics, have a very small (about several wavelengths) core region with maximum intensity of field oscillations and unique space distributions of polarization states, energy densities, and energy fluxes. The three–dimensional localization makes it possible to use these fields as structural elements to form various complex electromagnetic and elastic fields. In particular, localized fields can be combined into a complex field structure, such as a diffraction grating. This makes them promising tools to control laser radiation.

1. Introduction

During the last two decades, a number of so-called localized wave solutions to the scalar and vector homogeneous wave equations has been found (see, for example, [1–22] and references therein). In particular, these exact solutions include focus wave modes [1, 2], moving Gaussian [3] and Bessel–Gauss [4] pulses, electromagnetic missiles [5], Bessel and Bessel–Gauss beams [6–9], acoustic [10] and electromagnetic [11, 12] directed energy pulse trains, etc. They describe localized, slowly decaying transmission of electromagnetic and acoustic energy and appear to have great potential for numerous applications.

It is of prime importance that finite–energy and finite–aperture localized fields can be realized physically [11, 12, 18]. To this end, Ziolkowski proposed to use an array composed of independently addressable elements [15]. The existence of acoustic directed energy pulse trains was confirmed for ultrasonic waves in water [10, 13]. Recently, Saari and Reivelt proposed an approach to optical implementing of localized wave fields [21, 22].

Of the mathematical techniques which are used now in the analysis of various localized fields, plane wave expansions occupy a prominent place.

S. Zouhdi et al. (eds.), Advances in Electromagnetics of Complex Media and Metamaterials, 363–383.

They provide a very convenient and general approach to both constructing and investigating localized solutions. In particular, by using the space–time Fourier transform, Donnely and Ziolkowski developed a method for obtaining separable and non-separable localized solutions of constant coefficient homogeneous partial differential equations [16, 17]. It is essential that many types of localized fields in a source–free space, such as the focus wave modes [19], are composed of backward and forward propagating homogeneous plane waves.

The above–mentioned solutions have been much investigated, mainly, in connection with the problem of localized transmission of electromagnetic and acoustic energy. However, a different type of localized fields — three–dimensional standing waves — also may have important practical applications.

By using expansions in plane waves, we have proposed [23, 24] an approach for obtaining families of orthonormal beams and various localized fields, defined by a given set of orthonormal scalar functions on a two– or three–dimensional manifold (beam manifold). This approach makes it possible to obtain exact solutions to the corresponding homogeneous wave equations for any linear field. Its potentialities have been illustrated for the cases of electromagnetic waves in free space [23–29] and complex media [24–27], elastic waves in isotropic and anisotropic solids [30–33], sound waves in an ideal liquid [34], and weak gravitational fields [28]. In all these cases, we have treated the fields defined by the spherical harmonics.

The presented families of orthonormal electromagnetic beams can be applied, in particular, to characterizing electromagnetic fields and complex media [26, 29]. The localized fields, defined by the spherical harmonics, have a very small (about several wavelengths) core region with maximum intensity of field oscillations and unique space distributions of polarization states, energy densities, and energy fluxes. Outside the core, the intensity of oscillations rapidly decreases in all directions.

In Ref. [35], we have proposed another technique for obtaining localized exact solutions of linear field equations. It can be considered as a generalization of the earlier presented approach [24], that has extended potentialities for characterizing and designing localized fields.

The three–dimensional localization makes it possible to use these fields as structural elements to form various complex electromagnetic and elastic fields. In particular, it was shown [30] that localized elastic fields can be combined into a complex field structure, such as an ultrasonic diffraction grating. This makes them promising tools to control laser radiation.

In this paper, we illustrate this approach by calculating optical properties of an isotropic medium subjected to localized elastic fields composed of transverse eigenwaves. Since such elastic fields bear some similarities [33] to

the electromagnetic fields, localized microwave fields can be used similarly in electro–optics.

2. Basic Equations

2.1. ELASTIC EIGENWAVES IN AN ISOTROPIC MEDIUM

In an isotropic elastic medium with Lame modules λ_L and μ_L, the Hooke law takes the form [36]

$$\sigma = \lambda_L (\operatorname{div} \mathbf{u})\, \mathbf{1} + 2\mu_L \gamma, \tag{1}$$

where σ is the stress tensor, γ is the deformation tensor, $\mathbf{u}$ is the displacement vector, and $\mathbf{1}$ is the unit dyadic. In a Cartesian basis $(\mathbf{e}_i)$, γ has the components

$$\gamma_{ij} = \frac{1}{2}\left(\frac{\partial u_i}{\partial x_j} + \frac{\partial u_j}{\partial x_i}\right). \tag{2}$$

In the case of time–harmonic elastic fields, the time average kinetic w_K and elastic w_E energy densities, and the time average energy flux density vector $\mathbf{S}$ are given by [36]

$$w_K = \frac{1}{4}\varrho\omega^2|\mathbf{u}|^2, \qquad w_E = \frac{1}{4}\operatorname{Re}(\sigma_{ik}\gamma_{ik}^*), \qquad \mathbf{S} = \frac{\omega}{2}\operatorname{Re}(i\sigma^*\mathbf{u}), \tag{3}$$

where ϱ is the medium density, ω is the angular frequency, and σ^* is the complex conjugate to σ.

To compose time–harmonic orthonormal beams, normalized to the energy flux through a plane σ_0, and various localized fields in isotropic and anisotropic elastic media, we use the six–dimensional eigenwave amplitude [30, 31]

$$\mathbf{W}_0 = \begin{pmatrix} \mathbf{u} \\ \mathbf{f} \end{pmatrix}, \qquad \mathbf{f} = \sigma\mathbf{q} = i(\mathbf{q}\cdot c\cdot\mathbf{k})\mathbf{u}, \tag{4}$$

where $\mathbf{q}$ is the unit normal to σ_0, $\mathbf{k}$ is the wave vector, $(\mathbf{a}\cdot c\cdot\mathbf{b})_{im} = a_j c_{ijlm} b_l$, (c_{ijlm}) are the elastic modules, and summation over repeated indices is carried out from 1 to 3.

For an eigenwave in isotropic medium, Eqs. (1), (2) and (4) result in

$$\gamma = \frac{ik}{2}(\hat{\mathbf{k}}\otimes\mathbf{u} + \mathbf{u}\otimes\hat{\mathbf{k}}), \tag{5}$$

$$\sigma = ik[\lambda_L(\hat{\mathbf{k}}\cdot\mathbf{u})\mathbf{1} + \mu_L(\hat{\mathbf{k}}\otimes\mathbf{u} + \mathbf{u}\otimes\hat{\mathbf{k}})], \tag{6}$$

$$\mathbf{f} = ik[\lambda_L(\hat{\mathbf{k}}\cdot\mathbf{u})\mathbf{q} + \mu_L(\mathbf{u}\cdot\mathbf{q})\hat{\mathbf{k}} + \mu_L(\hat{\mathbf{k}}\cdot\mathbf{q})\mathbf{u}], \tag{7}$$

where $\hat{\mathbf{k}} = \mathbf{k}/k$ is the unit wave normal, and $k = 2\pi/\lambda = \omega/v$ is the wave number, λ is the wavelength, v is the phase velocity, and $\otimes$ is the tensor product. Longitudinal and transverse elastic eigenwaves have the phase velocities $v_1 = \sqrt{(\lambda_L + 2\mu_L)/\varrho}$ and $v_2 = \sqrt{\mu_L/\varrho}$, respectively.

2.2. ELASTIC BEAMS DEFINED BY THE SPHERICAL HARMONICS

In Refs. [30–33], we have presented various families of time–harmonic orthonormal beams and localized fields in an isotropic solid medium. They are defined by the spherical harmonics Y_j^s as

$$\begin{aligned}\mathbf{W}_j^s(\mathbf{r},t) &= \exp(-i\omega t)\int_0^{2\pi} d\varphi \int_0^{\theta_2} \exp[i\mathbf{r}\cdot\mathbf{k}(\theta,\varphi)] \\ &\quad \times Y_j^s(\theta,\varphi)\nu(\theta,\varphi)\mathbf{W}(\theta,\varphi)\sin\theta d\theta, \end{aligned} \tag{8}$$

where

$$\hat{\mathbf{k}} = \mathbf{k}/k = \mathbf{e}_r = \sin\theta'(\mathbf{e}_1\cos\varphi + \mathbf{e}_2\sin\varphi) + \mathbf{e}_3\cos\theta', \tag{9}$$

$$\theta' = \kappa_0\theta, \qquad 0 < \kappa_0 \leq 1. \tag{10}$$

Here, $\mathbf{e}_r = \mathbf{e}_r(\theta',\varphi)$ is the radial basis vector of the spherical coordinate system, θ' and φ are the polar and the azimuthal angles, κ_0 is some given parameter.

For the fields under consideration, the value $Y_j^s(\theta,\varphi)$ of function Y_j^s at given θ and φ specifies the intensity and the phase of the partial eigenwave with the unit wave normal $\hat{\mathbf{k}}(\theta,\varphi) = \mathbf{e}_r(\theta',\varphi)$. These fields are composed of plane waves propagating into the solid angle $\Omega = 2\pi(1 - \cos\kappa_0\theta_2)$.

The amplitude function for beams composed of longitudinal waves is given as [30, 32]

$$\mathbf{W}(\theta,\varphi) \equiv \begin{pmatrix} \mathbf{u} \\ \mathbf{f} \end{pmatrix} = \begin{pmatrix} \mathbf{e}_r \\ ik(\lambda_L\mathbf{e}_3 + 2\mu_L\cos\theta'\mathbf{e}_r) \end{pmatrix}, \tag{11}$$

where $k = \omega/v_1$ and $\mathbf{q} = \mathbf{e}_3$.

Transverse eigenwaves propagating in an isotropic medium have two–dimensional amplitude subspaces, thus providing a great scope for designing various localized fields. In particular, one can set two linearly independent amplitude functions by [30, 33]

$$\mathbf{W}(\theta,\varphi) = \begin{pmatrix} \mathbf{e}_{\theta'} \\ ik\mu_L\,(-\sin\theta'\mathbf{e}_r + \cos\theta'\mathbf{e}_{\theta'}) \end{pmatrix}, \tag{12}$$

$$\mathbf{W}(\theta,\varphi) = \begin{pmatrix} \mathbf{e}_\varphi \\ ik\mu_L\cos\theta'\mathbf{e}_\varphi \end{pmatrix}, \tag{13}$$

where

$$\mathbf{e}_{\theta'} = \cos\theta'(\mathbf{e}_1 \cos\varphi + \mathbf{e}_2 \sin\varphi) - \mathbf{e}_3 \sin\theta', \tag{14}$$

$$\mathbf{e}_{\varphi} = -\mathbf{e}_1 \sin\varphi + \mathbf{e}_2 \cos\varphi, \tag{15}$$

and $k = \omega/v_2$. This gives two different families of beams (u_M beams and u_A beams), composed of eigenwaves with the meridional and the azimuthal orientations of the displacement vector $\mathbf{u}$, respectively.

Similarly, in the case of electromagnetic plane–wave superpositions in an isotropic medium, two independent amplitude functions can be set as

$$\mathbf{W}(\theta, \varphi) = \begin{pmatrix} Z_0 \mathbf{e}_{\theta'} \\ \mathbf{e}_{\varphi} \end{pmatrix}, \tag{16}$$

$$\mathbf{W}(\theta, \varphi) = \begin{pmatrix} Z_0 \mathbf{e}_{\varphi} \\ -\mathbf{e}_{\theta'} \end{pmatrix}, \tag{17}$$

where $Z_0 = \sqrt{\mu/\epsilon}$, ϵ is the dielectric permittivity and μ is the magnetic permeability.

3. Optical properties of an isotropic medium subjected to a localized elastic field

3.1. CLASSIFICATION OF BEAMS DEFINED BY THE SPHERICAL HARMONICS

It follows from Eqs. (8)–(10) that the set of plane waves forming the beam $\mathbf{W}_j^s$ — the beam base — is prescribed by the parameters θ_2, κ_0 and the normalized amplitude function $\mathbf{W} = \mathbf{W}(\theta, \varphi)$. The latter specifies the polarizations of partial eigenwaves. The beam state function $\nu = \nu(\theta, \varphi)$ plays an important role in setting the contribution of each eigenwave to the total field. By assigning all these parameters and functions in various ways, one can obtain a multitude of orthonormal beams and localized fields. The major types of these plane–wave superpositions can be classified as follows.

1. **Orthonormal beams with $\theta_2 = \pi/2$, $\kappa_0 = 1$, and $\Omega = 2\pi$.** They are composed of plane waves propagating into a given half space and comprise two separate sets of orthonormal beams, defined by the spherical harmonics Y_j^s with even and odd j, respectively. These beams are normalized to the time average energy flux N_Q through the plane σ_0. In this case, the beam state function $\nu(\theta, \varphi)$ reduces to a constant

$$\nu_2 = \frac{1}{\pi}\sqrt{\frac{N_Q}{\varrho v_2^3}}. \tag{18}$$

2. **Orthonormal beams with $\theta_2 = \pi$, and $\kappa_0 \leq 1/2$.** These beams are composed of plane waves propagating into the solid angle $\Omega = 2\pi(1-\cos\kappa_0\pi) \leq 2\pi$. They comprise a complete system of orthonormal beams, defined by the whole set of spherical harmonics. In this case, the beam state function depends only on θ as

$$\nu(\theta) = \nu_2 \sqrt{\frac{\kappa_0 \sin \kappa_0\theta}{2\sin\theta}}. \tag{19}$$

3. **Three–dimensional standing waves with $\theta_2 = \pi$, $\kappa_0 = 1$, $\Omega = 4\pi$, and $\nu = \nu_2/\sqrt{2}$.** They are formed from plane waves of all possible propagation directions. This family consists of " **storms**", defined by the zonal spherical harmonics Y_j^0, and **"whirls"** defined by the other Y_j^s ($s \neq 0$). For the storms, the time average energy flux is identically zero at all points. The whirls have circular energy flux lines lying in the planes orthogonal to $\mathbf{e}_3$.
4. **Localized fields with $\pi/2 < \theta_2 < \pi$, $\kappa_0 = 1$, $2\pi < \Omega < 4\pi$, and $\nu = \text{const}$.** These fields are highly localized and have non-vanishing normal and radial components of $\mathbf{S}$. They include localized fields with spiral lines of energy flux — **"tornadoes"**. The later are defined by Y_j^s with $s \neq 0$.
5. **Finite–energy evolving sound storms, whirls, and tornadoes.** They can be obtained by the frequency integration as

$$\breve{\mathbf{W}}_j^s(\mathbf{r},t) = \frac{1}{\omega_+ - \omega_-} \int_{\omega_-}^{\omega_+} \mathbf{W}_j^s(\mathbf{r},t)d\omega. \tag{20}$$

The solutions, which are defined by the spherical harmonics Y_j^s with a non-zero s, describe rotating elastic fields.

A similar classification is valid for electromagnetic plane–wave superpositions.

3.2. PHOTOELASTICITY IN AN ISOTROPIC MEDIUM

Let us consider a homogeneous isotropic solid medium with refractive index n_0. Owing to the photoelastic effect, this medium becomes inhomogeneous non-stationary and anisotropic. It is described by the dielectric permittivity tensor field $\epsilon = \epsilon(\mathbf{r},t)$. Usually, the induced optical anisotropy is very small, and ϵ^{-1} is defined as [37]

$$\epsilon^{-1} = \frac{1}{{n_0}^2}\mathbf{1} + A, \tag{21}$$

where

$$A = p_{12}\,(\operatorname{div}\mathbf{u})\,\mathbf{1} + 2p_{44}\,\gamma, \tag{22}$$

p_{12} and p_{44} are the photoelastic constants.

In the case of shear waves, i.e., superpositions of transverse elastic eigenwaves, $\operatorname{div}\mathbf{u} = \gamma_{11} + \gamma_{22} + \gamma_{33} = 0$. Hence, Eq. (21) becomes

$$\epsilon^{-1} = \frac{1}{{n_0}^2}\mathbf{1} + 2p_{44}\gamma. \tag{23}$$

The tensors ϵ and γ have the same system of eigenvectors, and their eigenvalues ϵ_i and γ_i are related as

$$\frac{1}{\epsilon_i} = \frac{1}{{n_0}^2} + 2p_{44}\gamma_i, \qquad i = 1, 2, 3. \tag{24}$$

Since the perturbation of the dielectric permittivity tensor caused by the elastic field is small, the local values of refractive indices can be approximated as

$$n_{\pm} = n_0 - {n_0}^3 p_{44}\beta_{\pm}, \tag{25}$$

where $\beta_{\pm}$ are the eigenvalues of the tensor

$$\beta = -\mathbf{n}^{\times}\gamma\mathbf{n}^{\times}. \tag{26}$$

Here, $\mathbf{n}^{\times}$ is antisymmetric tensor dual to the unit wave normal $\mathbf{n}$. Since $\mathbf{n}^{\times}\mathbf{E} = \mathbf{n}\times\mathbf{E}$ and $\mathbf{1} = \mathbf{e}_i\otimes\mathbf{e}_i$, $\mathbf{n}^{\times}$ can also be denoted by $\mathbf{n}\times\mathbf{1} \equiv (\mathbf{n}\times\mathbf{e}_i)\otimes\mathbf{e}_i$.

4. Complex field structures

4.1. FIELD GRATINGS

The three–dimensional localization makes it possible to use the presented fields as structural elements to form various complex electromagnetic and elastic fields. By way of illustration, let us consider a field defined as

$$\mathbf{W}'(\mathbf{r}, t) = \sum_{n=M_1}^{N_1}\sum_{m=M_2}^{N_2}\sum_{l=M_3}^{N_3}\mathbf{W}_j^s(\mathbf{r} - \mathbf{a}_{nml}, t - \tau_{nml}), \tag{27}$$

$$\mathbf{a}_{nml} = n\mathbf{a}_1 + m\mathbf{a}_2 + l\mathbf{a}_3, \tag{28}$$

$$\tau_{nml} = n\tau_1 + m\tau_2 + l\tau_3, \tag{29}$$

where $\mathbf{W}_j^s(\mathbf{r}, t)$ is set by Eq. (8), $\mathbf{a}_j$ and τ_j are some given spatial and temporal shifts.

The translated fields $\mathbf{W}_j^s(\mathbf{r} - \mathbf{a}_{nml}, t - \tau_{nml})$ form a family of wavelets with $\mathbf{W}_j^s(\mathbf{r}, t)$ as the mother wavelet. If the lengths of the shift vectors $\mathbf{a}_j$ $(j = 1, 2, 3)$ are sufficiently large, the field $\mathbf{W}'$ will constitute a field grating, where each element has only reasonably small deviations from its initial

form. Moreover, the prior investigation of a single localized field permits to use copies of this field with small spatial and time shifts in designing complex electromagnetic and elastic fields.

4.2. LOCALIZED SHEAR WAVES IN THE FUSED QUARTZ

In Appendix, we present some graphic illustrations for the case of localized shear waves in the fused quartz that has parameters $n_0 = 1.46$, $v_1 = 5969$ m/s, $v_2 = 3753$ m/s, $\varrho = 2.203$ g/cm^3, $p_{12} = 0.27$, and $p_{44} = -0.0745$. In all illustrations, the elastic waves are time–harmonic fields of frequency 0.5 GHz. They are described in terms of the dimensionless coordinates $x' = x^1/\lambda$, $y' = x^2/\lambda$ and $z' = x^3/\lambda$, where $\mathbf{r} = x^i \mathbf{e}_i$ and $\lambda = 2\pi v_2/\omega$ is the wavelength.

Figs. 1 and 2 (Appendix I) illustrate the distinctions between variations of refractive indices, induced by the u_M and u_A orthonormal beams. Components of the tensor $A = \epsilon^{-1} - \mathbf{1}/{n_0}^2$ induced by the u_M and u_A elastic storms are presented in Figs. 3–6 (Appendix II) and 7–8 (Appendix III), respectively. Figs. 9–14 (Appendix IV) illustrate the properties of a cubic grating composed of u_M elastic beams.

Parameter κ_0 (10) exerts control over the beam divergence and the dimensions of the beam cross-section at the plane $z' = 0$. The smaller κ_0 is, the more collimated is the beam, but the cross-section becomes larger (see Figs. 15 and 16, Appendix V).

The beams defined by the zonal spherical harmonics Y_j^0 ($j = 0, 1, \ldots$) have axially symmetric instantaneous fields, whereas other beams, defined by Y_j^s with $s \neq 0$, comprise a family of rotating fields [24, 30–34]. Some of such electromagnetic and elastic fields have spiral energy flux lines. They can induce chiral inhomogeneities in isotropic media. Figs. 17–21 and 22 (Appendix VI) illustrate chiral structures induced by a single orthonormal elastic beam with $j = s = 1$ and a two–dimensional grating composed of such beams, respectively.

5. Conclusion

The electromagnetic and elastic plane–wave superpositions under consideration have a number of distinguishing features. Owing to a wide angular spectrum, they possess a very high degree of three–dimensional localization. This makes it possible to obtain large values of induced inhomogeneities (variations of the dielectric permittivity tensor) in small domains about several wavelengths by using beams of moderate energy flux. The proposed approach provides a broad spectrum of tools to design localized fields, i.e., to build–in symmetry properties of oscillating fields, to govern both

size and form of localization domains. Localized fields can be combined as constructive elements to obtain complex field structures, such as induced chiral structures and one–, two–, or three–dimensional field gratings. All this makes electromagnetic and elastic localized fields promising tools to control laser radiation.

References

1. Brittingham, J.N. (1983) Focus waves modes in homogeneous Maxwell's equations: Transverse electric mode, *J. Appl. Phys.* **54**, pp. 1179–1189.
2. Sezginer, A. (1985) A general formulation of focus wave modes, *J. Appl. Phys.* **57**, pp. 678–683.
3. Ziolkowski, R.W. (1985) Exact solutions of the wave equation with complex source locations, *J. Math. Phys.* **26**, pp. 861–863.
4. Overfelt, P.L. (1991) Bessel–Gauss pulses, *Phys. Rev.* **A44**, 3941–3947.
5. Wu, T.T. (1985) Electromagnetic missiles, *J. Appl. Phys.* **57**, pp. 2370–2373.
6. Durnin, J. (1987) Exact solutions for nondiffracting beams. 1. The scalar theory, *J. Opt. Soc. Am.* **A4**, pp. 651–654.
7. Gori, F., Guattari, G. and Padovani, C. (1987) Bessel–Gauss beams, *Optics Comm.* **64**, pp. 491–495.
8. Durnin, J., Miceli, J.J. and Eberly, J.H. (1988) Comparison of Bessel and Gaussian beams, *Opt. Letters* **13**, pp. 79–80.
9. Belsky, A.M. (2000) *Optics of Coherent Light Beams*, Belarusian State University, Minsk.
10. Ziolkowski, R.W., Lewis, D.K. and Cook, B.D. (1989) Evidence of localized wave transmission, *Phys. Rev. Lett.* **62**, 147–150.
11. Ziolkowski, R.W. (1989) Localized transmission of electromagnetic energy, *Phys. Rev.* **A39**, 2005–2033.
12. Shaarawi, A.M., Besieris, I.M. and Ziolkowski, R.W. (1989) Localized energy pulse trains launched from an open, semi-infinite, circular waveguide, *J. Appl. Phys.* **65**, 805–813.
13. Ziolkowski, R.W. and Lewis, D.K. (1990) Verification of the localized wave transmission effect *J. Appl. Phys.* **68**, 6083–6086.
14. Ziolkowski, R.W. and Tippett, M.K. (1991) Collective effect in an electron plasma system catalyzed by a localized electromagnetic wave *Phys. Rev.* **A43**, 3066–3072.
15. Ziolkowski, R.W. (1991) Localized wave physics and engineering, *Phys. Rev.* **A44**, 3960–3984.
16. Donnelly, R. and Ziolkowski, R.W. (1992) A method for constructing solutions for homogeneous partial differential equations: localized waves, *Proc. Roy. Soc. London* **A437**, 673–692.
17. Donnelly, R. and Ziolkowski, R.W. (1993) Designing localized waves, *Proc. Roy. Soc. London* **A440**, 541–565.
18. Ziolkowski, R.W., Besieris, I.M. and Shaarawi, A.M. (1993) Aperture realizations of exact solutions to homogeneous wave equations *J. Opt. Soc. Am.* **A10**, 75–87.
19. Shaarawi, A.M., Ziolkowski, R.W. and Besieris, I.M. (1995) On the evanescent fields and the causality of the focus wave modes, *J. Math. Phys.* **36**, 5565–5587.
20. Ziolkowski, R.W. (1995) Electromagnetic localized waves that counteract Coulomb repulsion to catalyze a collective electron–packet state, *Phys. Rev.* **E52**, 5338–5343.

21. Saari, P. and Reivelt, K. (1997) Evidence of X–shaped propagation invariant localized light waves, *Phys. Rev. Lett.* **79**, 4135–4138.
22. Reivelt, K. and Saari, P. (2000) Optical generation of focus wave modes, *J. Opt. Soc. Am.* **A17**, 1785–1790.
23. Borzdov, G.N. (1999) New types of electromagnetic beams in complex media and vacuum, in C.C. Peñalosa and B.S.Rawat (eds.), *Proc. 7th Int. Symp. Recent Advan. Microwave Techn.*, Málaga, Spain, pp. 169–172.
24. Borzdov, G.N. (2000) Plane–wave superpositions defined by orthonormal scalar functions on two– and three–dimensional manifolds, *Phys. Rev.* **E61**, 4462–4478.
25. Borzdov, G. N. (2000) New types of orthonormal electromagnetic beams in complex media and free space, in A.M. Barbosa and A.L. Topa (eds), *Proc. Bianisotropics 2000*, Lisbon, Portugal, pp. 55–58.
26. Borzdov, G. N. (2000) The application of orthonormal electromagnetic beams to characterizing complex media, in A.M. Barbosa and A.L. Topa (eds), *Proc. Bianisotropics 2000*, Lisbon, Portugal, pp. 11–14.
27. Borzdov, G. N. (2000) Localized electromagnetic fields in complex media and free space, in A.M. Barbosa and A.L. Topa (eds), *Proc. Bianisotropics 2000*, Lisbon, Portugal, pp. 59–62.
28. Borzdov, G.N. (2001) Localized electromagnetic and weak gravitational fields in the source–free space, *Phys. Rev.* **E63**, 036606(10).
29. Borzdov, G.N. (2001) Orthonormal beams with applications to characterizing electromagnetic fields and complex mediums, *Int. J. Electron. Commun. (AEÜ)* **55**, 224–232.
30. Borzdov, G.N. (2001) Elastic orthonormal beams and localized fields with applications to control laser radiation, in A. Lakhtakia, W.S. Weiglhofer and I.J. Hodgkinson (eds.), *Proc. SPIE* **4467** *(Complex Mediums II: Beyond Linear Isotropic Dielectrics)*, San Diego, USA, pp. 57–68.
31. Borzdov, G.N. (2001) Elastic and sound orthonormal beams and localized fields in linear mediums: I. Basic equations, *J. Phys.* **A34**, 6249–6257.
32. Borzdov, G.N. (2001) Elastic and sound orthonormal beams and localized fields in linear mediums: II. Superpositions of longitudinal elastic plane waves in an isotropic medium, *J. Phys.* **A34**, 6259–6267.
33. Borzdov, G.N. (2001) Elastic and sound orthonormal beams and localized fields in linear media: III. Superpositions of transverse elastic plane waves in an isotropic medium, *J. Phys.* **A34**, 6269–6279.
34. Borzdov, G.N. (2001) Elastic and sound orthonormal beams and localized fields in linear media: IV. Superpositions of sound plane waves in an ideal liquid, *J. Phys.* **A34**, 6281–6289.
35. Borzdov, G.N. (2002) Designing localized electromagnetic fields in a source–free space, *Phys. Rev.* **E65**, 066612(16).
36. Fedorov, F.I. (1968) *Theory of Elastic Waves in Crystals*, Plenum Press, New York.
37. Dieulesaint, E. and Royer, D. (1974) *Ondes élastiques dans les solides. Application au traitement du signal*, Masson, Paris.

Appendix

I. Refractive index variations in the central cross-section of the u_M and u_A orthonormal elastic beams

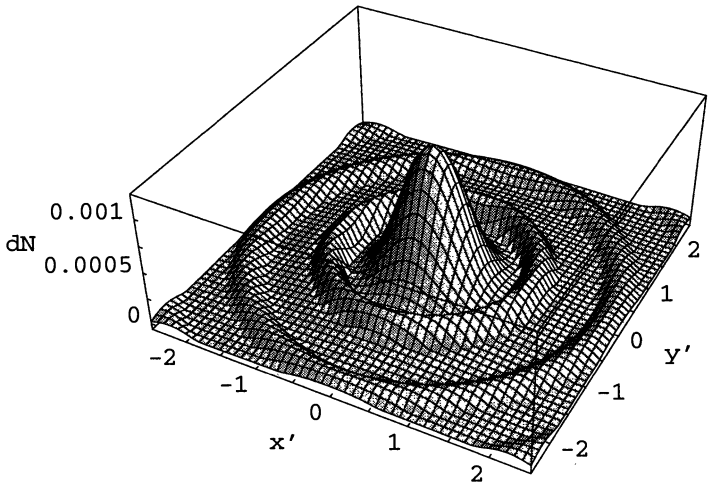

Figure 1. Refractive index variation $dN = n_+ - n_0$; u_M beam defined by the spherical harmonics Y_0^0; $\theta_2 = \pi/2$; $\kappa_0 = 1$; $\nu = \nu_2$; $N_Q = 0.5W$; $\mathbf{n} = \mathbf{e}_3$; $z' = 0$; $\omega t = \pi/2$.

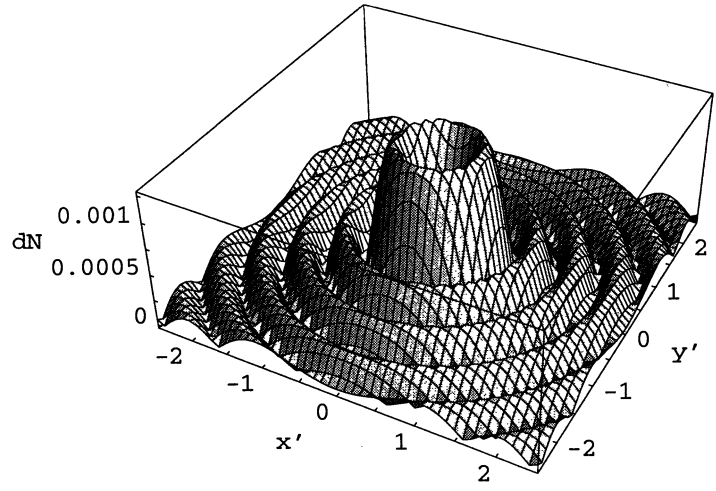

Figure 2. Refractive index variation $dN = n_+ - n_0$; u_A elastic beam defined by the spherical harmonics Y_0^0; the parameters are the same as those in Fig. 1.

II. Non-vanishing components of the tensor $A = \epsilon^{-1} - 1/{n_0}^2$ induced by the u_M elastic storm

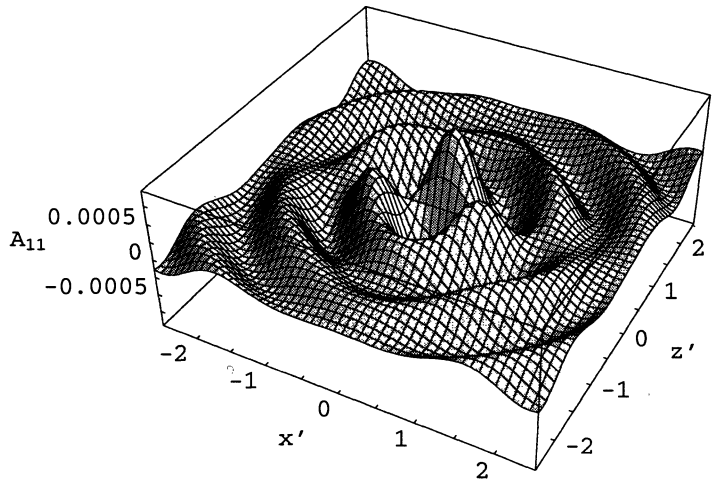

Figure 3. Component $A_{11} = (\epsilon^{-1})_{11} - 1/{n_0}^2$; u_M storm defined by the spherical harmonics Y_0^0; $\theta_2 = \pi$; $\kappa_0 = 1$; $\nu = \nu_2/\sqrt{2}$; $N_Q = 0.5W$; $y' = 0$; $t = 0$.

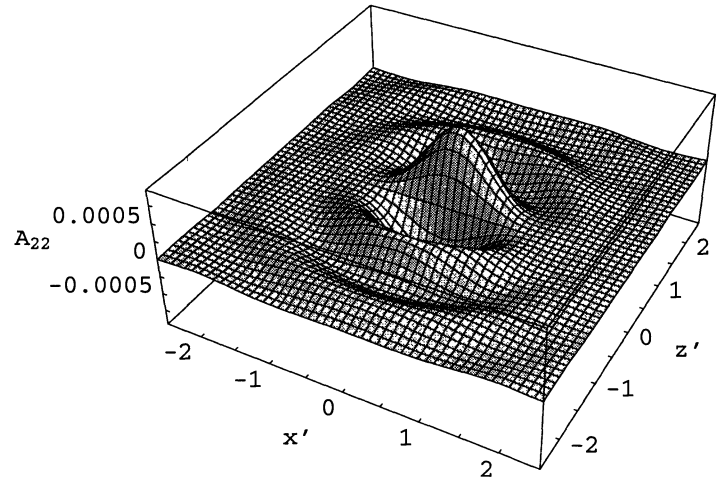

Figure 4. Component $A_{22} = (\epsilon^{-1})_{22} - 1/{n_0}^2$; the parameters are the same as those in Fig. 3.

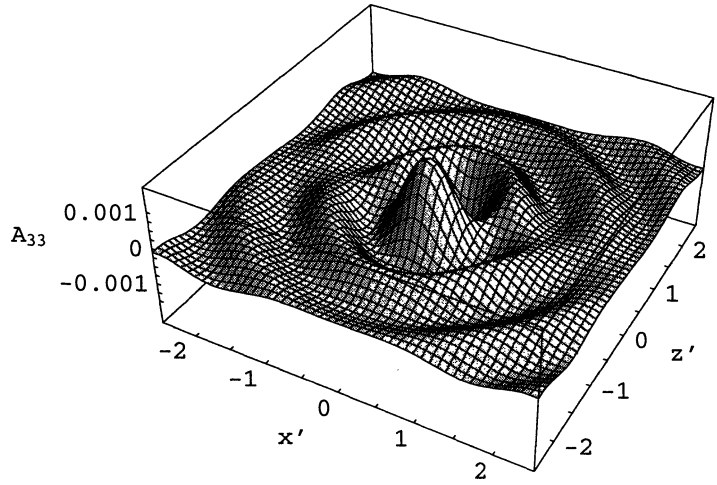

Figure 5. Component $A_{33} = (\epsilon^{-1})_{33} - 1/{n_0}^2$; the parameters are the same as those in Fig. 3.

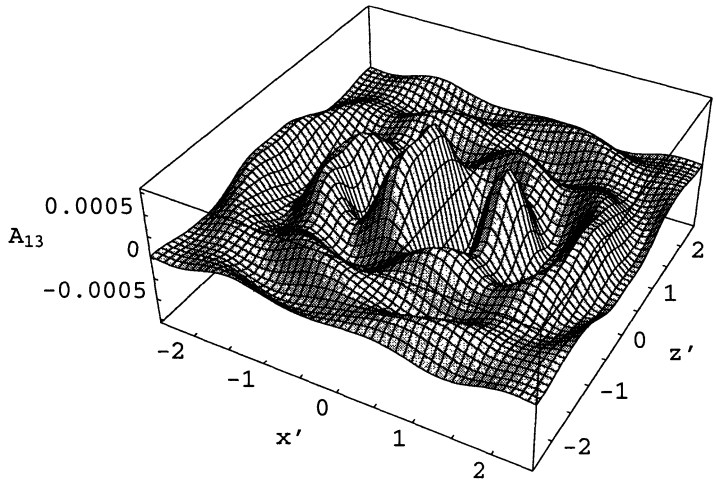

Figure 6. Component $A_{13} = A_{31} = (\epsilon^{-1})_{13}$; the parameters are the same as those in Fig. 3.

III. Non-vanishing components of the tensor $A = \epsilon^{-1} - 1/{n_0}^2$ induced by the u_A elastic storm

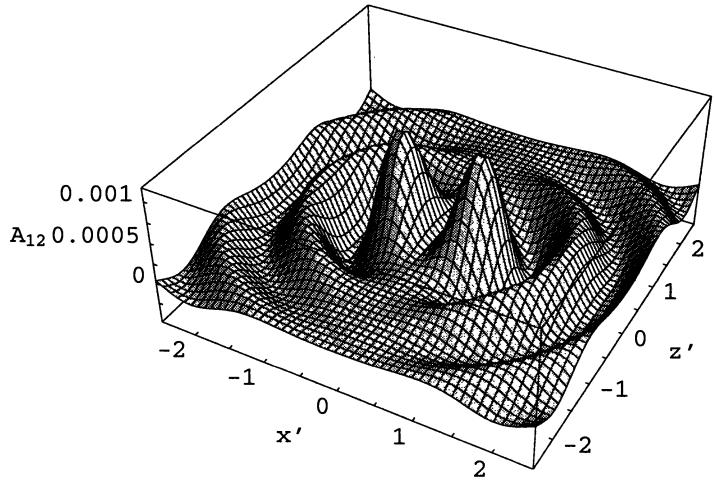

Figure 7. Component $A_{12} = A_{21} = (\epsilon^{-1})_{12}$; u_A storm defined by the spherical harmonics Y_0^0; $\theta_2 = \pi$; $\kappa_0 = 1$; $\nu = \nu_2/\sqrt{2}$; $N_Q = 0.5W$; $y' = 0$; $\omega t = \pi/2$.

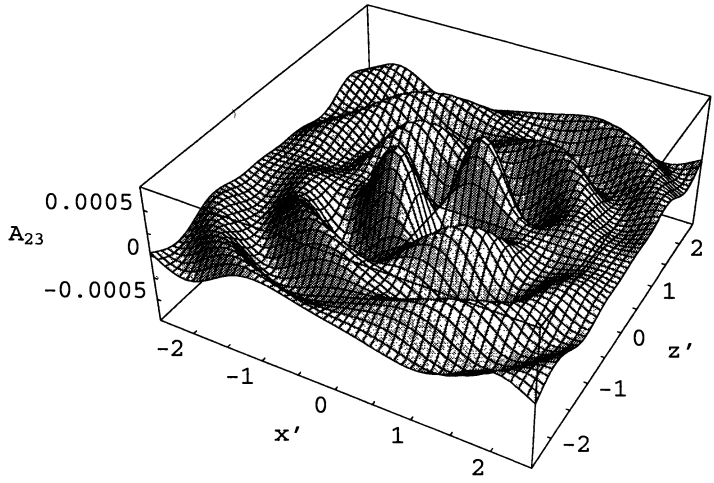

Figure 8. Component $A_{23} = A_{32} = (\epsilon^{-1})_{23}$; the parameters are the same as those in Fig. 7.

IV. Non-vanishing components of the tensor $A = \epsilon^{-1} - 1/{n_0}^2$ and refractive index variations in the central cross-section of the cubic grating composed of u_M elastic beams

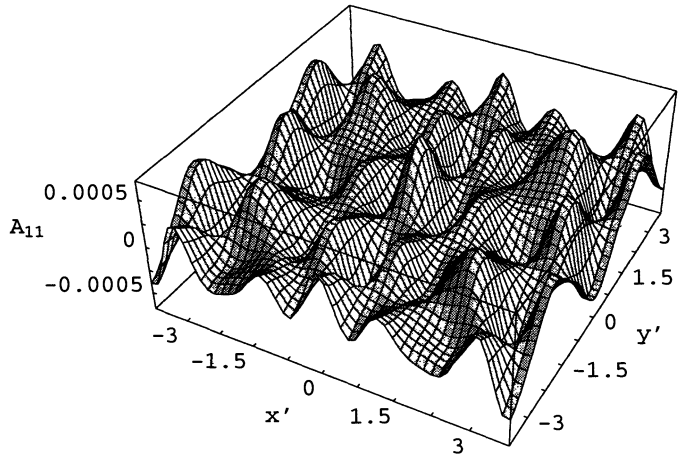

Figure 9. Component $A_{11} = (\epsilon^{-1})_{11} - 1/{n_0}^2$; Cubic grating composed of u_M elastic beams defined by the spherical harmonic Y_0^0; $\theta_2 = \pi$; $\kappa_0 = 0.5$; $\nu = \nu(\theta)$ (19 $N_Q = 0.5W$; $z' = 0$; $\omega t = \pi/2$; $M_1 = M_2 = M_3 = -7$; $N_1 = N_2 = N_3 = 7$; $\mathbf{a}_i = 2\lambda\epsilon$ $\omega\tau_i = \pi$; $i = 1, 2, 3$.

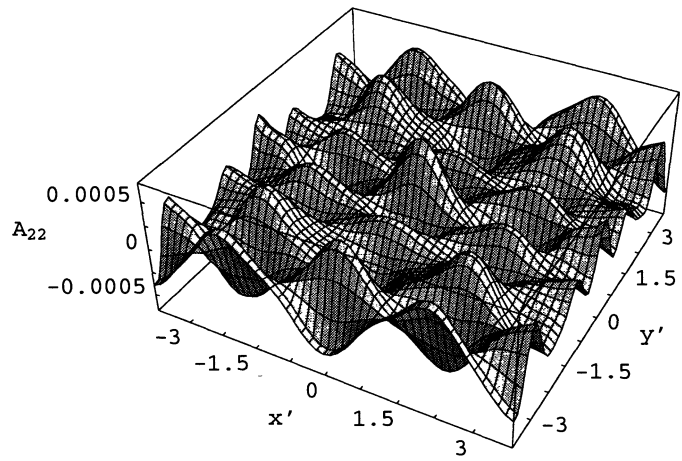

Figure 10. Component $A_{22} = (\epsilon^{-1})_{22} - 1/{n_0}^2$; the parameters are the same as those in Fig. 9.

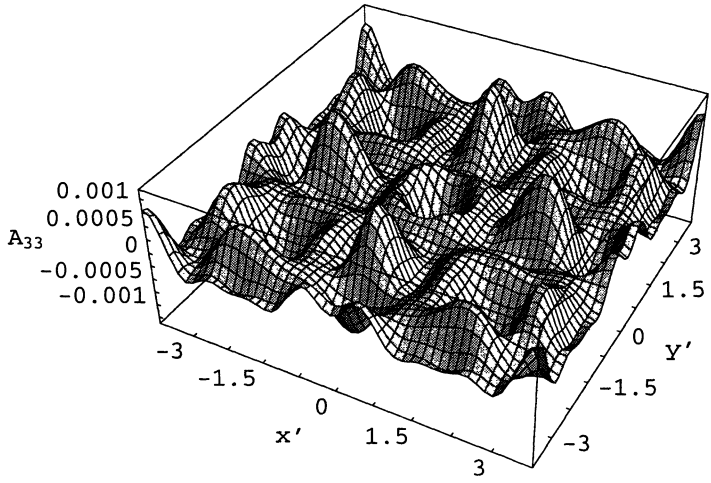

Figure 11. Component $A_{33} = (\epsilon^{-1})_{33} - 1/{n_0}^2$; the parameters are the same as those in Fig. 9.

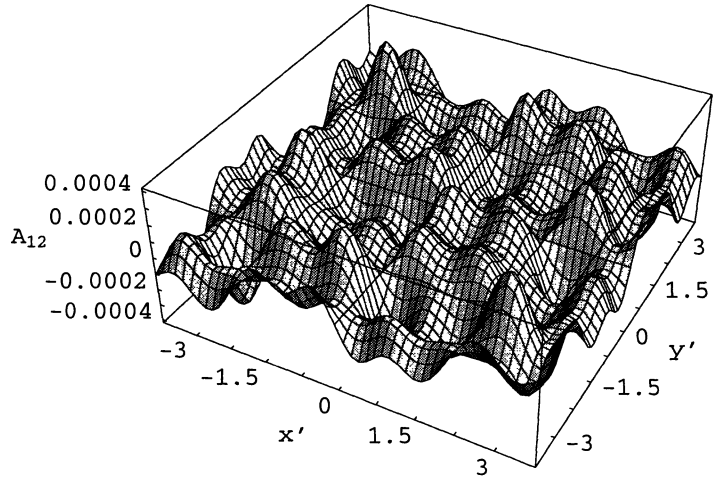

Figure 12. Component $A_{12} = A_{21} = (\epsilon^{-1})_{12}$; the parameters are the same as those in Fig. 9.

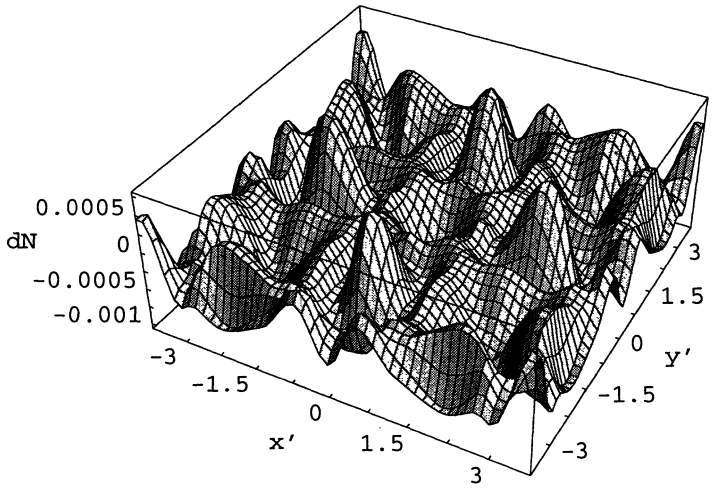

Figure 13. Refractive index variation $dN = n_- - n_0$; the parameters are the same as those in Fig. 9.

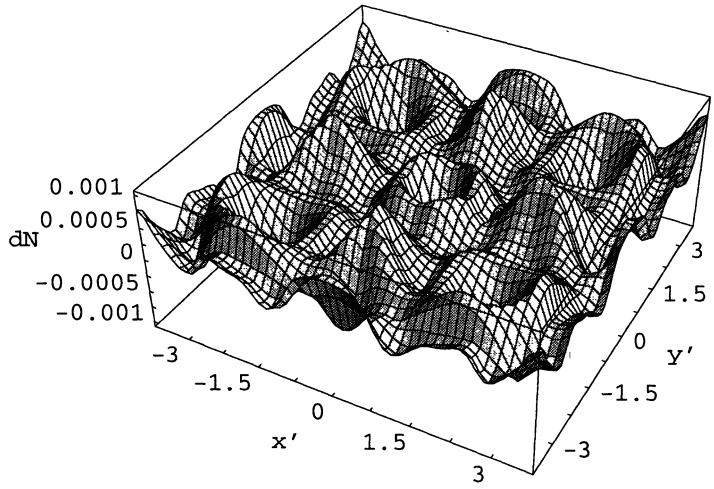

Figure 14. Refractive index variation $dN = n_+ - n_0$; the parameters are the same as those in Fig. 9.

V. Non-vanishing components of the tensor $A = \epsilon^{-1} - 1/{n_0}^2$ induced by the u_A orthonormal beam with $\kappa_0 = 0.15$

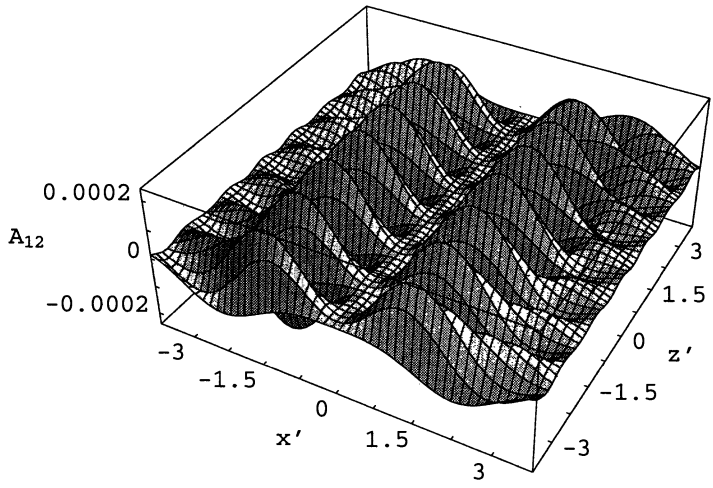

Figure 15. Component $A_{12} = A_{21} = (\epsilon^{-1})_{12}$; u_A orthonormal beam defined by the spherical harmonics Y_0^0; $\theta_2 = \pi$; $\kappa_0 = 0.15$; $\nu = \nu(\theta)$ (19); $N_Q = 5W$; $y' = 0$; $t = 0$.

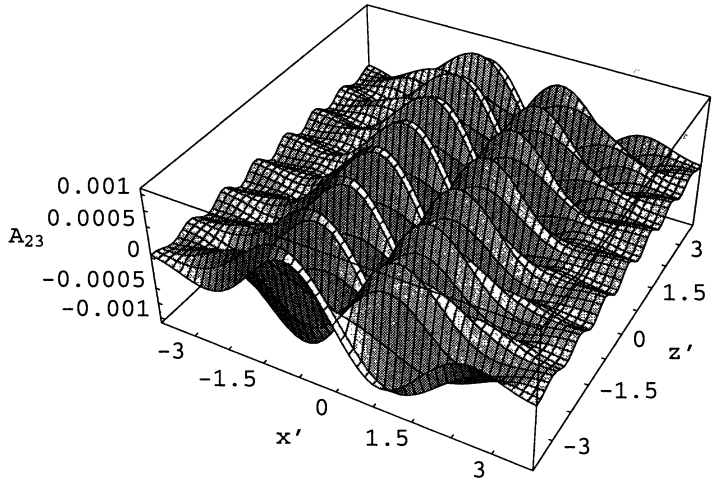

Figure 16. Component $A_{23} = A_{32} = (\epsilon^{-1})_{23}$; the parameters are the same as those in Fig. 15.

VI. Induced chiral structures

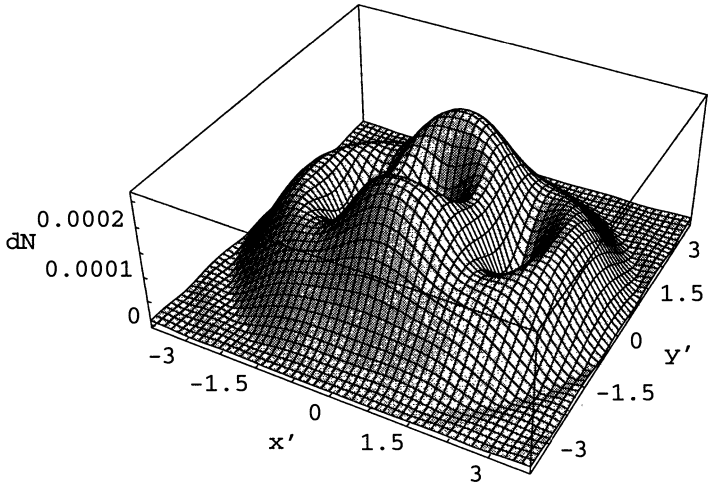

Figure 17. Refractive index variation $dN = n_+ - n_0$ in the plane $z' = 0$; u_A elastic beam defined by the spherical harmonics Y_1^1; $\theta_2 = \pi$; $\kappa_0 = 0.15$; $\nu = \nu(\theta)$ (19); $N_Q = 5W$; $\mathbf{n} = \mathbf{e}_3$; $t = 0$.

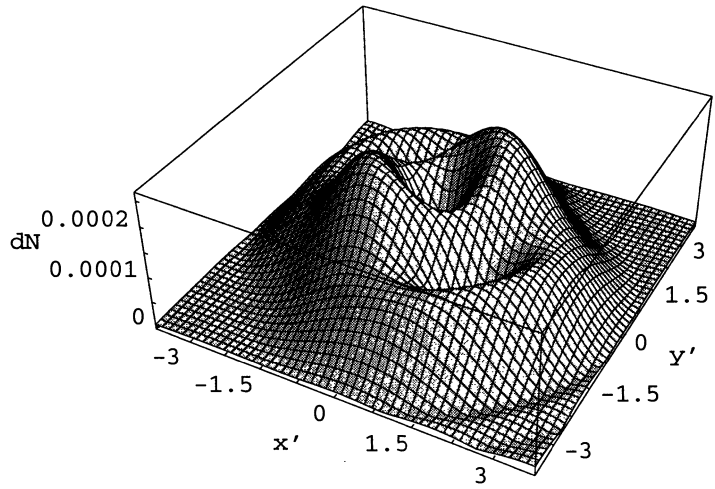

Figure 18. Refractive index variation $dN = n_+ - n_0$ in the plane $z' = 0.125$; the other parameters are the same as those in Fig. 17.

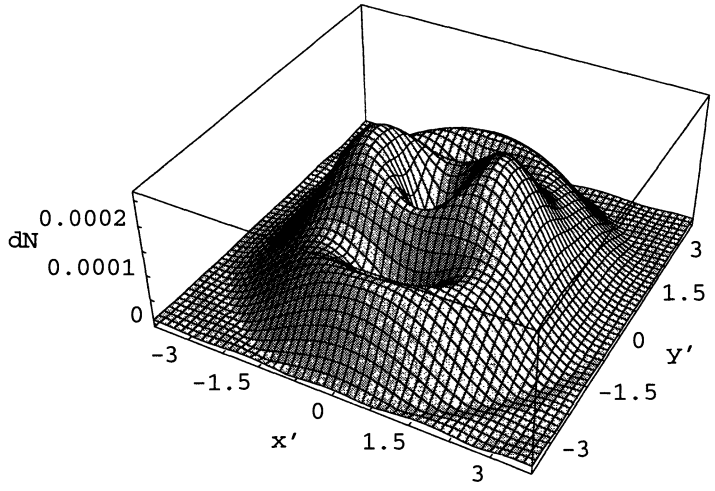

Figure 19. Refractive index variation $dN = n_+ - n_0$ in the plane $z' = 0.25$; the other parameters are the same as those in Fig. 17.

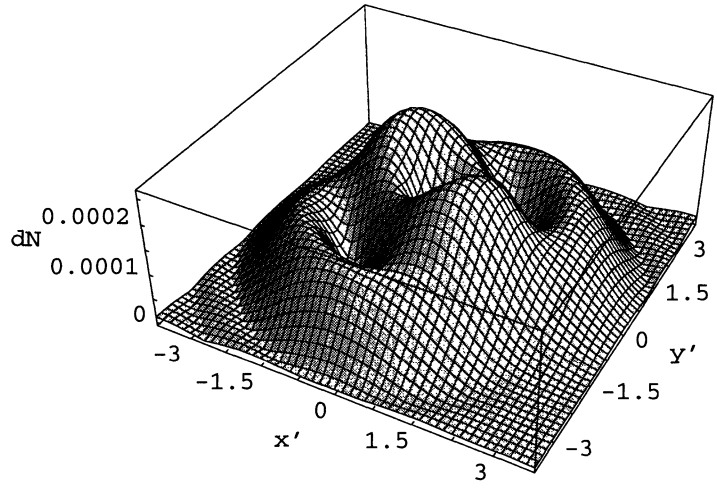

Figure 20. Refractive index variation $dN = n_+ - n_0$ in the plane $z' = 0.375$; the other parameters are the same as those in Fig. 17.

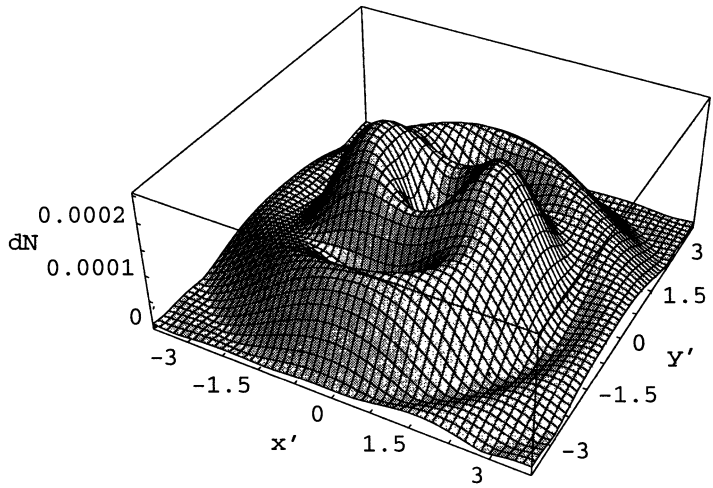

Figure 21. Refractive index variation $dN = n_+ - n_0$ in the plane $z' = 2.375$; the other parameters are the same as those in Fig. 17.

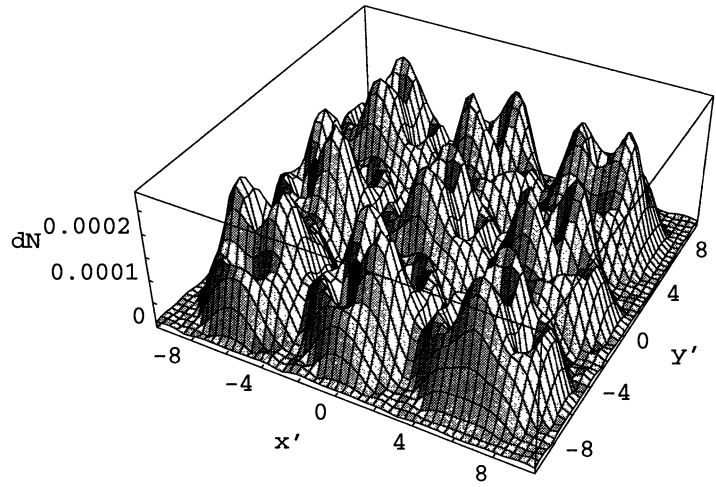

Figure 22. Refractive index variation $dN = n_+ - n_0$; two–dimensional grating composed of u_A elastic beams defined by the spherical harmonics Y_1^1; $\theta_2 = \pi$; $\kappa_0 = 0.15$; $\nu = \nu(\theta)$ (19); $N_Q = 5$ W; $z' = 0$; $t = 0$; $M_1 = M_2 = -1$; $N_1 = N_2 = 1$; $M_3 = N_3 = 0$; $\mathbf{a}_i = 6\lambda\mathbf{e}_i$; $\omega\tau_i = \pi/4$; $i = 1, 2$; $\mathbf{a}_2 = 0$; $\tau_3 = 0$.

EXCITONIC COMPOSITES

G. YA. SLEPYAN and S. A. MAKSIMENKO
Institute for Nuclear Problems, Belarus State University, Bobruiskaya 11, 220050 Minsk, Belarus, e-mail: maksim@inp.minsk.by

AND

A. HOFFMANN and D. BIMBERG
Institut für Festkörperphysik, Technische Universität Berlin, Hardenbergstr. 36, 10623 Berlin, Germany

Abstract. A new class of composite materials, excitonic composite, has been considered by the example of a collection of identical semiconductor quantum dots (QDs). The QD is modeled by a spatially confined exciton interacting with external electromagnetic field. A self-consistent microscopic local-field theory for an isolated arbitrary shaped QD has been developed. A Hamiltonian of the system has been formulated in terms of the acting field with a separate term responsible for the effect of depolarization. Relations between local and acting fields in QD have been derived in the dipole approximation for both strong and weak confinement regimes with the account for pronounced spatial nonlocality of the electromagnetic response in the latter regime. Homogenezation procedures have been carried out for both cases and expressions for the effective dielectric function have been derived. It has been shown that the nonlocality changes components of the polarizability tensor but does not change the general representation of the scattering operators as compared to the strong confinement regime.

1. Introduction

Fascinating electronic and optical properties of spatially confined nanostructures irreducible to properties of bulk media, and great potentiality of such structures in engineering applications have motivated permanent extension of their study. Among a variety of new results in this field, the recent progress in the synthesis of sheets of nano-scale 3D confined narrow-gap insertions in a host semiconductor, quantum dots (QDs), is of a special interest. Indeed, QD-based structures provide practical realization of the idea proposed by Dingle and Henry [1] to use structures with size quantization of charge carriers in one or more directions as active media of double heterostructure laser. Such a laser will show radically changed

S. Zouhdi et al. (eds.), Advances in Electromagnetics of Complex Media and Metamaterials, 385–402.

characteristics as compared to conventional quantum well (QW) lasers [2, 3]. Kirstaedter *et al.* [4] demonstrated very low threshold current density and its practically complete temperature insensitivity in InGaAs/GaAs QD laser up to 180 K. Ultrahigh material and differential gain, orders of magnitude exceeding those in QW lasers in a spectral range far beyond those available for conventional strained InGaAs-GaAs QWs, has been experimentally confirmed [5]. The large body of recent results on physical properties of QDs and their utilization for the QD laser design has been accumulated in Ref. [5]. Recently QDs have been proposed to serve as nodes of a quantum network that store and process quantum information being transmitted between nodes by entangled states of photons (see, e.g., [6] and references therein).

The key peculiarities of QD heterostructures are related to spatial confinement of the charge carrier motion and intrinsic spatial inhomogeneity. Since the inhomogeneity scale is much less than the optical wavelength, inclusions (QDs) can be treated as *electrically small* objects and electromagnetic response of such heterogeneous structures, *composites*, can be evaluated by means of effective medium theory [7]. Application of effective medium approach to 3D arrays of QDs has been presented in Refs. [8, 9, 10, 11]. In many cases, however, a planar array of QDs with intrinsic 2D periodicity of characteristic period much less than the optical wavelength, can be treated as more adequate and realistic model [5]; a general method for evaluation of electromagnetic response of planar arrays of QDs has been presented in Ref. [12]. This method, conventionally referred to as the effective boundary condition method, has been originally developed for microwaves and antenna theory (see, e.g., [13] and references therein), and has found a wide application in these fields.

Effective medium theory must be modified to include specific properties of excitons, coupled electron-hole states, which define the QD response (by this reason, further we speak about excitonic composites). First, the excitonic composite is constituted by resonant particles and, consequently, is characterized by a resonant response; moreover, inverse population is possible owing to the discrete energy spectrum of excitons. Thus, *excitonic composite is a resonant active system.* Another specific property of excitonic composites is appeared owing to the quantum nature of excitons: the exciton Bohr radius can either exceed the QD radius ($a_B \gg R_0$, strong confinement regtime) or be much less ($a_B \ll R_0$, weak confinement regime). In the later case, often realized in experiments, the QD electromagnetic response becomes *nonlocal*: constitutive relations for the polarization of the QD medium takes the form of integral operators. Peculiarities of the excitonic composite are in the focus of the presented paper. Constitutive relations for a QD accounting for the nonlocality have been derived in

Refs. [14, 15, 16]. In our paper we solve the Maxwell equations imposed to constitutive relations of such a type.

2. Excitonic composite in the strong confinement regime

2.1. LIGHT-MATTER INTERACTION HAMILTONIAN FOR A SINGLE QD

Let an isolated QD be exposed to classical electromagnetic field. Further such a QD is modeled as a strongly confined in space two-level quantum oscillator. Obviously, QD is essentially multilevel system. However, contribution of transitions lying far away from a given resonance can be approximated by a nonresonant dielectric function ε_h. We shell assume ε_h to be equal to the dielectric function of host semiconductor. Thus, in our model interaction of quantum oscillator with external electromagnetic field occurs inside a homogeneous boundless medium characterized by the dielectric function ε_h. For our consideration it is essential that ϵ_h can be assumed to be frequency independent and real-valued. This allows us to put $\varepsilon_h = 1$ without loss of generality. Substitutions in final expressions $c \to c/\sqrt{\varepsilon_h}$ and $\boldsymbol{\mu} \to \boldsymbol{\mu}/\sqrt{\varepsilon_h}$ for the speed of light and the oscillator dipole moment, respectively, will restore the case $\epsilon_h \neq 1$.

In the strong confinement regime the Coulomb interaction is assumed to be negligible, so that electrons and holes in QD are moved independently and spatial quantization is entailed by the interaction of the particles with the QD boundary. In this section we aim at the development of the Hamilton formalism, which would describe the system "QD + electromagnetic field" taking into account the role of QD boundaries. Apparently, the most sequential and rigorous approach to the problem is based on the concept of spatially varying interaction coefficient [17]. However, utilization of the approach for systems with the stepwise interaction coefficient meets the problem that the Hamilton equations are inapplicable at the discontinuity. The same problem exists in macroscopic electrodynamics of stratified media. By analogy, introducing a transient layer and reducing its thickness, one can obtain boundary conditions complimentary to the Hamilton equations. However, in practical use, the approach described turned out to be too complicated and was realized for the only simplest case: interaction of a material layer with normally incident light [17]. Note that even in this simplest case the local field effects are left beyond the consideration.

As applied to QDs, in our paper we develop a more constructive approach which utilizes the property of QDs to be electrically small. This property allows us to assume local and acting fields to be homogeneous inside the QD. In fact, this implies that we introduce a spatial averaging of the electric field over the QD volume. The approach enables us to solve the problem considering fields only inside the QD. Moreover, it proves to

be possible to examine separately, to a certain extent, the electromagnetic field and the particles. On the other hand, the simplification restricts the analysis to the strong confinement regime; the theory should be drastically modified to include inhomogeneity and nonlocality into consideration.

In the framework of the above stated approximation, the system "QD + electromagnetic field" is described by the Hamiltonian $H = H_0 + H_{IL}$, where $H_0 = \epsilon_e a_e^\dagger a_e + \epsilon_g a_g^\dagger a_g$ is the Hamiltonian of the carriers motion, $\epsilon_{g,e}$ are the energy eigenvalues, $a_{g,e}^\dagger$ and $a_{g,e}$ stand for the creation and annihilation operators (here and below indices e and g correspond to the excited and ground states of electron, respectively). These operators satisfy the anticommutative relations usual for fermions. The term H_{IL} describes interaction with the electromagnetic field. In this paper we use a 3D Cartesian coordinate system $\mathbf{u}_i$ $(i = x, y, z)$ with the unit vector $\mathbf{u}_x$ parallel to the electron-hole pair dipole moment: $\boldsymbol{\mu} = \mu \mathbf{u}_x$. In the chosen coordinates the term H_{IL} takes the form as follows:

$$H_{IL} = -V \widehat{P}_x E_{Lx}\,, \tag{1}$$

where $\widehat{P}_x = V^{-1}(-\mu b^\dagger + \mu^* b)$ is the polarization operator, the operators $b^\dagger = a_g a_e^\dagger$ and $b = a_g^\dagger a_e$ are the creation and annihilation operators for electron-hole pairs, V is the QD volume. Thus, we define the light-matter interaction Hamiltonian in the dipole approximation [18], i.e., we reject a negligibly small term proportional to $\mathbf{A}^2$. Such an approximation is valid, at least, in the vicinity of the exciton resonance [19]). Here and below we mark operators by the label "$\widehat{\ }$" if it is necessary to distinguish them from their macroscopically averaged values denoted by the same letters. We use underlined letters to mark tensors. Note that our model also describes higher excitonic modes; in that case operators $b^\dagger$ and b move up the exciton into the next energy level and return it back.

The field inside QD, $\mathbf{E}_L$, involved in Eq. (1), is different from the external acting field $\mathbf{E}_0$(see Fig. 1). Since we postulate the QD to be electrically small, and, as consequence, the field inside QD to be homogeneous, this difference is determined by the depolarization field [20]. To evaluate the depolarization field, we start with the frequency–domain integral relation defined inside the QD [21],

$$\mathbf{E}_L(\mathbf{r}) = \mathbf{E}_0(\mathbf{r}) + (\nabla\nabla\cdot + k^2) \int\limits_V \mathbf{P}(\mathbf{r}') G(\mathbf{r} - \mathbf{r}')\, d^3\mathbf{r}' \tag{2}$$

which follows from the Maxwell equations. Here $G(\mathbf{r}) = \exp(ik|\mathbf{r}|)/4\pi|\mathbf{r}|$ is the vacuum Green function, $\mathbf{P} = \langle \widehat{\mathbf{P}} \rangle$ is the macroscopic polarization. This relation couples the local $\mathbf{E}_L(\mathbf{r})$ and the acting $\mathbf{E}_0(\mathbf{r})$ fields inside the QD. Letting the QD to be electrically small, we can neglect retardation in this

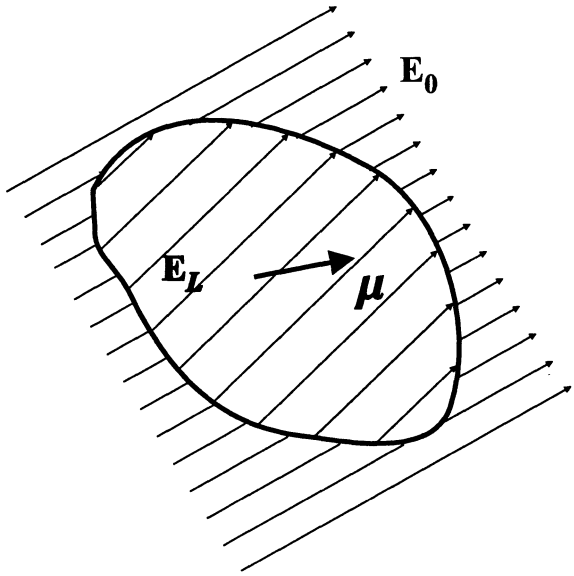

Figure 1. Correlation between acting and local fields in electrically small scatterer. Local field is assumed to be homogeneous.

equation and reduce it to

$$\mathbf{E}_L(\mathbf{r}) = \mathbf{E}_0(\mathbf{r}) + \nabla\nabla \cdot \int_V \mathbf{P}(\mathbf{r}') \frac{d^3\mathbf{r}'}{|\mathbf{r} - \mathbf{r}'|} . \tag{3}$$

Also, the above made approximation allows us to suppose the acting field and, consequently, the polarization $\mathbf{P}$ to be constant over the QD volume. As a result, Eq. (3) is transformed to

$$\mathbf{E}_L = \mathbf{E}_0 - 4\pi \underline{\mathbf{N}} \mathbf{P} . \tag{4}$$

Here $\underline{\mathbf{N}}$ is the depolarization tensor with its components defined by

$$N_{\alpha\beta} = -\frac{1}{4\pi} \frac{\partial^2}{\partial r_\alpha \partial r_\beta} \int_V \frac{d^3\mathbf{r}'}{|\mathbf{r} - \mathbf{r}'|} , \tag{5}$$

where $r_\alpha = x, y, z$. This tensor is symmetrical [21] and depends only on the shape of the scattering object, i.e., QD. For instance, for a sphere $\underline{\mathbf{N}} = \underline{\mathbf{I}}/3$. For an spheroid the tensor $\underline{\mathbf{N}}$ is diagonal in a basis related to the spheroid's axes [20]:

$$N_{ZZ} = \frac{e^2 + 1}{e^3} (e - \arctan e) , \quad N_{XX} = N_{YY} = \frac{1}{2} (1 - N_{ZZ}) , \tag{6}$$

where $e = \sqrt{a_{el}^2/b_{el}^2 - 1}$ is the spheroid eccentricity, a_{el} and b_{el} are the spheroid semiaxes in the $X0Y$ plane and the Z-direction, respectively. These formulae hold true for both disklike ($a_{el} > b_{el}$) and cigarlike spheroids ($a_{el} < b_{el}$). Infinite stretching of the spheroid ($a_{el}/b_{el} \to 0$) results in $N_{ZZ} \to 0$, $N_{XX} \to 1/2$ and Eq. (6) reproduce the polarizabilities of the cylinders (see, e.g., [8]). It should be noted that for an arbitrary three-axis ellipsoid, the tensor $\underline{\mathbf{N}}$ does not depend on the coordinates. Consequently, the local field $\mathbf{E}_L(\mathbf{r})$ is also constant over the QD volume. For non-ellipsoidal QDs, the tensor $\underline{\mathbf{N}}$ and, thus, the local field become spatially inhomogeneous what contradicts to the basic assumption used under formulation of the Hamiltonian. To eliminate the contradiction, we should average relation (4) over the QD volume. This leads us again to Eq. (4) with $\mathbf{E}_L$, $\mathbf{E}_0$, $\mathbf{P}$ = const and

$$N_{\alpha\beta} = -\frac{1}{4\pi V} \iint\limits_{V\,V} \frac{\partial^2}{\partial r_\alpha \partial r_\beta} \frac{d^3\mathbf{r} d^3\mathbf{r}'}{|\mathbf{r} - \mathbf{r}'|} \,. \tag{7}$$

Returning to the co-ordinate system related to the QD dipole momentum, Eq. (4) can be rewritten by

$$E_{Lx} = E_{0x} - 4\pi N_x P_x \,, \tag{8}$$

where the depolarization coefficient N_x is as follows: $N_x = (\boldsymbol{\mu} \cdot \underline{\mathbf{N}}\boldsymbol{\mu})/|\mu|^2 \equiv (\mathbf{u}_x \cdot \underline{\mathbf{N}}\mathbf{u}_x)$. In view of the above consideration, the total Hamiltonian is represented by

$$H = H_0 + H_{I0} + \Delta H \,, \tag{9}$$

where

$$H_{I0} = -V\widehat{P}_x E_{0x} \tag{10}$$

and

$$\begin{aligned} \Delta H &= 4\pi N_x P_x(-\mu b^\dagger + \mu^* b) \\ &= \frac{4\pi}{V} N_x(\mu^* b - \mu b^\dagger)(\mu^* \langle b\rangle - \mu\langle b^\dagger\rangle) \,. \end{aligned} \tag{11}$$

Thus, in the total Hamiltonian we have separated contribution of the interaction of electron-hole pairs with acting field, H_{I0}, from contribution of depolarization, ΔH. Such a separation allows us to include the local field effects into consideration without explicit solution of the electrodynamical boundary-value problem. This is of special importance when we come to the quantization of the electromagnetic field. Note that the quantity ΔH is expressed in terms of dynamic variables of the particle motion. Thus, coefficient N_x contains complete information about electromagnetic interaction.

2.2. EQUATIONS OF MOTION

Let $|\tilde{\psi}(t)\rangle$ be the wavefunction of the system "QD + electromagnetic field". In the interaction representation this system is described by the Schrödinger equation

$$i\hbar\frac{\partial|\psi\rangle}{\partial t} = H_{int}|\psi\rangle \tag{12}$$

with $H_{int} = \exp(iH_0t/\hbar)(H_{I0} + \Delta H)\exp(-iH_0t/\hbar)$ and $|\psi(t)\rangle = \exp(iH_0t/\hbar)|\tilde{\psi}(t)\rangle$. We represent then $|\psi(t)\rangle$ by the sum as follows

$$|\psi(t)\rangle = A(t)|e\rangle + B(t)|g\rangle\,,$$

where $A(t)$ and $B(t)$ are coefficients to be found, $|g\rangle$ and $|e\rangle$ are the wavefunctions of QD in ground and excited states, respectively. Taking into account the well-known identities $b^\dagger|e\rangle = b|g\rangle = 0$ and $b|e\rangle = |g\rangle$, $b^\dagger|g\rangle = -|e\rangle$, from Eq. (12) we obtain the set of equations of motion

$$\begin{aligned} i\hbar\frac{\partial A}{\partial t} &= (4\pi N_x P_x - E_{0x})\mu B e^{i\omega_0 t}\,,\\ i\hbar\frac{\partial B}{\partial t} &= (4\pi N_x P_x - E_{0x})\mu^* A e^{-i\omega_0 t}\,, \end{aligned} \tag{13}$$

with macroscopic polarization determined by

$$P_x = \langle\tilde{\psi}|\hat{P}_x|\tilde{\psi}\rangle = \frac{1}{V}\mu^* A(t)B^*(t)e^{-i\omega_0 t} + \text{c.c.}\,. \tag{14}$$

Further we restrict ourselves to the slow-varying amplitude approximation. For that aim, we present the acting field by $E_{0x} = \mathrm{Re}[\mathcal{E}(t)\exp(-i\omega t)]$ with $\mathcal{E}(t)$ as a slow-varying amplitude. Then, taking relation (14) into account and neglecting the fast-oscillating terms in Eq. (13), we derive final expressions for equations of motion:

$$\begin{aligned} i\hbar\frac{\partial A}{\partial t} &= \hbar\Delta\omega A|B|^2 - \frac{1}{2}\mathcal{E}(t)\mu B e^{i(\omega_0-\omega)t}\,,\\ i\hbar\frac{\partial B}{\partial t} &= \hbar\Delta\omega B|A|^2 - \frac{1}{2}\mathcal{E}^*(t)\mu^* A e^{-i(\omega_0-\omega)t}\,, \end{aligned} \tag{15}$$

where

$$\Delta\omega = \frac{4\pi}{\hbar V}N_x|\mu|^2\,. \tag{16}$$

These equations constitute a basic self-consistent system describing the interaction of QD with electromagnetic field. The consistency is provided by the depolarization-induced first terms in the right-hand parts of the equations. Physically, system (15) is analogous to the Bloch equations

for optically dense media derived in Ref. [22]. The relaxation can easily be included into Eqs. (15) either by introduction of the phenomenological transverse and longitudinal relaxation times [22] or by corresponding modification of initial Hamiltonian (9).

2.3. POLARIZABILITY OF A SINGLE QD IN THE STRONG CONFINEMENT REGIME

The case of excited QD can be analyzed using equations (15) with the initial conditions $A(0) = 1$ and $B(0) = 0$ imposed. In linear approximation with respect to electromagnetic field we can put $A(t) \approx 1$. Physically, this means that we restrict the analysis to temporal intervals essentially less than the relaxation time of the given resonant state. In such a situation, Eqs. (15) are simplified and reduced to

$$i\hbar\frac{\partial B}{\partial t} = \hbar\Delta\omega B - \frac{1}{2}\mathcal{E}^*(t)\mu^* e^{i(\omega_0-\omega)t}\,. \tag{17}$$

For time-harmonic excitation, i.e., for $\mathcal{E}(t) = \mathcal{E}$ =const, this equation is exactly integrable:

$$B(t) \approx -\frac{\mathcal{E}^*\mu^*}{2\hbar(\omega_0 - \Delta\omega - \omega)}\left[e^{-i(\omega_0-\omega)t} - e^{-i\Delta\omega t}\right] \tag{18}$$

with $\Delta\omega$ determined by Eq. (16). Thus, one can see that the local fields (depolarization) leads to the shift $\Delta\omega$ of the resonant frequency. This shift was predicted in a number of papers [23, 24, 10] on the basis of different phenomenological models. In Refs. [8, 9] it has been predicted and experimentally verified that this shift in anisotropically shaped QDs provides polarization splitting of the gain band. Note also that the depolarization effect has been proposed by Gammon *et al.* [25] as a hypothesis explaining the experimentally observed polarization-dependent splitting of the PL spectrum of single anisotropically shaped QD.

Eq. (16) is identical to that obtained in Refs. [8, 9]. In order to demonstrate it we should make a substitution $|\mu|^2 \to |\mu_0|^2/3$ where μ_0 is the matrix element of the dipole moment of a corresponding bulk sample (coefficient $1/3$ is appeared as a result of orientational averaging in bulk samples). We should also take into account the spin degeneracy of electron-hole pairs which results in duplication of $\Delta\omega$. This is because the total polarization of the system is provided by superposition of two partial polarizations corresponding to two spin components. Then, expressing macroscopic polarization in terms of $B(t)$, we find

$$P_x = \frac{1}{8\pi}\alpha_{xx}(\omega)\mathcal{E}\left[e^{-i\omega t} - e^{-i(-\Delta\omega+\omega_0)t}\right] + \text{c.c.}\,, \tag{19}$$

where

$$\alpha_{xx}(\omega) = \frac{4\pi|\mu|^2}{\hbar V(\omega + \Delta\omega - \omega_0)} \tag{20}$$

is the component of the QD polarizability tensor. Phenomenological consideration for QD modeled as single-resonance medium with the Lorentz dispersion $\varepsilon(\omega) = \varepsilon_h + g_0/(\omega - \omega_0)$ [8, 9] gives the same result if we put $g_0 = 4\pi|\mu|^2/\hbar V$. This means that the Hamiltonian defined by Eqs. (9)–(11) comprises that phenomenological model as a particular case.

For a ground-state QD, the initial conditions has the form as follows: $A(0) = 0$, $B(0) = 1$. Applying to this case the above presented procedure, we obtain

$$A(t) \approx \frac{\mathcal{E}\mu}{2\hbar(\omega_0 + \Delta\omega - \omega)} \left[e^{i(\omega_0 - \omega)t} - e^{-i\Delta\omega t}\right]. \tag{21}$$

Thus, for the ground state the local field effects manifest themselves in the same shift $\Delta\omega$ of the resonance but with the opposite sign. If we introduce now into consideration a finite radiation linewidth, interaction of a ground-state QD with the electromagnetic field corresponds to the absorption, while interaction with an excited QD corresponds to the case of stimulated emission. In other words, the optical absorption and gain of an isolated QD could be distinguished owing to the depolarization shift, blue in the former case and red in the latter one.

2.4. HOMOGENIZATION PROCEDURE

In the strong confinement regime the homogenization procedure for excitonic composites is carried out in ordinary way with the account for the depolarization. Electromagnetic properties of composites are usually modeled in the framework of the effective-medium approach, which implies electromagnetic field averaging over material inhomogeneities. Thus, a homogeneous medium with effective constitutive parameters, such as conductivity, susceptibility, permittivity, instead a composite is being considered. The effective parameters are expressed in terms of the generic and the geometrical parameters of the inclusions and the host medium. The general approach for estimating the effective constitutive parameters of a composite material is as follows: First, the field scattered by a single inclusion in the host medium is found; then, the scattering contributions from all inclusions are summed and averaged over a vanishingly small region. For this approach to hold, all inclusions must be electrically small, i.e., their linear size must be small comparing with the wavelength. Having linear extension of the spatial inhomogeneity of the order of several nanometers, QD–based structures completely satisfy the above condition in the visible

range. This justifies applicability of the effective medium approach to the description of the electromagnetic response properties of QD arrays.

There is a large number of different modifications of the effective medium theory [7]. Among them, we choose the Maxwell Garnett approach as it is based on rigorous solution of the integral equations of macroscopic electrodynamics for composites with small volume fraction of inclusions ($f_V < 0.4-0.5$, [7]); i.e., a weak modification of the electronic spectrum and the gain of QD ensemble is assumed as compared to that of individual QD. In the framework of the Maxwell Garnett approach a composite medium comprising a regular ensemble of uniform in size, electrically small dielectric inclusions dispersed in a host dielectric material is characterized by the effective permittivity tensor as follows [26]:

$$\underline{\varepsilon}_{eff}(\omega) = \underline{\mathbf{I}} + f_V \underline{\boldsymbol{\alpha}}(\omega) \left[\underline{\mathbf{I}} - f_V \underline{\boldsymbol{\delta}}\underline{\boldsymbol{\alpha}}(\omega)\right]^{-1} , \tag{22}$$

where $\underline{\mathbf{I}}$ is the unit tensor, $\underline{\boldsymbol{\alpha}}(\omega)$ is the polarizability tensor of single QD with components defined by Eq. (20), and $\underline{\boldsymbol{\delta}}$ is the lattice tensor completely determined by geometry of the array. The notation $\underline{\boldsymbol{\delta}}\,\underline{\boldsymbol{\alpha}}$ stands for the inner tensor product, $(\underline{\boldsymbol{\delta}}\,\underline{\boldsymbol{\alpha}})^j_k = \delta^j_l \alpha^l_k$.

Eq. (22) states that the QD ensemble comprises an optically anisotropic medium even if both QD and host materials are isotropic. Thus, we predict *electromagnetic* anisotropy of the electromagnetic response in QD arrays due to diffraction of the electromagnetic field by inclusions. In Ref. [26] it has been shown that, assuming linear size of the lattice elementary cell to be much less than the wavelength, components of the lattice tensor are given by the integrals over the elementary cell volume Ω as follows:

$$\delta_{ij} = -\frac{3}{4\pi}\int\limits_{\Omega} \frac{r_i r_j}{r^5} d^3\mathbf{r} \quad \text{if} \quad i \neq j\,, \quad \text{and} \quad \delta_{ii} = -\frac{1}{4\pi}\int\limits_{\Omega} \frac{3r_i^2 - r^2}{r^5} d^3\mathbf{r}\,. \tag{23}$$

Here $\mathbf{r}$ is the radius vector of a point inside the elementary cell and $r = |\mathbf{r}|$; indices i and j stand for the Cartesian components x, y, z. Note that the lattice tensor (23) is found without any reference to specific properties of QDs as quantum-mechanical objects.

3. Excitonic composite in the weak confinement regime

3.1. POLARIZABILITY OF A SINGLE QD

Let us now study the role of nonlocality in electromagnetic response of an isolated QD. Again, we decompose the total Hamiltonian of the system "QD+electromagnetic field" into two parts, $H = H_0 + H_{IL}$, with H_{IL} responsible for the light-matter interaction. As different from the previous

case, in the weak confinement regime Coloumb interaction contributes to the Hamiltonian H_0. The Hamiltonian H_{IL} contains an external field averaged over the crystalline lattice of the QD material. Here we apply the Coloumb calibration for the the vector potential $\nabla \cdot \mathbf{A} = 0$ which implies electromagnetic field to be transverse. In that case, $H_{IL} = -i\mathbf{A}\mathbf{p}/mc$, where e, m are the electron charge and mass, respectively, $\mathbf{p} = -i\hbar\nabla$ is the momentum operator. The charge carrier motion in QD is described by the Liuwille equation $i\hbar\partial\rho/\partial t = [H, \rho]$ for the density matrix ρ, which we will solve to the linear approximation with respect to electromagnetic field. For complex–valued amplitudes one finds:

$$P_\alpha(\mathbf{r}) = \int\limits_V \chi_{\alpha\beta}(\mathbf{r}, \mathbf{r}', \omega) E_\beta(\mathbf{r}') d^3\mathbf{r}', \tag{24}$$

where

$$\chi_{\alpha\beta}(\mathbf{r}, \mathbf{r}', \omega) = \left(\frac{e\hbar}{m\omega}\right)^2 \sum_{p,n} (\rho_{0n} - \rho_{0p}) \left[\frac{1}{\hbar\omega + \epsilon_n - \epsilon_p} - \frac{1}{\hbar\omega - \epsilon_n + \epsilon_p}\right]$$
$$\times \Psi_p^*(\mathbf{r}) \nabla_\alpha \Psi_n(\mathbf{r}) \Psi_n^*(\mathbf{r}') \nabla'_\beta \Psi_p(\mathbf{r}'), \tag{25}$$

$\epsilon_{n,p}$ and $\Psi_{n,p}(\mathbf{r})$ stand for the eigenvalues and eigenfunctions of the Hamiltonian H_0, respectively, while quantities $\rho_{0n,p}(\mathbf{r})$ are the eigenvalues of the unperturbed density matrix.

Let us estimate contribution of excitons to the QD polarizability. For that aim, we put $\rho_{0n} = 0$ and $\rho_{0p} = 1$ into Eq. (25) assuming thus that n–th state is an exciton while p–th one is the ground state. Exciton and ground–state wavefunctions are as follows [27]

$$\Psi_n = \sum_{j',j} F_j(\bar{\mathbf{j}}) \Phi(\mathbf{j}_r) W_j^c(\mathbf{r}_j) \prod_{i \neq j} W_i^v(\mathbf{r}_i), \qquad \Psi_p = \Psi_g = \prod_i W_i^v(\mathbf{r}_i), \tag{26}$$

with $W_j^{c,v}(\mathbf{r}_j)$ as the Wannier functions of the conduction and valence bands, respectively. The function $\Phi(\mathbf{j}_r)$ describes the electron–hole relative motion with $\mathbf{j}_r \equiv j - j'$ while $F_j(\bar{\mathbf{j}})$ characterizes the center–of–mass motion of the exciton with $\bar{\mathbf{j}} \equiv (m_e j + m_h j')/(m_e + m_h)$; $m_{e,h}$ are the electron and hole effective masses, respectively.

Carrying out averaging over the infinitesimal volume in the atomic scale, from Eq. (24) one can obtain

$$\langle \mathbf{P}^{ex}(\mathbf{r}) \rangle = \sum_n (\boldsymbol{\mu} \otimes \boldsymbol{\mu}) \Phi^2(0) \left[\frac{1}{\hbar\omega + \epsilon_n - \epsilon_g} - \frac{1}{\hbar\omega - \epsilon_n + \epsilon_g}\right]$$
$$\times F_n(\mathbf{r}) \int\limits_V F_n(\mathbf{r}') \mathbf{E}(\mathbf{r}') d^3\mathbf{r}', \tag{27}$$

where the symbol $\otimes$ marks a diadic product of vectors. If QD comprises an isotropic material, orientational averaging in it leads to the change $(\boldsymbol{\mu} \otimes \boldsymbol{\mu}) \rightarrow |\boldsymbol{\mu}_0|^2 \delta_{ij}/3$, where δ_{ij} is the Kronecker symbol. In that case, anisotropy of the QD electromagnetic response arises as a result of anisotropy of the QD shape (or, in composites, as result of anisotropy of array).

Consider scattering of an initial electromagnetic field $\mathbf{E}_0(\mathbf{r})$ by an isolated QD assuming the background permittivity of the QD to be equal to the permittivity of the host medium ε_h. Thus, we neglect the image-potential effects. For the analysis we make use again Eqs. (2)–(3) with the substitution $k \rightarrow k_1 = k\sqrt{\varepsilon_h}$. However, unlike the strong confinement regime, now polarization of QD is related to the local electric field $\mathbf{E}_L(\mathbf{r})$ by means of a linear integral operator. Restricting ourselves to the exciton component of polarization, one come to the following relation [16]

$$\mathbf{P}(\mathbf{r}) \approx DF(\mathbf{r})\boldsymbol{\Lambda}\,, \tag{28}$$

where

$$D \approx \frac{2}{3}|\boldsymbol{\mu}|^2 \frac{\Phi^2(0)}{\hbar\omega + \epsilon - \epsilon_g}\,, \qquad \boldsymbol{\Lambda} = \int_V F(\mathbf{r})\mathbf{E}_L(\mathbf{r})d^3\mathbf{r}\,. \tag{29}$$

Index n of the excitonic mode in the coefficient D is omitted for simplicity. Multiplier 2 in the expression for D takes into account spin degenerating of excitonic modes. Note that Eq. (28) defines very special type of nonlocality: the integral operator in it has degenerated kernel with degeneration order equal to unit. In view of that, integral differential equations (2) and (3) turn out to be equivalent to the integral Fredholm equations with degenerated kernels. For arbitrary degenerating order, such equations are reduced to systems of algebraic equations [28]; in our case, presence of a degenerated kernel makes possible analytical consideration of the nonlocality problem. First, Eq. (3) allows us to find vector $\boldsymbol{\Lambda}$ omitting the procedure of evaluation of the local electromagnetic field $\mathbf{E}_L(\mathbf{r})$ inside QD; to do this, let us multiply Eq. (3) by the function $F(\mathbf{r})$ and integrate it over the QD volume. Then, solving Eq. (2) by the method presented in Ref. [12], we derive the expression for the Hertz potential in the far zone:

$$\boldsymbol{\Pi}^e = \frac{V}{4\pi r} e^{ik_1 r} \underline{\boldsymbol{\alpha}} \mathbf{E}_0\,, \tag{30}$$

where polarizability tensor of an isolated QD $\underline{\boldsymbol{\alpha}}$ is expressed by

$$\underline{\boldsymbol{\alpha}} = \frac{4\pi}{V} DM^2 \left(\underline{\mathbf{I}} - D\underline{\mathfrak{F}}\right)^{-1}\,, \tag{31}$$

with $M = \int_V F(\mathbf{r})d^3\mathbf{r}$. The tensor $\underline{\mathfrak{F}}$, which describes the role of the QD depolarization, is given by its components as

$$\mathfrak{F}_{\alpha\beta} = 4\pi \int_V \int_V F(\mathbf{r}')F(\mathbf{r})\frac{\partial^2}{\partial r_\alpha \partial r_\beta} G(\mathbf{r}-\mathbf{r}')d^3\mathbf{r}'d^3\mathbf{r}\,. \tag{32}$$

Using the Puasson equation for the Green function $G(\mathbf{r})$, we obtain the important normalization condition

$$\mathfrak{F}_{xx} + \mathfrak{F}_{yy} + \mathfrak{F}_{zz} = 4\pi \int_V F^2(\mathbf{r})d^3\mathbf{r}\,. \tag{33}$$

This equality can be used to control the accuracy of numerical integration of complicated expressions (32).

Thus, we have shown that the special law of the nonlocality (28) inherent to an isolated QD admits description of the electromagnetic field scattering by the QD using the polarizability tensor independent on the incident field structure. In other words, the nonlocality changes values of the polarizability tensor components but does not change the general representation of the scattering operators as compared to the strong confinement regime.This result allows extension of the Maxwell Garnett approach to 3D composites constituted by QDs in the weak confinement regime.

3.2. EFFECTIVE CONSTITUTIVE RELATIONS FOR EXCITONIC COMPOSITES

Let the composite comprises a regular 3D lattice of identical QDs with $\mathbf{h}_\tau$ as the lattice vector. As before, the starting point of the analysis is the integral equations for the electric field inside the QD:

$$\mathbf{E}_L(\mathbf{r}+\mathbf{h}_\tau) = \mathbf{E}_0^{(\tau)}(\mathbf{r}+\mathbf{h}_\tau) + (\nabla\nabla\cdot + k_1^2)\mathbf{\Pi}_\tau^e(\mathbf{r})\,, \tag{34}$$

where

$$\mathbf{\Pi}_\tau^e(\mathbf{r}) = D\mathbf{\Lambda}_\tau \int_V \frac{e^{ik_1|\mathbf{r}-\mathbf{h}_\tau-\mathbf{r}'|}}{|\mathbf{r}-\mathbf{h}_\tau-\mathbf{r}'|} F(\mathbf{r}')d^3\mathbf{r}'\,, \tag{35}$$

$$\mathbf{E}_0^{(\tau)}(\mathbf{r}+\mathbf{h}_\tau) = \mathbf{E}_0(\mathbf{r}+\mathbf{h}_\tau) + \sum_\nu{}' (\nabla\nabla\cdot + k_1^2)\mathbf{\Pi}_\nu^e(\mathbf{r})\,, \tag{36}$$

prime in the summation excludes the term with $\nu = \tau$, $\mathbf{E}_0(\mathbf{r})$ is the incident field. The quantity $\mathbf{\Lambda}_\tau$ is given by

$$\mathbf{\Lambda}_\tau = \int_V F(\mathbf{r}+\mathbf{h}_\tau)\mathbf{E}_L(\mathbf{r}+\mathbf{h}_\tau)d^3\mathbf{r} = \int_V F(\mathbf{r})\mathbf{E}_L(\mathbf{r}+\mathbf{h}_\tau)d^3\mathbf{r}\,.$$

Under derivation of this equation we made use the property of the excitonic wavefunction of the composite to be periodical $F(\mathbf{r}+\mathbf{h}_\tau)=F(\mathbf{r})$. We also neglect overlapping of excitonic wavefunctions. Then we come to the infinite system of integral equations for infinite set of lattice vectors $\mathbf{h}_\tau$.

Electromagnetic field outside the QD, in the region $\mathbf{r}\notin V$, is presented by:

$$\begin{aligned}\mathbf{E}(\mathbf{r}) &= \mathbf{E}_0+\sum_\nu(\nabla\nabla\cdot+k_1^2)\mathbf{\Pi}_\nu^e(\mathbf{r})\,,\\ \mathbf{H}(\mathbf{r}) &= \mathbf{H}_0-ik_1\varepsilon_h\sum_\nu\nabla\times\mathbf{\Pi}_\nu^e(\mathbf{r})\,,\end{aligned}\tag{37}$$

where

$$\mathbf{\Pi}_\nu^e(\mathbf{r})=DM\frac{e^{ik_1|\mathbf{r}-\mathbf{h}_\nu|}}{|\mathbf{r}-\mathbf{h}_\nu|}(\underline{\mathbf{I}}-D\underline{\mathfrak{F}})^{-1}\mathbf{\Lambda}_\nu=\frac{V}{4\pi M}\frac{e^{ik_1|\mathbf{r}-\mathbf{h}_\nu|}}{|\mathbf{r}-\mathbf{h}_\nu|}\underline{\boldsymbol{\alpha}}\mathbf{\Lambda}_\nu\,.$$

No we can apply the Maxwell Garnett procedure to the excitonic composite. For that aim, we introduce mean fields by averaging of microscopic fields over the elementary cell volume Ω. For mean fields we obtain expressions analogous to expressions (37) with

$$\mathbf{\Pi}_\nu^e(\mathbf{r})\to\widetilde{\mathbf{\Pi}}_\nu^e(\mathbf{r})=\frac{f_V}{4\pi M}\underline{\boldsymbol{\alpha}}\mathbf{\Lambda}_\nu\int\limits_\Omega\frac{\exp\{ik_1|\mathbf{r}-\mathbf{h}_\nu-\boldsymbol{\eta}|\}}{|\mathbf{r}-\mathbf{h}_\nu-\boldsymbol{\eta}|}d^3\boldsymbol{\eta}\,.\tag{38}$$

To complete the procedure we should couple the mean field with the local one acting inside the QD. We found

$$\mathbf{E}_L(\mathbf{r}+\mathbf{h}_\nu)=\langle\mathbf{E}(\mathbf{r}+\mathbf{h}_\nu)\rangle-\frac{f_V}{4\pi M}\left(\nabla\nabla\cdot\int\limits_\Omega\frac{1}{|\mathbf{r}-\boldsymbol{\eta}|}d^3\boldsymbol{\eta}\right)\underline{\boldsymbol{\alpha}}\,\mathbf{\Lambda}_\nu\,.\tag{39}$$

Multiplying this equation by $F(\mathbf{r})$, after integration over the QD volume we derive the equality

$$\mathbf{\Lambda}_\nu=M\,(\underline{\mathbf{I}}-f_V\underline{\boldsymbol{\delta}}\,\underline{\boldsymbol{\alpha}})^{-1}\,\langle\mathbf{E}(\mathbf{h}_\nu)\rangle\,,\tag{40}$$

where $\underline{\boldsymbol{\delta}}$ is the tensor given by its components:

$$(\underline{\boldsymbol{\delta}})_{ij}=-\frac{1}{4\pi M}\int\limits_V\int\limits_\Omega F(\mathbf{r})\frac{\partial^2}{\partial r_i\partial r_j}\frac{1}{|\mathbf{r}-\boldsymbol{\eta}|}d^3\boldsymbol{\eta}d^3\mathbf{r}\,.\tag{41}$$

Further we follow to the conventional procedure of the electrodynamics of composite media: Eq. (40) obtained for a discrete set of points $\mathbf{r}=\mathbf{h}_\nu$ is extended to all space. After that, this equation presents a generalization of the Mossotti–Clausius factor to the excitonic composite. Peculiar property

of such composites is that the relation between mean and acting fields is nonlocal. Note that the condition $k\Omega^{1/3} \ll 1$ allows us the change

$$\widetilde{\Pi}^{e}_{N}(\mathbf{r}) \to \frac{1}{4\pi M} f_V \underline{\boldsymbol{\alpha}} \int\limits_{\Omega} \boldsymbol{\Lambda}(\mathbf{h}_\nu + \boldsymbol{\eta}) \frac{\exp\{ik_1|\mathbf{r} - \mathbf{h}_\nu - \boldsymbol{\eta}|\}}{|\mathbf{r} - \mathbf{h}_\nu - \boldsymbol{\eta}|} d^3\boldsymbol{\eta}\,.$$

In this case, macroscopic polarization of the excitonic composite is expressed by $\mathbf{P} = (\underline{\varepsilon}_{eff}/\varepsilon_h - 1)\langle \mathbf{E} \rangle / 4\pi$ with $\underline{\varepsilon}_{eff}$ determined by equation (22) and tensors $\underline{\boldsymbol{\alpha}}$ and $\underline{\boldsymbol{\delta}}$ given by Eqs. (31) and (41), respectively. This allows us to conclude that the excitonic composite in the weak confinement regime is equivalent to a homogeneous anisotropic medium with the tensorial dielectric function $\underline{\varepsilon}_{eff}$ and unit permeability.

4. Cubic lattice of spherical QDs: comparison of the weak and strong confinement regimes

Let a collection ofv uniform spherical QDs of the radius R_0 constitutes a cubic lattice. Exciton wavefunction for an isolated spherical QD is as follows (see, e.g., [23]):

$$F(\mathbf{r}) \equiv F_{nlm}(\mathbf{r}) = C_{nl} Y_{lm}(\theta, \varphi) J_{l+1/2}\left(\kappa_{nl} \frac{\rho}{R_0}\right) \frac{1}{\sqrt{\rho}},$$

where $Y_{lm}(\theta, \varphi)$ is the spherical harmonics, $J_\nu(x)$ is the Bessel function, ρ, θ, φ are the spherical co-ordinates, κ_{nl} is the n-th root of the Bessel function $J_{l+1/2}(x)$, indices n and l define the working mode in the oscillator spectrum. Coefficient $C_{nl} = \sqrt{2}[R_0 J_{l+3/2}(\kappa_{nl})]^{-1}$ provides orthonormalization of functions F_{nlm}. Further we restrict ourselves to the case $l = m = 0$; in this case $Y_{00}(\theta, \varphi) = 1/2\sqrt{\pi}$. Let the dipole moment of the QD is oriented along the x-axis; in this case polarizability tensor is characterized by the xx–component. By integration in Eqs. (32) we obtain $M^2 = 32\pi R_0^3/\kappa_{n0}^2$, $\Im_{xx} = 4\pi/3$. Since for a sphere all directions are equivalent, identical results are obtained for zz - and yy-components. It can easily be shown that the components satisfy the equality (33). Choosing excitonic mode with another set of numbers n, l, m we obviously obtain another magnitude of components $\Im_{\alpha\alpha}$ and, consequently, another magnitude of the polarizability tensor $\underline{\boldsymbol{\alpha}}$ (31). Thus, we come to peculiar property of the weak confinement regime: depolarization depends on the excitonic mode number. This property follows from the nonlocality of the exciton polarization. Unlike that, in the strong confinement regime depolarization tensor (5) is completely determined by the QD geometry.

For the particular case of the cubic lattice, a special approach based on the the trace theorem $(\underline{\delta})_{xx} + (\underline{\delta})_{yy} + (\underline{\delta})_{zz} = 1$ can be applied. Taking into

account isotropy of cubic lattice we find $(\underline{\delta})_{xx} = (\underline{\delta})_{yy} = (\underline{\delta})_{zz} = \delta = 1/3$. This result, together with the previous ones, allows us to evaluate depolarization shift of the exciton resonant frequency in the weak confinement regime:

$$\Delta\omega = -\frac{4}{9}\left(\frac{R_0}{a_B}\right)^3 g_0 \,. \tag{42}$$

The formula $\Phi(r) = (1/\pi a_B^3)^{1/2} \exp(-r/a_B)$ [27] has been utilized under derivation of the shift; a_B is the exciton Bohr radius. This shift is different from that given by Eq. (16) for spherical QDs in the strong confinement regime: $\Delta\omega = -g_0/3\varepsilon_h$. Thus we state another peculiar property of the weak confinement regime: radial dependence of the depolarization shift.

5. Conclusion

In our paper we have developed effective medium theory of 3D inhomogeneous semiconductor heterostructure — excitonic composite, constituted by QDs imbedded in a transparent host medium. We have started with the self-consistent microscopic local-field theory for an isolated arbitrary shaped QD. In our approach we introduce into Schrödinger equation depolarization field induced by an external electromagnetic field, and combine this idea with the second quantization technique for electron-hole pairs. As a result, we succeeded in deriving of general self-consistent nonlinear equations for the system "QD + classical electromagnetic field". In the linear approximation, our approach reproduces microscopically the depolarization shift of the QD gain band and, in anisotropically shaped QDs, polarization dependent splitting of this band.

Both types of the exciton localization, strong and weak confinement regimes have been considered. Pronounced nonlocality is characteristic of the latter regimes. The basic result is that in both cases excitonic composite is described by spatially local constitutive relations although electromagnetic response of an isolated QD in the weak confinement regime is spatially nonlocal. The nonlocality manifests itself in specific dependence of the effective constitutive parameters on the geometry and electronic properties of single QD.

To conclude, let us dwell on possible ways of the further development of the theory presented. In our consideration we have restricted ourselves to a simplest model of the excitonic composite: perfect lattice of identical QDs, whereas experimentally available structures show intrinsic size dispersion and periodicity violation. These effects may be characterized by a distribution function and taken into account by a theory of irregular

excitonic composites. Elaboration of such a theory is the topical question. Another essential restriction of the analysis presented is that nonclassical light-matter interaction has been left beyond the analysis. Quantum nature of the light interacting with an excitonic composite is expected to be of importance for many problems where collections of excitons are involved: quantum computing, electromagnetic fluctuations, *etc.* In general, quantum electrodynamics provides necessary formalism for investigation of the problem. However, since QDs are electrically small inhomogeneities with inherent energy dissipation (absorption or gain) and dispersion, canonical quantization scheme of the electromagnetic field becomes invalid: dissipation results in that the operators corresponding to the Maxwell equations turn out to be non-Hermitian. To avoid this difficulty, a quantization scheme which involves auxiliary fields has been proposed in Ref. [18]. The theory elaborated in our paper allows synthesis with that quantization scheme and, thus, creates necessary basis for investigation of quantum optics of excitonic composites.

Acknowledgments

The research is partially supported through the NATO Science for Peace Program under project SfP-972614.

References

1. Dingle, R. and Henry, C. H. Quantum effects in heterostructure lasers, U.S. Patent No. 3982207, 21 September 1976.
2. Arakawa, Y. and Sakaki, H. (1982) Multidimensional quantum well lasers and temperature dependence of its threshold current, *Appl. Phys. Lett.* **40**, pp. 939-941.
3. Asada, M., Miyamoto, Y. and Suematsu, Y. (1986) Gain and the threshold of three dimensional quantum dot lasers, *IEEE J. Quant. Electr.* **32**, pp. 1915-1933.
4. Kirstaedter, N., Ledentsov, N. N., Grundmann, M., Bimberg, D., Ustinov, V. M., Ruvimov, S. S., Maximov, M. V., Kop'ev, P. S., Alferov, Zh. I., Richter, U., Werner, P., Gosele, U., and Heydenreich, (1994) Low threshold, large T0 injection laser emission from (InGa)As quantum dots, *J Electron. Lett.* **30** pp. 1416-1418.
5. Bimberg, D., Grundmann, M., and Ledentsov, N. N. (1999) *Quantum dot heterostructures*, John Wiley & Sons, Chichester.
6. Kilin, S. Ya. (1999) Quantum information, *Phys.-Uspehi* **42**, pp. 435-452.
7. Lakhtakia, A. (ed.) (1996) *Selected papers on linear optical composite materials.* SPIE Optical Engineering Press, Bellingham, WA.
8. Slepyan, G. Ya., Maksimenko, S. A., Kalosha, V. P., Ledentsov, N. N., Bimberg, D., and Alferov, Zh. I. (1999) Polarization splitting of the gain band in quantum wire and quantum dot arrays, *Phys. Rev. B* **59**, pp. 1275-1278.
9. Maksimenko, S. A., Slepyan, G. Ya., Kalosha, V. P., Maly, S. V., Ledentsov, N. N., Herrmann, J., Hoffmann, A., Bimberg, D., and Alferov, Zh. I. (2000) Electromagnetic response of 3d arrays of quantum dots, *J. Electronic Materials*, **29**, pp. 494-503.

10. Maksimenko, S. A., Slepyan, G. Ya., Ledentsov, N. N., Kalosha, V. P., Hoffmann, A., and Bimberg, D., (2000) Light confinement in a quantum dot, *Semiconductor Sci. and Techn.* **15**, pp. 491-496.
11. Maksimenko, S. A., Slepyan, G. Ya., Kalosha, V. P., Ledentsov, N. N., Hoffmann, A., and Bimberg, D. (2001) Size and shape effects in electromagnetic response of quantum dots and quantum dot arrays, *Mat. Sci. Engineer. B* **82**, pp. 215-217.
12. Slepyan, G. Ya., Maksimenko, S. A., Kalosha, V. P., Hoffmann, A., and Bimberg, D. (2001) Effective boundary conditions for planar quantum-dot structures, *Phys. Rev. B* **64**, No 125326.
13. Ilyinsky, A. S., Slepyan, G. Ya., and Slepyan, A. Ya. (1993) *Propagation, Scattering and Dissipation of Electromagnetic Waves* Peter Peregrinus, London.
14. Cho, K. (1999) Mechanisms for LT splitting of polarization waves: a link between electron-hole exchange interaction and depolarization shift, *J. Phys. Soc. Japan* **68**, pp. 683-691.
15. Ajiki, H. and Cho, K. (2000) Longitudinal and transverse components of excitons in a spherical quantum dot, *Phys. Rev. B* **62**, pp. 7402-7412.
16. Fu, Y., Willander, M., and Ivchenko, E. L. (2000) Photonic dispersions of semiconductor-quantum-dot-array-based photonic crystals in primitive and face-centered cubic lattacies, *Superlattices and Microstructures*, **27**, pp. 255-264.
17. Drummond, P. D. and Hillery, M. (1999) Quantum theory of dispersive electromagnetic modes, *Phys. Rev. A* **59**, pp. 691-707.
18. Vogel, W., Welsch, D.-G., and Wallentowitz, S. (2001) *Quantum optics. An introduction*, Willey-VCH, New York.
19. Savona, V., Hradil, Z., Quattporani, A. and Schwendimann, P. (1994) Quantum theory of quantum-well polaritons in semiconductor microcavities, *Phys. Rev. B* **49**, pp. 8774-8779.
20. Landau, L. D. and Lifshitz, E. M. (1960) *Electrodynamics of continuous media*, Pergamon Press, Oxford.
21. Kleinman, R. E. (1978) Low frequency electromagnetic scattering, in P. L. E. Uslenghi (ed.) *Electromagnetic scattering*, Academic Press, New York, pp. 1-28.
22. Bowden, C. M. and Dowling, J. P. (1993) Neardipole-dipole effects in dense media: Generalized Maxwell-Bloch equations, *Phys. Rev. A* **47**, pp. 1247-1251.
23. Schmitt-Rink, S., Miller, D. A. B. and Chemla, D. S. (1987) Theory of the linear and nonlinear optical properties of semiconductor microcrystallites, *Phys. Rev. B* **35**, pp. 8113-8125.
24. Hanewinkel, B., Knorr, A., Thomas, P. and Koch, S. W. (1997) Optical near-field response of semiconductor quantum dots *Phys. Rev. B* **55**, pp. 13715-13725.
25. Gammon, D., Snow, E. S., Shanabrook, B. V., Katzer, D. S. and Park, D. (1996) Fine structure splitting in the optical spectra of single GaAs quantum dots, *Phys. Rev. Lett.* **76**, pp. 3005-3008.
26. Khiznjak, N. A. (1986) *Integral equations of macroscopic electrodynamics* Naukova Dumka, Kiev, in Russian.
27. Hanamura, E. (1988) Very large optical nonlinearity of semiconductor microcrystallites, *Phys. Rev.* B **37**, pp. 1273-1279.
28. Courant, R. and Hilbert, D. (1966) *Methods of mathematical physics*, Vol.1, Interscience Publ. New York.

OPTICAL ANISOTROPY OF THE CRYSTALS AT THE NONUNIFORM FIELDS

R. VLOKH and M. KOSTYRKO
Institute of Physical Optics
23 Dragomanov Str., 79005, L'viv, Ukraine
E-mail: vlokh@ifo.lviv.ua

Abstract. In this paper a review of the parametrical crystallooptical effects at the influence of the nonhomogeneous fields is presented. It is shown that the parametrical crystallooptics at the static nonhomogeneous fields is the particular branch of the nonlinear optics in which spatial dispersion is taken into account. The coupling spatial dispersion phenomena and gradient crystallooptical effects are shown on the phenomenological level as well as description of the influence of the multicomponent fields on the behavior of the optical indicatrix is realized. It is shown that the mechanical bending and twisting deformations could be described as axial second rank tensor. The experimental investigations of the influence of the nonuniform mechanical strain and temperature field on the refractive and gyrotropy properties of $LiNbO_3$ and $NaBi(MoO_4)_2$ crystals are presented.

1. Introduction

Last time special interest displays to factors, which takes into account a real media structure. Complex approach to this problem enables to explain nature and mechanisms of already known phenomena, to obtain scientific information, bearing upon interaction of electromagnetic radiation with media of diverse structure (distant from idealized models). Firstly it was believed that the nonlinear optical phenomena arise in media only at sufficiently high field power of the light wave. However, from the point of view of nonlinear electrodynamics, to them one can attribute also effects, which appear in sufficiently weak light fields. This is so called parametrical nonlinear phenomena, which arise in media, the parameters of which change under the action of external influences (electric and magnetic field, mechanical strain, etc.) [1]. Among them can be pointed out so called gradient effects – that is – effects, caused by the presence of spatial dispersion. Today gradient crystallooptics comes forward as partial branch of nonlinear optics.

S. Zouhdi et al. (eds.), Advances in Electromagnetics of Complex Media and Metamaterials, 403–417.

2. Phenomenological analysis of the influence of the nonhomogeneous actions on optical properties of crystals

2.1. SYMMETRY ASPECTS OF PARAMETRIC OPTICAL PHENOMENA AT NONHOMOGENEOUS INFLUENCE

Possibility of existence of different effects into first turn follows from symmetry transformations. We shall model some possible types of nonhomogeneities, for example, of the electric field.

1. Spiral distribution of equal on absolute value vectors of electric field E will possess $\infty 2$ symmetry. Axial tensor of second rank possesses such symmetry. So, the lowering of crystals symmetry at propagating through them of intensive circular polarized wave can be represented as superposition of symmetry elements of axial-tensor action with symmetry elements of crystal.

2. Spiral distribution of polar vectors, which gradually changes on absolute value, possesses symmetry of rotative cone – ∞. This action always can cause the optical activity in medium.

3. A nonhomogeneous vector field, that is not changed in direction, but evenly changes in absolute value, will possess symmetry m (E vector and direction of its change is in plane m). At such action optical activity can arise, crystal symmetry will lower to group m or 1. Then the optical indicatrix will have a view of ellipsoid of general type and can rotate around crystalophysical axis, which is perpendicular to plane of symmetry in m group, or around all axes in 1 group. Regarding optical activity at twisting, its appearing admits in crystals of all symmetry groups. Actually axial-tensor action always leads to lowering of crystal symmetry to optically active state. It may be noticed, that at any nonhomogeneous actions the optical activity, that is ellipticity of eigen waves, is ought to arise [2].

2.2. POLARIZATION CHARACTERISTICS OF CRYSTALLINE MEDIUM WITH THE ACCOUNT OF FIELDS' GRADIENTS

In presence of effects of spatial dispersion the correlation for polarization of crystalline medium could be written in the form:

$$P_i=\chi_{ij}E_j+d_{ijk}E_jE_k+\gamma_{ijk}\partial E_j/\partial x_k+R_{ijkl}E_l\partial E_j/\partial x_k+... \qquad (1)$$

Two last terms in expression (1) describe the optical activity and electrogyration effect [3, 4]. The optical activity may be represented as bilinear effect, whereas electrogyration is, perhaps, first known effect of gradient nonlinear optics [5]. Taking into account different gradient invariants in correlation (1) one can foresee and define the existence conditions of new gradient effects, connected with spatial dispersion [6, 7]. Medium polarization at linear electrogyration effect can be represented as follows:

$$^{nl}P_i^{\omega}=R_{ijkl}E_l\partial E_j/\partial x_k = ie_{ikm}\gamma_{mjl}E_j^{o}E_k^{\omega}k_l \qquad (2)$$

where γ_{mil} is axial tensor of the third rank, e_{ikm} is Levi-Civita tensor. Then we get:

$$^{nl}P_i^{\omega}=R_{ijkl}E_l^{\omega}\partial E_j^{0}/\partial x_k \quad (3)$$

and $$\Delta a_{ij}=R_{ijkl}\partial E_k/\partial x_l \quad (4)$$

So-called electrogyration light diffraction is possible:

$$^{nl}P_i^{\omega\pm\Omega}=ie_{ikm}\gamma_{mjl}E_k^{\omega}E_j^{\Omega}k_l. \quad (5)$$

Phenomena of gradient parametrical crystal optics can appear also in fields of another nature. So, for example, well-known piezogyration effect [8-10] is described by following expression:

$$^{nl}P_i^{\omega}=\theta_{ijmkl}\sigma_{kl}^{0}\partial E_j^{\omega}/\partial x_m=ie_{ijn}\theta_{nmkl}\sigma_{kl}^{0}E_j^{\omega}k_m \quad (6)$$

and $$\Delta g_{nm} = \theta_{nmkl}\sigma_{kl} \quad (7)$$

At the propagation of acoustic wave with frequency Ω in acentric medium, a light diffraction on the grate, formed on the imaginary part of dielectric permitivity, must arise:

$$^{nl}P_i^{\omega\pm\Omega}=\theta_{ijmkl}\sigma_{kl}^{0}\partial E_j^{\omega}/\partial x_m=ie_{ijn}\theta_{nmkl}\sigma_{kl}^{\Omega}E_j^{\omega}k_m \quad (8)$$

This effect was for the first time observed in quartz crystals and called acoustogyration light diffraction [11].

The effect of optical activity appearance in centrosymmetrical $NaBi(MoO_4)_2$ crystals under the influence of twisting deformation was also observed [12]. This effect is connected with arising of nonhomogeneous mechanical strains in crystal because piezogyration can not appear in centrosymmetrical crystals:

$$^{nl}P_i^{\omega}=S_{ijklmn}\partial\sigma_{kl}^{0}/\partial x_m\partial E_j^{\omega}/\partial x_n=ie_{ijr}k_{nrkml}\partial\sigma_{kl}^{0}/\partial x_m E_j^{\omega}k_n \quad (9)$$

and $$\Delta g_{rn} = k_{rnklm}\partial\sigma_{kl}/\partial x_m \quad (10)$$

where tensor k_{rnklm}, according to its symmetry $\varepsilon[V^2][V^2]V$, differs from zero even in isotropic medium. So, optical activity is a suitable tool for control and investigation of nonuniformly strained state of media [13, 14].

Nonhomogeneous mechanical strains also lead to the changes of refractive properties of crystals. This phenomenon was called gradient piezooptics effect and it can be described by the expression [7]:

$$\Delta a_{ij} = K_{ijklm}\partial\sigma_{kl}/\partial x_m, \quad (11)$$

where K_{ijklm} is polar tensor of 5-th rank.

2.3. INFLUENCE OF THE MULTICOMPONENT FIELDS ON OPTICAL INDICATRIX

For the description of effects of parametric crystallooptics (electro- and piezooptics) usually optical indicatrix is used. External influences can cause turnings of optical indicatrix around its axes. As far as we know, cases of inducing by external influence the turning of indicatrix around only one axis were considered up-to-now. This may be explained by the circumstance, that to bring ellipsoid equation to canonical view (to obtain correlation for changed principal refraction indexes) at the turnings of indicatrix around two or three axes in extant view is practically impossible. But the turning around the third coordinate axis must be observed at turnings presence of any geometrical figure around two coordinate axes. In crystallooptics, the turning of indicatrix around the third coordinate axis can be unconnected with the existence of a respective field component, which should induced it, or tensor components, for example, electrooptics or piezooptics tensor constants. Then such indicatrix turning is reasonable to describe as non-direct turning, so far as it must be described over its turnings around two other axes.

As we established, at inducing of the turning of characteristic refraction indexes surface around two axes by external influence always the turning around the third axis appears. So, for example, at the turning of optical indicatrix around y and z axes the axis x′ does not belong to the plane xy, neither to the plane xz (as in the case of turning around one axis), that one can describe with the help of correlation for angles between projection of axis x′ on the plane yz and axis z:

$$\alpha' = \pi - \arccos \frac{\{\xi_2/2\pi\}}{\left(\{\xi_2/2\pi\}^2 + \{\xi_3/2\pi\}^2\right)^{1/2}} \qquad (12)$$

The angle α' may be used for quantitative description of non-direct turning of optical indicatrix around the third axis [15].

Let us consider some possible cases of correlation between angles ξ_2 and ξ_3 in the formula (12): 1) $\xi_2 = \xi_3$, then $\alpha'_1 = 3\pi/4$;2) $\xi_2 << \xi_3$, then $\alpha'_2 \approx \pi/2$; 3) $\xi_2 >> \xi_3$, then $\alpha'_3 \approx \pi$. All of these cases are depicted on figure 1. It is visible, that non-direct turning is most essential at close values of the angles ξ_2 and ξ_3; if one of the angles is far from the other, then non-direct turning is insignificant.

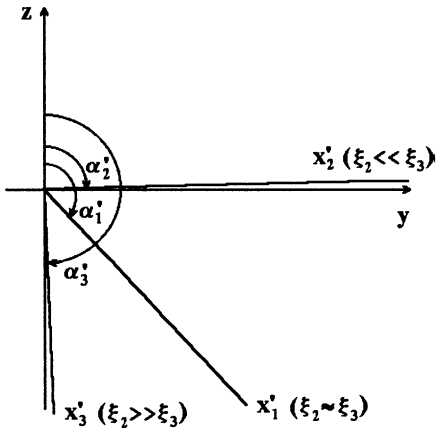

Figure 1. Non-direct turning for diverse correlations between angles ξ_2 and ξ_3.

2.4. TENSOR DESCRIPTION OF GRADIENT PIEZOGYRATION AND PIEZOOPTICS

The phenomena of gradient piezooptics and piezogyration consist in changing of polarization (a_{ij}) and gyration (g_{ij}) constants proportional to the gradient of mechanical strain and are described by the correlations [7]:

$$\Delta a_{ij} = K_{ijklm} \partial \sigma_{kl} / \partial x_m \, , \; \Delta g_{ij} = k_{ijklm} \partial \sigma_{kl} / \partial x_m \qquad (13)$$

As we established, some simplifications are possible in the case of twisting and bending. The tensor of gradient piezooptics at twisting and bending with internal symmetry $[V^2]V^2$ η_{ijln} has the fourth rank. Then we can write down

$$\Delta a_{ij} = \eta_{ijln} (\mathrm{Rot}\sigma)_{nl} \qquad (14)$$

(analogous correlation just for Δg_{ij}).

As one can see, antisymmetrical tensor $\mathrm{Rot}(\sigma)_{nl}$ contains only the diagonal components of tensor of strains, which are connected with bending and does not contain strains, which are connected with twisting. In this case we shall once more lower the rank of tensor, which is used for the link between polar vector, which describes the two-coordinate bending, and tensor of polarization constants:

$$\Delta a_{ij} = \theta_{ijp} a_p .$$

So, twisting and bending deformation can be described by axial tensor of second rank [16]. The diagonal components of this tensor describe crystal twisting around crystallophysical axes, and nondiagonal ones - bending. Antisymmetrical part of axial tensor of second rank describes so-called two-coordinate bending.

3. Light interaction in crystals at static nonuniform influences

3.1. INFLUENCE OF NONUNIFORM MECHANICAL ACTIONS ON OPTICAL PROPERTIES OF CRYSTALS

3.1.1. *Distribution of optical indicatrix turning in $LiNbO_3$ crystals at twisting*

The turning of optical indicatrix at scanning by laser ray in xy-crossing in the $LiNbO_3$ crystal was investigated at the application of the torsion moment around z axis [13]. The distribution of optical indicatrix turnings (fig. 2) possesses special directions, which coincides with crystallophysical axes x and y. Obtained results coincide with theoretically predicted but an interesting peculiarity exists: at transition from the xy and x-y quadrants to -xy and -x-y, respectively, optical indicatrix turns to angle 90° with the saving of the orientation of long axis (fig. 2, on insert). This situation corresponds to the crystallophysical x axis interchanging with y axis, because in the unity system of coordinates the turning angle of optical indicatrix can not be more, than 45°.

3.1.2. *Neutral birefringence point and neutral birefringence line in $LiNbO_3$ crystals at twisting*

The twisting of the crystals was realized by the pair of forces applied to the opposite faces of the samples. The measuring of birefringence was carried out by Senarmont method.

From the equation of optical indicatrix for $LiNbO_3$ crystals, which belong to symmetry group 3m, at presence of shift strains σ_{31} and σ_{32} (it corresponds to the configuration of experiment k||Z, M||z), one can derive:

$$\Delta n \approx \frac{p_{14}\sqrt{e_{32}^2+e_{31}^2}}{a_{11}\sqrt{a_{11}}} = p_{14}\sqrt{e_{32}^2+e_{31}^2}\,n_1^3 \qquad (16)$$

Obviously, the dependence of induced birefringence on coordinates is determined by dependences of strains σ_{32} and σ_{31} on coordinates, which are proportional to x and y, respectively. Because $\sigma_{32}=\sigma_{31}=0$ only in the point x=0, y=0, then $\Delta n=0$ only in this point (fig. 3).

From the equation of optical indicatrix for $LiNbO_3$ crystals at presence of shift strains σ_{12} and σ_{31} (it corresponds to the configuration of experiment k||z, M||x), one can write down induced birefringence for optical ray, which propagates above (y>0) and below (y<0) plane y=0, as:

$$\Delta n_+ \approx 2n_1^3\pi_{56}\sigma_{31} \text{ and } \Delta n_- \approx -2n_1^3\pi_{56}\sigma_{31} \qquad (17)$$

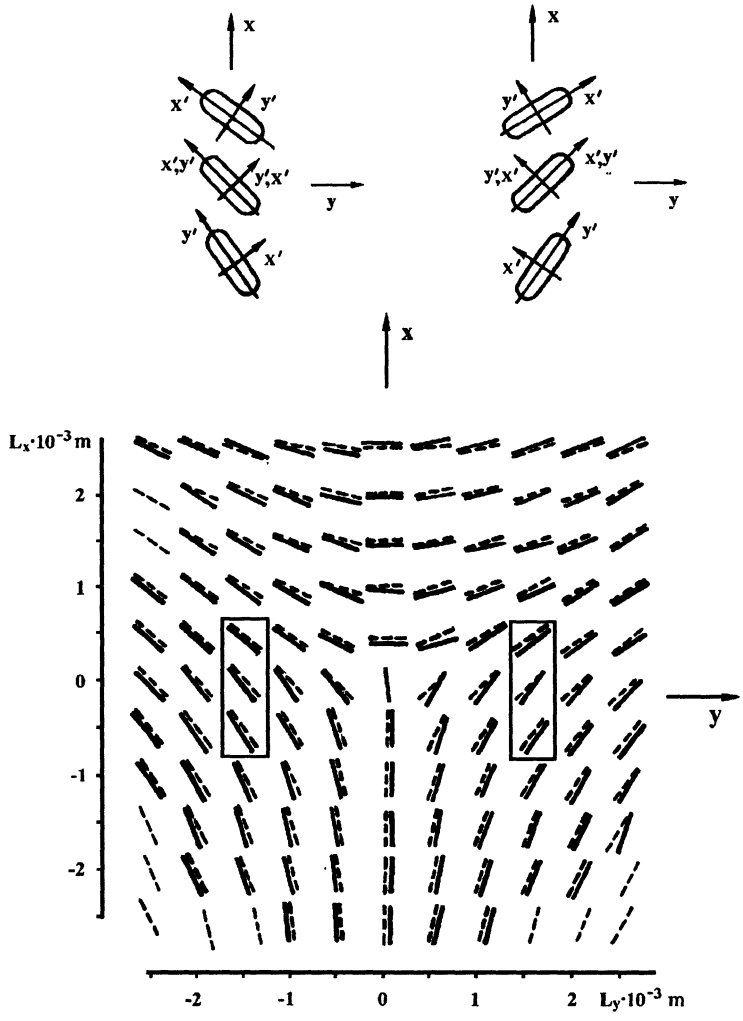

Figure 2. Distribution of optical indicatrix turnings at constant twisting moment on xy - crossing of $LiNbO_3$ crystal. Theoretically calculated orientations of optical indicatrix are marked by strokes. On the insert - the turn of optical indicatrix to angle 90° with the saving of orientation of long axis at transition from quadrants xy and x-y to quadrants -xy and -x-y, respectively. x and y axes orientation of undeformed crystal is marked by arrows.

It is visible, that the dependence of induced birefringence on coordinate is determined by the dependence of strain σ_{31} on coordinate. Because at y=0 σ_{31}=0, then Δn=0, that is observed on the experiment (fig. 4).

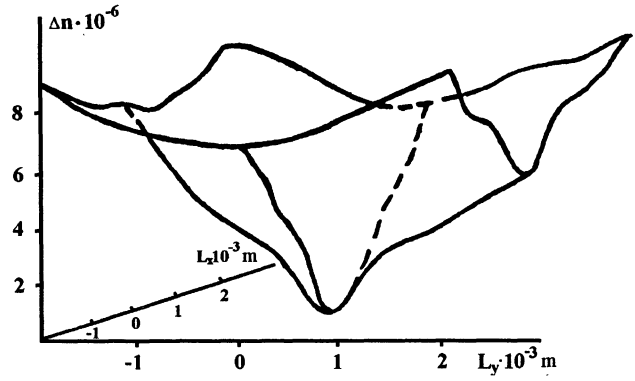

Figure 3. Distribution of the birefringence induced by constant twisting moment M=1.68×10^3 N/m on xy-crossing of $LiNbO_3$ crystal (λ=632.8 nm), (k | | z, M | | z).

In the result of carried out investigations we obtain dependencies of birefringence on the twisting moment (fig. 5 – for the configuration of experiment k||z, M||x; for the configuration of experiment k||z, M||z dependencies were qualitatively similar) and distributions of induced birefringence on samples crossing (fig. 3 and 4). It was established that birefringence does not arise only in the case, when an optical ray propagates through the geometrical center of square crossing - neutral birefringence point (fig. 3) or in plane y=0 - neutral birefringence line (fig. 4) in dependence of configuration of experiment, in all other cases the birefringence induced by twisting increases at displacement of optical ray from crystal crossing center [13, 17].

3.1.3. *Distribution of birefringence in $LiNbO_3$ crystals at bending*

Bending deformation is as well as twisting deformation one of the simplest nonhomogeneous deformations. Firstly bending moment was applied to the samples by a three-point method. Obtained results for the turning of indicatrix and induced birefringence essentially distinguish from theoretically calculated ones.

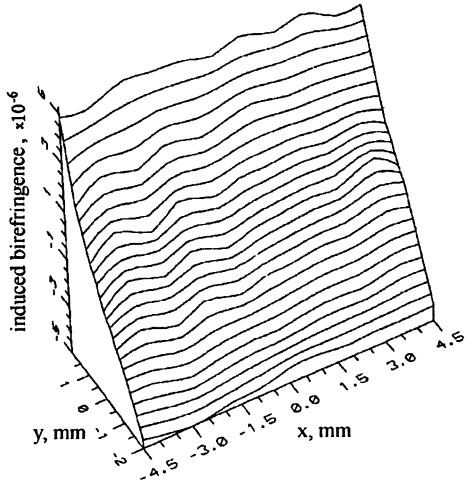

Figure 4. Distribution of induced by constant twisting moment $M=3.008\times10^3$ N/m birefringence on xy-crossing of the $LiNbO_3$ crystal (λ=632.8 nm), (k | | z, M | | x).

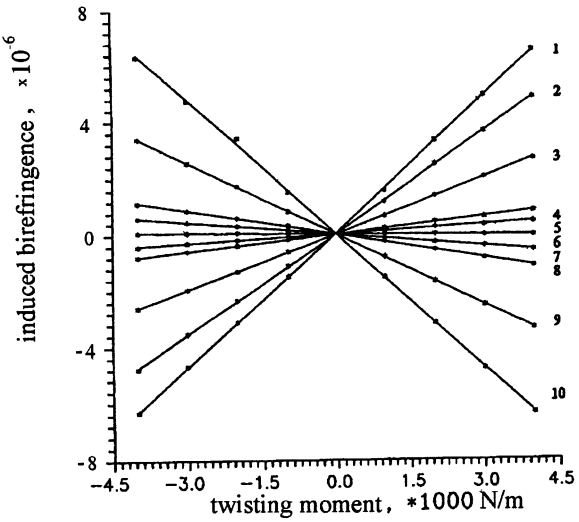

Figure 5. Dependence of the birefringence on twisting moment at different distances L from line y=0 $LiNbO_3$ crystals xy-crossing (λ=632.8 nm). Ly= -1998 μm (1), -1332 μm (2), -666 μm (3), 0 μm (4), 166.5 μm (5), 333 μm (6), 499.5 μm (7), 666 μm (8), 1332 μm (9), 1998 μm (10), (k | | z, M | | x).

In connection with this we used a so-called single-arm method of the bending application and thinner sample. The turning of optical indicatrix was not observed; obtained distribution of induced birefringence (fig. 6) corresponds to our calculation, especially a so-called neutral birefringence line (line of absence of induced birefringence) was observed. It is necessary to note, that the essential deviations from theoretically predicted dependencies were observed on sample edges - in places of pasting up and loading, and thus in these regions additional strains exist.

In the result of carried out study the distribution of induced birefringence on samples crossing (fig. 6) was obtained [18, 19]. Birefringence does not arise in that case, when an optical ray propagates in the plane y=0 - neutral birefringence line, as well as at displacement of optical ray from plane y=0 induced by bending birefringence increases.

3.1.4. *Torsion-gyrational effect (gradient piezogyration) in $NaBi(MoO_4)_2$ crystals*
From the symmetry point of view the lowering of crystal symmetry to the noncentrosymmetrical group causes the appearing of gyration in the centrosymmetrical crystals. The change or appearing of the gyration at crystals twisting (torsion-gyrational effect) can be described by the correlation

$$\Delta g_{ij}=\xi_{ijkl}M_{kl}, \qquad (18)$$

where ξ_{ijkl} is a polar tensor of 4-th rank, M_{kl} is a symmetrical axial tensor of 2-nd rank. Most comfortable from the point of view of founding of the torsion-gyrational effect is an experiment with using single-axis centrosymmetrical crystals at light propagation along optical axis and twisting crystal around it, because under such twisting neutral birefringence point should exist and linear birefringence should not mask an investigated effect.

Torsion-gyrational effect was observed in $NaBi(MoO_4)_2$ crystals, which belong to the group of the symmetry 4/m, at propagation of linearly-polarized light along optical axis. As it was found out, the dependence of component of gyration tensor g_{33} on the value of applied moment is linear and its sign changes at the change of twisting direction (fig. 7). On the base of obtained experimental results the component of torsion-gyration tensor was calculated – $\xi_{3333}=3.7\times10^{-11}$ m/N [12].

As well as data about twisting-polarization tensor coefficients is absent, it is impossible to estimate the role of a secondary electrogyration in torsion-gyrational effect.

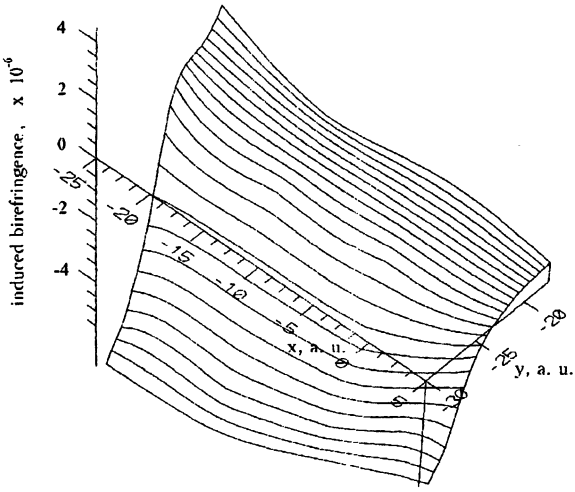

Figure 6. Distribution of induced birefringence on xy-crossing of $LiNbO_3$ crystal at mechanical bending (case of the single-arm bending).

3.2. INFLUENCE OF THE TEMPERATURE GRADIENT ON THE REFRACTIVE PROPERTIES OF THE $LiNbO_3$ CRYSTALS

The study of the influence of nonhomogeneous temperature distribution on the crystallooptical properties is very interesting from the point of view of the stability of operating elements of different optoelectronical devices in the natural environment. Gradient thermooptical effect is described by third rank polar tensor. Other gradient phenomena such as gradient electrooptical and gradient piezooptical effects are described by the fourth and fifth rank tensors respectively and therefore should be smaller than the gradient thermooptical effect.

There are only some reports about the experimental study of this effect [20-22]. The authors [22] have observed the appearance of a birefringence in $LiNbO_3$ crystals with light being propagated and a thermal gradient applied along the Z-axis. However, as it follows from the point group of symmetry for $LiNbO_3$ crystal, such a thermal gradient cannot induce the birefringence along the optical axis. Therefore, the origin of the thermal gradient effect is not clearly understood yet. It is obvious that thermal flows should exist in different directions in the case of a temperature gradient. It means that this experiment possesses time dynamics as well as the appearance of non-homogeneous mechanical strains.

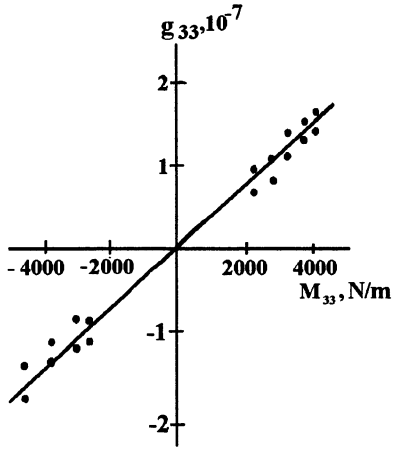

Figure 7. Dependence of gyration tensor component g_{33} on value of twisting moment M_{ij} for $NaBi(MoO_4)_2$ crystals for configurations of experiment k | | z, M | | z.

Thus, we have used a CCD camera to study the gradient thermooptical effect. In this paper we study the gradient thermooptical effect in $LiNbO_3$ crystals by the imaging polarimetry technique described in [23]. Temperature gradient was created by the Peltier semiconductor cooler and electrical heater. To provide uniform temperature on the sample faces thermo conductive paste was used. Using this paste also allows to avoid the sample gripping as well as an appearance of additional stresses caused by thermal expansion. The magnitude of temperature gradient was $2.25 \cdot 10^4$ K/m and the magnitude of temperature difference was 68.5 K.

Two samples were studied in this work (x=4.10mm, y=3.85mm and z=5.46mm and x=4.91mm, y=2.31mm and z=5.00mm). In both cases light was propagated along the Z-axis. Temperature gradient was created in the X- and the Y-direction respectively. The topographical maps of induced birefringence across the sample aperture at the different values of thermal gradient $\partial T/\partial y$ and $\partial T/\partial x$ were obtained and the dependencies of induced birefringence on temperature gradient were calculated (fig. 8 and 9) [24]. The calculated coefficients are $r_{22}=(4.61\pm0.49)\times10^{-12}$ *m/K* for the $\partial T/\partial x$ case and $r_{22}=(4.85\pm0.43)\times10^{-12}$ *m/K* for the $\partial T/\partial y$ case.

Thus, the phenomenological description of gradient thermooptical effect is proposed. The gradient thermooptical effect in $LiNbO_3$ crystal was studied experimentally. The topographical maps of induced phase differences at the different temperature gradients are obtained using the imaging polarimetry technique. The change of phase difference at the different thermal gradient was observed. The dependencies of induced birefringence Δn_z on thermal gradients

$\partial T/\partial x$ and $\partial T/\partial y$ were obtained and the coefficients of gradient thermooptical effect were calculated.

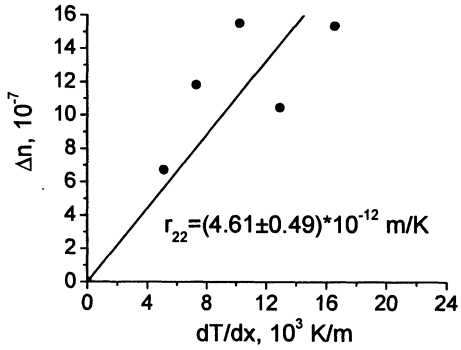

Figure 8. Dependence of induced birefringence on thermal gradient $\partial T/\partial x$ (first sample).

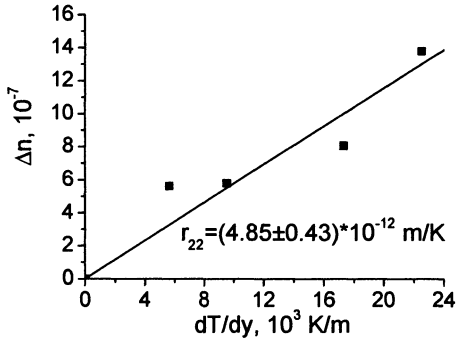

Figure 9. Dependence of induced birefringence on thermal gradient $\partial T/\partial y$ (second sample).

4. Conclusion

Phenomenological analysis of nonlinear optical phenomena caused by nonhomogeneous fields (so called gradient effects) was made. On the base of relation between crystal medium polarization on the optical frequency and gradient of the field with different nature as well as on the base of the symmetry approach it was shown that the electrogyration effect was the first founded phenomena of the gradient nonlinear optics. The existence condition of the new different crystallooptical effects induced by the gradients of fields was analyzed.

It was shown that bending and torsion strains could be described by the axial tensor of the second rank. The presentation of the turning of the optical indicatrix at the multicomponent field influence by the axial vector permits to show, that at the presence of turning of the indicatrix around two crystallophysical axes there always should exist the turning around the third axis. The relation that describes the angle of this turning was derivated and analyzed.

The experimental investigations of mechanical twisting and bending influence on optical properties of crystals were made and the distributions of optical indicatrix, conoscopic pictures and birefringence in $LiNbO_3$ crystals were analyzed. The experimental study permits to find out and to investigate predicted by theory gradient piezogyration effects on the example of $NaBi(MoO_4)_2$ crystals. These investigations testify that the optical topography method of investigation of the distribution of the gyrotropy induced by the gradient strains allows determining peculiarities of nonuniform strained state. The gradient crystallooptical effects could be applied in the operation of optical radiation and in the optical method of the orientation of crystal.

The gradient thermooptical effect in $LiNbO_3$ crystal was studied experimentally. The topographical maps of induced phase differences at the different temperature gradients are obtained using the imaging polarimetry technique. The change of phase difference at the different thermal gradient was observed. The dependencies of induced birefringence Δn_z on thermal gradients $\partial T/\partial x$ and $\partial T/\partial y$ were obtained and the coefficients of gradient thermooptical effect were calculated.

5. References

1. Vlokh, O. (1984) *The spatial dispersion phenomena in the parametrical crystallooptics*, Vyscha shkola, Lviv.
2. Vlokh, R. (1989) Symmetry and tensor description of refractive and gyrotropic properties of crystals at nonhomogeneous influences, *Ukrainian Journal of Physics* **7**, 1000-1002.
3. Zheludev, I.S. (1964) Third rank axial tensors and described by them physical phenomena, *Krystallographiya* **9**, 501-505.
4. Vlokh, O. (1970) Electrooptical activity in quartz crystals, *Ukrainian Journal of Physics* **15**, 759-763.
5. Vlokh, O.G., Zheludev, I.S. (1980) Diploma of the State commettee of the pathents and discoveries of the USSR № 211 "Electrogyration phenomena in crystals" (published in (1979) *Information Bulletin* **29**, 3).
6. Vlokh, R.O. (1989) Parametrical optical effects of circularly polarized waves in crystals, *Dielectrics and semiconductors* **36**, 3-5.
7. Vlokh, R. (1991) Nonlinear medium polarization with the gradient invariants accounting, *Phys. Stat. Sol. (b)* **168**, k. 47-50.
8. Vlokh, O.G., Crushelnickaya, T.D. (1970) Fourth rank axial tensors and quadratic electrogyration, *Kristallographiya* **15**, 587-589.
9. Chandrasekhar, S. (1961) Optical rotary dispersion of crystals, *Proc. Roy. Soc. (A)* **259**, 531-551.

10. Vlokh, R.O., Pyatak, Yu.A., Skab, I.P. (1988) Acoustogyrational light diffraction in quartz crystals, *Abs. of the 4-th Soviet workshop "Ferroelastics (properties and application)" (Dnipropetrovsk, 1988)*, 186-189.
11. Vlokh, R.O., Pyatak, Yu.A., Skab, I.P. (1989) Acoustogyrational light diffraction in quartz crystals, *Izvestia of Academy of Science of USSR (ser. phys.)* **53**, 1339.
12. Vlokh, R., Skab, I., Kostyrko, M., Guzandrov, A. (1998) The crystallooptics effects in $NaBi(MoO_4)_2$ induced by nonhomogeneous strain, *Abs. IV Ukrainian-Polish Meeting on Phase transitions and Ferroelectric Physics, Dnipropetrovsk (Ukraine), 15-19 June 1998,* 79.
13. Vlokh, R., Kostyrko, M., Skab, I. (1998) Principle and application of crystallo-optical effects induced by inhomogeneous deformation, *Japan J. Appl. Phys.* **37**, 5418-5420.
14. Vlokh, R., Kostyrko, M., Skab, I. (1996) Torsion optical methods and gears to operate the optical radiation and to measure the physical quantities, *Abstr. of 3rd European Conference on Application of Polar Dielectrics (ECAPD-3), Bled (Slovenia), 26-29 August 1996*, 70.
15. Vlokh, R.O., Kostyrko, M.Ye., Skab, I.P. (1997) Indirect rotation of the optical indicatrix under external influences, *Ukrainian Journal of Physics* **47**, 311-313.
16. Vlokh, R.O., Kostyrko, M.Ye., Skab, I.P. (1997) Description of gradient piezogyration and piezooptics caused by twisting and bending, *Kristallographiya* **42**, 1087-1089.
17. Vlokh, R., Kostyrko, M., Skab, I. (1997) The observation of "neutral" birefringence line in $LiNbO_3$ crystals under torsion, *Ferroelectrics* **203**, 113-117.
18. Vlokh, R., Kostyrko, M. (1996) The torsion and bending influence on the optical properties of $LiNbO_3$ crystals, *Abstr. of XXII International School and III Polish-Ukrainian Meeting on Ferroelectrics Physics, Kudova Zdroj (Poland), 16-20 September 1996.*
19. Vlokh, R.O., Kostyrko, M.Ye., Skab, I.P. (1999) Principle and application of crystallooptical effects induced by inhomogeneuos deformation, *Abstr. of 1st Ukrainian Workshop on Ferroelectrics and Related Materials, Lviv (Ukraine), 26-28 August 1999*, 22.
20. Luh, Y.S., Byer, L. (1986) Peculiar properties of domain structure in $LiNbO_3$ crystals, *J. Crystal Growth* **78**, 135.
21. Wang, H., Hu, X., Zhou, W. (1985) The influence of temperature nonuniformity on the optical properties of $LiNbO_3$ crystals, *Japan J. Appl. Phys.* **24**, Suppl. 242-275.
22. Fujishiro, K., Nakamura, T., Uesu, Y. et.al. (1995) The influence of temperature gradients on refringent properties of $LiNbO_3$ crystals, *Ferroelectrics* **168**, 193.
23. Krupych, O.M., Berezhnyi, I.V., Vlokh, O.G. (1998) Automatic Jones matrix imaging polarimeter, *Herald of State Univ. "L'viv Politechnika"* **348**, 3-11.
24. Vlokh, R., Krupych, O., Kostyrko, M., Netolya, V., Trach, I. (2001) Gradient thermooptical effect in $LiNbO_3$ crystals, *Ukrainian J. of Physical Optics* **2**, No. 3, 154-158.

VII.

APPLICATIONS OF COMPLEX MEDIA AND OTHER META-MATERIALS

SELF-ADAPTIVE MATERIAL SYSTEMS *

L. R. ARNAUT
National Physical Laboratory
Center for Electromagnetic and Time Metrology
Queens Road, Teddington TW11 0LW
United Kingdom

Abstract. The concept, realization and properties of self-adaptive material (SAM) systems are presented. Reflection, transmission and radiation characteristics are analyzed using array techniques and effective medium theory. Optimal control techniques are used to yield the transfer function of the SAM controller for a specified cost function.

Key words: multi-functional materials, structured materials, adaptive control.

1. Introduction

Important new developments continue to be made in the field of micro- and nanostructured passive electromagnetic (EM) materials and surfaces. While this progress increases the potential of such 'metamaterials' ever further, inherent and fundamental restrictions exist on their practical performance and applicability. The limitations on available and suitable candidate constituent materials, the fixation of the effective constitutive parameters of the medium once realized, the inevitable tolerances and uncertainties associated with parameters and dimensions of the host medium and inclusions, etc., suggest that one could search for yet more versatile types of EM materials, or new ways to implement them and adjust their properties.

With advances in micro-electronics, signal processing, adaptive antenna methods, etc., adaptive engineered materials become feasible that exhibit unusual or adjustable reflection, transmission, absorption or polarization transformation properties. One possible realization is a hybrid passive/active material system, in which sensors, T/R modules, power hybrids, beamformers, micro-actuators, etc. are integrated with control logic into a single system that presents itself as a single *self-adaptive material* (SAM) system

* This work was supported by the *NPL* Strategic Research Programme (project nr. 9SRPE040).

S. Zouhdi et al. (eds.), Advances in Electromagnetics of Complex Media and Metamaterials, 421–438.

to a distant observer. Its characteristics can be changed according to different needs, variable circumstances or multiple observers separated in space, frequency or time (Fig. 1). Such a system no longer restricts a material to its physico-chemical, geometrical and configurational properties at the time of implementation. Instead, the incorporation of controllers, microsensors and microactuators results in a system with a user-specified response that can be treated as an effective medium. Moreover, the transfer function (i.e., excitation vs. response characteristic) of a SAM is no longer fixed or manually controlled by the user or designer, but automatically adjusted in accordance with the characteristics of the incident wave, so as to yield the desired macroscopic response (object function). This function becomes an integral part of the constitutive description. This concept of a SAM holds the prospect of the ultimate tailored or multi-functional material. Of course, the interest is mainly in the implemention of response functions that are otherwise difficult or impossible to achieve with conventional materials at the wavelengths and field strengths of interest.

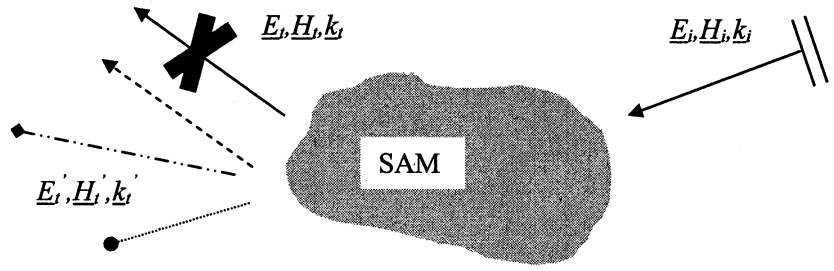

Figure 1. Concept of a self-adaptive material (SAM) system. The naturally scattered wave $(\underline{E}_t, \underline{H}_t, \underline{k}_t)$ (solid outward arrow), for the SAM in its passive state, is suppressed by its controlled active sources. The artificially stimulated EM response $(\underline{E}_t', \underline{H}_t', \underline{k}_t')$ (other outgoing arrows) can be adapted to different observers and is a function of the properties of the incident wave $(\underline{E}_i, \underline{H}_i, \underline{k}_i)$.

Conventional passive materials typically exhibit a linear response for sufficiently weak excitation fields. By combining active and passive inclusions into a single entity, the constitutive properties of the SAM become dependent on the incident field itself. Thus, to the external observer a SAM is a fundamentally nonlinear medium. Such a system has the ability to reduce its local entropy (information contents) [2]. Interpreted in an electromagnetic context, a SAM cannot be a single, homogeneous material, because the latter can only respond to its environment without reducing its information contents, viz., scattering properties. Thus, SAMs are necessarily mixtures of electromagnetically different compounds. As will be shown,

the self-adaptivity is maximally efficient at low frequencies ($kL \ll 1$). This complements passive media, whose ability to transform or condition incident waves based on interaction with a (micro)structured medium is most prominent only at sufficiently high frequencies ($kL \sim 1$).

2. Adaptive control of radiation by pair of sources

2.1. COUPLED SOURCES

Fundamental to SAM operation is the response of a pair of coupled dipole sources. A primary (master) source s generates an 'unwanted' radiated field, e.g., an incident wave excites a Rx antenna (sensor) and scatters part of the incident field. The impressed or induced current or voltage in s is then used to drive a Tx antenna (slave source or actuator a) to yield the desired overall, i.e., combined field (Fig. 2).

To this end, a control and optimization strategy can be formulated by defining a cost function for an EM quantity of interest. This function is then evaluated at a specified location and distance of observation, or across some spatial region of interest. In one important case, the cost function is specified for the radiated power at a given field point or through a spherical surface in the far field of the s/a pair. Other object functions can often also be expressed in the form of the minimization of an energy functional.

2.2. SINGLE DIRECTION OF OBSERVATION

For two small sources of volumes V_α ($\alpha = s, a$) and electric current densities $\underline{J}_\alpha$, which are spaced a distance $\underline{d} = d\underline{1}_x$ apart, the radiated fields follow as $(\underline{E}_\alpha, \underline{H}_\alpha) = \int\int\int_V (\underline{\underline{G}}_{ee_\alpha}, \underline{\underline{G}}_{me_\alpha}) \cdot \underline{J}_\alpha \mathrm{d}V$.

Consider first the minimization of the radiated power in a single direction, at arbitrary distance from the sources. The complex Poynting vector $\underline{S} = (\underline{E}_a + \underline{E}_s) \times (\underline{H}_a + \underline{H}_s)^*$ for the instantaneous power of the pair is

$$\underline{S} = \int\int\int_{V_a+V_s} \left[\underline{J}_a^T \;\; \underline{J}_s^T \right] \cdot \begin{bmatrix} \underline{\underline{G}}_{ee_a} \\ \underline{\underline{G}}_{ee_s} \end{bmatrix} \mathrm{d}V' \times \int\int\int_{V_a+V_s} \left[\underline{\underline{G}}^*_{me_a} \;\; \underline{\underline{G}}^*_{me_s} \right] \cdot \begin{bmatrix} \underline{J}_a^* \\ \underline{J}_s^* \end{bmatrix} \mathrm{d}V', \tag{1}$$

where the superscripts T and $*$ denote transposition and complex conjugation, respectively. For dipole radiation, (1) can be re-expressed as

$$\underline{S} = \left[\underline{p}_a^T \;\; \underline{p}_s^T \right] \cdot \begin{bmatrix} \underline{\underline{A}}_{aa} & \underline{\underline{A}}_{as} \\ \underline{\underline{A}}_{sa} & \underline{\underline{A}}_{ss} \end{bmatrix} \cdot \begin{bmatrix} \underline{p}_a^* \\ \underline{p}_s^* \end{bmatrix}, \tag{2}$$

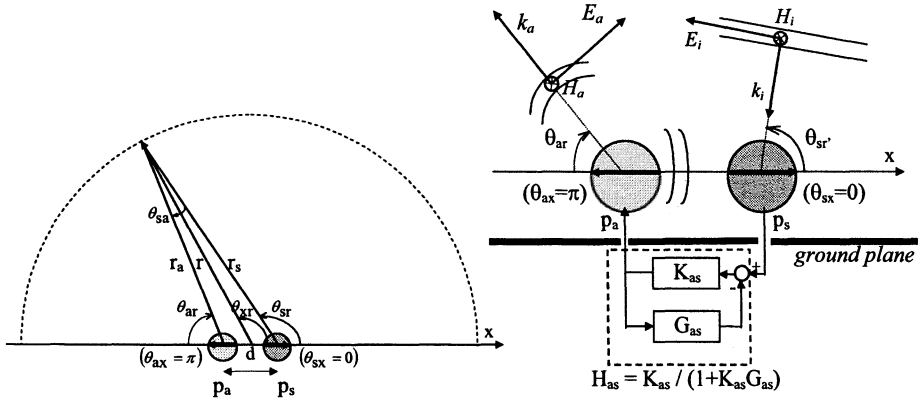

Figure 2. (a) Adaptive control of radiation by primary (master) source s by secondary (slave) source a, with relative source spacing d and observation point at distance r; (b) adaptive control of scattering.

with $\underline{\underline{\underline{A}}}_{\alpha\beta} \triangleq \underline{\underline{\underline{G}}}^T_{ee_\alpha} \times \underline{\underline{\underline{G}}}^*_{me_\beta}$ as defined in [1]. Instead of directly minimizing $S \equiv ||\underline{\underline{S}}||$, it is generally easier to minimize

$$S^2 = \underline{p}_s^T \cdot \underline{\underline{\underline{B}}}_{ss} \cdot \underline{p}_s^* + \underline{p}_s^T \cdot \underline{\underline{\underline{B}}}_{sa} \cdot \underline{p}_a^* + \underline{p}_a^T \cdot \underline{\underline{\underline{B}}}_{as} \cdot \underline{p}_s^* + \underline{p}_a^T \cdot \underline{\underline{\underline{B}}}_{aa} \cdot \underline{p}_a^*, \tag{3}$$

where

$$\begin{aligned} \underline{\underline{\underline{B}}}_{\alpha\beta} = {} & (\underline{\underline{\underline{A}}}^\dagger_{s\alpha} \cdot \underline{p}_s^*) \cdot (\underline{p}_s^T \cdot \underline{\underline{\underline{A}}}_{s\beta}) + (\underline{\underline{\underline{A}}}^\dagger_{s\alpha} \cdot \underline{p}_s^*) \cdot (\underline{p}_a^T \cdot \underline{\underline{\underline{A}}}_{a\beta}) + \\ & (\underline{\underline{\underline{A}}}^\dagger_{a\alpha} \cdot \underline{p}_a^*) \cdot (\underline{p}_s^T \cdot \underline{\underline{\underline{A}}}_{s\beta}) + (\underline{\underline{\underline{A}}}^\dagger_{a\alpha} \cdot \underline{p}_a^*) \cdot (\underline{p}_a^T \cdot \underline{\underline{\underline{A}}}_{a\beta}), \end{aligned} \tag{4}$$

$$\begin{aligned} \underline{\underline{\underline{A}}}_{\alpha\beta} = {} & \frac{\exp[-jk(r_\alpha - r_\beta)]}{(4\pi)^2 (r_\alpha r_\beta)^3 \epsilon_o \sqrt{\mu_o \epsilon_o}} [jkr_\beta(1 - jkr_\beta)] \times \\ & \left\{ \left[3(1 + jkr_\alpha) + (jkr_\alpha)^2 \right] \underline{\underline{\underline{X}}}_{\alpha\beta} - \left[1 + jkr_\alpha + (jkr_\alpha)^2 \right] \underline{\underline{\underline{Y}}}_{\beta} \right\}, \end{aligned} \tag{5}$$

$$\underline{\underline{\underline{X}}}_{\alpha\beta} \triangleq \underline{1}_{r_\alpha} \underline{1}_{r_\beta} \underline{1}_{r_\alpha} - (\underline{1}_{r_\alpha} \cdot \underline{1}_{r_\beta}) \sum_{\gamma=x,y,z} \underline{1}_{r_\alpha} \underline{1}_\gamma \underline{1}_\gamma, \tag{6}$$

$$\underline{\underline{\underline{Y}}}_{\beta} \triangleq \sum_{\gamma=x,y,z} \left[\underline{1}_\gamma \underline{1}_{r_\beta} \underline{1}_\gamma - (\underline{1}_\gamma \cdot \underline{1}_{r_\beta}) \sum_{\delta=x,y,z} \underline{1}_\gamma \underline{1}_\delta \underline{1}_\delta \right], \tag{7}$$

in which $\underline{1}_\gamma$ and $\underline{1}_\delta$ are Cartesian unit vectors. For given $\underline{p}_s$ and $\underline{1}_a$, (3) is quadrilinear in the complex control variable $p_a = |p_a| \exp(j\phi_a)$. Local and absolute extremes of S^2 are reached for the roots $p_{a,\text{opt}}$ of $\partial S^2/\partial p_a = 0$. For far-field radiation observed in the direction of $\underline{r}$ with arbitrary θ_{ar}, coplanar $\underline{p}_s$ and $\underline{p}_a$ located at $\underline{r}_s$ and $\underline{r}_a$, it follows after calculation that the magnitude W of $\underline{W} = (1/2)\Re[\underline{E} \times \underline{H}^*]$ is minimum provided

$$p_{a,\text{opt}} = -\frac{A_{sa}}{A_{aa}}\, p_s = -\frac{\sin\theta_{sr}}{\sin\theta_{ar}} \exp(-jkd\cos\theta_{xr}) p_s \triangleq H_{as,\text{opt}} p_s, \qquad (8)$$

where $\cos\theta_{uv} \triangleq \underline{1}_u \cdot \underline{1}_v$ and $\theta_{as} \triangleq \theta_{ar} + \theta_{rs}$. The oriented angles θ_{uv} are measured from $\underline{1}_u$ to $\underline{1}_v$. The reference direction $\underline{1}_x$ is taken as being parallel to the line connecting the centers of both dipoles and is directed from a to s. The mutual coupling between s and a, which is of paramount importance, can be explicitly taken into account [1].

The transfer function $H_{as,\text{opt}}$ in (8), which links p_s with p_a (Fig. 3a), specifies a two-stage optimum serial or parallel PID controller $H_{as,\text{opt}}(\sigma) = K_c(\sigma)(1 + \sigma\tau_1)^2/(1 + \sigma\tau_2)^2$, where $\sigma = j\omega$ and $\tau_1 < \tau_2$ or $\tau_1 > \tau_2$ for a low-pass or high-pass implementation, respectively, and $K_c(0) = -\sin\theta_{sr}/\sin\theta_{ar}$. For parallel $\underline{1}_a$ and $\underline{1}_s$, (8) defines two nearly anti-parallel complex vectors, i.e., two identical polarization ellipses whose phasors are separated in phase by $kd\cos\theta_{xr} + \pi$. Fig. 4a shows $|H_{as,\text{opt}}|$ as a function of the orientations of the dipoles with respect to $\underline{1}_x$. The phase of $H_{as,\text{opt}}$ is near 180 deg for all angles of orientation. As expected, $H_{as,\text{opt}} \approx -1$ for $\theta_{ax} = \theta_{sx}$ and for $\theta_{ax} + \theta_{sx} = \pi$.

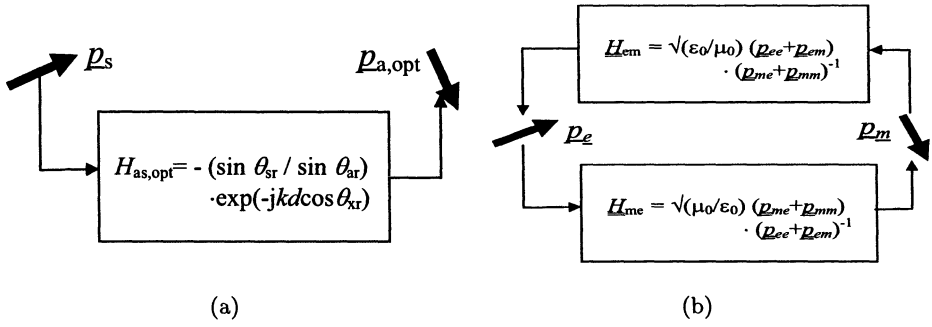

Figure 3. (a) Transfer function between pair of linked dipoles; (b) bianisotropic particle modelled as an intrinsically coupled pair of dipoles, using forward and backward coupling dyadics $\underline{\underline{H}}_{me}$ and $\underline{\underline{H}}_{em}$.

The minimum cumulative radiated power $W_{\min}(\underline{r})$, as observed *in the direction of observation* $\underline{1}_r$ is found to be zero, regardless of the values of θ_{ar}, θ_{sr}, kd and θ_{xr}, although the $\underline{p}_{a,\text{opt}}$ required to achieve this minimum

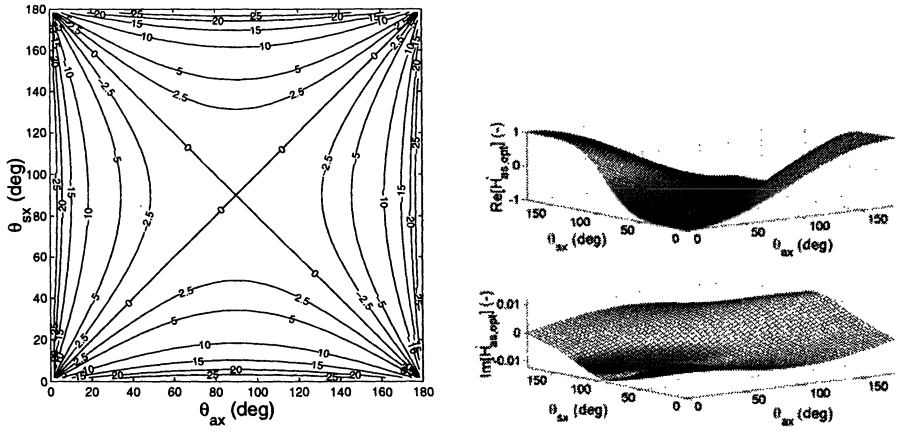

(a) (b)

Figure 4. (a) Magnitude of transfer function $|H_{as,\mathrm{opt}}|$ (dB), optimized for a single direction of observation, as a function of θ_{ax} and θ_{sx}; (b) transfer function $H'_{as,\mathrm{opt}}$ (linear) for total integrated radiated power as a function of θ_{ax} and θ_{sx} with $kd = 0.02$.

does depend on each one of these quantities. Thus, perfect active field cancellation (zero total radiated power) is possible for the far field in an arbitrary *single* direction.

For near-field and boundary-zone fields, the optimization is considerably more complex. For the special case of isotropic sensors and actuators, minimization of the near-field power in a single direction is now achieved for

$$\underline{p}_{a,\mathrm{opt}} = -(3\underline{1}_{r_a}\underline{1}_{r_a} - \underline{\underline{I}})^{-1} \cdot (3\underline{1}_{r_s}\underline{1}_{r_s} - \underline{\underline{I}}) \exp(-jkd)\underline{p}_s. \tag{9}$$

Parenthetically, the use of transfer functions to describe material coupling effects is not limited to the extrinsic (explicit) coupling of separate active and passive sources. For example, for plane-wave excitation (i.e., $\underline{E} = \sqrt{\mu_o/\epsilon_o}\underline{H}$) of a single bianisotropic particle, which is characterized in the dipolarizability approximation by

$$\underline{p}_e = \epsilon_o \underline{\underline{p}}_{ee} \cdot \underline{E} + \sqrt{\mu_o \epsilon_o}\, \underline{\underline{p}}_{em} \cdot \underline{H}, \quad \underline{p}_m = \sqrt{\mu_o \epsilon_o}\, \underline{\underline{p}}_{me} \cdot \underline{E} + \mu_o \underline{\underline{p}}_{mm} \cdot \underline{H}, \tag{10}$$

the intrinsic magneto-electric coupling can be formally described by dyadics $\underline{\underline{H}}_{me}$ and $\underline{\underline{H}}_{em}$ specified in Fig. 3b. In this case, however, the description is purely formal because the fields, rather than $\underline{p}_m$ or $\underline{p}_e$, are the true sources of excitation for $\underline{p}_e$ or $\underline{p}_m$, respectively.

2.3. TOTAL INTEGRATED RADIATED POWER

Without additional precautions, the decrease of radiated power in one direction $\underline{1}_r$ usually comes at the expense of an increase in another one. This is in general undesirable because it reduces the overall self-adaptivity and, hence, the SAM efficiency. However, it is possible to obtain a reduction of radiated power across an entire user-specified solid angle. For example, for the 2D problem of a circular boundary of observation of radius $r \gg d$ in the plane of two collinear dipoles ($\theta_{ax} = \theta_{sx} = 0$ or π) centered around $(\underline{r}_a + \underline{r}_s)/2$ (Fig. 2a), the total power crossing this boundary and associated transfer function are obtained as

$$\frac{W'_{\text{tot,min}}}{W_s} = 1 + 9\left[\frac{j_1(kd)}{kd}\right]^2 = \frac{(kd)^2}{5} - \frac{(kd)^4}{100} + \ldots, \tag{11}$$

$$H'_{as,\text{opt}} = -3\frac{j_1(kd)}{kd} = -\left[1 - \frac{(kd)^2}{10} + \ldots\right], \tag{12}$$

where $j_1(x) = \sin(x)/x^2 - \cos(x)/x$ is the spherical Bessel function of the first kind and first order. Thus, to leading order, a quadratic dependence of $W'_{\text{tot,min}}/W_s$ on kd is found. Parallel arrangements constitute, in effect, quadrupole SAMs. Unlike strictly parallel dipoles (doublets), the collinear arrangement does not produce an additional magnetic moment and, hence, yields a lower total radiated power. For either case, zero backscattering in the retro-direction occurs.

Fig. 4b shows $H'_{as,\text{opt}}(\theta_{ax},\theta_{sx})$ for $kd = 0.02$. On a linear scale, small deviations from (anti-)parallelism are seen to be not critical to the optimal tuning of $\Re[H'_{as,\text{opt}}]$. Fig. 5a shows the associated $W'_{\text{tot,min}}(\theta_{ax},\theta_{sx})/W_s$. The superiority of strictly parallel and anti-parallel dipoles, and the worst case of perpendicular dipoles are clearly noticed. The near-minima for $\theta_{sx} = \theta_{ax}$ are seen to be stable with respect to misalignment errors for the dipoles. Plotting $H'_{as,\text{opt}}(kd)$ for a few relative orientations shows that most (although not all) cases require the optimum controller to steer in anti-phase when $kd \to 0$ [$H'_{as,\text{opt}}(kd) \to -1$]. As kd increases, the controller gradually switches off in the mean [$|H'_{as,\text{opt}}(kd)| \to 0$], i.e., active control becomes increasingly ineffective at shorter wavelengths. Fig. 5b shows $W'_{\text{tot,min}}(kd)/W_s$. For $kd \to 0$, collinear parallel dipoles yield a power reduction by a factor 3 (~ 4.77 dB) better than strictly parallel dipoles.

2.4. OMNIDIRECTIONAL POWER REDUCTION

A reduction of radiated power in a chosen direction should preferably not increase the power radiated in other directions. For an arbitrary far-field

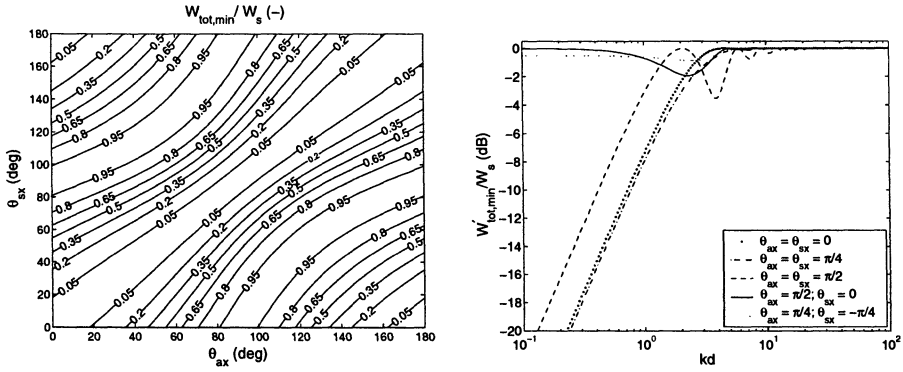

(a) (b)

Figure 5. Normalized density of total radiated power $W'_{\text{tot,min}}/W_s$ associated with $H'_{as,\text{opt}}$ (a) as a function of θ_{ax}, θ_{sx} and (b) as a function of kd.

location $\underline{r}' = r'\underline{1}_{r'}$ relative to a primary source whose radiation has been minimized for the single direction $\underline{1}_r$, it can be shown [1] that the criterion $0 \leq kd < kd_{\max} = (1/2)\cos^{-1}[\sin\theta_{sr}/(2\sin\theta_{ar})]$ guarantees for such an increase not to occur for *any* direction away from the optimization direction (omnidirectional power reduction). For parallel dipoles, this limit is independent of the relative direction of $\underline{1}_r$: in this case, $0 \leq kd < \pi/6$. Then, the maximum power ratio for radiation in any direction, viz., $2[1-\cos(2kd)]$, is smaller than 1 and decreasing for increasing kd. The power is increasingly being diverted via the actuator towards the T/R module of the SAM, or converted to reactive power.

3. Arrays of interleaved sources

3.1. ADAPTIVE CONTROL FOR SAM ARRAYS

The results for a single source pair can be extended to an arbitrary configuration of multiple sources. For N_α sources $\underline{p}_{\alpha_i}$, each type α forming source vectors $\left[\underline{p}_\alpha\right]$, the far-field power radiated in a single direction is minimized for $\left[\underline{p}_{a,\text{opt}}\right] = -\left[\underline{\underline{A}}_{aa}\right]^{-1} \cdot \left[\underline{\underline{A}}_{sa}\right] \cdot \left[\underline{p}_s\right]$, where $\left[\underline{\underline{A}}_{\alpha\beta}\right]$ is an $N_\alpha \times N_\beta$-matrix of tryads $\underline{\underline{A}}_{\alpha_i,\beta_j}$ $(i = 1,\ldots,N_\alpha,\ j = 1,\ldots,N_\beta,\ \alpha,\beta = s \text{ or } a)$.

By configuring the s and a elements in a spatially symmetric way, equal flexibility is achieved in scanning and beamforming (wave conditioning) for both incident and radiated waves, allowing for a reciprocal SAM. To this end, the lay-out can be chosen, for example, as a 2D array of size $2M \times 2N$

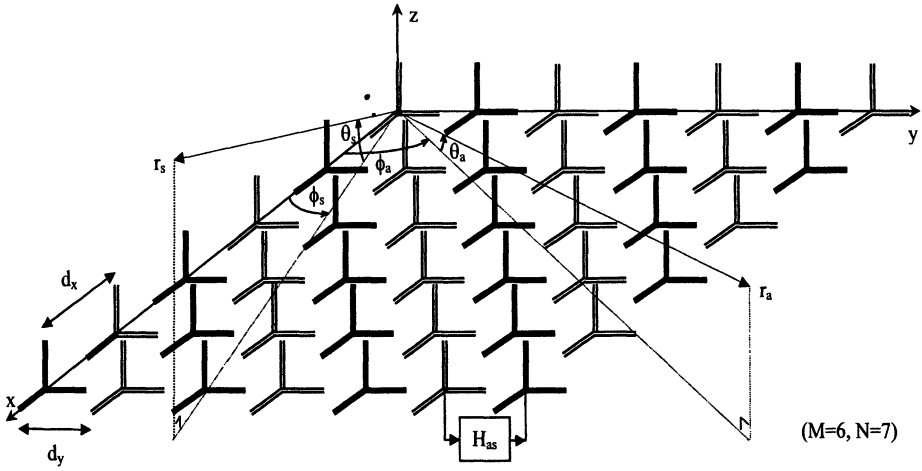

Figure 6. Planar chequered array of interleaved primary and secondary sources.

having a 'chessboard' pattern, in which a 'black' subarray of active elements a is interleaved with a 'white' subarray of sensors s (Fig. 6).

If $l_s, l_a \not\ll d$ then details of the current distribution along the elements affect the mutual coupling. If $l_s, l_a \ll d < k^{-1}$ then the SAM operates as an effective medium in quasi-static regime. In view of the results for a source pair, this ensures efficient control but inefficient radiation, unless element loading is introduced. Based on the single-element fields $\underline{E}_\alpha$, the total field for the actuator array is

$$\underline{E}_{a,\mathrm{tot}} = \frac{\sin(MkT_{ax}d_x)}{\sin(kT_{ax}d_x)} \frac{\sin(NkT_{ay}d_y)}{\sin(kT_{ay}d_y)} \{1 + \exp[jk(T_{ax}d_x + T_{ay}d_y)]\} \times$$
$$\exp\left[jk\left(T_{ax}(M-1)d_x + T_{ay}(N-1)d_y\right)\right] \underline{E}_a \triangleq f_a(T_{ax}, T_{ay})\underline{E}_a. \quad (13)$$

The corresponding expression for $\underline{E}_{s,\mathrm{tot}} = f_s(T_{sx}, T_{sy})\underline{E}_s$ follows by replacing $T_{ax,y}$ by $T_{sx,y}$ and $\{1 + \exp[jk(T_{ax}d_x + T_{ay}d_y)]\}$ by $[\exp(jkT_{sx}d_x) + \exp(jkT_{sy}d_y)]$ in (13), respectively. The direction cosines $T_{\alpha x}$ and $T_{\alpha y}$ are taken with reference to the 'look' directions (i.e., the axes of the main beams for the s and a arrays), and linear phase tapers $\varphi_{\alpha x}$ and $\varphi_{\alpha y}$ control these directions.

The far-field radiated power in a direction defined by θ_{xr} is minimized by a controller now defined by

$$\left[\underline{p}_{a,\mathrm{opt}}\right] = -\frac{f_s^*}{f_a^*}\frac{A_{sa}}{A_{aa}}\left[\underline{p}_s\right] \triangleq H_{as,\mathrm{opt,array}}\left[\underline{p}_s\right]. \quad (14)$$

The associated minimum power is $|f_s|^2$ times the value of $W_{\text{min,pair}}$ for a source pair. For $kd_x, kd_y \ll 1$:

$$W_{\text{min,array}} = \frac{1}{2}\left(A_{ss} - A_{sa}A_{as}/A_{aa}\right)|f_s p_s|^2 \approx (MN)^2\left[4 + (kT_{sx}d_x + kT_{sy}d_y)^2\right]\operatorname{sinc}^2(MkT_{sx}d_x)\operatorname{sinc}^2(NkT_{sy}d_y)W_{\text{min,pair}}. \quad (15)$$

3.2. SPECTRAL-DOMAIN GREEN FUNCTION

If the spatial distribution of the current $\underline{I}_{00}(l) \equiv I_{00}(l)\underline{1}_l$ in the reference sensor element at $x = y = 0$ is accurately known, then the radiated field can be calculated from the vector potential of the individual active and passive arrays [3, 4]. For the chequered configuration, the field scattered and radiated by both subarrays is thus obtained as

$$\begin{aligned}\underline{E}_t(\underline{r}) &= \int_0^l \frac{Z_0 \exp\left[-jk\left[\underline{r} - \underline{r}''(l)\right]\cdot\underline{1}_{s_\pm}\right]}{2d_x d_y s_z}\left\{\left(\underline{1}_{s_\pm}\underline{1}_{s_\pm} - \underline{\underline{I}}\right) + \right. \\ &\qquad \left.\mathcal{H}_{as}\left(\underline{1}'_{s_\pm}\underline{1}'_{s_\pm} - \underline{\underline{I}}\right)\right\}\cdot\underline{I}_{00}[\underline{r}''(l)]\mathrm{d}l \\ &= \left[\underline{\underline{I}} + \mathcal{H}_{as}\left(\underline{1}'_{s_\pm}\underline{1}'_{s_\pm} - \underline{\underline{I}}\right)\cdot\left(\underline{1}_{s_\pm}\underline{1}_{s_\pm} - \underline{\underline{I}}\right)^{-1}\right]\cdot\underline{E}_s(\underline{r}), \end{aligned} \quad (16)$$

with

$$\mathcal{H}_{as} \triangleq (s_z/s'_z)H_{as}\exp(jkd_x s'_x)\exp\left[-jk\underline{r}\cdot(\underline{1}'_{s_\pm} - \underline{1}_{s_\pm})\right], \quad (17)$$

where $\underline{1}^{(\prime)}_{s\pm} = (s_x^{(\prime)}, s_y^{(\prime)}, \pm s_z^{(\prime)})$ is the unit vector in the forward (upper sign) or specular (lower sign) scattering direction w.r.t. the incident wave for the subarray of sources s (unprimed) or a (primed). Equation (17) characterizes the SAM electric-electric Green dyadic function $\underline{\underline{G}}^{\text{SAM}}_{ee}(\underline{r}|\underline{r}'')$ through $\underline{E}_t(\underline{r}) = \int_0^l \underline{\underline{G}}^{\text{SAM}}_{ee}(\underline{r}|\underline{r}'')\cdot\underline{I}_{00}[\underline{r}''(l)]\mathrm{d}l$, and $\underline{\underline{G}}^{\text{SAM}}_{me}(\underline{r}|\underline{r}'')$ follows in a similar manner. Thus, the array control is accounted for by the field coupling factor $\mathcal{H}_{as}$ between the Rx and Tx subarrays. Special cases include the control of radiation in the forward direction ($\underline{1}'_s = \underline{1}_{s_+}$), retro-direction ($\underline{1}'_s = -\underline{1}_{s_+}$) and specular direction ($\underline{1}'_s = \underline{1}_{s_-}$).

3.3. SAM IMPEDANCE AND EQUIVALENT PERMITTIVITY

The self-impedance Z_A of the SAM array for the main Rx and Tx beams with no grating lobes is

$$Z_A = \frac{Z_0\mathcal{P}\mathcal{P}^t\,\underline{1}_l\cdot\left[\left(\underline{\underline{I}} - \underline{1}_{s_\pm}\underline{1}_{s_\pm}\right) + \mathcal{H}^0_{as}\left(\underline{\underline{I}} - \underline{1}'_{s_\pm}\underline{1}'_{s_\pm}\right)\right]\cdot\underline{1}_l}{2d_x d_y s_z}, \quad (18)$$

where $\mathcal{H}_{as}^{0} \equiv \mathcal{H}_{as}^{0'} - j\mathcal{H}_{as}^{0''} \triangleq \mathcal{H}_{as}(|\underline{r}| = 0)$ and Z_s is the impedance of the s subarray. Equation (18) can be written as $Z_A \triangleq Z_s(1 + \mathcal{K}_{as})$, where

$$\mathcal{K}_{as} = \mathcal{H}_{as}\underline{1}_l \cdot \left(\underline{\underline{I}} - \underline{1}'_{s_\pm}\underline{1}'_{s_\pm}\right) \cdot \left(\underline{\underline{I}} - \underline{1}_{s_\pm}\underline{1}_{s_\pm}\right)^{-1} \cdot \underline{1}_l \tag{19}$$

is a coupling factor between both subarrays which depends on their respective 'look' directions. The current shape factors $\mathcal{P}^{(t)} \triangleq I_{00}^{-1}(\underline{r}_0) \int_L I_{00}^{(t)}(l)\mathrm{d}l$ depend on the details of the current distribution along the array elements in question, for the Rx (Tx) mode [4]. For nonmagnetic homogenizable SAM arrays, (18) can be formally equated to $\sqrt{\mu_o/(\epsilon_o\epsilon_r)}$ for $z < 0$, whence the equivalent refractive index of the SAM is

$$\sqrt{\epsilon_r} = \frac{2d_x d_y s_z}{\mathcal{P}\mathcal{P}^t\, \underline{1}_l \cdot \left[\left(\underline{\underline{I}} - \underline{1}_{s_\pm}\underline{1}_{s_\pm}\right) + \mathcal{H}_{as}^{0}\left(\underline{\underline{I}} - \underline{1}'_{s_\pm}\underline{1}'_{s_\pm}\right)\right] \cdot \underline{1}_l}. \tag{20}$$

For retro-radiation and specular radiation, assuming x-directed linear elements, we have $Z_A = Z_0\mathcal{P}\mathcal{P}^t(1 - s_x^2)(1 + \mathcal{H}_{as}^{0})/(2d_x d_y s_z)$ and

$$\epsilon_r \equiv \epsilon_r' - j\epsilon_r'' = \frac{(2d_x d_y s_z)^2 \exp\left\{j2\tan^{-1}\left[\mathcal{H}_{as}^{0''}/\left(1 + \mathcal{H}_{as}^{0'}\right)\right]\right\}}{\left(\mathcal{P}\mathcal{P}^t\right)^2 (1 - s_x^2)^2 \left[\left(1 + \mathcal{H}_{as}^{0'}\right)^2 + \left(\mathcal{H}_{as}^{0''}\right)^2\right]}. \tag{21}$$

For collinear $\underline{p}_s$ and $\underline{p}_a$, we obtain for (8) $H_{as} = -\exp(-jkd_x s_x \sin\theta_{nr})$ $= -\exp\left(-jkd_x \sin\theta_{nr}\cos\phi_{nr}\right)$. Consequently, for retro-radiation, $\mathcal{H}_{as}^{0} = -H_{as}\exp(-jkd_x s_x) = \exp[-jkd_x s_x(1 + \sin\theta_{nr}\cos\phi_{nr})]$, and for specular radiation, $\mathcal{H}_{as}^{0} = -H_{as}\exp(jkd_x s_x)$.

3.4. SAM RADIATION AND REFLECTION COEFFICIENTS

By expressing the excitation of the s array in terms of the incident field $\underline{E}_i$ instead of the induced current I_{00}, the vector radiation[1] coefficient $\underline{E}_t/E_i$ of the array can be calculated based on (16). In the Appendix, the coefficient of specular reflection for passive arrays [4] is generalized to radiation and scattering by hybrid active/passive arrays. This can be done for arbitrary directions of observation in the principal planes. In the absence of adaptive control [$H_{as} = +\exp(jkd)$], the radiated fields are the usual reflected (scattered) fields. For retro-radiation ($\underline{1}'_s = -\underline{1}_s$, i.e., $\underline{1}'_\perp = -\underline{1}_\perp$, $\underline{1}'_\parallel = +\underline{1}_\parallel$):

$$\underline{E}_t(\underline{r}) = -\frac{Z_0\left(1 + \mathcal{H}_{as}\right)\exp\left(-jk\underline{r}\cdot\underline{1}_s\right)}{2d_x d_y s_z(Z_A + Z_L)} \times$$

[1] Since space waves can be radiated by SAMs in any direction, not just in specular direction, the term 'radiation coefficient' is introduced here, as a generalization of the notions of reflection and transmission coefficients.

$$\Big[(1-\mathcal{H}_{as})\,E_{i,\perp}\mathcal{P}_\perp\mathcal{P}_\perp^t\underline{1}_\perp + (1-\mathcal{H}_{as})\,E_{i,\perp}\mathcal{P}_\perp\mathcal{P}_\parallel^t\underline{1}_\parallel$$
$$+ (1+\mathcal{H}_{as})\,E_{i,\parallel}\mathcal{P}_\parallel\mathcal{P}_\perp^t\underline{1}_\perp + (1+\mathcal{H}_{as})\,E_{i,\parallel}\mathcal{P}_\parallel\mathcal{P}_\parallel^t\underline{1}_\parallel\Big]. \qquad (22)$$

In this case, the retro-reflection matrix is

$$\begin{bmatrix} r_{\perp,\perp} & r_{\perp,\parallel} \\ r_{\parallel,\perp} & r_{\parallel,\parallel} \end{bmatrix} = -\frac{Z_0\,(1+\mathcal{H}_{as})\,\mathcal{P}\mathcal{P}^t}{2d_xd_ys_z(Z_A+Z_L)} \times$$
$$\begin{bmatrix} (1-\mathcal{H}_{as})\,(\underline{1}_\perp\cdot\underline{1}_l)^2 & (1+\mathcal{H}_{as})\,(\underline{1}_\perp\cdot\underline{1}_l)(\underline{1}_\parallel\cdot\underline{1}_l) \\ (1-\mathcal{H}_{as})\,(\underline{1}_\perp\cdot\underline{1}_l)(\underline{1}_\parallel\cdot\underline{1}_l) & (1+\mathcal{H}_{as})\,(\underline{1}_\parallel\cdot\underline{1}_l)^2 \end{bmatrix}. \qquad (23)$$

For TE incidence in the principal plane ($\underline{1}_\perp\cdot\underline{1}_l=\pm1$, $\underline{1}_\parallel\cdot\underline{1}_l=0$), at an angle of incidence $\theta_i=\cos^{-1}(s_z)$:

$$r_{\perp,\perp} = -\frac{Z_0\,(1-\mathcal{H}_{as}^2)\,\mathcal{P}\mathcal{P}^t}{2d_xd_y(Z_A+Z_L)\cos\theta_i}, \qquad (24)$$

whereas for TM polarization:

$$r_{\parallel,\parallel} = -\frac{Z_0\,(1+\mathcal{H}_{as})^2\,\mathcal{P}\mathcal{P}^t(\underline{1}_\parallel\cdot\underline{1}_l)^2}{2d_xd_y(Z_A+Z_L)\cos\theta_i}. \qquad (25)$$

For forward radiation ($\underline{1}'_s=+\underline{1}_s$), the coefficients $(1-\mathcal{H}_{as})$ in (23) are to be replaced by $(1+\mathcal{H}_{as})$.

3.5. NUMERICAL RESULTS

Fig. 7 shows the dependencies of the TE reflection coefficient of an infinite chequered SAM array on s/a-spacing kd, angle of incidence θ_i, and element load impedance Z_L, all for the case of specular radiation. Strictly parallel interconnections are confirmed to yield slightly larger magnitudes of the reflection coefficients compared to collinear arrangements, on average. Element loading profoundly affects the obtainable minimum reflected power. Further analytical and numerical results are given in [1].

4. Adaptive control of scattering

If the primary source s is one of scattering of an external incident plane wave, this wave is usually incident onto a as well, causing additional parasitic scattering and mutual coupling which must be accounted for. In general, $\underline{p}_{a,\mathrm{tot}}$ consists of several contributions, viz., $\underline{p}_{a,\mathrm{ctl}}$ impressed by the controller, $\underline{p}_{a,\mathrm{inc}}$ induced by the plane wave and $\underline{p}_{a,s}$ induced by the nearby sensors (s/a mutual coupling): $\underline{p}_{a,\mathrm{tot}}=\underline{p}_{a,\mathrm{ctl}}+\underline{p}_{a,\mathrm{inc}}+\underline{p}_{a,s}$. Likewise, $\underline{p}_{s,\mathrm{tot}}$

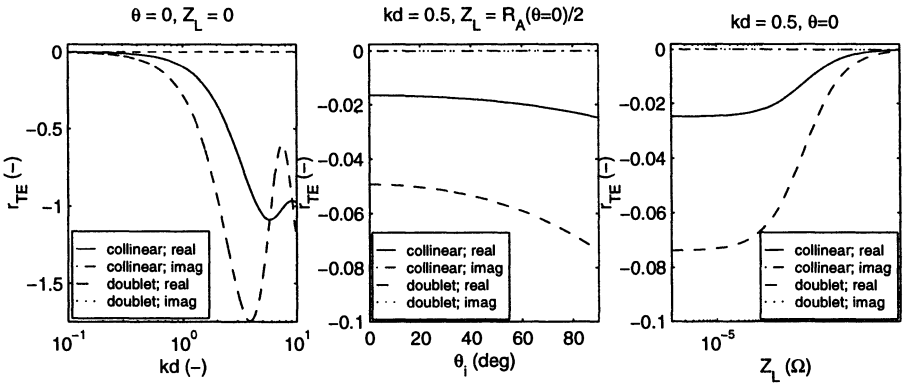

Figure 7. TE reflection coefficient for specular radiation off chequered sensor/actuator array, for collinear and parallel interconnections, (a) as a function of spacing kd for $0.1 \leq kd \leq 10$, $Z_L = 0$, $\theta_i = 0$; (b) as a function of incidence angle θ_i for $0 \leq \theta_i < \pi/2$, $kd = 0.5$, $Z_L = R_A/2$; and (c) as a function of element load impedance Z_L for $10^{-6}\,\Omega \leq Z_L \leq 10^{-1}\,\Omega$, $kd = 0.5$, $\theta_i = 0$.

consists of three contributions, although an impressed source moment $\underline{p}_{s,\mathrm{src}}$ is usually absent in the adaptive control of scattering here considered, i.e., $\underline{p}_{s,\mathrm{tot}} = \underline{p}_{s,\mathrm{inc}} + \underline{p}_{s,a}$. Since $||\underline{p}_s|| \ll ||\underline{p}_a||$ in SAMs, the contribution of $\underline{p}_{a,s}$ is usually negligible, but $\underline{p}_{s,a}$ can be significant. If $\underline{p}_s$ and $\underline{p}_a$ are blind to one another, then

$$\begin{aligned}\underline{p}_{a,\mathrm{ctl}} &= -\frac{\sin\theta_{sr}}{\sin\theta_{ar}} \exp\left(-jkd\cos\theta_{xr}\right) \times \\ &\qquad \left\{1 + \frac{\sin\theta_{ar}}{\sin\theta_{sr}} \frac{\sin\theta_{ar'}}{\sin\theta_{sr'}} \exp\left[jkd\left(\cos\theta_{xr} + \cos\theta_{xr'}\right)\right]\right\} \underline{p}_{s,\mathrm{inc}} \\ &\triangleq -\frac{\sin\theta_{sr}}{\sin\theta_{ar}} \exp(-jkd\cos\theta_{xr})\underline{p}_{s'}, \end{aligned} \tag{26}$$

which may be interpreted as an actively controlled perturbed scatterer s', with nonlocal perturbation due to the presence of the nearby source a. The associated minimum radiated power in the direction $\underline{1}_r$ is again zero, as for uncoupled sources. For zero retro-reflection ($\theta_{xr'} = \theta_{xr}$),

$$\underline{p}_{a,\mathrm{ctl}} = -\left[\frac{\sin\theta_{sr}}{\sin\theta_{ar}} \exp\left(-jkd\cos\theta_{xr}\right) + \frac{\sin\theta_{ar}}{\sin\theta_{sr}} \exp\left(jkd\cos\theta_{xr'}\right)\right] p_{s,\mathrm{inc}}, \tag{27}$$

which for parallel dipoles further reduces to $p_{a,\mathrm{ctl}} = -2\cos\left(kd\cos\theta_{xr}\right)\underline{p}_{s,\mathrm{inc}}$, i.e., a purely real $H_{as,\mathrm{sc}}$. For zero specular reflection ($\theta_{xr'} = \pi - \theta_{xr}$),

$$\underline{p}_{a,\mathrm{ctl}} = -\left(\frac{\sin\theta_{sr}}{\sin\theta_{ar}} + \frac{\sin\theta_{ar'}}{\sin\theta_{sr'}}\right) \exp\left(jkd\cos\theta_{xr}\right)\underline{p}_{s,\mathrm{inc}}. \tag{28}$$

If the dipoles are parallel, then $p_{a,\mathrm{ctl}} = -2\exp(jkd\cos\theta_{xr})\,p_{s,\mathrm{inc}}$.

Fig. 8 shows the optimum $H_{as,\mathrm{sc}}(\theta_{xr}, \theta_{xr'})$ as defined by (26) for collinear dipoles ($\theta_{ar^{(\prime)}} = \theta_{sr^{(\prime)}}$) with $kd = 5\pi/4$. Both its in-phase and quadrature components now maximally vary between -2 and $+2$, i.e., covering double the range of $H_{as,\mathrm{opt}}$ for a single radiating source (cf. Fig. 5), because the controller must now account for scattering by both s and a.

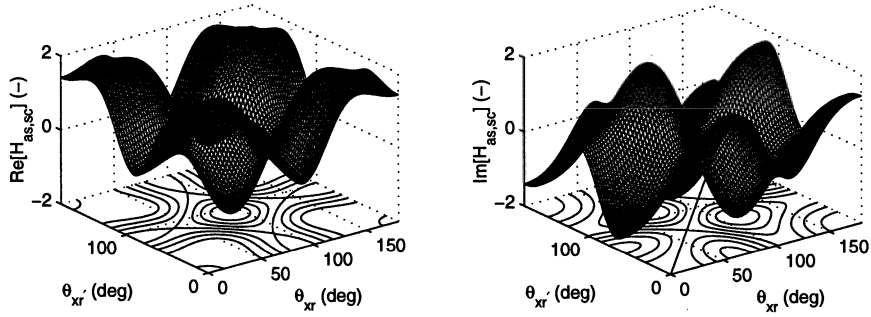

Figure 8. Real and imaginary parts of optimum control transfer function $H_{as,\mathrm{sc}}$ for adaptive control of scattering as a function of θ_{xr} and $\theta_{xr'}$ for parallel dipoles ($\theta_{ar^{(\prime)}} = \theta_{sr^{(\prime)}}$) and $kd = 5\pi/4$.

5. Effective medium theory for random SAMs

5.1. MICROSCOPIC CONSTITUTIVE MODELLING OF SOURCE PAIR

We return to the s/a pair to determine its dipolarizability. The induced electric dipole moment is $\underline{p}_e = (j\omega)^{-1}\int_L I(l)\mathrm{d}l \triangleq \epsilon_0 \underline{\underline{p}}_{ee} \cdot \underline{E}_i$. With $\mathcal{P}^{(t)}$ as defined above and $I_{00}(\underline{r}_0) = V/(Z_{00} + Z_L)$ for an induced voltage V:

$$\underline{\underline{p}}_{ee,\mathrm{pair}} = \frac{\mathcal{P}\mathcal{P}^t\left[\underline{\underline{I}} + \mathcal{H}_{as}\left(\underline{1}'_s\underline{1}'_s - \underline{\underline{I}}\right)\cdot\left(\underline{1}_s\underline{1}_s - \underline{\underline{I}}\right)^{-1}\right]\cdot(\underline{1}_l\underline{1}_l)}{j\omega\epsilon_0\,(Z_{00} + Z_L)}. \tag{29}$$

For example, for randomly oriented pairs of short identical dipoles, i.e., $\mathcal{P}^{(t)} = l/2$, $Z_{00} = (j\omega C)^{-1}$ and $\langle\underline{1}_s^{(\prime)}\underline{1}_s^{(\prime)}\rangle = \langle\underline{1}_l\underline{1}_l\rangle = \underline{\underline{I}}/3$, this yields an average dipolarizability

$$\left\langle \underline{\underline{p}}_{ee,\mathrm{pair}} \right\rangle = \frac{(1+\mathcal{H}_{as})l^2C}{12\epsilon_o(1+j\omega Z_L)}\underline{\underline{I}}, \tag{30}$$

where C is the equivalent capacitance of the dipole element.

5.2. EFFECTIVE PERMITTIVITY

Since a SAM was found to operate most efficiently in the quasi-static regime (kl_α, $kd \ll 1$), a description in the framework of effective medium theory (EMT) is feasible. When considering each s/a pair to form a single SAM particle of specific orientation and dipolarizability (29), $\underline{\underline{\epsilon}}_{\text{eff}}$ may be calculated directly from the Lorenz–Lorentz formula. However, this formulation is known to be sufficiently accurate only for relatively low particle densities. On the other hand, the two-phase asymmetric Bruggeman formula for ϵ_{eff} [5] appears to be well suited to high-density mixtures of conducting particles, which are typical for efficient implementations of SAMs, but requires the individual particle permittivities to be known. The latter formulation has been extended in [1] to deal with multi-phase mixtures. The SAM can be considered as a three-phase mixture of particles with respective dipolarizabilities $\underline{\underline{p}}_{ee}$ and $\underline{\underline{H}}_{as,\text{opt}} \cdot \underline{\underline{p}}_{ee}$ inside a host medium. In order to apply the result, the relationship between the particle's dipolarizability and its equivalent permittivity is needed. To this end, consider spherically symmetric s and a of equal size l as particles with isotropic dipolarizabilities ($\underline{\underline{p}}_{\alpha,ee} = p_{\alpha,ee}\underline{\underline{I}}$). The principal components of their permittivity follow from $p_{\alpha,ee} = 3V_\alpha(\epsilon_\alpha - \epsilon_o)/(\epsilon_\alpha + 2\epsilon_o)$ as:

$$\frac{\epsilon_{\alpha_{ii}}}{\epsilon_h} = \frac{V_\alpha + (1 - N_{\alpha_{ii}}/\epsilon_{A,r})p_{\alpha,ee}}{V_\alpha - (N_{\alpha_{ii}}/\epsilon_{A,r})\, p_{\alpha,ee}}, \qquad (i = x, y, z), \tag{31}$$

valid for $l \ll \lambda_h/(2\pi)$, i.e. $V \ll \lambda_h^3/(48\pi^2)$, where λ_h is the ambient wavelength, $N_{\alpha_{ii}} = 1/3$ are depolarization factors and $\epsilon_{A,r}$ is the apparent permittivity. With $\underline{p}_s = \epsilon_o \underline{\underline{p}}_{s,ee} \cdot \underline{E}_i$ and $\underline{p}_a = \epsilon_o H_{as} \underline{\underline{p}}_{s,ee} \cdot \underline{E}_i$, it follows that

$$\frac{\epsilon_s}{\epsilon_h} = \frac{V_s + [1 - (N_{s_{ii}}/\epsilon_{\text{eff},r})]\, p_{s,ee}}{V_s - (N_{s_{ii}}/\epsilon_{\text{eff},r})\, p_{s,ee}}, \quad \frac{\epsilon_a}{\epsilon_h} = \frac{V_a + [1 - (N_{a_{ii}}/\epsilon_{\text{eff},r})]\, H_{as} p_{s,ee}}{V_a - (N_{a_{ii}}/\epsilon_{\text{eff},r})\, H_{as} p_{s,ee}}, \tag{32}$$

for $p_{a,ee} < 3V_a < 2|H_{as}|p_{s,ee}$. Equation (32) can then be used with the three-phase Bruggeman formula to yield ϵ_{eff}.

Fig. 9 shows $(\epsilon_{\text{eff}}/\epsilon_o)$ and $(\epsilon_{\text{eff}}/\epsilon_h)$ as a function of the volume loading fraction $v_p \equiv 2v_s \equiv 2v_a$, for a mixture of spherical isotropic s/a particles forming an effective composite SAM. In this example, $p_{s,ee} = (7.5 - j0.1) \times 10^{-8}$ m^3, $V_s = V_a = 10^{-7}$ m^3 and $kd = 0.02$. The particles are encapsulated by a Kapton matrix for which $\epsilon_h/\epsilon_o = 3.48(1 - j0.008)$. Both the Maxwell–Garnett (MG) and asymmetric Bruggeman (AB) results are shown. For comparison, the effective permittivity for the same SAM in its passive state ($H_{as} \to 1$) is also shown. The effective permittivity shifts from (ϵ_h/ϵ_o) or 1 at $v_p = 0$ to 1 or $(\epsilon_h/\epsilon_o)^{-1}$ at $v_p = 1$.

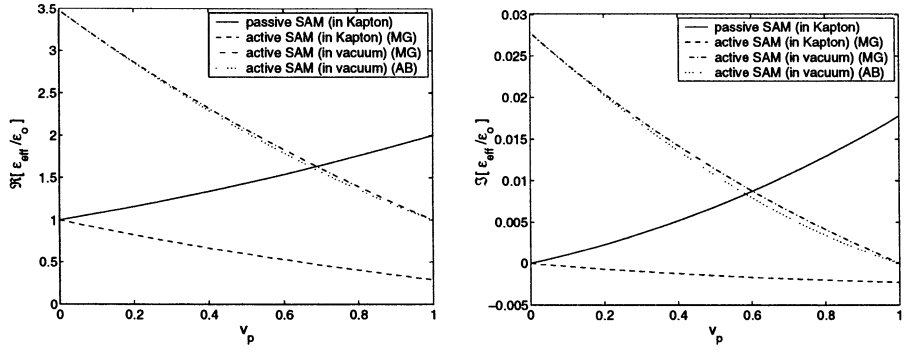

Figure 9. (a) Real and (b) imaginary parts of complex effective permittivity as a function of volume loading fraction v_p of sensor/actuator pairs for $kd \to 0$ relative to host medium or free space, for passive and active SAM, using Maxwell–Garnett (MG) and asymmetric Bruggeman (AB) mixing rules.

Fig. 10 shows the reflection coefficient for a free-standing single layer of effective SAM at normal incidence, compared to the corresponding reflection for the passive SAM and host medium only. This confirms the result in Fig. 7 that high particle densities (implying small s/a spacings) are required to obtain a substantial reduction in reflection. For example, a reduction by 20 dB compared to the reflection at $v_p = 0$ requires $v_p = 0.87$.

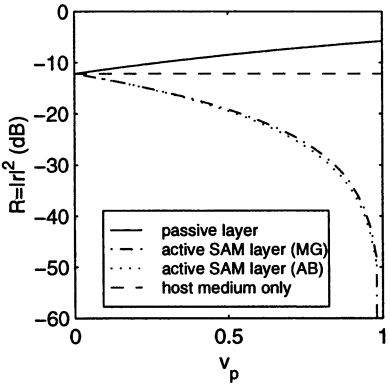

Figure 10. Reflection coefficient as a function of loading fraction of sensor/actuator pairs for $kd \to 0$, for passive and active SAM, using Maxwell–Garnett (MG) or asymmetric Bruggeman (AB) mixing rules.

A scattering-matrix formalism has been developed [1] that enables the frequency dependence of the reflection and transmission a SAM layer to be calculated. At long wavelengths, the contribution of scattering by an

efficient s/a pair is negligible compared to that by absorption in the overall attenuation (extinction) budget. The formalism is valid because we consider complex scattering coefficients, provided that each particle can be assumed to be excited by the external incident wave. Details on practical aspects of the implementation of SAMs based on antenna array technology can also be found in [1].

6. Conclusions

In this paper, we discussed the mechanism and implementation of a self-adaptive material (SAM) system, by considering adaptive control of a primary (master) source of uncontrolled radiation by a juxtaposed secondary (slave) source. The system was found to have its highest control efficiency, but lowest radiation efficiency when operated at relatively low frequencies. Only one but fundamental aspect, viz., the minimization of radiated power according to a user-specified criterion was analyzed in detail. This primary action is needed in order to suppress the natural (passive) EM response for a conventional material or scatterer. Any chosen secondary function may then be further added, through superposition or modulation of the secondary sources, using standard adaptive array techniques. In this way, SAMs may find application as an enhancement of conventional VHF, RF, microwave or millimeter-wave materials (e.g., tunable, wide-band or adaptive absorbing or shielding media), by adding new capabilities (e.g., Raman surfaces, nonspecular reflection, retro-directive glory, etc.) or by extending their capabilities to handle different signals simultaneously or in distinct manners (e.g., dual polarization or frequency, adaptive anisotropy, spectral or angular filtering, etc.).

The present analysis can also be used in connection with purely passive or purely active linear media consisting of paired elements that are connected via general transfer functions H_{as} (e.g, by introducing microscopic feedback in a pair of particles).

Appendix: SAM radiation coefficients

Based on the electric field integral and the reciprocity theorem, the field radiation coefficient can be expressed in terms of the control and configurational characteristics of the SAM array. We decompose $\underline{E}_t(\underline{r})$ in (16) in components parallel and perpendicular to the plane of incidence [4]:

$$\underline{E}_t(\underline{r}) = -\frac{\mathcal{P}I(\underline{r}_0)\ Z_0 \exp\left[-jk(\underline{r}-\underline{r}_0)\cdot\underline{1}_s\right]}{2d_x d_y s_z} \times \left[\left(\underline{1}_s\underline{1}_s - \underline{\underline{I}}\right) + \mathcal{H}_{as}\left(\underline{1}'_s\underline{1}'_s - \underline{\underline{I}}\right)\right]\cdot\underline{1}_l$$

$$= -\frac{V Z_0 \exp\left[-jk(\underline{r}-\underline{r}_0)\cdot\underline{1}_s\right]}{2d_x d_y s_z (Z_A+Z_L)} \times \left[\left(\mathcal{P}_\perp \underline{1}_\perp + \mathcal{P}_\parallel \underline{1}_\parallel\right) + \mathcal{H}_{as}\left(\mathcal{P}_\perp \underline{1}'_\perp + \mathcal{P}_\parallel \underline{1}'_\parallel\right)\right], \quad (33)$$

where we have omitted the subscripts '$\pm$' for simplicity. Here, $\underline{1}_\perp \triangleq (\underline{1}_n \times \underline{1}_s)/|\underline{1}_n \times \underline{1}_s|$, $\underline{1}_\parallel \triangleq \underline{1}_\perp \times \underline{1}_s$ and $\underline{1}'_{\parallel,\perp} = \left(\underline{1}'_s \underline{1}'_s - \underline{\underline{I}}\right)\cdot\left(\underline{1}_s \underline{1}_s - \underline{\underline{I}}\right)^{-1}\cdot \underline{1}_{\parallel,\perp}$ are unit vectors parallel and perpendicular to the plane of incidence for the sensors and to the plane of secondary radiation for the actuators, respectively, and $\underline{1}_n \equiv -\underline{1}_z$ is the unit vector along the inward normal to the SAM array. The array impedance Z_A is given by (18) and we furthermore allowed for a load impedance Z_L per array element. The total field (33) can be expressed in terms of $\mathcal{P}$ for general 3D incidence and radiation [1]. When specialized to radiation and scattering in the same plane as the plane of incidence, i.e., $\underline{1}'_\perp = \underline{1}_\perp$ and $\underline{1}'_\parallel = \underline{1}_\parallel$, then the components of the total field $\underline{E}_t = E_{t_\perp}\underline{1}_\perp + E_{t_\parallel}\underline{1}_\parallel$ are

$$E_{t_{\perp,\parallel}}(\underline{r}) = -\frac{Z_0\,(1+\mathcal{H}_{as})^2\,\mathcal{P}\mathcal{P}^t \exp\left(-jk\underline{r}\cdot\underline{1}_s\right)}{2d_x d_y s_z (Z_A+Z_L)}\,(\underline{E}_i\cdot\underline{1}_l)\left(\underline{1}_{\perp,\parallel}\cdot\underline{1}_l\right), \quad (34)$$

which implicitly defines the radiation coefficients $E_{t_\perp}/E_i$ and $E_{t_\parallel}/E_i$. Important special cases such as specular, forward and retro-radiation are discussed in Sec. 3.

References

1. Arnaut, L. R. Adaptive control and optimization of electromagnetic radiation, attenuation and scattering using self-adaptive material systems. *NPL Report CETM/RFMW/DGSS/000505,* May 2000; *IEEE Trans. Antennas Propag.,* to be published (2003).
2. Culshaw, B. *Smart Structures and Materials.* Artech House, 1996, Sec. 1.3.
3. Munk, B. A. and Burrell, G. A. Plane wave expansion for arrays of arbitrarily oriented piecewise linear elements and its application in determining the impedance of a single linear antenna in a lossy half-space; *IEEE Trans. Antennas Propag.,* vol. 34 nr. 3 (1979), pp. 331–343.
4. Munk, B. A. *Frequency Selective Surfaces: Theory and Design.* Wiley, 2000, Ch. 4.
5. Arnaut, L. R. Statistical characterization of complex media in random fields; *Int. J. Electron. Commun. (Archiv Elektr. Übertr.),* vol. 55 nr. 4 (2001), pp. 211–223.

ELECTROMAGNETIC FIELD SOLUTION IN CURVED STRUCTURES WITH LOCAL BIANISOTROPIC LOADING MEDIA

L.VEGNI, A. ALÙ, and F. BILOTTI
University of Roma Tre – Department of Electronic Engineering
Via della Vasca Navale, 84 – 00146 – Rome – Italy

Abstract. This contribution addresses the solution of the electromagnetic field in conformal geometries with local bianisotropic loading materials. The electromagnetic field solution is investigated both in the spatial and in the spectral domain in the generalized orthogonal curvilinear reference system. Finally, a novel set of transmission line equations are carried out to solve the electromagnetic field in integrated conformal structures involving bianisotropic media.

1. Introduction

The employment of unconventional media (inhomogeneous, chiral, bianisotropic, etc.) as substrates for integrated circuits has been deeply investigated in the last few years. Both theoretical and technological aspects concerning such materials have been considered and a lot of interesting features in the microwave frequency range have been pointed out. More in detail, a special interest has been focused by the authors on the possibility to improve antenna and circuit compactness for a fixed working frequency by employing chiral and bianisotropic materials [1]-[3].

On the other hand, in several research fields, including aircraft, spacecraft and land vehicle applications, integrated circuits have to be mounted on curved surfaces, in order to improve both aerodynamical and electrical performances. For this reason, conformal antennas and transmission lines have received recently much attention in the open technical literature and a lot of work has been performed from both the theoretical and the experimental point of view ([4] and references therein).

Complex geometries, even if they can be properly modelled in one of the orthogonal reference systems, introduce some analytical difficulties in the solution of the electromagnetic field [5]-[6]. Particularly, to decouple differential equations and derive closed form solutions for the electromagnetic field is not a straightforward matter. Moreover, if we want to investigate the electromagnetic features of conformal structures in presence of bianisotropic media, analytical difficulties increase very much, due to the presence of the magneto-electric effect. Differential equations to be solved in such a case are coupled equations (containing

S. Zouhdi et al. (eds.), Advances in Electromagnetics of Complex Media and Metamaterials, 439–448.

more than one field component) and some mathematical tricks must be used to obtain closed-form expressions for the electromagnetic field.

In this paper, we will present in a unified formulation some new theoretical developments on the solution of the electromagnetic field in conformal structures. The general formulation here derived in the case of bianisotropic media and generalized orthogonal geometries, can be used as an useful tool when particular structures and, thus, particular combinations of material and geometry have to be analyzed. The structure of the paper is given in the following. In section 2 a brief description of the generalized orthogonal curvilinear reference system and a detailed justification for its employment in the present analysis will be discussed. In section 3 the solution of the electromagnetic field in the spatial domain in presence of linear, isotropic, homogeneous media will be treated and discussed showing in which reference systems it is possible to find closed form solutions and in which ones a numerical solution is unavoidable. In section 4 the latter problem will be overcome and the possibility to find out closed form solutions in the spectral domain will be investigated and further discussed giving a generalization of the Fourier transform in curvilinear coordinates. In section 5 the presence of complex materials will be considered and a new set of transmission line equations in the generalized orthogonal curvilinear reference system will be derived showing their successful application in the analysis of conformal structures both in the spatial and in the spectral domain.

2. Generalized Orthogonal Curvilinear Reference System

Conformal structures are usually mounted on curved surfaces. Sometimes it is possible to approximate a generally curved finite surface by means of a portion of a single or a double curvature canonical surface (cylindrical or spherical). In many cases, instead, when the component dimensions are comparable with the surface curvature, in order to obtain good results, it is no longer possible to simplify the problem reducing the curvature to a canonical one. In such cases, a general and rigorous theory is needed.

Limiting our analysis to surfaces which can be described in orthogonal geometries, we can consider such surfaces as coordinate ones in the generalized orthogonal curvilinear reference system. The orthogonal unit vectors $\hat{\mathbf{q}}_1, \hat{\mathbf{q}}_2, \hat{\mathbf{q}}_3$ describing this reference system are depicted in Figure 1. As shown in [7], if the spatial coordinates associated with the reference system are expressed as q_1, q_2, q_3, the volume element (see Figure 1) is given by $dV = h_1 h_2 h_3 dq_1 dq_2 dq_3$, where h_1, h_2, h_3 are the so called metric factors (functions of all the three spatial coordinates q_1, q_2, q_3).

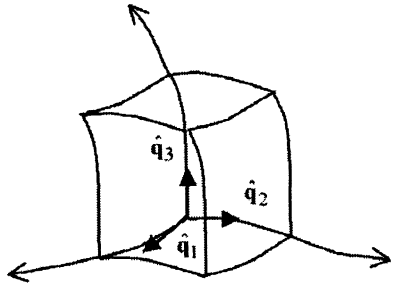

Figure 1 Generalized orthogonal curvilinear reference system

It is very convenient to develop a general theory for conformal integrated structures in the generalized orthogonal curvilinear reference system now presented. Such system, in fact, contains as particular cases sixteen reference systems, among which there are some very common and canonical ones, as reported in Table I. Spatial variables and scale factors associated to each reference system are also reported in the table. It has to be observed that some reference systems require also the assignment of some geometrical parameters indicated as a, b, and c [7].

3. Spatial Domain Field Solution in Linear, Isotropic and Homogeneous Media

Assuming a time harmonic dependence exp[jωt], and considering a source free region, Maxwell's equations in a linear, isotropic, homogeneous medium can be written as:

$$\begin{cases} \nabla \times \mathbf{E} = -j\omega\mu\mathbf{H} \\ \nabla \times \mathbf{H} = j\omega\varepsilon\mathbf{E} \\ \nabla \bullet \mathbf{E} = 0 \\ \nabla \bullet \mathbf{B} = 0 \end{cases}.$$

Vectorial wave equations for the electric and magnetic fields are, in this case, of the Helmholtz kind:

$$\begin{aligned} \nabla^2\mathbf{E} + k^2\mathbf{E} &= \mathbf{0} \\ \nabla^2\mathbf{H} + k^2\mathbf{H} &= \mathbf{0} \end{aligned}. \qquad (1)$$

The main goal, now, is to solve analytically these vectorial equations in order to express in a closed form the electromagnetic field inside the conformal structure. To this end, the first problem to be considered is the reduction of the vectorial Helmholtz equation to scalar uncoupled differential equations. The next one, then, is to find an analytical solution for the obtained scalar equations. The solutions of these two problems here proposed are summarized in Table II.

TABLE I. Reference systems contained in the generalized orthogonal curvilinear reference system.

Reference System	Spatial Variables			Metric Factors		
	q_1	q_2	q_3	h_1	h_2	h_3
Cartesian	x	y	z	1	1	1
Circular Cylindrical	ρ	ϕ	z	1	ρ	1
Parabolic Cylindrical	u	v	z	$\sqrt{u^2+v^2}$	$\sqrt{u^2+v^2}$	1
Elliptic Cylindrical	u	v	z	$a\sqrt{\sin^2 v+\sinh^2 u}$	$a\sqrt{\sin^2 v+\sinh^2 u}$	1
Spherical	r	θ	ϕ	1	r	r sin θ
Prolate Spheroidal	ξ	η	ϕ	$a\sqrt{\sin^2\eta+\sinh^2\xi}$	$a\sqrt{\sin^2\eta+\sinh^2\xi}$	$a \sin\eta \sinh\xi$
Oblate Spheroidal	ξ	η	ϕ	$a\sqrt{\sin^2\xi+\sinh^2\eta}$	$a\sqrt{\sin^2\xi+\sinh^2\eta}$	$a \cos\xi \cosh\eta$
Parabolic	u	v	ϕ	$\sqrt{u^2+v^2}$	$\sqrt{u^2+v^2}$	uv
Conic	λ	μ	ν	1	$\frac{\sqrt{\mu^2-\nu^2}\lvert\lambda\rvert}{\sqrt{\mu^2-a^2}\sqrt{b^2-\mu^2}}$	$\frac{\sqrt{\mu^2-\nu^2}\lvert\lambda\rvert}{\sqrt{\nu^2-a^2}\sqrt{\nu^2-b^2}}$
Paraboloidal	λ	μ	ν	$\frac{\sqrt{(\mu-\lambda)(\nu-\lambda)}}{2\sqrt{a^2-\lambda}\sqrt{b^2-\lambda}}$	$\frac{\sqrt{(\lambda-\mu)(\nu-\mu)}}{2\sqrt{a^2-\mu}\sqrt{b^2-\mu}}$	$\frac{\sqrt{(\lambda-\nu)(\mu-\nu)}}{2\sqrt{a^2-\nu}\sqrt{b^2-\nu}}$
Ellipsoidal	λ	μ	ν	$\frac{\sqrt{(\mu-\lambda)(\nu-\lambda)}}{2\sqrt{a^2-\lambda}\sqrt{b^2-\lambda}\sqrt{c^2-\lambda}}$	$\frac{\sqrt{(\lambda-\mu)(\nu-\mu)}}{2\sqrt{a^2-\mu}\sqrt{b^2-\mu}\sqrt{c^2-\mu}}$	$\frac{\sqrt{(\lambda-\nu)(\mu-\nu)}}{2\sqrt{a^2-\nu}\sqrt{b^2-\nu}\sqrt{c^2-\nu}}$
Bipolar	u	v	z	$\frac{a}{\cosh v-\cos u}$	$\frac{a}{\cosh v-\cos u}$	1
Bispherical	u	v	ϕ	$\frac{a}{\cosh v-\cos u}$	$\frac{a}{\cosh v-\cos u}$	$\frac{a \sin u}{\cosh v-\cos u}$
Toroidal	u	v	ϕ	$\frac{a}{\cosh u-\cos v}$	$\frac{a}{\cosh u-\cos v}$	$\frac{a \sinh u}{\cosh u-\cos v}$
Cardioid Cylinder	μ	ν	z	$\left(\mu^2+\nu^2\right)^{-3/2}$	$\left(\mu^2+\nu^2\right)^{-3/2}$	1
Tangent Sphere	μ	ν	ψ	$\frac{1}{\mu^2+\nu^2}$	$\frac{1}{\mu^2+\nu^2}$	$\frac{\mu}{\mu^2+\nu^2}$

TABLE II. Solution of the vectorial Helmholtz equation in the reference systems reported in Table I.

Reference System	1st Problem: Scalar Equation		2nd Problem: Analytical Solution
	Direct Projection	Borgnis' Potentials	Solution by Factorization
Cartesian	YES	YES	YES
Circular Cylindrical	YES	YES	YES
Parabolic Cylindrical	YES	YES	YES
Elliptic Cylindrical	YES	YES	YES
Spherical	NO	YES	YES
Prolate Spheroidal	NO	YES	NO
Oblate Spheroidal	NO	YES	NO
Parabolic	NO	YES	NO
Conic	NO	YES	YES
Paraboloidal	NO	YES	NO
Ellipsoidal	NO	YES	NO
Bipolar	YES	NO	YES
Bispherical	NO	NO	NO
Toroidal	NO	NO	NO
Cardioid Cylinder	NO	NO	NO
Tangent Sphere	NO	NO	YES

The first problem can be solved either by direct projection of the vectorial equation on the three coordinate directions (it has solution in five reference systems only) or by following the more general Borgnis' potentials theory (scalar equations to be solved can be found in eleven reference systems, including the previous five ones). As shown in [8], the Borgnis' potential functions U and V can be successfully introduced in those reference systems whose metric factors satisfy the following two conditions:

$$\begin{cases} h_3 = 1 \\ \dfrac{\partial}{\partial q_3}\left(\dfrac{h_1}{h_2}\right) = 0 \end{cases}. \tag{2}$$

It can be proved that in such reference systems (see Table I and Table II) the overall electromagnetic field can be expressed in terms of the Borgnis' potentials U and V as follows:

$$\begin{cases} E_1 = \dfrac{1}{h_1}\dfrac{\partial^2 U}{\partial q_3 \partial q_1} - j\omega\mu\dfrac{1}{h_2}\dfrac{\partial V}{\partial q_2} \\ E_2 = \dfrac{1}{h_2}\dfrac{\partial^2 U}{\partial q_2 \partial q_3} + j\omega\mu\dfrac{1}{h_1}\dfrac{\partial V}{\partial q_1}, \\ E_3 = \dfrac{\partial^2 U}{\partial q_3^2} + k^2 U \end{cases} \quad \begin{cases} H_1 = \dfrac{1}{h_1}\dfrac{\partial^2 V}{\partial q_3 \partial q_1} + j\omega\varepsilon\dfrac{1}{h_2}\dfrac{\partial U}{\partial q_2} \\ H_2 = \dfrac{1}{h_2}\dfrac{\partial^2 V}{\partial q_2 \partial q_3} - j\omega\varepsilon\dfrac{1}{h_1}\dfrac{\partial U}{\partial q_1}, \\ H_3 = \dfrac{\partial^2 V}{\partial q_3^2} + k^2 V \end{cases}$$

while the Borgnis' potentials satisfy the following two equations:

$$\begin{aligned} \nabla_t^2 U + \frac{\partial^2 U}{\partial q_3^2} + k^2 U = 0 \\ \nabla_t^2 V + \frac{\partial^2 V}{\partial q_3^2} + k^2 V = 0 \end{aligned}, \tag{3}$$

where $\nabla_t^2 = \dfrac{1}{h_1 h_2}\left[\dfrac{\partial}{\partial q_1}\left(\dfrac{h_2}{h_3}\dfrac{\partial}{\partial q_1}\right) + \dfrac{\partial}{\partial q_2}\left(\dfrac{h_1}{h_2}\dfrac{\partial}{\partial q_2}\right)\right]$.

The last column on the right side of Table II shows the reference systems in which a closed-form solution, obtained through the separation of variables (i.e. factorization), is possible.

4. Spectral Domain Field Solution in Conventional Materials

According to the theory up to now developed, separable closed-form solutions for the electromagnetic field can be found in the spatial domain in five reference systems only. In order to extend the family of orthogonal curvilinear reference systems for which closed forms are available, it is convenient to continue our analysis in the spectral domain.

Given a conformal integrated structure in the generalized reference system as in Figure 2, in the following we will explore the possibility to define a 2D spectral integral transform on the coordinate surface orthogonal to the $\hat{\mathbf{q}}_3$ direction. Such a transform, in the general case, is not of the Fourier kind (as in Cartesian reference system) and depends on the specific reference system we are considering.

A convenient integral representation in an unbounded region can be expressed using a continuous set of solutions of the scalar Helmholtz equation in those reference systems (the eleven ones previously mentioned) where it is possible to solve analytically such an equation. The solutions of the scalar Helmholtz equations, in fact, satisfy the completeness and orthogonality requirements we need for an integral transform. The general expression of this spectral transform is reported below, where the integration limits are not indicated, since their values depend on the particular reference system we are considering.

$$\tilde{\psi}(k_{q1}, k_{q2}, q_3) = \int\int \psi(q_1, q_2, q_3) K(q_1, q_2, k_{q1}, k_{q2}) h_1 h_2 dq_1 dq_2 \,. \qquad (4)$$

In the Cartesian case (where solutions of the scalar Helmholtz equation are expressed in terms of complex exponential functions), of course, this spectral transform turns into the very well known Fourier one. Applying (4), the scalar coupled partial differential equations derived by projecting the vectorial wave equation on the principal axes become ordinary ones involving derivatives with respect to the untransformed spatial variable (that one along $\hat{\mathbf{q}}_3$).

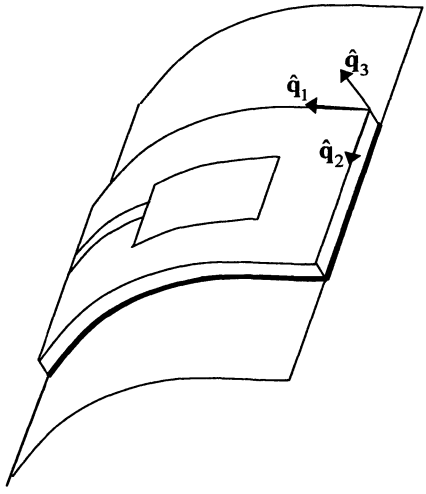

Figure 2. Integrated conformal structure in the generalized orthogonal curvilinear reference system. Please, note that any surface belongs to a coordinate one.

It can be shown that, after a further derivation with respect to q_3, it is possible to combine the coupled equations in order to derive a single scalar differential equation containing only one field unknown in the spectral domain. The main point to emphasize, now, is that the last equation can be solved analytically in terms of the spatial solutions $Q_3(q_3)$ of the factored scalar Helmholtz equation.

5. Local Bianisotropic Media: Generalized Transmission Line Equations

When considering local bianisotropic media as substrates for integrated conformal structures, vectorial wave equations for **E** and **H** fields are no longer as in (1). They are much more complex equations and the theory up to now developed cannot be applied as well. The constitutive relations for the media we are considering in this section, assuming a time harmonic variation law, can be written as:

$$\begin{cases} \mathbf{B} = \underline{\boldsymbol{\mu}}(q_1, q_2, q_3) \bullet \mathbf{H} + \underline{\boldsymbol{\beta}}(q_1, q_2, q_3) \bullet \mathbf{E} \\ \mathbf{D} = \underline{\boldsymbol{\alpha}}(q_1, q_2, q_3) \bullet \mathbf{H} + \underline{\boldsymbol{\varepsilon}}(q_1, q_2, q_3) \bullet \mathbf{E} \end{cases},$$

where $\underline{\varepsilon}, \underline{\alpha}, \underline{\beta}, \underline{\mu}$ are the constitutive tensors. More in detail, $\underline{\varepsilon}, \underline{\mu}$ are the permittivity and permeability tensors, respectively, while the two tensors $\underline{\alpha}, \underline{\beta}$ take into account the coupling effect between the electric and the magnetic field (magneto-electric effect).

In order to solve the electromagnetic field in a conformal structure containing complex media, we derive here the so-called generalized transmission line equations [9]-[10]. Starting from the curl Maxwell's equations

$$\begin{cases} \nabla \times \mathbf{E} = -j\omega\left(\underline{\mu} \bullet \mathbf{H} + \underline{\beta} \bullet \mathbf{E}\right) \\ \nabla \times \mathbf{H} = j\omega\left(\underline{\alpha} \bullet \mathbf{H} + \underline{\varepsilon} \bullet \mathbf{E}\right) \end{cases},$$

we adopt, firstly, the following normalizations:

$$\begin{cases} \overline{\mathbf{E}} = \underline{\mathbf{K}} \bullet \mathbf{E} \\ \overline{\mathbf{H}} = \underline{\mathbf{K}} \bullet \mathbf{H} \end{cases}, \quad \underline{\nabla}_r = \frac{1}{jk_0}\underline{\nabla}, \quad \begin{cases} \underline{\varepsilon}_r = \varepsilon_0^{-1}\underline{\varepsilon} \\ \underline{\mu}_r = \mu_0^{-1}\underline{\mu} \end{cases}, \quad \begin{cases} \underline{\alpha}_r = c_0\underline{\alpha} \\ \underline{\beta}_r = c_0\underline{\beta} \end{cases},$$

where $k_0 = \omega\sqrt{\varepsilon_0\mu_0}$, $c_0 = 1/\sqrt{\varepsilon_0\mu_0}$, and

$$\underline{\mathbf{K}} = \begin{pmatrix} h_1 & 0 & 0 \\ 0 & h_2 & 0 \\ 0 & 0 & h_3 \end{pmatrix}, \quad \underline{\nabla} = \begin{pmatrix} 0 & -\partial/\partial q_3 & \partial/\partial q_2 \\ \partial/\partial q_3 & 0 & -\partial/\partial q_1 \\ -\partial/\partial q_2 & \partial/\partial q_1 & 0 \end{pmatrix}.$$

Doing so, the curl Maxwell's equations can be rewritten in the following compact form:

$$\begin{cases} \left(\underline{\nabla}_r + \underline{\overline{\beta}}_r\right) \bullet \overline{\mathbf{E}} = -\underline{\overline{\mu}}_r \bullet Z_0\overline{\mathbf{H}} \\ \left(\underline{\nabla}_r - \underline{\overline{\alpha}}_r\right) \bullet Z_0\overline{\mathbf{H}} = \underline{\overline{\varepsilon}}_r \bullet \overline{\mathbf{E}} \end{cases},$$

where $Z_0 = \sqrt{\mu_0/\varepsilon_0}$ and $\underline{\overline{\nu}} = h_1h_2h_3\underline{\mathbf{K}}^{-1} \bullet \underline{\nu} \bullet \underline{\mathbf{K}}^{-1}$, where $\underline{\nu} = \underline{\varepsilon}_r, \underline{\mu}_r, \underline{\alpha}_r, \underline{\beta}_r$.

Eliminating the longitudinal components of the fields (with respect to $\hat{\mathbf{q}}_3$ direction), after some tedious algebra, the following telegraphist-like equations for the transverse fields ($\overline{\mathbf{E}}_t, \overline{\mathbf{H}}_t$) are derived:

$$\begin{cases} \dfrac{\partial \overline{\mathbf{E}}_t}{\partial \overline{q}_3} = \underline{\overline{\mathbf{A}}} \bullet \overline{\mathbf{E}}_t + \underline{\overline{\mathbf{Z}}} \bullet \overline{\mathbf{H}}_t \\ \dfrac{\partial \overline{\mathbf{H}}_t}{\partial \overline{q}_3} = \underline{\overline{\mathbf{Y}}} \bullet \overline{\mathbf{E}}_t + \underline{\overline{\mathbf{B}}} \bullet \overline{\mathbf{H}}_t \end{cases}, \tag{5}$$

where $\overline{q}_i = jk_0q_i$ (i=1,2,3). The elements of matrices in (5) have a very

complicated form and depend on the constitutive parameters, on the scale factors and on the derivatives with respect to the transverse variables. The elements of $\underline{\bar{\mathbf{A}}}$ and $\underline{\bar{\mathbf{Z}}}$ are reported in the following, while those ones of the other two matrices $\underline{\bar{\mathbf{Y}}}$ and $\underline{\bar{\mathbf{B}}}$ can be easily derived by using the duality principle:

$$
\begin{cases}
A_{11} = -\bar{\beta}_{21} - D^{(2,3)}_{-1,\bar{\beta}}\left(\dfrac{\bar{\alpha}_{33}}{\bar{\Delta}} D^{(3,1)}_{-2,\bar{\beta}} + \dfrac{\bar{\mu}_{33}}{\bar{\Delta}}\bar{\varepsilon}_{31}\right) - \bar{\mu}_{23}\left(\dfrac{\bar{\varepsilon}_{33}}{\bar{\Delta}} D^{(3,1)}_{-2,\bar{\beta}} + \dfrac{\bar{\beta}_{33}}{\bar{\Delta}}\bar{\varepsilon}_{31}\right) \\
A_{12} = -\bar{\beta}_{22} + D^{(2,3)}_{-1,\bar{\beta}}\left(\dfrac{\bar{\alpha}_{33}}{\bar{\Delta}} D^{(3,2)}_{+1,\bar{\beta}} - \dfrac{\bar{\mu}_{33}}{\bar{\Delta}}\bar{\varepsilon}_{32}\right) + \bar{\mu}_{23}\left(\dfrac{\varepsilon_{33}}{\bar{\Delta}} D^{(3,2)}_{+1,\bar{\beta}} - \dfrac{\bar{\beta}_{33}}{\bar{\Delta}}\bar{\varepsilon}_{32}\right) \\
A_{21} = \bar{\beta}_{11} - D^{(1,3)}_{+2,\bar{\beta}}\left(\dfrac{\bar{\alpha}_{33}}{\bar{\Delta}} D^{(3,1)}_{-2,\bar{\beta}} + \dfrac{\bar{\mu}_{33}}{\bar{\Delta}}\bar{\varepsilon}_{31}\right) + \bar{\mu}_{13}\left(\dfrac{\bar{\varepsilon}_{33}}{\bar{\Delta}} D^{(3,1)}_{-2,\bar{\beta}} + \dfrac{\bar{\beta}_{33}}{\bar{\Delta}}\bar{\varepsilon}_{31}\right) \\
A_{22} = \bar{\beta}_{12} + D^{(1,3)}_{+2,\bar{\beta}}\left(\dfrac{\bar{\alpha}_{33}}{\bar{\Delta}} D^{(3,2)}_{+1,\bar{\beta}} - \dfrac{\bar{\mu}_{33}}{\bar{\Delta}}\bar{\varepsilon}_{32}\right) - \bar{\mu}_{13}\left(\dfrac{\bar{\varepsilon}_{33}}{\bar{\Delta}} D^{(3,2)}_{+1,\bar{\beta}} - \dfrac{\bar{\beta}_{33}}{\bar{\Delta}}\bar{\varepsilon}_{32}\right)
\end{cases},
$$

$$
\begin{cases}
Z_{11} = -\bar{\mu}_{21} - D^{(2,3)}_{-1,\bar{\beta}}\left(\dfrac{\mu_{33}}{\bar{\Delta}} D^{(3,1)}_{+2,\bar{\alpha}} - \dfrac{\bar{\alpha}_{33}}{\bar{\Delta}}\bar{\mu}_{31}\right) - \bar{\mu}_{23}\left(\dfrac{\bar{\beta}_{33}}{\bar{\Delta}} D^{(3,1)}_{+2,\bar{\alpha}} - \dfrac{\bar{\varepsilon}_{33}}{\bar{\Delta}}\bar{\mu}_{31}\right) \\
Z_{12} = -\bar{\mu}_{22} + D^{(2,3)}_{-1,\bar{\beta}}\left(\dfrac{\mu_{33}}{\bar{\Delta}} D^{(3,2)}_{-1,\bar{\alpha}} + \dfrac{\bar{\alpha}_{33}}{\bar{\Delta}}\bar{\mu}_{32}\right) + \bar{\mu}_{23}\left(\dfrac{\bar{\beta}_{33}}{\bar{\Delta}} D^{(3,2)}_{-1,\bar{\alpha}} + \dfrac{\bar{\varepsilon}_{33}}{\bar{\Delta}}\bar{\mu}_{32}\right) \\
Z_{21} = \bar{\mu}_{11} - D^{(1,3)}_{+2,\bar{\beta}}\left(\dfrac{\mu_{33}}{\bar{\Delta}} D^{(3,1)}_{+2,\bar{\alpha}} - \dfrac{\bar{\alpha}_{33}}{\bar{\Delta}}\bar{\mu}_{31}\right) + \bar{\mu}_{13}\left(\dfrac{\bar{\beta}_{33}}{\bar{\Delta}} D^{(3,1)}_{+2,\bar{\alpha}} - \dfrac{\bar{\varepsilon}_{33}}{\bar{\Delta}}\bar{\mu}_{31}\right) \\
Z_{22} = \bar{\mu}_{12} + D^{(1,3)}_{+2,\bar{\beta}}\left(\dfrac{\bar{\mu}_{33}}{\bar{\Delta}} D^{(3,2)}_{-1,\bar{\alpha}} + \dfrac{\bar{\alpha}_{33}}{\bar{\Delta}}\bar{\mu}_{32}\right) - \bar{\mu}_{13}\left(\dfrac{\bar{\beta}_{33}}{\bar{\Delta}} D^{(3,2)}_{-1,\bar{\alpha}} + \dfrac{\bar{\varepsilon}_{33}}{\bar{\Delta}}\bar{\mu}_{32}\right)
\end{cases},
$$

where $D^{(j,k)}_{\pm i,\bar{\beta}} = \partial / \partial \bar{q}_i \pm \bar{\beta}_{jk}$, $D^{(j,k)}_{\pm i}(\bar{\alpha}) = \partial / \partial \bar{q}_i \pm \bar{\alpha}_{jk}$, $\bar{\Delta} = \bar{\mu}_{33}\bar{\varepsilon}_{33} - \bar{\alpha}_{33}\bar{\beta}_{33}$ and $\bar{v}_{ij}$ are the elements of tensor $\underline{\bar{\mathbf{v}}}$.

It is worth noting that in those reference systems in which it is possible to define a 2D spectral transform (see Section 5), the four matrices in equation (5) no longer contain derivatives with respect to the transverse spatial variables (they are replaced, in fact, by simple products) and become algebraic matrices. In such cases, it is straightforward to solve the electromagnetic field in the spectral domain and to calculate the spectral dyadic Green's function of the conformal structure depicted in Figure 2. Once the Green's function is known analytically, the main radiation and/or transmissive features of the conformal structure can be derived.

Finally, equations (5) can be straightforwardly employed, without applying a 2D spectral transform, in the numerical solution of the electromagnetic field inside a conformal structure by the so called *Method of Lines* (MoL). This method, introduced in electromagnetic problems by Pregla [11], allows to obtain a very fast

semi-analytical solution by discretizing the conformal structure with a proper set of lines.

6. Conclusions

In this paper, the solution of the electromagnetic field in integrated structures characterized by curved geometries and local bianisotropic loading materials has been addressed both in the spatial and in the spectral domain exploiting the generalized orthogonal curvilinear reference system. Finally, a novel set of transmission line equations, very useful in the analytical determination of the spectral Green's function of conformal structures and in the implementation of the numerical procedure called Method of Lines, have been derived.

7. References

1. Bilotti, F., Toscano, A., Vegni, L. (2002) FEM-BEM Formulation for the Analysis of Cavity Backed Patch Antennas on Chiral Substrates, *IEEE Trans. Antennas Propagat* **AP-50**, (to appear: Dec 2002 issue).
2. Bilotti, F., Vegni, L., Toscano, A. (2003) Radiation and Scattering Features of Patch Antennas with Bianisotropic Substrates, *IEEE Trans. Antennas Propagat.* **AP-51**, (to appear: Feb 2003 issue).
3. Scamarcio, G., Bilotti, F., Toscano, A., Vegni, L. (2001) Broad Band U-Slot Patch Antenna Loaded by Chiral Material *J. Electromag. Waves Applicat.* **15**, 1303-1317.
4. Wong, K. L., (1999) *Design of Nonplanar Microstrip Antennas and Transmission Lines*, Wiley Series in Microwave and Optical Engineering, K. Chang Ed., John Wiley and Sons, Inc., New York, NY.
5. Vegni, L., Alù, A., Bilotti, F. (2001) Some New Theoretical Developments on Conformal Integrated Antenna Theory *invited paper Proc. 16th International Conference on Applied Electromagnetics and Communications* (ICECOM'01), 120-123, Dubrovnik, Croatia, October 1-3.
6. Bilotti, F., Vegni, L., Alù, A. (2001) Generalized Transmission Line and Helmholtz Equations for the Analysis of Integrated Conformal Antennas and Circuits *Proc. International Conference on Electromagnetics in Advanced Applications* (ICEAA'01), 259-262, Turin, Italy, September 10-14.
7. Morse, P. M., Feshbach, H. (1953) *Methods of Theoretical Physics*, International Series in Pure and Applied Physics. McGraw-Hill, New York.
8. Borgnis, E., Papas, C. H. (1958) Electromagnetic Waveguides and Resonators, in *Encyclopedia of Physics*, **XVI**, Springer Verlag, Berlin.
9. Schelkunoff, S. A. (1952) Generalised Telegraphist's Equation for Waveguide *Bell Syst. Tech. J.*, 784-801, July issue.
10. Bresler, A. D., Joshi, G. H., Marcuvitz, N. (1958) Orthogonality Properties of Modes in Passive and Active Uniform Waveguides *J. Applied Phys.***29**, 794-799.
11. Pregla, R., Pascher, W. (1989) The Method of Lines in T. Itoh (ed.), *Numerical Techniques for Microwave and Millimeter Wave Passive Structures*, J. Wiley Publ., New York, pp. 381-346.

DIELECTRIC SUBSTRATES ANISOTROPY EFFECTS ON THE CHARACTERISTICS OF MICROSTRIP STRUCTURES

MOHAMED ESSAAIDI AND OTMAN EL MRABET
Electronics and Microwaves Group
Faculty of Science, Abdelmalek Essaadi University
P. O. Box 2121 Tetuan 93000 Morocco

Abstract. In this paper, we present an extension of the 3-D FDTD method based on **D**, **E**, **B** and **H** fields to handle arbitrary anisotropic media characterized by both a permittivity and a permeability tensors. This analysis was not possible for many FDTD simulators due to the lack of convenient absorbing boundary conditions (ABCs). Using the FDTD Method with Generalized Material-independent perfectly matched-Layer (GMIPLM) ABCs, based on the unsplit formulation, the behavior of the characteristics of microstrip structures printed on general anisotropic dielectric substrates is studied as a function of the optical axis rotation angle of this substrate.

1. Introduction

The Finite Difference Time Domain (FDTD) Method was originally proposed by K. S. Yee [1] and has been extensively used for a very wide variety of electromagnetic problems [2] ranging from microwave circuits analysis and design problems to those concerned with the simulation of electromagnetic waves radiation and scattering. Evidently, this is one of the most powerful simulation and CAD technique for solving several electromagnetic problems in the time domain and / or the frequency domain since it only suffices to perform a Fast Fourier Transform to obtain the frequency response on a wide frequency range from the time domain results. In order to limit the computation space for open electromagnetic problems, such those related with radiation and scattering problems, absorbing boundary conditions (ABCs) should be implemented. These particular boundary conditions consist in limiting the studied computational space by EM waves absorbing walls. Therefore, these ABCs work exactly like the walls of an anechoic chamber which absorb most of the electromagnetic power impinging on them and can reflect a very small amount of it without a significant impact on the accuracy of this model's results. One of the most important milestones in the history of the FDTD was the development of the so called perfect matching layers (PML) absorbing boundary condition which have been introduced by Berenger [3-4] and which have received a special interest in the specialized literature. Later on, several other improved PML based ABCs have also been

S. Zouhdi et al. (eds.), Advances in Electromagnetics of Complex Media and Metamaterials, 449–460.

proposed in the literature such as the uniaxial PML (UPML) and the general material independent PML (GMIPML) [5-7]. These latter PML versions have allowed a very efficient truncation of the computation space especially for materials with anisotropic and non-linear properties. This fact certainly contributed to enlarging the scope of the electromagnetic problems that can be dealt with using the FDTD efficiently.

Microstrip structures are very important microwave components for microwave integrated circuits (MICs) and Monolithic MICs (MMICs). They can fulfill several functions such as transmission lines, interconnects, filters, power dividers, resonators and antennas. CAD tools for these structures should take into account all the geometrical and physical parameters characterizing them to allow their accurate design. Hence, since anisotropy is an inherent characteristic to many dielectric materials that are used as substrates for these structures it should be taken into account in the numerical model used for their CAD. However, anisotropy cannot be seen only as a disadvantage or an anomaly in these materials whose impact on their overall characteristics and performances should be assessed correctly in order to allow an accurate prediction of their characterizing parameters or their efficient CAD. It should be also considered as another parameter, or another degree of freedom in their relevant EM problems, allowing to control and tune their characteristics.

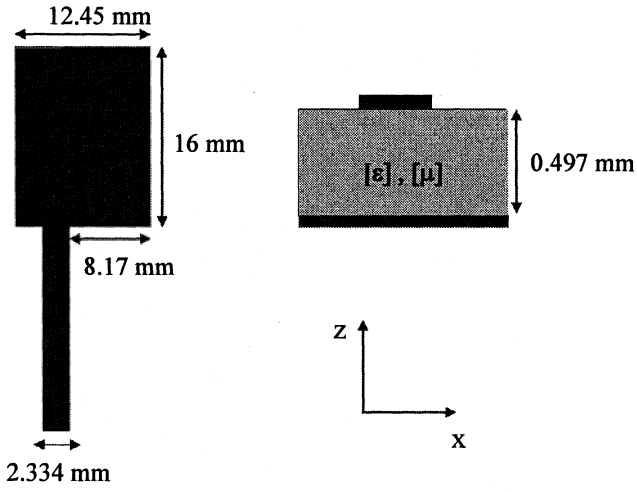

Figure 1. Microstrip patch antenna printed on anisotropic substrate

For the sake of illustration, the FDTD with the GMIPML absorbing boundary conditions are implemented for the analysis of a microstrip patch antenna printed on a general anisotropic dielectric substrate (Figure 1). The behavior of the return loss of this structure as a function of the permittivity and permeability tensors' elements is studied in depth allowing to capture efficiently their effects on its performances. The main result highlighted in this study shows the possible monitoring of these performances by means of the permittivity and permeability tensors' elements. So, in the case of the studied microstrip patch antenna the operating frequency band can be tuned through the tensors elements. This result is very important since this can be achieved by means of ferromagnetic materials, for instance, for which the permeability tensor elements' values can be controlled by a biasing static magnetic field.

2. Maxwell's equations in 3-D arbitrary anisotropic media

In the case of anisotropic media, considering **D-H** and **B-E** fields representations Maxwell's equations can be written as follows:

$$\frac{\partial D_x}{\partial t} = \frac{\partial H_z}{\partial y} - \frac{\partial H_y}{\partial z} \tag{1.1}$$

$$\frac{\partial D_y}{\partial t} = \frac{\partial H_x}{\partial z} - \frac{\partial H_z}{\partial x} \tag{1.2}$$

$$\frac{\partial D_z}{\partial t} = \frac{\partial H_y}{\partial x} - \frac{\partial H_x}{\partial y} \tag{1.3}$$

$$\frac{\partial B_x}{\partial t} = \frac{\partial E_y}{\partial z} - \frac{\partial E_z}{\partial y} \tag{1.4}$$

$$\frac{\partial B_y}{\partial t} = \frac{\partial E_z}{\partial x} - \frac{\partial E_x}{\partial z} \tag{1.5}$$

$$\frac{\partial B_z}{\partial t} = \frac{\partial E_x}{\partial y} - \frac{\partial Ey}{\partial x} \tag{1.6}$$

It is worth noting that the PML formulation based on **D-H** and / or **B-E** fields representations has been shown to be an optimal choice for anisotropic media since it allows important savings on computation resources [7]. This formulation has been developed only for electrically anisotropic substrate (i.e. considering a permittivity tensor). In this paper, we are going to extend this formulation to

anisotropic substrates characterized by both a permittivity tensor and a permeability tensor.

In order to update the **E** and **H** fields' components the following constitutive relations can be used,

$$\mathbf{H} = (1/\mu_0)[\mu]^{-1}\mathbf{B} \tag{2.1}$$

$$\mathbf{E} = (1/\varepsilon_0)[\varepsilon]^{-1}\mathbf{D} \tag{2.2}$$

where ε_0 and μ_0 are respectively vacuum's permittivity and permeability. As an illustrative example we give here only the expressions for the x components of the EM field, namely, E_x and H_x which can be written as follows :

$$E_x = \frac{\varepsilon_{yy}\varepsilon_{zz} - \varepsilon_{yz}\varepsilon_{zy}}{\Lambda} D_x + \frac{\varepsilon_{xz}\varepsilon_{zy} - \varepsilon_{xy}\varepsilon_{zz}}{\Lambda} D_y + \frac{\varepsilon_{xy}\varepsilon_{yz} - \varepsilon_{xz}\varepsilon_{yy}}{\Lambda} D_z \tag{3.1}$$

$$H_x = \frac{\mu_{yy}\mu_{zz} - \mu_{yz}\mu_{zy}}{\Delta} B_x + \frac{\mu\varepsilon_{xz}\mu_{zy} - \mu_{xy}\mu_{zz}}{\Delta} B_y + \frac{\mu\varepsilon_{xy}\mu_{yz} - \mu_{xz}\mu_{yy}}{\Delta} B_z \tag{3.2}$$

with,

$$\Lambda = \varepsilon_0 (\varepsilon_{xx}\varepsilon_{yy}\varepsilon_{zz} + \varepsilon_{xy}\varepsilon_{yz}\varepsilon_{zx} + \varepsilon_{xz}\varepsilon_{yz}\varepsilon_{zy} - \varepsilon_{xz}\varepsilon_{yy}\varepsilon_{zx} - \varepsilon_{xy}\varepsilon_{yx}\varepsilon_{zz} - \varepsilon_{xx}\varepsilon_{yz}\varepsilon_{zy})$$

$$\Delta = \mu_0 (\mu_{xx}\mu_{yy}\mu_{zz} + \mu_{xy}\mu_{yz}\mu_{zx} + \mu_{xz}\mu_{yz}\mu_{zy} - \mu_{xz}\mu_{yy}\mu_{zx} - \mu_{xy}\mu_{yx}\mu_{zz} - \mu_{xx}\mu_{yz}\mu_{zy})$$

$$[\varepsilon] = \begin{bmatrix} \varepsilon_{xx} & \varepsilon_{xy} & \varepsilon_{xz} \\ \varepsilon_{yx} & \varepsilon_{yy} & \varepsilon_{yz} \\ \varepsilon_{zx} & \varepsilon_{zy} & \varepsilon_{zz} \end{bmatrix} \tag{4.1}$$

$$[\mu]=\begin{bmatrix} \mu_{xx} & \mu_{xy} & \mu_{xz} \\ \mu_{yx} & \varepsilon_{yy} & \varepsilon_{yz} \\ \mu_{zx} & \mu_{zy} & \mu_{zz} \end{bmatrix} \tag{4.2}$$

Using the central difference approximation for the space and time derivatives and the averaging approximation procedure in space for **D;** equation (2.1), for example, can be written in the FDTD form as follows :

$$\begin{aligned} E_x^n(i+0.5,j,k) &= \frac{\varepsilon_{yy}\varepsilon_{zz}-\varepsilon_{yz}\varepsilon_{zy}}{\Lambda} D_x^n(i+0.5,j,k) + \frac{\varepsilon_{xz}\varepsilon_{zy}-\varepsilon_{xy}\varepsilon_{zz}}{4\Lambda} \\ &.(D_y^n(i,j-0.5,k) + D_y^n(i,j+0.5,k) + D_y^n(i+1,j-0.5,k) + \\ &D_y^n(i+1,j+0.5,k)) \\ &+ \frac{\varepsilon_{xy}\varepsilon_{yz}-\varepsilon_{xz}\varepsilon_{yy}}{4\Lambda}(D_z^n(i,j,k-0.5)+D_z^n(i,j,k+0.5) \\ &+ D_z^n(i+1,j,k-0.5)+D_z^n(i+1,j,k+0.5)) \end{aligned} \tag{5}$$

Furthermore, a special updating equation on the perfect electric conducting (PECs) planes, ensuring that the tangential electric field $\mathbf{E}_t$ is equal to zero on them, is used. A more detailed description of this technique can be found in [4]. If the PEC is located inside the mesh domain (e.g. at the metallic microstrip line located at $k = k_0$ along the z-direction) we can write :

$$\begin{aligned} &D_x^n(i+0.5,j,k_0) = \\ &-\frac{(\varepsilon_{xz}\varepsilon_{zy}-\varepsilon_{xy}\varepsilon_{zz})}{4\Lambda(\varepsilon_{yy}\varepsilon_{zz}-\varepsilon_{yz}\varepsilon_{zy})}(D_y^n(i,j-0.5,k_0)+D_y^n(i,j+0.5,k_0) \\ &D_y^n(i+1,j-0.5,k_0)+D_y^n(i+1,j+0.5,k_0)) \\ &-\frac{(\varepsilon_{xy}\varepsilon_{yz}-\varepsilon_{xz}\varepsilon_{yy})}{4\Lambda(\varepsilon_{yy}\varepsilon_{zz}-\varepsilon_{yz}\varepsilon_{zy})}(D_z^n(i,j,k_0-0.5)+D_z^n(i,j,k_0+0.5) \\ &D_z^n(i+1,j,k_0-0.5)+D_z^n(i+1,j,k_0+0.5)) \end{aligned} \tag{6}$$

However, if the PEC is located exactly on the mesh truncation (i.e. the ground plane at k = 0), the above expression can be written,

$$
\begin{aligned}
D_x^n(i+0.5,j,0) &= -\frac{(\varepsilon_{xz}\varepsilon_{zy}-\varepsilon_{xy}\varepsilon_{zz})}{4\Lambda(\varepsilon_{yy}\varepsilon_{zz}-\varepsilon_{yz}\varepsilon_{zy})}(2D_y^n(i,j-0.5,1)-D_y^n(i,j-0.5,2) \\
&2D_y^n(i+1,j+0.5,1)-D_y^n(i,j+0.5,2)+2D_y^n(i+1,j-0.5,1) \\
&-D_y^n(i+1,j-0.5,2)+2D_y^n(i+1,j+0.5,1)-2D_y^n(i+1,j+0.5,2)) \\
&-\frac{(\varepsilon_{xy}\varepsilon_{yz}-\varepsilon_{xz}\varepsilon_{yy})}{4\Lambda(\varepsilon_{yy}\varepsilon_{zz}-\varepsilon_{yz}\varepsilon_{zy})}(3D_z^n(i,j,0.5)-D_z^n(i,j,1.5) \\
&+3D_z^n(i+1,j,0.5)-D_z^n(i+1,j,0.5))
\end{aligned}
\tag{7}
$$

The theoretical formulation based on the FDTD method, which has been developed through the different equations presented above, can be used efficiently to model microstrip structures printed on anisotropic substrates.

3. Absorbing boundary conditions

As mentioned earlier, absorbing boundary conditions are essential for efficient implementation of the FDTD method. Basically, these conditions are used to truncate the computation space of the studied electromagnetic problem. Though, in the literature we can find references to Murs's [8] and Higdon's [9] ABCs, we limit our discussion in this section to the widely used perfect matching layers PML ABCs.

3.1 BERENGER'S PML MEDIUM

In order to bring EM wave reflection on a material interface to zero level, a material with a magnetic conductivity σ^* and an electric conductivity σ filling half space is used. A TE_z -polarized plane wave is incident on the interface between air and this material such that :

$$\vec{H}^{inc} = \hat{z}H_0 \exp(-j(\beta_x^i x - \beta_y^i y) \tag{8}$$

and it is propagating with an angle θ^i with respect to the x-direction.

The EM fields in the two regions can be expressed as,

$$\vec{H}_1 = \hat{z}H_0(1+\Gamma e^{2j\beta_x^i x})e^{-j\beta_x^i x - j\beta_y^i y} \tag{9.1}$$

$$\vec{E}_1 = \left[-\hat{x}\frac{j\beta_y^i}{\omega\varepsilon_1}\left(1+\Gamma e^{2j\beta_x^i x}\right)+\hat{y}\frac{j\beta_x^i}{\omega\varepsilon_1}\left(1+\Gamma e^{2j\beta_x^i x}\right)\right]H_0 e^{-j\beta_x^i x - j\beta_y^i y} \tag{9.2}$$

for $x < 0$, and

$$\vec{H}_2 = \hat{z}H_0\tau e^{-j\beta_x^t x - j\beta_y^t y} \tag{9.3}$$

$$\vec{E}_1 = \left[-\hat{x}\frac{j\beta_y^t}{\omega\varepsilon_2\left(1+\frac{\sigma}{j\omega\varepsilon_2}\right)}+\hat{y}\frac{j\beta_x^t}{\omega\varepsilon_2\left(1+\frac{\sigma}{j\omega\varepsilon_2}\right)}\right]H_0 e^{-j\beta_x^t x - j\beta_y^t y} \tag{9.4}$$

for $x > 0$.

where Γ and τ are reflection and transmission coefficients respectively.

It can be easily demonstrated that if $\mu_1 = \mu_2$ and $\varepsilon_1 = \varepsilon_2$ then $\Gamma = 0$. Furthermore, we can prove that the wave speed in Berenger's medium is identical to that in medium 1. Also, despite the fact that the medium is lossy the wave is dispersionless.

This medium has been used with limited success to terminate FDTD lattices since it is matched to the interior region only for normally incident waves. Therefore, oblique incidence waves partially reflect back into the computation region and corrupt the solution. Consequently, the absorbing medium should be placed sufficiently far away from any source or discontinuity such that the incident waves are planar and quasi-normally impinging on the interface. This is impractical for large or elongated domains. Berenger [4] introduced another technique to remedy this problem consisting in adding an additional degree of freedom through splitting the transverse fields into two orthogonal components so that the medium can be matched at oblique incidence. Thus, if a wave impinges at the interface between the air and the perfectly matched layer, it is perfectly transmitted for all polarizations, all frequencies and all angles of incidence.

3.2 ANISOTROPIC PML ABSORBING MEDIUM

We can consider the split-field PML introduced by Berenger as a hypothetical medium. Since the coordinates depend on the loss terms this medium should be anisotropic. This kind of absorbing medium was first discussed by Sacks et al. [10]. For a single interface this medium is considered to be uniaxial with resepct to the electric and magnetic properties. These ABCs are also refered to as uniaxial perfectly matching layers UPML. Furthermore, Berenger's split field PMLs and the UPML have the same propagation characteristics since they both result in the same wave equation.

3.3. PML FORMULATION BASED ON D-H FIELDS FOR ARBITRARY ANISOTROPIC DIELECTRIC MEDIA

This is [5-7] one of the most efficient PML formulations used for the truncation of computation space in the FDTD method.

As an illustrative example of this formulation, let's suppose that the substrate is composed of arbitrary anisotropic dielectric material. For such a medium, Maxwell's equations (inside the PML) considering a D-H fields based formulation can be written,

$$\vec{\nabla} x \vec{H} = \hat{\varepsilon}^D \frac{\partial \vec{D}}{\partial t} \tag{10.1}$$

$$\vec{D} = [\varepsilon]\vec{E} \tag{10.2}$$

$$\vec{\nabla} x \vec{E} = -\mu_0 \hat{\varepsilon}^D \frac{\partial \vec{H}}{\partial t} \tag{10.3}$$

where $[\varepsilon]$ is the permittivity tensor of the substrate which can be expressed in a form similar to that given by (4.1). $\hat{\varepsilon}^D$ is the material-independent diagonal tensor used in the PML which is given by,

$$\hat{\varepsilon}^D = \begin{bmatrix} \frac{s_y^D s_z^D}{s_x^D} & 0 & 0 \\ 0 & \frac{s_x^D s_z^D}{s_y^D} & 0 \\ 0 & 0 & \frac{s_x^D s_y^D}{s_z^D} \end{bmatrix} \tag{11}$$

where, $$s_v^D = 1 + \frac{\sigma_v^D}{j\omega}, \quad v = x,y \text{ or } z$$

4. Numerical results

As an illustration of this study, we consider a microstrip patch antenna (Figure 1) printed on an anisotropic substrate with optical axes laying in the x-y plane. Under this latter condition, the permittivity and permeabilty tensors are given respectively by [10],

$$\varepsilon_{xx} = \varepsilon_1 \cos^2\theta + \varepsilon_2 \sin^2\theta \tag{12.1}$$

$$\varepsilon_{yy} = \varepsilon_1 \tag{12.2}$$

$$\varepsilon_{zz} = \varepsilon_1 \sin^2\theta + \varepsilon_2 \cos^2\theta \tag{12.3}$$

$$\varepsilon_{xz} = \varepsilon_{zx} = (\varepsilon_1 - \varepsilon_2) \sin\theta \cos\theta \tag{12.4}$$

$$\varepsilon_{xy} = \varepsilon_{yx} = \varepsilon_{yz} = \varepsilon_{zy} = 0 \tag{12.5}$$

where $\varepsilon_1 = 2.31$ and $\varepsilon_2 = 2.19$ and θ represents the angle between the optical axis and the x-direction.

$$\mu_{xx} = \mu_1 \cos^2\varphi + \mu_2 \sin^2\varphi \tag{13.1}$$

$$\mu_{yy} = \mu_1 \sin^2\varphi + \mu_2 \cos^2\varphi \tag{13.2}$$

$$\mu_{zz} = \mu_1 \tag{13.3}$$

$$\mu_{xy} = \mu_{yx} = (\mu_2 - \mu_1) \sin\varphi \cos\varphi \tag{13.4}$$

$$\mu_{xz} = \mu_{zx} = \mu_{yz} = \mu_{zy} = 0 \tag{13.5}$$

where $\mu_1 = 2.0$ and $\mu_2 = 2.2$ and φ represents the angle between the optical axis and the x-direction.

The studied patch antenna has been already analyzed by D. M. Sheen et al. [12] considering isotropic substrate. It is represented by an FDTD simulation mesh comprised of 58 × 80 × 22 cells in the x-, y- and z-directions, respectively. The cell size is defined by $\Delta x = 0.3891$ mm, $\Delta y = 0.400$ mm and $\Delta z = 0.1985$ mm and the corresponding time step was $\Delta t = 0.4$ ps. The microstrip feed line was 27 cells long and was excited by a voltage source with a Gaussian profile and 30-GHz bandwidth. The GMIPML media layers were placed five cells from the edge of the patch antenna and ten cells above its surface. The GMIPML slabs were eight-cells

thick, the normal theoretical reflection coefficient R(0) was 10^{-4} and the power of the conductivity distribution m = 4.

Figure 2 depicts the studied microstrip patch antenna return loss versus frequency. For this case, the dielectric substrate is considered to be a non magnetic anisotropic material with a permittivity tensor similar to that given by (12). For $\theta = 0$ we approach the isotropic case which has been already studied in reference [10]. A comparison with the results presented in this reference shows a very good agreement. Furthermore, changing this material's optical angle from 0 to $\pi/2$ rad affects very slightly the resonant frequencies of this microstrip structure, especially for the first resonance. These frequencies decrease when θ varies from 0 to $\pi/2$ rad.

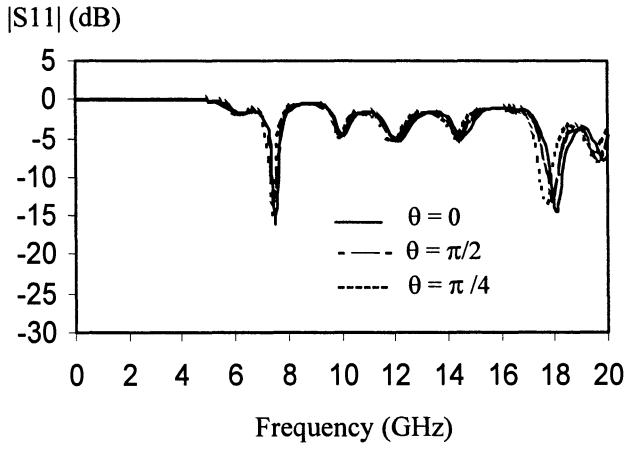

Figure 2. Return loss of the anisotropic microstrip patch antenna vs. frequency, with $\varepsilon_1 = 2.31$, $\varepsilon_2 = 2.19$

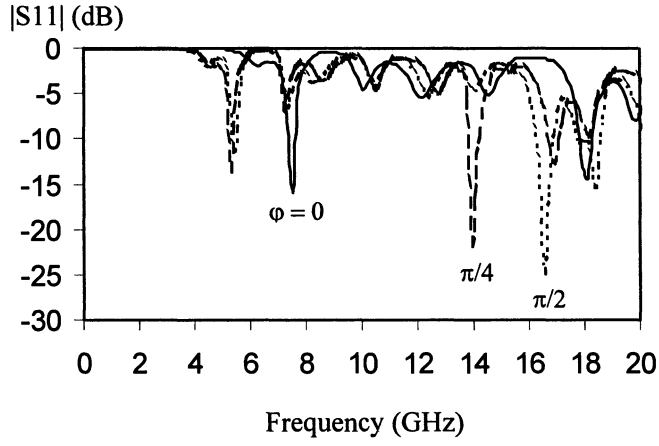

Figure 3. Return loss of the anisotropic microstrip patch antenna vs. frequency, with $\mu_1 = 2.0$ and $\mu_2 = 2.2$

In Figure 3 we investigate the behavior of the return loss of the studied microstrip patch antenna as a function of the permeability tensor's elements. Compared to the results presented in figure 2, we see that the resonant frequencies experience a very important shift towards lower frequencies when φ varies from 0 to π/2 rad. Furthermore, the greatest decrease is observed for $\varphi = \pi/4$ rad especially for the second resonance peaks between 14 and 18 GHz. Thus, using ferromagnetic materials, for example, the permeability tensor's elements could be used to tune the operating frequencies of this antenna over a wide range of frequencies.

5. Conclusions

In this paper we have extended the 3-D FDTD method based on **D, E, B,** and **H** fields representation to model microstrip structures printed on anisotropic dielectric substrates. The influence of anisotropy effects on the return loss of a microstrip patch antenna printed on an anisotropic dielectric substrate has been treated as an illustrative example. It has been found that anisotropic effects can be very significant. Therefore, they should be taken into account in the model to allow an accurate design of these structures. Moreover, anisotropic materials can be used as a means to control microstrip structures' characteristics.

6. References

1. Yee, K. (1966) Numerical Solution of Initial Boundary Value Problems Involving Maxwell's Equations in Isotropic Media, *IEEE Trans. Antennas and Propagation* **14**, 302-307.
2. Taflove, A. (1998) *Advances in Computational Electromagnetics : The Finite-Difference Time-Domain Method*, Artech House, Boston-London.
3. Berenger, J. P. (1994) A Perfectly Matched Layer for the Absorption of Electromagnetic Waves, *J. comput.Phy.* **114**, 185-200.
4. Berenger, J. P. (1997) Improved PML for the FDTD Solution of wave-structure interaction problems, *IEEE Trans. Antennas and Propagation* **45**, pp. 466-473.
5. Gedney, S. D. (1996) An Anisotropic Perfectly Matched Layer-absorbing Medium for the Truncation of FDTD Lattices, *IEEE Trans. Antennas and Propagation* **44**, pp.1630-1639.
6. Zhao, A. P. (1998) Unsplit-Field Formulations for Generalised Material Independent PML Absorbers, *IEEE MTT-S microwave Symp. Dig.* **2**, 496-472.
7. Zhao, A.P. et al. (1999) An Efficient FDTD Algorithm for the analysis of Microstrip Patch Antennas Printed on a General Anisotropic Dielectric Substrate, *IEEE Trans. Microwave Theory and Techniques* **47**,1142-1146.
8. Mur, G.(1981) Absorbing Boundary Conditions for the Finite-Difference Approximation of the Time Domain Electromagnetic Field Equations, *IEEE Trans. Electromagnetic Compatibility* **23**, pp. 377-382.
9. Higdon, R. L. ((1986) Absorbing Boundary Conditions for Difference Approximations to the Multidimensional Wave Equation, *Mathematics of Computation* **47**, pp. 437-459.
10. Sacks, Z. S., Kingsland, D. M., Lee, R. and Lee, J. F. (1995) A Perfectly Matched Anisotropic Absorber for Use As An Absorbing Boundary Condition, *IEEE Trans. Antennas and Propagation* **43**, pp. 1460-1463.
11. Chen, Y. and Becker, B. (1993) Dispersion characteristics of Open and Shielded Microstrip Lines Under a Combined Principal Axes Rotation of Electrically and Magnetically Anisotropic Substrates, *IEEE Trans. Microwave Theory and Techniques* **41**.
12. Sheen, D. M., Ali, S. M., Abouzahra, M. D. And Kong, J. A. (1990) Application of the Three-Dimensional Finite-Difference Time-Domain Method to the Analysis of Planar Microstrip Circuits, *IEEE Trans. Microwave Theory and Techniques* **38**, pp. 849-857.

THEORETICAL AND EXPERIMENTAL LIMITATIONS OF CHIRAL MICROWAVE ABSORBERS

O. REYNET and O. ACHER
CEA Le Ripault
BP 16 - 37260 MONTS
acher@ripault.cea.fr

Abstract. Constitutive relations of chiral media are used to derive integral relations on the reflection coefficient of chiral microwave absorbers. The result of our calculation allow us to rigorously extend Rozanov's bound to metal-backed chiral multilayered slabs. Experimental data are given and a comparison between the performances of chiral and conventional dielectric microwave absorbers is made.

1. Introduction

A significant research effort has been dedicated to the investigation of the microwave properties of chiral media over the last 20 years [5, 11, 12]. Chiral materials were suspected to exhibit several attractive properties, and in particular they were advocated for making radar absorbers. The experimental properties of chiral absorbers have been reported [7, 13]. Though chiral materials with significant maximal absorption have been reported, it is not evident that these results indicate a significant breakthrough compared to existing absorbing materials [3, 4]. Indeed, the interest for chiral absorbers seems to have decreased for the last years. However, the nature of the limitations of chiral absorbers has not yet been understood. It may be due to technical difficulties in manufacturing them with a high level of performance. It may also be due to a still imperfect understanding of how to use the chirality parameter as an adjustable parameter in multilayer absorbers. Alternatively, this may be attributed to more fundamental limitations.

Recently, significant progress have been made in establishing bounds on the ultimate performance of conventional radar absorbers [1, 8, 9]. These bounds have been derived from the causality principle. Rozanov's bound gives the ultimate thickness to bandwidth ratio for a dielectric absorber. For thin magnetic absorbers, the minimal amount of magnetic material necessary to achieve a given absorption spectrum has been derived [1]. It has been

S. Zouhdi et al. (eds.), Advances in Electromagnetics of Complex Media and Metamaterials, 461–470.

shown [2] that a single layer chiral absorber cannot exceed Rozanov bound. However, this demonstration did not rule out the possibility that chiral materials may be more competitive than conventional dielectric absorbers when inserted in a multilayer structure.

One aim of this paper is to extend Rozanov's bound to multilayers comprising any number of chiral materials. Another aim is to give some comparisons between the experimental performances reported for chiral absorbers, and the theoretical bounds presented here.

We first establish the reflection coefficient of a wave incoming under normal incidence on a chiral slab or on a chiral multilayer backed by a metallic plate. Then, we rigorously adapt the derivation of Rozanov's bound to chiral multilayers. Some measurements on a commercially available dielectric absorber are then detailed and we retrieve some experimental results on chiral absorbers. We show that the experimental limitation is consistent with the bound we derived. We conclude on the expected properties of chiral absorbers compared to conventional dielectric absorbers.

2. Theoretical approach

2.1. WAVE PROPAGATION IN CHIRAL MEDIA

In this paper, constitutive relations of chiral media are noted :

$$\vec{D} = \varepsilon \vec{E} + jg\vec{H} \tag{1}$$

and

$$\vec{B} = \mu \vec{H} - jg\vec{E}. \tag{2}$$

where μ, ε and g are complex scalar numbers and functions of the wavelength $\lambda = c_o/f$, where c_o is the speed of light in the vacuum. It is important to note that when $|\lambda| \longrightarrow \infty$, the value limit of g is zero, otherwise static electromagnetic fields would be complex vectors.

For plane waves in a chiral medium, there are two eigen-polarizations: Right Circular (RCP) and Left Circular (LCP). From Maxwell's equations we derive associated wave vectors :

$$k_r = \omega(g + \sqrt{\varepsilon\mu}) \tag{3}$$

and

$$k_l = \omega(-g + \sqrt{\varepsilon\mu}). \tag{4}$$

2.2. REFLECTION COEFFICIENT

We first derive the reflection coefficient for a chiral monolayer backed by a metallic plate for each eigen-polarization. A plane monochromatic wave is assumed to be normally incident on the chiral layer. The reflection coefficient is then

$$\rho = \frac{Z - Z_0}{Z + Z_0}. \tag{5}$$

The expression of the first order development in d/λ of the reflection coefficient will be useful for deriving bounds of allowed properties. When the thickness d of the chiral layer is small compared to the wavelength, the expression of this coefficient at the first order in d/λ is

$$\rho_+ = -1 + j\frac{4\pi}{\lambda}\left(\mu + gc_o\sqrt{\frac{\mu}{\varepsilon}}\right)d \tag{6}$$

for a right circular polarization and

$$\rho_- = -1 + i\frac{4\pi}{\lambda}\left(\mu - gc_o\sqrt{\frac{\mu}{\varepsilon}}\right)d \tag{7}$$

for a left circular polarization. Here, c_o stands for the speed of light in vacuum.

This result can be extended to a multilayered structure (Fig. 1) using transformation matrix [10]. For either RCP (+) or LCP (-) polarization, a matrix relates the complex E and H fields at the interface m, as a function of the fields at the interface (m-1)

$$\begin{bmatrix} E_{m-1} \\ H_{m-1} \end{bmatrix} = [A_{m\pm}] \begin{bmatrix} E_m \\ H_m \end{bmatrix} \tag{8}$$

where

$$A_{m_\pm} = \begin{bmatrix} \cos(k_m d_m) & jz_m \sin(k_m d_m) \\ \frac{j}{z_m}\sin(k_m d_m) & \cos(k_m d_m) \end{bmatrix}. \tag{9}$$

and $k_m = k_r$or $k_m = k_l$.

We note A the following matrix

$$A_\pm = \begin{pmatrix} a_{11} & a_{12} \\ a_{21} & a_{12} \end{pmatrix} = [A_1][A_2]\cdots[A_m] \tag{10}$$

that describes the relation between the fields inside a multilayered screen.

An effective input impedance for the layer combination can be defined as

$$Z_\pm = \frac{a_{11}z_m + a_{12}}{a_{22} + a_{21}z_m} \tag{11}$$

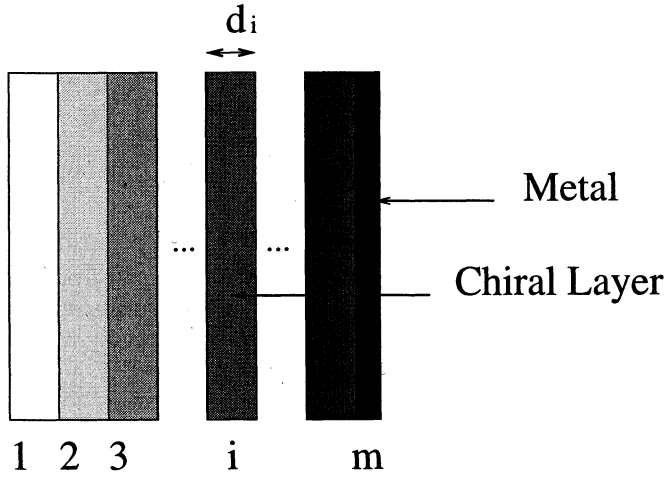

Figure 1. Chiral multilayer backed by a metallic plate.

where z_m is equal to zero because the last layer is metallic. The total reflection coefficient is found to be

$$\rho_{\pm} = \frac{Z_{\pm} - Z_0}{Z_{\pm} + Z_0} \tag{12}$$

for each RC(+) and LC(-) polarization.

In particular, this holds for a multilayer including chiral layers and isotropic conventional layers. Then, if the thickness d_i of each layer is small compared to the wavelength, the reflection coefficient of the multilayer at the first order in d/λ is

$$\rho_{\pm} = -1 + j\frac{4\pi}{\lambda}\sum_{i=1}^{n}(\mu_i \pm g_i c_o\sqrt{\frac{\mu_i}{\varepsilon_i}})d_i. \tag{13}$$

3. Theoretical results

3.1. CAUCHY'S THEOREM

In the following, the index +/- referring to either RCP or LCP will be omitted, as the derivation can be carried on both expressions. The electromagnetic fields are assumed to have the $exp(j\omega t)$ time dependence, and therefore $\rho(\lambda)$ is analytic in the upper half-plane of complex λ [6]. $\rho(\lambda)$ may

have nulls in the upper-half plane and $ln(\rho(\lambda))$ is not an analytical function in the upper half plane. Following Rozanov [9], we introduce an ancillary function ρ'

$$\rho'(\lambda) = \rho(\lambda)\Pi(\lambda) \tag{14}$$

with

$$\Pi(\lambda) = \frac{\prod_{i=1}^{n} (\lambda - \lambda_i^*)}{\prod_{i=1}^{n} (\lambda - \lambda_i)} \tag{15}$$

where the λ_i are the nulls in the upper-half plane of $\rho(\lambda)$ and * stands for the complex conjugation. The function $\ln \rho'(\lambda)$ is analytical over the upper half plane.

Applying Cauchy's theorem to this function on the closed contour C (Fig. 2) consisting in the whole axis of real wavelength and the closing upper semi-circle C_∞ yields

$$\int_C \ln(\rho')d\lambda = \int_C \ln(\rho)d\lambda + \int_C \ln \Pi(\lambda)d\lambda = 0. \tag{16}$$

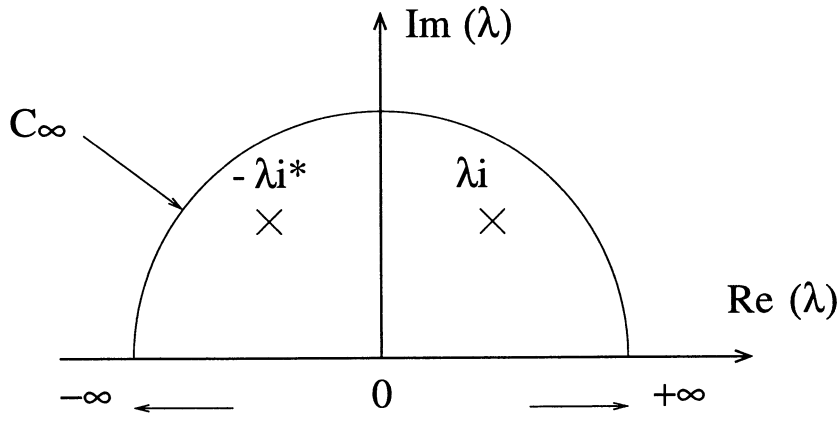

Figure 2. Complex plane and nulls of $\rho(\lambda)$ in the upper half plane

The integral over the upper semi-circle are first calculated. These integrals are easy to derive :

$$\int_{C\infty} \ln \Pi(\lambda) d\lambda = -2\pi \sum_{i=1}^{n} Im(\lambda_i) \tag{17}$$

The quantity on the right side of Eq. (17) is negative or null, because the complex λ_i are in the upper half plane. From Eq. (6), it can be derived that

$$\int_{C\infty} \ln(\rho) d\lambda = 4\pi^2 \left(\mu_s + g_s c_o \sqrt{\frac{\mu_s}{\varepsilon_s}} \right) d \tag{18}$$

where μ_s, ε_s and $g_s$stand for the static values of μ,ε and g.

The integrals over the real axis are then calculated. As causality and analicity are strongly connected [6], it can be shown that :

$$\rho^*(\lambda) = \rho(-\lambda^*) \tag{19}$$

For real wavelength, this relation becomes $\rho^*(\lambda) = \rho(-\lambda)$. As a consequence :

$$\int_{-\infty}^{+\infty} \ln(\rho) d\lambda = \int_{0}^{+\infty} \ln(\rho^* \rho) d\lambda = 2 \int_{0}^{+\infty} \ln |\rho| d\lambda. \tag{20}$$

Besides, it can be noticed that if λ_i is a null of ρ, then $-\lambda_i^*$ is also a null of ρ. This implies that $\Pi(-\lambda^*) = \Pi^*(\lambda)$, and for real frequencies, $\Pi(-\lambda) = \Pi^*(\lambda)$. It follows that

$$\int_{-\infty}^{+\infty} \ln \Pi d\lambda = \int_{0}^{+\infty} \ln \Pi \Pi^* d\lambda = 2 \int_{0}^{+\infty} \ln |\ \Pi\ | d\lambda. \tag{21}$$

As the module of Π is 1, this integral is null :

$$2 \int_{0}^{+\infty} \ln \mid \Pi \mid d\lambda = 0. \tag{22}$$

Thus, for a Dällenbach screen, we derive that

$$-\int_{0}^{\infty} \ln |\rho(\lambda)| d\lambda \leq 2\pi^2 \left(\mu_s + g_s c_o \sqrt{\frac{\mu_s}{\varepsilon_s}} \right) d \tag{23}$$

For a multilayered screen, we obtain

$$-\int_0^\infty \ln|\rho(\lambda)|d\lambda \leq 2\pi^2 \sum_{i=1}^{n} (\mu_{s_i} \pm g_{s_i} c_o \sqrt{\frac{\mu_{s_i}}{\varepsilon_{s_i}}}) d_i. \tag{24}$$

As the static limit of the chirality parameter g is zero, the previous result simplifies into :

$$-\int_0^\infty \ln|\rho(\lambda)|d\lambda \leq 2\pi^2 \sum_{i=1}^{n} \mu_{s_i} d_i. \tag{25}$$

This bound applies to the reflection coefficient of any metal-backed chiral multilayered screen. It means that Rozanov's bound is the same for magnetodielectric and chiral media.

4. Experimental results and discussion

Previous results do not mean that chirality is useless to design microwave absorbers. In fact, chirality might be a solution to reach this bound. Therefore we calculate the integrals of the logarithm of the reflection coefficient to compare the performance of a chiral medium and a dielectric medium. The results are reported in table I.

TABLE I. Characteristics of dielectric and chiral absorbers

Material References	Units	DFS10	Chiral 1 [13]	Chiral 2 [4]
Thickness d	mm	1.6	11.2	5
Investigation band	GHz	2-18	10-18	14.5-17.5
$2\pi^2 d$	mm	31.5	220	99
$\int_{\lambda\,\min}^{\lambda\,\max} \ln\|\rho\|d\lambda$	mm	30.6	22	6

The Eccosorb DSF 10® is a commercially available dielectric absorber from Emerson&Cuming. Its thickness is 1,6 mm. The reflection coefficient of a 300x300mm^2 plate of this material has been measured in the Dällenbach configuration in the 2-18 GHz range. The maximum absorption is located near 10 GHz. The integral (25) is computed in the wavelength range 17 mm to 150 mm from the experimental measurements. It is compared to

the Rozanov's bound $2\pi^2 d$. We observe that the absorption over the investigated range reaches 97% of the bound. This result is coherent with Rozanov's work predicting that the bound can not be exceeded, but also indicates that materials with microwave properties pretty close to this bound can be manufactured.

It is important to notice that the integration in (25) is performed on the wavelength, whereas it is more common to give absorption results as a function of the frequency. For that reason, the reflection coefficient R in dB has been represented both as a function of the frequency (Fig. 3) and of the wavelength (Fig. 4).

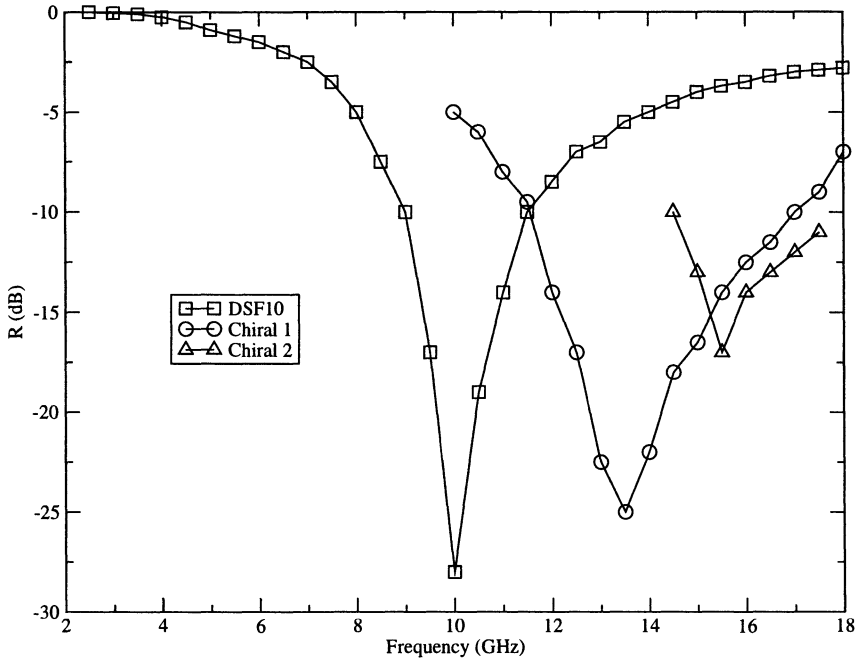

Figure 3. Reflection coefficient of dielectric DSF10 and two chiral materials versus frequency.

We were able to find the reflection coefficients of two chiral media in the literature [4, 13]. They are represented on Figs 3 and 4. The integral of the absorption over the wavelength has been computed for each material in the measurement bandwidth.

The first material reaches 10% of the bound and the second 6% (see table I). This is coherent with our prediction that this bound can not be exceeded with chiral materials. Indeed, it appears that the absorption properties

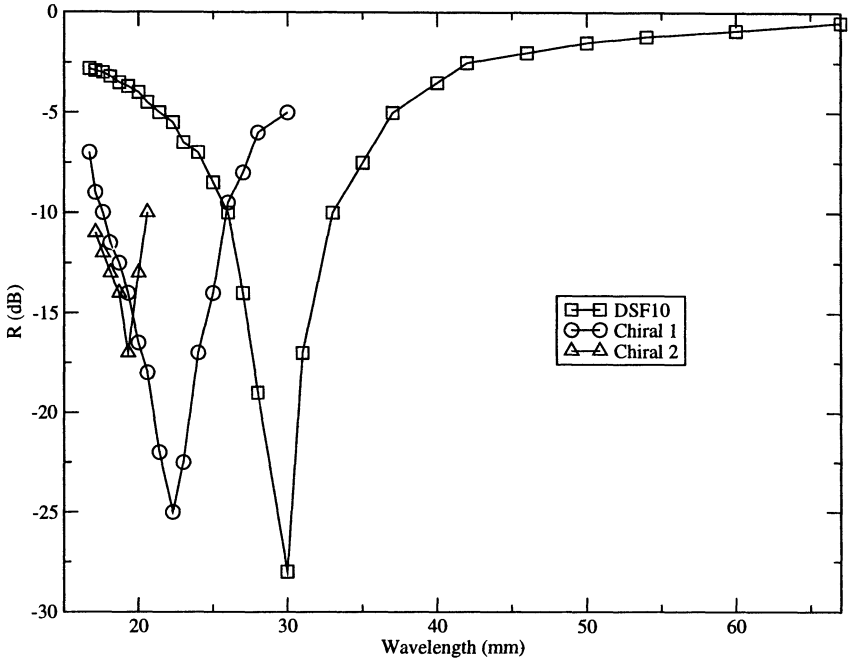

Figure 4. Reflection coefficient of dielectric DSF10 and two chiral materials versus wavelength.

lie far below this bound. This may be partly attributed to the limited measurement bandwidth : the integral over the whole frequency range is expected to be somewhat larger than the integral over the measurement bandwidth. However, it may also be attributed to the thickness and design of chiral materials which are not optimized.

5. Conclusion

It has been shown that for chiral media, the bound of the integral of the logarithm of the reflection coefficient over the wavelength is the same as for conventional magneto-dielectric media. Experimental results confirm that the measured properties of chiral absorber are below this bound. This suggests that no breakthrough is to be expected in the absorption properties of multilayered chiral absorbers. However, it does not exclude that chiral materials may be convenient to obtain specific spectral responses, or may be useful for other purposes.

Acknowledgements

We are grateful to Alain Froger and Nicolas Malléjac for precious comments on the manuscript, to A. Sihvola and S. Zouhdi for fruitful discussions.

References

1. Acher, O. and A. Adenot: 2000, 'Bounds on the dynamic properties of magnetic materials'. *Phys. Rev. B* **62**(17).
2. Brewitt-Taylor, C.: 2000, 'Fundamental limitation on the performance of chiral radar absorbing materials'. In: A. Barbosa and A. Topa (eds.): *Bianisotropics 2000.* Lisbon, Portugal.
3. Cloethe, J., M. Bingle, and D. Davidson: 2001, 'The role of chirality and resonance in synthetic microwave absorbers'. *Int. J. Electron. Commun.* **55**(4), 233–239.
4. Cloethe, J., S. Kuehl, and M. Bingle: 1998, 'The absorption of electromagnetic waves at microwave frequencies by synthetic chiral and racemic materials'. *Int. J. Of Applied Electromagnetics and Mechanics* **9**, 103–114.
5. Jaggard, D., A. Mickelson, and C. Papas: 1978, 'On electromagnetic waves in chiral media'. *Appl. Phys.* **18**, 211–216.
6. Nussenzveig, H.: 1972, *Causality and Dispersion Relations*, Mathematics in science and engineering. New-York and London: Academic Press.
7. Ro, R., V. Varadan, and V. Varadan: 1991, 'Parametric experimental study of microwave absorption in chiral composites'. In: *Microwave Theory and Application in Materials Processing. Annual meeting of the American Ceramic Society*, Vol. 21. Cincinnati, Ohio, pp. 531–538.
8. Rozanov, K.: 1998, 'Ultimate thickness to bandwidth ratio of radar absorbers'. *IVTAN* **1**, 422.
9. Rozanov, K.: 2000, 'Ultimate thickness to bandwidth ratio of radar absorbers'. *IEEE Trans. Ant. Prop.* **48**(8), 1230.
10. Ruck and Barrick: 1990, *Radar Cross Section Handbook*, Vol. 2.
11. Serduykov, A., I. Semchenko, S. Tretyakov, and A. Sihvola: 2001, *Electromagnetics of Bi-anisotropic Materials Theory and Applications*, Electrocomponent Science Monographs. Gordon and Breach Science.
12. Sihvola, A. and I. Lindell: 1995, 'Material effects in bi-anisotropic electromagnetics'. *IEICE Trans. Electron.* **E78-C**(10), 1383–1390.
13. Varadan, V., A. Lakhtakia, and V. Varadan: 1988, 'Principles of microwave interaction with polymeric and organic materials'. *Mat. Res. Soc. Symp. Proc.* **124**, 59–67.

LIST OF CONTRIBUTORS

O. ACHER
Laboratoire Matériaux Magnétiques et Hyperfréquences
CEA Le Ripault
BP. 16, F-37260 MONTS, France

E. ALTSHULLER
Saratov State University
Astrakhanskaya str. 83, Saratov, Russia

A. ALÙ
Department of Electronic Engineering
University of Roma Tre
Via della Vasca Navale, 84 – 00146, Rome, Italy

L.R. ARNAUT
National Physical Laboratory
Center for Electromagnetic and Time Metrology
Queens Road, Teddington TW11 0LW, United Kingdom

A.M. BARBOSA
Instituto de Telecomunicações
Instituto Superior Técnico
Av. Rovisco Pais, 1, 1049-001 Lisboa, Portugal

A.Y. BIJAMOV
Tbilisi State University
Chavchavadze Ave., 380028 Tbilisi, Georgia

F. BILOTTI
Department of Electronic Engineering
University of Roma Tre
Via della Vasca Navale, 84 – 00146, Rome, Italy

D. BIMBERG
Institut für Festkörperphysik
Technische Universität Berlin
Hardenbergstr. 36, 10623 Berlin, Germany

F.G. BOGDANOV
Tbilisi State University
Chavchavadze Ave., 380028 Tbilisi, Georgia
& Georgian Technical University
Kostava Str., 380075 Tbilisi, Georgia

A.N. BORZDOV
Department of Theoretical Physics
Belarusian State University
Fr. Skaryny avenue 4, 220050 Minsk, Belarus

G.N. BORZDOV
Department of Theoretical Physics
Belarusian State University
Fr. Skaryny avenue 4, 220050 Minsk, Belarus

N.N. DADOENKOVA
Donetsk Physical & Technical Institute
National Academy of Sciences of Ukraine
72, R. Lyuxemburg str., 83114 Donetsk, Ukraine

O. EL MRABET
Electronics and Microwaves Group
Faculty of Science, Abdelmalek Essaadi University
P. O. Box 2121, Tetuan 93000, Morocco

N. ENGHETA
Department of Electrical and Systems Engineering
University of Pennsylvania
Philadelphia, Pennsylvania 19104, USA

D. ERNI
Swiss Federal Institute of Technology
CH-8092 Zurich, Switzerland

M. ESSAAIDI
Electronics and Microwaves Group
Faculty of Science, Abdelmalek Essaadi University
P.O. Box 2121, Tetuan 93000, Morocco

E.A. EVDISHCHENKO
Shubnikov Institute of Crystallography
Russian Academy of Sciences
Leninskii pr. 59, Moscow 117333, Russia

E.A. FEDOSENKO
Department of General Physics
Gomel State University
Sovyetskaya Str. 104, 246019 Gomel, Belarus

V. GUSYATNIKOV
Saratov State University
Astrakhanskaya str. 83, Saratov, Russia

C. HAFNER
Swiss Federal Institute of Technology
CH-8092 Zurich, Switzerland

A. HOFFMANN
Institut für Festkörperphysik
Technische Universität Berlin
Hardenbergstr. 36, 10623 Berlin, Germany

V.E. KAGANOVICH
Department of General Physics
Gomel State University
Sovyetskaya Street 104, 246019 Gomel, Belarus

D.D. KARKASHADZE
Tbilisi State University
Chavchavadze Ave., 380028 Tbilisi, Georgia

S.A. KHAKHOMOV
Department of General Physics
Gomel State University
Sovyetskaya Str. 104, 246019 Gomel, Belarus

K.K. KONSTANTINOV
Shubnikov Institute of Crystallography
Russian Academy of Sciences
Leninskii pr. 59, Moscow 117333, Russia

A.F. KONSTANTINOVA
Shubnikov Institute of Crystallography
Russian Academy of Sciences
Leninskii pr. 59, Moscow 117333, Russia

M. KOSTYRKO
Institute of Physical Optics
23 Dragomanov Str., 79005 L'viv, Ukraine

A. LAKHTAKIA
Department of Engineering Science and Mechanics
Pennsylvania State University, University Park
PA 16802-6812, USA

I.L. LYUBCHANSKII
Donetsk Physical & Technical Institute
National Academy of Sciences of Ukraine
72, R. Lyuxemburg str., 83114 Donetsk, Ukraine

M.I. LYUBCHANSKII
Donetsk Physical & Technical Institute
National Academy of Sciences of Ukraine
72, R. Lyuxemburg str., 83114 Donetsk, Ukraine

T.G. MACKAY
School of Mathematics
University of Edinburgh
The King's Buildings, Edinburgh EH9 3JZ, United Kingdom

S.A. MAKSIMENKO
Institute for Nuclear Problems
Belarus State University
Bobruiskaya 11, 220050 Minsk, Belarus

R. MARQUÉS
Departamento de Electricidad y Electrónica
Universidad de Sevilla
Av. Reina Mercedes s/n, 41012 Sevilla, Spain

J. MARTEL
Departamento de Física Aplicada 3
Universidad de Sevilla
Av. Reina Mercedes s/n, 41012 Sevilla, Spain

S.I. MASLOVSKI
Radio Laboratory
Helsinki University of Technology
P.O. Box 3000, FIN-02015 HUT, Finland

F. MEDINA
Departamento de Electricidad y Electrónica
Universidad de Sevilla
Av. Reina Mercedes s/n, 41012 Sevilla, Spain

A.M. MERZLIKIN
Institute of Theoretical and Applied Electromagnetism (ITAE), JIHT
Russian Academy of Sciences
Izhorskaya 13/19, Moscow 127412, Russia

F. MESA
Departamento de Física Aplicada 1
Universidad de Sevilla
Av. Reina Mercedes s/n, 41012 Sevilla, Spain

Y. MOROZOV
Radio Laboratory
Helsinki University of Technology
P.O. Box 3000, FIN-02015 HUT, Finland
on leave from Institute of Radio Engineering and Electronics
Russian Academy of Sciences
Zelyonaya str. 38, Saratov 410019, Russia

B.V. NABATOV
Shubnikov Institute of Crystallography
Russian Academy of Sciences
Leninskii pr. 59, Moscow 117333, Russia

I.S. NEFEDOV
Radio Laboratory
Helsinki University of Technology
P.O. Box 3000, FIN-02015 HUT, Finland
on leave from Institute of Radio Engineering and Electronics
Russian Academy of Sciences
Zelyonaya str. 38, Saratov 410019, Russia

C.R. PAIVA
Instituto de Telecomunicações
Instituto Superior Técnico
Av. Rovisco Pais, 1, 1049-001 Lisboa, Portugal

S. PROSVIRNIN
Institute of Radio Astronomy
Krasnoznamennaya Street 4, Kharkov 61002, Ukraine

Th. RASING
Research Institute for Materials
University of Nijmegen
6525 ED Nijmegen, The Netherlands

O. REYNET
Laboratoire Matériaux Magnétiques et Hyperfréquences
CEA Le Ripault
BP 16, F-37260 MONTS, France

I.V. SEMCHENKO
Department of General Physics
Gomel State University
Sovyetskaya Str. 104, 246019 Gomel, Belarus

E.A. SHAPOVALOV
Department of Physics
Donetsk National University
24, Universitetskaya str., 83055 Donetsk, Ukraine

A. SIHVOLA
Electromagnetics Laboratory
Helsinki University of Technology
P.O. Box 3000, FIN-02015 HUT, Finland

C.R. SIMOVSKI
Radio Laboratory
Helsinki University of Technology
P.O. Box 3000, FIN-02015 HUT, Finland
On leave from State Institute of Fine Mechanics and Optics
Sablinskaya, 14, 197101, St. Petersburg, Russia

G. YA. SLEPYAN
Institute for Nuclear Problems
Belarus State University
Bobruiskaya 11, 220050 Minsk, Belarus

A.L. TOPA
Instituto de Telecomunicações
Instituto Superior Técnico
Av. Rovisco Pais, 1, 1049-001 Lisboa, Portugal

S.A. TRETYAKOV
Radio Laboratory
Helsinki University of Technology
P.O. Box 3000, FIN-02015 HUT, Finland

L.VEGNI
Department of Electronic Engineering
University of Roma Tre
Via della Vasca Navale, 84 – 00146, Rome, Italy

V.G. VESELAGO
Moscow Institute of Physics and Technology
9 Institutski per. Dolgoprudny, Moscow district 141700, Russia

A.P. VINOGRADOV
Institute of Theoretical and Applied Electromagnetism (ITAE), JIHT
Russian Academy of Sciences
Izhorskaya 13/19, Moscow 127412, Russia

R. VLOKH
Institute of Physical Optics
23 Dragomanov Str., 79005 L'viv, Ukraine

W.S. WEIGLHOFER
Department of Mathematics
University of Glasgow
University Gardens, Glasgow G12 8QW, Great Britain

R.S. ZARIDZE
Tbilisi State University
Chavchavadze Ave., 380028 Tbilisi, Georgia

S. ZOUHDI
Laboratoire de Génie Electrique de Paris *LGEP-Supélec*
Plateau de Moulon, 91192 Gif-Sur-Yvette Cedex, France

Index